HiTASC

AD-A267 022

4 |||||||||||||||||||||||||||

High Temperature Advanced Structural Composites

Rensselaer Polytechnic Institute
Troy, N. Y. 12180-3590

Final Report

Book 1 of 3: *Executive Summary and Intermetallic Compounds*

DTIC
ELECTE
JUL 19 1993
S E D

University Research Initiative

Sponsored by: The Defense Advanced Research Projects Agency

Monitored by: Office of Naval Research
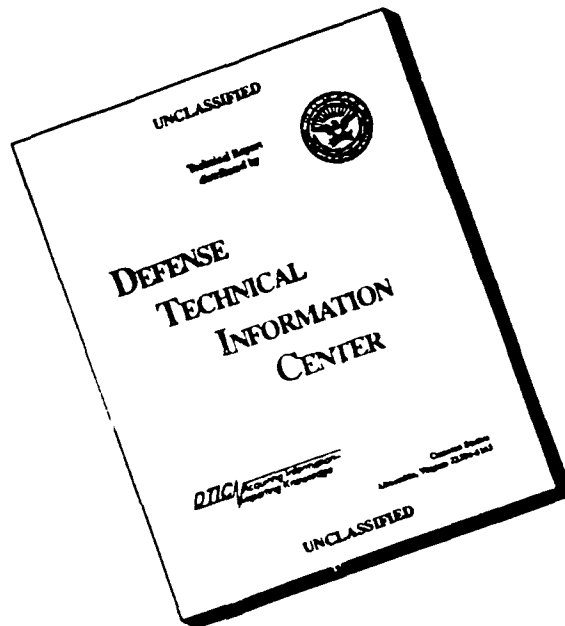
93-16145
||||||||||||||||||||||||||||

93 7   1

DISCLAIMER NOTICE

THIS DOCUMENT IS BEST QUALITY AVAILABLE. THE COPY FURNISHED TO DTIC CONTAINED A SIGNIFICANT NUMBER OF PAGES WHICH DO NOT REPRODUCE LEGIBLY.

FINAL REPORT
University Research Initiative
Contract No. N00014—86—K—0770
October 1, 1986 — June 13, 1992

High Temperature Advanced Structural Composites

vol. 1 of 3

sponsored by
Office of Naval Research and
Defense Advanced Research Projects Agency

Accesion For		
NTIS CRA&I		☒
DTIC TAB		☐
U..announced		☐
Justification		
By		
Dist ibution /		
Availability Codes		
Dist	Avail and / or Special	
A-1		

DTIC QUALITY INSPECTED 5

REPORT DOCUMENTATION PAGE

Form Approved
OMB No. 0704-0188

1a. REPORT SECURITY CLASSIFICATION	1b. RESTRICTIVE MARKINGS
Unclassified	

2a. SECURITY CLASSIFICATION AUTHORITY	3. DISTRIBUTION / AVAILABILITY OF REPORT
2b. DECLASSIFICATION / DOWNGRADING SCHEDULE	Unrestricted

4. PERFORMING ORGANIZATION REPORT NUMBER(S)	5. MONITORING ORGANIZATION REPORT NUMBER(S)

6a. NAME OF PERFORMING ORGANIZATION	6b. OFFICE SYMBOL (If applicable)	7a. NAME OF MONITORING ORGANIZATION
Center for Composite Materials and Structures Rensselaer Polytechnic Institute		Office of Naval Research

6c. ADDRESS (City, State, and ZIP Code)	7b. ADDRESS (City, State, and ZIP Code)
Rensselaer Polytechnic Institute Troy, NY 12180-3590	800 North Quincy Street Arlington, VA 22217-5000

8a. NAME OF FUNDING / SPONSORING ORGANIZATION	8b. OFFICE SYMBOL (If applicable)	9. PROCUREMENT INSTRUMENT IDENTIFICATION NUMBER
Advanced Research Projects Agency		#N00014-86-K-0770

8c. ADDRESS (City, State, and ZIP Code)	10. SOURCE OF FUNDING NUMBERS			
	PROGRAM ELEMENT NO.	PROJECT NO.	TASK NO.	WORK UNIT ACCESSION NO.
1400 Wilson Blvd. Arlington, Virginia 22209				

11. TITLE (Include Security Classification)

High Temperature Advanced Structural Composites

12. PERSONAL AUTHOR(S) George J. Dvorak and R. Judd Diefendorf

13a. TYPE OF REPORT	13b. TIME COVERED	14. DATE OF REPORT (Year, Month, Day)	15. PAGE COUNT
Final	FROM 861001 TO 920613	930402	748

16. SUPPLEMENTARY NOTATION

17. COSATI CODES			18. SUBJECT TERMS (Continue on reverse if necessary and identify by block number)
FIELD	GROUP	SUB-GROUP	High temperature composites, Fibers, Matrices, Interfaces, Processing, Thermomechanical and Environmental behavior

19. ABSTRACT (Continue on reverse if necessary and identify by block number)

Final results obtained on the High Temperature Advanced Structural Composites Program at Rensselaer Polytechnic Institute are described in three volumes. Volume one contains the Executive Summary and reprints of papers on Intermetallic Compounds. Volume two contains reprints of papers on Ceramic Matrix Composites, Fiber Processing and Properties and on Interfaces. The third volume contains reprints of papers on Mechanics.

20. DISTRIBUTION / AVAILABILITY OF ABSTRACT	21. ABSTRACT SECURITY CLASSIFICATION
☒ UNCLASSIFIED/UNLIMITED ☐ SAME AS RPT. ☐ DTIC USERS	Unclassified

22a. NAME OF RESPONSIBLE INDIVIDUAL	22b. TELEPHONE (Include Area Code)	22c. OFFICE SYMBOL
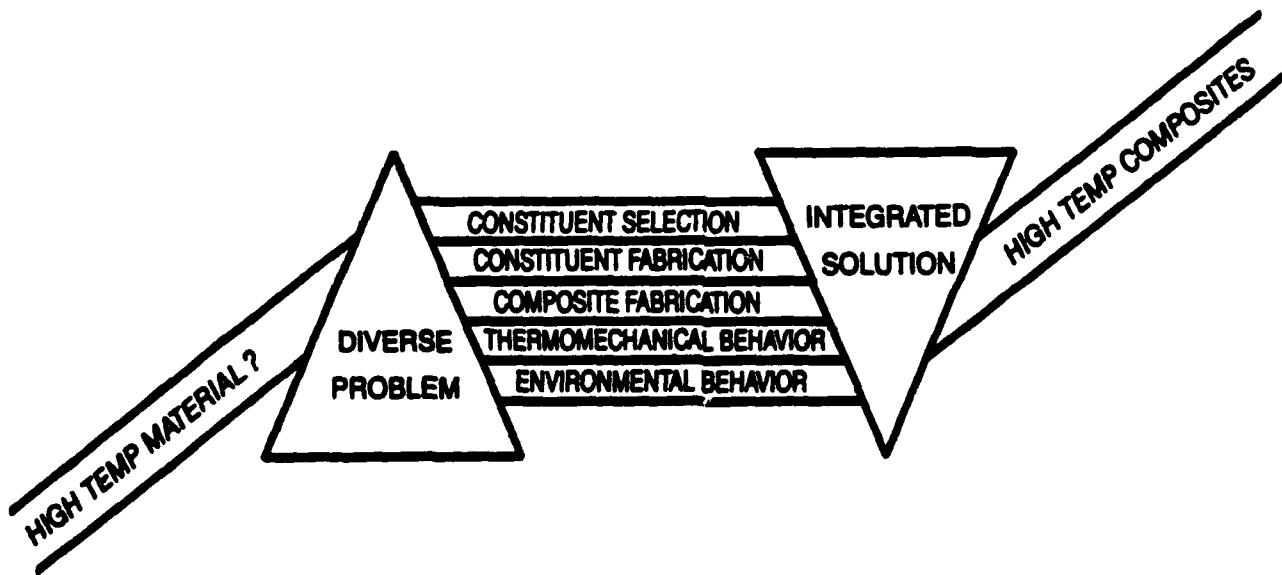
DD Form 1473, JUN 86 Previous editions are obsolete.

HiTASC

HIGH TEMPERATURE ADVANCED STRUCTURAL COMPOSITES

RENSSELAER POLYTECHNIC INSTITUTE
TROY, N.Y. 12180-3590

FINAL REPORT

University Research Initiative
CONTRACT NO. N00014–86–K–0770
OCTOBER 1, 1986 – JUNE 13, 1992

Volume 1 of 3

HiTASC

HIGH TEMPERATURE ADVANCED STRUCTURAL COMPOSITES

Professor George J. Dvorak
Program Director

Professor R. J. Diefendorf
Program Director (1986–1989)

Program Monitors

RENSSELAER POLYTECHNIC INSTITUTE

Troy, N.Y. 12180

SUMMARY

OF

TABLE OF CONTENTS

BOOK 1

TABLE OF CONTENTS

EXECUTIVE SUMMARY

INTERMETALLIC COMPOSITES

PROCESSING

Shaw, K.G., Misiolek, W.Z., and German, R.M., "The Properties of Plasma Atomized NiAl Powders," Advances in Powder Metallurgy — 1991, MPIF, Princeton, NJ, 6, 1991, pp. 159–166.

Misiolek, W.Z. and German, R.M., "Economical Aspects of Experiment Design for Compaction of High Temperature Composites," Proceedings of the American Society for Composites Sixth Technical Conference, Albany, NY 1991, pp. 1002–1011.

Misiolek, W.Z., Sopchak, N.D., and German, R.M., "Pressure Assisted Reactive Sintering of NiAl/TiB$_2$," Processing and Fabrication of Advanced Materials for High Temperature Applications, The Minerals, Metals & Materials Society, 187–192 (1992).

Wegmann, M.R., Misiolek, W.Z., and German, R.M., "Injection Molding and Reactive Sintering of Ni$_3$Al," Advances in Powder Metallurgy — 1991, MPIF, Princeton, NJ, 2, 1991, pp. 175–180.

Stoloff, N.S. and Alman, D.E., "Innovative Processing Techniques for Intermetallic Matrix Composites," Materials Research Society Symposium Proceedings, Vol. 194, Materials Research Society, Pittsburgh, PA, 1990, pp. 31–43.

Stoloff, N.S. and Alman, D.E., "Powder Processing of Intermetallic Alloys and Intermetallic Matrix Composites," Materials Science and Engineering, A144 (1991) 51–62.

Alman, D.E. and Stoloff, N.S., "Powder Fabrication of Monolithic and Composite NiAl," The International Journal of Powder Metallurgy, 27, 29–41 (1990).

Misiolek, W.Z. and German, R.M., "Processing of Continuous Fiber Reinforced NiAl Matrix Composite," Advances in Powder Metallurgy — 1991, MPIF, Princeton, NJ, 6, 1991, pp. 167–176.

Bose, A., Page, R.A., Misiolek, W., and German, R.M., "Reactive Sintering and Reactive Hot Isostatic Pressing of Iron Aluminides," Advances in Powder Metallurgy — 1991, MPIF, Princeton, NJ, 6, 1991, pp. 131–146.

German, R.M., Bose, A., Alman, D., Murray, J., Korinko, P., Oddone, R., and Stoloff, N.S., "High Temperature Intermetallic Alloys and Intermetallic Matrix Composites by Powder Processing," PM Into the 1990's The Institute of Metals, International Conference on Powder Metallurgy, Wembley Conference Centre, London, U.K., 1990, pp.310–323.

Alman, D.E. and Stoloff, N.S., "Fabrication of Intermetallic Matrix Composites by Powder Injection Molding (PIM) Techniques," High Temperature – Low Density P/M Alloys, TMS, Warrendale, PA, 1991, pp. 109–125.

Alman, D., Dibble, A., Bose, A., German, R.M., and Stoloff, N.S., "Powder Processing of Intermetallic Matrix Composites," Processing of Ceramic and Metal Matrix Composites, Pergamon Press, NY, 1989, pp. 217–227.

MECHANICAL PROPERTIES

Alman, D.E., Shaw, K.G., Stoloff, N.S., and Rajan, K., "Fabrication, Structure and Properties of $MoSi_2$–Base Composites," Materials Science and Engineering A, accepted for publication, 1992 (28 pp).

Alman, D.E. and Stoloff, N.S., "Processing and Properties of Intermetallic Matrix Composites," Materials Research Society Symposium Proceedings, Vol. 213, Materials Research Society, Pittsburg, PA, 1991, pp. 989–1000.

Alman, D.E., Stoloff, N.S., and Otsuki, M. "Powder Processing and Mechanical Properties of Intermetallic Matrix Composites," Intermetallic Composites, Proc. of JIMIS–6, The Japan Institute of Metals, Sendai, 1991, pp. 891–899.

Alman, D.E. and Stoloff, N.S., "Consolidation and Mechanical Behavior of Intermetallic Matrix Composites," Advanced Composite Materials, Ceramic Transactions, Vol. 19, The American Ceramic Society, Westerville, OH, 1991, pp. 831–842.

Alman, D.E. and Stoloff, N.S., "Fabrication and Mechanical Properties of Powder Injection Molded Intermetallic Matrix Composites," American Society for Composites, Sixth Technical Conference, Technomic Publishing Co., Lancaster, PA, 1991, pp. 390–399.

Alman, D.E. and Stoloff, N.S.. "Effect of Ductile Phase Reinforcement Morphology on Toughening of $MoSi_2$," presented at the MRS Spring '92 Conference, San Francisco, CA, April, 1992. To be published in Intermetallic Matrix Composite II, MRS, Pittsburgh, PA (6 pp.).

Bose, A., Camus, G., German, R.M., Duquette, D.J., and Stoloff, N.S., "Tensile Properties of Ordered and Disordered Ni_3Fe Intermetallic Compound and Composite," International Journal of Powder Metallurgy, (in press) (13 pp.).

ENVIRONMENT AND OXIDATION

Camus, G.M., Duquette, D.J., and Stoloff, N.S., "Fatigue/Creep Interactions in Ni_3Al–Base Alloys," Materials Research Society Symposium Proceedings, Vol. 133, Materials Research Society, Pittsburgh, PA, 1989, pp. 579–584.

Camus, G.M., Stoloff, N.S., and Duquette, D.J., "The Effect of Order on Hydrogen Embrittlement of Ni_3Fe," Acta Metall., Vol. 37, pp. 1497–1501 (1989).

Bose, A., Camus, G., German, R.M., Duquette, D.J., and Stoloff, N.S., "Influence of Long Range Order on Ni_3Fe and Ni_3Fe–Y_2O_3 Composites," Journal of Materials Research, Materials Research Society, 1990 (22 pp.).

Camus, G.M., Duquette, D.J., and Stoloff, N.S., "Effect of an Oxide Dispersion on the Hydrogen Embrittlement of a Ni$_3$Al Base Alloy," J. Mater. Res., Vol. 5, Materials Research Society, Pittsburgh, PA, 1990, pp. 950–954.

Camus, G.M., Duquette, D.J., and Stoloff, N.S., "The Influence of Test Frequency, Temperature and Environment on the Fatigue Resistance of an Ni$_3$Al–B/Cr/Zr Intermetallic Alloy," Journal of Materials Research, Vol. 7, Materials Research Society, Pittsburgh, PA, 1992, pp. 313–320.

Matuszyk, W., Camus, G., Duquette, D.J., and Stoloff, N.S., "Effects of Temperature and Environment on the Tensile and Fatigue Crack Growth Behavior of a Ni$_3$Al–Base Alloy," Met. Trans., 21A, pp. 2967–2976 (1990).

Fish, J.S. and Duquette, D.J., "Isothermal and Cyclic Oxidation of TiAl Composites," 3rd International Conference on High Temperature Oxidation and Protection of Materials, Marseilles, France, 1992, (in press) (13 pp.).

Korinko, P.S. and Duquette, D.J., "Oxidation of Powder Processed NbAl$_3$ Matrix Composites," Materials Research Society Symposium Proceedings, Vol. 194, Materials Research Society, Pittsburgh, PA, 1990, pp. 423–428 (7 pp.).

Korinko, P.S., Alman, D.E., Stoloff, N.S., and Duquette, D.J., "Oxidation of Powder Processed NiAl and NiAl/TiB$_2$ Composites," Presented at the MRS Spring 92 Conference, San Francisco, CA, April 1992. To be published in Intermetallic Matrix Composites II, MRS, Pittsburgh, PA, (1993).

EXECUTIVE SUMMARY

I. MATERIALS

The University Research Initiative on High Temperature Structural Composites, supported by DARPA/ONR over a five–year period, had several objectives related to the materials. The first was to identify intermetallic and ceramic matrix materials and suitable fiber reinforcements for new composite systems. The second objective was to develop suitable processing techniques for composite production. Finally, a major portion of the program was devoted to modeling and characterization of composite systems fabricated in our laboratories.

A. INTERMETALLIC COMPOUNDS

Several intermetallic compounds were identified early in the program as suitable candidates for composite matrix materials. These included Ni_3Al, $TiAl$, Nb_3Al, Al_3Ta, $MoSi_2$, $NiAl$, Fe_3Al and $TaTiAl_2$. Theoretical predictions of thermodynamic stability of these compounds with various oxide, carbide and boride reinforcements indicated that TiB_2 and Al_2O_3 were stable in contact with most of these compounds. In the latter stages of the program ductile niobium reinforcements were selected for study due to the ineffectiveness of ceramic reinforcements *as toughening agents*.

1. Processing

A major accomplishment in the early stages of our program was the identification of reactive sintering or self propagating high temperature synthesis (SHS) as a reliable means

1

of preparing appreciable quantities of the intermetallic compounds from their elemental constituents. Once the process variables (principally powder size and shape) were optimized, and the magnitude of the exotherm was measured for each system, preparation of composites reinforced with ceramic particles or fibers was easily accomplished. A variant on the technique, known as reactive hot isostatic pressing (RHIP), was developed to improve densefication of the composites. However, when it was clearly established that these particulate or short, randomly oriented fibers were ineffective for improving ductility or toughness, a new powder technique was introduced. Powder injection molding (PIM), a process well known for polymeric materials, was adapted to the intermetallic systems, and we were successful in producing aligned short fiber components of NiAl and $MoSi_2$ with Al_2O_3. Later work with continuous fibers (principally Nb) incorporated with $MoSi_2$ was accomplished by hand lay-up techniques.

Another approach to preparing intermetallic matrix composites utilized a plasma spray unit to co-deposit $MoSi_2$ and Al_2O_3 layers. Another vapor phase technique, chemical vapor deposition, was carried out under subcontract to prepare $MoSi_2/SiC$ laminates. Plasma spray of several other intermetallic compounds and their composites was carried out as follows:

Ni_3Al; Ni_3Al/Al_2O_3 laminates

Fe_3Al; Fe_3Al/Al_2O_3 laminates

Ni; Ni/Al_2O_3 particles

In general little oxidation was noted, densities between 85 and 100% of theoretical were obtained and numerous non-equilibrium defects were observed by transmission election microscopy.

In conjunction with the experimental work on plasma spray, a numerical model has been developed to simulate the plasma process. This code aids in the determination of proper particle sizes and plasma conditions which need to be satisfied to produce dense deposits.

2. Mechanical Properties

Limited evaluation of mechanical properties was carried out on both matrix and composite materials. Hardness, compression, bend, tensile, fatigue and creep–fatigue studies were carried out on several systems. Significant toughening of the intermetallics was achieved only when continuous, aligned metallic fibers were incorporated into a $MoSi_2$ matrix. However, substantial strengthening of NiAl was achieved with TiB_2 particles and with several solid solution alloying elements, principally Hf. It was shown that dispersion weakening could occur when TiB_2 particles were added to a Hf–alloyed NiAl matrix, confirming work reported elsewhere on different composite systems. Compression creep experiments on $MoSi_2$ reinforced with Nb particles showed a sharp increase in creep rate due to the particles. Temperatures ranged from 1323–1724K and stress levels studied were 10–100 MPa. Linear creep with time was noted for the $MoSi_2$ matrix.

3. Environmental Effects

Intermetallic compounds often display appreciable sensitivity to gaseous or liquid environments. In particular, Ni_3Al, Fe_3Al and Ti_3Al are severely embrittled by hydrogen at low temperatures, and Ni_3Al is embrittled by oxygen at high temperatures. Therefore, several investigations of the influence of hydrogen on particulate–reinforced intermetallics,

including a Ni$_3$Al,Cr,Zr alloy, Fe$_3$Al and a model Ni$_3$Fe system were carried out. These tests showed that particulate or fibrous reinforcements do not significantly alter environmental susceptibility. Similarly, oxygen at elevated temperatures was found to be a severe embrittler of the Ni$_3$Al,Cr,Zr alloy at elevated temperatures. Fatigue crack growth measurements were carried out at several test temperatures and at several test frequencies. The relative importance of creep and environmental effects on crack growth rates was established.

4. Oxidation

Isothermal and cyclic oxidation experiments were carried out on γTiAl , NbAl$_3$, NiAl , MoSi$_2$ and their composites. These studies are described below:

a. TiAl and Composites

The oxidation behavior of gamma TiAl containing 40 wt.% (54 at.%) aluminum was studied at 950 to 1070°C in air. The effects of niobium and alumina reinforcements on the oxidation of TiAl also were studied over this temperature range.

Alumina was chosen as a reinforcement because of a low CTE mismatch with the matrix (8x10^{-06} /°C vs. 11x10^{-06} /°C) and an inherent chemical compatibility with gamma TiAl. Three types of Al$_2$O$_3$ fibers were used, as were Al$_2$O$_3$ particles. FP and PRD166 (Al$_2$O$_3$ + ZrO$_2$) fibers were chopped to lengths of 3mm and Saffil fibers were supplied in lengths of 200μm. The chopped fibers were mixed with the elemental titanium and aluminum powders, cold isostatically pressed, pre—reacted at 800°C, and then consolidated

4

by hot isostatically pressing at 1350°C. After fabrication, the composites were fully dense and X-ray diffraction confirmed that the matrix was gamma TiAl.

The specific weight gain of the PRD166 reinforced composites was greater than that of the monolithic TiAl and increased proportionally with the volume fraction of reinforcement. It is believed that stress-assisted diffusion, occurring at the high fabrication temperature and pressure, produces a zirconia sheath at the perimeter of the fibers and dopes the matrix with zirconium. Zirconia, in which oxygen diffuses rapidly, allows rapid oxygen diffusion along the fibers and subsequent oxidation of the surrounding matrix. This localized oxidation is responsible for the increased weight gain in the TiAl-PRD166 composites.

A fiber-matrix reaction occurred at some of the fibers, predominantly at fiber clusters, during oxidation at 950, 1020 and 1070°C in air. The reaction grows at a parabolic rate, produces Al_2O_3 precipitates in the matrix and dopes the matrix with zirconium.

The matrix-PRD166 reaction results from localized internal oxidation at fiber clusters, not from an inherent chemical fiber-matrix incompatibility. Electron microscopy shows that the fiber ends are not covered by an oxide film, thus allowing a constant supply of oxygen to the reaction zone surrounding the fibers. Zirconium, which diffused into the matrix during fabrication, increases the oxygen diffusion in TiAl and, consequently, promotes internal oxidation. The internal oxidation along the PRD166 fibers may be suppressed by heat treating in vacuum or increasing the aluminum content of the matrix from 40 to 48 wt.%.

In contrast to the PRD166–containing composites, TiAl reinforced with FP fibers, Saffil fibers, or Al_2O_3 powder did not exhibit increased weight gain during oxidation, as compared to monolithic TiAl, or any internal oxidation. The lack of internal oxidation in these composites indicates that the fiber–matrix reaction is dependent on zirconium for enhanced oxygen diffusion along the fibers and in the TiAl matrix. In composites containing FP or Saffil fibers, the alumina reinforcement reduces the matrix surface area available for oxidation and, thereby, improves their isothermal oxidation resistance.

The oxide adherence on monolithic TiAl during cyclic oxidation is poor, as indicated by the spalling and subsequent rapid weight gain. In contrast, none of the composites exhibited any spalling. Oxide adherence on Ti–Al alloys appears to be associated with the ability to form a continuous alumina film and the absence of a thick external TiO_2 scale. Alumina reinforcements in TiAl promote the formation of a continuous Al_2O_3 film, which leads to improved oxide adherence and superior cyclic oxidation resistance, as compared to monolithic TiAl.

b. NbAl₃ and Composites

The oxidation characteristics of reactively sintered NbAl₃ were analyzed. Reactively sintered NbAl₃ has parabolic oxidation behavior at 1000°C and forms a layered oxide, with alternating bands of Al_2O_3 and $NbAlO_4$. A phase transformation to Nb_2Al occurs as the NbAl₃ is oxidized. This result is in agreement with those of Perkins and others who examined pack aluminised and cast NbAl₃.

The oxidation behavior of reactively hot isostatically pressed (RHIP) NbAl₃ and RHIP NbAl₃ reinforced with Saffil was studied between 1000 and 1400°C. The oxidation

resistance of the composites is improved at 15% Saffil but harmed at 5% Saffil compared to the monolithic RHIP. Hot pressed NbAl₃ was found to be more oxidation resistant than the RHIP materials.

c. NiAl and Composites

The oxidation behavior of NiAl and NiAl matrix composites was examined between 800 and 1200° C. The mass changes were detected with a continuously recording Cahn microbalance.

The mass change after 50 hours for RHIP NiAl and RHIP NiAl and RHIP NiAl reinforced with 10 and 20% random FP alumina fibers was determined. These results show that the oxidation resistance is not affected by the inclusion of the fibers, although the bulk surface area was used for the calculations rather than the effective surface area of the NiAl. Use of the effective surface area would have resulted in an increase of the specific mass change.

The mass change after 50 hours for the RHIP NiAl is not deleteriously affected by the inclusion of HfB_2 at 800 and 1000° C. However, at 1200° C the composite exhibits a two times increase in weight compared to the monolithic material. The composites reinforced with 20% HfB_2 have a two times weight increase at 800 and 1000° C and a 10 times increase at 1200° C compared to monolithic NiAl.

NiAl reinforced with TiB_2 has worse oxidation resistance at all volume fractions and temperatures when compared to monolithic NiAl. There is also an apparent discontinuity in the weight change data that occurs between 1000 and 1200° C. This discontinuity is

most likely due to a change in the oxide that is formed since the phase diagram indicates liquid phase formulation at 1050° C.

The oxidation data were fitted to a parabolic equation and a rate constant was determined. The rate constants were in agreement with the mass change data for all the samples examined. Al_2O_3 has a negligible effect on the rate constant. The rate constant for $NiAl/10\%$ HfB_2 is lower at 800 and 1000° C than monolithic NiAl. The rate constants for the TiB_2 reinforced composites scale with the volume fraction of the reinforcement.

d. MoSi₂ and Composites

Cyclic oxidation experiments were carried out on $MoSi_2$ and $MoSi_2$–Nb fibrous composites at 1200° C. Initial degradation of the composites were a result of Nb fibers on the surface oxidizing. As time progressed, cracks developed in the matrix due to the volumetric expansion associated with the formation of niobium oxide.

B. CERAMIC MATRIX COMPOSITES

1. Thermochemical Calculations

The thermochemical computations during the course of this program developed programs based on the principles of free–energy–minimization for the systems involved. The number of different high temperature materials investigated exceeds 100, and the associated reactions, thermochemically analyzed, amount to several hundred different processes.

A computational thermodynamic analysis of group IV, V and VI transition metal borides, carbides, nitrides, and oxides established the thermal stability limits of these materials. For selected boundary conditions, these computations yielded the relative stabilities of compounds in the different classes investigated. The results of this analysis provided the basis for a large number of specific investigations dealing with critical processes of high temperature ceramic materials. These are summarized in the following.

* Evaluation of thermal stabilities and surface recession rates of borides, carbides, nitrides, and oxides of boron, aluminum and silicon and of MgO, BeO, Y_2O_3, and CeO_2.

The results of this work revealed the expected lifetimes of materials under various temperature conditions.

* Computation of volatility (partial pressure) diagrams for various oxides and nitrides, e.g., Al_2O_3, MgO, BeO, ZrO_2, SiO_2, BN, AlN, and Si_3N_4.

The resulting phase diagrams established quantitative boundary conditions in terms of temperature and atmospheric conditions.

* Computation of phase stability diagrams for the systems Si–N–O, B–N–O, Si–C–N–O, and others.

This is an application of stability computations to important ternary and quarternary systems.

*   Computation of environmental stability (oxidation, nitridation, vaporization) for borides, carbides, nitrides, and oxides of various refractory metals.

This analysis is concerned with the simultaneous occurrence of oxidation, nitridation, and mass loss (vaporization).

*   Thermochemical compatibility of C, SiC, Si_3N_4, TiB_2, and Al_2O_3 reinforcements with various oxides, borides, and nitrides based matrices and coatings.

*   Chemical compatibility and environmental stability of TiB_2, ZrB_2, and HfB_2 with Al_2O_3, TiO_2, ZrO_2, and HfO_2.

*   Analysis of chemical compatibility of SiC, TiB_2, and Al_2O_3 reinforcements with nickel aluminides (Ti_3Al, TiAl, and $TiAl_3$).

*   Environmental stability and chemical compatibility of various reinforcements in molybdenum disilicide matrix.

The above topics deal with important interfacial reactions which determine the practical limitations of composite materials.

*   Estimation of thermal expansion behavior of various refractory carbides and nitrides, e.g., TiC, ZrC, HfC, VC, NbC, TaC, TiN, and ZrN.

The last topic provided the basis for the further development of equations for the estimation of the thermal expansion of selected materials.

The combined results of the thermochemical analysis of high temperature ceramic materials and interactions provided important and new insights into the thermal and environmental behavior of these materials. The results also demonstrate the importance and practical value of thermochemical computations for the application and modification of existing materials, and for the synthesis of new materials. The agreement between predicted behavior and experimental observations of investigated systems supports the validity of our theoretical approach and of the thermodynamic data employed for these computations.

2. Thermal Stability and Processing

A brief summary of the key results obtained for the several different projects conducted with organometallic precursors follows:

a. Preparation of High–Yield Precursors to Stoichiometric SiC

Our work in this area has focused on the preparation of polymeric precursors to SiC that contain a stoichiometric ratio of Si to C hydrogen as essentially the only additional component. Two different routes to polymers having the approximate formulae, "$[SiH_2CH_2]$", were discovered, leading, respectively, to highly branched and linear polycarbosilanes. Both polymers were found to have high ceramic yields, after thermal processing, and gave near–stoichiometric SiC on pyrolysis under nitrogen.

The first approach developed employs Mg as a coupling agent and Cl_3SiCH_2Cl as the starting material. The resultant "chloro polymer" (nominally, "$[SiC]_2CH_2]$" was converted to the hydridopolymer "$[SiH_2CH_2]$", by reduction with $LiAlH_4$. A patent

application covering this process and the hydrido polymer as a new composition of matter was submitted on behalf of Rensselaer to the US Patent Office in July 1990 by the AKZO Corporation in exchange for an exclusive license.

A structural analysis of this polymer by NMR methods have revealed a complex, highly branched structure, resulting from the ternary functionality of the Cl_3Si end of the monomer unit. Despite this branching, the polymer is not appreciably crosslinked and remains liquid and highly soluble in hydrocarbon solvents. This "$[SiH_3CH_2]$" polymer undergoes crosslinking through loss of H_2 above ca. 200°C, eventually forming a gel, and then a glass, which is insoluble and exhibits a high char yield on pyrolysis under N_2 to 1000°C (ca. 80%).

The second approach that we have developed to obtain a "$[SiH_2CH_2]$" polymer involves the ring–opening polymerization of tetrachlorodisilacyclobutant, $[SiCl_2CH_2]_2$. The resultant "chloropolymer" is again reduced to the hydridopolymer with $LiAlH_4$. In this case, however, the product polycarbosilane is a high molecular weight linear polymer that contains the $[SiH_2CH_2]_n$ repeat unit. This polymer is also a liquid at room temperature, is soluble in hydrocarbons, and undergoes pyrolysis under N_2 to give stoichiometric SiC in yields approaching the theoretical value (up to 91%) by 1000°C. This polymer is currently available only in small quantities by a relatively low yield process and is not expected to be competitive in the short term with our branched "$[SiH_2CH_2]$" polymer as a source of SiC for composite fabrication. In the longer term this may change, as we are continuing to explore alternative, low cost, high yield approaches to the $[SiCl_2CH_2]_2$ monomer.

Both of these methods are fundamentally new approaches for SiC precursor preparation. The new polycarbosilanes so obtained undergo a novel thermally induced

crosslinking process that involves elimination of H_2 from SiH_n groups on the polymer backbone. They show considerable promise as high yield precursors to stoichiometric SiC and, in the case of the branched polymer, as a viable source of SiC coatings and matrices for composites.

b. Studies of Preceramic Polymer Pyrolyses

These studies have focused on two different organosilicon precursors, a vinylic polysilane (Y–12044) previously marketed by Union Carbide, and the "[SiH$_2$CH$_2$]" polymer described above. Pyrolysis of both polymers gives an amorphous "SiC" ceramic on pyrolysis under N_2 to 1000°C; however, the SiC obtained from the commercial vinylic polysilane contains ca. 17% excess C and undergoes a significant weight loss on heating in air above ca. 700°C whereas the "[SiH$_2$CH$_2$]" polymer gives a virtually pure SiC product that shows no weight loss on heating in air at high temperatures. In our studies of the polymer–to–ceramic conversion process, solid state NMR, as well as other chemical and microstructural analysis methods were used to follow the micro– and macroscopic changes occurring in the sample on heating in N_2. The NMR studies were aided by collaboration with Prof. G. Maciel of Colorado State University and a joint postdoctoral associate, Dr. Paul Marchetti, both of whom are experts in solid state NMR spectroscopy. In these studies ^{29}Si, ^{13}C, and ^{1}H NMR spectroscopy was used to follow the local structural changes occurring during the curing (thermosetting) and subsequent pyrolysis stages during the conversion. Key findings include the identification of vinyl coupling initiated by Me$_3$Si radical formulation as the main thermosetting mechanism in the case of the vinyl–substituted polymer, whereas the "[SiH$_2$CH$_2$]" polymer apparently thermosets through interchain Si–Si bonding after loss of H_2 from the SiH$_x$ groups on heating. At higher temperatures in both polymers the "SiC" network structure develops through

13

radical coupling reactions after loss of H_2 (and, in the case of the vinylic polysilane, hydrocarbons and volatile organosilanes) from both the Si and the C atoms of the polymer. Among the important practical consequences of this study is the finding that loss of H_2 from SiH_x (x > 2) groups can provide an effective crosslinking mechanism above 200°C and, therefore, that C—containing functionalities such as vinyl groups are not necessary for effective thermosetting of SiC precursors.

c.   Application of Preceramic Polymers to Obtain Novel Ceramic Compositions and Nanocrystalline Composites

We have found that both homogeneous solid solutions and nanoscale composite mixtures of SiC with AlN can be obtained on pyrolysis of mixtures of the polycarbosilanes and dialkylaluminum amides (as the AlN precursor) and that the ceramic yield of the polycarbosilane is generally enhanced in the presence of the AlN precursor. This opens up the possibility of using the "$[SiH_7CH_2]$" precursor not only as a source of SiC coatings and matrices for ceramic composites but also for the preparation of other mixed—component ceramic systems that may be more advantageous than SiC alone as a matrix, coating of fiber material. In particular, alloying of SiC with AlN has been reported to improve its microstructural stability, inhibiting the exaggerated grain growth that is known to contribute to the loss of strength typically observed for commercial "SiC" fibers at high temperatures (1200–1800°C).

We also have explored the use of both precursor mixtures and specially prepared single component precursors in the preparation of nanocrystalline composites of AlN/Si_3N_4, BN/Si_3N_4, and BN/TiN. We have demonstrated that such precursors can be used to obtain extremely fine—grained, homogeneously mixed composite powders of these

crystalline ceramic phases. Such mixed—phases ceramics may have application as matrices for SiC—reinforced composites or as tough monolithic materials in their own right.

d. CVD of Interphase Layers for Composites

In the area of CVD of fiber coatings for high temperature composites, we have developed an effective process for coating SCS—6 SiC fibers with yttria and have demonstrated that such a coating is effective in inhibiting reaction of the SiC with Ni during the fabrication of SCS—6—reinforced Ni_3Al matrix composites by reactive sintering. In this study, the conditions for obtaining a uniform adherent coating of yttria on the SCS—6 fiber by using a tris—betadiketonate complex as the CVD source were determined and SiC/Ni_3Al composites were prepared by reactive sintering from Ni and Al powder mixtures. The presence or absence of a reaction between the fiber and the matrix was determined by means of SEM and scanning electron microprobe methods after sectioning the composites both perpendicular to and along the length of the SCS—6 fibers. This approach to the production of protective fiber coatings using betadiketonate complexes should be generally applicable to a wide range of other oxides, such as ZrO_2, Al_2O_3, and Sc_2O_3.

We also have explored the use of cyclic organosilicon and organoaluminum compounds as single—source precursors *, SiC and AlN respectively, both of which ceramic materials hold promise for fiber coatings or CVI—produced matrices in high temperature structural composites.

Detailed studies have been initiated of the gas phase chemistry occurring on deposition of AlN using the cyclic organoaluminum amide, $[Me_2AlNH_2]_3$, a compound

which we had previously identified as a suitable single source precursor to AlN. Our objective is to understand the precursor–to–ceramic conversion process, so as to enable the effective use of this precursor in the deposition of AlN on SiC fiber. Key results include the development of a molecular beam apparatus for time–of–flight measurements on the base phase species and its application in the identification of a dimeric form for this precursor in the gas phase at elevated temperatures. These results indicate a rapid equilibrium between monomer, dimer and trimer analogous to that which we had previously observed in solution.

3. Mechanical Properties of Ceramics and CMC

Mullite ($3Al_2O_3$, $2SiO_2$) was selected for study as a matrix for ceramic matrix composites because of a high melting point, 1890°C, and a low density, 3.15 g/cc. High purity mullite with and without glass at the grain boundaries and second–phase alumina was synthesized by a sol–gel method.

Three compositions of chemically pure mullite powders were synthesized with controlled phase compositions, densified into pellets, and creep tested at temperatures in the range of 1200 to 1600°C. Apparent creep activation energies of 740–820 kJ/mol and stress exponents of 1.2–1.6 were measured in air on the fine grained ($\leq$ 1μm) mullites. Mullites containing glass crept about an order of magnitude faster than the crystalline compositions. Samples of "single crystal" mullite were found to contain impurities and glass, and crept at approximately the same rates as the polycrystalline mullite–with–glass composition. Mullite creep literature has been reviewed and related to microstructure and test technique.

The compressive creep behavior of three aluminosilicate compositions containing fine–grained ($\leq 1\mu m$) mullite were measured in air at 1470–1725K and 15–100 MPa. The mullite with second phase corundum was the most creep resistant, closely followed by the single–phase mullite, which was about an order to magnitude slower than mullite containing second phase glass. The creep activation energies (740–820 kJ/mol), stress exponents (1.2–1.6), the magnitudes of the creep rates and the microstructural observations by SEM and TEM were used to interpret the likely controlling creep mechanisms: diffusional control in the crystalline compositions, and viscous flow of the glassy grain boundary phase in the composition containing glass.

Primary creep was observed except at the highest temperatures before the creep rate decreased to a steady state, linear creep rate. Significant changes in density or grain size did not occur during the tests, which were maintained at total strains of less than 5%. At approximately equal grain sizes (~0.8 μm) and densities (92–95% of theoretical), the samples containing glass crept more rapidly than the single phase samples, which crept more rapidly than the sample containing α–Al_2O_3. The observation that the creep of mullite containing corundum is slower than that of single phase mullite is in contrast to previous results probably due to differences in microstructure. Our samples contained elongated corundum particles ˜6 μm long by 0.5–1 μM diameter; previously tested samples contained roughly equiaxed corundum particles with grain sizes approximately equal to that of the mullite matrix.

Selected creep measurements were made on samples prepared from commercial mullite powders from the United States (VISTA), France (Baïkowski) and Japan (Chichibu). The creep rates for these glass–containing mullites were the same or slightly faster than those of the RPI samples containing glass, and the commercial samples are less chemically homogeneous according to EDS back–scattered electron results.

Mullite "single crystals" grown by a Czochalski process were obtained. Glass pockets were found by optical microscopy. Creep tests showed a pronounced primary creep stage under most conditions, and a creep rate close to that of the polycrystalline mullite containing glass. Samples have been annealed in order to dissolve the glass in mullite, which has a 2:1 composition.

A study of the microstructural evolution of single–phase mullite and mullite/α–Al_2O_3 under load free conditions was made at 1423K, 1840K and for 1–80H. The significant changes in the microstructure were a small increase in density ($\leq$1% TD), and a small increase in mullite grain size. After a 100h hold, the mullite grain size in the single–phase mullite should increase from an initial 0.5 μm at 1423K and to 2.0 μm at 1840K. The elongated α–Al_2O_3 grains decreased in aspect ratio (from ~9–4) during the heat treatments.

Microstructural examination of the samples containing glass with SEM and TEM revealed equiaxed, rounded mullite grains surrounded by the intergranular glass at grain boundaries and triple points. The mullite grains in the single phase and mullite plus corundum samples were equiaxed and occasionally elongated, with straight or slightly curved grain boundaries. No second phase glass was found in the single phase samples or in the mullite containing corundum. The corundum was located at grain boundaries. Occasional dislocations were observed in all of the compositions in both the deformed samples and in the undeformed samples. Evidence of cavitation was not observed, except in the crept samples containing glass at higher strains.

The evolution of the grain size distribution of mullite samples was studied after heating at temperatures up to 1700°C. The grain size distributions were log–normal both

before and after heating. The activation energy for grain growth was found to be about 260 kj/mole, and the grain size grew proportional to square root of time.

The mullite creep literature has been reviewed. The test and characterization procedures have been documented, since small differences in the procedures as well as the samples may have a pronounced effect on the creep rate. Literature data for mullite containing glass were replotted after reducing the literature data to a common grain size and temperature or stress. Nearly all of the replotted data for mullites containing glass were found to fall on a single line which had an activation energy close to the activation energy of viscous flow. The reduced data for the single phase mullites showed more scatter than did the mullites containing glass. Evidence exists that some of this difference is due to differences in microstructure, specifically chemical homogeneity and grain structure, which can be affected by processing.

C. FIBER PROCESSING AND PROPERTIES

1. Processing

Direct measurements of transverse coefficients of thermal expansion have been performed on single carbon fibers. Although axial properties of carbon fibers are well known, only "guesstimates" of the transverse properties were used in the past for micromechanical modeling. The usual assumption of transverse isotropy was found experimentally to be invalid for higher modulus pitch precursor carbon fibers, as the thermal expansion was found to differ by as much as a factor of three in various radial directions. While the transverse coefficients of thermal expansion could be semiquantitatively predicted from a fiber's microtexture, the inability to properly account

19

for the pores/cracks requires that the coefficients still be determined experimentally at present. This phase of the program has allowed the determination of the transverse properties of carbon fibers.

Chemical vapor deposition has been used for fabrication of creep resistant fibers, and the infiltration of higher strain to failure matrices. Extensive efforts have been made to properly model the flow, temperature, and concentrations for fiber fabrication. At present, a complete calculation from first principles cannot be made because of excessive computational time. However, within five to ten years, the computational capability should be available. For infiltrated matrix depositions, the research has shown that design fiber architecture for manufacturing as well as mechanical properties could drastically reduce deposition time. The complete description of fiber architectures, designed for manufacturing, was not completed. However, even with present 2–D fabric composite preforms, a two–step deposition procedure, optimized for the two main void distributions, reduced deposition times to tens of hours from hundreds. Finally, infiltrations using multiple crack stopping interfaces, such that an internal lamellar microstructure resulted, produced a doubling of the matrix failure strain.

2. Mechanical Characterization of Fibers at High Temperatures

The goals of this project were to develop advanced techniques for the mechanical characterization of fibers at elevated temperatures, and to utilize these techniques for the detailed characterization of candidate fibers for high temperature reinforcement of composite materials. Two original instruments were designed, constructed and utilized.

The first instrument consists of a six station high temperature fiber creep facility which utilizes direct ohmic heating of the fibers. The fiber temperature is measured using a two wavelength optical pyrometer with a computer interface. The pyrometer is mounted on a precision, stepper motor driven, rotary table which is also interfaced to the computer. This setup enables the use of a single pyrometer for the simultaneous creep data acquisition on up to six fibers. In addition, the rotary table provides a precise means by which to automatically aim the pyrometer at the fiber. This feature eliminates a major source of errors associated with fiber temperature measurements. A closed loop PID control scheme is implemented whereby the temperature error signal is fed to a high voltage DC power supply which controls the current passing through the fiber. In practice long term temperature stability of ± 1 C is achieved at temperatures of 1600 C. Fiber deformation is measured directly by fixing one end of the fiber to the core of an LVDT, which is also interfaced to the computer. The ends of the fibers are secured in water–cooled aluminum quench blocks. The temperature gradient over the entire length of the fiber (which is 15 inches) is less than 30 C at an operating temperature of 1600 C. This provides an exceptionally long isothermal gage length and contributes to the high precision of the instrument. Creep experiments were generally conducted in an argon environment.

The second instrument is a heated wall, dynamic mechanical apparatus which is capable of resolving both the in–phase (storage or elastic modulus) and out–of–phase (loss or viscous modulus) components of the dynamic modulus as a function of both temperature and frequency. A linear motor with a DC bias to maintain fiber tension is connected to one end of the fiber, and is driven by a DC coupled power amplifier, whose drive signal is derived from a computerized Fourier transform type of phase angle analyzer. This apparatus has an operating range of from room temperature to 1600 C and frequency range from 0.1 to 25 Hz. The resolution on loss factor is 0.0005 or better, as confirmed by completely elastic fibers run at room temperature.

Both systems have been used to characterize SCS–6 SiC fibers. A complete set of creep curves have been obtained between 1100 and 1500 C, at several levels of stress. It is found that the creep is a linear viscoelastic process, and is fully recoverable within certain limits of stress and temperature. In addition, the coefficient of thermal expansion has been obtained vs. temperature. It is found that there is an anomalous contraction at ca. 1370 C, for heating rates of 15 C/min. The kinetics and hysteresis in length associated with this phenomenon have been studied extensively. It is believed that the anomalous contraction is due to the melting of excess silicon within the SIC structure. Dynamic data on these fibers have been obtained from 1100 to 1500 C using a variety of heating and loading paths. It is found that the viscous component of the modulus begins to grow rapidly above 1200 c. An algorithm has been developed for the determination of isothermal gage length data from the parabolic temperature profile data obtained in the heated wall system. The dynamic data emphasize the short time scale responses of the fiber, whereas the creep data emphasize the long time scale behavior. Taken together, these data provide a comprehensive data base for the evaluation of these fibers as a suitable high temperature reinforcement.

It is noted in closing that the techniques we have developed are now being used to evaluate new fiber systems, including YAG fibers and alumina fibers.

D. INTERFACES

Several studies were carried out aimed at characterizing and understanding the factors involved in the kinetics and energetics of the formulation and stability of fiber–matrix interfaces. The results of three studies, one on the Al–SiC system, one on Ti Alloy–Al$_2$O$_3$ systems, and one on interface formation by sputter deposition, are summarized below.

1. Aluminum on Silicon Carbide

The interface studied was formed by the deposition of aluminum on the (0001) faces of SiC single crystal platelets. The process was carried out in ultrahigh vacuum, with aluminum being deposited by physical vapor deposition onto the clean SiC surface. Depositions were carried out for a range of deposition times and surface temperatures. The deposition process was characterized by in situ Auger electron spectroscopy, measuring the Auger peaks for Al, Si and C after increments of aluminum deposition. After deposition, temperature programmed desorption (TPD) was used to characterize the binding energy of the aluminum to the substrate, and the deposit was depth profiled using argon ion bombardment to determine the extent of Al penetration into the SiC lattice. Annealing studies were also carried out, using Auger electron spectroscopy to characterize changes in the Al binding states at the surface.

At low substrate temperatures (below 300°) the deposit grew by the Vollmer–Weber mechanism, with islands of solid Al forming on an otherwise nearly clean SiC surface. Plots of the intensity of the various Auger peaks vs deposition time, show that, as surface temperature increases, fewer nuclei form, leading to a more gradual decrease in Si and C Auger features as deposition proceeds. At temperatures above 300°C, there is a reaction between the Al and the SiC. This is shown by a shift in the Al LVV Auger transition energy. Depth profiles taken after disorption of the unreacted aluminum showed that this reaction involved only the top most atomic layer of the SiC, with Al atoms replacing Si in this layer. TPD studies showed zero–order desorption kinetics, with a desorption energy of 148 Kj/mol for desorption from heavy deposits of aluminum, while light deposits showed first–order kinetics with a desorption energy of 178 Kj/mol. This behavior is also consistent with the evaporation of an island deposit on top of a reacted layer.

23

While this study provided significant information on the kinetics and energetics of the interface formation, it was not capable of forming thick layers that would be useful in studying the long—term stability of the Al/SiC interface, and was not pursued further.

2. Titanium Alloys on Al₂O₃

This study was aimed at characterizing interface stability in titanium aluminide/sapphire composites. Samples were prepared by sputter deposition of the desired metal or interm⸱ 'lic onto flat, single crystal samples after sapphire. Typically, the layer deposited was 1000 – 2000 A thick. After deposition, samples were annealed for a range of times and temperatures. The annealing process was carried out in ultrahigh vacuum to avoid introducing oxygen into the sample from the free surface. After annealing, the samples were analyzed by Rutherford backscattering spectroscopy (RBS) and by Auger depth profiling to characterize the extent of reaction or interdiffusion at the metal—oxide interface. Results for the various combinations studies are summarized below.

Auger spectra taken in the course of the depth profile run on an annealed Ti/Al₂O₃ sample indicated that the aluminum Auger peak in the 60 eV region was split, showing contributions from both metallic aluminum and oxidized aluminum, Al³⁺. Accordingly, all depth profile studies recorded these two contributions independently.

There was a general trend for the reactions to become thermodynamically more favorable as the oxidation state of the titanium in the oxide product decreased.

The results obtained clearly indicate that the titanium—Al₂O₃ interface is highly reactive, even at relatively low temperatures. Use of intermetallic matrixes such as TiAl or

TiTaAl$_2$ greatly reduces the tendency toward interfacial reactions, with the interface stability increasing with the addition of tantalum.

3. Fiber Coating by Sputter Deposition

A preliminary study was made to determine the feasibility of depositing protective coatings on fibers or fiber tows by reactive sputter deposition using a hollow cathode configuration. In this technique, a magnetically confined discharge produces ions that remove material from a target by ion bombardment. In physical sputtering, the material removed is redeposited on the growth surface. In reactive sputtering a second gas that will react with the material being deposited is added to the system, to produce a deposit of the reaction product. This technique makes it possible to deposit refractory materials such as nitrides or borides at temperatures close to ambient.

This system was tested in the deposition of titanium onto 3mm diameter carbon rods, and onto the fibers of a carbon fiber tow, containing approximately 1000 fibers, each about 7 μm diameter. Deposition onto the carbon rod resulted in the formation of a deposit of pure titanium at a deposition rate of 750 nm/minute. In the case of the fiber tow, it was found that fibers separate from one another due to the electrostatic repulsion associated with surface charge buildup during exposure to the plasma in the hollow cathode cell.

An initial study of reactive sputter deposition was also carried out in this system, using N$_2$ as the sputtering gas to produce a TiN coating. Results indicated the formation of a non-stoichiometric TiN$_x$, with x less than unity. It is felt that this non-stoichiometry is due to inadequate control of the N$_2$ gas pressure during the sputtering process.

4. Facilities Development

During the course of the program a major effort was made to upgrade our facilities for the production and characterization of samples containing metal–refractory interfaces, including lamellar composite samples, coated fibers and samples for the study of interface strength and stability.

Two systems have been constructed for sample fabrication. One of these, a research CVD system optimized for deposition using organometallic precursors, was developed using funding provided as part of a grant from the New York State Energy Research and Development Agency. The second, a research sputter deposition system, was developed under DARPA funding.

The sputter system is a tree–target system, capable of both rf and dc magnetron sputtering. It is equipped with facilities for pumping into the ultrahigh vacuum range, rapid switching from one material to another using a shutter system, sample introduction without breaking vacuum, and feedback control of deposition rate and sputtering gas composition. This system has been used successfully to deposit $MoSi_2/Al_2O_3$ multilayer structures, and can be used with the hollow cathode configuration described previously for reactive sputter coating of refractory materials onto fibers or fiber tons.

In this characterization area, an x–ray photoelectron spectroscopy (XPS or ESCA) system has been installed, and is currently being used to analyze both the $MoSi_2/Al_2O_3$ multilayers mentioned above, and to extend the previous studies of interfaces between intermetallics and refractory materials.

5. Soft Layer Interfaces

The focus of this study is the analysis of "soft layers" interfaces in ceramic matrix composites as a mean of improving strain to failure capability. The approach taken here is to first evaluate the stress field for various crack configurations, then the compliance of the sample can be computed. Several conclusions were drawn from this study: 1) for the "soft layer" interface concept to be effective the maximum maximum interface strength should be very low. For instance in a ceramic with a fracture toughness of 0.3 Pa.m1/2 $\ldots$ a soft layer distance of a $=$ 10 microns the maximum interface strength was found to be 60 MPa. 2) A limiting soft layer disbonding length can be determined for a given interface strength. For instance, for the same ceramic with an interface strength of 33 MPa, the toughening mechanism will be effective if the interface debonds over a length 4a. 3) For a given crack size and interface spacing the stress at which the crack will propagate to the interface can be determined based on the J–Integral concept. 4) using a finite element model of the matrix with a crack having propagated to the interface, significant improvement in compliance can be demonstrated. For example, when the interface has debonded one third of the length of the sample, a 50% improvement in sample compliance can be obtained.

II. MECHANICS

The mechanics program was conducted, in part, to support the material selection and predict the behavior of different material systems. Both micromechanical and macroscopic studies were conducted on ductile and brittle matrix systems.

A. MICROMECHANICAL MODELING

The micromechanical analysis work was concerned with the behavior of ceramic and intermetallic systems subjected to mechanical loads and to thermal cycles. The general objective was to examine the thermomechanical compatibility, to develop methods for reliable prediction of overall properties and of local stress and strain fields in the phases under prescribed thermomechanical loads, and to explore techniques for reduction of local stress concentrations.

With regard to brittle systems, we have developed analytical approaches to modeling of coated fiber systems. Both exact and approximate techniques were used. For example, using Dvorak's discovery of the properties of uniform fields in heterogeneous media, we were able to derive exact connections between mechanical and thermal stress and strain fields in two and three–phase fibrous systems. These connections proved useful in the understanding of such diverse phenomena as evaluation of coefficients of thermal expansion, response of yield surfaces to thermal changes, and conversions of thermal changes to mechanical loading in inelastic deformation. Among the approximate techniques we have chosen the Mori–Tanaka approximation in studies of coated fiber systems. We extended the original formulation to three–phase systems and incorporated cylindrically orthotropic fiber properties, as well as changes of elastic constants with

temperature. To make the results useful to designers, we have extended the above results to laminates and outlined a technique for constructing failure maps that define a permissible loading range in the laminate overall stress space such that a specified magnitude of fiber, matrix, or interface strength is not exceeded. The maps are constructed in a dimensionless stress space in which the laminate stresses are normalized by the assigned strength values. Therefore, the maps can be easily adjusted to reflect different values of local strengths. Specific examples of the maps were constructed for the SCS6–Ti$_3$Al, (0/±45)$_s$ laminate.

For the purposes of thermomechanical compatibility, the fiber coatings of choice should have a high coefficient of thermal expansion in the transverse plane, and a low transverse Young's modulus. Thicker coating are more efficient in reducing thermal stresses, but they also elevate local stress concentrations in the matrix under transverse normal loads.

In a related study, we examined several approximate methods for evaluation of overall elastic properties of composite materials, and established limits to their applicability that were not defined previously.

In our studies of ductile systems, we developed the novel transformation field analysis technique for elastic–plastic, viscoelastic, and viscoplastic composite systems. In this method, all inelastic as well as thermal strains, phase transformation, and any other such deformations are regarded as eigenstrains, or transformation strains applied to an otherwise elastic composite. Their effect is superimposed with mechanical load effects. Both the transformation and mechanical strains are analyzed with certain influence

functions derived from elasticity solutions, which are therefore constant during inelastic deformation. The influence functions permit formulation of governing equations for incremental solutions of inelastic loading problems. The procedure has been used both with such approximate techniques as the self-consistent and Mori-Tanaka methods, and the finite element method associated with unit cell models. In the approximate methods, we have identified and corrected errors in the widely used self-consistent model originally proposed by Hill. In the finite element method, we found greater efficiency with the new formulation. Also, since the governing equations are written as a separate system, there is no need to program specific inelastic constitutive equations into the finite element program used in the composite analysis. At most, one needs an elastic program for finding the transformation influence functions.

These analytical techniques were applied to evaluation of local fields caused by fabrication in unidirectional and laminated SCS6/Ti$_3$Al and SCS6/Ni$_3$Al systems. For the unidirectional materials, we performed a simulation of the HIP process of the two systems with and without coated fibers. The coatings reduced initial stresses, but also elevated local stresses in the matrix for certain mechanical loading directions, such as transverse tension and shear. Moreover, we examined the effect of the ratio of the axial and transverse stresses applied in the HIP process. Significant reduction of internal stresses was found for a modified HIP process that applied a high transverse and low or absent axial pressure. In the laminates, we described the shape, position and kinematic motion of bimodal yield surfaces during cooling from the fabrication temperature in the two systems with the (0/±45)$_s$ layup. No inelastic deformation was detected during unconstrained cooling from a stress-free state in the SCS6/Ti$_3$Al, but there was a significant rearrangement of the yield surfaces that would affect inelastic deformation in the plies

30

under subsequent mechanical loading. The more extensive matrix–dominated yielding was favored at high temperatures.

B. THERMOVISCOPLASTIC ANALYSIS OF MMC

The objective of this task was to develop analysis tools using a "unified" constitutive equation, the viscoplasticity theory based on overstress (VBO). In unified theories all inelastic deformation is considered rate dependent, and creep and plasticity are not separately accounted for. Unified models have been developed during the past two decades and have been used with success to model the high temperature deformation behavior of isotropic materials.

A thermal orthotropic VBO was developed which allowed for variable Poisson's ratio and was shown to have desirable properties for thermal cycling. The theory permits specialization to cubic symmetry, transverse isotropy, and isotropy. It has been applied to simulate the behavior of single crystals made of a Nickel base superalloy. With the basic representation of material behavior accomplished, application to composite laminates followed.

In a modification of classical laminate theory, each ply is represented by the orthotropic VBO. To show the capability of the theory, the material constants of the theory were adjusted to approximately simulate composite behavior. One metal matrix composite called MMC2 was patterned after the Al_2O_3/Ni_3Al composite which shows an increase in transverse strength with temperature before the strength decreases. MMC1 has the same properties as MMC2 except that the strength continuously decreases with temperature. Thermal and mechanical behavior was simulated for in–phase and

out—of—phase cycling by numerically integrating the resulting nonlinear first order differential equations and plotting the results.

We introduced a comparably simple analysis tool which could be used for high temperature design in the same manner as the classical laminate theory is used for elastic behavior. Owing to the continuum representation of each ply, the theory is not capable of reproducing thermal—inelastic coupling which was shown to be important by Dvorak.

1. VBO and the Vanishing Fiber Diameter Model

To avoid this deficiency a simple composite model, the vanishing fiber diameter model (VFD) of Dvorak and Bahei—El—Din was introduced and combined with VBO. Although all of the published work deals with VFD, other composite models have been combined with VBO, such as Mori—Tanaka and Dvorak's bimodal theory in the PhD thesis of Yeh. The difficulty of applying advanced constitutive equations to high temperature composites lies in the small number of experimental data for fibers and the matrix, such as the effect of loading rates on the stress—strain behavior, the creep, and the relaxation behaviors. To perform numerical experiments, it is necessary to make reasonable guesses to be able to represent the constitutive behavior.

The theory of VBO and VFD is given by Yeh and Krempl (1992a). In this paper, the governing equations for thermal analysis of a single ply of fibrous metal matrix composites are derived. VBO is for cyclic neutral behavior (under symmetric cycling the hysteresis loop closes after one cycle) and for limited (primary) creep in the quasi linear region of the stress—strain diagram. The prediction of VBO is compared to that of an equivalent rate—independent plasticity theory and correspondence in simple tests is

32

established. It is also shown that the viscoplasticity theory models path dependent hardening, a typical plasticity phenomenon, although no yield surface and no loading and unloading conditions are used. In a companion paper, Yeh and Krempl (1992b), the theory is specialized for simple tensile or shear tests to show the predicted influence of volume fraction on the stress–strain and primary creep behavior. As expected, very little time dependence was predicted in the fiber direction. In the transverse direction creep is significant. Also, the variation of total Poisson's ratio during monotonic loading and during creep has been computed and there is general agreement with sparse experimental results.

2. VBO/VFD with Static Recovery of State

All the analyses reported so far were for a VBO model which exhibited only primary creep at stress levels corresponding to the quasi linear region of the stress–strain diagram. It is known from the high temperature creep behavior of monolithic materials that in these regions secondary and tertiary creep can occur. Under a separate program we have been developing a VBO theory which can model such behavior. A static recovery of state term must be introduced in the growth law for the state variables following the Baily/Orowan concep; of hardening/recovery competition in secondary creep. This has been done by Majors and Krempl (1991) for modified Cr–Mo steel. It is shown that secondary creep in the quasi elastic regions can be reproduced together with other phenomena found in our experiments. These experiments include strain rate changes and repeated relaxation tests at 538°C. If such tests would have been available for the matrix of a metal matrix composite, the theory could have been applied. However, such tests could not be found. To shown the capability of the theory, a hypothetical composite MMC3 was created consisting of the Cr–Mo steel matrix with a tungsten fiber. With this composite,

numerical experiments were performed which simulated the behavior of the unconstrained composite during cool–down. The residual stresses between fiber and matrix were shown to depend on cool–down temperature history. Hold–times at temperatures where recovery of state is active were most beneficial in reducing residual stresses at room temperature. An optimal temperature history was found which led to a residual stress reduction of 20% compared to uniform cooling (Yeh and Krempl, 1993).

In preparation for life–time analyses of metal matrix composites, a three–dimensional incremental damage accumulation law was developed. Its correlation and predictions compared favorably with scarce experimental data (Yeh and Krempl, 1993a). Such incremental laws can be combined with incremental constitutive laws such as VBO for life–predictions of composites under low–cycle fatigue conditions.

Additional references:

"The Influence of Cool–Down Temperature Histories on the Residual Stresses in Fibrous Metal Matrix Composites," N.–M. Yeh and E. Krempl, 1993, to appear in J. of Composite Materials.

"An Incremental Life Prediction Law for Multiaxial Creep–Fatigue Interaction and Thermomechanical Loading," N.–M. Yeh and E. Krempl, 1993a, to appear in American Society for Testing and Materials STP 1191.

III.   DEGREES GRANTED UNDER DARPA PROGRAM

David E. Alman, Ph.D., December 1992.
"The Effect of Ductile Phase (Nb) Reinforcement Morphology on the Mechanical Behavior of an Intermetallic Matrix (MoSi$_2$)," (Stoloff).

C. Amato, Ph.D., January 1993.
"The Thermal Decomposition Chemistry of an Aluminum Nitride Precursor, [(CH$_3$)$_2$AlNH$_2$]$_3$, Revealed by Molecular Beam Mass Spectrometry," (Interrante).

John Beale, M.S., 1989.
"High Temperature Dynamic Mechanical Characterization of AVCO SCS–6 SiC Fibers," (Sternstein).

Ronald P. Boisvert, M.S., May 1988.
"Ceramic Matrix Composites Via Organometallic Precursors," (Diefendorf).

Tungyang Chen, Ph.D., July 1990.
"Selected Problems in Micromechanics of Fibrous Composites," (Dvorak).

Sharathchandra Dakshinamurthy, Ph.D., (not completed).
(Rajan).

John Fish, Ph.D., August 1992.
"Oxidation of Aluminides," (Duquette).

Richard B. Hall, Ph.D., October 1990.
"Matrix–Dominated Thermoviscoplasticity in Fibrous Metal–Matrix Composite Materials," (Dvorak).

Anne Hynes, Ph.D., expected 1993.
"Creep of Mullite," (Doremus).

Andrea Kazmer, Ph.D., December 1992.
"Oxidative Stabilization of Bulk Carbonaceous Materials," (Diefendorf/Stoloff).

Paul Korinko, Ph.D., December 1992.
"Oxidation Behavior of Ti and Nb Aluminides," (Duquette).

Bryan Lagos, M.S., May 1991.
"Studies in Reactive Spatter Deposition onto Carbon Fiber Tows Using a Cylindrical Hollow Cast Cathode Magnetron," (Hudson).

Edgar Lara–Curzio, Ph.D., 1992.
"High Temperature Mechanical and Structural Characterization of Composite CVD SiC Fibers," (Sternstein).

D. Larkin, Ph.D., March 1991.
Part I. "Application of CVD–ypbria for the Protection of SCS–6 Silicon Carbide Fibers and a Reactively Sintered Nickel Aluminide Matrix Composite."
Part II. "CVD–Pyrolysis Studies of Various 1,3–Substituted 1,3–Disilacyclobutanes and Applications as Single–Source CVD Precursors to Silicon Carbide," (Interrante).

Carolyn Lee, M.S., 1988.
"Microstructure and Grain Growth of Mullite Prepared by the Sol–gel Method," (Doremus).

K.D. Lee, Ph.D., August 1989.
"An Orthotropic of Theory of Viscoplasticity Based on Overstress for Thermomechanical Deformation and Its Application to Laminated Metal Matrix Composites," (Krempl).

Lazhar Mazlout, Ph.D., December 1991.
"Synthesis of High Performance Titanium Diboride Fibers by Chemical Vapor Disposition," (Stoloff).

Joseph Montrym, M.S., September 1988.
"Oxidation of Ni_3Al Intermetallics," (Duquette).

Dung A. Ngo, M.S., December 1987.
"Analysis of Thermal and Mechanical Properties of High Temperature Composites," (Bauchau).

Lisa A. Puleo, M.S., 1987.
"Grain Growth and Microstructural Observations of Hydroxylapatite and Silicon Nitride," (Doremus).

James J. Scott, M.S., May 1992.
"Hydrogen Embrittlement of Intermetallic Based Composites," (Duquette).

Rahul S. Shah, Ph.D., May 1991.
"Modeling and Analysis of High Temperature Inelastic Deformation in Metal Matrix Composites," (Dvorak).

Karl Shaw, Ph.D., December 1992.
"Particle Size Effects During Plasma Spraying and Atomization," (German/MacCrone).

Robert Shinavski, Ph.D., (not completed).
(Diefendorf/Hillig).

Shainn–Shyong Tzeng, Ph.D., November 1992.
"Structure and Property Relationship in Carbon Fibers," (Diefendorf).

C.W. Whitmarsh, Ph.D., July 1991.
"Synthesis and Characterization of Si–H Containing Polycarbosilanes as Precursors to Silicon Carbide," (Interrante).

H.J. Wu, Ph.D., December 1992.
"The Preparation of Poly(silapropylene) and Poly(silaethylene) via Ring–Opening Polymerization and the Study of Pyrolysis of Poly(silaethylene) to Silicon Carbide," (Interrante).

N.M. Yeh, Ph.D., December 1991.
"Thermoviscoplastic Analysis of Metal–Matrix Composites," (Krempl).

INTERMETALLIC COMPOUNDS

PROCESSING

THE PROPERTIES OF PLASMA ATOMIZED NiAl POWDERS

K. G. Shaw, W. Z. Misiolek, and R. M. German*

Rensselaer Polytechnic Institute
Department of Materials Engineering
Troy, NY 12180

*effective summer 1991, Brush Chair in Materials,
Engineering Science and Mechanics Dept., Pennsylvania State University
University Park, PA 16802

ABSTRACT

Nickel aluminum powders have been fabricated using two different plasma
atomization techniques: spheroidization of pre-alloyed powders and agglomeration
by mechanical alloying and subsequent spheroidization of elemental powders. These
powders have also been fabricated by reactively sintering elemental powder and
ultra-centrifugation. The properties of these powders are compared with respect
to morphology, size and microstructure using electron microscopy, laser light
scattering particle size determination and X-ray diffraction. Measurement of the
grain size and diffraction pattern is used to estimate the rapid solidification
and possible formation of glassy phases.

INTRODUCTION

As the technology and processing of NiAl advances there is a need for metal
injection molding grade NiAl powders. These powders should have a mean particle
diameter of approximately 10 μm, be spherical, and possess a fine microstructure
which enhances sintering. The mechanical properties, specifically the ductility
of NiAl, are known to improve as the average grain size remains below 8 μm [1].
It is the intent of this study to characterize the properties of plasma atomized
NiAl powders with respect to creation of the desired particle size and fine
microstructure.

It is well known that plasma atomization is a technique which produces
rapidly solidified powders [2-5]. The cooling rates involved with this technology
are generally slightly higher than gas atomization [6] and can exceed 1×10^5 K/sec.
Certainly at this cooling rate a fine microstructure will develop, however it is
not clear whether an ordered, disordered or glassy microstructure will form as the
NiAl re-solidifies. The effect of the rapidly solidified microstructure on the
sintering behavior is also not well documented. To gain some insight to the
answers of these questions various NiAl powders have been fabricated and analyzed
with respect to the phase stability of the ordered NiAl structure.

EXPERIMENTAL

Commercial NiAl powders (mean particle diameter of 83 μm) were ball milled in hexane for 48 hours with zirconia balls at 100 RPM. The milling process decreased the size of the powder to a mean diameter of 14 μm. The milled powders were then plasma atomized subsonically with a 28 kW argon plasma. The configuration of the plasma atomizer is shown in Fig. 1. The atomization chamber was kept under an inert argon atmosphere. The oxygen content of this atmosphere was measured during the atomization using an oxygen detector and found to be 4 ppm. The apparent and tap densities were measured. The shape of the powders was determined using electron microscopy and the size of the fabricated powders was determined using laser light scattering.

Alternatively, elemental nickel and aluminum powders were mechanically alloyed using an attritor mill. This mechanical alloying process was used to bond the elemental powders together for subsequent reaction induced in the plasma without the use of organic binders as denoted in the PRMS (Plasma Melt and Rapid solidification) process used by Johnson et. al. [7]. These agglomerated elemental powders were then plasma atomized using the same atomization conditions as above. The last group of powders were fabricated by reactively sintering elemental nickel and aluminum powders at 973 K in vacuum and using ultra-centrifugation to mill the powders down to the appropriate size. Consequently five types of powders may be compared with the above fabrication sequence; commercial, ball milled, BMPS (ball milled and plasma spheroidized), MAPS (mechanically alloyed and plasma spheroidized), and RSUC (reactively sintered and ultra-centrifuged) powders.

RESULTS

Shown in Fig. 2 are the electron micrographs of the fabricated powders. As can be seen a dramatic size reduction has occurred in the processed powders. The BMPS process has created the desired spherical particle shape. The MAPS powders have not adequately reacted as evidenced by the non-spherical shape of these powders. The RSUC powders are faceted indicative of the brittle fracture occurring from the action of the high speed rotor against the feedstock material. One may also see some fragmented fine particles produced by the high energy collision between the rotor and NiAl. The laser light scattering size distributions of the fabricated powders are compared in Fig. 3.

To check for the formation of glassy phases diffractometer patterns were taken for each of the fabricated powders. These results are shown in Fig. 4. Observation of the low scattering angle intensities reveals that no glassy phases are present. One may measure the strain caused by the milling by measuring the line broadening. All of the powders except for the MAPS powder have diffraction patterns common to the CsCl structure.

The microstructures of the rapidly solidified BMPS and commercial powders were determined by electron microscopy after cross-section, polish and etching. These micrographs are illustrated in Fig. 5. One can see that the rapid solidification has decreased the grain size to approximately 4 μm from 35 μm in the commercial powders. For the rapidly solidified powders, the grain size is smallest near the particle surface indicative of the high cooling rate at the surface.

Finally, to check the sintering behavior of the powders, the powders were tapped into an alumina crucible and sintered at 1673 K for 1 hour in vacuum. The densification was determined. These results are shown in Fig. 6. A summary of the measured powder properties is given in Table 2. These results indicate that the

internal strain caused by milling has a greater effect on sintering than the fine microstructure caused from the rapid solidification. The RSUC powder exhibited the best sintering behavior and also possessed the greatest internal strain as measured by X-ray diffraction.

SUMMARY

It is possible to form MIM grade powders using the plasma atomization process. Currently the MAPS process is not producing the desired material, perhaps due to the volatilization of aluminum prior to the reactive formation of NiAl causing lack of stoichiometry in the fabricated MAPS powder or because of transient effects during the reactive sintering between the nickel and aluminum. The RSUC produces a desirable powder of approximately the proper morphology, however the grain structure of these powders is not refined in the process.

Nickel aluminide re-solidifies in a columnar microstructure. No glassy or disordered phases were observed. The refined microstructure does aid sintering, however the magnitude of this effect is not greater than any enhanced sintering mechanisms caused by the cold work during milling or ultra-centrifugation. It is felt that to take full advantage of the plasma atomized powders densification should be aided by hot isostatic pressing at relatively lower temperatures and short times to reduce grain growth and preserve the fine grain size present in the fabricated powders.

REFERENCES

1. E. M. Schulson and D. R. Barker, "A Brittle to Ductile Transition in NiAl of a Critical Grain Size," *Scr. Metall.*, Vol. 17, (1983), 519.

2. W. A. Johnson, N. E. Kopatz and E. B. Yoder, "Fine Powders by Plasma Processing," *Progress in Powder Metallurgy*, Vol. 42, ed. E.A. Carlson, and G. Gaines (Princeton, NJ: Metal Powder Industries Federation, 1986), 775-789.

3. R. F. Cheney and E. R. Seydel, "The Production of Rapidly Solidified Ultrafine Metal and Ceramic Powders," *Physical Chemistry of Powder Metals Production and Processing*, ed. W. Murray Small (Warrendale, PA: The Minerals, Metals & Materials Society, 1989), 297-307.

4. R. F. Cheney, F. J. Mower, C. L. Moscatello. *U.S. Patent No. 3909241.* (1975).

5. R. F. Cheney, R. L. Daga, R. M. German and A. Bose, "Heavy Alloys from Rapidly Solidified Powders," *Proceedings of the 1988 International Powder Metallurgy Conference*, Vol. 19, (Princeton, NJ: Metal Powder Industries Federation, 1988), 155-169.

6. G. H. Gessinger. *Powder Metallurgy of Superalloys.* Butterworth & Co., London, (1984), 32.

7. W. A. Johnson, N. E. Kopatz and E. B. Yoder, "Plasma Processing Technologies for Production of Fine Spherical Refractory Metal (Alloy) Powders," *International Journal of Refractory & Hard Metals*, Vol 8, No. 1, (March 1989), 41-48.
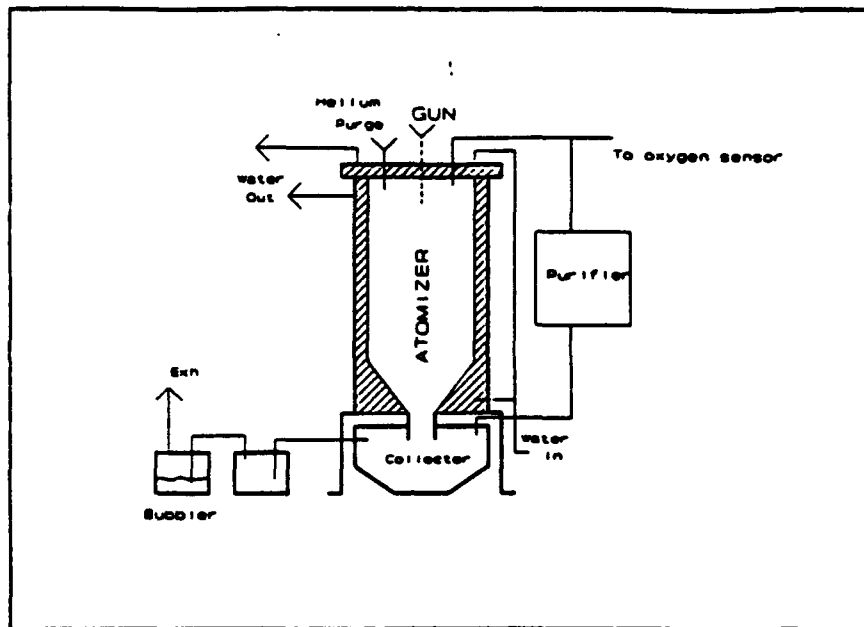
Figure 1
Schematic of the plasma atomization system. The atomizer is approximat
8 feet tall and supports an inert atmosphere.

Table 1 Comparison of fabrication processes		
Abbreviated Process Name	Expanded Process Name	Process Description
BM	Ball-Milled	Ball mill in hexane with zirconia balls
BMPS	Ball-milled Plasma Spheroidized	Inject milled powder into a D.C. plasma jet
MA	Mechanically Alloyed	Mechanically alloy in an attritor mill and with hexane blanket
MAPS	Mechanically Alloy Plasma Spheroidized	Inject mechanically alloyed powder into a D.C plasma jet
RSUC	Reactively Sintered Ultra-centrifuged	Reactively sinter and ultra-centrifuge the powder at 20000 RPM

162
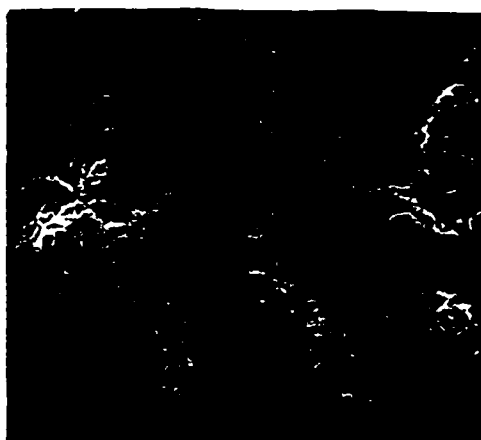
Commercial Powder

40 µm

Ball-Milled Powder

10 µm

SMPS
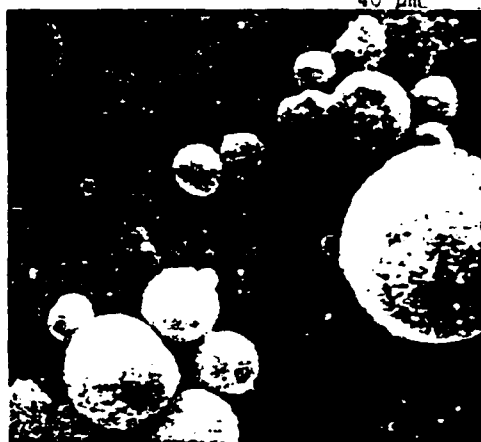
10 µm

Mechanically Alloyed

30 µm

MAPS

15 µm
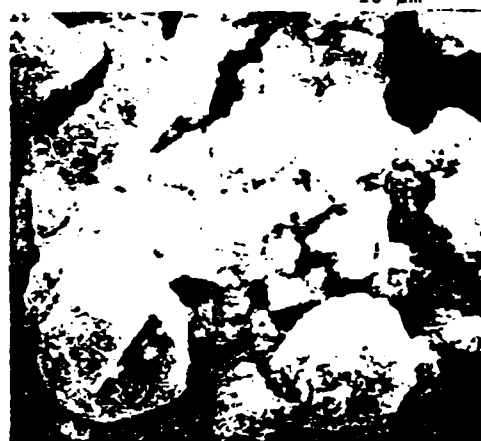
RSUC

10 µm

Figure 3
Electron micrographs of the fabricated powders.

163

Comparison of Size Distributions
Laser light scattering analysis

Comparison of Size Distributions
Laser light scattering analysis
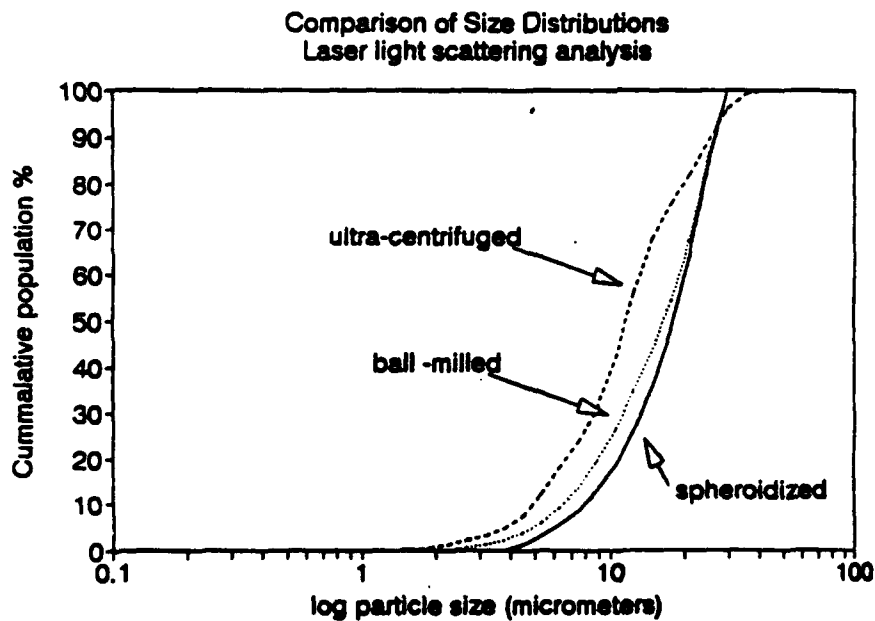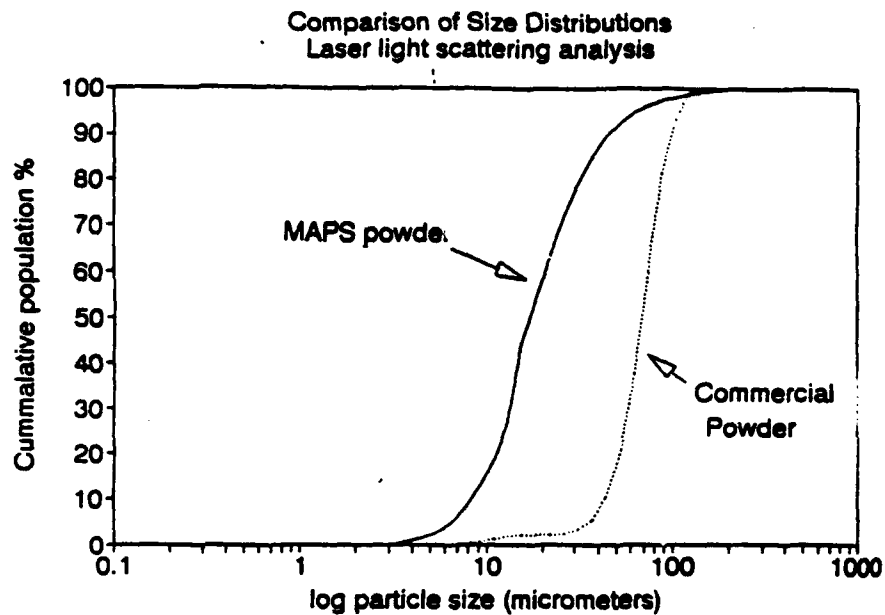
Figure 3

Laser light scattering analysis of the particle sizes of the fabricated powders

164
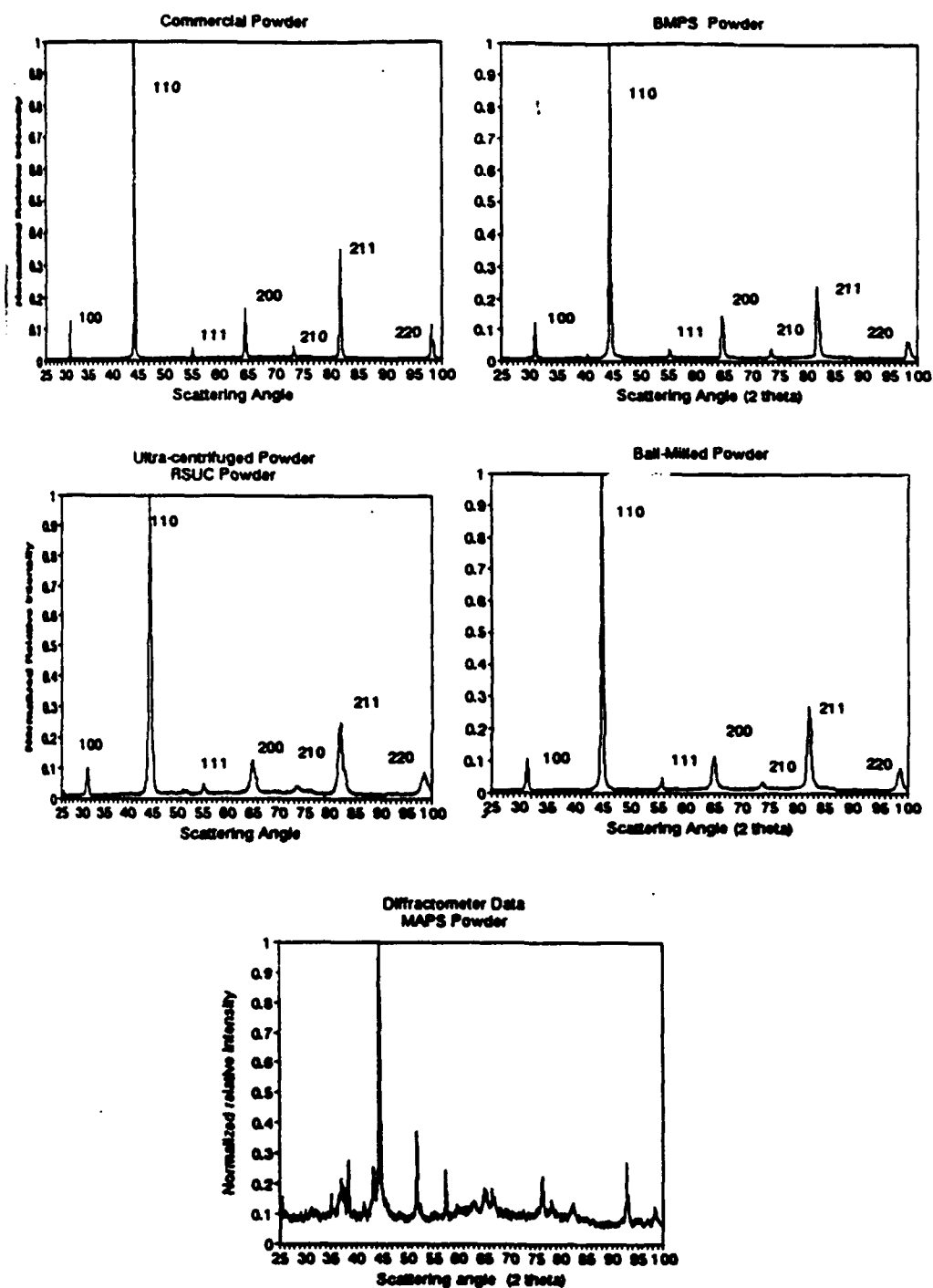
Figure 4
X-ray diffractometer powder patterns of the fabricated powders.

BMPS Powder

Commercial Powder

2 μm

30 μm
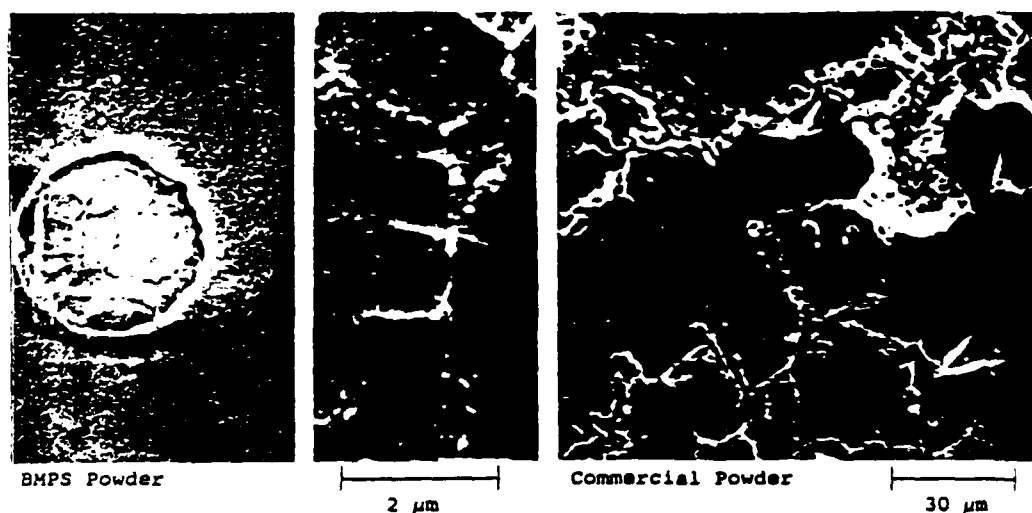
Figure 5

Cross sections of BMPS (ball-milled and plasma spheroidized) and commercial powders showing refined grain structure from the plasma atomization.

Table 2

Summary of Powder Characteristics					
Powder	Mean Diameter (μm)	Linewidth (Δ2θ) at 2θ	Apparent Density (g/cm³)	Tap Density (g/cm³)	Sintered Density (g/cm³)	Densifi-cation %
Commer-cial	93	0.2° 81.75°	1.78	2.65	2.70	1.6
Milled	17.5	0.6° 82.105°	2.39	2.94	3.55	20.9
Atomized BMPS	17	0.2° 81.905°	1.94	2.50	3.25	22.3
RSUC	12	0.8° 82.05°	2.35	3.09	3.92	30.0

Densification defined as $(\rho_s - \rho_g)/(\rho_t - \rho_g)$, where ρ_s is the sintered density, ρ_g is the green density and ρ_t is the theoretical density.

Economical Aspects of Experiment Design for Compaction of High Temperature Composites

W. Z. MISIOLEK AND R. M. GERMAN

ABSTRACT

This paper focuses on the application of an factorial experimental design method to the fabrication of an advanced material. A high temperature composite NiAl/30vol%TiB$_2$ was compacted using hot isostatic pressing (HIP). Due to the HIP process variables, a full factorial approach to these studies would be very labor intensive. The powder price and the high cost of processing were other reasons to employ an economical experimental design method. This method allows the comprehensive investigations of the densification process based on the Taguchi method. It considers material parameters, such as, particle size, particle size ratio, and hot isostatic pressing variables of pressure, temperature, and time. The subsequent statistical analysis of the results permitted conclusions based on results of 9 instead of 81 tests.

INTRODUCTION

Intermetallic compounds have great potential in structural engineering applications due to their oxidation resistance and high strength at elevated temperatures. Among all intermetallics, the aluminides have received the most attention because of their low density. Extensive research has been done on nickel aluminides to improve their intrinsic brittleness and evaluate possible fabrication methods [1-5]. Compounds based on NiAl, including alloys and composites, show more potential than Ni$_3$Al because of their higher melting temperatures (1911 K for NiAl versus 1663 K for Ni$_3$Al) and lower density (5.86 g/cm^3 for NiAl versus 7.50 g/cm^3 for Ni$_3$Al). Extensive studies have been undertaken on NiAl [2,6-14] which show possible improvements of its properties by using composites technology. The addition of a ceramic phase like TiB$_2$ improves mechanical properties, such as high temperature strength and hardness [2,7]. The objective

W. Z. Misiolek, Materials Engineering Department,
Rensselaer Polytechnic Institute, Troy, New York 12180-3590
R. M. German, Engineering Science and Mechanics Department,
Pennsylvania State University, University Park, PA 16802

of this work was to study fabrication, microstructure, and mechanical properties of a NiAl matrix composite with 30 vol % of particulate TiB₂ as a reinforcing phase. The choice of 30 vol % of reinforcing phase was made to achieve continuity of the ceramic phase within the consolidated microstructure. Although this composite material has poor oxidation resistance at elevated temperatures, nevertheless, expected improvement of mechanical properties offset the need to coat the final product with monolithic NiAl. This study concentrates on hot isostatic pressing (HIP) of prealloyed powders as the production technology. Variables such as particle size and particle size ratio were studied in the material system. The experimental matrix was based on orthogonal array method proposed by Taguchi [15]. Hot isostatic pressing was conducted under various temperature, pressure, and time parameters, which enable optimization of the densification process [16].

EXPERIMENTAL PROCEDURES

The powders used for this investigations are described in Table I. They were purchased with average particle sizes of 82 μm for NiAl and 13 μm for TiB₂, and then ball milled to smaller particle sizes. The average particle sizes after milling are given in parentheses. They were measured using a laser light scattering particle size analyzer. To form the composite, NiAl and TiB₂ powders of the desired sizes were weighed to form composite with 30 vol% of reinforcing ceramic phase and mixed for 30 minutes in a turbula mixer.

Table I
Powder Characteristics

	NiAl	TiB₂
Vendor	Cerac Inc.	ICD Group Inc.
Shape	blocky, irregular	sponge, irregular
Average Particle Size (μm)	82 (52, 49, 44, 36, 27, 18)	13 (6)

The NiAl powder was milled to mean particle sizes of 49 μm, 36 μm and 18 μm, while the TiB₂ powder particles were reduced to 6 μm. The milling used balls made of partially stabilized zirconia. Hexane was used to minimize oxidation during milling. The particle size ratios (NiAl/TiB₂) for these samples were 8.2, 6.0, and 3.0, respectively. To avoid difficulty with compaction, ejection, and sample handling, the powder was compacted directly in stainless steel cylinders used later as HIP cans. These HIP samples of 12.6 mm outside diameter were degassed for several hours at a temperature of 570 K prior to being welded under vacuum.

The experiment was designed using the orthogonal array method proposed by Taguchi [15]. Key process parameters, such as

particle size, particle size ratio, and hot isostatic pressing variables such as temperature, pressure, and time were selected as the main factors in the densification process. These controllable process factors and their levels are shown in Table II. The TiB_2 average particle size was constant at 6 μm. The NiAl powder was 49 μm, 36 μm, and 18 μm, and as a result the powder particle size ratio (NiAl/TiB_2) also varied.

Table II
Controllable Factors of HIP Process

Controllable Factor	Levels		
NiAl particle size (μm)	49	36	18
Temperature (K)	1373	1423	1473
Pressure (MPa)	100	135	170
Time (h)	1	2	4

RESULTS

A typical microstructure for the fully dense composite is presented in Figure 1. The results of density and hardness measurements together with HIP process parameters are shown in Table III. The results for experiments 1 to 9 are representative for the experiment designed for the three levels of studied factors (See Table II). This allows analysis of the L_9 orthogonal array since it is the most efficient orthogonal design to accommodate four factors at three levels. This array specifies nine experimental runs, but the aim is to find the best of $3^4=81$ combinations that exist. This way the designed experiment is statistically balanced and its results are presented in Tables III and IV. The experiments 10 to 12 were run as confirmation tests for the proposed model and their results are also presented in Table III. The relationship between predicted and measured density is presented in Figure 2.

Statistical analyses permit building a mathematical model for HIP compaction of NiAl + 30 vol% TiB_2. Density (σ) is a function of NiAl particle size (TiB_2 powder average size was constant and equal 6 μm) and the HIP parameters of pressure, temperature, and hold time. The equation representing this

.
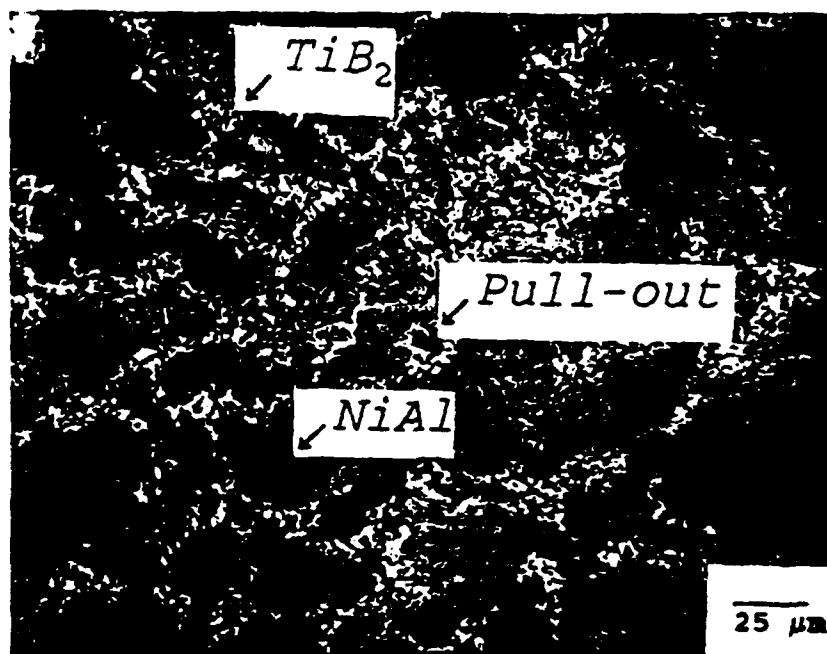
Fig. 1. Microstructure of test #3 HIP sample; 49 μm NiAl and 6 μm TiB$_2$, at 1473 K, under 170 MPa, for 4 h, with 100% of theoretical density.
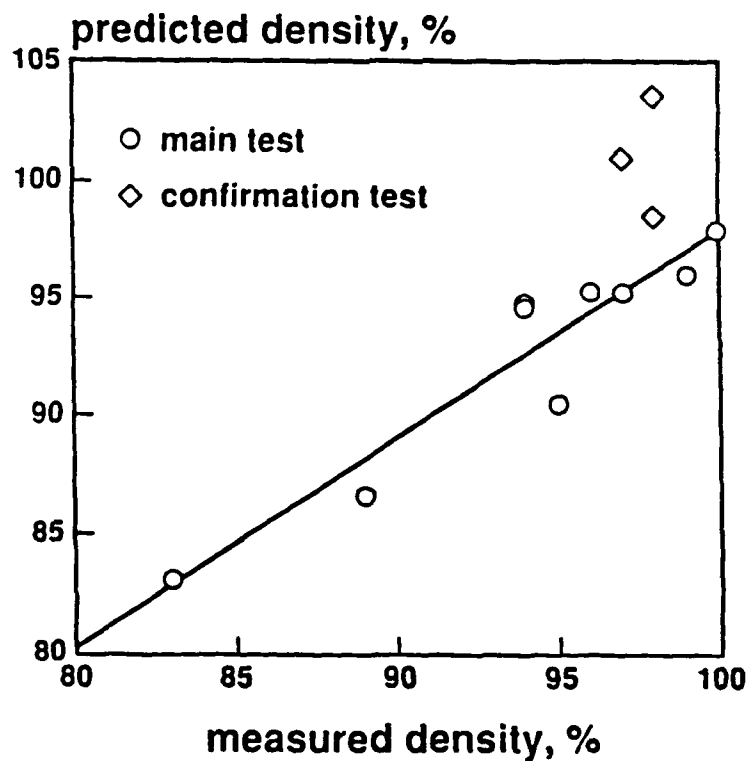
Fig. 2. The relationship between predicted and measured density for HIP NiAl + 30vol% TiB$_2$ composite.

relationship is as follows:

$$\ln (\sigma) = 0.106 \ln (P) + 0.037 \ln (t) - 0.056 \ln (D)$$
$$- 1168/T + 5.0 \tag{1}$$

where:
P = HIP pressure (MPa)   T = HIP temperature (K)
t = HIP hold time (h)   D = NiAl particle size (μm)

Table III
Experimental Results

Test #	NiAl Powder Size D [μm]	HIP			Percent of Theoretical Density %	HRC
		Temp. T [K]	Press. P [MPa]	Time t [h]		
1	49	1373	100	1	83	6.5
2	49	1423	135	2	95	36.2
3	49	1473	170	4	100	47.0
4	36	1423	135	4	94	42.5
5	36	1473	170	1	94	48.0
6	36	1373	100	2	89	22.3
7	18	1373	170	2	97	44.9
8	18	1423	100	4	96	47.4
9	18	1473	135	1	99	49.9
10	18	1473	170	1	98	53.3
11	18	1473	170	2	97	53.1
12	18	1473	170	4	98	51.5

Table IV
Statistical Parameters of the Experiment

Parameter	Density Function	Hardness Function
Correlation Coefficient	0.946	0.934
Significance	0.0001	0.0000
Standard Error of Estimate	1.8%	5.3%

The mathematical formula for hardness (H) in HRC as a function of NiAl particle size, HIP variables (temperature, pressure, hold time) and composite density based on the results of the twelve tests (1 to 12) can be presented in the form of a logarithmic equation:

$$\ln(H) = -0.143 \ln(D) - 1930/T + 0.105 \ln(P) + 0.064 \ln(t) + 9.07 \ln(\sigma) - 36.4 \qquad (2)$$

where: σ = composite density (%), and P, D, T and t are defined in Equation (1).

The relationship between predicted and measured hardness for the HIP NiAl/30vol%TiB$_2$ composite is presented in Figure 3. Equation (1) is a very functional formula and can be used for calculation of composite final density. It also can be employed to find an interaction between two process variables for a certain final density when two other process parameters are constant. For example, for a definite material system it is possible to calculate pressure - temperature conditions, which for a particular hold time, will result in certain final density. Three curves are presented on the pressure vs. temperature graph in Figure 4. They represent hold times of 1 hour, 2 hours, and 4 hours, which for given pressure - temperature conditions result in a final composite density of 98%.

DISCUSSION
The results obtained in this study give valuable information on the densification of NiAl/TiB$_2$ composites using the HIP process. Analysis of the results presented in Table III shows the evident role of the NiAl particle size. The combination of pressure, temperature, and time variables can lead to good quality material with a final density of 97% of theoretical or higher. This material was obtained in confirmation experiments (test #10, #11, and #12). The hardness measurements (See Table III) showed a good correlation with the density results and processing temperature. A higher hardness was achieved with higher processing temperatures (test #3, #5, and #9) with a large role of particle size. NiAl powder with an

predicted hardness, HRC

measured hardness, HRC
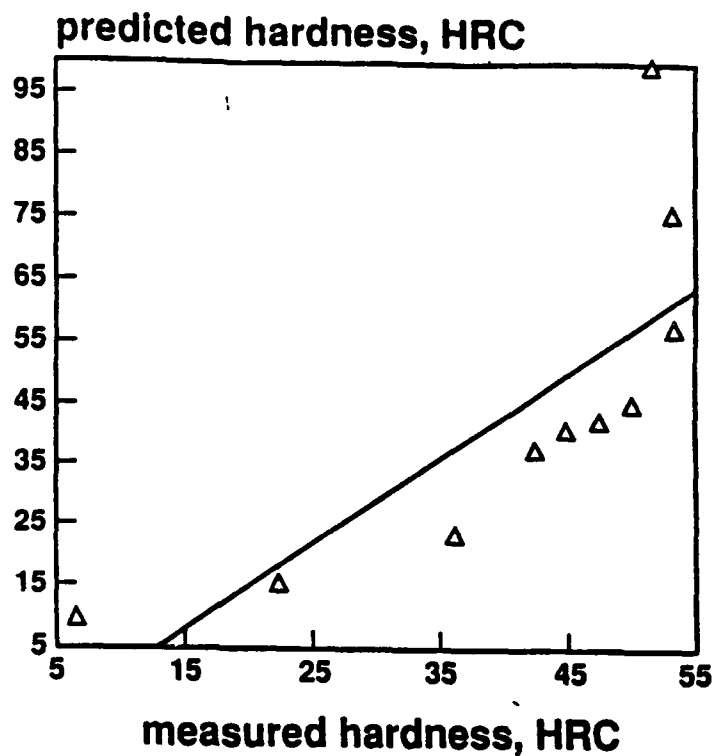
Fig. 3. The relationship between predicted and measured Rockwel
C hardness for HIPed NiAl + 30 vol% TiB$_2$
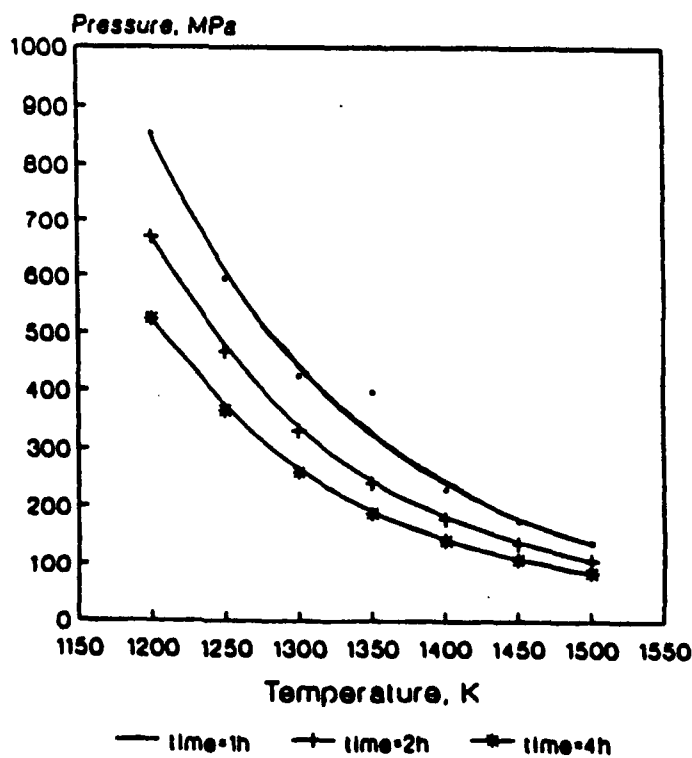
Fig. 4. Pressure - temperature HIP conditions to obtain 98%
dense NiAl + 30vol% TiB$_2$ material at a given hold time

average particle size of 36 μm was consolidated at the same
temperature (1473 K) and under the same pressure (170 MPa) as
the 49 μm NiAl powder, and gave the same hardness readings of 47
to 48 HRC even though it was held at a high temperature and
pressure for only 1 hour instead of 4 hours, as was used for the
49 μm NiAl compound. A sample made of 18 μm NiAl powder and
consolidated for only 1 hour at 1473 K, under a lower pressure
of 135 MPa resulted in a higher hardness, 49.9 HRC.

A mathematical model represented by Equation (1) allows
design of a HIP experiment in such a way as to obtain the
desired density as presented in Figure 4. The plot in Figure 2
and the statistical analysis data presented in Table IV show the
accuracy of the model, which was built on the base of nine
statistically design experiments. By knowing the effect of the
HIP parameters, such as temperature, pressure and time on the
densification process and by using different NiAl powder sizes,
one can tailor the process parameters to achieve the desired
mechanical properties. This model was confirmed by experiments
listed in Table III as 10, 11 and 12. For these temperatures and
pressures the final densities are very close or below the
calculated values. For example, the density calculated for 10
test is 98.5% while the measured value is 98%, for tests 11 and
12 the calculated densities are above 100% while the measured
values are 97% and 98% respectively. There is a physical
limitation of 100% density which is not incorporated into the
mathematical relationship. Nevertheless, this equation is
valuable and gives general information about densification of
composite materials over a wide range of process variables. The
mathematical model can be built for *any desired variables and in*
the case of a small variable range it will match the
experimental results accurately.   Figure 2 shows good
correlation between measured and predicted density in the range
from 80% to 100%. Equation (2) allows us to calculate hardness
of fabricated composite material when material data and process
variables together with final density are known. This model
shows good correlation up to a predicted hardness of 55 HRC.
Above this value the calculations are higher than measured
mainly due to a longer HIP hold time, which at elevated
temperature favors the recovery process. As a result the
material, which was held for longer time shows lower hardness.

CONCLUSIONS

1. The experimental design method allowed us to perform a
   significantly reduced number of tests in order to achieve
   vital information about densification of a NiAl/TiB$_2$ composite
   by the HIP process.

2. Mathematical models for the HIP densification process and for
   final hardness of the NiAl + 30 vol% TiB$_2$ composite have been
   proposed.

3. A significant impact of HIP temperature on the

densification mechanism and composite hardness has been noted.

4. The powder size has a dramatic influence on the densification of the $NiAl/30vol\%TiB_2$ composite.

REFERENCES
1. V. K. Sikka,"Processing Technology for Nickel Aluminides", Proceedings of Materials Research Society Symposium, Materials Research Society, Pittsburgh, PA, vol. 81, 1987, 487-493.
2. D. Alman et al.,"Powder Processing of Intermetallic Matrix Composites", Symposium on Advances in Processing and Application of Ceramic and Metal Matrix Composites, Canadian Institute of Metallurgists, Halifax, August 20-24, 1989.
3. R. M. German and A. Bose,"Fabrication of Intermetallic Matrix Composites", Materials Science and Engineering, 1989, vol. A107, 107-116.
4. B. H. Rabin, A. Bose and R. M. German, "Processing Effects on Densification in Reactive Sintering of Nickel-Aluminum Powder Mixtures", Modern Developments in Powder Metallurgy, Metal Powder Industries Federation, Princeton, NJ, vol. 20, 1988, 511-529.
5. R. M. German,"Transient Thermal Effects in the Synthesis of Intermetallic Alloys", TMS Meeting, Anheim, CA, February 18-22, 1990.
6. J. A. Patchett and G. J. Abbaschian,"Kinetics and Mechanism of Formation of Al-Ni Intermetallics", Proceedings of Materials Research Society Symposium, Materials Research Society, Pittsburgh, PA, vol. 81, 1986, 135-141.
7. J. D. Rigney, P. S. Khadkikar, J. J. Lewandowski and K. Vedula, "Strength and Toughness of Composite Materials Based on Nickel Aluminide Matrices", Proceedings of Materials Research Society Symposium, Materials Research Society, Pittsburgh, PA, vol. 133, 1989, 603-608.
8. S. Nourbakhsh et al.,"Pressure Casting of Ni_3Al/Al_2O_3 Composites", Proceedings of Materials Research Society Symposium, Materials Research Society, Pittsburgh, PA, vol.133, 1989, 459-464.
9. J. D. Whittenberger, S. Kumar, S. K. Mannan and R. K. Viswanadham ,"Slow Plastic Deformation of Extruded $NiAl-10TiB_2$ Particulate Composites at 1200 and 1300 K", Journal of Materials Science Letters, vol. 9, 1990, 326-328.
10. R. K. Viswanadham, J. D. Whittenberger, S. K. Mannan and B. Sprissler, "Elevated Temperature Slow Plastic Deformation of $NiAl/TiB_2$ Particulate Composites", Proceedings of Materials

Research Society Symposium, Materials Research Society, Pittsburgh, PA, vol.120, 1988, 89-94.

11. E. M. Schulson and D. R. Barker, "A Brittle to Ductile Transition in NiAl of a Critical Grain Size", Scripta Metallurgica, vol. 17, 1983, 519-522.

12. E. P. George and C. T. Liu, "Brittle Fracture and Grain Boundary Chemistry of Microalloyed NiAl", Journal of Materials Research", vol. 5, 1990, No 4, 754-762.

13. D. B. Miracle, S. Russell and C. C. Law, "Slip System Modification in NiAl", Proceedings of Materials Research Society Symposium, Materials Research Society, Pittsburgh, PA, vol.133, 1989, 225-230.

14. W. Z. Misiolek and R. M. German, "Fabrication of NiAl/TiB$_2$ Intermetallic Composites", Advances in Powder Metallurgy, Metal Powder Industries Federation, Princeton, NJ, vol. 2, 1990, 161-172.

15. G. Taguchi, <u>Introduction to Quality Engineering</u>, Kraus International Publications, 1986, White Plains, N.Y.

16. A. M. Laptev, N. V. Samarov and S. V. Podlesny, "Theory and Optimization of Hot Isostatic Pressing", Powder Metallurgy International, vol.22, 1990, No 2, 23-25.

Pressure Assisted Reactive Sintering of NiAl/TiB$_2$

W. Z. Misiolek[*], N. D. Sopchak[*], and R. M. German[**]

[*]Materials Engineering Department
Rensselaer Polytechnic Institute
Troy, NY 12180-3590

[**]Department of Engineering Science and Mechanics
Pennsylvania State University
University Park, PA 16802

Abstract

Reactive sintering techniques use a transient liquid phase for the formation of a compound. This method has been successfully applied to the fabrication of several materials, such as borides, carbides, nitrides, silicides, intermetallics and composites. The work presented here focuses on the use of reactive powder processing techniques to fabricate the intermetallic matrix composite NiAl/30vol%TiB$_2$. First experiments showed a possibility of reactive sintering of NiAl/TiB$_2$ composite. The final density (approximately 60% of theoretical value) was not satisfactory. To enhance the densification mechanism, reactive sintering was conducted under simultaneous pressurization. A special heated die was built for this experiment, which served as a hot press when used on a mechanical testing machine. This design enabled us to compact the powders in the hot die and then spark the powder mixture to start the reaction to obtain a wave of liquid phase moving through the sample for consolidation.

Introduction

The reactive sintering technique has been used to create compounds, but the addition of pressure to reactive sintering has not been given much consideration[1-4]. For some systems, such as ceramics and composites, there is a need for pressure in order to obtain full density. This can be achieved by reactive sintering of powers which are hot pressed at the same time. Pressure assisted reactive sintering (PARS) has a number of benefits, while still obtaining desired properties, which can only be obtained by hot isostatic pressing (HIPing). Cycle time is on the order of minutes rather than hours like for HIPing. PARS is a high strain rate process comparable to forging, whereas HIPing is a low strain rate process with creep as the main densification mechanism. HIPing also requires the additional preceding operation of sintering of the part to greater than 95% of theoretical density or else the use of a container. PARS is a more attractive process due to its efficiency from a production point of view. The efficiency of the process can be measured by the amount of energy required, the processing time, and the amount of material needed to aid in the processing. This efficiency in turn reduces part cost. The above mentioned advantages of hot pressing of powder mixtures shows the need for more study in the field.

The objective of this project is to study the feasibility of this processing route to achieve full density composite materials. The experiment performed and its results enable us to gain knowledge about the interaction between different process variables. This learning can then be applied to hot pressing and reactive sintering of different material systems.

Experimental Procedure

Elemental nickel, aluminum, titanium, and boron powders were weighed in proportion to form $NiAl/30volTiB_2$ composite. The powders used for this experiment are characterized in Table I. They were mixed together in Turbula mixer for 30 minutes. Then the composite powder was loaded into the specially designed hot press, degassed at an elevated temperature, and then reacted under pressure. The processed samples were removed and density was measured.

The first generation hot press consisted of a conventional hydraulic press and a cylindrical stainless steel double action die and punch set, which is shown in Fig. 1. The die had a radial ports for a thermocouple. One of the punches was drilled to insert an ignition element, which allowed us to initiate the reaction. The outside of the die was coated with an insulating ceramic, then wrapped with resistance heating elements followed by an outer layer of thermal insulation.

The heating rate and temperature were controlled by regulating the current to the heating elements. The problem found with this series of experiments was that once the reaction started, the shrinkage due to sintering happened so fast that the conventional hydraulic press could not respond fast enough. As a result, the sintering occurred with no pressure applied to the

sample. These results were similar to those found in conventional reactive sintering. In both cases the samples were only in the region of 60% of the theoretical density.

Table I.
Powder Characteristics

Powder	Mean Particle Size	Vendor	Vendor Designation
Nickel	17μm	Inco	123
Aluminum	10μm	Valimet	H3
Titanium	30μm	Micro Metals	Ti-020
Boron	40μm	Cerac	
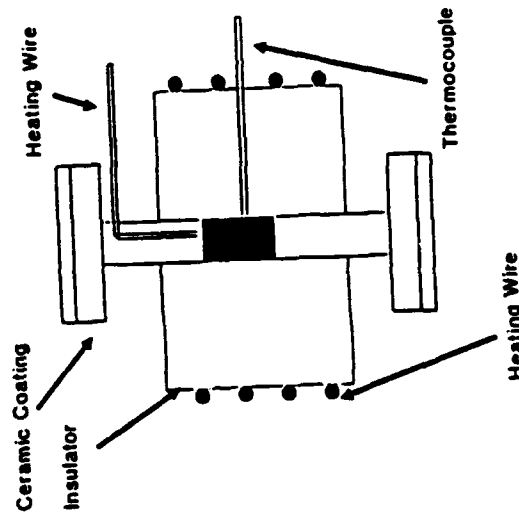
Fig. 1. Schematic of first generation die

The second generation used the same die and punch set-up but utilized a Gleeble 1500, which is a mechanical testing machine capable of controlling temperature and force in a very precise manner. The benefit is that the Gleeble monitors the system 120 times a second, thus effectively responding and applying constant force, which results in constant pressure. These experiments yielded higher densities, in the region of 68% of theoretical.

The third generation hot press used a conventional, double action cylindrical, stainless steel die with the thermocouple

188

189

welded to the outside of the die, and standard punches. The punches were covered by an electrically conducting lubricant, which allowed the heating by the resistance heating of the Gleeble. Similarly, the force/pressure was controlled by the Gleeble. To achieve sufficient information, the factorial method was used in designing the set of experiments. An experimental matrix was set up to study three major factors: pressure, degassing time, and temperature. Each variable was studied at two levels. The process parameters and the final densities are presented in Table II.

Table II

Process Parameters and results

Experiment #	Pressure (MPa)	Degassing Time (min)	Degassing Temperature °C	Percent of Theoretic. Density
1	105	15	300	81.6
2	105	30	350	80.3
3	175	15	350	83.4
4	175	30	300	84.4

Through these process variables, as well as running the experiment in vacuum, greatly improved final densities were achieved. These parameters yielded densities in the region of 80% of theoretical, which is reported in Table 2. The force applied to the sample and the displacement of the punches (stroke) is presented as a function of time in Figure 2.

An additional experiment has been conducted which appear to support these findings. A sample with the same cycle used in the third set of experiments, but with an applied pressure of 211 MPa resulted in density of 86% of theoretical value.

Discussion

The results gathered in the last set of experiments and the additional experiment indicate that pressure is a major factor. The graph shown in Figure 2 demonstrates the reaction taking place in the form of rapid shrinkage. The stroke rises very rapidly when the reaction wave advances through the sample. Then further densification takes place due to the hot deformation process. To achieve higher densities it is necessary to also study process parameters other than pressure, degassing temperature and time. The focus should be put on particle size ratio, heating rate, and the delay time to apply pressure after the reaction has started. To achieve this flexibility, a new die has to be built. The information that could be obtained is necessary for scaling up the process to higher volumes of reacting powders. To achieve full densities in reactive sintered samples some changes need to be done to the existing die design. The die should probably be split with a graphite lining, thus

allowing better escape of trapped gases. It would also allow more dynamic heating rates, because the region being heated would have the same cross-sectional area as the punches, which carry the current.
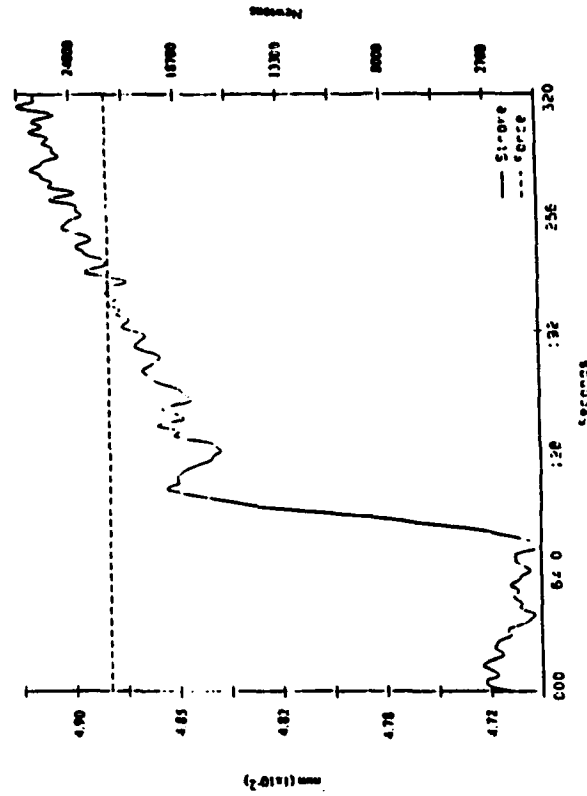
Fig. 2. Stroke and force as a function of time

Summary

Sintering reaction of the nickel, aluminum, titanium, and boron powders is exothermal by nature and leads to the formation of 60% dense composite material. Pressure has to be applied in a dynamic manner during the sintering reaction to result in a high density material. Studies of pressure assisted reactive sintering conducted on the mechanical dynamic testing machine indicate that pressure is a major parameter in this process.

191

190

References

1. R. M. German, Powder Metallurgy Science (Metal Powder Industries Federation, Princeton, NJ, 1984).

2. N. D. Sopchak, "Pressure Assisted Reactive Sintering: A New Method of Manufacturing Advanced Materials", Proceedings of 5th National Conference on Undergraduate Research, University of North Carolina Asheville, 1991.

3. D. M. Sims, A. Bose, and R. M. German, "Reactive Sintering of Nickel Aluminide", Progress in Powder Metallurgy, vol. 43, ed. C. L. Freeby and H. Hjort, Metal Powder Industries Federation, Princeton, NJ, 1987, p. 575-596.

4. R. M. German, "Transient Thermal Effects in the Synthesis of Intermetallic Alloys", to be published.

5. D. E. Alman and N. S. Stoloff, "Powder Fabrication of Monolithic and Composite NiAl", The International Journal of Powder Metallurgy, Vol. 27, No. 1, 1991, P. 29-41.

6. K. Sun and P. Tibbits, "Rapid Resistive Consolidation of YBa$_2$Cu$_3$O$_7$ Powder", Journal of Material Shaping Technology, Vol. 8, No. 4, 1990, p.219-223.

192

Injection Molding and Reactive Sintering of Ni₃Al

Markus R. Wegmann, Wojtek Z. Misiolek,
and Randall M. German*

Materials Engineering Department, RPI,
Troy, NY 12180-3590

*Engineering Science and Mechanics Department,
Pennsylvania State University,
University Park, PA 16802

Abstract

This study investigates the application of powder injection molding and reactive sintering to the fabrication of Ni₃Al. Low density and good resistance to corrosion and oxidation at high temperatures make Ni₃Al an attractive material for many applications. Injection molding permits a large degree of flexibility in shaping a component, but places tight size and shape restrictions on the metal powder in question. Prealloyed Ni₃Al powder with the required particle size and shape is not available, so elemental nickel and aluminum powders with suitable particle characteristics were mixed with binder and injection molded. The compacts were debound using a combination of solvent vapor and thermal debinding treatments and densified using reactive sintering in either a dry hydrogen atmosphere or under vacuum. Initial experiments showed severe shape distortion during sintering in either atmosphere. Further investigation revealed that the shape distortion is a strong function of the thermal debinding cycle and of thermal gradients set up in the compacts during sintering. Final densities for samples sintered in hydrogen are low at approximately 70% of theoretical, but the samples sintered under vacuum are significantly more dense.

Introduction

The high oxidation resistance at elevated temperatures and low density of intermetallic Ni₃Al make it a suitable candidate for applications such as heat engines which require good high temperature performance and low weight. The numerous small and complex shaped components likely to be encountered in such an application lend themselves to forming by powder injection molding (PIM), which offers good shaping flexibility without the large energy expenditure and waste associated with traditional machining processes. Cost and energy savings are also demonstrated advantages of reactive sintering, a relatively simple and energetically undemanding consolidation process which uses readily available elemental powders. The motivation for this work is to combine these processing advantages of PIM and reactive sintering in fabricating Ni₃Al components.

Reactive Sintering

Self-propagating high-temperature synthesis (SHS) operates on the principle

that an exothermic reaction may drive itself to completion if it produces sufficient exothermic energy[1-3]. Once the reaction is initiated, a combustion wave propagates through the reactant compact, leaving behind the product. If a transient liquid phase forms during the reaction, synthesis and densification can be manipulated to occur simultaneously.[1] This special case of SHS is called reactive sintering. Figure 1 shows four consecutive moments in the combustion wave propagation through a compact of nickel and aluminum powders. The violence and speed of the reaction make acceptable shape retention difficult to achieve.
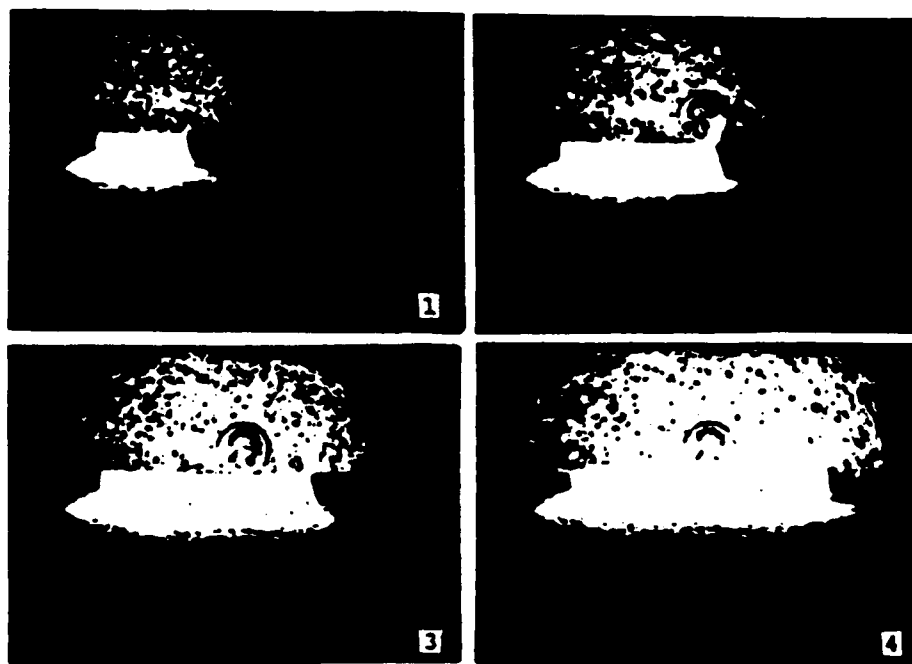
Figure 1. Propagation of the combustion wave through a Ni$_3$Al compact. Frames are separated by 2 sec.

In this work the reactant compact is a mixture of elemental nickel and aluminum powders near the Ni$_3$Al stoichiometry. Ignition is achieved by heating the mixture to a temperature where the reaction occurs spontaneously. As the compact is heated to the first eutectic temperature at approximately 910 K, intermetallic phases are generated around the nickel particles by solid-state diffusion. Liquid Al is formed at the first eutectic temperature and this liquid surrounds and consumes the nickel particles in the combustion wavefront. The aluminide precipitates behind the wavefront, forming the final densified product. The highly exothermic character of the reaction is manifested in a temperature rise of approximately 1500K in the reaction zone.

Methodology

The nickel and aluminum powders were chosen on the basis for their suitability for injection molding and reactive sintering. The injection molding process dictates a spherical particle shape and a size smaller than 25μm for good flow characteristics. Reactive sintering requires small particle sizes to aid intermixing and to sustain the connectivity of phases in the combustion wave[3]. To date two Ni$_3$Al stoichiometry powder systems have been combined with an organic binder, described in Table I; System 1 is a 64 vol% powder feedstock with 15.5μm

Al and 8.5μm Ni powders (1.8 : 1 particle size ratio), and System 2 is a 55 vol%
powder feedstock with 4.0μm Al and 4.0μm Ni particle sizes (1 : 1 particle size
ratio). Powder characteristics are listed in Table II.

Table I
Binder Composition

Component	Weight Percent (wt.%)
paraffin wax	69
polypropylene	20
carnauba wax	10
stearic acid	1

Table II
Powder Characteristics

Material	Vendor/Designation	Particle size (μm)
Nickel	Novamet 4SP	8.5
Aluminum	Valimet H-10	15.5
Nickel	Novamet 4SP -10μm	4.0
Aluminum	Valimet H-3	4.0

Tensile test and bend test specimen pairs of both systems were produced with
a Techmire Model CEM-01 injection molding machine. Two different setup geometries
were considered for the subsequent processing steps, the specimens being either
placed flat on a porous alumina substrate, or embedded in 5μm alumina wicking
powder within a crucible. Debinding was achieved using solvent vapor debinding
with heptane followed by thermal debinding under hydrogen. A dilatometry test
confirmed the onset of the combustion wave at 910 K, and reactive sintering was
performed under either hydrogen or vacuum.

Results
     After sintering the influence of the setup geometry on the final product was
visually striking, as demonstrated in Figure 2. Apparently the low thermal
conductivity of the porous alumina substrate delays the reaction initiation in the
lower part of the compact. Thus, densification and shrinkage occurs first along
the top surface, causing the samples to bow upward. By embedding the specimens
in alumina wicking powder such temperature gradients are avoided, resulting in
much better shape retention, and so the substrate approach was abandoned. Shape
retention needs to be improved further by manipulation of the remaining processing
parameters.
     A major problem with simply heating the compacts to the reaction temperature
was controlling the location of the reaction initiation. Figure 3 depicts a pair
of test specimens whose sintering cycle resulted in pronounced surface features,
and it shows clearly the random nature of the starting point. A passive ignitor
in the form of a small copper plate was the solution. The plate is embedded
alongside the compact with one end touching the compact at the desired ignition
point and the other end protruding above the alumina powder into the furnace

177

substrate wicking powder
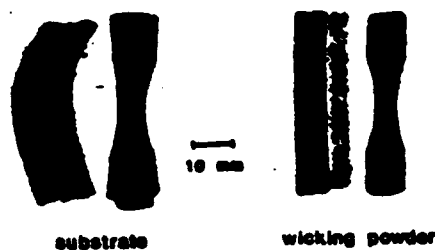
Figure 2. The effect of setup geometry on overall shape retention.

reaction initiation

10mm
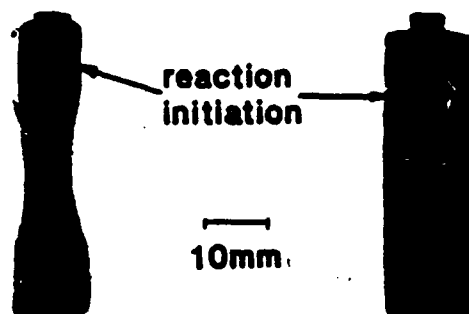
Figure 3. Photograph of specimens showing points of reaction initiation.

atmosphere. The high thermal conductivity of the copper plate causes the contact point to reach the desired temperature first and the reaction proceeds from there.

The highest densities achieved for either system with similar debinding and sintering processes were approximately 84% of theoretical, falling well short of the 95%+ desired. The pertinent debinding and sintering profiles are shown in Figure 4. Despite its nine percent lower loading, System 2 with a 1 : 1 alumina to nickel particle size ratio densified as much as System 1 with a 1.8 : 1 particle size ratio. This indicates that System 2 with the small aluminum would densify somewhat more if its volume fraction of powder were equivalent to that of System 1 with the large Al particles. This bears out previous results[2] which showed that with aluminum particles larger or equivalent in size to the nickel particles, the network of liquid aluminum during combustion is discontinuous and consequently densification is localized and accompanied by pore formation.

178
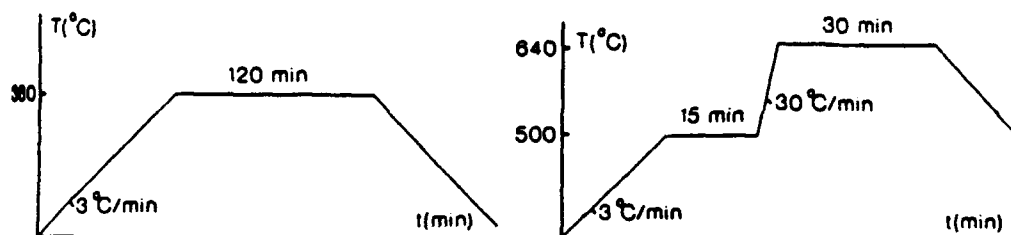
Figure 4. Temperature profiles used to achieve 84% of theoretical density. (a) Thermal debinding under dry hydrogen. (b) Sintering under vacuum.
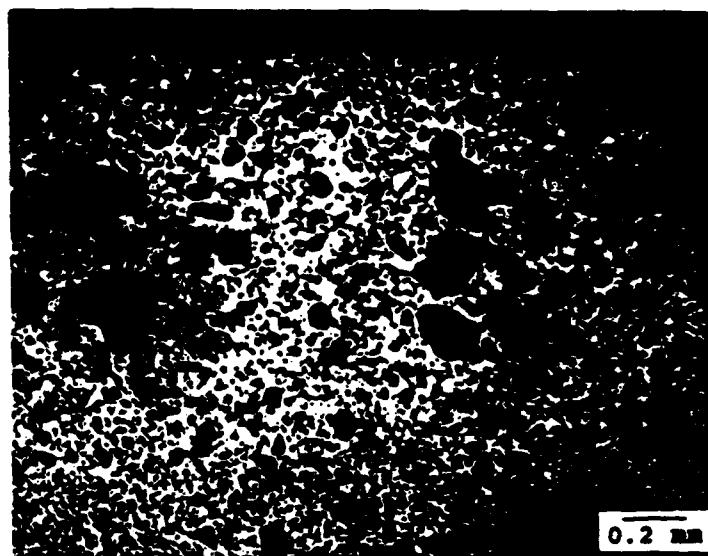
Figure 5. Pore structure of reactive sintered Ni_3Al, 82% dense.

Those compacts sintered under vacuum consistently exhibited a density 10% higher than those sintered under hydrogen. This indicates that pockets of gas inhibit densification, but since hydrogen is soluble in Ni_3Al, the resulting pores were expected to be rather small[2]. Pores too large to be attributed to particle size ratio considerations or entrapped gas were observed in all the sintered compacts. A sample micrograph is shown in Figure 5. The most likely origin of these pores is vaporizing pockets of residual binder, probably polypropylene, in the combustion wave. A 1.5 hour hold at 773K was incorporated into the sintering cycle in an attempt to purge the polymer. However, at only 130 K below the eutectic temperature, solid-state diffusion was greatly accelerated and no reactants remained at the end of the hold. The path being followed now is the use of a binder whose components will be removed from the compacts below about 500K.

Conclusions
    Combining powder injection molding and reactive sintering to produce intermetallic Ni_3Al is proving to be quite a challenge. Control has been established over shape retention and reaction initiation. Sintering under vacuum

seems to be a requisite for higher densities. However, a shortfall in density remains an open issue, with particle sizes and binder choices seeming to be the key to the solution. Current work is focusing on the use of a lower temperature binder and smaller aluminum particles to aid the connectivity of the liquid phase, and the application of pressure to the compacts during the reactive sintering process.

References
[1] Z. A. Munir, "Synthesis of High Temperature Materials by Self-Propagating Combustion Methods," Ceramic Bulletin, 16 [2] (1988), 342-349.
[2] R. M. German, "Transient Thermal Effects in the Synthesis of Intermetallic Alloys," in press.
[3] A. Bose, B. H. Rabin, and R. M. German, "Reactive Sintering of Nic Aluminide to Near Full Density," Powder Met. Inter, 20 [3] (1988), 25-30.

INNOVATIVE PROCESSING TECHNIQUES FOR INTERMETALLIC MATRIX COMPOSITES

N.S. STOLOFF AND D.E. ALMAN
Materials Engineering Department, Rensselaer Polytechnic Institute,
Troy, NY 12180-3590

INTRODUCTION

Although intermetallics based upon aluminum or silicon tend
to have a very attractive combination of low density and excellent
oxidation resistance, they suffer from lack of adequate creep strength
and, in most cases, from inadequate ductility and toughness. It
has been recognized for several years that an approach which could
simultaneously solve both problems, without degrading other properties,
is to utilize the intermetallics as matrices for composite materials.
The consequence has been an explosion of interest in two-phase intermetallic-
based alloys, as is manifested in the current symposium.
With the exception of some early work by Seybolt[1], intermetallic
matrices have been utilized for composites only for the past 5-6
years; the first published reference to systematic studies of fibrous
composites dates from the proceedings of an MRS conference in Dec.
1986[2]. Thus the published literature is much sparser than, for
example, on ceramic matrix composites which have been under development
for a much longer period. Nevertheless, there are now an appreciable
number of intermetallic matrices that have been reinforced with fibers
or particles. This paper introduces a session on processing of intermetallic
matrix composites, and is intended to survey a broad range of innovative
processing techniques. Further details will be provided in the individual
papers of this and other sessions.

OVERVIEW OF PROCESSING TECHNIQUES

Because of the relatively high melting points and extreme brittleness
of most intermetallic compounds utilized as matrices, as well as
other significant advantages, there has been enormous effort devoted
to powder metallurgical techniques. In this category we include
reactive sintering of elemental or elemental plus prealloyed powders[3-7],
reactive hot pressing[8], reactive HIPing[5-7], injection molding[4-9],
the XD process[10-14], dynamic compaction of powders[15-18], mechanical
alloying[19-21] the powder cloth method[2,24,25] and, of course,
traditional hot pressing techniques[22,23]. Most recently a process
consisting of mixing a combination of alloy rod or tubing with matrix
alloy powder to provide macroscopic plus microscopic toughening has
been developed by UTRC and labelled. Microstructurally toughened
composites[26]. Among all the powder processes, only injection molding,
reactive hot pressing and the microstructural toughening procedure
have produced aligned composites.
In order to overcome the inherent limitations of most powder
techniques in providing aligned composites two other major categories
of composite preparation have been studied and are reviewed in this
paper. These are vapor deposition processing (CVD, CVI[27-29] or
plasma spraying[30]) to produce monolithic, fibrous or laminated
structures, and liquid metal infiltration[31-34].

POWDER PROCESSING

Reactive Consolidation

Several variants of reactive sintering have been employed to consolidate intermetallic matrix composites. All incorporate fibers or particles in a mixture of at least some elemental powders, although prealloyed powders also may be present to dampen the reaction[7]. The basis of all reactive sintering processes is the formation of a liquid phase as a result of an exothermic reaction between elemental powders present in the mixture. The liquid phase accelerates consolidation, and is consumed during the process[3]. The reaction may proceed with no pressure (reactive sintering, RS), with isostatic pressure (reactive hot isostatic pressing, RHIP) or unidirectional pressure (reactive hot pressing, RHP). A flow chart for RHIP of NiAl is shown in Fig. 1. This procedure generally has been utilized to produce particulate-reinforced and random-fiber reinforced intermetallics. A typical microstructure of NiAl-20v%TiB$_2$ composites shown in Fig. 2, while compressive flow stresses vs temperatu: :r several composites are shown in Fig. 3[7]. Al$_3$Ta composites . 10v% Safill

1   Ni+Al were mixed to stoichiometric proportions.

2   Compacts were CIPed to a green density of approximately 70% theoretical.

3   Vacuum encapsulated in 304 stainless steel.

4   RHIPed
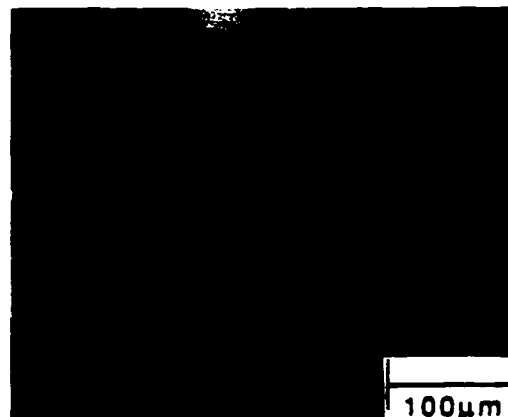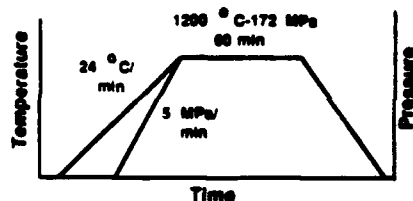
Fig. 1   Flow chart for RHIP of NiAl.   Fig. 2   Microstructures of NiAl-20v%TiB$_2$.
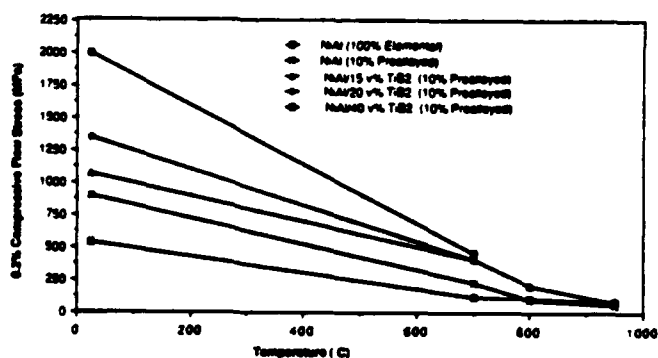
Fig. 3   Compressive flow stresses vs temperature for NiAl-TiB$_2$.

fibers, randomly oriented, have been consolidated by RHIP at 1200°C, with a pressure of 172MPa. However, damage to the fibers occurred during processing; this can be alleviated by reducing pressure during the RHIP cycle[6,7].

With $NbAl_3$, best sintering densification occurs with a 9μm niobium powder formed by hydride-dehydride and a 30μm aluminum (helium atomized) powder[4,35]. The mixed powders are compacted at 200MPa giving a 77% green density, heated to 500°C for degassing, then heated at 15 K/min to 1200°C and held at that temperature for 1 h. The resulting product is 95% dense and essentially pure $NbAl_3$. Reactive HIPing follows a similar processing route with a 170MPa pressure giving 98% density. The incorporation of 30 v% short randomly oriented, Saffil Al_2O_3 fibers gives a composite with a Rockwell hardness of 87 HRA in contrast with HRA 72 for the monolithic $NbAl_3$. However, the composites are almost as brittle as $NbAl_3$.

Anton[8] has employed RHP to produce both continuous and random fiber Al_2O_3 reinforced Al_3Ta. Toughness and strength improvements were achieved with the former only.

In some cases reactive sintering has been used as a precursor to conventional HIPing in order to produce prealloyed powders. For example, attempts to form γ-TiAl directly by RTS were frustrated by formation of Al_3Ti, which inhibited diffusion and full consolidation[4,36]. Therefore, RS was used to prepare prealloyed Al_3Ti+Ti+Al mixtures which were subsequently consolidated to nearly full density.

The key to successful reactive consolidation is the use of fine powders, the existence of a finite controllable exotherm and the lack of formation of intervening compounds (as in the Al-Ti system cited above). When full density is not achieved by RS, subsequent consolidation by HIP can be employed, although in these cases a single stage RHIP operation is more efficient.

Processing conditions which influence the reaction between the constituent powders alter the amount, distribution, and duration of the liquid[37]. However, unlike in other sintering studies, time at temperature is not a significant factor since the process occurs rapidly once the liquid forms. The role of the various process parameters can be explained in terms of their effects on the liquid phase.

Sintering atmosphere plays a role in determining the sintered density is explained by heat conduction and entrapped gas effects[9]. Heat is carried away from the compact during reaction by the higher thermal conductivity of a gas vs vacuum. Vacuum is the best environment, especially for TiAl[36], $NbAl_3$[35], and $TaAl_3$[6].

Injection Molding

Reactive consolidation may also be applied to injection molding, a process increasingly being applied to monolithic and composite metallic based materials[37]. In injection molding a mixture of powders, short fibers and a binder is extruded through a tapered die to achieve fiber alignment. Extrusion must be performed above the softening temperature of the binder. After extrusion the binder is removed (thermally or by wicking action) and the compact is consolidated to approximately full density by HIPing. Apart from the alignment of fibers, which is achieved only when particles and fibers are very small in diameter (~10μm), this process offers the possibility of producing complex P/M parts. However, the principal disadvantages are the difficulty of complete binder removal and the inability to produce continuous fiber-reinforced composites. Nevertheless, fully dense Al_2O_3-reinforced composites of NiAl and $MoSi_2$ have been produced successfully by this method, as shown in Fig. 4[39].

Mechanical Alloying

Mechanical alloying is a powder process involving high energy milling of (dry) powders of a generally ductile matrix with ceramic particles. Although mechanically alloyed nickel and aluminum alloys have been widely studied and commercially applied, relatively little work has been done on mechanical alloying of intermetallics.

Seybolt[1], in 1966, first produced dispersions of Al_2O_3, ThO_2 or Y_2O_3 in NiAl and Al_2O_3 in FeAl by ball milling. The latter alloy displayed a 400% increase in rupture strength over the matrix alloy alone.

Later work at Oak Ridge National Lab was done with B-doped Ni_3Al, mechanically alloyed with 1% Al_2O_3[40]. The resultant fine grain size actually caused a weakening of the base alloy at high temperatures. Later work on mechanical alloying of the same Ni_3Al-base alloy with several oxides produced a brittle alloy when tested at 510°C[19]. These early attempts at mechanical alloying all suffered from an excess in size and quantity of oxide particles relative to that needed for dispersion strengthening. With better process control Strothurs and Vedula[21] were able to mechanically alloy FeAl with Y_2O_3, resulting in a good combination of strength and ductility at room temperature.

More recently still, Benn et al[20] have consolidated several intermetallics based upon the Ni_3Al, NiAl or Ni_3Al+NiAl matrices. The use of elemental powders in the initial charge led to the production of very fine mechanically alloyed powders which were canned and extruded at 1150°C in preparation for mechanical testing.

Reaction milling has been described as a hybrid process combining both mechanical alloying and chemical reactions[41]. A composite of NiAl with very small AlN particles was inadvertently produced by Luton et al[42] when they attempted to mill NiAl with Y_2O_3 in liquid nitrogen. Compressive tests at 1300°K showed that the NiAl/AlN composite is at least twice as strong as NiAl-10%TiB_2 over a strain rate range of 10^{-7} to $2x10^{-4}s^{-1}$. Whittenberger[41] has suggested that high energy milling in different liquid or gaseous environments should be studied as a means of producing other reaction milled composites.

XD PROCESSING

The XD process developed by Martin Marietta has generally been utilized to produce multiphase alloy powders which are subsequently hot pressed to full density at temperatures of the order of 1450°C in graphite dies[10-14]. The process can incorporate both hard (strengthening) and soft (toughening) phases of various sizes. Morphologies ranging from whiskers to platelets can be obtained by appropriate process control. The XD process also is compatible with casting and fabrication techniques; investment casting, forgings, extrusions and rolled sheets have been produced. The most common reinforcement has been TiB_2, which has been incorporated as 1 um diameter particles into TiAl, $TiAl+Ti_3Al$, NiAl, NiAl/Ni_2AlTi and CoAl matrices in the form of a weakly bonded compact. After synthesis the samples usually are broken up, milled and then consolidated by hot pressing or HIPing[41]. Typical microstructures and mechanical properties of hot pressed NiAl-TiB_2 compacts are shown in Fig. 5[41].

A method that appears to be similar to the XD process of Martin Marietta has been developed by GTE Products Corp[43].

Powder Cloth Process
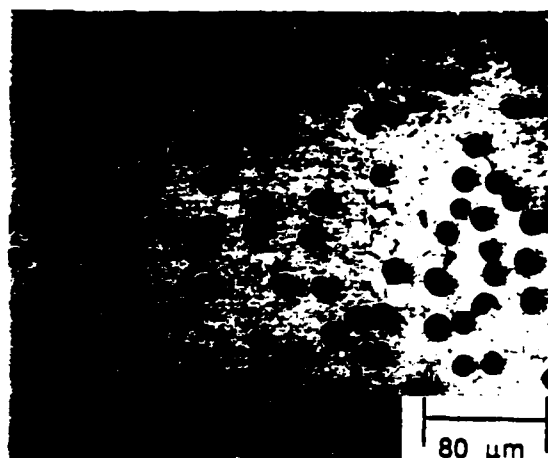
Fig. 4 Aligned NiAl/Al$_2$O$_3$ by injection molding.
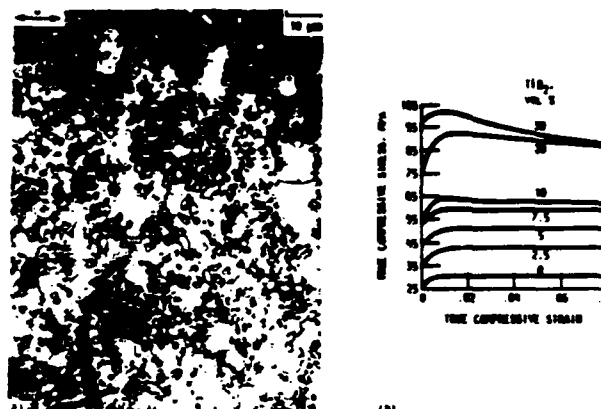
Fig. 5 Microstructure and mechanical properties
of XD-NiAl-TiB$_2$.[41]

The powder cloth method was the first reported to fabricate intermetallic matrix composites. Brindley described the technique and provided some mechanical property data for continuous fiber (Ti$_3$Al+Nb)/SiC[2 and Fe-40Al/W and NiAl/W composites[51].

In this method, see Fig. 6, the intermetallic alloy powder (which may be produced by atomization or by pulverization of meltspun ribbon) is mixed with a powdered Teflon binder (most successful results were obtained in the range 4-11%) and Stoddard solution (high grade kerosene). The mixture, after most of the Stoddard solution is evaporated, has a dough-like consistency. The dough is rolled into thin sheets with a stainless steel rolling pin. The balance of the Stoddard solution is evaporated from the rolled sheet, which is then trimmed to size for hot pressing.

The fiber matrix is prepared by winding a continuous fiber on a drum mounted in a lathe[51]. When the desired fiber spacing and mat width have been achieved, the lathe is stopped and the mat is coated with a polymer-base binder such as polymethyl methacralate (PMMA) in a solvent base. After evaporation of the solvent the fiber
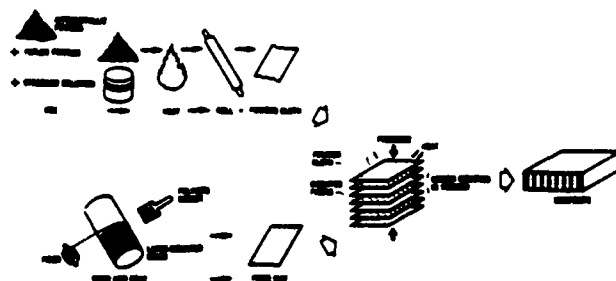
Fig. 6 Powder cloth method[24].

mat is removed from the drum and cut to size in preparation for hot
pressing. The desired number of fiber plies is obtained by stacking
alternate layers of powder cloth and fiber mat. Vacuum hot pressing
is used for final consolidation; a dynamic vacuum and liquid nitrogen
cooled trap to retain organics during binder removal are necessary
for best results. As in injection molding, complete binder removal
is required to avoid contamination of the composite with carbon or
other constituents such as flourine in the binder.

Most of the work reported for the powder cloth method has involved
a two phase Ti_3Al+Nb matrix with up to 40v% SCS6 SiC fibers. Although
these composites can be produced with no contamination from the binder
and have superior strength/density ratios to wrought and to single
crystal superalloys from room temperature to 1000°C, several problems
have been encountered. A complex multi-layered reaction zone, containing
TiC, Ti_3AlC and Ti_5Si_3 forms at the fiber-matrix interface[25].
This brittle region may cause degradation of properties when the
composites is operated for extended periods of time at elevated temperatures.
When oxygen contents of matrix powders are high, e.g. 0.11w%, composite
tensile strengths are reduced at room temperatures. Also, thermal
cycling of oxygen-rich (0.15w%) composites results in the formation
of cracks at the fiber-matrix interface after three thermal cycles
from 23 to 985°C. This is a consequence of the high thermal expansion
mismatch and limited room temperature ductility of fibers and matrix.
Low oxygen content (0.052-0.06w%) composites showed good strength
retention at 23°C after 5 to 10 thermal cycles between 85 and 815°C[24].
In summary, the powder cloth method can be successfully used to produce
a variety of continuous fiber reinforcements, including varied orientations
of the plies, with little or no binder contamination. However, composite
performance is sensitive to the depth of any reaction zone and to
high residual interstitial contents.

HIGH ENERGY RATE FORMING

Pulsed power, high energy kinetic energy storage devices, eg.
rail guns, have been used to fabricate monolithic α_2 and γ titanium
aluminides as well as composites containing ceramic or intermetallic
particulate reinforcements[15-18]. Processing is generally achieved
by discharge of a single high energy pulse through a pressurized
powder blend. Both solid-state and liquid phase assisted consolidation
of Ti_3Al with AlN, TiB_2 and TiAl reinforcements has been accomplished[17,18].
Applied pressures ranged between 210 and 420MPa and the specific
energy inputs varied between 3200 and 4800 kJ/kg. The fairly uniform
interface (about 5µm thick) between an 80-20 mixture of Nb-stabilized
α_2 and γ, respectively, is shown in Fig. 7[17]. TEM microanalysis

Fig. 7 Interface between α_2 and γ in kinetic
energy discharge compact[17].

showed depletion of Nb in the matrix and Nb transport forwards the
particles of γ. This techrique has been used also to consolidate
Ti$_3$Al+Nb/SiC particulate composites. Reaction products in this case
were analysed to be TiC and TiSi$_2$, the latter associated with regions
of localized matrix melting at high energy inputs. At lower inputs
this product could be avoided.

MICROSTRUCTURALLY TOUGHENED COMPOSITES[26]

The last powder technique to be described in this paper involves
the mixing of alloy tubing with a particle-reinforced matrix blended
as powders. Final consolidation is accomplished by extrusion or
forging. A schematic of the process is shown in Fig. 8. The principal
advantage of this system is the potential for large energy absorption
due to the two dimensional crack stopping ability of the macroscopic
tubing[26]. There is also the potential for relatively isostropic
properties. Finally, the composites are easily fabricable to final
shape. Examples of composite systems produced at UTRC by this method
is a matrix consisting of B$_4$C particles in NiAl, reinforced by tubes
of 304 stainless steel. The overall composite density is equal to
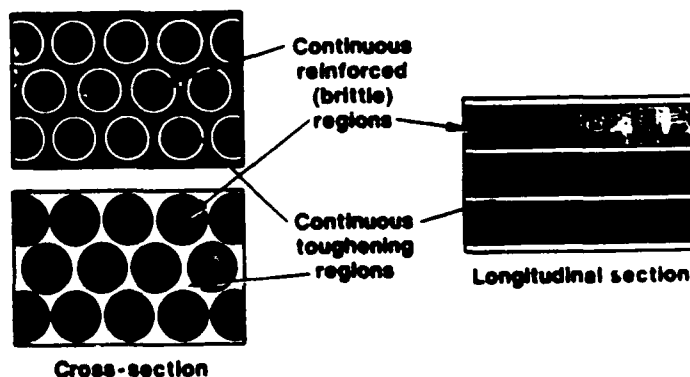
Fig. 8 Microstructurally toughened composites[26].

that of NiAl alone, ∿6g/cc. The composite had a notched bar impact
energy of 74 ft lbs (100J) compared to 0.2 ft lbs (0.27J) for NiAl[26].
This alloy displayed 28% elongation at room temperature and 21% at
825°C. This composite system has been scaled up to 1.25cm thick
x 150cm long plate. Recently, the technique has been successfully
extended to MoSi$_2$ and 25v% Al$_2$O$_3$ particles as the matrix, reinforced
by 50v% tubes of Nb-1Zr. The calculated toughness K$_a$=35ksi√in =
32MPa√m is about 10x higher than that of MoSi$_2$.

MELT PROCESSING

Pressure Casting

Pressure casting is one of the few techniques that have been
successfully utilized to produce continuous fiber-reinforced composites.
TiAl, Fe$_3$Al and Ni$_3$Al base composites, reinforced with Al$_2$O$_3$ fibers,
have been prepared by Nourbakhsh and co-workers[31-34]. The process
involves melting of the matrix alloy under vacuum in a crucible placed
above a preform containing up to 60 vol% fibers. The fibers and
matrix alloy are heated simultaneously but separately. When the
desired temperature (100°C above the matrix melting point) is reached,
the liquid metal is poured onto the fibers. Argon gas is then admitted;
gas pressure forces the melt, usually with an additive to facilitate
wetting, to infiltrate the fibers. A typical cross section of a
composite produced by this method is shown in Fig. 9 for a Ni$_3$Al/Al$_2$O$_3$
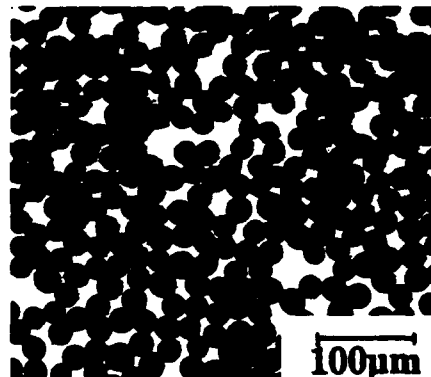
Fig. 9 Cross section of pressure cast
Ni$_3$Al/Al$_2$O$_3$ continuous composite[38].

composite[38]. Interfacial reactions are more likely with this process
than with most powder processes due to the higher temperatures involved.
Reactions in Ti$_3$Al/Al$_2$O$_3$ lead to the formation of dislocations within
the matrix near the interface and penetration of fiber grain boundaries
by the liquid. However, Ni$_3$Al-base alloys (IC-50 and IC-218) displayed
no reaction layer[32].

A key issue in all composite consolidation processes is the
nature of the bond between reinforcement and matrix. Ni$_3$Al/Al$_2$O$_3$
particulate composites prepared from powder displayed very poor bonding
and consequently poor mechanical properties[3,5]. The addition of
small amounts of Ti to Ni-base melts provides good bonding with Al$_2$O$_3$
fibers such as PRD-166 or FP, unless substantial amounts of aluminum
are present in the melt, as in the case of Ni$_3$Al[32]. Diffusion
of Ti into the fiber is suggested to be responsible for good bonding
and Al apparently inhibits such diffusion[32]. Additions of Y also

have been tried with some success[33]. Therefore, the problem of poor bonding with intermetallic matrices has not been fully solved even with the pressure casting technique.

Directional Solidification of Eutectics

Preparation of intermetallic matrix composites by directional solidification of eutectic alloys had, in the past, been reported by several workers[44,45]. There is now renewed interest in eutectic solidification to prepare composites with high melting constituents such as Mo-Mo$_5$Si$_3$[46], Nb-Nb$_5$Si$_3$[47,48] and NiAl-Re[49].

VAPOR PHASE PROCESSING

Arc Spray Method

NASA-Lewis Research Center developed the arc-spray method for composite fabrication[50]. The process begins with winding of a continuous fiber on a drum mounted in a lathe. Fiber spraying is obtained by movement of the lathe crosshead relative to the drum. The drum is placed in the arc-spray chamber, which is evacuated and back-filled with argon. An arc is struck between wires of matrix material, causing tips of the feed wire to melt. The molten metal is atomized by high pressure argon and sprayed on the drum surface. To provide an even coating, the drum is rotated and translated during service. The drum is then removed from the arc chamber; the arc-sprayed monotype is removed and cut to size for subsequent consolidation by hot pressing.

This process eliminates the need for organic binders, which are sources of contamination, but the necessity to provide matrix material as a wire is a serious limitation for most intermetallics, which are typically brittle. Also, contamination during spraying, especially by oxygen, is possible.

Chemical Vapor Deposition

Thin films of several intermetallic compounds: Nb$_3$Al, Nb$_2$Al, NbAl$_3$ and MoSi$_2$ as well as two phase alloys of Nb$_2$Al+NbAl$_3$ and MoSi$_2$ on SiC laminates have been made by chemical vapor synthesis.

MoSi$_2$ has been produced by CVD under atmospheric and reduced pressure conditions, with the following reaction:

$$MoCl_5(g)+2SiCl_4(g)+6.5H_2(g)+MoSi_2(s)+13HCl \quad [28,29]. \tag{1}$$

Deposition can be accomplished in the range 700-1400°C. Similarly, SiC can be produced by CVD using any one of several reactions, including the following:

$$CH_3SiCl_3(g)+H_2(g) \rightarrow SiC(s)+HCl(g)+H_2(g) \tag{2}$$
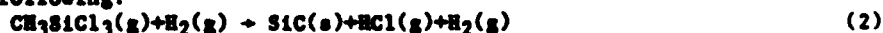
The deposition range of 1100-1400°C is compatible with that for MoSi$_2$.

Recently, laminates of MoSi$_2$ and SiC have been produced by CVD[28] and are undergoing tests.

Apart from choice of substrate and deposition temperature, gas pressure and flow rates of reactants affect deposition rate, microstructure and density of the layers.

Filament Coating

Several methods exist to produce fibrous composites by a series of steps dealing with coatings on fibers. Such coatings may be applied

by CVD, plasma spray or by a sol-gel process. An example of a sequential coating and winding process is shown in Fig. 10[52]. In this case
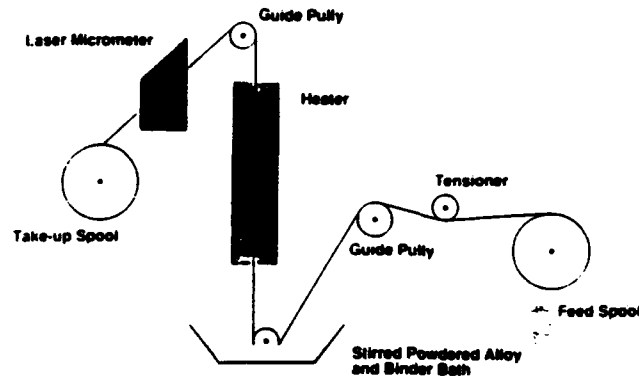
Fig. 10 Sequential coating-winding process[52].

W alloy fibers are coated with alumina and then a powdered tantalum aluminide alloy/binder mixture. The fibers are wound on a mandrel and dried; monotypes are then cut from the mandrel and stacked in a hot press cavity. The binder is burned out prior to hot pressing.

Low Pressure Plasma Spray

Metal and ceramic matrix composites, e.g. Ni-50Cr/NiCrAlY and superalloy/Al_2O_3 laminates, have been produced by a low pressure plasma spray technique[30]. This method could easily be adapted to produce intermetallic matrix composites as well. Layered structures are built up as discontinuous laminates, by spraying a powder blend of two or more different compositions. Alternatively, a continuous laminate can be produced by using two plasma guns traversing across a rotating cylindrical mandrel.

DISCUSSION

As a consequence of high melting points and brittle behavior displayed by most intermetallics of interest for high temperature applications, powder processes have been the most widely used. Powder processing is versatile in that virtually any alloy-reinforced combination can be blended in the solid state and then consolidated at elevated temperatures. Also, complex shapes can be produced readily. Reactive processing offers the further advantages of utilization of elemental powders, which are cheaper and more readily available than prealloyed powders. Low furnace temperatures and very rapid densification are further very significant advantages for variants of reactive sintering. Although it is possible to obtain fully dense monolithic intermetallics by reactive sintering, the strengthening of the compact and inhibition of the exothermic reaction by the reinforcements usually requires the application of pressure during or subsequent to reactive sintering to remove all porosity. To date, the greatest success in producing intermetallic composition by reactive processing has been achieved

with Ni₃Al, NiAl and Al₃Ta matrices, reinforced with either particles or fibers. In spite of these successes, certain inherent limitations in the reactive sintering process will restrict its application to relatively few intermetallic matrices.

One may cite also the difficulties associated with HIPing which often accompanies or succeeds reactive processing: most notable are the need for ductile canning materials which do not react with the powders and the need to seal cans carefully. The low costs associated with reactive sintering can quickly be overcome by the expenses associated with welding HIP cans of expensive and reactive metals, such as Ti and Nb.

The XD process is proprietary and, therefore, it is difficult to comment upon its future utility. It is apparent that TiB₂ is relatively inert in many intermetallics, especially aluminides, and that fully dense material can be made with very fine TiB₂ particle sizes; interfaces are very clean. However, it is unclear whether other reinforcements can be successfully prepared in-situ. The principal limitation to XD processing is its restriction to particulate reinforced composites. For maximum tensile and creep strengths as well as toughness, either continuous fibers or lamellae are required.

The latter can be readily produced by two powder processes: microstructurally toughened composites and the powder cloth method, as well as by the pressure casting technique. Each process have been applied to only a few intermetallics to date, but it seems that there are few limits to the combinations of fiber and matrix which can be utilized to produce continuous composites. Of course, the higher temperatures inherent in melt processing of composites gives rise to greater energy costs, higher liklihood of chemical reaction and increased possibility of thermal mismatch strains. While the powder cloth and microstructurally toughened composite methods rely on lower process temperatures, reaction zones are not precluded, and contamination by oxygen must be carefully avoided in the powder cloth method.

Mechanical alloying has thus far proven to be a relatively unreliable technique for producing particulate reinforced composites.

Vapor deposition techniques are still in their infancy. Although the need for appropriate precursors for matrix and reinforcement is a significant limitation for CVD, the method can be used to prepare both continuous fiber and lamellar composites. The volume fraction can be varied within wide limits by control of deposition rates on fibers or as lamellae. The CVD process is particularly well suited to very high melting compounds which would be extremely difficult to melt. As in powder processing, contamination by oxygen may be a serious handicap unless great care is used in designing and using the reaction chamber. Plasma spray techniques are not handicapped by the need for chemical precursors as in CVD, and higher deposition rates can be expected. However, where very thin lamellae are needed CVD offers better process control and, most likely, higher purity as well.

The kinetic energy storage devices utilized at the University of Texas dramatically illustrates the inherent versatility of powder processes. However, the rarity of such machines and the small sizes of samples produced to date makes it difficult to predict whether kinetic energy discharge is a viable technique to prepare intermetallic matrix composites.

SUMMARY AND CONCLUSIONS

Many innovative techniques have been developed to produce intermetallic

matrix composites, of which several representative ones have been
summarized here. The majority of processes involve use of powders,
although increasing attention is being directed towards vapor phase
techniques. Most intermetallic composites produced to date are reinforced
by particulates or random fibers. However, several techniques have
been successfully employed to produce continuous fiber reinforcements.
Injection molding appears to be feasible to produce aligned short
fiber reinforced composites. The major success of the various new
processing techniques has been improved strength (monotonic and creep).
Ductile phase toughening also has been demonstrated in a few cases,
but much more work needs to be done to produce strong and tough composites.

ACKNOWLEDGMENTS

REFERENCES

1. A.U. Seybolt, Trans ASM 59, 860 (1966).
2. P.K. Brindley in High Temperature Ordered Intermetallic Alloys II,
    N.S. Stoloff et al, eds., MRS 81, Pittsburgh, PA, 1987, pp. 419-424.
3. A. Bose, B. Moore, N.S. Stoloff and R.M. German, J. Met. 40 (9), 14 (1988).
4. R.M. German, A. Bose and N.S. Stoloff in High Temperature Ordered
    Intermetallic Alloys III, C.T. Liu, et al, (eds.) MRS 133, Pittsburgh,
    PA, 1989, pp. 403-414.
5. B. Moore, A. Bose, R.M. German and N.S. Stoloff, in High Temperature/
    High Performance Composites, MRS 120, F.D.Lemkey et al eds., Pittsburgh,
    PA, 1988, pp. 51-56.
6. A.R. Dibble, M.S. Thesis, Rensselaer Polytechnic Institute, May 1989.
7. D.E. Alman, A. Dibble, B. Moore, A. Bose, R.M. German and N.S. Stoloff
    in Processing of Ceramic and Metal Matrix Composites, H. Mostaghaci,
    ed., Pergamon Press, NY, 1989, pp. 217-227.
8. D.L. Anton in High Temperature/High Performance Composites, MRS, F.D.
    Lemkey, et al, MRS 120, F.D.Lemkey, et al, eds., Pittsburgh, PA, 1988,
    pp. 57-64.
9. A. Bose and R.M. German, Adv. Mater. Manuf. Proc. 3, 37 (1988).
10. L. Christodoulou, P.A. Parrish and C.R. Crowe, in High Temperature/
    High Performance Composites, MRS 120, F.D.Lemkey, et al, eds., 1988,
    Pittsburgh, PA, pp. 29-34.
11. R.K. Viswanadham, J.D. Whittenberger, S.K. Mannan and B. Sprissler,
    in High Temperature/High Performance Composites, MRS 120, 1988, F.D. Lemkey,
    et al, eds., Pittsburgh, PA, pp. 89-94.
12. J.D. Whitttenberger, R.K. Viswanadham, S.K. Mannan and K.S. Kumar,
    J. Mater. Res. 4, 1164 (1984).
13. J.D. Whittenberger, R.S. Viswanadham, S.K. Mannan and B. Spissler,
    J. Mater Sci, 25, 35 (1990).
14. J.D. Whittenberger, S.K. Mannan and K.S. Kumar, Scripta Met, 23, 2055 (1989).
15. H.L. Marcus, D.L. Bourell, Z. Eliezer, C. Persad and W. Weldon,
    Journal of Metals, Vol. 39, (12) (1987).
16. C. Persad, S. Raghunathan, B.-H. Lee, D.L. Bourell, Z. Eliezer and H.L.
    Marcus, MRS 120, Pittsburgh, PA, F.D. Lemkey, et al (eds.), 1988, pp. 23-28.
17. C. Persad, B.-H. Lee, C.-J. Hou, Z. Eliezer and H.L. Marcus, in High
    Temperature Ordered Intermetallic Alloys III, MRS 133, C.T. Liu, et al
    (eds.), Pittsburgh, PA, 1989, pp. 717-722.
18. Z. Eliezer, B.-H.Lee, C.-J. Hou, C. Persad, and H.L. Marcus, Metal and

Ceramic Matrix Composites: Processing, Modeling and Mechanical Behavior, R.B. Bhagat, et al (eds.) TMS, Warrendale, PA, 1990, pp. 401-412.

19. J.S.C. Jang and C.C. Koch, Scripta Met., 22, 677 (1988).

20. R.C. Benn, P.K. Mirchandani and A.S. Watwe, in Proc P/M 88, Modern Developments in Powder Metallurgy, APMI.

21. K. Vedula, R.J. Lauf and C.A. Wells, ECUT Quarterly Rpt, 1985, July 1-Sept 30, Oak Ridge National Lab, p. 56.

22. G.E. Fuchs in High Temperature Ordered Intermetallic Alloys III, C.T. Liu et al, eds., MRS 133, Pittsburgh, PA, 1989, pp. 615-620.

23. C.G. McKamey, G.L. Povirk, J.A. Horton, T.N. Tiegs and E.K. Ohriner, in High Temperature Ordered Intermetallic Alloys III, C.T. Liu et al, eds., MRS Symposia 133, Pittsburgh, PA 1989, pp 609-614.

24. P.K. Brindley, P.A. Bartolotta and S.J. Klima, Investigation of a SiC/Ti-24Al-11Nb Composite, NASA TM -100956, 1988.

25. S.F. Baumann, P.K. Brindley and S.D. Smith, "Reactive Zone Microstructure in a Ti₃Al+Nb/SiC Composite", TMS Fall Mtg, Sept 26-29, Chicago, IL 1988.

26. V.C. Nardone, UTRC, presented at DARPA program review, P&W Aircraft, W. Palm Beach, FL, Mar 1, 1990.

27. J.H. Norman and G.R. Reynolds "Chemical Vapor Synthesis of Niobium Aluminides", AFWAL-TR-88-4166, Oct 1988.

28. Y. Mehrohtra, A.K. Kuruvilla and N.S. Stoloff, Materials Technologies Corp, unpublished.

29. G.H. Reynolds, et al, DARPA/ONR Program Review, Pratt & Whitney Aircraft, W. Palm Beach, FL, Feb 27, 1990.

30. P.A. Seiers, M.R. Jackson, R.L. Mehan and J.R. Rairden, GE CR&D Rpt 85CRD001, Jan 1985.

31. S. Nourbakhsh, F.L. Liang and H. Margolin, Met Trans A, 21A, 213 (1990).

32. S. Nourbakhsh, F.L. Liang and H. Margolin, in High Temperature Ordered Intermetallic Alloys III, C.T. Liu, et al (eds.) MRS 133, Pittsburgh, PA, 459 (1989).

33. S. Nourbakhsh, F.L. Liang and H. Margolin, in Processing of Ceramic and Metal Matrix Composites, H. Mostaghci, ed., Pergamon Press, NY 1989, pp 195-205.

34. S. Nourbakhsh, L.L. Liang and H. Margolin, J. Phys E: Sci Instrum 21, 898 (1988).

35. J. Murray, MS Thesis, RPI, Troy, NY 1989.

36. R. Oddone, MS Thesis, RPI, Troy, NY 1989.

37. R.M. German and A. Bose, Mat Sci & Eng, A107, 107 (1989).

38. S. Nourbakhsh and H. Margolin, Met Trans A, 20A, 2159 (1989).

39. D.E. Alman and N.S. Stoloff, submitted to Int J Powder Met, (1990).

40. R.J. Lauf and C.A. Wells, ECUT Quarterly Report, 1985, July 1-Sept 30, Oak Ridge National Lab, p. 56.

41. D. Whittenberger in Solid State Powder Processing, A.H. Clauer and J.J. Barbadillo, Eds. 1990, p. 137.

42. M. Luton, C.S. Jayanth, M.M. Disko, S. Matras and J. Vallone in Multicomponent Untrafine Structures, MRS 132, Pittsburgh, PA, 1989, p. 79.

43. M.P. Sayre and W.A. Johnson "Aluminum Based Composite Powders and Process for Conducting Same", U.S. Patent No. 4,755,221, July 5, 1988.

44. J. L. Walter and H.E. Cline, Met Trans, 1, 1970, p. 1221.

45. T. Ishii, D.J. Duquette and N.S. Stoloff, Acta Met 29, 1981, p. 1467.

46. S. Mazdiyasni and D.B. Miracle, this symposium.

47. M.G. Mendiratta and D.M. Dimiduk, in High Temperature Ordered Intermetallic Alloys III, C.T. Liu et al (eds.) MRS 120, Pittsburgh, PA, 1989, pp. 441-446.

48. M.G. Mendiratta, this symposium.

49. D.P. Mason, D.C. Van Aken and J.G. Webber, Univ of Michigan, this symposium.

50. G.K. Watson, J.W. Pickens, R.D. Noebe, P.K. Brindley and S.L. Draper in HIGH TEMP Review 1988, NASA Publ 10025, p. 215.

51. P.K. Brindley and P.A. Bartolotta in HIGH TEMP Review 1988, NASA Publ. 10025, p. 225.

52. M.J. Maloney, DARPA/ONR program review, Pratt and Whitney Aircraft, W. Palm Beach, FL, Feb 27, 1990.

Powder processing of intermetallic alloys and intermetallic matrix composites

N. S. Stoloff and D. E. Alman

Materials Engineering Department, Rensselaer Polytechnic Institute, Troy, NY 12180-3590 (U.S.A.)

Abstract

This presentation covers the use of powder metallurgy for the formation of monolithic intermetallics and intermetallic matrix composites. A notable development has been the fabrication of homogeneous high density compacts from elemental powders by reactive sintering. A variant process involving simultaneous pressurization in a hot isostatic press, termed reactive hot isostatic pressing, is applicable to those compounds that prove difficult to consolidate by pressureless reactive sintering. This paper describes the effects of various processing factors on fabrication of compounds including Ni_3Al, $NiAl$, $TaAl_3$, $MoSi_2$ and their composites. A key concern is with processing effects on microstructure, selection of compatible ceramic reinforcing phases, and whisker alignment through injection molding.

1. Introduction

Intermetallic compounds are being studied as possible high temperature oxidation-resistant structural materials for aerospace and turbine applications. Aluminides are particularly attractive, with a low density, high strength, good corrosion and oxidation resistance, non-strategic elements and relatively low cost. In some cases these intermetallics exhibit improved strength with increasing temperature [1]. Coupled with relatively high melting temperatures, these attributes make for interesting high temperature materials. Most importantly, recent research has demonstrated improved ductility in some intermetallic systems [2-4]. Thus fabricability and reliability have been improved, leading to new interest in the use of these compounds as matrices for composites.

Sintering is ideal for the fabrication of complex-shaped high performance intermetallic alloys. This research considers reactive sintering and reactive hot isostatic compaction as fabrication routes for the production of aluminide compounds and composites from mixed elemental powders. In this paper, the basic principles of reactive sintering will be reviewed and applications to aluminides detailed, including a presentation of mechanical properties and processing variants. In addition, other powder techniques to produce similar composites will be discussed.

2. Overview of reactive processing

Our research has emphasized reactive sintering for forming several aluminides. In general, reactive sintering involves the formation of a transient liquid phase [5, 6]. The initial compact is composed of mixed powders which are heated to a temperature where they react to form a compound product. Often the reaction occurs on the formation of a first liquid, typically a eutectic liquid at the interface between contacting particles. Figure 1 shows a schematic binary phase diagram for a reactive sintering system, where a stoichiometric mixture of A and B powders is
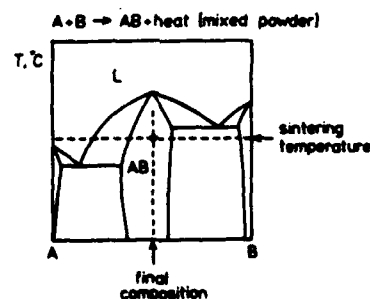
Fig. 1. Schematic binary phase diagram.

TABLE 1

Comparison of thermodynamic data for reactively sintered intermetallics

Inter-metallic	ΔH_f, 298 K (kcal mol^{-1})	Solubility X in Al (vol.%)	Solubility Al in X (vol.%)	Liquid (vol.%)
Al$_3$Ta	−22.7	1.3	11	73
NiAl	−28.3	17	20	60
Ni$_3$Al	−36.6	17	20	37
NbAl$_3$	−28.1	50	50	74
TiAl	−19.3	3	23	55

used to form an intermediate compound product AB. At the lowest eutectic temperature a transient liquid forms and spreads through the compact during heating. Heat is liberated because of the thermodynamic stability of the high melting temperature compound. Consequently, reactive sintering is nearly spontaneous, once the liquid forms. By appropriate selection of temperature, particle size, green density and composition, the liquid becomes self-propagating through the compact and persists for only a few seconds. Like other transient liquid phase sintering treatments, the liquid provides a capillary force on the structure which leads to densification [6]. However, if the solubilities are unbalanced, swelling can occur owing to the formation of Kirkendall porosity. Table 1 summarizes thermodynamic data and solubility limits for several components prepared by this method [7].

During slow heating, solid state interdiffusion can generate intermetallic phases at the interfaces, e.g. during the sintering of TiAl. Such compounds inhibit the subsequent reaction when the liquid forms; thus reactive sintering is sensitive to processing parameters such as heating rates, interfacial quality, green density and particle size. Because of the rapid spreading and reaction of the liquid, pore formation at prior particle sites is common, especially in systems with large aluminum particle sizes and large exotherms. Furthermore, dimensional control proves difficult if an excess of liquid is formed. Because of such problems, the applications of reactive sintering have been limited. However, as demonstrated here, the process is well suited to forming dense intermetallic compound structures.

Reactive sintering has been applied in various forms to produce NiAl, Ni$_3$Al, TaAl$_3$, NbAl$_3$ and TiAl. In one variant, compound formation and densification are achieved in separate steps by mixing elemental powders, reacting, pulverization
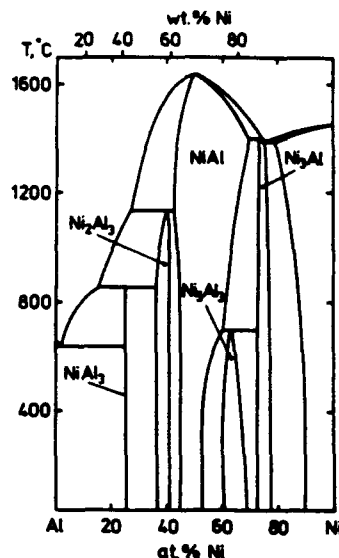
Fig. 2. Al–Ni binary phase diagram [10].

(grinding), compaction and subsequent sintering. Variations on this basic scheme involved hot pressing and pressure-assisted sintering. Stoichiometry control is important and is often achieved using an excess of the more volatile ingredient or intermediate chemical leaching to remove unreacted constituents. The current reactive sintering approach circumvents these problems by using commercial elemental powders, low processing temperatures, short process cycles with a classic press and sinter technology. Small particle sizes generally proved most useful [8, 9].

3. Reactive consolidation of specific alloys

3.1. Ni$_3$Al

Figure 2 shows the Al–Ni binary phase diagram [10]. The Al–Ni system is characterized by five intermetallic compounds, of which two have been the focus of research: Ni$_3$Al and NiAl.

For Ni$_3$Al, reactive sintering near the lowest eutectic temperature (640 °C) is most appropriate. Nickel and aluminum powders are randomly mixed in a stoichiometric ratio. The powder particles should be small to aid intermixing; they are compressed to create good particle–particle contact [8]. During heating to the first eutectic temperature (640 °C), solid state interdiffusion generates intermetallic phases and some self-heating. At the first eutectic temperature, liquid forms and rapidly spreads throughout the structure. The liquid consumes the elemental
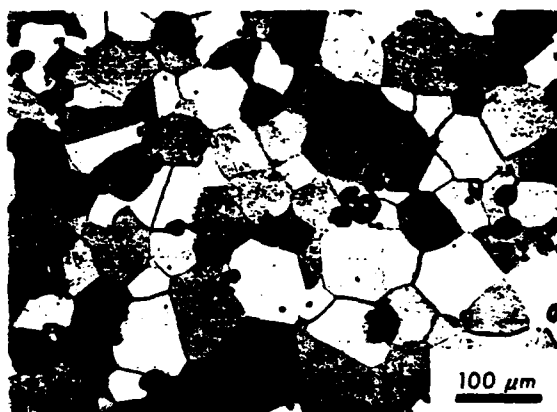
Fig. 3. Microstructure of reactively sintered Ni₃Al.

Fig. 4. Effect of particle size on densification of Ni₃Al [5].

powders and forms a precipitated Ni_3Al solid behind the advancing liquid interface. Interdiffusion of aluminum and nickel is very rapid in the liquid phase and the formation of the compound generates heat which further accelerates the reaction. If the reaction is controlled, then the compound will be nearly dense and suitable for containerless hot isostatic pressing (HIP) to full density [8].

Samples of nearly stoichiometric composition (86.7 wt.% Ni) were sintered in vacuum for 600 s at 750 °C using a heating rate of 30 K min⁻¹. The microstructure shows a small amount of porosity and two distinct phases; the grain size is approximately 30 μm (Fig. 3). The reactively sintered material was annealed at 1350 °C for 1 h to homogenize it; the result was a single phase. Microprobe line scans confirmed that the composition was uniform throughout the sample. Transmission electron microscopy substantiated that the product was ordered Ni_3Al.

Differential thermal analysis and dilatometry were used to understand the character of the reactive sintering process. In the unreacted powder a large exotherm was evident at approximately 600 °C, demonstrating the onset of reactive sintering. In the reacted sample, no further exotherm and only an endotherm was evident when the sample melted, indicating total consumption of the ingredients in the reactive sintering process. The first eutectic temperature in the Al–Ni system is at 640 °C (Fig. 2) and aluminum melts at 660 °C; thus the exotherm occurs prior to liquid formation and the compact undergoes self-heating, leading to rapid liquid formation. Dilatometry results correlated with the differential thermal analysis, indicating that the reaction

begins below approximately 600 °C. Furthermore, under optimum conditions the duration of the reaction appears to be approximately 2 s [5].

In view of the self-heating during reaction, experiments were performed to determine the maximum temperature needed for densification with the 30 K min⁻¹ heating rate to various maximum temperatures and a subsequent 900 s hold time using two aluminum particles sizes: 3 and 30 μm (Fig. 4) [5]. Temperatures below 550 °C resulted in higher porosities, most probably because no liquid was formed. At temperatures in the 550–600 °C range, good densification was obtained. With higher temperatures there was a gradual increase in swelling. Thus the optimum reaction temperature is relatively low. It should be noted that generally the 3 μm aluminum powder provided less densification than the 30 μm powder.

Another important variable was sintering atmosphere. Vacuum provided a much higher density than did hydrogen or argon at a 30 K min⁻¹ heating rate.

Composites of Ni_3Al with chopped Dupont FP Al_2O_3 fibers (20 μm in diameter) or particles of Y_2O_3 or Al_2O_3 have been prepared by the methods outlined above. In general, poor wetting of fibers led to low tensile strengths and ductilities of the compacts [11]. Therefore this line of research was terminated.

3.2. NiAl

The exothermic reaction between nickel and aluminum at the stoichiometric NiAl composition is so vigorous (see Table 1) that melting and loss of specimen shape commonly occur during reactive sintering. As a consequence it is usually necessary to mix 10–25% of pre-alloyed NiAl powders with the elemental powders to dampen the reaction. The optimum amount of pre-alloyed powder depends on the particle size distribution of the pre-alloyed powder [9]. Alternatively, an

inert phase such as TiB$_2$ or Al$_2$O$_3$ (as particles or fibers) can be used for the same purpose.

The optimum method to consolidate NiAl matrix composites appears to be by reactive hot isostatic pressing (RHiP), employing the cycle shown in Fig. 5. The RHIP temperature of 1200 °C is much higher than that used for Ni$_3$Al, although it is possible to consolidate (inhomogeneously) NiAl at lower temperatures. A typical microstructure of RHIP NiAl is shown in Fig. 6(a).
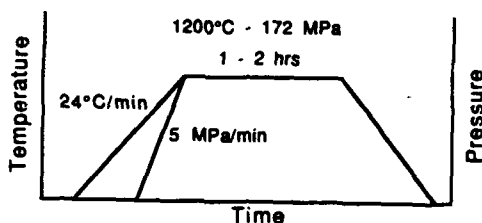
Fig. 5. RHIP cycle for NiAl [9].
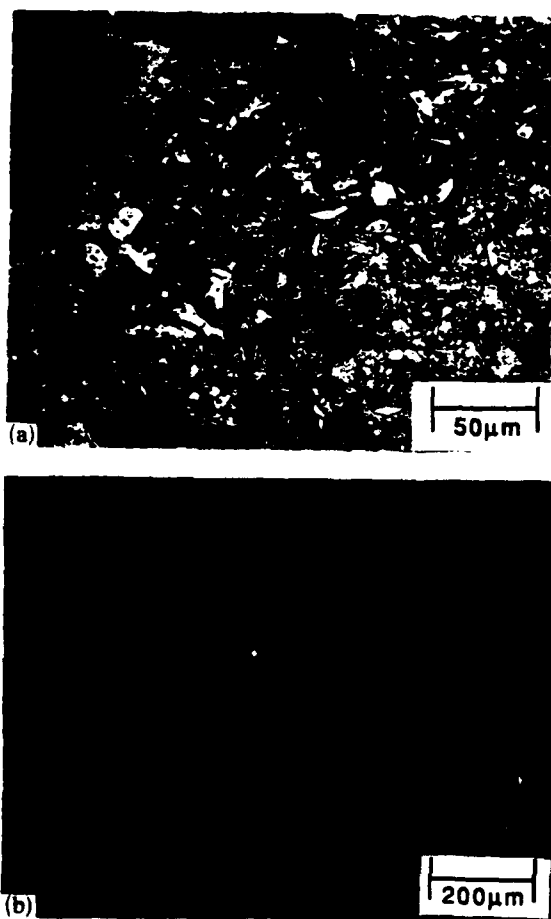
Fig. 6. Microstructure of alloys obtained by RHIP: (a) NiAl; (b) NiAl-20vol.%TiB$_2$.

The RHIP process also has been successfully employed to produce NiAl reinforced with 10 and 20 vol.% TiB$_2$ (Fig. 6(b)). The tensile properties of RHIP NiAl and NiAl-TiB$_2$ alloys are shown in Fig. 7 [9]. It should be noted that appreciable strengthening occurs even though the TiB$_2$ particles are relatively coarse. This is a consequence of two factors: a refinement of grain size due to the TiB$_2$ and incorporation of surface oxides from the powders in the compact. Strengthening is also greater than would be predicted from the rule of mixtures, using the data for TiB$_2$ of Mandorf et al. [12].

3.3. Al$_3$Ta

Attempts to densify Al$_3$Ta by pressureless reactive sintering have been unsuccessful [13]. Samples swelled rather than densifying at all sintering temperatures and at several aluminum contents. The degree of swelling increased with increased finishing temperature, increased particle size, decreased degassing temperature and decreased heating rate. The particle size ratio had less of an effect than did the average size of the particle; thus an aluminum-to-tantalum powder size ratio of 3 to 1 did not minimize swelling as predicted by Kusy [14]. Generally, the sintered density increased as the green density increased.
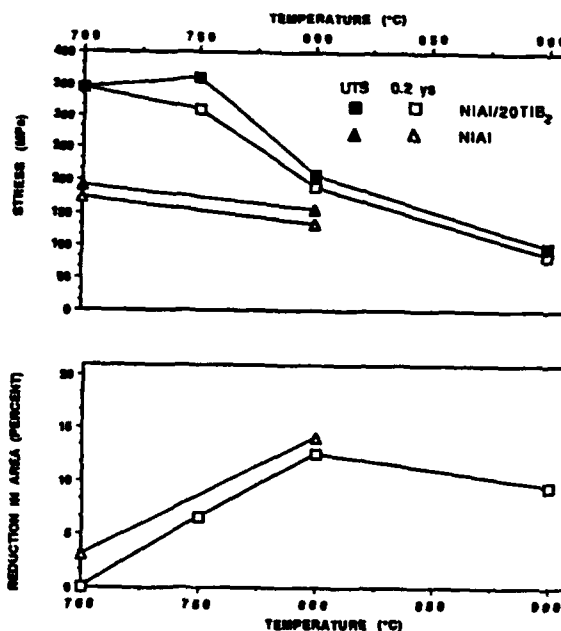
Fig. 7. Effect of temperature on the tensile properties of NiAl and NiAl-20vol.%TiB$_2$. All tests were performed in air except that for 900 °C which was performed in vacuum.

The failure of the reactive sintering (RS) technique for Al_3Ta led to a series of experiments on RHIP. For all experiments 10 μm tantalum and aluminum powders were mixed, cold pressed to high green densities and outgassed for at least 10 h at 500 °C, and a 35 °C min^{-1} heating rate to the hold temperature was maintained.

HIP at 1200 °C proved successful in providing fully dense homogeneous samples at 23 at.% Al, as shown in Fig. 8(a). Lower HIP temperatures left some unreacted tantalum. At 24 and 25 at.% Al, some second phase (Al_2Ta) was observed, even after RHIP at 1200 °C, in agreement with a recent phase diagram for this system [15]. A small quantity of oxide, 1 vol.%, was observed at prior particle boundaries, indicating that outgassing was not complete. Anton [16] has suggested that outgassing is effective only when the material is vibrated to allow escape of the gases.

Samples with 8 at.% Fe were also fabricated by RHIP. Fully dense samples containing two phases were obtained after a 1200 °C cycle (see Fig. 8(b)). The matrix is Al_3Ta with a ternary distributed phase.

Additions of reinforcing phases (TiB_2 powders on Al_2O_3 fibers) dramatically increased processing problems [13]. Particulates agglomerated even when methanol was used as a dispersant. Samples tested to fracture after cold isostatic pressing (CIP) had lower green densities than monolithic samples cold isostatically pressed to the same pressure. This problem was less severe with TiB_2 particles than with fibers; problems with CIP mixtures containing fibers also have been noted in Al_3Ti-base alloys. This problem can be avoided by using an organic binder to mix powders and fibers. The porosity of hot isostatically pressed material (1200 °C; 172 MPa) increased with increasing percentage reinforcement. The tantalum-rich phase Al_2Ta was observed in samples with FP Al_2O_3 fibers; only very small amounts of Al_2Ta were found in compacts containing TiB_2 or Saffil fibers. The latter appeared to agglomerate at prior particle boundaries but were distributed better than the FP fibers. Both types of Al_2O_3 fiber fractured during processing at pressures of 172 MPa; lower pressures lessened this problem. Also, Saffil fibers exhibited roughening, suggesting that the fibers were deforming at 1200 °C

3.4. $MoSi_2$

Attempts to process $MoSi_2$ reactively from elemental powders in our laboratory have not been successful. Extensive porosity was noted after attempts to use RHIP at 1600 °C and 83 MPa in a glass container. Therefore only composites made by injection molding of pre-alloyed powders have been produced, as described in the following section.

It should be noted that reactive sintering of $MoSi_2$-based composites has been accomplished by Smelser and coworkers [17]. SiC reinforcements (up to 20 vol.%) were sintered in various mixtures of molybdenum, silicon, chromium, titanium and $CrSi_2$. The reactants (other than molybdenum and silicon) greatly enhanced densification at temperatures as low as 1400 °C.

4. Injection molding

Reactive consolidation also may be applied to injection molding, a process increasingly being used for the powder processing of both mono-
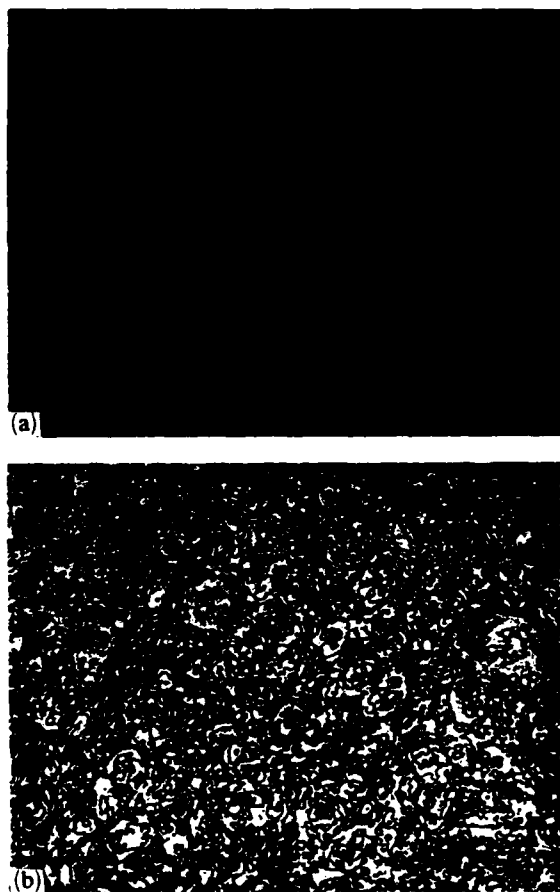
Fig. 8. Microstructures of Al_3Ta alloys obtained by RHIP: (a) $Al_{73}Ta_{27}$; (b) $Al_{67}Fe_8Ta_{25}$.

56
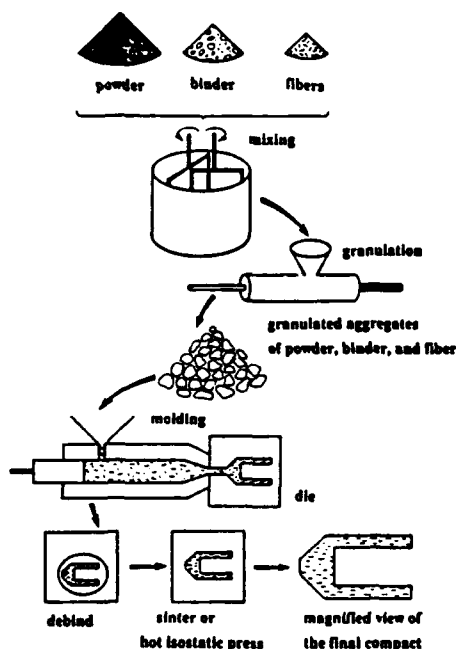
Fig. 9. Schematic diagram of the injection-molding process.
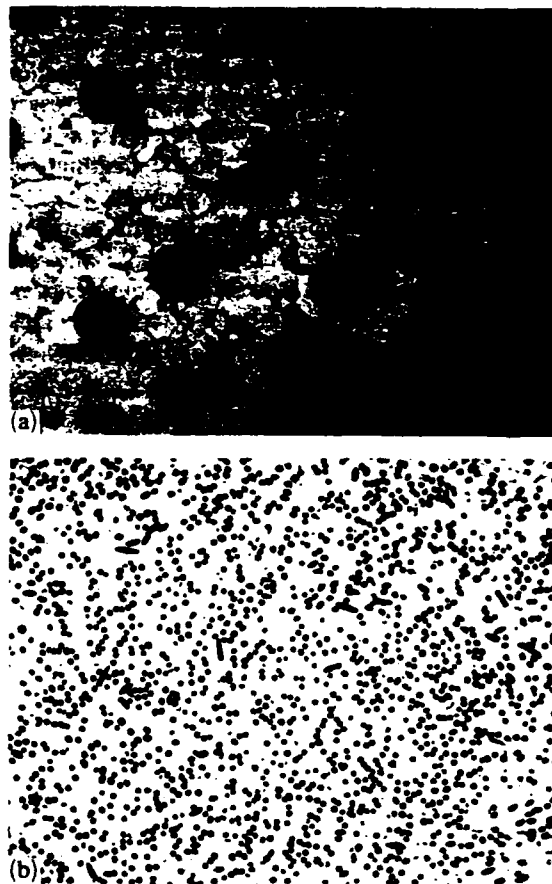

Fig. 10. Microstructures of injection-molded composites: (a NiAl-15vol.%Al$_2$O$_3$; (b) MoSi$_2$-20vol.%Al$_2$O$_3$.
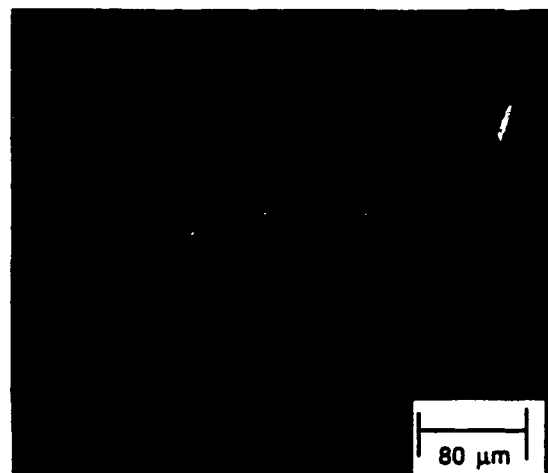
Fig. 11. Crack deflection by fibers in NiAl-Al$_2$O$_3$.

lithic and composite alloys [18]. In injection molding, a mixture of powders, short fibers and a binder is extruded through a tapered die to achieve fiber alignment (Fig. 9) [8]. Extrusion must be performed above the softening temperature of the binder. After extrusion the binder is removed (thermally or by wicking action) and the compact is consolidated to approximately full density by HIP. Apart from the alignment of fibers, which is achieved only when particles and fibers are very small in diameter (10 μm), this process offers the possibility of producing complex powder metallurgy (P/M) parts. However, the principal disadvantages are the difficulty of complete binder removal and the inability to produce continuous-fiber-reinforced composites. Nevertheless, fully dense Al$_2$O$_3$-reinforced composites of NiAl have been produced successfully by this method, as shown in Fig. 10(a) for NiAl-Al$_2$O$_3$ and in Fig. 10(b) for MoSi$_2$-Al$_2$O$_3$. The latter composite was made from prealloyed powders. There was some evidence that the Al$_2$O$_3$ fibers inhibited crack propagation in the NiAl matrix (Fig. 11).

Attempts to injection mold 10 μm aluminum and tantalum powders and 10 vol.% FP fibers resulted in some alignment near specimen centers, but not at the edges. Smaller powders did not lead to improved alignment. RHIP consoli-

dated the composite with some porosity, possibly owing to a low green density. However, this experiment showed that the binder did not contaminate the exothermic reaction.

5. Other powder-processing techniques

5.1. XD^TM processing

The XD™ process developed by Martin Marietta has generally been utilized to produce multiphase alloy powders which are subsequently hot pressed to full density at temperatures of the order of 1450 °C in graphite dies [19–22]. The process can incorporate both hard (strengthening) and soft (toughening) phases of various sizes. Morphologies ranging from whiskers to platelets can be obtained by appropriate process control. The XD process also is compatible with casting and fabrication techniques; investment casting, forgings, extrusions and rolled sheets have been produced. The most common reinforcement has been TiB$_2$, which has been incorporated as particles 1 μm in diameter into TiAl, TiAl + Ti$_3$Al, NiAl, NiAl-Ni$_2$AlTi and CoAl matrices in the form of a weakly bonded compact. However, other ceramic reinforcements (carbides, nitrides and silicides) have been incorporated into Nb–Ti–Al matrices [23]. After synthesis the samples are usually broken up, milled and then consolidated by hot pressing or HIP [24]. Typical mechanical properties of hot-pressed NiAl–TiB$_2$ compacts are shown in Fig. 12 and compared with properties of other Ni–Al alloys [24].

5.2. Powder cloth process

The powder cloth method was the first reported to fabricate intermetallic matrix composites. The techniques have been described and some mechanical property data provided for continuous fiber (Ti$_3$Al + Nb)–SiC by Brindley [25] and for (Fe–40at.%Al)–W and NiAl–W composites by Brindley & Barlotta [26].

In this method (Fig. 13) the intermetallic alloy powder (which may be produced by atomization or by pulverization of melt-spun ribbon) is mixed with a powdered Teflon binder (the most successful results were obtained in the range 4–11 vol.%) and Stoddard solution (high grade kerosene). The mixture, after most of the Stoddard solution has been evaporated, has a dough-like consistency. The dough is rolled into thin sheets with a stainless steel rolling pin. The balance of the Stoddard solution is evaporated from the rolled sheet, which is then trimmed to size for hot pressing.

The fiber matrix is prepared by winding a continuous fiber on a drum mounted in a lathe. When the desired fiber spacing and mat width have been achieved, the lathe is stopped and the mat is coated with a polymer-base binder such as polymethylmethacralate in a solvent base. After evaporation of the solvent the fiber mat is removed from the drum and cut to size in prep-
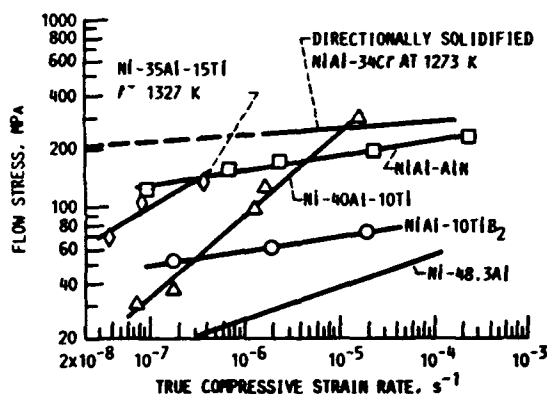
Fig. 12. Flow stress of Ni–Al alloys near 1300 K [24].
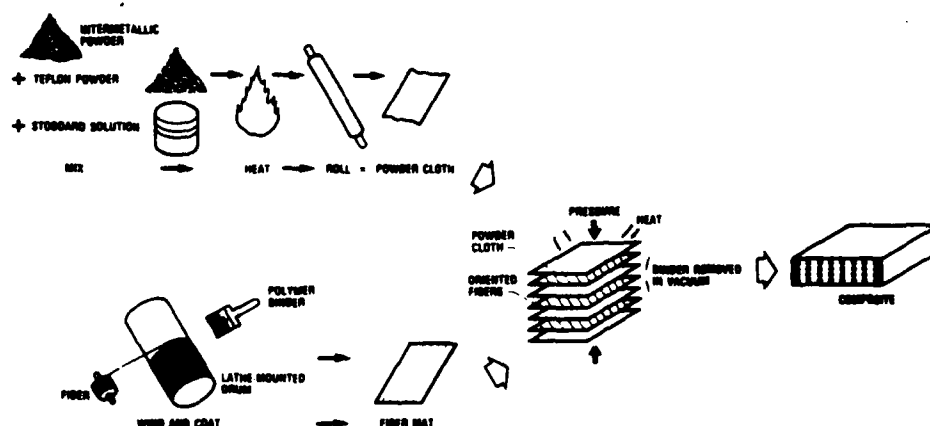
Fig. 13. Schematic diagram of the powder cloth method [26].

aration for hot pressing. The desired number of fiber plies is obtained by stacking alternate layers of powder cloth and fiber mat. Vacuum hot pressing is used for final consolidation; a dynamic vacuum and liquid-nitrogen-cooled trap to retain organics during binder removal are necessary for best results. As in injection molding, complete binder removal is required to avoid contamination of the composite with carbon or other constituents such as fluorine in the binder.

Most of the work reported for the powder cloth method has involved a two-phase $Ti_3Al + Nb$ matrix with up to 40 vol.% SCS6 SiC fibers, as shown in Fig. 14 [26]. Although these composites can be produced with no contamination from the binder and have superior strength-to-density ratios to wrought and to single-crystal superalloys from room temperature to 1000 °C, several problems have been encountered. A complex multilayered reaction zone, containing TiC, Ti_3AlC and Ti_5Si_3 forms at the fiber–matrix interface [27]. This brittle region may cause degradation of properties when the composites are operated for extended periods of time at elevated temperatures. When oxygen contents of matrix powders are high, e.g. 0.11 wt.%, composite tensile strengths are reduced at room temperatures. Also, thermal cycling of oxygen-rich (0.15 wt.%) composites results in the formation of cracks at the fiber–matrix interface after three thermal cycles from 23 to 985 °C. This is a consequence of the high thermal expansion mismatch and limited room temperature ductility of fibers and matrix.

5.3. Mechanical alloying

Mechanical alloying is a powder process involving high energy milling of (dry) powders of a generally ductile matrix with ceramic particles. Although mechanically alloyed nickel and aluminum alloys have been widely studied and commercially applied, relatively little work has been done on the mechanical alloying of intermetallics.

Early attempts at mechanical alloying suffered from an excess in size and quantity of oxide particles relative to that need for dispersion strengthening. With better process control Strothers and Vedula [28] were able to alloy FeAl mechanically with Y_2O_3, resulting in a good combination of strength and ductility at room temperature. More recently still, Benn et al. [29] have consolidated several intermetallics based upon the Ni_3Al, NiAl or $Ni_3Al + NiAl$ matrices.

The use of elemental powders in the initial charge led to the production of very fine mechanically alloyed powders which were canned and extruded at 1150 °C in preparation for mechanical testing.

5.4. Reaction milling

Reaction milling has been described as a hybrid process combining both mechanical alloying and chemical reactions [24]. A composite of NiAl with very small AlN particles was inadvertently produced by Luton et al. [30] when they attempted to mill NiAl with Y_2O_3 in liquid nitrogen. Compressive tests at 1300 K showed that the NiAl–AlN composite is at least twice as strong as NiAl–10vol.%TiB_2 over a strain rate range from 10^{-7} to 2×10^{-3} s^{-1} (Fig. 12) [24]. Whittenberger [24] also has reported that small-diameter AlN particles are twice as effective as TiB_2 particles in strengthening NiAl between 1200 and 1400 K. The AlN particles, which surround the NiAl grains, form as a result of a chemical reaction between aluminum and nitrogen which is incorporated into the matrix during cryomilling.

6. Processes involving ductile reinforcements

The processes described above have almost exclusively been applied to composites strengthened by brittle ceramic particles or fibers (with the exception of high energy rate forming). However, several techniques have been utilized to incorporate ductile particles, fibers or tubes into a brittle matrix so as to improve toughness. A few examples follow.
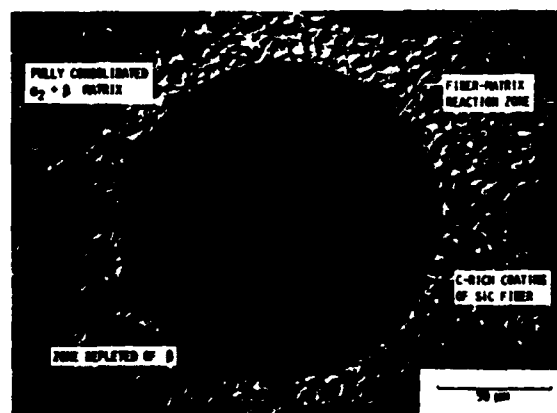
Fig. 14. Microstructure of (Ti$_3$Al + Nb)–SiC composite [26].

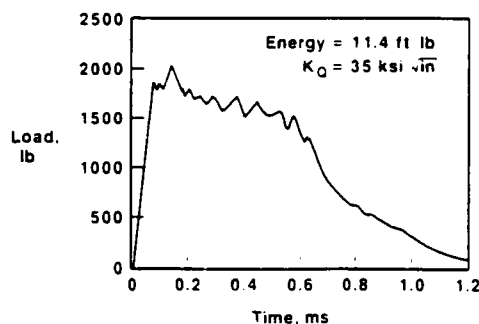Fig. 15. Charpy impact curve for microstructurally toughened $(MoSi_2-Al_2O_3-(Nb-Zr)$ composites [31].

Fig. 16. Microstructure of $TaTiAl_2-Al_2O_3$ composite produced by HIP pre-alloyed powders at 1200 °C [37].

6.1. Microstructural toughening

A combination of ductile phase toughening and hard particle strengthening has been reported by Nardone and coworkers [31, 32]. Thin-walled tubes of ductile metals have been mixed with powders and a binder to produce multiphase alloys capable of stopping cracks in more than one direction. Composites of $(NiAl + B_4C)$-type 304 stainless steel tubes and $(MoSi_2-Al_2O_3)-(Nb-1wt.\%Zr)$ tubes have been produced with substantial increase in toughness relative to the monolithic matrices, as shown in the Charpy curve for the latter (Fig. 15)[31].

6.2. Vacuum hot pressing

Hot pressing of elemental powders (reactive hot pressing or, more commonly, of pre-alloyed powders), has been widely utilized to prepare intermetallic matrix composites. Anton [33] has reported the processing and properties of $Al_3Ta-Al_2O_3$ composites prepared from elemental powders, while others have utilized hot pressing to prepare ductile phase-toughened alloys such as Nb_5Si_3-Nb [34], TiAl–Ti-33at.%Nb [35] and $MoSi_2-Nb$ [36]. Hot pressing and HIP are well suited to the preparation of composites from pre-alloyed powders, as shown in Fig. 16 [37].

7. Discussion

Certain advantages and disadvantages are inherent in powder processing. The most notable advantage is the much lower furnace temperatures than required for melting (even though exothermic reactions may drive the compact temperature to well above the melting point). In addition, powder processing is flexible, in that a range of sizes and shapes can be produced either from elemental powders, which are cheap, or from pre-alloyed powders, which are not. Also, the powder process provides finer-grained, more homogeneous material than can be achieved in most melting operations. An added advantage, especially with anisotropic alloys, is the ability to cool compacts with little or no cracking compared with that seen in arc-melted buttons.

These advantages are somewhat counterbalanced by the increased likelihood of incorporating impurities, especially oxygen, that can be very detrimental to mechanical behavior. Porosity can be a problem but is usually easily overcome by HIP. With respect to grain size, the fine grain size inherent with powder processing is advantageous for low temperature strength and toughness but is undesirable for good high temperature creep resistance. Nevertheless, the inherent versatility of powder processes has led to the many innovative techniques that have been applied to or developed for intermetallic matrix composites. We shall now consider specific aspects of the various processes described earlier.

The key to successful reactive consolidation is the use of fine powders, the existence of a finite controllable exotherm and the lack of formation of intervening compounds (as in the Al-Ti system cited above). When full density is not achieved by RS, subsequent consolidation by HIP can be employed, although in these cases a single-stage RHIP operation is more efficient.

The significant role of the sintering atmosphere in determining the density of aluminides during reactive sintering is explained by heat conduction and entrapped gas effects [5]. Heat is carried away from the compact during reaction by the higher thermal conductivity of a gas vs.

vacuum. Furthermore, because of the speed of the reaction, there is not time for adsorbed vapors and the atmosphere captured in the pores to escape. Hydrogen has a higher solubility in Ni_3Al than argon has. Thus with hydrogen trapped in the pores there is some opportunity for gas escape even after the pores have sealed during densification. Hydrogen was found to be better than argon with two heating rates; however, vacuum is the best environment, especially for TiAl [38], $NbAl_3$ [39] and $TaAl_3$ [13].

Heating rate effects on transient liquid phase sintering have been explained based on solid state interdiffusion prior to liquid formation [5]. With a slow heating rate there is more solid state reaction, resulting in less liquid. Indeed, the intermetallic products formed by solid state interdiffusion may actually inhibit liquid formation at the reaction temperature. Typically, higher heating rates are beneficial when sintering involves a transient liquid. However, too rapid a heating rate gives a loss of process control and with massive samples proves difficult to sustain with any uniformity. Also, as the heating rate increases, the reactivity of the liquid increases, thereby decreasing process control. Therefore intermediate heating rates prove most successful.

It is interesting to compare mechanical properties of intermetallic alloys prepared by other powder-processing methods with the results obtained by reactive sintering and its variants.

Particulate-reinforced composites of NiAl have been prepared by Jha and Ray [40] and by Seybolt [41]. Tensile properties, where available, are compared in Table 2. It should be noted that the strengths achieved with 20 vol.% TiB_2 particles in our work are comparable with the 5 vol.% ThO_2 alloy used by Seybolt and higher than the 2.7 vol.% TiB_2 material used by Jha and Ray. Such sketchy data seem to indicate that reactive synthesis is capable of developing properties comparable with those achieved by other methods. Comparison of the compressive strength of NiAl containing 20 vol.% TiB_2 by XD [24] and by reactive synthesis leads to a similar conclusion. It should be remembered that the various processing techniques lead to different grain sizes and impurity contents, which will produce effects beyond those of particle size, shape and volume fraction.

8. Summary

Several powder consolidation methods have been described, with emphasis on reactive processing. Densification during reactive consolidation has been applied successfully to several aluminides and has the potential to be used for other intermetallic systems. Full density often is achieved only when HIP is employed subsequent to or concurrently with reactive sintering, especially in systems with a weak exotherm or in two-

TABLE 2

Tensile properties of NiAl at elevated temperatures

Alloy	Condition	Temperature (°C)	$\dot{\varepsilon}$ (s^{-1})	Yield strength (MPa)	Ultimate tensile strength (MPa)	Reduction in area (%)	Reference
Ni–49wt.%Al	RS + HIP (20% pre-alloyed)	700	1.67×10^{-4}	173	191	3	Present study
		800	1.67×10^{-4}	135	154	14	Present study
Ni–49wt.%Al–20vol.%TiB$_2$	RS + HIP (20% pre-alloyed)	700	1.67×10^{-4}	394	344	0	Present study
		750	1.67×10^{-4}	310	360	6.5	Present study
		800	1.67×10^{-4}	190	207	12.5	Present study
		900	1.67×10^{-4}	86	99	9.4	Present study
Ni–50wt.%Al	P/M extruded	850	4.2×10^{-5}		75		[41]
		1000	4.2×10^{-5}		20		[41]
Ni–50wt.%Al–5vol.%ThO$_2$	P/M extruded	850	4.2×10^{-5}		150		[41]
		1000	4.2×10^{-5}		80		[41]
Ni–50wt.%Al	Cast	700	—		134	12.3^a	[42]
		815	—		105	24.5^a	[42]
		925	—		66	27.2^a	[42]
Ni–50wt.%Al–2.7vol.%TiB$_2$	RS, extruded	760	8.4×10^{-5}	209	251	64.7	[40]

^{a}Measured elongation.

phase systems. Reactive sintering is favored also by the use of fine powders and controlled atmospheres. Reactive HIP of injection molded fibrous composites is a feasible method of producing aligned intermetallic matrix composites. Mechanical properties of NiAl–TiB$_2$ composites prepared by reactive synthesis compare well with properties achieved by other powder processes.

Acknowledgments

References

1 N. S. Stoloff, *Int. Metall. Rev.*, 29 (1984) 123–167.
2 K. Aoki and O. Izumi, *J. Jpn. Inst. Met.*, 43 (1979) 1190–1193.
3 C. T. Liu and V. Sikka, *J. Met.*, 38 (5) (1986) 19–21.
4 A. I. Taub, S. C. Huang and K. M. Chang, in C. C. Koch, C. T. Liu and N. S. Stoloff (eds.), *High Temperature Ordered Intermetallic Alloys, Materials Research Society Symp. Proc.*, Vol. 39, Materials Research Society, Pittsburgh, PA, 1985, p. 221.
5 D. M. Sims, A. Bose and R. M. German, *Prog. Powder Metall.*, 43 (1987) 575.
6 R. M. German, *Liquid Phase Sintering*, Plenum, New York, 1985, p. 157.
7 I. Barin, O. Knacke and O. Kubaschewski, *Thermochemical Properties of Inorganic Substances*, Springer, Berlin, 1977.
8 R. M. German and A. Bose, *Mater. Sci. Eng. A, 107* (1989) 107–116.
9 D. E. Alman and N. S. Stoloff, *Int. J. Powder Metall., 27* (1991) 29.
10 M. Hansen and K. Anderko, *Constitution of Binary Alloys*, 2nd edn., McGraw-Hill, New York, 1958.
11 B. Moore, *M.S. Thesis*, Rensselaer Polytechnic Institute, 1988.
12 V. Mandorf, J. Hartwig and E. J. Seldin, in A. U. Ault, W. G. Barclay and M. P. Munger (eds.), *High Temperature Materials II*, Wiley-Interscience, New York, 1961, pp. 455–467.
13 A. Dibble, *M.S. Thesis*, Rensselaer Polytechnic Institute, 1989.
14 R. P. Kusy, *J. Appl. Phys.*, 48 (12) (1977) 5301–5305.
15 P. R. Subramanian, D. B. Miracle and S. Mazdiyasni, to be published.
16 D. Anton, private communication, United Technologies Research Center, 1988.
17 M. R. Weiser, S. R. Smelser and J. J. Petrovic, in D. L. Anton, P. L. Martin, D. B. Miracle and R. M. McMeeking (eds.), *Intermetallic Matrix Composites, Materials Research Society Symp. Proc.*, Vol. 194, Materials Research Society, Pittsburgh, PA, 1990, pp. 53–58.
18 R. M. German, *Powder Injection Molding*, Metal Industries Federation, Princeton, NJ, 1990.
19 L. Christodoulou, P. A. Parrish and C. R. Crowe, in F. D. Lemkey, S. G. Fishman, A. G. Evans and J. R. Strife (eds.), *High Temperature/High Performance Composites, Materials Research Society Symp. Proc.*, Vol. 120, Materials Research Society, Pittsburgh, PA, 1988, pp. 29–34.
20 R. K. Viswanadham, J. D. Whittenberger, S. K. Mannan and B. Sprissler, in *High Temperature/High Performance Composites, Materials Research Society Symp. Proc.*, Vol. 120, Materials Research Society, Pittsburgh, PA, 1988, pp. 89–94.
21 J. D. Whittenberger, R. K. Viswanadham, S. K. Mannan and K. S. Kumar, *J. Mater. Res.*, 4 (1984) 1164.
22 J. D. Whittenberger, R. K. Viswanadham, S. K. Mannan and B. Spissler, *J. Mater. Sci.*, 21 (1990) 35.
23 R. M. Aikin, P. E. McCubbin and L. Christodoulou, in D. L. Anton, P. L. Martin, D. B. Miracle and R. M. McMeeking (eds.), *Intermetallic Matrix Composites, Materials Research Society Symp. Proc.*, Vol. 194, Materials Research Society, Pittsburgh, PA, 1990, pp. 307–314.
24 J. D. Whittenberger, in A. H. Clauer and J. J. Barbadillo (eds.), *Solid State Powder Processing*, 1990, p. 137.
25 P. K. Brindley, in N. S. Stoloff, C. C. Koch, C. T. Liu and O. Izumi (eds.), *High Temperature Ordered Intermetallic Alloys II, Materials Research Society Symp. Proc.*, Vol. 81, Materials Research Society, Pittsburgh, PA, 1987, pp. 419–424.
26 P. K. Brindley and P. A. Barlotta, *High Temperature Review, NASA Publ. 10025*, 1988, p. 225 (National Aeronautics and Space Administration).
27 S. F. Baumann, P. K. Brindley and S. D. Smith, Reactive zone microstructure in a Ti$_3$Al + Nb/SiC composite, *Metallurgical Society of AIME Fall Meet., Chicago, IL, September 26–29, 1988.*
28 S. Strothers and K. Vedula, *American Society for Metals Congr., Orlando, FL, September 1986.*
29 R. C. Benn, P. K. Mirchandani and A. S. Watwe, *Proc. Conf. on Modern Developments in Powder Metallurgy*, Vol. 21, American Powder Metallurgy Institute, New York, 1988, pp. 471–494.
30 M. Luton, C. S. Jayanath, M. M. Kisko, S. Matras and J. Vallone, in L. E. McCandlish, D. E. Polk, R. W. Siegel and B. H. Kear (eds.), *Multicomponent Ultrafine Microstructures, Materials Research Society Symp. Proc.*, Vol. 132, Materials Research Society, Pittsburgh, PA, 1989, p. 79.
31 V. C. Nardone, United Technologies Research Center, *Defense Advanced Research Projects Agency Program Review, P&W Aircraft, West Palm Beach, FL, March 1, 1990.*
32 V. C. Nardone, J. R. Strife and K. M. Prewo, in D. L. Anton, P. L. Martin, D. B. Miracle and R. M. McMeeking (eds.), *Intermetallic Matrix Composites, Materials Research Society Symp. Proc.*, Vol. 194, Materials Research Society, Pittsburgh, PA, 1990, pp. 205–210.
33 D. L. Anton, in F. D. Lemkey, S. G. Fishman, A. G.

62

Evans and J. R. Strife (eds.), *High Temperature/High Performance Composites, Materials Research Society Symp. Proc.*, Vol. 120, Materials Research Society, Pittsburgh, PA, 1988, pp. 57-64.

34 R. M. Nikkanti and D. M. Dimiduk, in D. L. Anton, P. L. Martin, D. B. Miracle and R. M. McMeeking (eds.), *Intermetallic Matrix Composites, Materials Research Society Symp. Proc.*, Vol. 194, Materials Research Society, Pittsburgh, PA, 1990, pp. 175-182.

35 G. R. Odette, G. Lucas, W. Scheckherd and E. H. Aigelfinger, *Materials Research Society Spring Meet., San Francisco, CA, April 16-21, 1990.*

36 L. Xiao, Y. S. Kim and R. Abbaschian, in D. L. Anton, P. L. Martin, D. B. Miracle and R. M. McMeeking (eds.), *Intermetallic Matrix Composites, Materials Research Society Symp. Proc.*, Vol. 194, Materials Research Society, Pittsburgh, PA, 1990, pp. 399-404.

37 L. W. Graham, unpublished, Rensselaer Polytechnic Institute, 1990.

38 R. Oddone, *M.S. Thesis*, Rensselaer Polytechnic Institute, 1989.

39 J. Murray, *M.S. Thesis*, Rensselaer Polytechnic Institute, 1989.

40 S. C. Jha and A. Ray, *J. Mater. Sci. Lett.*, 7 (1988) 285-288.

41 A. U. Seybolt, *Trans. Am. Soc. Met.*, 59 (1966) 860.

42 E. M. Grala, in J. H. Westbrook (ed.), *Mechanical Properties of Intermetallic Compounds*, Wiley, New York, 1960, p. 358.

Powder Fabrication of Monolithic and Composite NiAl

David E. Alman* and Norman S. Stoloff**

Reactive sintering, hot isostatic pressing and powder injection molding techniques were utilized for the processing of NiAl and several NiAl composites. It was necessary to control the exothermic reaction associated with reactive sintering and reactive HIPing (RHIP) by combining NiAl prealloyed powders with elemental Ni and Al powders. Once particulate composites of NiAl-TiB₂ were fabricated, compressive and tensile stress strain curves were established as a function of test temperature. NiAl-Al₂O₃ fibrous composites also were fabricated. Alignment of short fibers was accomplished by using powder injection molding techniques. Nearly perfect specimens were produced, indicating that this is a viable technique for the fabrication of aligned fibrous intermetallic matrix composites.

Introduction

The intermetallic compound NiAl displays a number of favorable properties for use at high temperatures. These include a high melting temperature (1640 °C), low density (5.86 g/cm³), and excellent oxidation resistance. However, NiAl is brittle at room temperature and has low strength at high temperatures.[1] One potential means of improving toughness is to utilize a fibrous second phase for reinforcement. Particulates also can be used for strength improvements. Powder metallurgical processes are useful in preparing such composites, as has been demonstrated in the Ti₃Al/SiC[2] and Al₃Ta/Al₂O₃[3] systems. Brindley[2] prepared Ti₃Al powder cloths from prealloyed powders; these cloths were interspersed with layers of continuous SiC fibers, and consolidated by hot pressing. Anton[3] infiltrated a Al₂O₃ fibrous preform with elemental Al and Ta powders. Consolidation of the composites or of the Al₃Ta matrix was performed by reactive hot pressing. A recent review article by Soloff and Alman[4] describes these and other innovative processing technniques for the fabrication of intermetallic matrix composites.

NiAl also has been investigated for use as a matrix for high temperature composites. Seybolt[5] mechanically alloyed NiAl with Al₂O₃, Y₂O₃ and ThO₂ particles. These particles improved the high temperature tensile properties of NiAl. The effects of fine TiB₂ (1 to 3 μm) particles on NiAl have been studied.[6,7,22,23] Martin Marietta's proprietary XD process has been employed to fabricate NiAl dispersed with 2.7 to 30 v/o TiB₂ particles.[6,22,23] These particles significantly improved the compressive strength of stoichometric NiAl; the addition of 30 v/o TiB₂ improved the compressive flow stress of NiAl from 25 MPa to 95 MPa at 1027 °C and a strain rate of 2 × 10⁻⁶ sec⁻¹.[6,22] The XD process also has been used to disperse fine TiB₂ particles in Ni-38.5 a/o Al,[24] NiAl/Ni₂AlTi alloys,[25] CoAl[6] and Ti-45 a/o Al.[26] Similarly, NiAl/2.7 v/o TiB₂,[7] fabricated by rapid solidification techniques, had a tensile yield stress of 208MPa as compared to 85MPa for monolithic NiAl at 760 °C. Not all efforts have been aimed at fabrication of particulate composites based on NiAl. Kumar et al.[6] also fabricated NiAl and NiAl/TiB₂ alloys reinforced with random Al₂O₃ whiskers. With 15 v/o whiskers the fracture toughness improved to 9MPa√m compared to 6MPa√m for monolithic NiAl. However, the scatter associated with the fracture toughness of the whisker-reinforced compo-

*Graduate Research Assistant and **Professor, Materials Engineering Department, Rensselaer Polytechnic Institute, Troy, New York 12180-3590, USA.

random input ⟶ oriented output
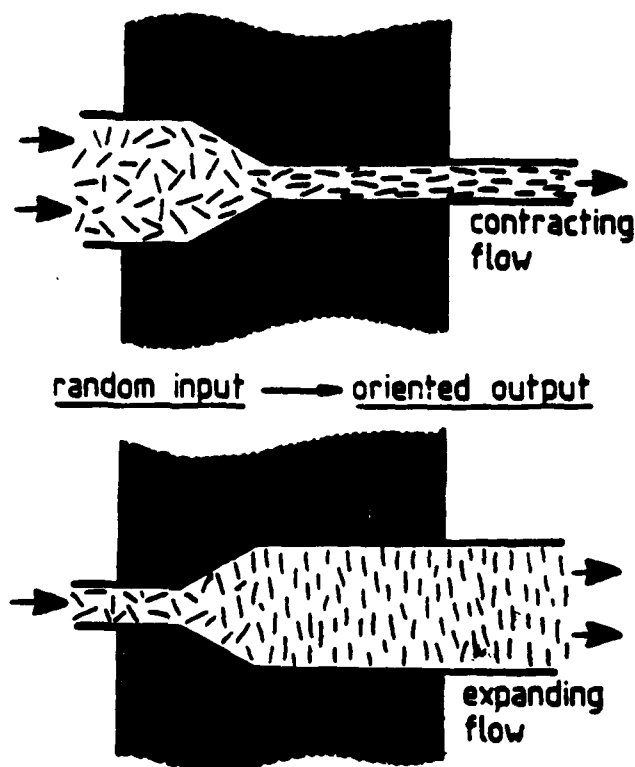
Figure 1. Fiber alignment by injection molding.[11]

site was significant. Earlier, Walters and Cline[6] had fabricated NiAl reinforced with Cr and Mo fibers by directional solidification techniques. Recently, Nathal et al.[9] consolidated NiAl+W reinforced with SiC fibers by the powder cloth method described previously.

This paper summarizes efforts to fabricate both particulate (TiB$_2$) composites and aligned chopped fibrous Al$_2$O$_3$ composites with a NiAl matrix using P/M techniques, such as reactive sintering and powder injection molding. Also reported are preliminary results on the mechanical behavior of these composites.

Background

Reactive sintering, also termed self propagating high temperature synthesis or gasless combustion, has been described elsewhere in detail for Ni$_3$Al.[10] This is a process in which an exothermic reaction between two or more elemental constituents of a powder compact provides enough heat to produce a liquid phase which markedly reduces sintering time. If isostatic pressure is applied during sintering the process is termed Reactive Hot Isostatic Pressing (RHIP).

Powder injection molding has been proposed as a method to achieve alignment of chopped fibers in a powder matrix.[11] This process consists of binder-assisted extrusion of the powders and fiber through a tapered die prior to consolidation to achieve fiber alignment, as depicted in Fig. 1.[11] Extrusion is performed at temperatures above the softening temperature of the binder. After extrusion, the binder is thermally removed and the powder is consolidated, resulting in an aligned fibrous composite. One advantage of a powder injection molding technique is that with the proper die design complex P/M parts can be produced. From a manufacturing point of view, this technique is superior to one that results in flat plates. The major disadvantage is that continuous reinforced composites cannot be produced.

Experimental Procedure

The characteristics of the powder, particles and fibers used in this study are summarized in Table I. For the fabrication of NiAl and NiAl/TiB$_2$, INCO-123 Ni powder and Valimet H-15 Al powders were used. Superior fiber alignment can be achieved with smaller particles,[11] so the Novamet 4SP Ni and smaller Valimet H-3 Al powders were chosen for experiments involving the fabrication of NiAl/Al$_2$O$_3$ fibrous aligned composites.

TABLE I. Material Characteristics

Powder	Size	Shape	Process	Vendor
Al	3μm	spherical	gas atomized	Valimet H-3
Al	15μm	spherical	gas atomized	Valimet H-15
Ni	3-7μm	spikey surface	carbonyl	INCO-123
Ni	<10μm	spherical	carbonyl	Novamet 4sp – 10μm
TiB$_2$	3μm	—	—	ICD Group
NiAl	– 325 mesh	angular	—	Cerac, Inc.
NiAl	92μm	angular	milled	RPI

Fibers	Vendor		Diameter	Length
Al$_2$O$_3$	Dupont-FP		20μm	5–30mm
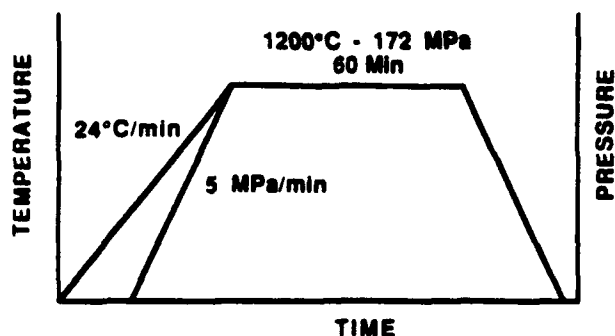
Figure 2. A typical RHIP cycle for NiAl.

Ni+Al. 15 Vol °₀ FP Fibers. 35 Vol°₀ Binder

As Extruded

As CIPed (208 MPa)

Figure 3. Sample produced by the binder-assisted extrusion technique.

Elemental powders were mixed to a composition corresponding to Ni-49 a/o Al (30 w/o Al). For composite specimens the appropriate amount of the reinforcement phase was blended with the matrix mixture. Mixing of the powder was performed in a turbula type mixer for 1 hour. Cylindrical compacts (0.5 grams, 6 mm in diameter) were pressed to 350MPa, with a resulting green density of approximately 75 percent of theoretical. These compacts were reactively sintered in vacuum (10^{-8} Pa) for 15 minutes at 700 °C. Experimentally, it was found that the vacuum (Varian M-4 diffusion pump system) did not deteriorate due to evolved gases until sample sizes approached 500 g. Sintered densities were determined by the water immersion technique and metallographic inspection. For material produced by RHIP, the mixed powders were cold isostatically pressed (CIP) to 210 MPa in a cylindrical polyurethane mold bag. The resulting specimens were approximately 12.7mm in diameter by 100mm long, weighing 50 grams and had a green density of approximately 70 percent of theoretical. These specimens were then vacuum encapsulated in 304 stainless steel. Prior to encapsulation the specimens were degassed in vacuum at 300 °C for 10 hours. RHIP conditions were 172 MPa, 750 °C or 1200 °C for 1 hour, Fig. 2.

Aligned fibrous composites were produced by adding a blend of Ni plus Al powders (Ni-49 a/o Al) and 15 v/o Al₂O₃ fibers to 35 v/o of a melted low molecular weight proprietary polymer binder. As a consequence of the small amount of powders used (approximately 50 grams total), mixing was performed manually in glass jars. A hand press was utilized for extrusion from a heated die (90 °C). The extrusion die was tapered from 12.7 to 1.5mm. The extruded "wires" (1.5mm in diameter) were then carefully placed in a polyurethane die and CIPed to 208MPa to produce specimens approximately 25.4mm long by 12.7mm in diameter, Fig. 3. The binder was removed by thermal debinding

(4 hours at 450 °C in flowing hydrogen). The samples were then reactively sintered as described above. The procedure is outlined in Fig. 4.

Results

The exothermic reaction associated with the reactive sintering of NiAl from elemental powders was uncontrollable. The heat that was generated was sufficient to melt the compacts, as shown in Fig. 5, and to destroy Al₂O₃ sintering crucibles. The microstructure of this material (Fig. 6) has the characteristics of a casting rather than the expected equiaxed P/M microstructure. Electron microprobe analysis revealed that the composition of the material was Ni-49 a/o Al and the small dark particles present were oxides associated with prior particle boundaries.

It was found by trial and error that the reaction could be diluted by mixing 10 to 25 % of prealloyed NiAl powder with the elemental powder, Fig. 7. The optimum amount of prealloyed powder needed to control the reaction was found to be dependent on the particle size distribution of the prealloyed powder. The NiAl powder purchased from Cerac had a more

```
MELT BINDER
     │
     ▼
MIX FIBER/POWDER
TO MELTED BINDER
     │
     ▼
EXTRUDE FIBER/POWDER
AND MELTED BINDER BLEND
THROUGH A TAPPERED DIE
TO ALIGN FIBERS
     │
     ▼
CIP EXTRUDED MATERIAL
TOGETHER
     │
     ▼
DEBIND
     │
     ▼
SINTER
```
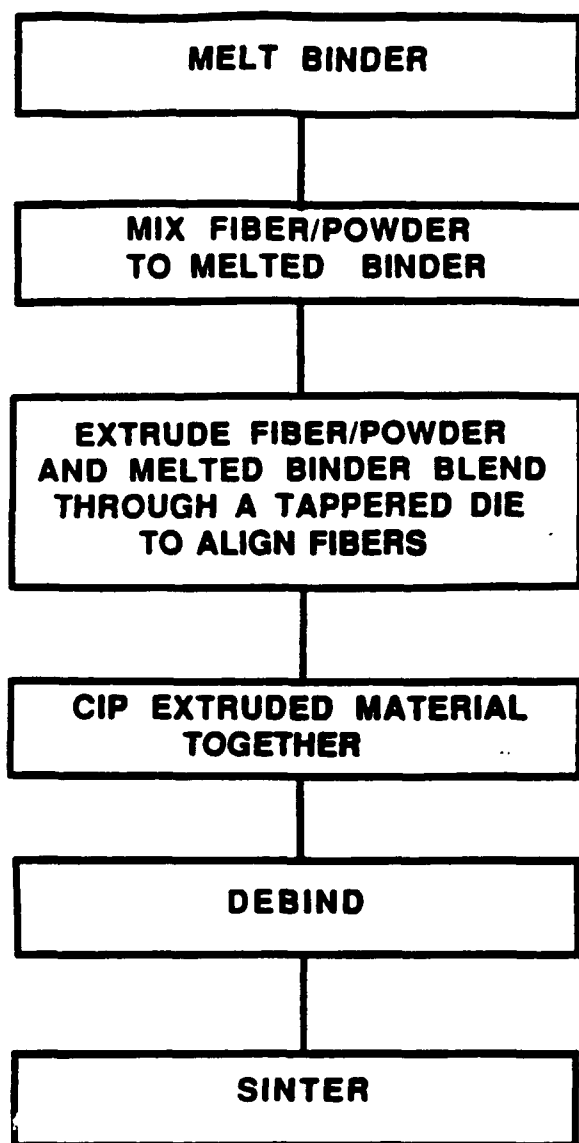
Figure 4. Outline of the binder-assisted extrusion technique.

Figure 5. NiAl tensile bars produced by reactively sintering Ni and Al powders. Top is a green bar, bottom two are as-sintered.
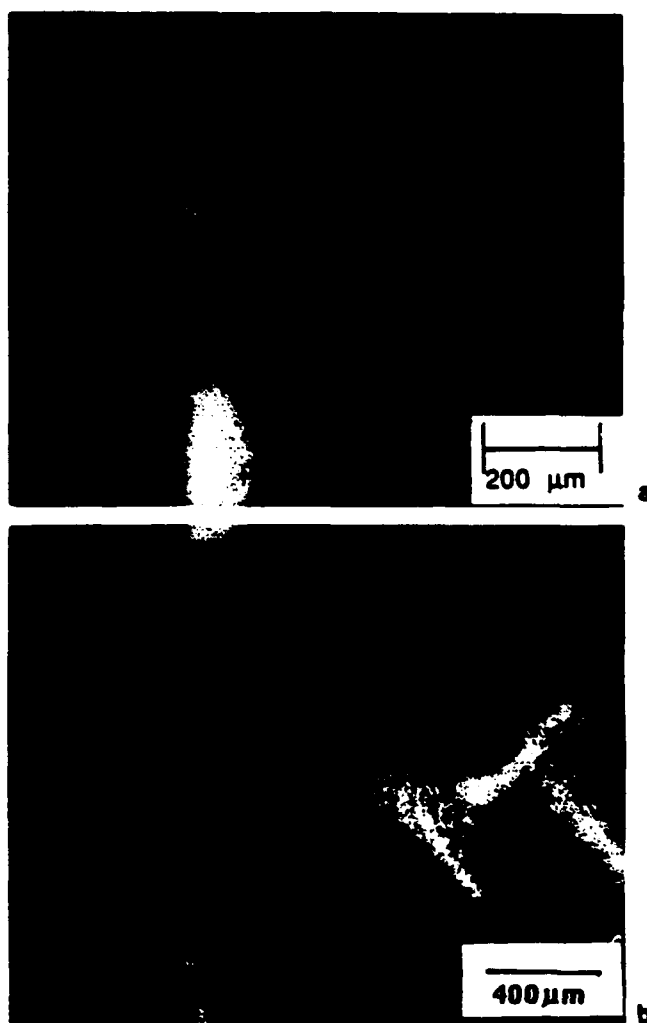
Figure 6. Microstructure of reactively sintered NiAl from Ni and Al powders. Reactively sintered while vacuum encapsulated in a thick walled stainless steel can followed by a HIP cycle (172MPa, 1 hr, 1200 °C). a) as polished b) etched, Kallings solution.

narrow particle size distribution than the powder milled at RPI. Therefore, blending was achieved with less Cerac powder than RPI powder. The first two bars in Fig. 8 show properties for reactively sintered NiAl with RPI and Cerac powders. Even though different optimum amounts of prealloyed powders were used, the properties are essentially equivalent.

The properties of intermetallic compounds are sensitive to impurity content.[12] Therefore, it was decided that in order to compare the properties of the NiAl with composite alloys, the amounts of prealloyed powders needed to be similar in both matrix and composite specimens. Fig. 8 also shows the effect of TiB_2 particles on the strength of reactive sintered NiAl.

a

b

c

Figure 7. Effect on shape retention of the addition of prealloyed NiAl powders to dilute the reaction between Ni and Al. (a) 10% prealloyed 90% elemental (b) 20% prealloyed 80% elemental (c) 25% prealloyed 75% elemental powders.

It is evident that TiB$_2$ hindered densification. Pressure had to be employed in the form of RHIP to produce fully dense specimens.

Typical microstructures of NiAl and NiAl/TiB$_2$ composites fabricated by RHIP at 750 °C and 1200 °C are shown in Figs. 9 and 10, respectively. Both monolithic and composite alloys fabricated at 750 °C and monolithic NiAl fabricated at 1200 °C were inhomogeneous. Electron microprobe analysis revealed that the light etching phase was Ni-45 a/o Al while the dark etching phase was Ni-50 a/o Al, both within the NiAl phase field. These alloys were homogenized at 1300 °C for approximately 6 hours in vacuum. The composition of the as-homogenized material was determined by electron microprobe to be approximately Ni-49 a/o Al. NiAl/TiB$_2$ alloys

RHIP at 1200 °C were found to be homogeneous in the as-fabricated condition and did not need to be heat treated.

Notice that the microstructure of the RHIP NiAl fabricated from the mixture of prealloyed and elemental powders had a more equiaxed grain structure than NiAl produced from elemental powders, cf. Figures 6 and 9. Also, the addition of TiB$_2$ particles acted to refine the grain structure of NiAl; 5 μm for the composite alloys vs. 30 μm for monolithic NiAl.

Compression tests for monolithic and TiB$_2$ reinforced NiAl alloys, RHIP at 1200 °C, were carried out as a function of test temperature. Compression flow stresses vs. temperature are plotted in Fig. 11. Note the rapid rise in yield stress with increasing TiB$_2$ content at room temperature. A portion of this strengthening
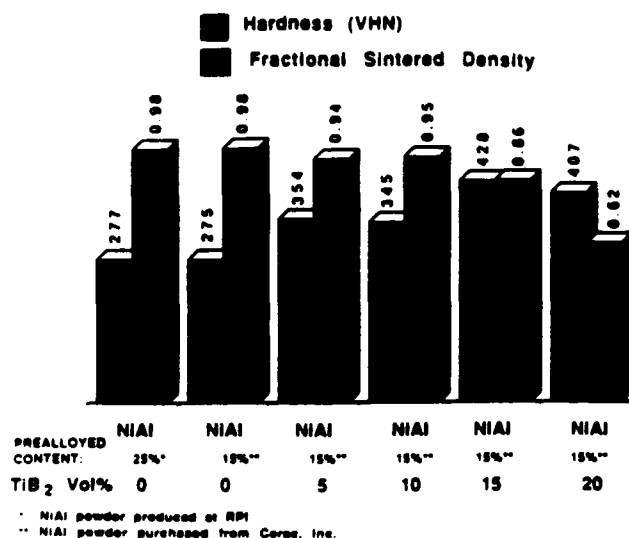
Figure 8. Effect off TiB₂ particles on the properties of reactively sintered NiAl.

can be attributed to the very fine grain size of the composite alloys. The remainder of the strengthing is due to the TiB₂ particles. Above 700 °C there is a rapid decrease of flow stress with temperature.

Large ingots (31.75mm in dia. by 75mm long, weighing 200 grams) of NiAl and NiAl/20TiB₂ were prepared for fabrication of tensile specimens. Mixed powders (Ni, Al, NiAl and TiB₂) were CIPed to 70% of theoretical density and encapsulated in 304 stainless steel. In light of the inhomogeneity of the RHIP materials, it was determined that these specimens should be reacted while attached to an active vacuum, followed by a conventional HIP cycle (1250 °C 4 hrs/ 172MPa), to remove residual porosity. A representative microstructure is shown in Fig. 12. NiAl/TiB₂ tensile specimens (Fig. 13) were produced by grinding; however, NiAl specimens had to be produced by
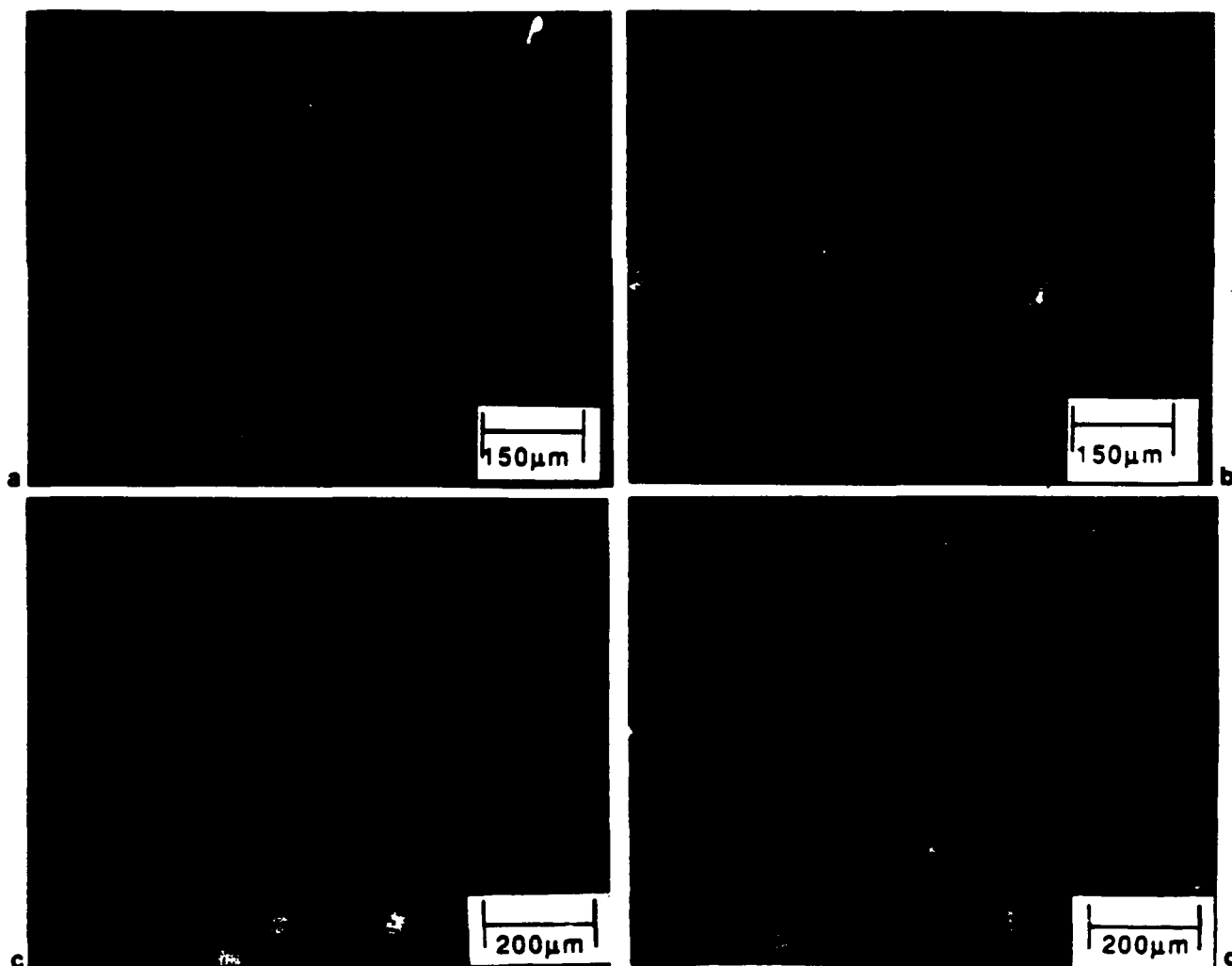
Figure 9. Microstructure of RHIP NiAl (10% prealloyed powder) (a) As RHIP 750 °C (b) RHIP 750 °C plus homogenization (c) As RHIP 1200 °C (d) RHIP 1200 °C plus homogenization (etched, Kallings solution).
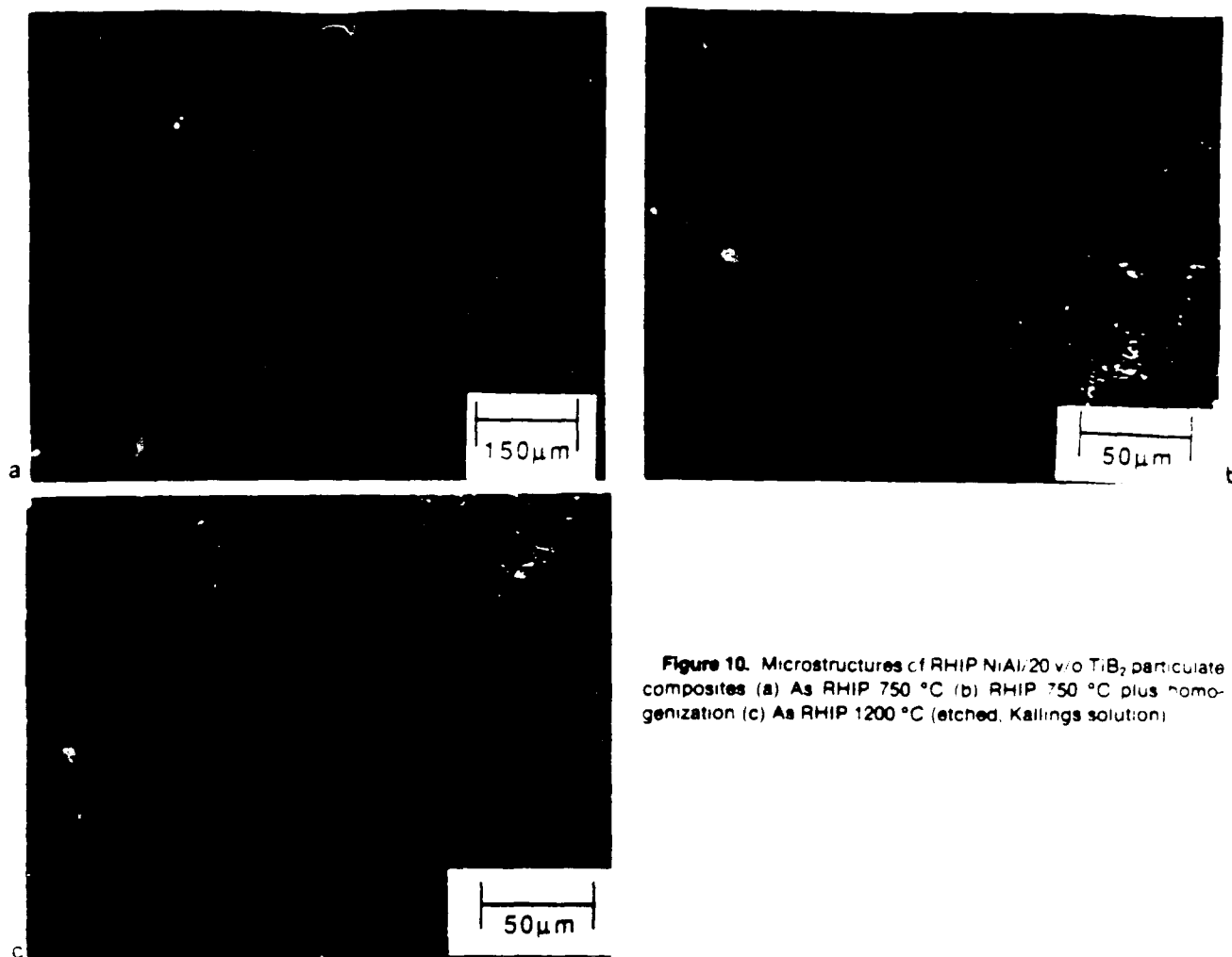
Figure 10. Microstructures of RHIP NiAl/20 v/o TiB₂ particulate composites (a) As RHIP 750 °C (b) RHIP 750 °C plus homogenization (c) As RHIP 1200 °C (etched, Kallings solution)
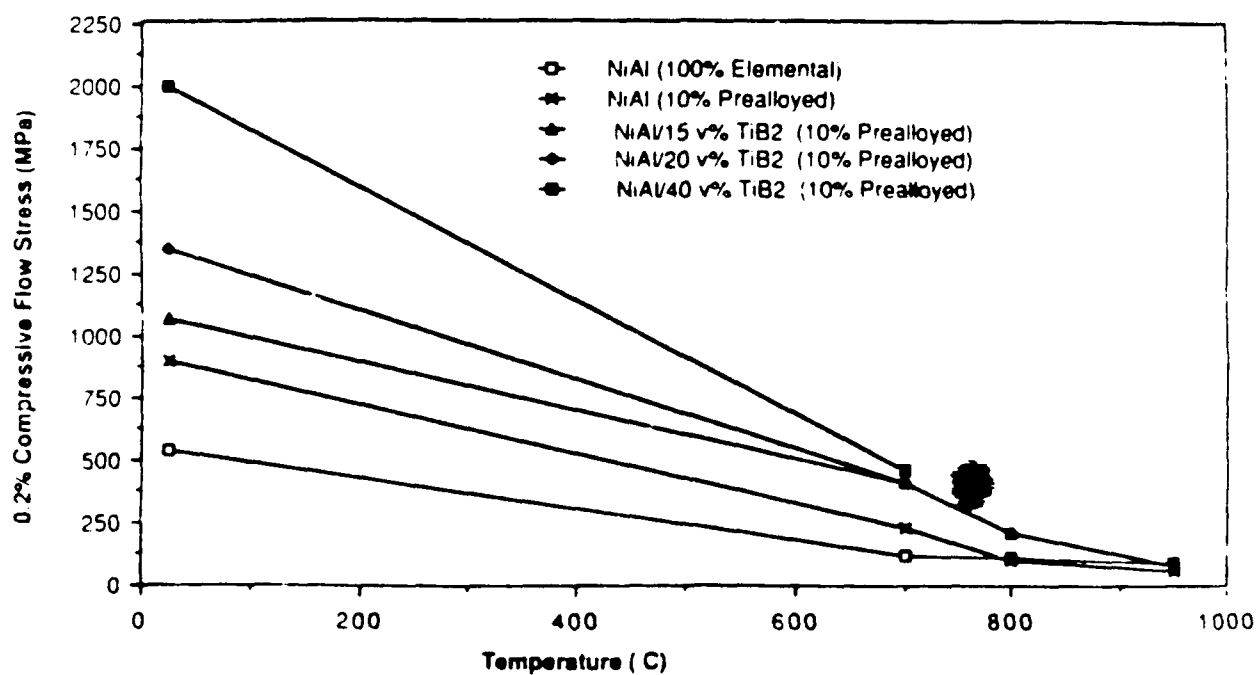
Figure 11. Effect of TiB₂ particles on the compressive properties of NiAl (RHIP 1200 °C). ε = 4 × 10⁻⁴/sec

Figure 14. Effects of TiB_2 particles on the elevated temperature tensile properties of NiAl, $\dot{\epsilon} = 1.67 \times 10^{-4} sec^{-1}$.
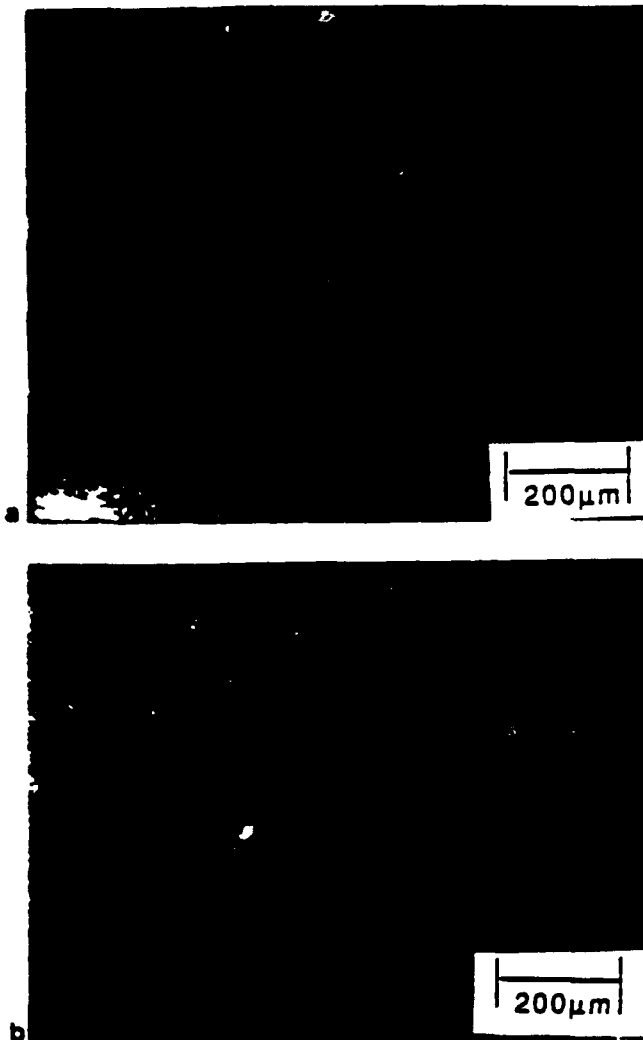
Figure 12. Microstructure of reactively sintered and HIPed material a) NiAl b) NiAl/20 v/o TiB_2.

electro discharge machining. Prior to testing the surfaces of the specimens were mechanically polished through 9 μm diamond. Figure 14 shows yield and ultimate tensile strengths, along with reduction in area, as a function of temperature for NiAl and NiAl/ 20 v/o TiB_2 composite. Most samples were tested in air except at 900 °C. Note the rapid drop in tensile strength with temperature for both matrix and composite.

Gauge dia 3.18 mm

dia 6.86 mm

19.1mm

25.4 mm
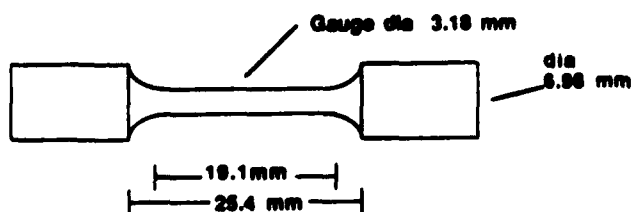
Figure 13. Cylindrical tensile specimen.

Fig. 15 shows the microstructure of an aligned fibrous composite, NiAl/15 v/o Al_2O_3, produced by binder-assisted extrusion and reactive sintering. The reinforcing phase was used to control the reaction, instead of prealloyed powders. Note the equaixed grain structure of the matrix, along with the nearly perfect fiber alignment and distribution. Also note the large residual pores remaining after reactive sintering. HIPing after reactive sintering produced fully dense specimens, as shown in Fig. 16.

Discussion

Control over the exotherm associated with the formation of NiAl was attained by adding a high melting temperature particulate to elemental powders. The latter acts as a heat sink for the heat that is generated from the reaction between Ni and Al. For the case of monolithic NiAl, prealloyed NiAl powder was used to dilute the reaction. Similar results were obtained for the combustion of TiC.[13] As the percentage of prealloyed TiC powder increased the maximum temperature of the reaction between Ti and C decreased. For reinforced NiAl alloys the reinforcement phase can also be used as a dilutant, as was the case with the NiAl/Al_2O_3 composites. While nearly fully dense monolithic NiAl could be reactively sintered, experience revealed that pressure-aided sintering
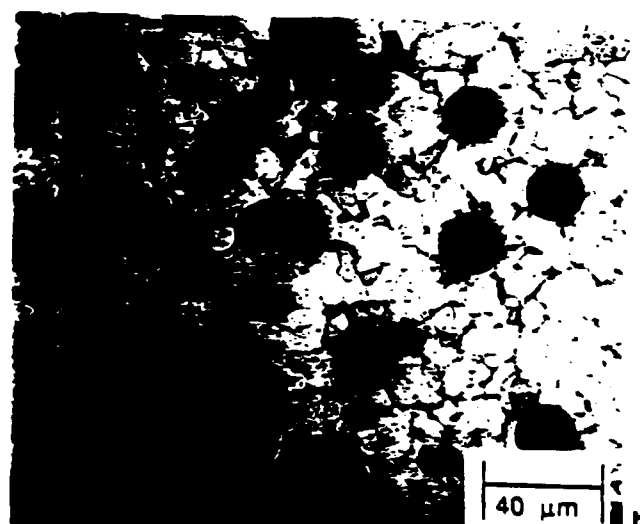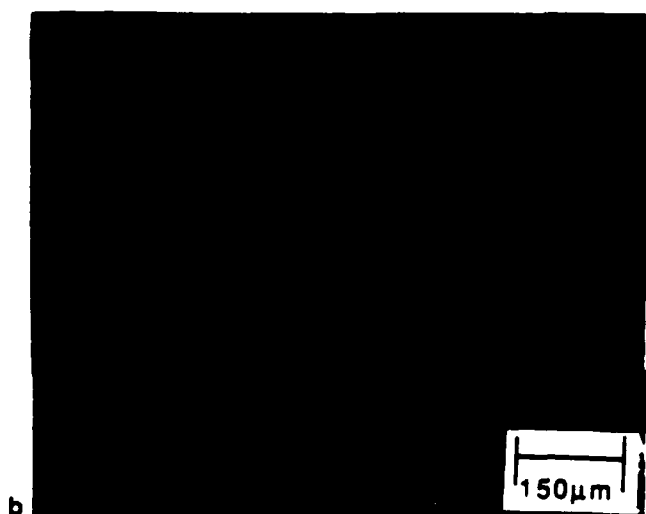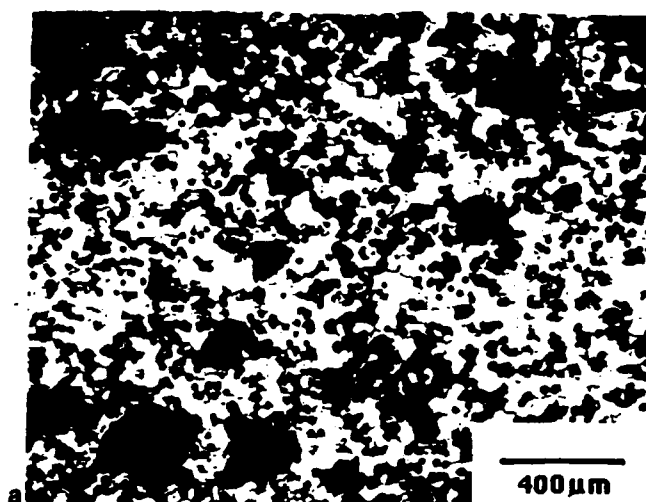
Figure 15. Microstructure at two magnifications of NiAl/15 v/o aligned Dupont FP Al₂O₃ fibers fabricated by binder assisted extrusion plus reactive sintering (etched, Kallings solution).

Figure 16. Fully dense microstructure of NiAl/15 v/o aligned FP fibers fabricated by binder-assisted extrusion plus reactive sintering, followed by a HIP cycle (172 MPa, 1200 °C, 1 hour). HIP sample was vacuum encapsulated in stainless steel. a) as polished b) etched, Kallings solution.

techniques (RHIP) are required to fabricate composites.

The application of pressure during reactive sintering (RHIP) caused the transient liquid phase to become non-uniformly dispersed, which lead to the inhomogenity. Similar inhomogeneities have been found during HIPing in the presence of a liquid phase in the W-Ni system.[14] Owing to its reduced grain size the NiAl/TiB₂ composite alloys fabricated at 1200 °C were homogeneous, since in ordered alloys grain boundary diffusion is more rapid than bulk diffusion. Even with the resulting fine grain size, a processing temperature of 750 °C proved too low to form homogeneous composite materials.

Somewhat surprising is the considerable strengthening from the addition of large (13μm) TiB₂ particles. Some of this strengthening arises from matrix grain size refinement, the grain size being reduced from 30μm to 5μm by the TiB₂ particles. However, a Hall-Petch analysis of the contribution from grain size refinement to strengthening can only account for a portion of the observed strengthening, see Table II.

A rule of mixtures calculation provides an upper limit for the strength of NiAl reinforced with TiB₂, assuming that there is no interaction (i.e. dislocation motion impedence) between the matrix and particles. Table III compares calculated and experimentally determined compressive yield strengths for NiAl/TiB₂

TABLE II. Contribution of Grain Refinement to Room Temperature Compressive Yield Stress

	Grain Size (μm)	Yield Stress (MPa)
NiAl (10% Prealloyed)	30	890
NiAl (10% Prealloyed) Calculated from Hall Petch*	5	1000
NiAl (10% Prealloyed) 15 v/o TiB₂-	5	1060
NiAl (10% Prealloyed) 20 v/o TiB₂	5	1350

*Hall Petch slope from Schulson[15]

TABLE III. Comparison of Room Temperature Compressive Strengths of NiAl and NiAl/TiB₂ and Rules of Mixtures Calculated Strengths

v/o TiB₂	Rule of Mixture Compressive Strength (MPa)	Experimentally Determined Compressive Strength (MPa)
0	—	1000*
20	1144	1350
40	1288	1915
100	—	1723**

*NiAl 5μm grain size calculated from Hall Petch relationship (Table II).
**Value for TiB₂ from Mandorf et al.[16]

alloys at room temperature. It is clear that some of the strengthening arises from interactions between the particles and the matrix.

Tables IV, V and VI compare compressive and tensile strengths of NiAl and NiAl particulate reinforced alloys fabricated by other techniques to materials produced by reactive synthesis. It is important to remember that

Figure 17. NiAl reinforced with 10 v/o FP fibers a) tensile bars b) cross section.

the properties of NiAl are sensitive to gr   ze, impurity content, deviations from stoichiom   d strain rate effects. Direct comparison, therefc   uld not be made. However, comparison of the   s in these tables clearly indicates that fine TiB₂ particles are needed to significantly strengthen NiAl at elevated temperatures. Also, NiAl fabricated by reactive synthesis has equivalent mechanical properties to materials produced by other techniques.

Results of the binder-assisted extrusion experiments indicate that this is a viable method for producing aligned fibrous composites. Near perfect alignment was achieved using the techniques described previously. Near net shape composites (NiAl/10 v/o Al₂O₃) have been produced by injection molding coupled with reactive sintering, Fig. 17. It is evident that pressure must be employed to produce fully dense composites. One problem has been damage to the fibers during powder processing. A fiber that is stiffer in the transverse direction (i.e., one with a tungsten core) might be less susceptible to damage during powder processing than the FP fiber.

Figure 18 compares microhardness values for alloys fabricated in this study. It is important to recall that a large poriton of the strengthening with TiB₂ is a result of grain size refinement of the matrix. The addition of Al₂O₃ fibers did not refine the grain size, so that values cannot be compared directly. Larger microhardness values were obtained with aligned fibers than for randomly oriented fibers. The behavior of cracks initiating from hardness indentations can be used to gauge the ability of the fibers to blunt cracks, and therefore, increase the toughness of the composite relative to the matrix alone. Figure 19 shows a crack initiating from a hardness indentation in a fully dense, random NiAl/Al₂O₃ composite. Note that the cracks propagate around and not through the fibers, indicating that the addition of Al₂O₃ fibers may improve the
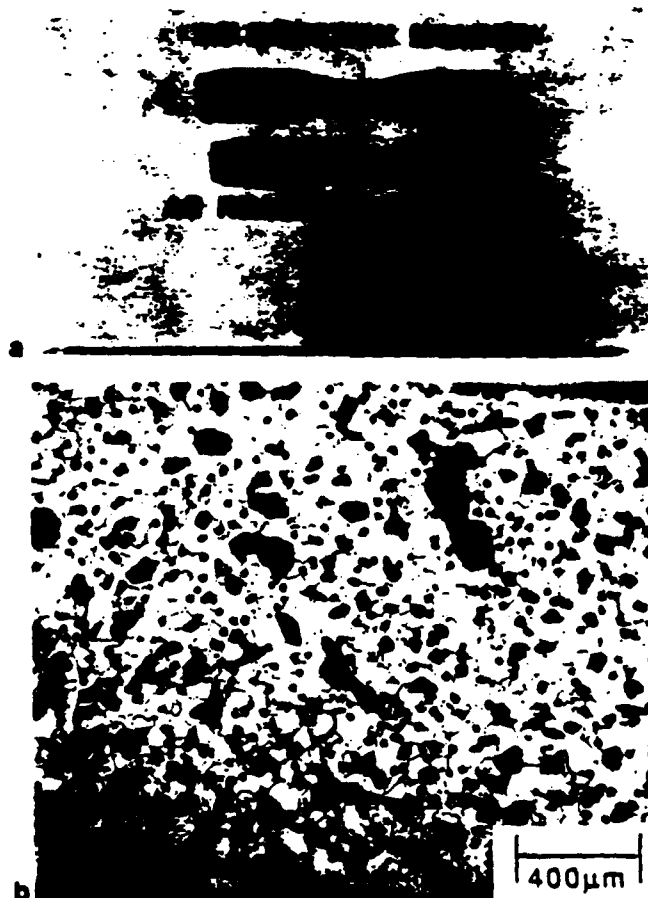
TABLE IV. Effect of Processing Condition and Grain Size on Compressive Yield Strength of NiAl at Ambient Temperature

Alloy	Condition	Grain Size (μm)	σ_{ys}(MPa)	Reference
48.9 Al	Cast	> 500	430*	Ball and Smallman[18]
49 Al	—	30	311	Schulson and Barker[19]
50 Al	VIM, HIP, extruded	50	290	Law and Blackburn[20]
50 Al	Hot Press, prealloyed	2000–3000	314**	Rigney et al.[17]
50 Al-10TiB$_2$	Hot Press, prealloyed	40	896**	Rigney et al.[17]
49 Al	RS, 0% prealloyed	30	544	present study
49 Al	RHIP, 10% prealloyed	30	890	present study
49 Al-15TiB$_2$	RHIP, 10% prealloyed	5	1060	present study
49 Al-20TiB$_2$	RHIP, 10% prealloyed	5	1350	present study

* 200°C
**in bend

TABLE V. Effect of Processing Condition, Temperature, and Strain Rate on Compressive Yield Strength of NiAl

Alloy	Condition	Temp (°C)	$\dot{\epsilon}$(sec^{-1})	σ_{ys}(MPa)	Reference
49 Al	RHIP, 10% prealloyed	700	4×10^{-4}	234	present study
		950	4×10^{-4}	62	present study
49 Al-20TiB$_2$	RHIP, 10% prealloyed	700	4×10^{-4}	406	present study
		950	4×10^{-4}	80	present study
50 Al	XD synthesis	927	2×10^{-4}	70*	Kumar et al.[6]
50 Al-20TiB$_2$	XD synthesis	927	2×10^{-4}	200	Kumar et al.[6]
50 Al	VIM, HIP, extruded	700	—	100	Law and Blackburn[20]
		900	—	50	Law and Blackburn[20]
49.2 Al	P/M, extruded	927	1.3×10^{-5}	45	Whittenberger[21]

*Extrapolation from data.

TABLE VI. Tensile Properties of NiAl at Elevated Temperature

Alloy	Condition	Temp (°C)	$\dot{\epsilon}$(sec^{-1})	σ_y(MPa)	σUTS (MPa)	R.A (%)	Reference
Ni-49 Al	RS + HIP	700	1.67×10^{-4}	173	191	3	present study
	(20% prealloyed)	800	1.67×10^{-4}	135	154	14	present study
49Al-20TiB$_2$	RS + HIP,	700	1.67×10^{-4}	344	344	0	present study
	(20% prealloyed)	750	1.67×10^{-4}	310	360	6.5	present study
		800	1.67×10^{-4}	190	207	12.5	present study
		900	1.67×10^{-4}	86	99	9.4	present study
50 Al	P/M extruded	850	4.2×10^{-6}		75		Seybolt[5]
		1000	4.2×10^{-6}		20		Seybolt[5]
50 Al-5ThO$_2$	P/M extruded	850	4.2×10^{-6}		150		Seybolt[5]
		1000	4.2×10^{-6}		80		Seybolt[5]
50 Al	Cast	700	—		134	12.3*	Grala[1]
		815	—		105	24.5*	Grala[1]
		925	—		68	27.2*	Grala[1]
50Al-2.7TiB$_2$	Rapid Solidify, extruded	760	8.4×10^{-6}	209	251	64.7	Jha and Ray[7]

*measured elongation

toughness of NiAl, confirming the results of Kumar et al.[6]

Conclusions

NiAl and NiAl matrix composites can be fabricated from a reactive synthesis approach as long as a component is present to dilute the exothermic reaction between Ni and Al. For monolithic NiAl, small additions of prealloyed NiAl to purely elemental powders are sufficient to control the reaction. The application of pressure during the reaction of the diluted mixture causes the initial liquid that forms to become nonuniformly dispersed, which leads to

Figure 18. Comparative microhardness for fully dense NiAl alloys.
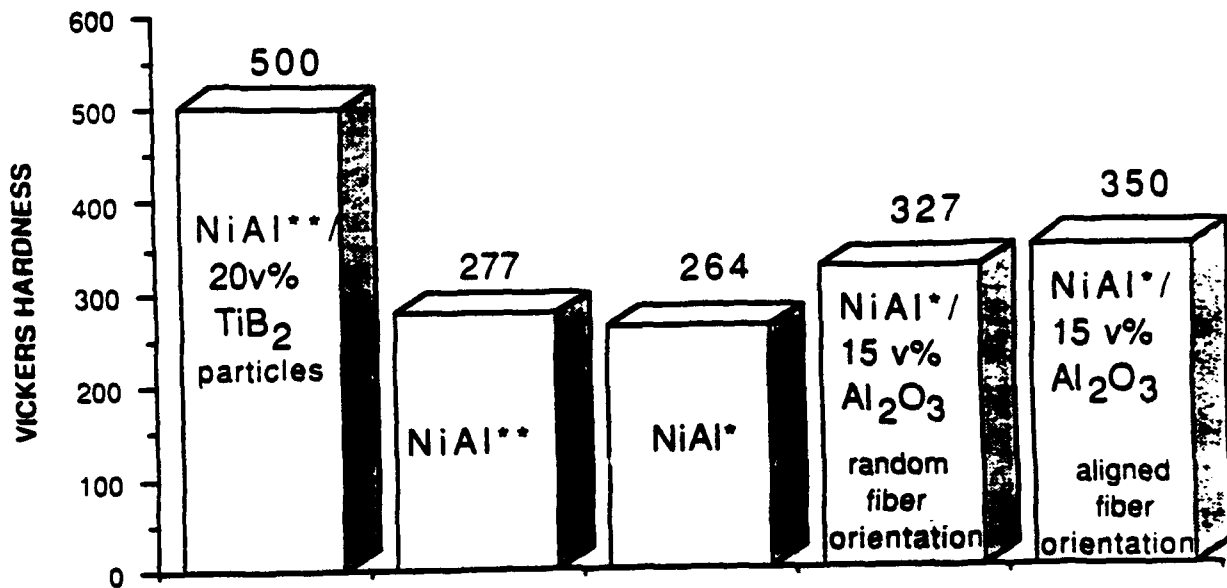
* fabrication route: 100% elemental powders (except for reinforcement phase) reactively sintered followed by HIP.
** fabrication route: Mixture of 90% elemental(Ni+Al) and 10% prealloyed (NiAl) powders RHIP.

inhomogeneities in the microstructure. Therefore, the optimal fabrication route for NiAl is by reactive sintering followed by HIP. Fabrication of composites can be achieved without the addition of prealloyed powder because the ceramic reinforcing phase acts as a heat sink.

Binder-assisted extrusion (powder injection mold is a viable method for production of aligned fibrou composites in an intermetallic matrix. Superior alignment is achieved with small spherical powders. Therefore, an elemental powder approach such as reactive synthesis is necessary for the production of
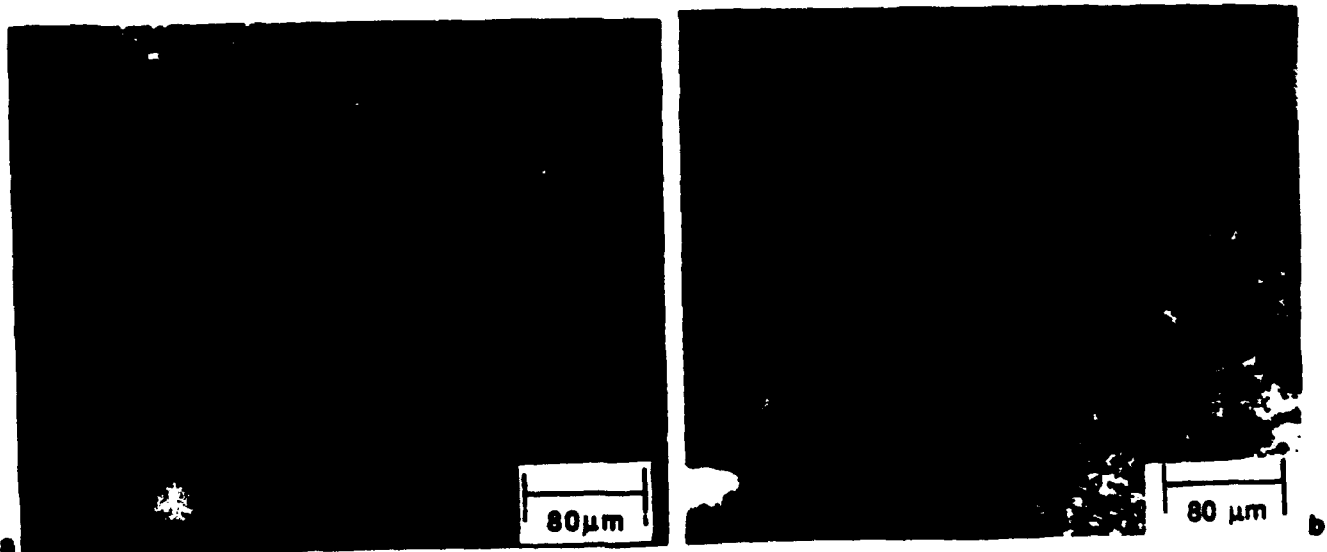
Figure 19. Two views of crack growth inhibition by Al₂O₃ fibers in NiAl.

these composites, since elemental powders are more readily available in a wider range of sizes, shapes, and purity.

NiAl and NiAl/TiB$_2$ composites fabricated by reactive synthesis had comparable strengths at low and intermediate temperatures to similar alloys produced by other techniques. Compressive and tensile tests revealed that the yield stress of NiAl can be increased with the addition of TiB$_2$. A large portion of this strengthening is attributed to grain size refinement. Fine TiB$_2$ particles are needed to strengthen NiAl significantly at elevated temperatures.

Microhardness tests reveal that Al$_2$O$_3$ fibers will strengthen NiAl, especially if the fibers are aligned. Crack paths arising from hardness indentations indicate that the addition of Al$_2$O$_3$ fibers may improve the toughness of NiAl.

Acknowledgment

References

1. E. M. Grala, *Mechanical Properties of Intermetallic Compounds*, 1960, edited by J. H. Westbrook, John Wiley and Sons, New York, p. 358.
2. P. K. Brindley, *High Temperature Ordered Intermetallic Alloys II*, 1987, edited by N. S. Stoloff, C. C. Koch, C. T. Liu and O. Izumi, Materials Research Society Symposia Proceedings, vol. 81, Materials Research Society, Pittsburgh, PA., p. 419.
3. D. L. Anton, *High Temperature/High Performance Composites*, 1988, edited by F. P. Lemkey, S. G. Fishman, A. G. Evans and J. R. Strife, Materials Research Society Symposia Proceedings, vol. 120, Materials Research Society, Pittsburgh, PA., p. 57.
4. N. S. Stoloff and D. E. Alman *Intermetallic Matrix Composites*, 1990, edited by D. L. Anton, R. McMeeking, D. Miracle and P. Martin, Materials Research Society Symposia Proceedings, vol. 194, Materials Research Society, Pittsburgh, PA., to be published.
5. A. U. Seybolt, Trans. ASM, 1966, vol. 59, p. 860.
6. K. S. Kumar, S. K. Mannan, J. D. Whittenberger, R. K. Viswanadham, and L. Christodoulou, *Nickel Aluminide/Titanium Diboride Composites Via XD Synthesis*, 1989, MML-TR-89-102(C). S. C. Jha and R. Ray, J. Mat. Sci. Lett, 1988, vol. 7, p. 285.
8. J. L. Walters and H. E. Cline, Metall. Trans., 1973, vol. 4, p. 33.
9. M. V. Nathal, R. D. Noebe, I. E. Locci, S. L. Draper and D. J. Gaydosh, in *HiTemp Review 1988*, NASA Conference Publication 10025, p. 235.
10. D. M. Sims, A. Bose and R. M. German, *Progress in Powder Metallurgy, Vol. 43*, 1987, compiled by C. L. Freeby and H. Hjort, Metal Powders Industries Federation, Princeton, NJ., p. 575.
11. R. M. German and A. Bose, Mat. Sci. Eng., 1989, vol. A 107, p. 107.
12. N. S. Stoloff, *High Temperature Ordered Intermetallic Alloys*, 1985, edited by C. C. Koch, C. T. Liu and N. S. Stoloff, Materials Research Society Symposia Proceedings, vol. 39, Materials Research Society, Pittsburgh, PA., p. 3.
13. S. D. Dummead, D. W. Readey, C. E. Semler and J. B. Holt, J. Amer. Ceramic Soc., 1989, vol. 72, p. 2318.
14. A. Frisch, W. A. Kaysser and G. Petzow, *Advances in Powder Metallurgy, Vol. 2*, 1989, compiled by T. G. Gasbarre and W. F. Jandesea, Metal Powder Industries Federation, Princeton, NJ, p. 431.
15. E. M. Schulson, *High Temperature Ordered Intermetallic Alloys*, 1985, edited by C. C. Koch, C. T. Liu and N. S. Stoloff, Materials Research Society Symposia Proceedings, vol. 39, Materials Research Society, Pittsburgh, PA., p. 183.
16. V. Mandorf, J. Hartwig and E. J. Seldin, *High Temperature Materials II*, 1961, edited by G. U. Ault, W. G. Barclay and H. P. Munger, Interscience, New York, p. 455.
17. J. D. Rigney, P. S. Khadkikar, J. J. Lewandowski and K. Vendula, *High Temperature Ordered Intermetallic Alloys III*, 1989, edited by C. T. Liu, A. I. Taub, N. S. Stoloff and C. C. Koch, Materials Research Society Symposia Proceedings, vol. 133, Materials Research Society, Pittsburgh, PA., p. 603.
18. A. Ball and R. E. Smallman, Acta Metall., 1966, vol. 14, p. 1349.
19. E. M. Schulson and D. R. Barker, Scr. Metall., 1983, vol. 17, p. 519.
20. C. C. Law and M. J. Blackburn, *Rapidly Solidified Lightweight Durable Disk Material*, 1987, AFWAL-TR-87-4102.
21. J. D. Whittenberger, J. Mat. Sci., 1987, vol. 22, p. 394.
22. J. D. Whittenberger, R. K. Viswanadham, S. K. Mannan and B. Sprissler, J. Mat. Sci., 1990, vol. 25, p. 35.
23. J. D. Whittenberger, S. Kumar, S. K. Mannan, and R. K. Viswanadham, J. Mat. Sci. Lett., 1990, vol. 9, p. 326.
24. J. D. Whittenberger, S. K. Mannan, and K. S. Kumar, Scr. Metall., 1989, vol. 23, p. 2055.
25. J. D. Whittenberger, R. K. Viswanadham, S. K. Mannan, and K. S. Kumar, J. Mat. Res., 1989, vol. 4, p. 1164.
26. L. Christodoulou, P. A. Parrish and C. R. Crowe, *High Temperature/High Performance Composites*, 1988, edited by F. P. Lemkey, S. G. Fishman, A. G. Evans and J. R. Strife, Materials Research Society Symposia Proceedings, vol. 120, Materials Research Society, Pittsburgh, PA., p. 29.

Processing of Continuous Fiber Reinforced NiAl Matrix Composite

W. Z. Misiolek[*],   R. M. German[**]

[*]Materials Engineering Department, R P I,
Troy, NY 12180

[**]Engineering Science and Mechanics Department,
Pennsylvania State University,
University Park, PA 16802

Abstract

The NiAl matrix composites are among the recently widely studied
materials due to their attractive properties such as high melting
temperature, low density and low cost. The goal of this research is
to study the processing of NiAl matrix composites reinforced with
NiAl/15vol%TiB$_2$ 1.5 mm diameter continuous fibers. The whole
composite material i.e., both the reinforcing fibers and the matrix
material are produced by extrusion of powder binder mixtures. The
next step is to layup the extrudates in a desired configuration and
then to cold isostatically press (CIP) them together. The binder is
removed from the green sample and the sample is sintered during a hot
isostatic pressing (HIP) operation. This fabrication method enables
us to tailor the properties of the manufactured composite material.
This can be done by controlling the fiber composition, fiber fraction
and their layout in the matrix. Extrusion gives us flexibility in
terms of fiber diameter, while the HIP process allows us to use
variable process parameters such as temperature, pressure and time.
These process parameters were varied and their influence on the
properties of the final product is discussed in the paper.

Introduction

The objective of this project was to study the feasibility of
the proposed technique to manufacture continuous fiber reinforced
composites. The manufacturing technique based on powder processing
gives us unlimited flexibility in terms of choice for matrix and
fiber material. The selection of NiAl for the matrix material and
NiAl/TiB$_2$ for the fiber was done based on prior mechanical and
oxidation data[1-3]. These materials have been studied extensively and
are well characterized.

Oxidation Studies

Systematic oxidation studies were performed on NiAl materi
obtained by hot isostatic pressing (HIP) of prealloyed powders a
elemental powders, which led to reactive hot isostatic pressi
(RHIP)³. Nickel aluminide (NiAl) was used as a matrix material a
it was reinforced with various amounts of TiB₂ particulate
NiAl/TiB₂ composites with 10, 20, and 30 volume % of reinforce
phase were fabricated with HIP and RHIP techniques. These samp
were exposed to air at 1073K, 1273K, and 1473K for several hours.
results of the oxidation tests performed at 1273K are presented
Figure 1. This graph shows specific weight gain as a function of ti
for various composites. The following symbols are used: PA
prealloyed powder, RS - reactive sintering (elemental powders), D
prealloyed powder obtained by XD process at Martin Marrieta Compa
and the number next to the symbol shows the amount of reinforci
phase used.
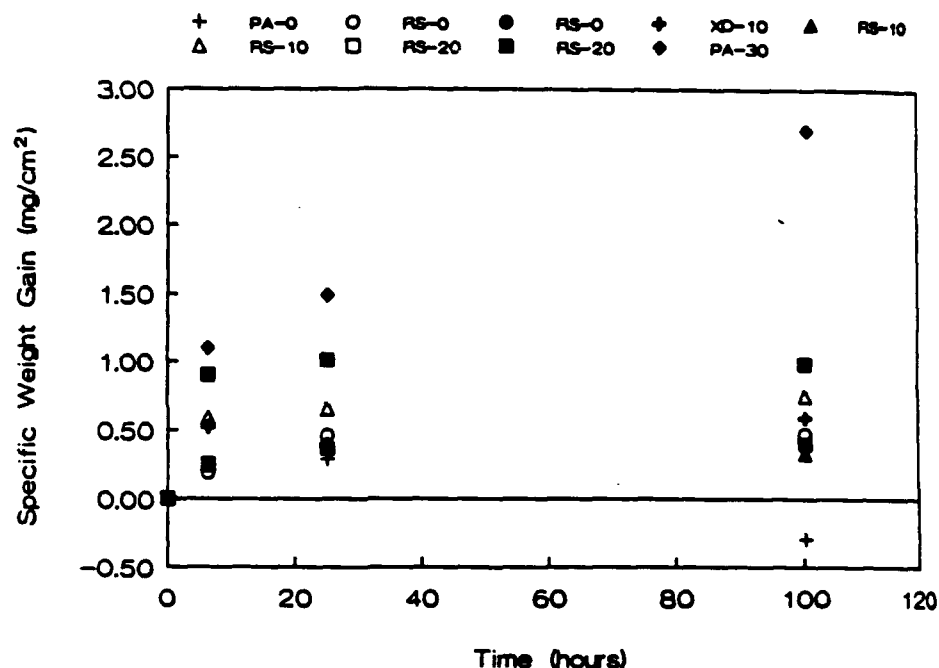
Figure 1. Specific weight gain of NiAl and NiAl/TiB₂ composites
a function of time in oxidation test performed at 1273K.

These results show behavior similar to most composites exce
for the samples with 30vol% of TiB₂. Due to the differe
manufacturing techniques used for these composites, only a genera
conclusion can be drawn. A straight comparison between oxidati
resistance of the HIP-ed prealloyed powders and the RHIP-ed element
powders based on the amount of reinforcing phase cannot be mad
There are important process and material variables, different f

xth of the fabrication methods, which have to be taken into account. The sample made from the prealloyed NiAl powder and HIP-ed to full density exhibits a hardness of 34.6 HRC, while NiAl material reinforced with 30vol% TiB$_2$ HIP-ed under the same parameters shows a hardness of 51.5 HRC. At this point a compromise was made between the improved mechanical properties and degraded oxidation resistance of NiAl/TiB$_2$ composites with higher fraction of the reinforcing TiB$_2$ phase. The relationship for oxidation resistance as a function of time is shown in Figure 1. The problem of losing oxidation resistance with an increasing amount of TiB$_2$ can be solved by using a different way of reinforcing the NiAl matrix. The goal was to use an intelligent processing route, which would allow us to improve the mechanical properties of the matrix with a significantly smaller fraction of TiB$_2$ than 30 volume percent.

Concept of Continuous Fiber Reinforced Composite

As a solution to the oxidation resistance problem, a continuous fiber reinforced composite (CFRC) was suggested. The idea was to use NiAl material as a matrix and to reinforce it with fibers made of NiAl/15 vol%TiB$_2$ composite. A schematic cross section of that composite with 20% fiber fraction is presented in Figure 2.

NiAl/15vol%TiB$_2$ Fiber

NiAl Matrix
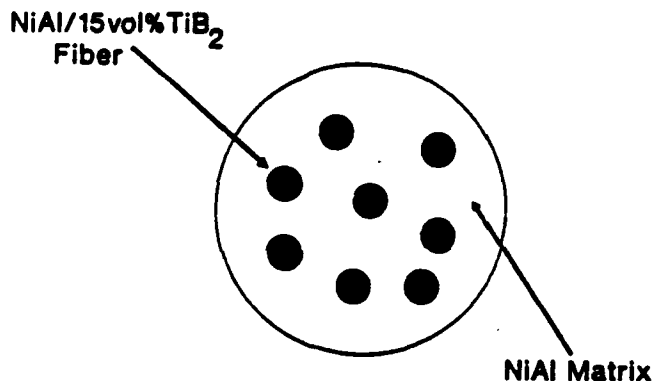
Sample Diameter	10.0 mm
Fiber Diameter	1.5 mm
Fiber Fraction	20.0 %

Figure 2. Composite cross section.

To produce such material a relatively complex fabrication method is required. First the selected powders were mixed with a binder to produce a feedstock. Then the feedstock was extruded through a conical die to form a fiber. This operation was used for different powder/binder mixtures to obtain fibers for the NiAl matrix and the NiAl/TiB$_2$ reinforcing material. In the next step straight fibers of

different composition were laid-up in a desired manner to form the
composite preform. The preform was then cold isostatically pressed
(CIP), which gave green strength to the fiber compound. The green
strength is desired due to fact that the sample had to be handled
during the debinding and HIP-ing operations. The next step was a
debinding procedure, which enabled us to remove the binder from the
fibers pressed together. After that step the sample was ready for the
final densification process. It was encapsulated under vacuum and
then HIP-ed. Final product testing included microstructural
observations, density, and hardness measurements. A flow chart of the
whole fabrication method for CFRC is shown in Figure 3.

```
┌─────────────────────────────┐
│    Powder/Binder Mixtures   │
└─────────────────────────────┘
               │
         ┌───────────┐
         │ Extrusion │
         └───────────┘
               │
   ┌──────────────────────┐
   │    Layup of Fibers of │
   │  Different Composition │
   └──────────────────────┘
               │
           ┌───────┐
           │ C I P │
           └───────┘
               │
         ┌───────────┐
         │ Debinding │
         └───────────┘
               │
           ┌───────┐
           │ H I P │
           └───────┘
               │
         ┌───────────┐
         │  Testing  │
         └───────────┘
```
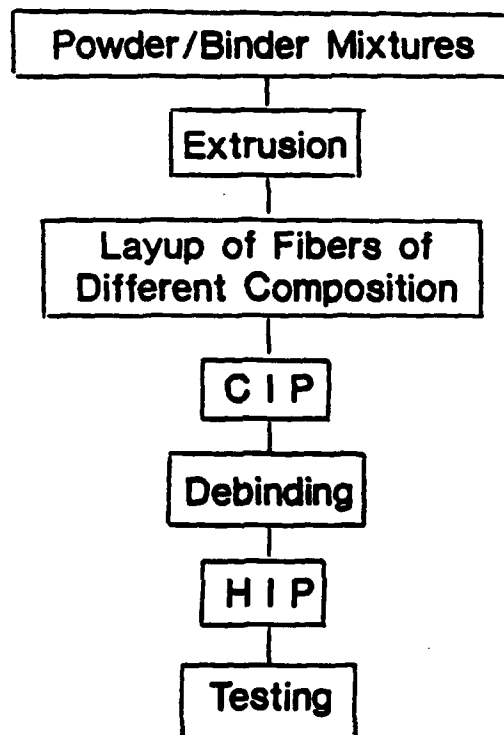
Figure 3. Flow diagram for powder processing of continuous fiber
reinforced composite.

Experimental and Results

Prealloyed NiAl and TiB_2 powders characterized in Table I were
used in the first experiments. There were mixed with an organic
binder, whose composition is shown in Table II. Powder loading for
NiAl/binder and NiAl/15vol%TiB_2 /binder mixtures was determined by
torque rheometer and the values were 55% and 46% respectively. Powder
binder mixtures were extruded through a 1.5 mm diameter conical die
at 393 K. The extrudates and the die are shown in Figure 4.

Table I

Powder Characteristic

Material	NiAl	TiB$_2$
Vendor	Cerac Inc.	ICD Group Inc.
Production Method	Ball Milled	Ball Milled
Mean Particle Size	18μm	4μm

Table II

Binder Composition

Composition of the binder	
Paraffin Wax	69%
Polypropylene	20%
Carnauba Wax	10%
Stearic Acid	1%

Figure 4. Extrudates and 1.5 mm diameter die.

The extrudates were warmed on a hot plate, which allowed the straightening of fibers made from the powder/binder mixtures. The extruded fibers were laid-up in the desired configuration and then cold isostatically pressed at 224 MPa. Then the sample was thermally debound in hydrogen following the schedule presented in Table III. This schedule also allowed presintering so sample handling did not cause a problem. The sample was placed in a stainless steel can, degassed at 625 K for 12 hours and then sealed under the vacuum. This way the prepared HIP can was placed in a HIP pressure chamber and processed for an hour at 1473 K under a pressure of 170 MPa. This processing route enables achievement of a fully dense material. The microstructure of the composite, shown in Figure 5, is almost homogenous in the whole cross section area.

Table III

Thermal Debinding Schedule; Hydrogen Atmosphere

Thermal Debinding Steps
1. Heating rate 2K/min
2. Hold for 300 min at 723K
3. Heating rate 10K/min
4. Hold for 60 min at 1473K
5. Cooling rate 20K/min down to room temperature
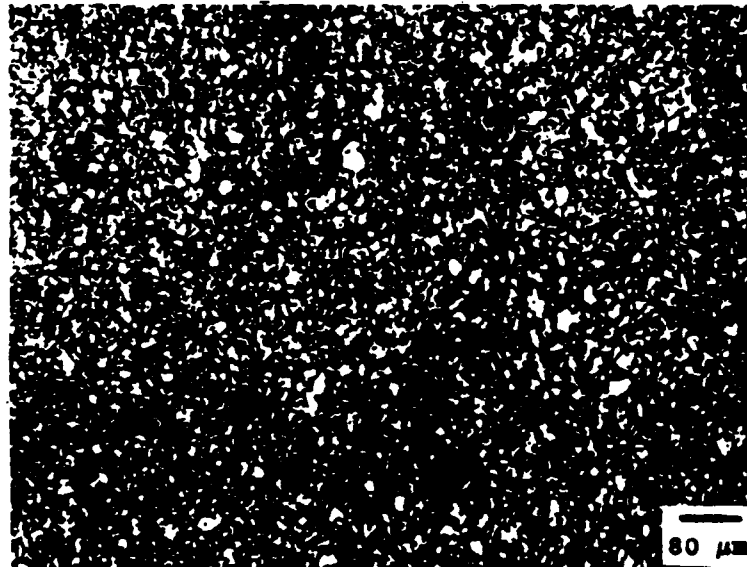
Figure 5. Microstructure of cross section area for a sample where the NiAl/TiB$_2$ fiber is homogenized into the matrix.

The TiB$_2$ particles were repositioned before they were sintered together. This resulted in almost even dispersion of TiB$_2$ particles in the whole matrix and in the loss of the fiber reinforced character of the composite material. In this situation we were dealing with a particle reinforced material instead of a fiber reinforced composite.

In the next set of experiments it was decided to replace the prealloyed NiAl powder with Ni and Al elemental powders to use the reactive sintering technique after debinding instead of presintering. The HIP process was used only to densify the fiber material, which had been sintered already and to enhance the sintering of fibers together. The powders used for reactive sintering are characterized in Table IV. These powders were mixed together in the proportion required for the NiAl composition. In order to control propagation of the reaction wave, 10% of prealloyed NiAl powder was added. These powders were mixed together for 30 minutes in a turbula mixer and then mixed with the organic binder described in Table II. The powder loading for this system was 64%. The same reinforcing fibers NiAl/15vol%TiB$_2$ were used. The extrusion and CIP conditions were identical to those for the first samples. The HIP process was performed for 30 minutes at 1473K under a pressure of 100 MPa. As a result, a sample with a very original microstructure was obtained. There are distinct microstructure differences between fiber and matrix material. The typical microstructure is shown in Figure 6. The microhardness measurements for both NiAl matrix and NiAl/TiB$_2$ fibers are presented in Table V.

Table IV

Powders characteristic for reactive sintering process

Material	Vendor/Grade	Production Method	Mean Particle Size
Ni	Novamet/4SP	Gas Atomization	4μm
Al	Valimet/H-3	Gas Atomization	3μm
NiAl	Cerac Inc.	Ball Milled	18μm
TiB$_2$	ICD Group Inc.	Ball Milled	4μm

173
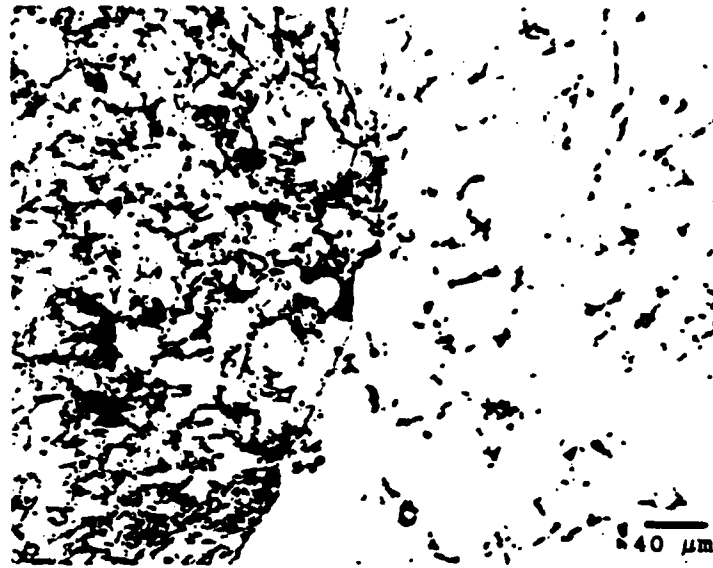
Fig 6. A NiAl/TiB$_2$ fiber NiAl matrix interface

Table V

Microhardness for NiAl matrix and NiAl/TiB$_2$ fiber material

Material	HV (100 g)	
	Readings	Mean Value
NiAl matrix	254 264 281 285 304 297 297 264 254	277.8
NiAl/TiB$_2$ fiber #1	421 401 421	414.3
NiAl/TiB$_2$ fiber #2	433 413 530	458.7
NiAl/TiB$_2$ fiber #3	464 421 401	428.7

Discussion

The second fabrication method involving reactive sintering proved to be a successful technique. The material obtained has a typical microstructure of a fiber reinforced composite. There is a distinct difference in microstructure and mechanical properties between fiber and matrix material (See Fig. 4 and Table V). Reactive sintering allows us to maintain the fiber structure. The HIP process is a very useful densification technique but has to be preceded by a sintering operation. Simultaneous application of temperature and pressure resulted in very extensive repositioning

of the particles and complete change of character of the reinforcing structure. The HIP-ed sample turned out to be reinforced by dispersed particles instead of aligned fibers. There are many aspects in this technology which should be studied further. The first eventual changes should be in the extrusion process. The matrix and fiber material can be extruded through the dies of different diameters. This would allow better packing density in the green stage and also help to layup fibers. The best solution is to use matrix fibers of larger diameter and reinforcing fibers of smaller diameter. The idea is to build a continuous network of large fibers with voids filled with smaller reinforcing fibers. This would significantly improve the packing density so important for the sintering process and also to assure better control of fiber alignment. This study was on the NiAl system but can be extended to other composites. The fiber and matrix composition can be easily changed and designed for current needs. It is also possible to introduce additional layer on the fiber surface, which can be made of a ductile material. The ductile reinforcing fibers could be made by traditional wire drawing technology and then placed in the intermetallic matrix. The proposed technology is very universal and gives freedom in designing composite properties through the matrix and fiber composition, their volume fraction and fibers layout in the matrix. The work on this processing technique should continue focusing on extrusion process and then on optimization of reactive sintering. After that, the obtained composites will be tested for mechanical properties and oxidation resistance.

Summary

The proposed technique for manufacturing continuous fiber reinforced composite by powder processing is very attractive due to its flexibility. The reactive sintering version of this technology gives a much better control over the composite microstructure, which influences properties. There is a need for further studies, especially in extrusion and sintering stage.

Acknowledgement

References

1. W.Z. Misiolek and R.M. German, Fabrication of NiAl/TiB$_2$ Intermetallic Matrix Composites, 1990 Advances in Powder Metallurgy, Metal Powder Industries Federation, Princeton, NJ, 1990, 161-172.
2. D.E. Alman and N.S. Stoloff, Powder Fabrication of Monolithic and Composite NiAl, International Journal of Powder Metallurgy, vol. 27, 1991, 29-41.
3. P. Korinko et al., "Oxidation Resistance of NiAl/TiB$_2$ Composites", to be publish.

REACTIVE SINTERING AND REACTIVE HOT
ISOSTATIC PRESSING OF IRON ALUMINIDES

A. Bose, R. A. Page, W. Misiolek* and R. M. German+

Engineering and Materials Sciences Division
Southwest Research Institute
San Antonio, TX - 78228

* Materials Research Center
Rensselaer Polytechnic Institute
Troy, NY - 12180

+ Engineering Science and Mechanics Department
Pennsylvania State University
University Park, PA 16802

ABSTRACT

Alloys based on iron aluminides are of interest due to their strength at elevated temperatures, good oxidation and sulfidation resistance, and low material cost. These intermetallic compounds are expected to be an inexpensive alternative for moderate temperature resistant alloys. Until now, the major thrust of research has been in the development of new alloys and a basic understanding of mechanical behavior. Relatively little effort has focussed on the processing of these materials.

Reactive sintering, a novel powder processing technique, has been successfully applied to fabricating nickel aluminides. In this paper, reactive sintering and reactive hot isostatic pressing (RHIP) of iron aluminides are discussed. This study included intentional variations in composition, powder types, powder size ratio, sintering temperatures, and degassing times. From reactive sintering experiments, an optimal combination of iron and aluminum particle sizes was selected for subsequent evaluation of composition and reactive hot isostatic compaction variables. The results demonstrated that full density could be achieved with a high aluminum content material processed by reactive hot isostatic compaction (RHIP). The maximum density obtained with an Fe_3Al composition was 91% of theoretical. This could be improved, however, by changing the processing parameters. Reactive sintering without simultaneous pressurization failed to give full densification in any of the compositions evaluated, largely due to a low enthalpy of compound formation. The results clearly demonstrate that reactive hot isostatic pressing can be a method of fabricating iron aluminides in an inexpensive manner.

INTRODUCTION

The promise of intermetallic compounds as structural components has been well documented in the literature [1,2]. Among all of the intermetallic compounds, the long range ordered aluminides, especially the nickel aluminindes, have been most extensively studied. Iron aluminides, which also possess extremely attractive properties like the nickel aluminides, have not been investigated to a great extent.

Alloys based on Fe_3Al and FeAl are of great interest, however, due to their good oxidation and sulphidation resistance and low material cost [3]. Presently, the majority of the heat resistant alloys are either nickel or cobalt based or high nickel and chromium containing steels. These alloys often suffer from chromium evaporation at high temperatures, exhibit very poor hot corrosion properties in sulphur-containing environments, and usually contain a number of expensive and strategic elements. On the other hand, intermetallic compounds between the Fe_3Al and FeAl composition exhibit good oxidation resistance and a fair amount of sulphidation resistance due to their ability to form a protective alumina coating at very low oxygen partial pressures [3]. Fe_3Al compounds also possess good strength at moderate temperatures, show around 2 to 5% ductility at room temperature, have lower densities compared to nickel or cobalt based alloys and steels, and do not depend on expensive and strategic elements. Improvements in creep properties of iron aluminides along with an excellent combination of other desirable mechanical properties can also be obtained in iron aluminide based composites with TiB_2 dispersoids [4,5]. Thus, this material offers extremely attractive property combinations like its more extensively studied counterpart, the nickel aluminides. Various processing techniques have been utilized for the fabrication of iron aluminide based intermetallic compounds. Conventional processes like casting and arc melting have been utilized to fabricate this compound. However, due to the inherent problems associated with the casting approaches, powder processing has been extensively used [6-9]. Powder processing also provides the opportunity of fabricating composites based on an iron aluminide matrix.

Recent powder metallurgy approaches for producing intermetallic compounds and composites based on intermetallic matrices generally favor conventional techniques, such as hot pressing, hot isostatic pressing, or hot extrusion of prealloyed powders [1-4,10,11]. Although, the success of these approaches is clearly established, there are the drawbacks of long process cycles, high process temperatures and considerable expense. A reactive processing approach could circumvent these problems by using commercial elemental powders and shorter process cycles. Reactive sintering and reactive hot isostatic processing are novel processing methods which have been successfully applied for producing near full density Ni_3Al intermetallic compounds [12,13]. It remains to be determined whether reactive processing can be extended to the fabrication of other intermetallic compounds. In general, reactive sintering of aluminides involves a transient liquid phase that is formed when the aluminum melts [14]. The initial compact is composed of mixed elemental powders which are heated to a temperature where they react to form the desired compound. Figure 1 shows a schematic binary phase diagram for a reactive sintering system, where a stoichiometric mixture of A and B powders is used to form an intermediate compound product AB [15]. The reaction occurs above the lowest eutectic temperature in the system, yet at a temperature where the desired compound is still solid. Heat is liberated due to the thermodynamic stability of the high melting temperature compound. Consequently, reactive sintering can be nearly spontaneous once the liquid forms, provided the heat liberated is sufficient to drive the reaction. The formation of molten aluminum provides a capillary force on the structure which can lead to rapid densification [14]. The reactive sintering process as envisioned for the present research on iron aluminide is similar to that used previously to produce high density nickel aluminides [16]. The phase diagram of a binary Ni-Al system is shown in Figure 2 [17,18]. Some of the similarities between the schematic binary phase diagram (Figure 1) and the Ni-Al phase diagram are quite obvious. Concerns about the applicability of the technique to the iron aluminides exist, however, due to the lower adiabatic temperature rise in this system and the unbalanced solubility between the iron and aluminum. If pressureless reactive sintering of the iron aluminides does not provide the desired level of densification due to the concerns described above, the chances of success in pressure assisted reactive sintering is extremely high. This paper describes the preliminary results of investigations on reactive sintering and reactive hot isostatic pressing of iron aluminides.

A+B → AB+heat (mixed powder)
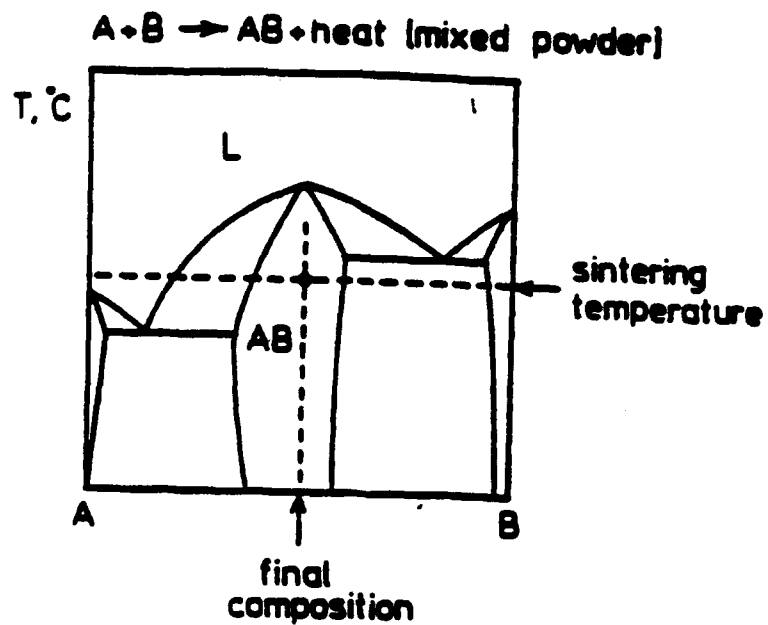
Figure 1. Schematic binary phase diagram for a reactive sintering system.
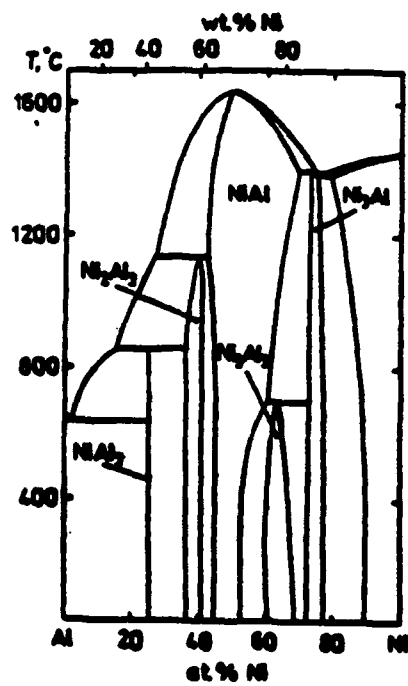
Figure 2. Binary Ni-Al phase diagram [17,18].

EXPERIMENTS AND RESULTS

Experimental Approach

The essential approach was to mix and compact elemental powders (inexpensive and easy to compact) and heat the mixture to a temperature at which the exothermic reaction occurred. Due to the low exotherm of the iron-aluminum mixture, it was felt that simultaneous application of pressure would be necessary during the reaction to obtain complete densification. However, to assess the optimal powder combination, screening experiments based on pressureless reactive sintering of mixed elemental powders were designed. The matrix of these screening experiments as designed to assess the influence of iron particle size, aluminum particle size, green density, degassing time, and maximum temperature on the degree of reaction, density, and structural integrity of the system. From these experiments, an optimal combination of iron and aluminum particle sizes was selected for subsequent evaluation of composition and reactive hot isostatic pressing variables. Sample characterization included shape retention, density, microstructure, and X-ray diffraction. Reactive hot isostatically pressed samples that exhibited good sintered densities were tested in tension (without the customary ordering treatment) at ambient temperature.

Screening Tests

Three different types of iron powders and three aluminum powders of different particle size and shape were selected for the initial experiments. The characteristics of all powders used in this research are presented in Table 1.

Initially the powders were mixed in a 3:1 atomic stoichiometry of iron to aluminum in a turbula mixer for 30 minutes. From these mixtures, 5g samples were die pressed in a 12.6 mm cylindrical die using zinc stearate as a die wall lubricant. Sixteen samples were prepared from each powder mixture, eight with a low green density and eight with a high green density. The variations in green density were achieved by variation of compacting pressure. The following code has been used to identify the powders:

> G: GAF iron powder
> S: Spheromet iron powder
> A: Atomet iron powder
> 3, 10, 30: H-3, H-10, H-30 aluminum powder

Thus, a sample designated as "S3" is one which was prepared from a mixture of Spheromet 60 iron powder with H-3 aluminum powder. The characteristics of the die-pressed green samples used for screening tests have been outlined in Table 2.

Two samples of each type were taken for each sintering run. Two different sintering temperatures together with two different degassing times were used. The sintering and degassing parameters are presented in Table 3. The GAF powder mixtures could not be die pressed or cold isostatically pressed (CIP'ed) without severe delamination. GAF iron powder mixed with H-3, H-10 and H-30 aluminum powder was, thus, reactively sintered only under schedule #1 (shown in Table 3) by spreading the powder mixture as a thin layer on top of a ceramic boat. The resultant sample was very porous, but had sufficient strength to prevent crumbling and easy milling. The GAF powder was, therefore, excluded from subsequent experiments. Reactive sintering of the remaining samples (S3, S10, S30, A3, A10 and A30) was carried out in accordance with the sintering and degassing parameters described in Table 3.

Table 1. Characteristics of all powders used in this investigation.

Property	Iron			Aluminum
Vendor	GAF Corp.	Quebec Metal Powders		Valimet
Grade	CIP-S-2000	Atomet 95	Spheromet 60	H-3 H-10 H-30
Fabrication Method	Carbonyl	Water Atomized	Gas Atomized	Gas Atomized
Average Particle Size	4μm	15μm	67μm	3μm 10μm 30μm

Table 2. Characteristics of the die-pressed green samples used for the screening tests.

Sample Code	Lower Green Density			Higher Green Density		
	Height (mm)	Density (%)	Compact. Pressure (MPa)	Height (mm)	Density (%)	Compact Pressure (MPa)
S 3	8.1	69	77.4	7.2	78	211.1
S 10	8.3	67	77.4	7.7	73	123.2
S 30	8.2	68	105.6	7.3	77	211.1
A 3	8.6	65	140.8	7.5	75	330.7
A 10	8.8	64	211.1	7.7	73	422.2
A 30	8.8	64	211.1	8.0	70	422.2

Table 3. Sintering and degassing parameters used for the screening experiments.

Run	Degassing		Sintering		Heat Rate
#	Temperature °C	Time min.	Temperature °C	Time min.	K/min.
1	500	60	800	20	30
2	500	240	800	20	30
3	500	60	1200	20	30
4	500	240	1200	20	30

135

Final density was evaluated only for the samples which showed the best shape integrity after the sintering process. A decrease in density, which is effectively a demonstration of the extreme Kirkendall effect associated with the unbalanced Fe-Al solubility, was characteristic of all of the reactive sintering experiments. The microstructures of the low green density samples reactive sintered under the conditions shown in Table 3 were examined; enabling the study of the influence of degassing and sintering parameters on microstructure. Two representative photomicrographs which demonstrate the effect of reactive sintering temperature are shown in Figures 3a and 3b. Figure 3a shows the microstructure of sample A10 reactive sintered at 800°C for 20 minutes (See Table 3, Run #2). Figure 3b shows the microstructure of sample A10 reactively sintered at 1200°C for 20 minutes (See Table 3, Run #4). Both the samples were degassed at 500°C for 2 hours before being heated to the sintering temperature at 30 K/min.

The final sintered products were characterized using conventional X-ray diffraction techniques. The 2θ diffraction angle was examined over the range of 25 to 100°. A constant scanning rate of 1.2°/minute for CuK$_\alpha$-radiation ($\lambda = 0.1542$ nm) was used. The full scale intensity was 1000 counts per second (cps). X-Ray analysis of two samples produced from powder mix A10 and reactive sintered at 800 and 1200°C provided insight into the compound formation ability of reactive sintered mixed elemental iron and aluminum powders. The X-ray peaks of the sample reactive sintered at 1200°C showed good correlation with the FeAl intermetallic compound and no evidence of a second phase. Thus, complete compound formation did occur during the pressureless reactive sintering process. On the other hand, the X-Ray analysis of the sample reactively sintered at 800°C showed evidence of some amount of unreacted iron indicating that the reaction had not proceeded to completion. One may conclude from these results that a high reactive sintering temperature is necessary in order to take the reaction to completion.

The screening experiments with various iron and aluminum particle sizes demonstrated success in generating the desired intermetallic compounds. The most dense and homogeneous structures were achieved in run #4 shown in Table 3. It was determined that the best reactivity and structural rigidity were attained using Atomet 95 iron powder (Quebec Metal Powders, mean size of 15 micrometers) and H-10 aluminum powder (Valimet, 10 micrometers mean size). However, all of the samples were very porous and definitely unsuitable for use as structural components. Green density had a small relative effect on the densification for this system, and the use of a maximum reaction temperature of 1200°C aided densification and compact integrity. The degassing time did not have a large influence on final density, but generally longer times were beneficial. To improve the sintered density, it was deemed necessary to apply pressure during the reaction or increase the aluminum content of the system so as to increase the exotherm and provide more liquid to aid densification. Consequently, pressureless reactive sintering of iron aluminides with increasing levels of aluminum content was conducted using the cycle described in Run #4 of Table 3.

Varied Composition Fe:Al Reactive Sintering

Reactive sintering experiments were run for the following Fe:Al atomic ratios: 75:25, 70:30, 60:40 and 50:50. Atomet 95 iron powder and Valimet H-10 aluminum powder were mixed in a turbula mixer for 30 minutes. A compact of 4g weight was die pressed in a 12.6 mm cylindrical die under a pressure of 172.5 MPa. Zinc stearate was used as a die wall lubricant. Sample characteristics in the green state are shown in Table 4.

The die pressed green samples were reactive sintered under the conditions described in Run #4 of Table 3. The sintered characteristics are shown in Table 5. The 50Fe:50Al composition exhibited the highest sintered density at 59% of theoretical. However, the 50Fe:50Al sample also had a higher green density (Table 4) to start with. Each of the compacts decreased in density, but none the less, exhibited good structural integrity. The microstructure of the 60Fe-40Al pressureless reactive sintered sample is shown in Figure 4. It is apparent from these results that pressureless
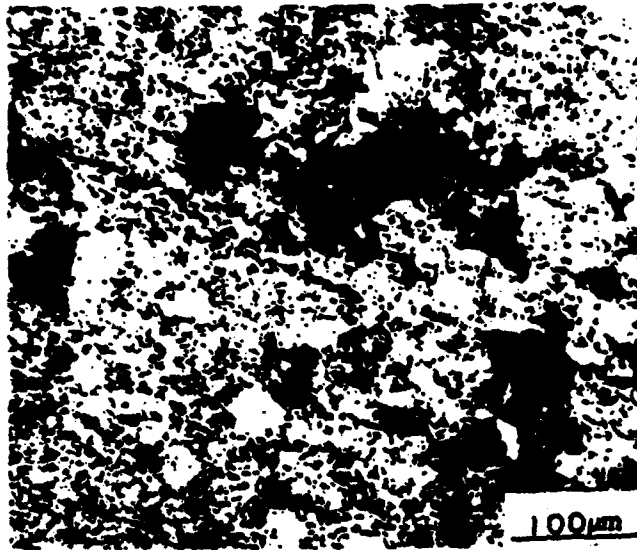
Figure 3a. Microstructure of 75Fe:25Al sample (A10), after pressureless reactive sintering for 3 minutes at 800°C (Table 3, Run #2).
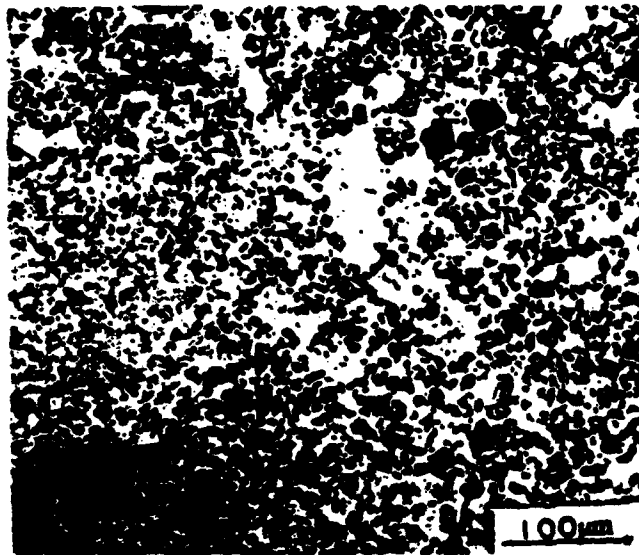
Figure 3b. Microstructure of 75Fe:25Al sample (A10) after pressureless reactive sintering for 3 minutes at 1200°C (Table 3, Run #4).

Table 4. Characteristics of the die-pressed green samples with varying Fe:Al ratio.

Fe : Al Ratio	Theoretical Density (g/cc)	Sample		
		Height (mm)	Diameter (mm)	Density (%)
75 : 25	7.15	7.7 7.7	12.7 12.7	57.2 57.2
70 : 30	6.98	7.7 7.9	12.7 12.7	58.6 57.1
60 : 40	6.61	8.2 8.2	12.8 12.8	57.4 57.4
50 : 50	5.29	8.8 8.9	12.7 12.7	67.7 66.9

Table 5. Properties of pressureless reactive sintered die-pressed samples with varying Fe:Al ratio. Sintering conditio⁻ i⁻ shown in Cycle #4 of Table 3.

Fe : Al Ratio	Dmin (mm)	⁻ax ⁻m)	Height (mm)	Weight (g)	Final Density (%)	Sinter Intact Y/N
75 : 25	12.7 12.8	13.2 13.1	8.5 8.7	4.00 3.99	49.7 50.0	Y Y
70 : 30	12.7 12.7	13.5 12.9	8.5 8.9	3.96 3.99	50.0 51.1	Y Y
60 : 40	12.8 11.7	13.7 11.9	9.3 9.9	3.96 3.95	48.0 47.0	Y Y
50 : 50	12.8 12.7	13.1 12.9	10.2 10.6	3.98 3.96	58.7 59.2	Y Y

Figure 4. Microstructure of 60Fe:40Al sample (A10), after pressureless reactive sintering in 20 minutes at 1200°C (Table 3, Run #4).

active sintering with aluminum contents up to 50 atomic % still did not result in the desired high density samples. Thus, to attain high densities, reactive hot isostatic pressing experiments were designed for samples with aluminum contents varying from 25 to 50 atomic percent.

Reactive Hot Isostatic Pressing (RHIP)

The reactive hot isostatic compaction experiments were conducted using a hybrid of the most successful reactive sintering cycle with the A10 powder mixture. These experiments consisted of cold isostatic compaction of four different compositions of the Fe:Al powder mixture (25, 30, 40 and 50 atomic percent aluminum) followed by hot isostatic compaction. The powder mixtures were cold isostatically pressed at 310 MPa in the form of cylindrical rods with densities varying from 53 to 66% of theoretical. Each of the CIP'ed samples were placed in one end sealed stainless steel cans, degassed at 500°C under vacuum for 12 hours and sealed in vacuum. These samples were then reactive hot isostatically pressed at a temperature of 1200°C under a pressure of 172 MPa. The schedule for reactive hot isostatic pressing is shown in Table 6. These conditions were applied to the powder mixtures of all four compositions.

The density after reactive hot isostatic compaction was measured as approximately 90% of theoretical for the 25, 30, and 40 at.% Al mixtures. For the 50 at.% Al composition, corresponding to FeAl, the measured density after reactive hot isostatic compaction was 104% of theoretical. This unusually high density indicates a possible loss of aluminum, probably through reaction with the stainless steel container. The 50 at.% Al specimen, when examined using optical metallography, exhibited a fairly homogeneous structure and no evidence of porosity. Photomicrographs of the HIP samples with 25 at.% aluminum and 50 at.% aluminum are shown in Figures 5a and 5b, respectively. The Fe-25Al sample exhibited fine porosity which was distributed throughout the matrix. X-Ray diffraction analysis was also carried out on the RHIP samples. These samples exhibited peaks which corresponded to the peaks of a stoichiometric FeAl intermetallic compound and no iron or aluminum peaks were detected. The reaction was thus deemed to be essentially complete.

Mechanical Properties

Two RHIP samples were selected for tensile property evaluation. One of the RHIP samples corresponded to the Fe₃Al composition, while the other was an FeAl (50:50 atomic percent) material. Tensile bars were machined from the HIP cans. The sample with the FeAl composition broke before testing, suggesting the extreme brittleness of the material. The Fe-25Al sample which corresponded to the Fe₃Al composition (the ordering treatment was not performed and the sample X-Ray peaks matched with the FeAl compound) was tested to failure under tension using a strain rate of 10-3 s⁻¹. The stress-strain curve for the sample is shown in Figure 6. The compound had a yield strength of 851 MPa (123.55 ksi) and an ultimate tensile strength of 979 MPa (142.11 ksi). The strain to failure was 2.7%. It should be pointed out that these results were obtained for a sample which was not fully dense. Thus, still better properties could be expected when the samples are fully densified by the proper reactive hot isostatic pressing conditions.

The sintered hardness was measured on selected samples and the ones of interest are given below:

75 Fe: 25 Al, RHIP: 36.8 +/- 0.6 HRC
70 Fe: 30 Al, RHIP: 35.8 +/- 0.7 HRC
50 Fe: 50 Al, RHIP: 48.9 +/- 4.0 HRC
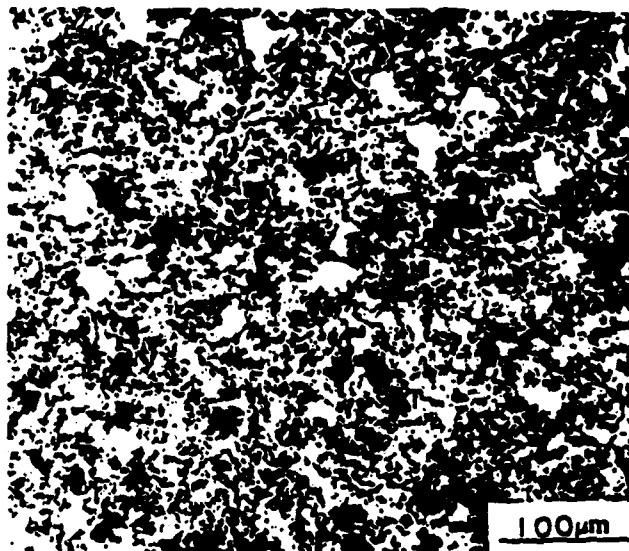
Figure 5a. Microstructure of 75Fe:25Al sample, reactive hot isostatically pressed at 1200°C, 172 MPa for 1 hour.
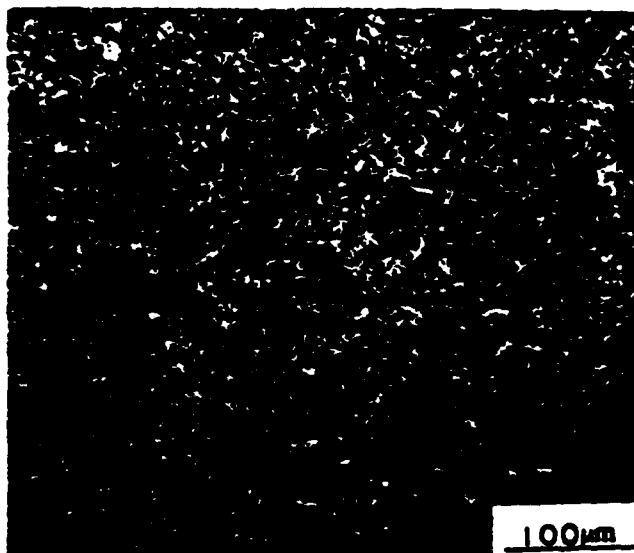
Figure 5b. Microstructure of 50Fe:50Al sample, reactive hot isostatically pressed at 1200°C, 172 MPa for 1 hour.

Table 6. Reactive hot isostatic pressing schedule.

Operation	Measurement	Time
Pressing	13.8 MPa	2 min.
Heating	1200°C	35 min.
Pressing	172 MPa	30 min.
Holding Temp. & Pressure	1200°C 172 MPa	60 min.
Depressurising & Cooling	6.9 MPa 300°C	60 min.
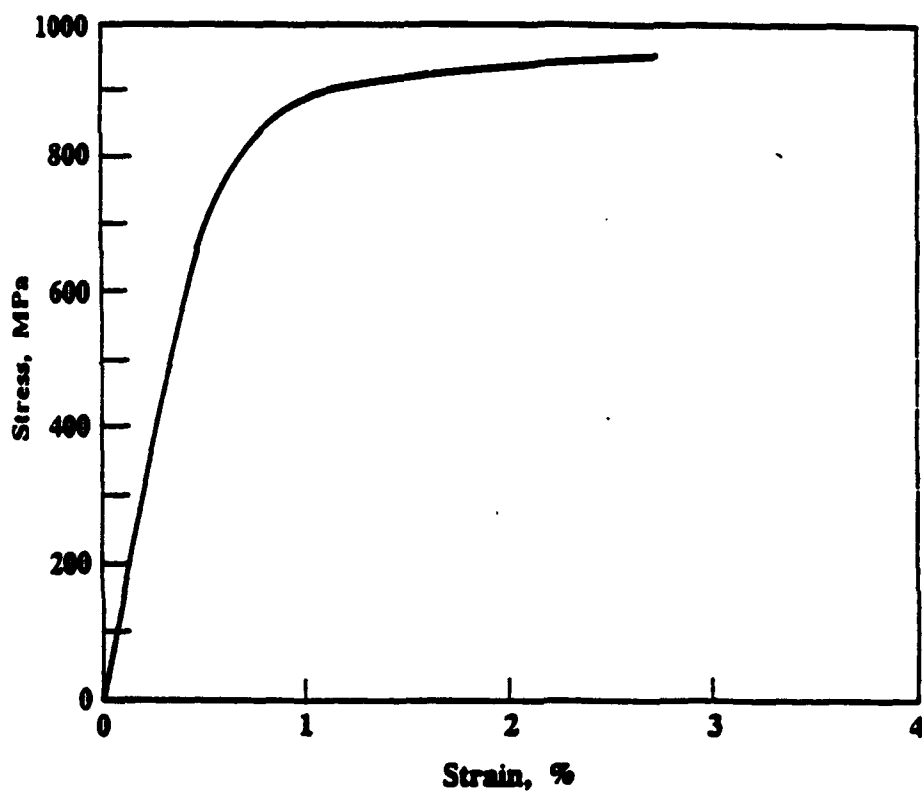
Figure 6. Engineering stress-strain curve for reactive hot isostatically pressed Fe₃Al intermetallic compound, tested in tension.

DISCUSSION

Reactive synthesis by sintering or hot isostatic compaction has been applied successfully the nickel-aluminum system. On the basis of this success, it was considered possible that anoth important system, namely the iron-aluminum system, could also be processed by reactive synthe from elemental powders. The binary Fe-Al phase diagram is shown in Figure 7 [19]. To gain a sea of the potential for reactive sintering of the iron aluminides, thermodynamic data were gathered t the Fe-Al binary system [20].

Over the temperature range from 500 to 800°C, the heat capacity of iron aluminide varies wi the test temperature _id alloy composition. At one atmosphere pressure, the low value is near 3 J/mol/K and the high value is near 54 J/mol/K, with a general increase in heat capacity with increas iron content and test temperature. For this analysis a mean value of 45 J/mol/K is acceptable is determining the potential adiabatic heating.

The enthalpy associated with alloying has been determined for Fe-Al alloys. For a referen temperature of 298 K, the enthalpy depends on the alloy composition as follows:

composition, at.% Fe	enthalpy, J/mol
25	-27,900
34	-26,200
50	-25,100
60	-20,000
70	-15,700
80	-11,000
90	-5,800

The enthalpy increases with temperature approaching twice these values by 1873 K. At th Fe_3Al composition, the melting temperature is approximately 1773 K, while the first eutectic in t system is located at 0.9 at.% Fe and 925 K, see Figure 7. Using the mean heat capacity and entha of reaction with the assumption that the reaction begins at the first eutectic gives the self-heat under adiabatic (ideal) conditions as roughly 300 K. With an initiation temperature of 925 K, th results in a maximum self-heating to 1225 K. Since the first intermetallic to form is Al_5Fe with melting temperature of 1430 K, this heating will be insufficient to cause melting. Consequent only transient liquid events are possible. Due to the large solubility gradient, the transient liqui results in pore generation at the prior aluminum particle sites, with surrounding Al_5Fe compoun and major compositional gradients.

On this basis, supplemental heating is needed to cause sintering of the structure (since th adiabatic temperature rise is insufficient to sustain the reaction). The poor solubility behavior (ve large aluminum solubility in iron and negligible solubility of iron in aluminum) results in compou formation that stabilizes the transient Kirkendall pores. In this study, sintering temperatures up 1200°C were selected to melt the intermetallics and allow formation of the desired Fe_3Al compou The results show that compound formation is incomplete when reactive sintering is carried out 800°C, while increasing the temperature to 1200°C results in the total consumption of all the stari elemental powders to form the reacted compound.

By contrast, the FeAl compound has a self-heating potential closer to 550 K. Thus, assum an initiation temperature of 925 K, under ideal conditions the reaction is able to self-heat to 1475 This should be just sufficient to melt

Al·Fe
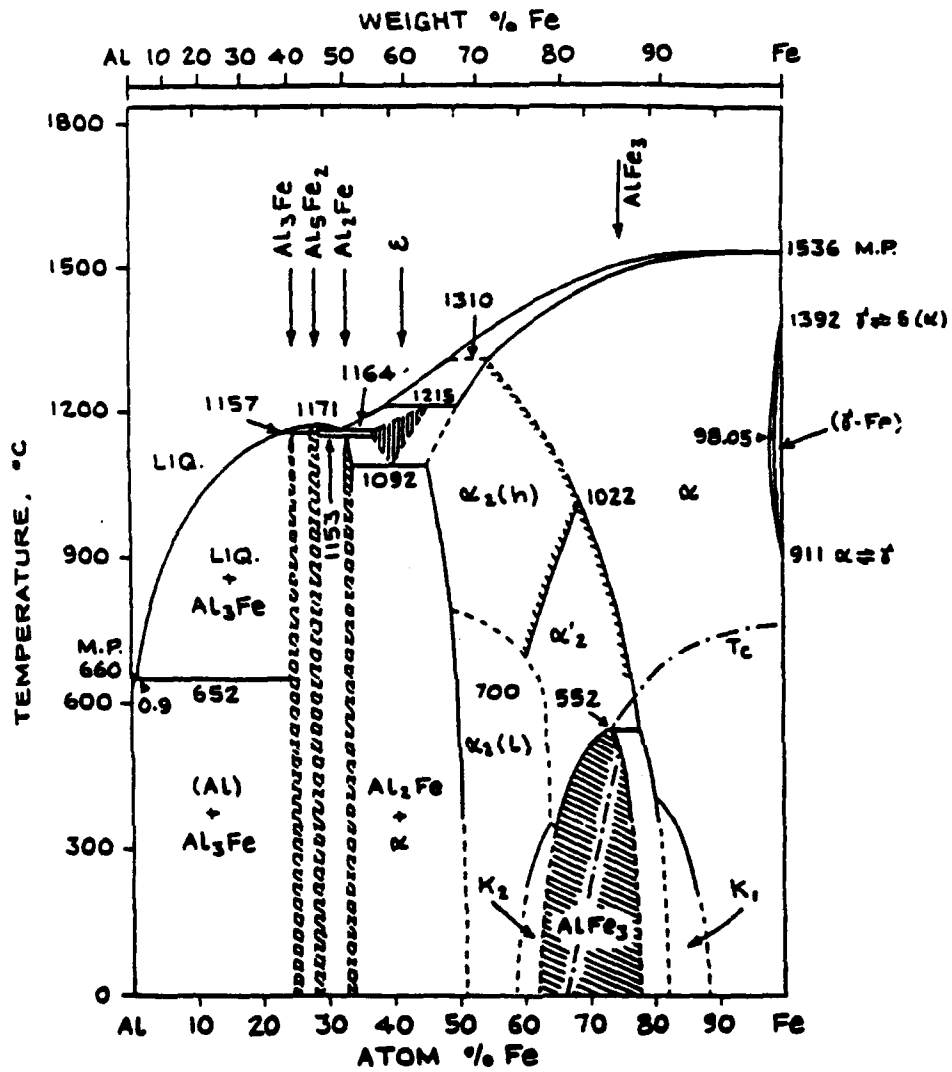
Figure 7. Iron-Aluminum phase diagram [13].

143

the FeAl or higher iron content compositions which require temperatures of 1488 K or higher. More rapid heating or hot compaction may provide opportunities for further densification and homogenization.

In the nickel-aluminum system, the exothermic heat is sufficient for significant densification. However, in the iron-aluminum system the heat of reaction is relatively small and more external heating is needed to sustain the compound formation reaction. So, even though the iron-aluminum system contains exothermic compounds and a low melting temperature liquid (aluminum) that allow transient liquid phase sintering, the low exotherm of the system does not sustain the reaction and densification. Further, the solubility of iron in molten aluminum is relatively low. As a consequence of an unbalanced solubility ratio (solubility of iron in aluminum is much lower than the solubility of aluminum in iron), Kirkendall pores are generated during interdiffusion. The pores form at prior aluminum particle sites and become stabilized by the high melting (low diffusion) surrounding intermetallic compounds. The application of an external stress via hot isostatic compaction is one means of offsetting the poor densification of this system.

Generally the most desirable situations for reactive sintering have temperature increases of 1500 K, roughly corresponding to H/C > 1500, where H is the reaction enthalpy and C is the heat capacity. It is obvious that the iron aluminides do not fulfil this requirement. On the other hand, this requirement is satisfied by the nickel-aluminides. Based on this it would be expected that pressureless reactive sintering of iron aluminides would not be successful. However, simultaneous application of pressure could produce the desired densification along with compound formation. This conclusion is well substantiated by the present investigation.

The RHIP sample of Fe$_3$Al composition showed excellent mechanical properties even though the sample had around 9% porosity (91% dense). The properties obtained, especially the yield strength, are higher than those reported in the literature [3]. Several factors could be responsible for the increased strength. The absence of the standard heat treatment of 1 hour at 850°C (for recrystallization) plus a seven day hold at 500°C (for DO3 ordering) could be responsible for influencing the mechanical properties. The compound formed shows X-Ray peaks that match with the FeAl compound instead of the Fe$_3$Al compound which would definitely require the ordering treatment. Small amounts of an alumina dispersion in the matrix could also be responsible for a part of the increased strength. It is likely that the mechanical properties of the material can be further improved by increasing the density of the compound. This can be achieved by proper manipulation of the reactive hot isostatic pressing parameters.

CONCLUSIONS

1. Full density for iron aluminides is attained with a high aluminum content (50 atomic percent aluminum) when processed by reactive hot isostatic compaction. It would also be possible to attain full density on compositions with lower aluminum content by increasing the RHIP temperature.

2. Reactive sintering without simultaneous pressurization fails to give full densification in the iron-aluminum system, due to a low enthalpy of compound formation and the unbalanced iron-aluminum solubility ratio.

3. The RHIP'ed iron aluminide with 25% aluminum content showed good mechanical properties compared to those reported in the literature, though the material was only 91% dense. Improving the density by proper selection of the RHIP conditions could further improve the mechanical properties of the iron aluminides.

4. The results of this study successfully demonstrate the feasibility of processing iron aluminides by a reactive processing approach.

144

REFERENCES

1. C. C. Koch, C. T. Liu and N. S. Stoloff (eds.), High-Temperature Ordered Intermetallic Alloys, Materials Research Society Symposium Proceedings, Vol. 39, Materials Research Society, Pittsburgh, PA, 1985.

2. N. S. Stoloff, Inter. Metal Rev., 1984, Vol. 29, pp. 123-135.

3. C. G. McKamey, C. T. Liu, S. A. David, J. A. Horton, D. H. Pierce, and J. J. Campbell, Development of Iron Aluminides for Coal Conversion Systems, ONRL/TM-10793, Oak Ridge National Laboratory, Oak Ridge, TN, July, 1988.

4. R. G. Bordeau, Development of Iron Aluminides, AFWAL-TR-87-4009, Air Force Wright Aeronautical Laboratories, Wright Patterson Air Force Base, Ohio, May 1987.

5. C. G. McKamey, J. A. Horton, and C. T. Liu, Mat. Res. Soc. Symp. Proc., Materials Research Society Symposium Proc., Materials Research Society, Pittsburgh, PA, 1987, Vol. 81, pp. 321-327.

6. W. M. Schulson, Inter. J. Powder Met., 1987, Vol. 23, pp. 25-32.

7. K. Vedula and J. R. Stephens, Powder Metallurgy 1986 State of the Art, W. J. Huppmann, W. A. Kaysser and G. Petzow (eds.), Verlag Schmid, Freiburg, West Germany, 1986, pp. 205-214.

8. A. Bose and R. M. German, Modern Developments in Powder Metallurgy, 1988, Vol. 18, pp. 299-314.

9. A. Bose, B. Moore, R. M. German, and N. S. Stoloff, J. Metals, 1988, Vol. 40, pp. 14-17.

10. A. Bose and R. M. German, Adv. Materials and Manufacturing Processes, 1988, V. 3, pp. 37-56.

11. P. K. Brindley, Mat. Res. Soc. Symp. Proc., Materials Research Society Symposium Proc., Materials Research Society, Pittsburgh, PA, 1987, Vol. 81, pp. 419-424.

12. B. Moore, A. Bose, R. M. German, and N. S. Stoloff, Mat. Res. Soc. Symp. Proc., 1988, Vol. 120, pp. 51-56.

13. R. M. German, A. Bose, D. Sims, U.S. Patent Number: 4,762,558, Date of Patent: August 9, 1988.

14. R. M. German, Liquid Phase Sintering, Plenum Press, New York, NY, 1985, Chapters 7 and 8.

15. R. M. German, J. Metals, 1986, Vol. 38, No. 8, pp. 26-29.

16. D. M. Sims, A. Bose, and R. M. German, Prog. Powder Met., 1987, Vol. 43, pp. 575.

17. M. Hansen and K. Anderko, Constitution of Binary Alloys, 2nd Edition, McGraw Hill, New York, New York, 1958.

18. I. M. Robertson and C. M. Wayman, Metallog., 1984, Vol. 17, p. 43.

19. O. Kubaschewski, Iron-Binary Phase Diagrams, Springer Verlag, 1982, pp. 5-9.

20. R. Hulton, P. D. Desai, D. T. Hawkins, M. Gleiser, and K. K. Kelly, Selected Values of the Thermodynamic Properties of Binary Alloys, ASM, Metals Park, Ohio, 1973, pp. 156-165.

18 HIGH TEMPERATURE INTERMETALLIC ALLOYS AND INTERMETALLIC MATRIX COMPOSITES BY POWDER PROCESSING

R. M. German, A. Bose, D. Alman, J. Murray, P. Korinko, R. Oddone and N. S. Stoloff

Materials Engineering Department, Rensselaer Polytechnic Institute Troy, New York 12180-3590 USA

ABSTRACT

Aluminide intermetallic compounds are the basis for high performance, high temperature materials of the future. This presentation covers the use of reactive powder processing techniques involving a transient liquid phase for the formation of monolithic aluminide intermetallics and intermetallic-matrix composites. A notable development has been the fabrication of homogeneous, high density compacts from elemental powders by reactive sintering. A variant process involving simultaneous pressurization in a hot isostatic press, termed reactive hot isostatic pressing, is applicable to those compounds that prove difficult to consolidate by pressureless reactive sintering. This paper describes the effects of various processing factors on fabrication of dense aluminides with primary emphasis on Ni_3Al. Results on the fabrication of several other aluminide compounds will be discussed, including NiAl, TiAl, $TaAl_x$, and $NbAl_x$. Current research is on the use of these aluminides as the matrix for high temperature composites. A key concern is with processing effects on microstructure, selection of compatible ceramic reinforcing phases, and whisker alignment through injection molding.

INTRODUCTION

Intermetallic compounds have emerged as the needed next generation of high temperature, oxidation resistant materials for aerospace and turbine applications. A recent surge of research on intermetallics has taken place as the ceramics have failed to live up to their promise and superalloys have apparently been exhausted [1,2]. The aluminide intermetallic compounds have the attractive characteristics of low density, high strength, good corrosion and oxidation resistance, nonstrategic elements, and relatively low cost. In some cases these intermetallics exhibit the unique characteristic of improved strength with increasing temperature. Coupled with relatively high melting temperatures, these attributes make for ideal high temperature materials. Most importantly, recent research has demonstrated ductility in some intermetallic systems. Thus, fabricability and reliability have been improved, leading to new interest.

Sintering is ideal for the fabrication of complex shaped, high performance intermetallic compound alloys [3,4]. This research considers reactive sintering and reactive hot isostatic compaction as fabrication routes for the production of aluminide compounds and composites from mixed elemental powders. These processes rely on a transient liquid phase to give densification and compound formation. In this presentation, the initial principles of reactive sintering will be developed and applications to aluminide compounds detailed, including a presentation of mechanical properties and processing variants.

BACKGROUND

Initial research focused on the processing of full density Ni₃Al. Subsequent efforts shifted to incorporation of whiskers in a nickel aluminide matrix [5-9]. Because processing difficulties are expected from thermal expansion mismatches and interfacial interactions, every effort is being made to keep processing temperatures low in this early research. Further, injection molding has been applied to attain the desired whisker dispersion and orientation in the matrix while forming complex shapes. Final densification for these composites is by a new process termed reactive hot isostatic compaction.

Within this framework, the research has emphasized reactive sintering as one process for forming several aluminides. In general, reactive sintering involves a transient liquid phase [10]. The initial compact is composed of mixed powders which are heated to a temperature where they react to form a compound product. Often the reaction occurs on the formation of a first liquid, typically a eutectic liquid at the interface between contacting particles. Figure 1 shows a schematic binary phase diagram for a reactive sintering system, where a stoichiometric mixture of A and B powders is used to form an intermediate compound product AB. At the lowest eutectic temperature a transient liquid forms and spreads through the compact during heating. Heat is liberated because of the thermodynamic stability of the high melting temperature compound. Consequently, reactive sintering is nearly spontaneous once the liquid forms. By appropriate selection of temperature, particle size, green density and composition, the liquid becomes self-propagating throughout the compact and persists for only a few seconds. Like other transient liquid phase sintering treatments, the liquid provides a capillary force on the structure which leads to densification [10-13]. However, if the solubilities are unbalanced, swelling can occur due to the formation of Kirkendall porosity.

During slow heating solid state interdiffusion can generate intermetallic phases at the interfaces. Such compounds inhibit the subsequent reaction when the liquid forms; thus, reactive sintering is sensitive to processing parameters such as heating rates, interfacial quality, green density, and particle size. Because of the rapid spreading and reaction of the liquid, pore formation at prior particle sites is common, especially in systems with large aluminum particle sizes and large exotherms. Furthermore, dimensional control proves difficult if an excess of liquid is formed. Because of such problems, the application of reactive sintering has been limited. However, as demonstrated here, the potential for reactive sintering is large and it is well suited to forming dense intermetallic compound structures.

Figure 2 shows the aluminum-nickel binary phase diagram. The system is characterized by five intermetallic compounds, with initial interest in this study on Ni3Al. For this system, reactive sintering treatments near the lowest eutectic temperature would be most appropriate (approximately 640°C). Figure 3 is a schematic diagram of the reactive sintering process. Nickel and aluminum powders are randomly mixed in a stoichiometric ratio. The powders have small particle sizes to aid intermixing and are compressed to create good particle-particle contact. During heating to the first eutectic temperature, solid state interdiffusion generates intermetallic compound phases and some self-heating. At the first eutectic temperature, liquid forms and rapidly spreads throughout the structure. The liquid consumes the elemental powders and forms a precipitated Ni₃Al solid behind the advancing liquid interface. Interdiffusion of nickel and aluminum is quite rapid in the liquid phase and the compound generates heat which further accelerates the reaction. If the reaction is controlled, then the compound will be nearly fully densified and suitable for containerless hot isostatic compaction to full density.

The concept of reactive sintering has been applied to several compounds in the past [14-19] and has been adapted to form NiAl, Ni₃Al, TaAl₃, NbAl₃, and TiAl in this research. In one variant, compound formation and densification are achieved in separate steps by mixing elemental powders, reacting, pulverization (grinding), compaction, and subsequent sintering. Variations on this basic scheme involve hot pressing and pressure assisted sintering. Stoichiometry control is important and is often achieved using an excess of the more volatile ingredient or intermediate chemical leaching to remove unreacted constituents. The current reactive sintering approach circumvents these problems by using commercial elemental powders, low processing temperatures, short process cycles with a classic press and sinter technology.

EXPERIMENTAL

The sintering research presented here emphasizes formation and densification of Ni₃Al where there is a large body of knowledge [5-10]. Parallel efforts on the other compounds will be summarized to illustrate the possible adaptations of the Ni₃Al techniques to other aluminides. The main process parameters were particle sizes of nickel and aluminum, stoichiometry, alloying, milling time, green density, maximum sintering temperature, heating rate, atmosphere, and duration of the sintering treatment. A basic processing scheme is outlined in Figure 4.

The characteristics of the nickel, niobium, titanium, and aluminum powders used for reactive sintering are given in Table 1. The aluminum has a minimum surface oxide due to the helium atomization process. Other aluminum particle sizes (3, 10, 30 and 95 micrometers) and powder types were examined, but the combination in Table 1 proved most successful in forming the Ni_3Al compound. For the other aluminides, small particle sizes proved generally most useful.

As part of this research the Ni:Al stoichiometry was varied from 84 to 90 wt.% Ni; the Ni_3Al stoichiometry corresponds to 86.7 wt.% Ni. The powders were mixed for 30 minutes in a turbula mixer. Various milling times were also applied to the powder using a high intensity vibratory mill to attain mechanical alloying. The carbonyl nickel powder is spiky and agglomerated, giving clusters over 20 micrometers is size. The mixed powders were compacted using a pressure between 200 to 330 MPa either by uniaxial die pressing or cold isostatic compaction, giving typical green densities near 70% of theoretical. Compact geometries included cylinders, transverse rupture bars, and flat tensile specimens.

Sintering was performed in a horizontal laboratory tube furnace capable of 1500°C and several atmospheres, including vacuum, dry argon, and dry hydrogen. Typically the specimens were loaded into an alumina crucible and inserted into a cold furnace. For vacuum sintering a pressure of 7×10^3 Pa was typical. Variations in degassing, heating rate, maximum temperature, and hold time were explored using either manual or automatic controls. The actual sample temperature was not measured, although parallel differential thermal analysis indicates considerable self-heating during sintering with temperatures exceeding 1300°C. From the reaction enthalpy and heat capacity the maximum self-heating is estimated at 1500 K. Through several experiments it was determined that temperatures from 550 to 750 C for times from 10 to 15 minutes gave nearly full density. Indeed, higher temperatures sometimes gave lower densities, due to swelling of entrapped gas. After sintering, the samples were furnace cooled. Some material was additionally heat treated at 1350°C for one hour in dry argon to further homogenize the microstructure.

Measurements consisted of shrinkage, densification, density, temperature rise, hardness, bend strength, tensile strength, and tensile elongation. Additionally, fracture surfaces were examined using scanning electron microscopy. X-ray diffraction and transmission electron microscopy were applied to the samples for phase identification and to determine ordering, and electron microprobe analysis was conducted to identify the phases and stoichiometry. Optical metallography provided insight to the phases and pores present during and after reactive sintering. Dilatometry and differential thermal analysis were employed to identify reaction temperatures and assess the speed of the reaction. In all cases, these analyses were performed using standard procedures typically with computer interfaced data acquisition.

Powder injection molding provides a novel and low-cost process for shaping composites from mixtures particles and ceramic whiskers. A schematic for the envisioned fabrication process is illustrated in Figure 5. In passing though an flow reduction or flow expansion area, the viscous mixture of particles and whiskers will undergo flow orientation as sketched in Figure 6. Under conditions of contraction flow, the acceleration of the mixture will tend to orient the whiskers along the flow direction, while an expanding flow will give perpendicular orientation. As illustrated in Figure 7, powder injection molding is a natural route to the fabrication of composites, since a wide range of metal-ceramic-polymer compositions are possible using this technology. For the composites, various ceramic particles, whiskers, and fibers were incorporated into the powder mixture, including Y_2O_3, Al_2O_3, TiB_2, and SiC. The composites included up to 30 vol.% ceramic phase. The particles were directly mixed with the elemental particles. The whiskers were aligned in the green microstructure using powder injection molding techniques with various wax-polymer binders. The fibers were manually aligned in the green microstructure. Debinding was by wicking and thermal degradation at temperatures below 500°C [9,20].

RESULTS

The initial results will emphasize the fabrication of monolithic Ni_3Al since this teaches the basic principles of aluminide fabrication using a transient liquid phase (reactive sintering) cycle. Beyond this detail the processing routes for several other aluminides and composites will be introduced on a selected basis.

Mechanical alloying resulted in agglomeration of the powders. As a consequence there was more difficulty in sustaining the reaction and attaining densification. Consequently, unmilled powders were used in the balance of the research.

The atmosphere effect on sintered density is shown in Figure 8, again using the 15 micrometers aluminum powder. With

the 3 K/min heating rate the samples sintered in argon and hydrogen swelled, resulting in low sintered densities. At a heating rate of 30 K/min densification occurred in all atmospheres, giving theoretical densities of 97.5% in vacuum, 96.4% in hydrogen and 93.1% in argon.

In light of the self-heating during reaction, experiments were performed to determine the maximum temperature needed for densification. Figure 9 shows example results for a 30 K/min heating rate to various maximum temperatures with a subsequent 15 minute hold time using three aluminum particle sizes. Temperatures below 550°C give higher porosities, most likely because no liquid is formed. At temperatures in the 550 to 600°C range there is good densification. With higher temperatures there is a gradual swelling phenomenon. Thus, the optimal reaction initiation temperature is relatively low. Note that generally the 3 micrometers aluminum powder gives less densification than the 30 micrometers powder. Indeed, the 15 micrometers aluminum powder proved optimal as illustrated in Figure 10. This figure further demonstrates the aluminum particle size effect by showing the final porosity versus aluminum particle size for compacts sintered at temperatures ranging from 550 to 750°C. A particle size near 15 micrometers is best, giving a final porosity less than 3%.

All of the above results are for a 3:1 atomic ratio of Ni to Al. Experiments were conducted to determine the effect of initial stoichiometry on the product using 10 micrometers aluminum powder. Maximum temperatures of 600 and 700°C were employed along with a 15 minute hold and 30 K/min heating rate in vacuum. Figure 11 shows the final porosity versus nickel content. A dramatic change in behavior exists near the intermetallic compound stoichiometry. The compacts slumped with the highest aluminum contents; thus, the reactive sintering process appears best suited to compositions close to the Ni$_3$Al stoichiometry.

After reactive sintering with a transient liquid phase, the microstructure shows a small amount of porosity and usually a major phase and possibly minor phases of incompletely reacted material. For stoichiometric Ni$_3$Al, the grain size after sintering is approximately 30 micrometers. The bulk hardness was 52 HRA and the microhardness was measured as 264 Knoop (100 g load), which agrees favorably with a value of 240 measured on a hot isostatically compacted and extruded prealloyed powder compact.

Chemical analysis after sintering gave the composition as 12.2% Al, 87.6% Ni (76.8 at.% Ni), with 0.02% Fe, 0.01% Si, 482 ppm O and 420 ppm C. Electron microprobe analysis was used to identify the two phases, giving Ni3Al as the major phase with an aluminum level of 24.3 at.%. The minor phase had an aluminum content of 34.8 at.%, approximately corresponding to the Ni$_2$Al$_3$ compound. Since the Ni$_2$Al$_3$ compound is unstable at temperatures over approximately 740°C, the reactive sintered material was annealed at 1350°C for one hour to attain homogenization. Microprobe scans confirmed the composition was uniform throughout the sample after annealing. Transmission electron microscopy substantiated that the product was ordered Ni$_3$Al.

Differential thermal analysis and dilatometry isolated the character of the reactive sintering process. Figure 12 shows dilatometer and differential thermal analysis scans performed on stoichiometric green powder compacts. In the unreacted powder a large exotherm was evident at approximately 600°C, demonstrating the onset of reactive sintering. This is slightly higher than the temperature of 550°C which gave good sintering. In the reacted sample, only an endotherm is evident when the sample melts, indicating total consumption of the ingredients in the reactive sintering process. The first eutectic temperature in the aluminum-nickel system is at 640°C and aluminum melts at 660°C; thus, the exotherm occurs prior to liquid formation and the compact undergoes selfheating, leading to rapid liquid formation. The dilatometry results correlated with the differential thermal analysis, indicating the reaction begins below approximately 600°C. Furthermore, under optimal conditions the duration of the reaction appears to be approximately two seconds. Consequently, studies involving time at the maximum temperature were not useful.

As a variant, elemental powders were mixed, cold isostatically compacted, evacuated, and heated under pressure using a hot isostatic press. This process is termed reactive hot isostatic pressing (RHIP). Using the same mixed elemental powders and a maximum temperature of 1100°C, pressure of 172 MPa, and hold time of 1 h resulted in full compact density. The final microstructure is shown in Figure 13, where the predominant phase is Ni$_3$Al, with some Ni$_2$Al$_3$ present. As noted above, this latter phase could be removed by annealing. With the successful development of reactive sintering and reactive hot isostatic pressing for Ni$_3$Al, some mechanical property assessments were performed. A summary of results is provided in Table 2. Improved properties were gained with boron doping, low temperature degassing, and post-sintering heat treatments. With boron doping at approximately the 0.1% level, and refined processing, the reactive sintered product proved to be superior to that possible using fusion metallurgy. Furthermore, preliminary oxidation tests indicate good resistance up to 900°C.

These results on Ni_3Al provide a basis for investigation of reactive sintering and reactive hot isostatic compaction of several other aluminides and intermetallic matrix composites. The many results on these systems can not be detailed here; however, in most instances direct variants on the above sintering processes have proven successful [21]. For example, composites with a Ni_3Al matrix reinforced with A120 whiskers have been fabricated using RHIP at 800°C, 180 MPa, for 0.5 h. After RHIP the compact is fully dense, but the microstructure is inhomogeneous. This indicates that pressure inhibits capillary induced liquid flow that normally occurs in reactive sintering. As indicated in Table 3, the composite showed increased strength, but decreased ductility as the alumina content increased. Examination of the fracture surface in Figure 14 shows preferential failure along the whisker-matrix interface. Other composites were fabricated using SiC fibers as reinforcing phases. During the reactive sintering step, the Ni_3Al attacked the SiC, leading to serious fiber degradation. Accordingly, the SiC fibers were coated with Y_2O_3 using chemical vapor deposition. With this coating the fiber successfully survived reactive sintering as illustrated by the fracture in Figure 15. This scanning electron micrograph shows the carbon core of the SiC fiber, and minimal attack at the fiber-matrix interface.

With $NbAl_3$ best sintering densification occurs with a 9 micrometer niobium powder formed by hydride-dehydride and a 30 micrometer aluminum (helium atomized) powder. The mixed powders are compacted at 200 MPa giving a 77% green density, heated to 500°C for degassing, then heated at 15 K/min to 1200°C and held at that temperature for 1 h. The resulting product is 95% dense and essentially pure $NbAl_3$. Reactive hot isostatic compaction follows a similar processing route with a 170 MPa pressure giving 98% density. The incorporation of 30 vol.% Al_2O_3 whiskers gives a composite with a Rockwell hardness of 87 HRA in contrast with HRA 72 for the monolithic $NbAl_3$. Likewise, similar processing has taken place to optimize the reactive consolidation of other aluminides.

Figures 16 and 17 show two other examples of the products from our powder processing research. Figure 16 is a full density composite of NiAl with TiB_2 as a reinforcing phase. This was fabricated using reactive hot isostatic pressing of elemental nickel and aluminum powders containing precompounded titanium diboride. The TiB_2 inhibits grain growth and contributes to substantial strengthening of the NiAl compound. Figure 17 shows the final microstructure of TiAl formed by reactive sintering followed by hot isostatic compaction. The composition contains 60 wt.% titanium and was formed by reacting elemental powders, milling the powders and hot isostatic compaction at 1350°C, 145 MPa for one hour. The product contains some oxides, but is otherwise dense and reasonably high in strength and exhibits some ductility.

DISCUSSION

The reactivity of the nickel and aluminum powders results in relatively high sintered densities with a low apparent sintering temperature and short sintering time. The high final densities occur because a transient liquid is present during the sintering cycle. Processing conditions which influence the reaction between the constituent powders alter the amount, distribution, and duration of the liquid. In transient liquid phase sintering, these factors are critical to the final sintered density and mechanical properties [11-13]. However, unlike other sintering studies, time at temperature is not a significant factor since the process occurs rapidly once the liquid forms. The role of the various process parameters can be explained in terms of their effects on the liquid phase.

Milling the powders decreased the sintered density because the liquid formed discontinuously in the microstructure. Also, an increase in the aluminum-nickel interfacial area due to milling increased the solid-state interdiffusion during heating, thereby reducing the amount of liquid during the reaction. Because of milling there is initial liquid and it is consumed faster during sintering. This concept is substantiated by the particle size experiments shown in Figure 10. A small aluminum particle size gives more rapid reaction (more interfacial area) and less densification. A coarse aluminum powder gives a poor distribution of liquid in the microstructure.

At the stoichiometric composition, aluminum constitutes 34 vol.% of the solid structure. This is insufficient to form an interconnected network of aluminum unless the aluminum particle size is less than the nickel particle size [10]. In the green compact, the nickel agglomerates are approximately 30 micrometers in intercept length, corresponding to a 45 micrometers diameter. According to Biggs [22], a particle size ratio of at least 2.4:1 (major phase diameter to minor phase diameter) is required at 34 vol.% to form a connected network in the minor phase. Thus, for 45 micrometers nickel agglomerates, an aluminum particle size below 19 micrometers is required. The optimal particle size for the aluminum (15 micrometers) was in agreement with this value. Thus, a connected aluminum matrix with minimal interfacial area is required for densification. Milling decreases the nickel particle size, thereby disrupting the aluminum connectivity.

The sintering atmosphere role in determining the sintered density is explained by heat conduction and entrapped gas effects. Heat is carried away from the compact during reaction by the higher thermal conductivity of a gas versus vacuum. Furthermore, because of the speed of the reaction, there is no time for adsorbed vapors and atmosphere captured in the pores to escape. Hydrogen has a higher solubility in Ni_3Al than argon. Thus, with hydrogen trapped in the pores there is some opportunity for gas escape even after the pores have sealed during densification. An examination of Figure 8 shows that hydrogen was better than argon with both heating rates; however, vacuum is superior, especially for TiAl, NbAl$_3$, and TaAl$_3$.

Heating rate effects on transient liquid phase sintering have been explained based on solid state interdiffusion prior to liquid formation [11-13]. With a slow heating rate there is more solid state reaction with subsequently less liquid. Indeed, the intermetallic products from solid state interdiffusion may actually inhibit liquid formation at the reaction temperature. Typically, higher heating rates are beneficial when sintering involves a transient liquid. However, there is a limit to the benefit of rapid heating rates. Too rapid a heating rate gives a loss of process control, and with massive samples proves difficult to sustain with any uniformity. Additionally, as the heating rate increases the reactivity of the liquid likewise increases, thereby decreasing process control. Hence, intermediate heating rates prove most reasonable.

A temperature over 550°C is required to optimally react nickel and aluminum powders. Higher temperatures are not of benefit since the reaction is fairly complete in short times as soon as a temperature near 600°C is attained. The calculated maximum 1500 K heating from the exothermic reaction is more than sufficient to attain the 640°C eutectic from a 550°C initiation temperature. Thus, the reaction is probably spontaneous during heating, independent of the final temperature and hold time. The heating rate is important only in its effect on outgassing and interdiffusion prior to the reaction. Likewise, particle size is of importance in determining the distribution of liquid in the microstructure. As sketched in Figure 18, if the liquid forms in isolated pools, then no long range capillary action is possible and swelling is expected [10-13,23]. Alternatively, a connected aluminum matrix will lead to rapid densification because of the long range capillary action. This concept also helps explain the stoichiometry results. With an excess of aluminum there is more liquid and an excess over that required to form Ni_3Al. The final porosity is fairly constant with an excess of aluminum, but slumping and shape loss are observed at 84% Ni. Alternatively, an excess of nickel reduces the amount of liquid and decreases the aluminum connectivity, thereby separating the liquid pools within the compact. For the experiments with a 10 micrometers aluminum powder, the calculated loss of connectivity for the aluminum would occur between 87 and 90 wt.% Ni, in agreement with the experimental observation. As a consequence, the high nickel content compositions fail to densify because of less liquid and a decreased connectivity of aluminum in the microstructure.

The composition of the second phase in the as-sintered compacts corresponds to Ni_2Al_3. This compound is stable over the approximate composition range of 32 to 37 at.% aluminum, which agrees well with our determination of 34.8 at.% Al. The one hour heat treatment at 1350°C effectively dissolves this phase, leaving the equilibrium compound Ni_3Al. The formation of the Ni_2Al_3 phase indicates that the reaction is not directly from nickel and aluminum to Ni_3Al, but involves formation of intermediate compounds. Removal of the residual porosity can be facilitated by hot isostatic compaction. With sintered densities over 92% of theoretical, the pore structure consists of closed pores and responds to containerless hot isostatic compaction to full density.

Variants on this reactive sintering process has been extended to several other intermetallic compounds. The elemental powders are available and provide experimental flexibility for the production of novel compositions and composites. Table 3 provides a summary of some of the other aluminides and aluminide-matrix composites that have been fabricated using similar processes.

SUMMARY

Much progress has been made in applying reactive sintering to the fabrication of aluminide intermetallics and composites using mixed elemental powders. Densities in excess of 97% of theoretical are possible through appropriate selection of particle sizes, composition, green density, heating rate, atmosphere, maximum temperature, and hold time. Although not all of these factors have been detailed here, the concept behind this exciting development has been outlined. It is clear that the sintered density depends on the amount of liquid formed at the first eutectic temperature and the connectivity of this liquid. In this sense, reactive sintering is analogous to transient liquid phase sintering. Because the liquid persists for only a short time, it is important that the several process parameters be carefully controlled to optimize the sintered density. Subsequent processing (heat treatment and containerless hot isostatic compaction) can then be used to remove the residual

porosity and homogenize the compact. A key to success is the formation of a fully interconnected liquid phase. This dictates the amount and particle size distribution of the constituents needed for optimal densification. The fabrication process is appropriate for the fabrication of intermetallic compounds and intermetallic-matrix composites.

ACKNOWLEDGMENTS

REFERENCES

1. C. C. Koch, C. T. Liu and N. S. Stoloff (eds.), High-Temperature Ordered Intermetallic Alloys, Materials Research Society, vol.39, Materials Research Society, Pittsburgh, PA (1985).

2. N. S. Stoloff, Inter. Metal Rev., 29:123-135 (1984).

3. W. M. Schulson, Inter. J. Powder Met., 23:25-32 (1987).

4. K. Vedula and J. R. Stephens, Powder Metallurgy 1986 State of the Art, W. J. Huppmann, W. A. Kaysser and G. Petzow (eds.), Verlag Schmid, Freiburg, West Germany, pp.205-214 (1986).

5. A. Bose, B. Moore, R. M. German and N. S. Stoloff, J. Metals, 40(9): 14-17 (1988).

6. D. M. Sims, A. Bose, and R. M. German, Prog. Powder Met., 43:575-596 (1987).

7. B. H. Rabin, A. Bose and R. M. German, Modern Developments in Powder Metallurgy, vol.21, P. U. Gummeson and D. A. Gustafson (eds.), Metal Powder Industries Federation, Princeton, NJ, pp.511-529 (1988).

8. A. Bose, B. H. Rabin and R. M. German, Powder Met. Inter., 20(3):25-30 (1988).

9. R. M. German and A. Bose, Mater. Sci. Eng., A107:107-116 (1989).

10. R. M. German, Liquid Phase Sintering, Plenum, New York, NY (1985).

11. W. H. Baek and R. M. German, Inter. J. Powder Met., 22:235-244 (1986).

12. W. H. Baek and R. M. German, Powder Met. Inter., 17:273-279 (1986).

13. R. M. German and J. W. Dunlap, Metall. Trans. A, 17A:205-213 (1986).

14. P. P. Turner and L. J. Jones, U.S. Patent 2,755,184, 17 July 1956.

15. E. Fitzer, U.S. Patent 2,877,113, 10 March 1959.

16. S. T. Zegler and J. B. Darby, U.S. Patent 3,084,041, 2 April 1963.

17. R. Maier, U.S. Patent 3,260,595, 12 July 1966. W.

18. J. Werner, M. C. McIlwain and J. P. Hammond, U.S. Patent 3,288,571, 29 November 1966.

19. L. S. Williams, U.S. Patent 3,353,954, 21 November 1967.

20. R. M. German, Powder Injection Molding, Metal Powder Industries Federation, Princeton, NJ (1989).

21. R. M. German, A. Bose and N. S. Stoloff, "Powder Processing of High Temperature Aluminides," presented at the 1988 Materials Research Society Meeting, Boston, December 1988, in press.

22. D. M. Biggs, Metal-Filled Polymers, S. K. Bhattacharya (ed.), Marcel Dekker, New York, NY, pp.165-226 (1986).

23. D. J. Lee and R. M. German, Inter. J. Powder Met. Powder Tech., 20:9-21 (1984).

A+B → AB+heat (mixed powder)
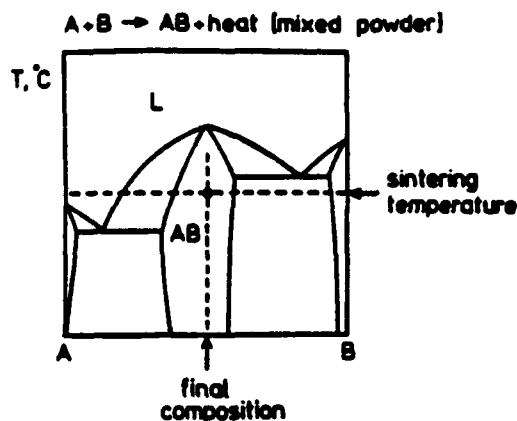
Fig. 1 A schematic binary phase diagram showing the characteristics necessary for formation of the AB intermetallic compound from mixed A and B constituent powders.
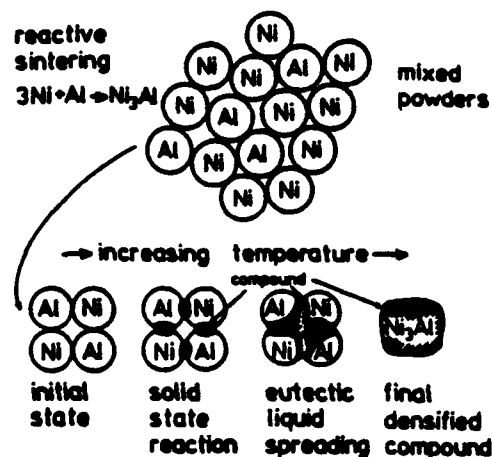
Fig. 2 The aluminum-nickel binary phase diagram.
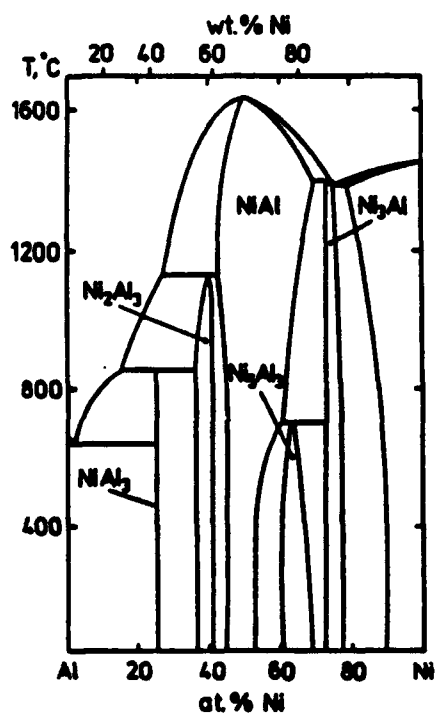
Fig. 3 A sketch of the reactive sintering process for forming Ni₃Al from mixed elemental Ni and Al powders. As temperature increases, first a solid state reaction occurs, with subsequently a rapid reaction when the eutectic liquid forms. The final product is a densified compound.

heat treat 1350°C, 1h, Ar
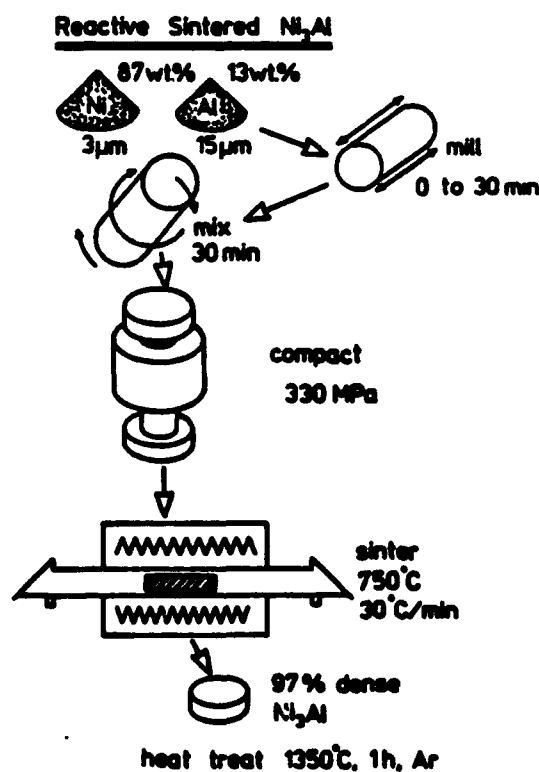
Fig. 4 An outline of the steps involved in forming reactive sintered Ni₃Al from mixed and milled elemental powders.

318
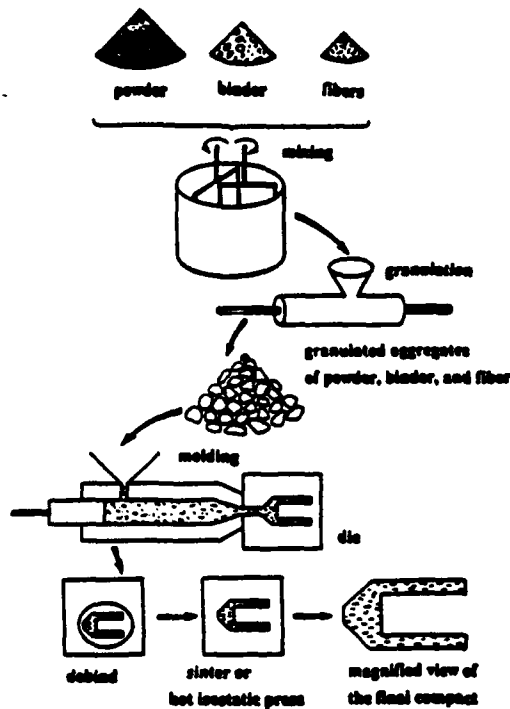
Fig. 5. A schematic of the envisioned powder injection molding process for forming aluminide matrix composites.

random input ⟶ oriented output

Fig. 6. Flow orientation of injection molded composite feedstocks, showing the possible control of whisker orientation by contraction or expansion of the flow channel.

Fig. 7 A sketch of the possible composite compositions (metal, ceramic, and polymer) that can be processed using powder injection molding techniques.
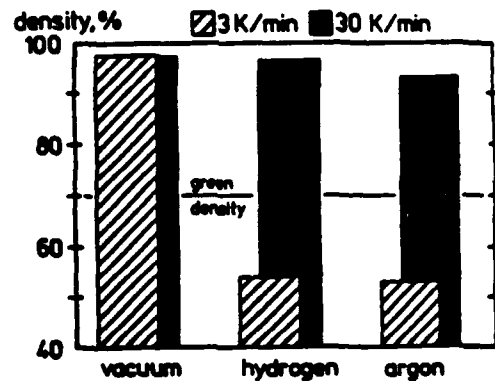
Fig. 8 Sintered density shown for two heating rates and three atmospheres for unmilled 15 micrometers aluminum.
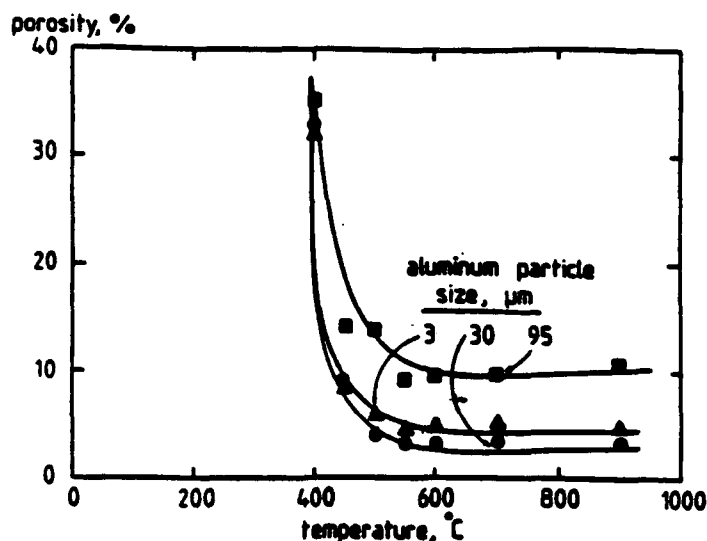
porosity, %

Fig. 9 The effect of the maximum sintering temperature
on porosity for three aluminum particle sizes.
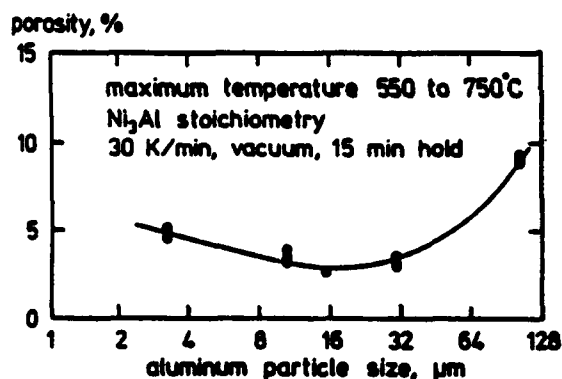
porosity, %

Fig. 10. Porosity as a function of the aluminum particle
size for various maximum furnace temperatures
between 550 and 750°C.
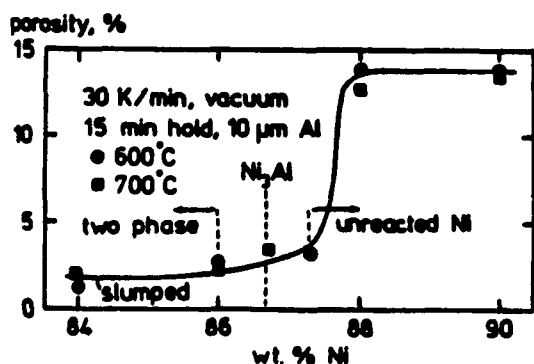
porosity, %

Fig. 11 The stoichiometry effect on porosity for reaction
sintered compositions near Ni$_3$Al using two maximum
temperatures.

shrinkage, %

heat flow
mJ/s
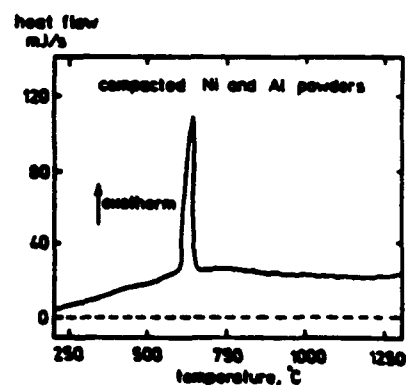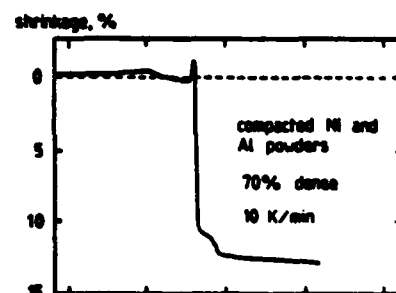
Fig. 12 The upper curve is the dilatometer scan and the
lower curve is the differential thermal analysis scan for
mixed nickel and aluminum powders showing the
reactive sintering exotherm at approximately 600°C.
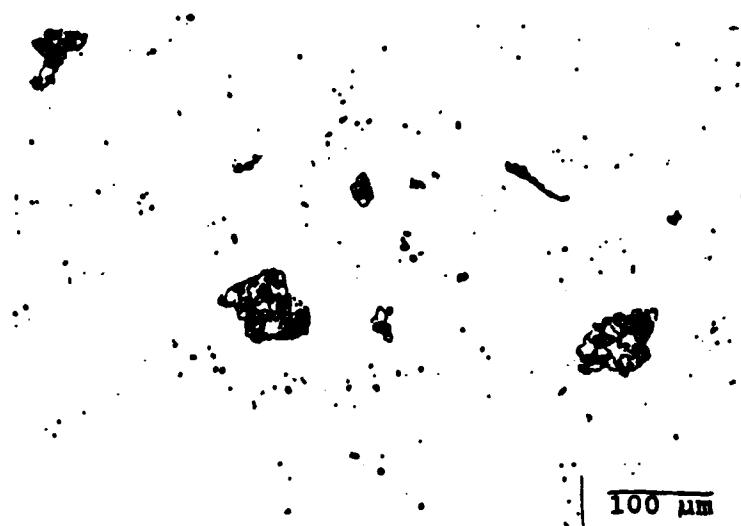
Fig. 13 An optical micrograph of full density product formed by reactive hot isostatic compaction of elemental nickel and aluminum powders, producing a major phase of Ni_3Al with a minor phase of Ni_2Al_3.

Fig. 14 A scanning electron micrograph of the fracture surface of a composite consisting of Ni_3Al as the matrix and Al_2O_3 whiskers, fabricated by RHIP.
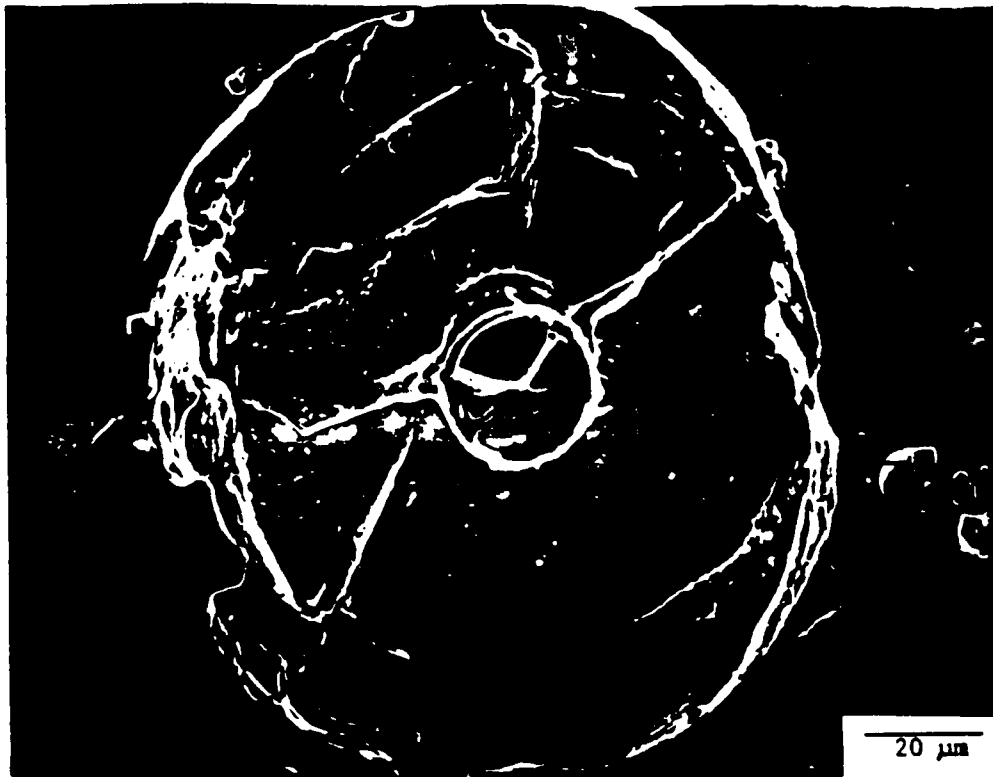
Fig. 15 Scanning electron micrograph of the interfacial
region in a Ni_3Al matrix phase composite with a yttria
coated SiC reinforcing fiber fabricated with minimal
fiber damage using reactive sintering.
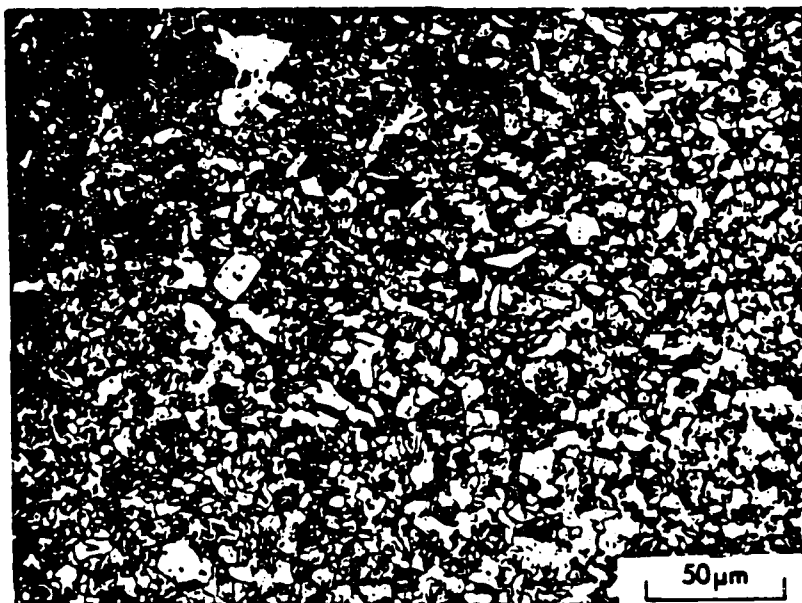
Fig. 16 An example microstructure of a NiAl matrix
composite reinforced with TiB_2 fabricated using reactive
hot isostatic compaction.
RHIP processed NiAl + TiB_2

Fig. 17 Optical micrograph of TiAl fabricated by a hybrid reactive sintering and reactive hot isostatic compaction process, using elemental powders and a maximum temperature of 1350°C and 145 MPa pressure. HIP TiAl (60 wt.% Ti, reactd milled, HIP) cycle = 1350 C, 1h, 145 MPa
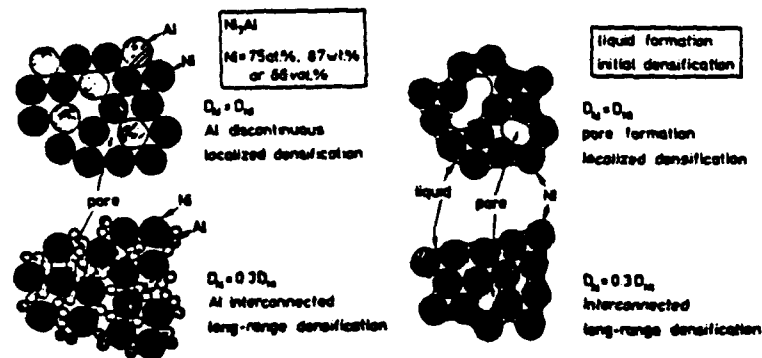
Fig. 18 A comparison of the green microstructure effect on local liquid formation and densification. Densification occurs when the Ni and Al are connected in the green microstructure prior to reactive sintering.

Table 1 Experimental powder characteristics

property	nickel	aluminum	niobium	titanium
vendor	INCO	Valimet	NRC	Micron Metal
designation	123	H-15	---	-325 mesh
powder type	carbonyl	gas atomized	hydride	sponge
purity, %	99.99	99.7	99.4	99.0%
FSSS size, micrometers	2.8	15.0	8.8	20
major impurities, ppm	Ca-10	Fe-1200	Ta-0.11%	O-0.15%
	Fe-30	water-200	O-0.38%	Cl-0.25%

Table 2 Mechanical properties of reactive sintered Ni3Al

process	yield strength, MPa	ultimate strength, MPa	elongation %
reactive sintered	270	270	1
same, B doped	353	682	12
RHIP, 800°C, 0.5 h, 104 MPa	---	363	0
same, B doped	265	727	10
RHIP, 1100°C, 1 h, 170 MPa	494	677	2
same, B doped, heat treated	591	827	5

Table 3 reactive processing results for aluminides and aluminide-matrix composites

compound	additive	process details	fractional density	strength, MPa
Ni$_3$Al	0.1% B	RHIP 1100°C, 1 h, 170 MPa	1.00	677
Ni$_3$Al	3% Al$_2$O$_3$	RHIP 800°C, 1 h, 170 MPa	1.00	548
Ni$_3$Al	20% Y$_2$O$_3$	RHIP 800°C, 1 h, 170 MPa	1.00	464
NiAl	-	RS 10% prealloyed 800°C	0.98	890 (c)
NiAl	15% TiB$_2$	RHIP 15% prealloyed 1200°C, 1 h, 170 MPa	1.00	1060 (c)
NiAl	20% TiB$_2$	RHIP 15% prealloyed 1200°C, 1 h, 170 MPa	1.00	1350 (c)
NbAl$_3$	-	RS 1200°C, 1 h	0.95	-
NbAl$_3$	30% Al$_2$O$_3$	RHIP 1200°C, 4 h, 170 MPa	0.98	-
TaAl$_3$	-	RHIP 1200°C	0.98	531
TaAl$_3$	8 at.% Fe	RHIP 1200°C	0.98	372
TiAl	-	RHIP 1370°C, 4 h, 170 MPa	1.00	533
TiAl	30% Al$_2$O$_3$	RHIP 1370°C, 3 h, 186 MPa	1.00	-

(c - indicates compressive test, all others are tensile)

FABRICATION OF INTERMETALLIC MATRIX COMPOSITES BY POWDER

INJECTION MOLDING (PIM) TECHNIQUES

D.E. Alman and N.S. Stoloff

Department of Materials Engineering
Rensselaer Polytechnic Institute
Troy, New York 12180-3590

Powder injection molding of the intermetallic matrix composites NiAl/
Al$_2$O$_3$ and MoSi$_2$/Al$_2$O$_3$ has been accomplished. The technique permits
alignment of short fibers and the production of near net shape specimens.
However, the volume fraction of reinforcement is limited by the powder
particle size and alignment is not as good as can be accomplished
by lay up of fibers or by liquid infiltration techniques. Binder
characteristics, including the ability to remove the binder, are
critical for success of the molding process. Limited mechanical
properties measurements carried out on injection molded composites
will be compared with properties of composites produced by other
techniques.

INTRODUCTION

Intermetallic compounds with low densities (<7.0 g/cm^3) and high melting temperatures ($>1600^\circ$C) are attractive for potential high temperature structural applications. However, before these compounds can be exploited for this purpose their low toughness and inadequate creep strength must be improved. Composite strengthening, in particular in the form of fibrous reinforcement, is an approach that can improve both toughness and creep strength. Thus, the fabrication and properties of intermetallic matrix composites are under intense investigation, as evidenced by a recent conference devoted to the subject[1]. Melt processing techniques have proven successful for the fabrication of fibrous reinforced intermetallic matrix composites. Walters and Cline[2] fabricated NiAl reinforced with Cr or Mo fibers, by directional solidification of eutectics. Nourbakhsh and co- workers[3-7] used pressure casting techniques to fabricate matrices based on nickel, iron, and titanium aluminides reinforced with Al$_2$O$_3$ continuous fibers. However, as the melting temperature of the matrix increases, powder methods for consolidation of composites become more attractive for obvious reasons.

Powder metallurgical techniques have been developed to fabricate aligned, continuous fibrous reinforced intermetallic matrix composites [8-10]. Ti$_3$Al+Nb reinforced with 40 volume percent SiC (SCS-6) fibers was fabricated by the powder cloth technique, which consists of preparing cloths of intermetallic matrix by rolling powder and a binder into thin sheets[8,9]. These matrix cloths are interspersed with fiber tapes. Once the binder is removed, consolidation of the composite is achieved by vacuum hot pressing. These composites displayed tensile behavior comparable to strengths calculated from the rule of mixtures, at test temperatures from above room temperature to 1100°C. At temperatures where the matrix exhibits limited ductility, fracture surfaces revealed fiber pullout, indicating that composite strengthening did improve fracture resistance. However, the major disadvantage of the powder cloth method is that flat plates only 0.075 cm thick have been produced. Nevertheless, this technique later was employed to fabricate NiAl/SCS-6 composites[11]. Anton[10] produced Al$_3$Ta reinforced with continuous Al$_2$O$_3$(DuPont PRD-166) by infiltrating a fibrous preform with elemental Al and Ta powders. Consolidation occured by reactive hot pressing. At room temperature, in four point bending, the continuous reinforced aligned composite showed improved strength and modulus over the matrix

alone and a random oriented chopped fiber composite. However, the
strengths were less than predicted by rule of mixtures calculations.
The fracture surface was characterized by fiber pullout in regions
were the fibers were agglomerated. The strength and modulus of the
random chopped fiber composite were worse than those of the matrix.
Powder Injection Molding (PIM) has been proposed as a route in which
chopped fibers can be aligned in an intermetallic matrix [12,13].
This method consists of passing a heated mixture of a polymer binder,
a matrix in powder form and chopped fibers through a tapered die
to achieve alignment. The extrusion is performed at temperatures
above the softening point of the polymer binder. With the proper
die design complex shapes can be fabricated. However the major problem
is that continuous reinforced composites can not be produced.
In the previous studies[12,13] no aligned short fibrous intermetallic
matrix composites were consolidated. Instead, powder characteristics
were defined for successful consolidation of composites by this technique.
Fine spherical powders are needed to produce alignment; also, powder
size dictates the volume fraction of reinforcement able to be aligned.
This study, therefore, was undertaken to consolidate intermetallic
matrix composites by PIM and to determine if aligned short fibers
can improve the mechanical properties of intermetallic compounds.

INTERMETALLIC MATRICES STUDIED

Two intermetallic compounds were investigated for matrices, NiAl
and MoSi$_2$. Phase diagrams for both systems are shown in Figure 1a)
and b), respectively. NiAl (ordered B2 crystal structure) was chosen
partly because of a large body of literature that exists detailing
the properties of this compound. Therefore, measurements of properties
can be compared to existing results. Also, beside a high melting
temperature (1640°C) and low density (5.86 g/cm^3), NiAl exhibits
excellent oxidation resistance. Depending on factors such as grain
size, deviations from stoichometery, strain rate, and impurity content,
the ductile to brittle transition has been reported to be between
about 400 and 600°C[18]. MoSi$_2$ (ordered noncubic C11b crystal structure)
warrants study due to its melting point alone (2000°C). It possesses
a low density (6.3 g/cm^3) and has useful oxidation resistance to
1700°C; however it exhibits the pest phenomenon below 600°C. The
ductile to brittle transition temperature of MoSi$_2$ is approximately
1000°C[19].
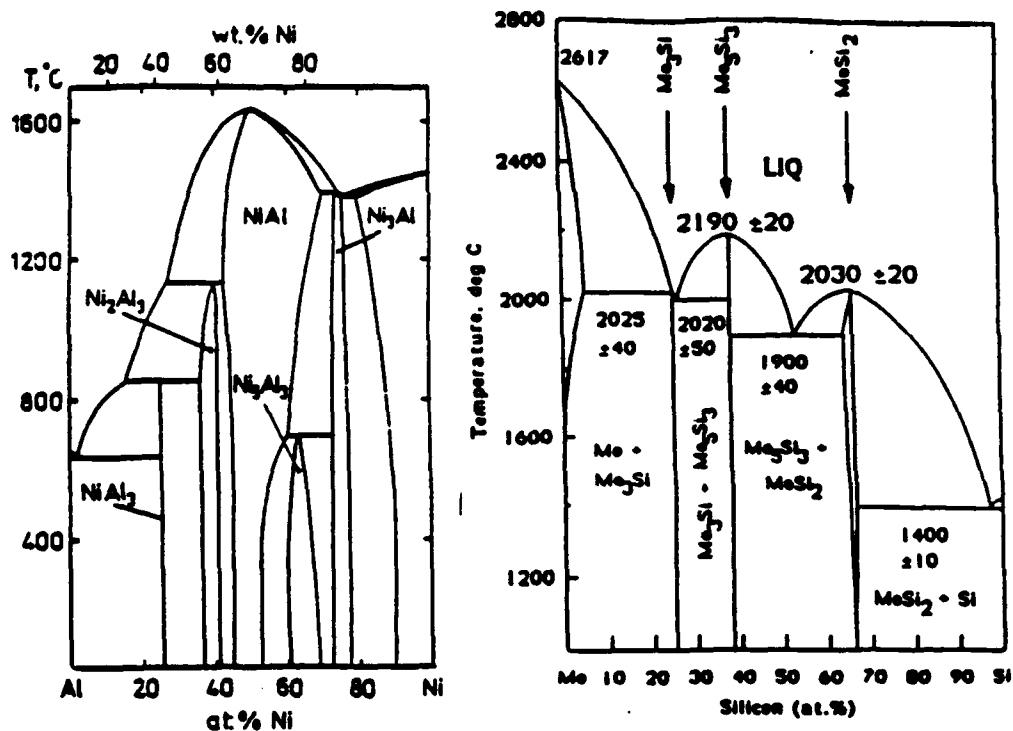
Figure 1   Phase diagrams for systems studied; a)Ni-Al; b)Mo-Si.

EXPERIMENTAL PROCEDURES

NiAl matrix composites were consolidated using reactive synthesis
techniques. Reactive synthesis consists of forming the compound
from elemental powders. During heating of the elemental powders
a transient liquid phase forms which is a consequence of the exotherm
associated with forming the compound. The liquid phase accelerates
diffusion and densification. This type of process also has been
termed self propagating high temperature synthesis (SHS). NiAl was
successfully fabricated by reactive sintering followed by HIP and
exhibited comparable mechanical properties to NiAl fabricated by
other techniques[14]. Since elemental powders are more readily available
in small sizes and spherical shapes than prealloyed powders and small
shperical powders are needed for alignment of fibers by PIM, reactive
synthesis is ideal for coupling with injection molding for the fabrication
of composites. MoSi$_2$ proved difficult to form by reactive processing;[15]
therefore, conventional HIPing of prealloyed MoSi$_2$ powders was employed
for consolidation.

Spherical Ni (Novamet 4SP-10μm) and Al (Valimet HO-3μm) were used
for reactive synthesis of NiAl. A blend of 70 weight percent (51

atomic percent) Ni to 30 weight percent Al was mixed in a turbula type mixer for 1 hour. The NiAl elemental powder was sized by the light scattering method to have an average diameter of approximately 8μm. Irregularly shaped $MoSi_2$ powder was obtained from Pratt and Whitney Aircraft Co. Division of United Technologies Corporation. This powder average diameter, determined by a light scattering technique was 4μm. Chopped Dupont FP Al_2O_3 fibers (density of 3.9 g/cm^3), 20μm in diameter, were used as the reinforcement phase. Fiber aspect ratios ranged between 10 and 100. This fiber was chosen primarily due to its commercial availability. Figure 2 shows SEM micrographs of the fibers and powders. The binder used was based on low molecular weight polypropylene, paraffin, carnauba wax, and stearic acid, and exact composition is proprietary. The softening point of the binder is approximately 90°C.

Uniform dispersion of fibers is necessary for maximum strengthening; therefore, proper blending of the fiber and powder is crucial. The chopped fibers tended to agglomerate, but an alcohol slurry was useful for dispersing the fibers. Appropriate amounts of powder were then added to the slurry of fibers and mixed in a turbula type mixer for 1 hour. The alcohol was then allowed to evaporate. Volume fractions of fibers ranged from 10 to 20 percent. The fiber powder mixture was added to melted binder while being mixed. For small quantities (50 g or less) mixing was performed by hand using a stirring rod. For larger amounts a double planetary type rotating mixer was employed. Typical loading of the feedstock was 70 and 65 percent by volume of solid (powder plus fiber) for NiAl and $MoSi_2$ respectively. For small quantities of material (50 g) the tapered die used for fiber alignment decreased from 1.27 to 0.15 cm. The extruded "wires" 0.15 cm in diameter were carefully placed in a polyeurethane mold and cold isostatically pressed (CIPed) at 208 MPa, to produce a cylindrical specimen 1.27 cm in diameter. This allowed for a significant size sample to be produced. Larger quantities of fiber powder and binder (200 g) were extruded from a heated die that was tapered from 5.08 to 1.27cm. This eliminated the need for CIPing and avoided any misalignment due to errors in placement of the "wires" in the CIP bag. A hand press was utilized for extruding from the dies which were preheated above the softening point of the binder (90°C). A reciprocating screw-type injection molding machine was used to produce
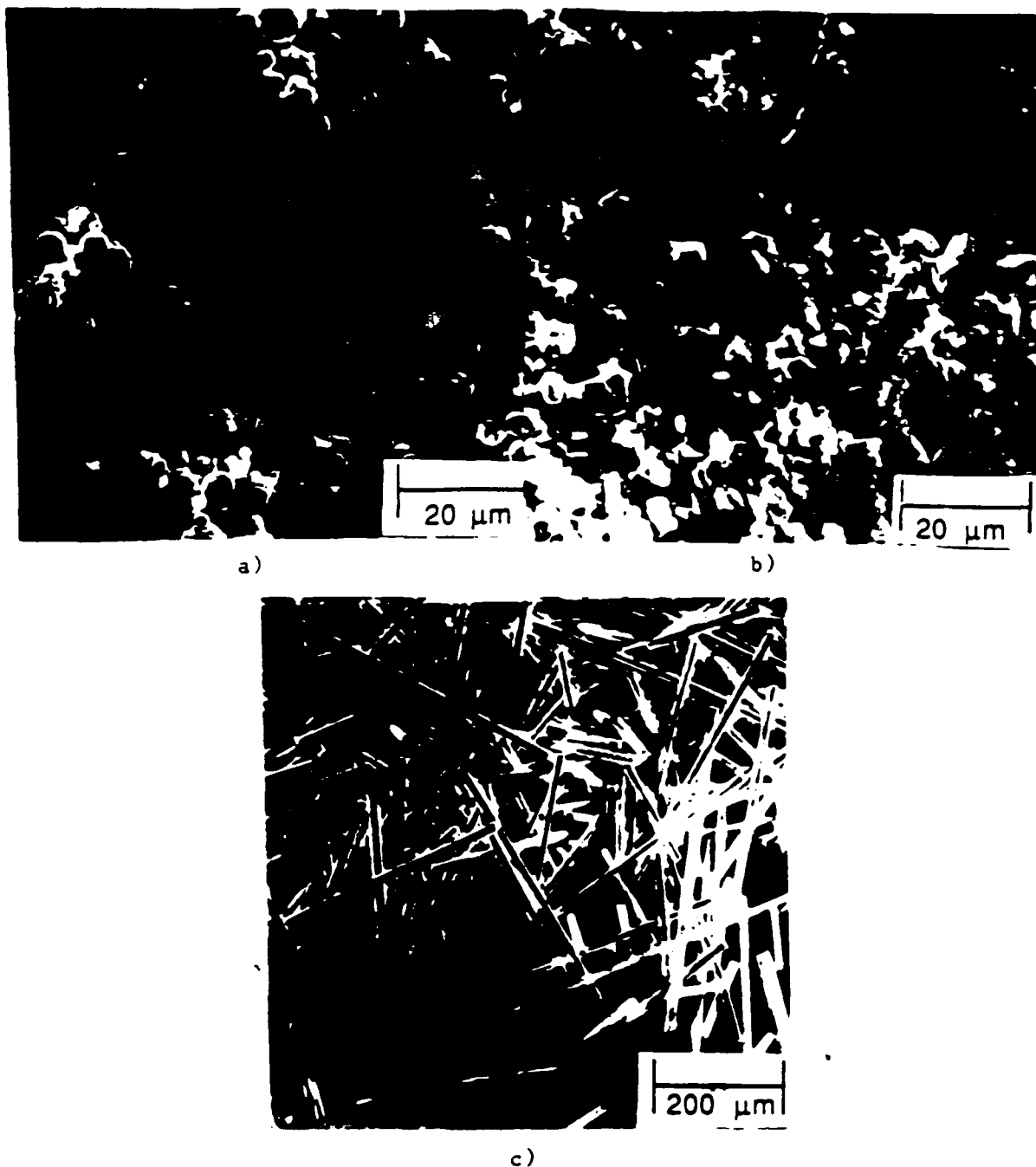
Figure 2   Powders and fibers employed in this study:a)Ni+Al;
b)MoSi$_2$; c)chopped DuPont FP Al$_2$O$_3$ fibers.

near net shape tensile and bend bars.   Figure 3 shows the different
samples produced.

All samples were placed in (Al$_2$O$_3$) wicking powder and debinding
was performed in flowing hydrogen. The debinding cycle consisted
of heating at 2°C/min to 450°C. After 300 minutes the NlAl composites
were allowed to furnace cool. After debinding, NiAl samples were
placed in a vacuum furnace and reactively sintered between 700°C
and 800°C for 15 minutes.

TENSILE BAR
DIE CAVITY

SPRUE/RUNNER/
GATE

BEND BAR
DIE CAVITY

2 cm
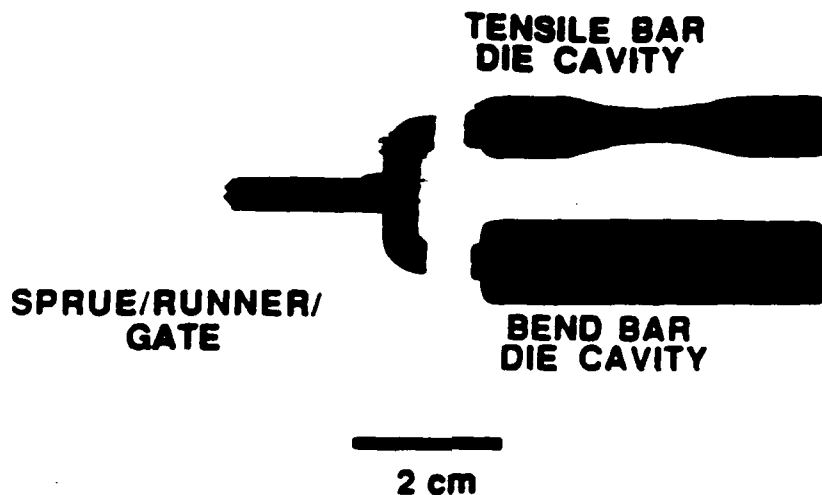
Figure 3   Samples produced by injection molding
machine.

At this point the specimens were prepared for consolidation by HIP.
This includes encapsulation and degassing. Samples were vacuum encapsulated
in stainless steel (304L) for NiAl and, owing to the higher melting
temperature of $MoSi_2$, either Ti or Nb. For Ti cans, the specimen
was wrapped with Nb foil to prevent any reaction between the can
and the specimen. Prior to sealing the can the specimens were outgassed
at 300°C for approximately 600 minutes. The HIPing conditions for
NiAl are as follows: 1200°C; 172 MPa for 60 or 120 minutes. For
$MoSi_2$, the conditions were either 1500°C or 1600°C, for Ti and Nb
cans respectively, and 172 MPa pressure for 2 hour. As a result of
possible thermal expansion mismatch between reinforcement phase and
matrix, cooling from consolidation temperatures may result in cracked
samples. Therefore, depressurization and cooling were carried out
slowly (from temperature to 300°C in 60 min. with the pressure decreasing
only as a result of temperature; over the next 60 min. depressurization
to atmospheric pressure and cooling to room temperature).

Matrix material alone also was consolidated. NiAl was fabricated
by reactive synthesis using the diluted mixture of Ni, Al and NiAl
powder described in a previous publication[14]. This mixture was
CIPed in a cylindrical polyurethane mold bag at 210 MPa. The CIP
bar was encapsulated and HIPed as described above. The $MoSi_2$ powder
did not CIP well; therefore, loose powder was poured into a Nb HIP
can. The can was vibrated for 1 hour to allow for the loose powder
to reach tap density. Samples were HIPed using the conditions listed
above for $MoSi_2$.
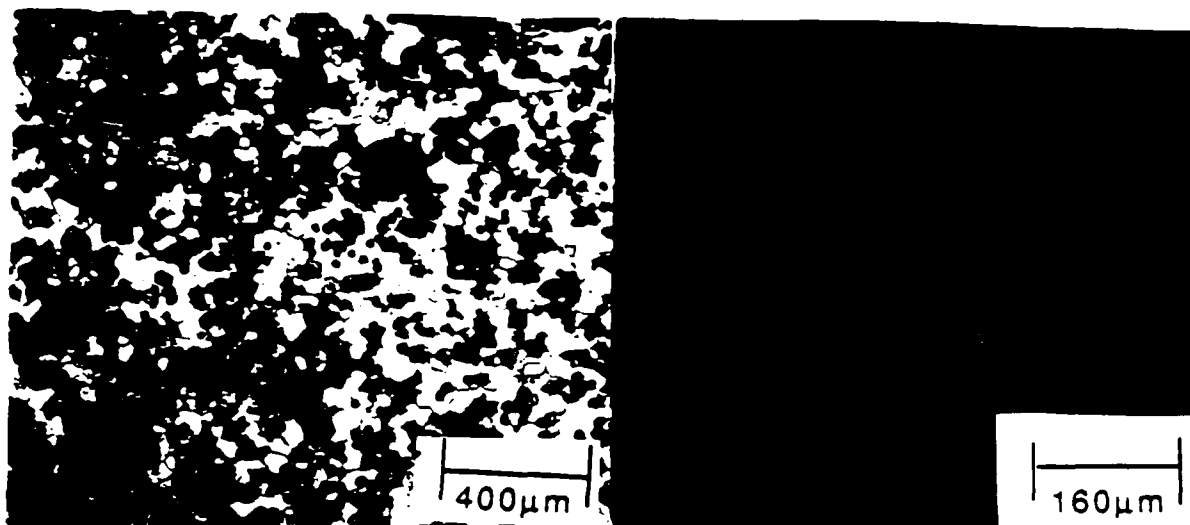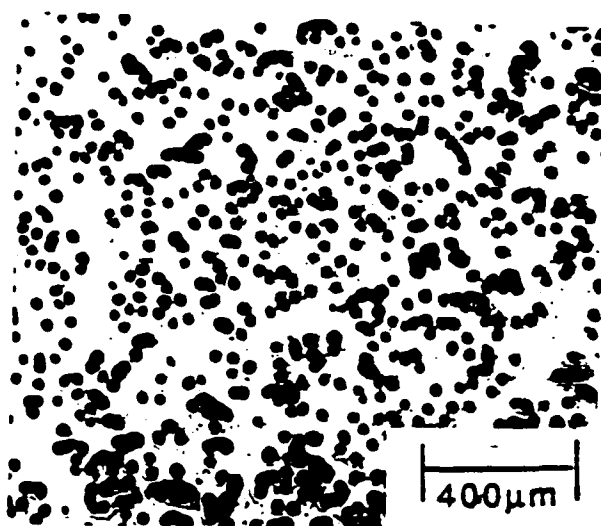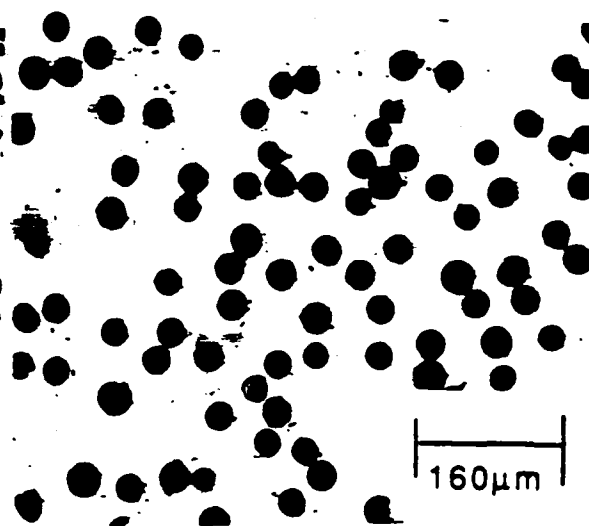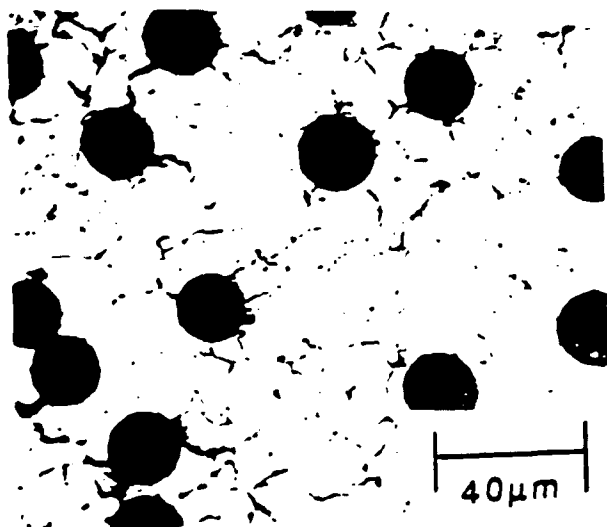
Figure 4 NiAl/15v%FP fabricated by extruding plus CIP method; a)as reactive sintered; b) as reactive sintered; c)as HIPed; d)as HIPed; e)as HIPed; etchant Kallings solution.

RESULTS AND DISCUSSION

Figure 4 shows cross sections of NiAl reinforced with 15v% Al$_2$O$_3$ fibers, produced by extruding from the small die and CIPing the wires together. Porosity remains in the microstructure after reactive sintering (Figs. 4a,b), indicating that pressure is necessary to consolidate the composites. The HIP cycle proved sufficient for densification (Figs. 4c-e).

Figure 5 shows microstructures of as-HIPed NiAl reinforced with 10 and 20 v% Al$_2$O$_3$ fibers. Extrusion was performed with the large die. An increased number of misaligned and agglomerated fibers are present in the 20 as opposed to the 10v% composite.

a)   b)
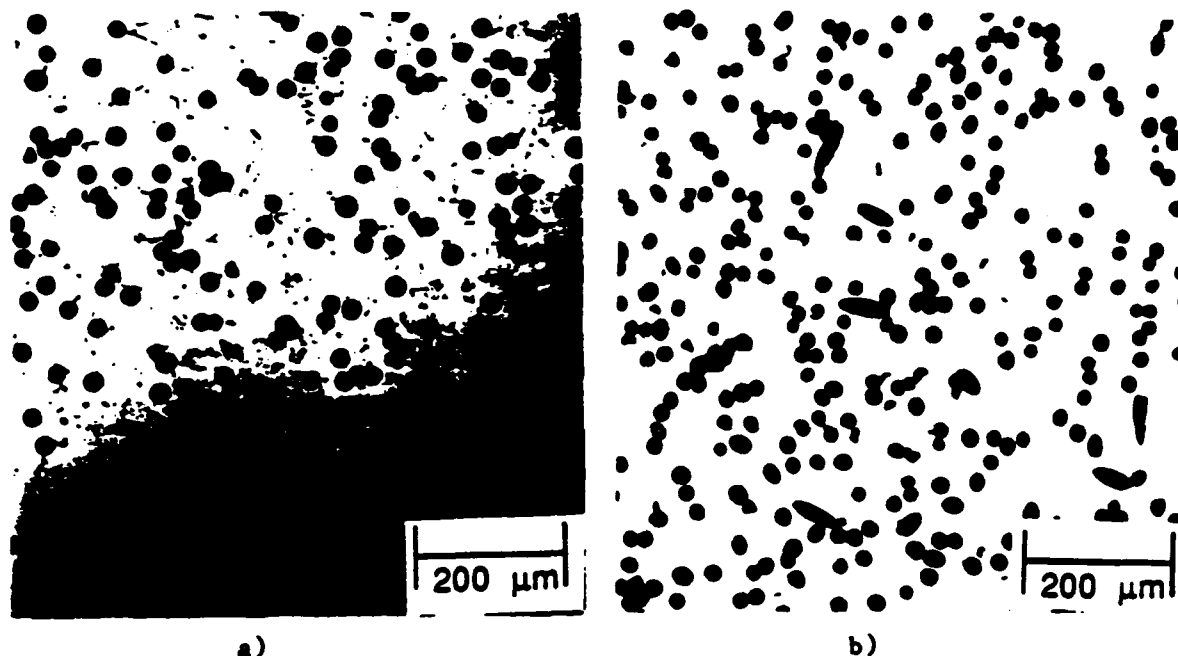
Figure 5   NiAl/FP fibers fabricated by the large extrusion method.
a)NiAl/10v%FP. b)NiAl/20v%FP.

A longitudinal section is shown in Fig 6. Note that the morphology of the fiber ends is either conical or square. This indicates that the alignment is not perfect. If 100 percent alignment existed, all the fiber ends would be square if the section were cut in the plane of the extrustion direction or conical if the section were not in plane. For comparison, a microstructure of Al$_3$Ta reinforced with 40v% Al$_2$O$_3$ fabricated by Anton[10] by hot pressing and sectioned at RPI is shown in Figure 7. Superior alignment was obtained by the hand layup technique of Anton. Another feature to notice, from the microstructures in Figs. 6 and 7, is the number of broken fibers that result from powder processing. It appears that more fibers are damaged in composites fabricated by PIM than by the hand layup technique.
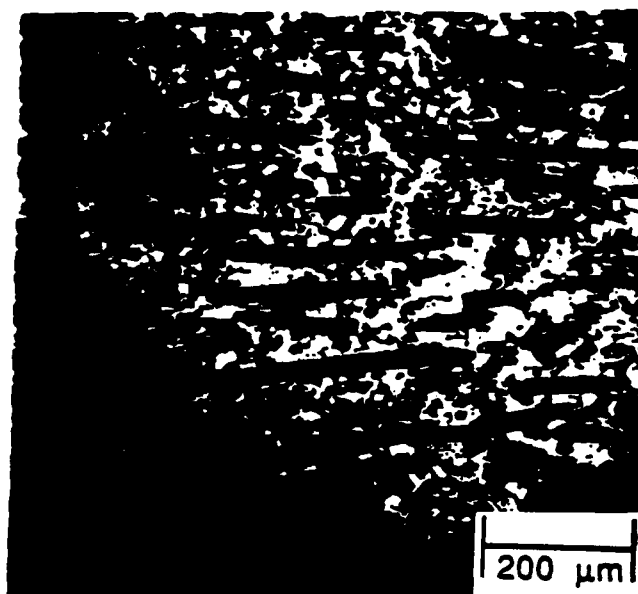
Figure 6   Longitudinal section of
NiAl/15v.FP. Etchant
Kallings solution.
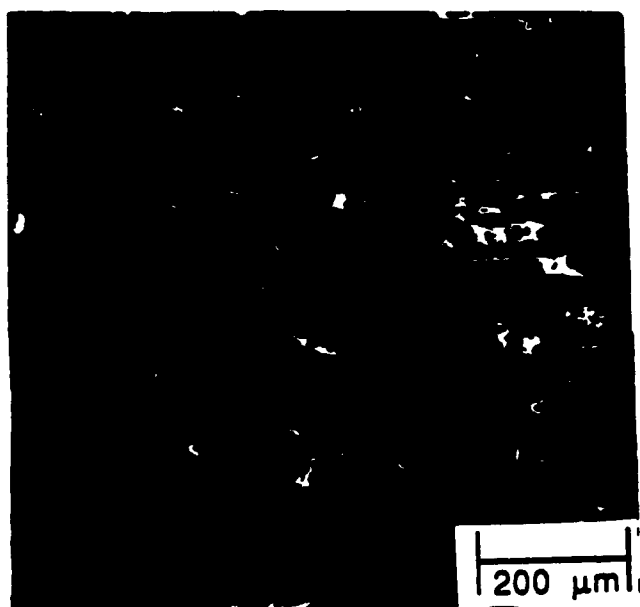
Figure 7   Longitudinal section of
Al₃Ta/40v% PRD-166
Al₂O₃ fibers fabricated
by Anton[10].Secondary
electron image.

The fibers follow the flow of the powder and binder well. Figure
8 shows a macrograph (8a) as well as a cross section (8b) of a reactive
sintered injection molded tensile bar. However, the complex shape
of the tensile bar becomes more difficult to encapsulate and therefore,
to date fully dense specimens have not been obtained.

Figures 4 through 8 indicate that reactive synthesis coupled with
PIM is a viable route for the consolidation of these composites.
The effectiveness of short fibers in improving the mechanical properties
of NiAl was determined by tensile tests. Cylindrical tensile bars,
3.18mm dia, were electrodischarge machined (EDM) from NiAl-15v% Al₂O₃
HIP bars. Tests were performed in air at a strain rate of 1.67×10^{-4}
sec^{-1} on a servohydraulic Instron machine. Prior to testing, the
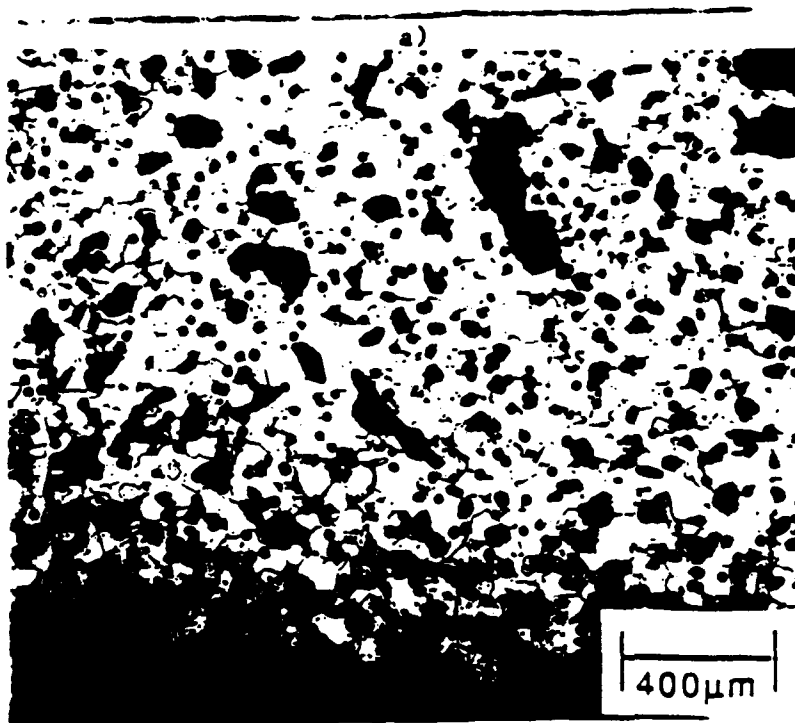
Figure 8   NiAl/10v%FP. a)Injection molded tensile bar. b)As
         reactive sintered microstructure. Etchant Kallings
         solution.

bars were mechanically polished through 9μm diamond. Results at
800°C, which is above the ductile to brittle transition for reactively
synthesized NiAl[14] are reported in Table 1. Modest increases in
strength resulted from the fibers, but the ductility was markedly
reduced. Fracture surfaces for NiAl and the composite are shown
in Figs. 9a) and b) respectively. Fiber pullout is prevalent in the
composite, with some fibers being totally separated from the matrix.
It appears that at this temperature a weak interface exists between
the fiber and matrix. However, a strong interface is required for
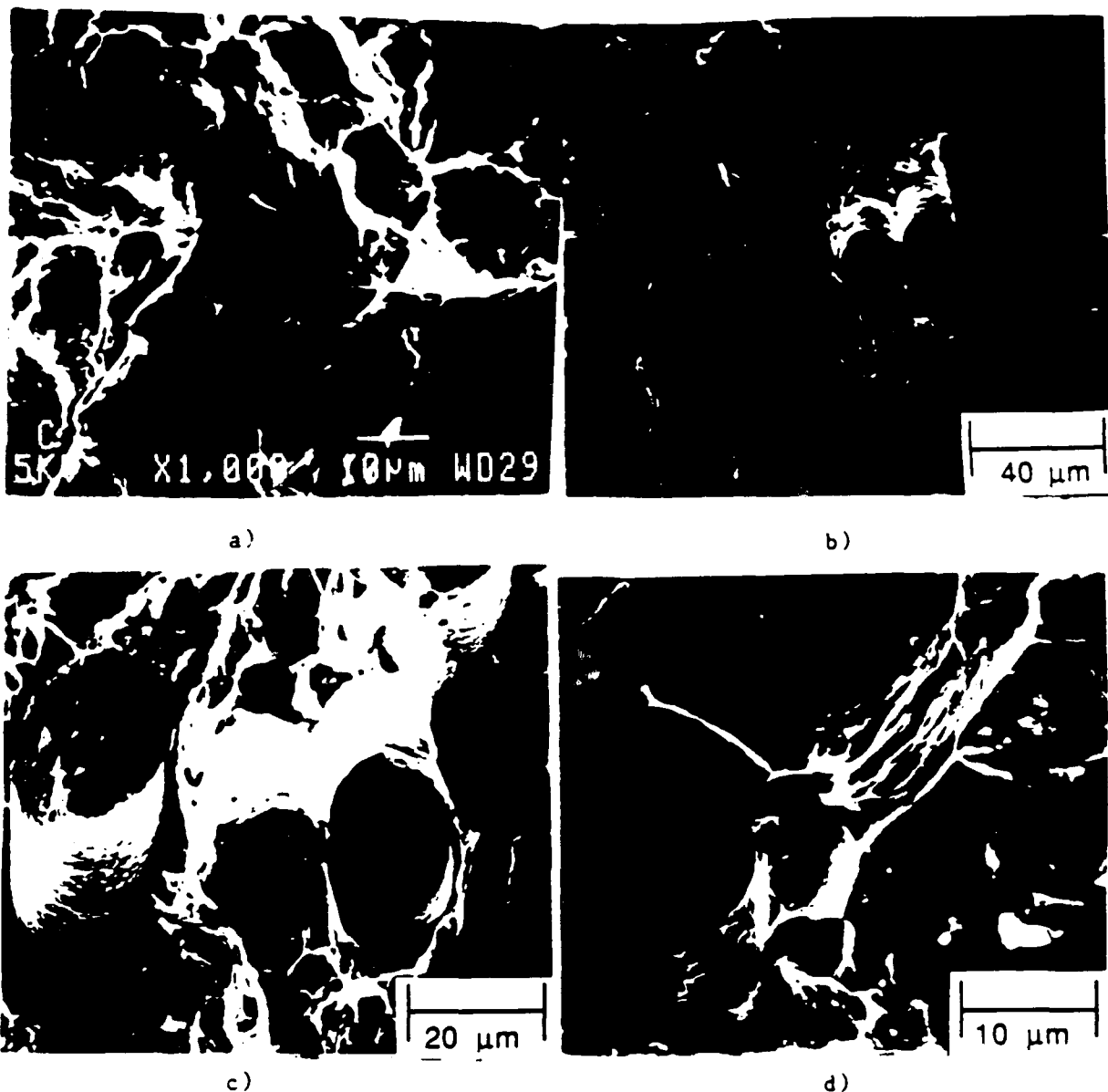
Figure 9   Fracture surfaces of NiAl and NiAl/15v%
           FP tested in tension at 800°C. a)NiAl;
           b-d)NiAl 15v%FP.

strengthening a ductile matrix by a brittle fiber.   Below the ductile
to brittle transition (<700°C)[14], the stress-strain curve of the
composite resembled that of a brittle material. Fracture in the matrix
was by cleavage, see Fig 10a).   However, fiber pullout was observed
on the fracture surface (Fig 10b).   The clam shell markings initiating
from the fibers on the fracture surface suggests that fiber failure
caused fracture, indicating a strong bond.   Also, the separation
between the matrix and fiber is not as extensive as it is at 800°C

TABLE 1
TENSILE PROPERTIES OF REACTIVELY PROCESSED NiAl MATRIX
COMPOSITES TESTED AT 800°C

	σ_{ys} (MPa)	σ_{UTS} (MPa)	Reduction Area (%)
NiAl	135	154	14
NiAl 15v% Al_2O_3 Fibers	142	163	3
NiAl 20v% TiB_2 Particles*	190	207	12.5

* see reference 14.

a)   b)
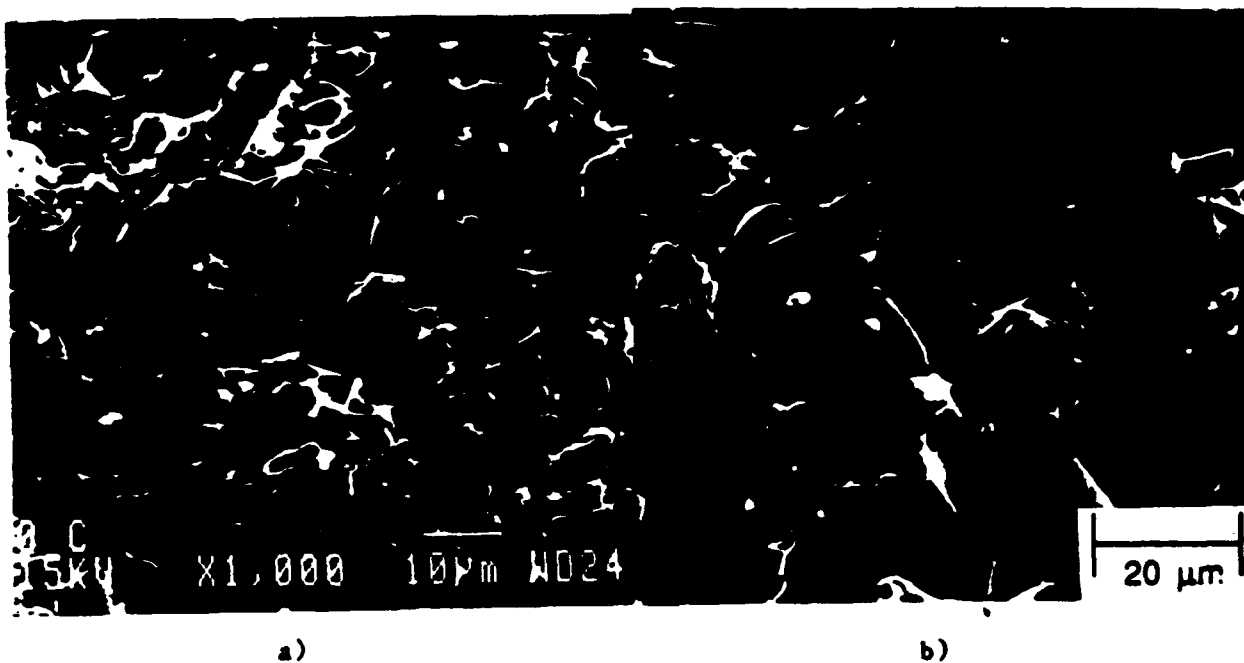
Figure 10   Fracture surfaces of NiAl and NiAl/15v%FP tested in tension
at 700°C (below DBTT) a)NiAl; b)NiAl 15v%FP.-

(compare Figs. 9 and 10), indicating that the strength of the interface
is increasing with decreasing temperature.   Composite properties
also are governed by the strength of the fiber matrix interface.
A weak interface is necessary for improvements in toughness for a
brittle fiber brittle matrix composite.

Included in Table 1 are values of strength and ductility for NiAl
reinforced with 15v% Al_2O_3 fibers and 20v% TiB_2 particles (13μm dia.)
fabricated by reactive synthesis[14].   It would appear that TiB_2
particles are more effective in improving high temperature strength
than the short Al_2O_3 fibers.

A degassing event occured during HIPing of injection molded $MoSi_2$ matrix composites which prevented consolidation. Since $MoSi_2$ could be densified using the HIP conditions described in the experimental section, it is not clear if this degassing event can be attributed to either the 1200°C hydrogen anneal or a chemical interaction between the binder and powders. A vacuum anneal (1000°C, 2 hours) prior to encapsulation was found to alleviate this degassing event. A microstructure of $MoSi_2$ reinforced with 10 or 20v%Al_2O_3 is shown in Figure 11. Due to lack of enough material only small specimens could be produced by the extrusion and CIP method. Room temperature hardness results indicate that Al_2O_3 might improve the toughness of $MoSi_2$. The hardness improved from 87.6 to 90.2 on the Rockwell "A" scale with the addition of the aligned fibers. Hardness values for powder processed $MoSi_2$ have been reported to range from 80 to 87 Rockwell "A"[16,17]. Figure 12 shows the actual indentations. While cracks propagated from the hardness indentation in the composite specimen, Fig. 12a), large craters of fractured material observed in the matrix were absent, Fig. 12b). These results indicate that the DuPont FP fiber may improve the fracture toughness of $MoSi_2$. Attempts to obtain a fracture toughness values from Vickers hardness indentations failed, as cracks did not propagate from the indentations.

CONCLUSIONS

$NiAl/Al_2O_3$ and $MoSi_2/Al_2O_3$ composites have been successfully produced by PIM, indicating that this is a viable technique for fabrication of fibrous intermetallic matrix composites. However, the resulting alignment is not perfect. The allowable volume fraction of fibers is limited. Misalignment and agglomeration increase as fiber volume fraction increases (Fig. 5). The DuPont FP fibers are damaged during powder processing, which reduce the aspect ratio of the fiber; a fiber on a tungsten or carbon core may be less susceptible to damage. Fine prealloyed powders will work as small elemental powders, as evidenced by the fabrication of $MoSi_2$ matrix composites from prealloyed powders. However, fine elemental powders are more readily available. Tensile test results indicate that the interface between the Al_2O_3 fibers and the matrix is not strong enough to strengthen NiAl above its ductile to brittle transition temperature. At this temperature a particulate is more effective in improving strength. Below the ductile to brittle transition the fibers did not toughen the matrix, even though fiber pull out was observed on the fracture surface. This possibly indicates that short fibers will not toughen this matrix.
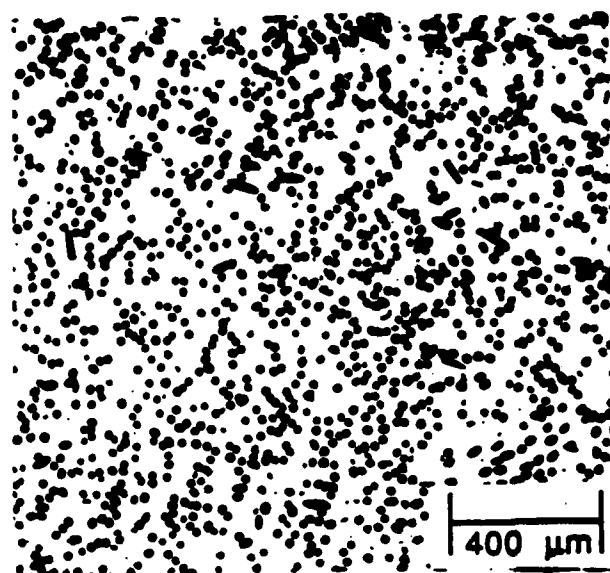
Figure 11   Microstructure of $MoSi_2/10v\%FP$ produced by PIM.

a)   b)
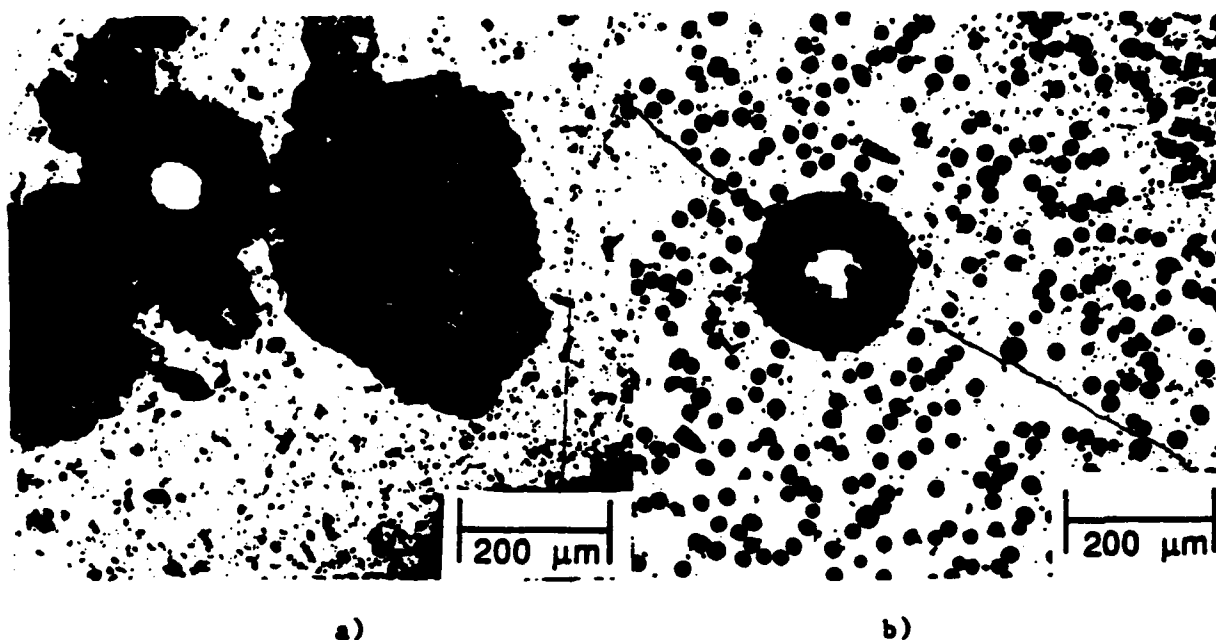
Figure 12   Rockwell "A" Hardness indentation in a)$MoSi_2$;
b)$MoSi_2/20v\%FP$.

However, interfacial characteristics of $NiAl/Al_2O_3$ must be explored
further, since the interface plays a major role in behavior of any
composite. Preliminary results (cracks initiating from hardness
indentations) indicate the DuPort FP Al_2O_3 fiber may improve the
toughness of $MoSi_2$.

REFERENCES

1. D.L. Anton, R. McMeeking, D. Miracle, and P. Martin, Intermetallic
   Matrix Composites, MRS 194, Pittsburgh, PA, 1990.

2. J.L. Walters and H.E. Cline, Met. Trans., 4, 33, (1973).

3. S. Nourbakhsh, F.L. Liang, and H. Margolin, Met. Trans A, 21A,
   213 (1990).

4. S. Nourbakhsh, F.L. Liang, and H. Margolin, in High Temperature
   Ordered Intermetallic Alloys III, C.T. Liu et al eds., MRS 133,
   Pittsburgh, PA, 1989, p 495.

5. S. Nourbakhsh, F.L. Liang, and H. Margolin, in Processing of
   Ceramic and Metal Matrix Composites, H. Mostaghci, ed., Pergamon
   Press, NY 1989, p 195.

6. S. Nourbakhsh, F.L. Liang and H. Margolin, J. Phys. E: Sci,
   Instrum, 21, 898 (1988).

7. S. Nourbaksh and H. Margolin, Met. Trans. A, 20A, 2159 (1989).

8. P.K. Brindley, in High Temperature Ordered Intermetallic Alloys
   II, N.S. Stoloff et al eds., MRS 81, Pittsburgh, PA, 1987, p
   419.

9. G.K. Watson, J.W. Pickens, R.D. Noebe, P.K. Brindley, and S.
   L. Draper, in Hi Temp Review 1988, NASA Conference Publication
   10025, 1988.

10. D.L. Anton, in High Temperature/High Performance Composites,
    F.D. Lemkey et al eds., MRS 120, Pittsburgh, PA, 1988, p 57.

11. I.E. Locci, R.D. Noebe, J.A. Moser, and M. Nathal, in High Temperature
    Ordered Intermetallic Alloys III, C.T. Liu et al eds., MRS 133,
    Pittsburgh, PA, 1989, p 639.

12. A. Bose and R.M. German, Material Sci. and Engr., A107, 107
    (1989).

13. A. Bose and R.M. German, Advanced Materials and Manufacturing
    Process, 3, 37 (1988).

14. D.E. Alman and N.S. Stoloff, Intl. J. of Powder Met., to be published Jan. 1991.

15. D.E. Alman and N.S. Stoloff, RPI, unpublished research.

16. R.D. Grintal, Powder Met..Bull-8, 18 (1957).

17. Materials and Methods, 43, 131 (1956).

18. A. Ball and R.E. Smallman, Acta Met, 14, 1349 (1966).

19. M.J. Maloney, DARPA/ONR Contract No. N00014-87-0862 Program Review, Pratt and Whitney Aircraft, W. Palm Beach, FL., Feb. 28, 1990.

Powder processing of intermetallic matrix composites

D. Alman, A. Dibble, A. Bose, R.M German, N.S. Stollof
Rensselaer Polytechnic Institute, Troy, New York 12180-3590, U.S.A.

B. Moore
General Electric Company, MAO, P.O. Box 1021, Schenectady, New York 12301, U.S.A.

ABSTRACT

Composites based upon the intermetallic compounds NiAl, Ni$_3$Al and Al$_3$Ta have
been consolidated by several novel techniques incorporating, at least in
part, reactive sintering or hot isostatic pressing of elemental powders.
This paper discusses the resulting microstructures and mechanical properties,
including hardness and tensile or compressive strengths as a function of
test temperature. The properties of the composites are compared to those
of the respective matrix materials, also prepared from powders by identical
techniques. The limitations as well as advantages of such processing techniques
are discussed.

KEYWORDS

Composite, fibers, grain size, hot isostatic pressing, intermetallic compound,
nickel aluminides, reactive sintering, tantalum aluminide.

INTRODUCTION

Intermetallic compounds, especially those containing large quantities of
aluminum, display a number of favorable properties for high temperature structural
use, including low density, high strength at elevated temperatures and excellent
oxidation resistance. However, most of the aluminides are brittle, which
leads to problems in consolidation and during service. One potential means
of improving ductility and/or toughness while increasing strength is to utilize
a fibrous second phase reinforcement. Particulates also can be used for
strength improvements, but usually at the expense of ductility. Powder metallurgical
processes are particularly useful in preparing such composites, as has already
been reported in the Ti$_3$Al/SiC (Brindley, 1987) and Al$_3$Ta/Al$_2$O$_3$ (Anton, 1988)
systems. This paper reviews efforts to produce both fibrous and particle
strengthened composites of Al$_3$Ta, Ni$_3$Al and NiAl by one or more methods based
upon either hot isostatic pressing (HIPing) or reactive sintering. The latter
refers to a process in which an exothermic reaction between two or more elemental
constituents of a powder compact provides enough heat to produce a liquid
phase which markedly reduces sintering time. If the process is carried out
without pressure, it is called reactive sintering. Processes which rely
upon application of uniaxial or isostatic pressure during reactive sintering
are labelled reactive hot pressing and reactive hot isostatic pressing, respectively.

An extensive discussion of the various processing techniques has appeared in previous publications (Moore et al, 1988; Bose et al, 1988, German and Bose,

ALLOY SYSTEMS STUDIED

The three alloy systems studied in this investigation are Ni_3Al, NiAl and Al_3Ta. Melting points, densities and crystal structure of these compounds are summarized in Table 1. NiAl and Al_3Ta are brittle at room temperature,

TABLE 1   INTERMETALLIC MATRIX ALLOYS

Alloy	Crystal Structure	Melting Pt °C	Density g/cc
$TaAl_3$	DO_{22}	1550	6.9
NiAl	B_2	1640	5.9
IC-218*	Ll_2	1390	7.5

* Ni_3Al,Cr,Zr+B

but NiAl undergoes a brittle to ductile (BD) transition at temperatures near 600°C. (No data are available concerning a BD transition in Al_3Ta.) The Ni_3Al alloy chosen for study, IC-218, is a two phase alloy that is ductile at all temperatures between 25°C and 800°C. The nominal composition of this alloy, which was developed at Oak Ridge National Laboratory, is Ni-8.2w%Al, 7.8%Cr, 0.8%Zr and 0.2%B.

Powders of the pure metals Ni, Al and Ta were obtained from various sources, as listed in Table 2. Previous research on Ni_3Al alloys prepared by reactive

TABLE 2   POWDER CHARACTERISTICS

	Size	Shape	Process	Vendor
Ta	4µm	angular	mechanically milled	Cabot
	10µm	angular	hydride/ dehydride	NRC
	-325	angular mesh	hydride/ dehydride	Fansteel
Al	3µm	spherical	gas atomized	Valimet, H-3
	10µm	spherical	gas atomized	Valimet, H-10
	30µm	spherical	gas atomized	Valimet, H-30
Ni	3-7µm	spiky surface	carbonyl	INCO-123

sintering had shown that maximum density of compacts is obtained with fine powders, in the range 10-15 µm (Bose et al, 1988). Therefore, starting powders were obtained in the finest sizes commercially available.

Al_2O_3 was chosen as the fibrous reinforcement for Al_3Ta and IC-218. For both IC-218 and NiAl varying volume fractions of TiB_2 particles were incorporated during consolidation of the alloy.

SINTERING TECHNIQUES

Obtaining dense monolithic samples of each alloy was the first objective
of this investigation. After extensive research it was found that reactive
sintering of elemental powders was not a suitable technique to prepare any
of the matrix alloys.

NiAl

In the case of NiAl, the exothermic reaction was uncontrollable, such that
the heat of reaction was sufficient to destroy crucibles or result in complete
melting of portions of the compact, as shown, for example, in Fig. 1. It
was found by trial and error that the reaction could be diluted by mixing
10 to 25% prealloyed NiAl powder with the elemental powders.

Near fully dense and near net shape Ni-49a%Al samples (0.5 grams wt cylindrical
pellets approximately 6mm in diameter, cold pressed to 70% of theoretical
density) could be produced from a mixture of elemental and prealloyed powders
by reactive sintering at 700°C in vacuum (10^{-6} torr) for 15 minutes. The
optimum amount of prealloyed NiAl powder needed to control the exotherm associated
with reactive sintering of Ni+Al was determined to be dependent on the particle
size distribution of the prealloyed powder. NiAl prealloyed powder was obtained
from two sources. One source was prereacted NiAl produced and milled at
RPI; the other source was prealloyed NiAl powder purchased from Cerac, Inc.
The Cerac NiAl powder possessed a more uniform particle size distribution,
and therefore blending was achieved with less Cerac NiAl powder than with
the RPI powder. The first two sets of bars in Fig. 2 show properties for
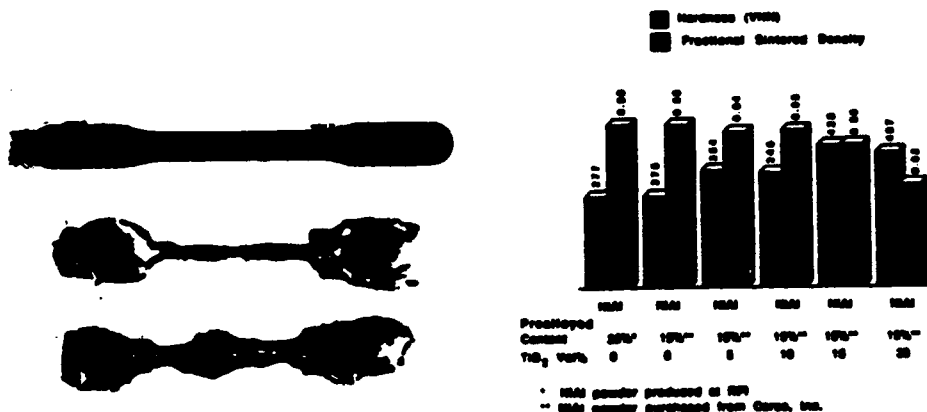
Fig. 1 Excessive reaction of elemental
Ni+Al powders.

Fig. 2 Effects of % prealloyed NiAl
and volume fraction of TiB$_2$
powders on sintered density of
NiAl.

active sintered NiAl with RPI and Cerac powder respectively. Even though
different optimum amounts of prealloyed powders were used, the sintered properties
is essentially equivalent with the two different powders. It was found
the TiB$_2$ powders added to the mixture hindered densification; the maximum
density obtained in a NiAl-TiB$_2$ alloy was 95% with 10v% TiB$_2$ and 15% prealloyed

powder (see Fig. 2). The influence of small amounts of alloying elements on reactively sintered NiAl/TiB$_2$ composites was also studied (see Fig. 3). No significant improvements in hardness or sintered density were noted with 1%Ta, 1%Nb or 5%Cr.

It became evident after obtaining many samples with large residual pores that to produce dense composites, hot isostatic pressing had to be employed. Fully dense microstructures of NiAl and NiAl/TiB$_2$ composites were produced by cold isostatic pressing followed by hot isostatic pressing in a 304 stainless steel can at 1200°C for 60 min at a pressure of 172MPa, using the process outlined in Fig. 4. Typical microstructures are shown in Figs. 5a)-d).
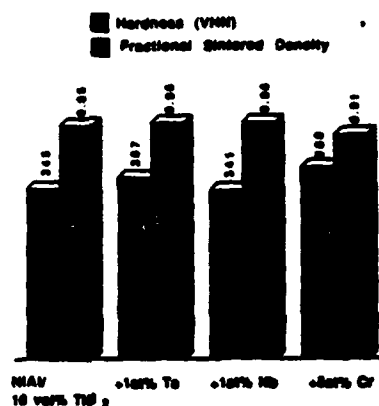
Fig. 3 Effects of alloying elements   Fig. 4 Schematic of HIP process
        on sintered density and   for NiAl.
        hardness of NiAl.
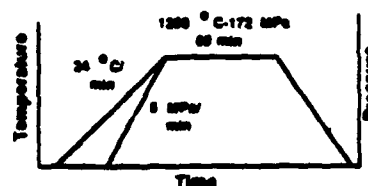
Note the more equiaxed grain structure produced from a mixture of prealloyed and elemental powders as opposed to the pure elemental powders. Also notice a more refined grain size with the addition of TiB$_2$ powders (5μm vs 30μm for monolithic NiAl.

Al$_3$Ta

Reactive hot isostatic pressing (RHIP) was utilized to fabricate samples of Al$_3$Ta. Control of the process conditions and particle sizes of the elemental powders affected the homogenization and densification of the intermetallic compound.

Since the exact composition of stoichiometric Al$_3$Ta was not clear from the literature, elemental powders of tantalum and aluminum were mixed in three ratios: 23, 24 and 25 at% Ta. Reactive sintering experiments showed that the optimum powder size was 10μm for both the aluminum and the tantalum powders. The powder mixtures were cold isostatically pressed at 200MPa into rods approximately 14 mm in diameter and 80 mm in height. The rods were inserted into stainless steel tubes lined with tantalum foil and coated with an Al$_2$O$_3$ slurry to prevent contamination from the can. The samples were evacuated and outgassed at 500°C for approximately 20 hours and then sealed under vacuum. Samples were produced by RHIPing at a pressure of 172MPa and temperatures of 700°C, 900°C
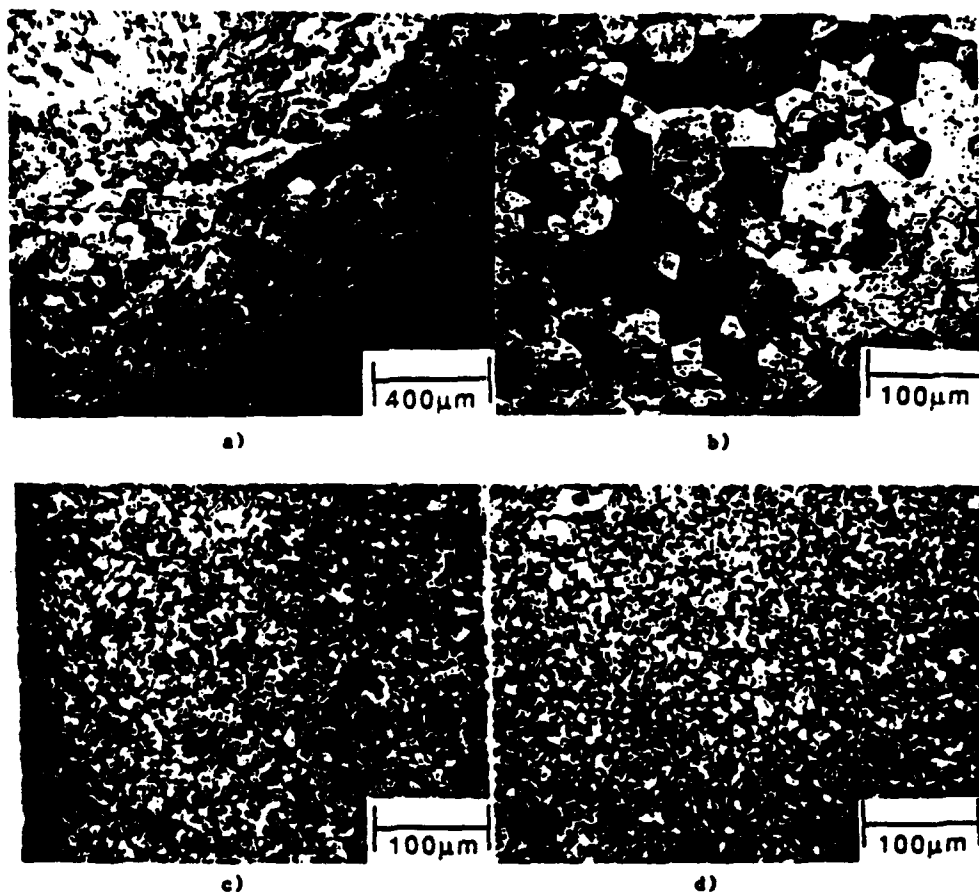
Fig. 5 Microstructures of NiAl+TiB$_2$. a) 0%TiB$_2$, g.s.30µm
        b) 10% prealloyed, 0%TiB, g.s.30µm, c) 10% prealloyed,
        15v%TiB$_2$, g.s.5µm, d) 10% prealloyed, 20v%TiB$_2$,
        g.s.5µm.

at 1200°C, for one hour. Dense, homogenous samples were formed at 23 at%
Ta and 1200°C, as shown in Fig. 6. Microprobe analysis confirmed that the
composition of Al$_3$Ta was approximately 23.3 at% Ta in agreement with a recently
revised phase diagram (Miracle, 1988). Lower temperatures and higher percentages
of tantalum results in incomplete reaction of the starting materials. Heat
treatment at 1100°C for ten hours or at 1200°C for four hours yielded a two
base microstructure which consisted of Al$_3$Ta and a phase identified as Al$_2$Ta
(Miracle, 1988).

Compacts containing 8at%Fe substituted for Al also were produced by similar
techniques. No change in crystal structure of the alloy was detected. Samples
containing 8at% Fe substituted for Al were produced by RHIPing at a pressure
of 172MPa and a temperature of 1100°C and then heat treated at 1200°C for
hours. The resulting microstructure consisted of two phases - a solid
solution Al$_3$Ta phase containing 0.5at% Fe and a ternary phase with a composition
of 32at%Ta, 56at%Al, and 12at%Fe.
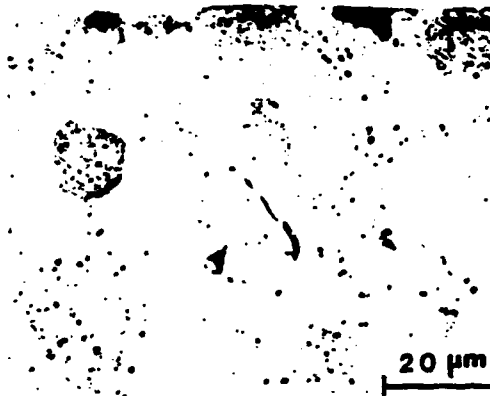
Fig. 6 Microstructure of Al$_3$Ta reactively
HIPed at 1200°C.

Composites with an Al$_3$Ta matrix also were fabricated by RHIPing. Compatibility
tests indicated that Al$_3$Ta did not react with Al$_2$O$_3$ during processing; therefore
two Al$_2$O$_3$ fibers, FP and Saffil, were selected for further study. Table 3
summarizes the properties of the FP and Saffil fibers. Using the optimum

TABLE 3 CHARACTERISTICS OF Al$_2$O$_3$ FIBERS

	PP	Saffil
length	5-30mm	70-200µm
diameter	20µm	3µm
density	3.9 g/cc	3.3 g/cc
tensile strength	1380MPa	2000MPa
Young's modulus	380GPa	300GPa
max powder diameter for 20 vol % fiber	23µm	4µm
source	DuPont	ICI

consolidation procedure described above, composites were fabricated with
10 vol% of randomly oriented fibers of each type. During processing, the
fibers fractured due to the high pressures. As the volume percent of fibers
was increased, the porosity and amount of second phase present also increased.
This was true for both the FP and the Saffil fibers, but was less severe
in the case of the smaller diameter Saffil. Most of the second phase which
appeared in the Saffil composites occurred around prior particle boundaries.
Representative microstructures are shown in Figs. 7a) and b).

In addition, work is in progress to align these fibers by injection molding.
This process requires the addition of about 40 vol% binder to the powder
mixture. The powder-binder mixture is injected through a die to obtain fiber
alignment and then heated to 450°C for 5 hours in hydrogen to remove the
binder. The samples are then RHIPed as described above. To date, a paraffin-
based liquid appears to be the best binder since it does not contaminate
the reaction in which Al$_3$Ta is formed.
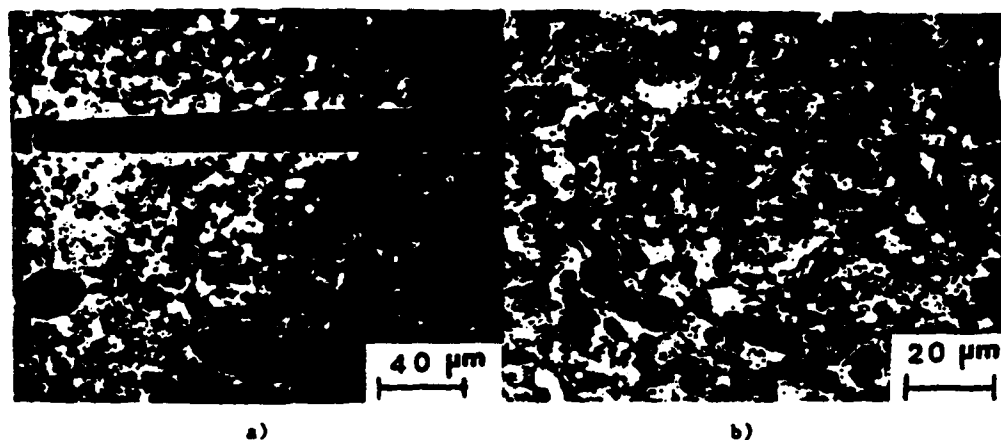
Fig. 7 Microstructures of Al₃Ta composites with 10v%
Al₂O₃ fibers a) FP Al₂O₃ b) Saffil.

Ni,Al,Cr,Zr+B (IC-218)

Prealloyed powder of the compound IC-218 was obtained from Homogeneous Metals,
Inc. Analysis of the -100 mesh powder revealed composition of 7.67w%Cr,
8.18%Al, 0.8%Zr, 0.2%B, with 7 ppm of N₂ and 73 ppm of O₂. TiB₂ powder used
in preparing some composites was obtained from Aerospace Corp. FP- Al₂O₃
fibers were obtained from Dupont Corp.

IC-218 and two types of composites with an IC-218 matrix were consolidated
by HIPing. The HIP cycle for the unreinforced matrix was 1100°C, 1 hr, at
a pressure of 172 MPa. The microstructure of IC-218 is shown in Fig. 8a).
Note that the microstructure consists of a γ' matrix with some disordered
second phase. IC-218 with 5v% of short Al₂O₃ fibers also was HIPed at 1150°C
and 172MPa pressure. A typical microstructure is shown in Fig. 8b). IC-218
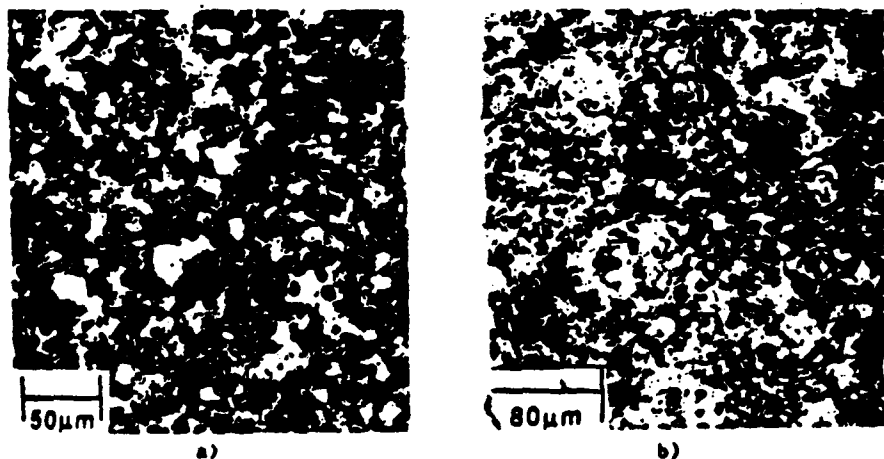
Fig. 8 HIPed microstructure of IC-218 a) matrix alloy
(HIPed at 1100°C) b) 5v%Al₂O₃ fibers (HIPed at 1150°C).

with varying volume fractions of 30um TiB$_2$ particles vs. HIPed at 1150°C for 30 min at a pressure of 172 MPa. The microstructure of a sample containin 10v%TiB$_2$ is shown in Fig. 9. Note that the TiB$_2$ forms a nearly continuous

100μm
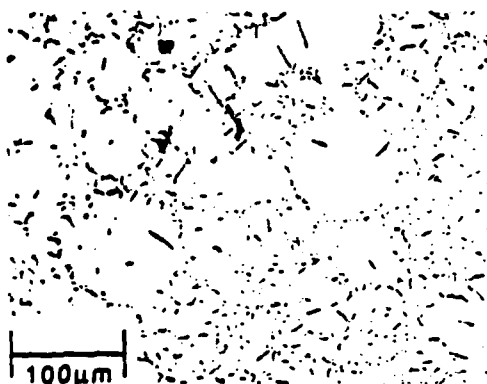
Fig. 9 Microstructure of IC-218 with 10v%TiB$_2$
particles, HIPed at 1150°C, 172MPa, 30 min.

phase at the grain boundaries. In general the TiB$_2$ had a needle-like or plate-like appearance.

STRENGTH MEASUREMENTS

The influence of microstructure and particle or fiber content on strength was carried out by a variety of mechanical tests.

NiAl

Compressive stress strain curves for Ni-49a% Al and several TiB$_2$-reinforced NiAl alloys were carried out as a function of test temperature. The results are shown in Fig. 10. Note the rapid rise in yield stress with increasing TiB$_2$ content. A portion of this strengthening is due to the very fine grain size (5 um) of the alloys containing 15 and 20% TiB$_2$ compared to the 30 um grain size of NiAl. The remainder of the strengthening is due to the effects of the TiB$_2$ particles. The strengthening due to TiB$_2$ persists to about 700°C; there is virtually no effect of TiB$_2$ on strength at 800 and 950°C.

IC-218

The tensile properties of IC-218 and IC-218 with 5v% Al$_2$O$_3$ fibers as a function of temperature are compared in Fig. 11. It can be seen that the fibers did not raise the yield stress and, by reducing ductility to near zero at all but room temperature, had a deleterious effect on ultimate tensile strength.

Tensile properties of IC-218/TiB$_2$ composites are shown in Fig. 12. Only the alloy containing 10%TiB$_2$ showed a higher yield strength than IC-218 at 25°C; however, at 600°C an increase in strength with 5% and 10% TiB$_2$ was noted. Note also in Fig. 12 the rise in yield stress with temperature that
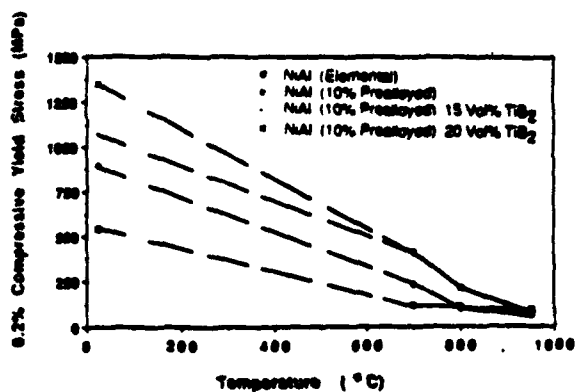
Fig. 10 Compressive yield stress vs temperature
         for NiAl alloys.
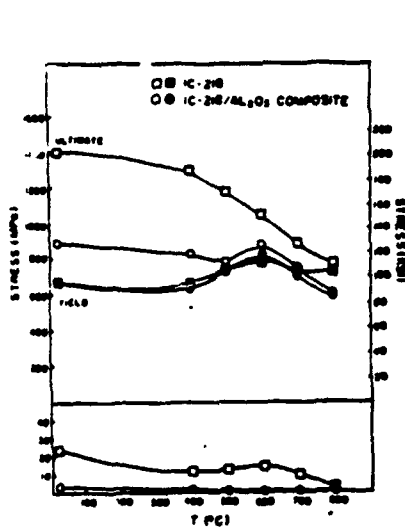
Fig. 11 Effect of temperature on
         tensile properties of IC-218
         and IC-218-5v%Al₂O₃ fibrous
         composites.
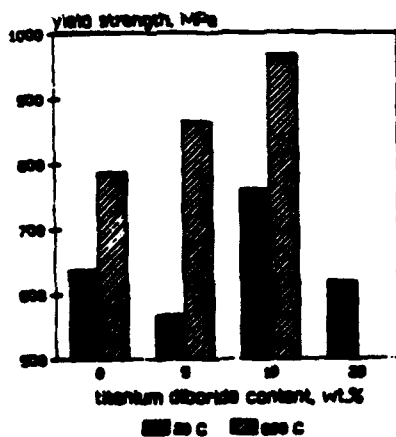
Fig. 12 Effect of temperature and
         TiB₂ content on tensile
         yield strength of IC-218.

characteristic of this alloy. The ductility decreased substantially with
% contents of TiB₂, the effect being greater with increasing %TiB₂.

strength of monolithic Al₃Ta has been measured in compression as a function

of temperature, see Table 4. Note the rapid weakening at elevated temperatures. The addition of 8%Fe replacing Al leads to a significant improvement in high temperature strength. Also, hardness tests have been carried out on several compositions. The Vicker's hardness of Al_3Ta was 369 DPH. This value varied little for the Al_3Ta which formed at various compositions or HIPing temperatures. The addition of fibers also had little effect upon the hardness. The hardness of the Al_2Ta phase which formed in some samples was approximately 450 DPH. The Vicker's hardness of the solid solution strengthened $Al_3Ta + Fe$ was 391 DPH. This hardness of the ternary phase with 12% Fe was 571 DPH.

TABLE 4   COMPRESSIVE PROPERTIES OF Al_3Ta ALLOYS

Alloy	Temp (C)	Yield Stress (MPa)
Al_3Ta	25	531
$Al_3Ta-8a%Fe$	25	372
$Al_3Ta-8a%Fe$	750	765
Al_3Ta	950	41
$Al_3Ta-8a%Fe$	950	198

DISCUSSION

Densification of intermetallic matrix composites can be accomplished by HIPing either elemental or prealloyed matrix material with compatible reinforcements. The consolidation conditions (temperature, pressure, time) do not substantially differ from those utilized for the matrix alone. However, the ability to achieve full density is inhibited somewhat by the presence of the reinforcements Reasons for similar processing cycles are the low volume frations of ceramic phases and the grain size refinement often observed after HIP of the composite. For many of the intermetallic compounds the primary densification mechanism involves grain boundary diffusion. Although the ceramic second phase inhibits densification, it has a beneficial grain size refinement effect. This latter change ensures more and shorter diffusion paths for densification. Because of the long range ordered structure of these compounds, the lattice diffusivity is low. Consequently, grain boundaries and grain boundary diffusion is necessary for rapid densification. Two of the three alloy systems studied, $Ni_3Al.Cr.Zr+B/TiB_2$ and $NiAl/TiB_2$ show considerable strengthening relative to the matrix alone. In the case of NiAl some of the strengthening arises from grain refinement, with the grain size being reduced from $30\mu m$ to $5\mu m$ by the TiB_2 particles. However, a Hall-Petch analysis of the contribution from grain size refinement to strengthening can account for only a portion of the observed strengthening, see Table 5. The balance is provided either by direct strengthening by the particles (unlikely due to their large size) or by impurity contamination, predominantly oxides on prior particle boundaries. Post-consolidation analyses of the NiAl compacts revealed an oxygen content of about 500 ppm. It is well known that the mechanical properties of intermetallic compounds are extremely sensitive to compositional variations, either Al content or impurity levels (Stoloff, 1985).

Contamination is only one of the problems affecting the properties of these composites. In the case of the fibrous composites $IC-218/Al_2O_3$, lack of wetting between fiber and matrix leads to premature nucleation of cracks at the fiber/matrix interfaces and severe loss of ductility. Two remedies are required: a dopant for better wetting and fiber alignment to allow the work of pull out to contribute to overall fracture resistance. Injection

TABLE 5 CONTRIBUTION OF GRAIN REFINEMENT TO STRENGTHENING
BY TiB₂ at 25°C.

	Grain Size (um)	Yield Stress (MPa)
NiAl (10% prealloyed)	30	890
NiAl (10% prealloyed) calculated from Hall Petch*	5	1000
NiAl (10% prealloyed) 15 vol % TiB₂	5	1060
NiAl (10% prealloyed) 20 vol % TiB₂	5	1350

* Hall Petch data from Schulson (1985)

molding offers some hope of overcoming the alignment problem, but contamination
from a polymeric-base binder must be avoided in the final product. Initial
efforts to develop injection molded composites have established that the
average powder particle diameter must be less than the fiber diameter to
accomplish alignment. Unfortunately, powders of the size required, of the
order of 10 μm or less, are either very expensive or unavailable. Reactive
processing using elemental powders remains an attractive route for densification
from injection molded small particles.

ACKNOWLEDGMENT

REFERENCES

Anton, D.L. (1988). In High Temperature/High Performance Composites, MRS
Symposia, V. 120, MRS, Pittsburgh, PA, 1988, 57-64.
Bose, A., B. Moore, N.S. Stoloff and R.M. German (1988). In PM Aerospace
Materials 1987, MPR Publ. Serv. Ltd, Shrewsbury, England, 4.1-4.13.
Crimp, P. (1987). In N.S. Stoloff and others (Eds.) High Temperature
Ordered Intermetallic Alloys II, MRS Symposia V. 81, MRS Pittsburgh, PA,
424.
German, R.M. and A. Bose (1989). Mat. Sci. and Eng., A107, 107-116.
Dimiduk, D. (1988). Wright Aeronautical Labs, Wright Patterson AFB, Ohio,
unpublished research.
Moore, B., A. Bose, R.M. German and N.S. Stoloff (1988). In P. Lemkey and
others (Eds.) High Temperature/High Performance Composites, MRS Symposia
120, MRS, Pittsburgh, PA, pp. 51-56.
Russell, K.R. (1985). In High Temperature Intermetallic Alloys, MRS Symposia
39, Pittsburgh, PA, pp. 193-204.
Schulson, E.M. (1985). In C.C. Koch and others (Eds) High Temperature Ordered
Intermetallic Alloys, MRS Symposia 39, MRS, Pittsburgh, PA, pp. 3-27.

INTERMETALLIC COMPOUNDS

MECHANICAL PROPERTIES

FABRICATION, STRUCTURE AND PROPERTIES OF

MoSi$_2$-BASE COMPOSITES

D.E. Alman, K.G. Shaw, N.S. Stoloff and K. Rajan

Rensselaer Polytechnic Institute

Materials Engineering Department

Troy, New York 12180-3590

November 4, 1991

Abstract

Several techniques have been employed to consolidate $MoSi_2$ composites reinforced either with Al_2O_3 or Nb. Powder injection molding was used to prepare $MoSi_2$ with aligned short FP Al_2O_3 fibers. Plasma spray was used to produce lamellar $MoSi_2$-Al_2O_3. Niobium particles, random short fibers and continuous fibers were incorporated into $MoSi_2$ by hot isostatic pressing. Microstructures and mechanical properties of the various composites are reported. Significant microscopic toughening was obtained with continuous Nb fibers, but at the expense of creep resistance.

1. Introduction

Many intermetallics are under intensive investigation as potential structural materials. Of these, $MoSi_2$ is perhaps the most interesting, because of its melting point (2030°C), excellent oxidation resistance and low density. However, efforts to develop $MoSi_2$ have been hampered by its extreme brittleness at temperatures below 1000°C, coupled with relatively low creep resistance. It has been recognized by most workers in the field that the best chance to solve these twin problems is through use of $MoSi_2$ as a composite matrix. However, the commercial ceramic fibers that are suitable for use as reinforcements are limited to SiC and Al_2O_3 (in various purities). Niobium fibers have been added to $MoSi_2$[1]. The addition of other metallic fibers such as W and Mo based alloys will likely strengthen $MoSi_2$. However, the addition of refractory metals is almost certain to lead to a degradation of oxidation resistance. With these cautions in mind, we, along with other investigators, have utilized a variety of processing techniques to prepare $MoSi_2$-base composites. In this paper we describe powder metallurgical and plasma spray techniques to prepare not only fiber reinforced samples, but also particulate reinforced composites as well as lamellar composites. Al_2O_3 and Nb were chosen as candidate ceramic and metallic reinforcements respectively, because of thermal expansion compatibility and availability of reinforcements.

2. Fabrication approaches

Several experimental techniques have been used for our

3

composite studies: hot isostatic pressing (HIPing) of $MoSi_2$-Nb particulate and random fiber composites, injection molding of $MoSi_2$-Al_2O_3 aligned short fiber composites, hand layup and HIPing of $MoSi_2$-Nb continuous fiber composites and plasma spraying of $MoSi_2$-Al_2O_3 lamellar composites. Since details of HIPing operations for $MoSi_2$/Al_2O_3 have been published previously [2], we will describe here only the injection molding and plasma spray processes, as well as HIPing of $MoSi_2$/Nb composites.

2.1 Injection Molding

Injection molding for fiber alignment consists of four basic steps, feedstock production, fiber alignment, debinding and consolidation. Feedstock preparation consists of mixing the powders and fibers with a polymer binder. Fiber alignment comprises injection of the feedstock through a nozzle. Injection is performed above the softening point of the polymer binder. The binder is then removed, either thermally or chemically. Final consolidation is accomplished by sintering or pressure aided sintering techniques. A schematic diagram of the process is shown in Fig. 1.

Uniform fiber distribution is crucial for toughness improvements in brittle matrices; therefore, the addition of fibers to the powders must be performed with great care. Twenty volume percent (13.5 wt%) chopped DuPont FP Al_2O_3 fibers ($20\mu m$ diameter) were mixed into the $MoSi_2$ powders (H.C. Stark-Grade C) in an alcohol slurry. Fiber aspect ratios ranged from 10 to 200. A turbula type mixer was employed for blending of the fibers and

4

powders in the slurry. Mixing occurred for 1 hour, after which the alcohol was allowed to evaporate. The binder used was based on low molecular weight polyproplylene, paraffin, carnauba wax, and stearic acid. Its softening point is approximately 90°C and density is 0.94 g/cm^3. The feedstock was prepared by mixing the powder/fiber blend into the melted binder. Mixing was performed for 30 minutes employing a double planetary type mixer. Approximately 30 percent by volume of feedstock was binder.

The fibers were aligned by extruding the feedstock through a tapered die. The die decreased in diameter from 12.7mm to 1.5mm. Extrusion was performed with the die preheated to 90°C. This produced wires that were 1.5mm in diameter by about 50mm long. These wires were carefully placed in a polyeurethane mold (12.7mm in diameter) and cold isostatically pressed to 208 MPa. This produced a cylindrical specimen about 12.7mm in diameter and 50mm long.

Thermal debinding was carried out with specimens placed in Al_2O_3 powder. The cycle consisted of heating at 2°C/min to 450°C and holding at temperature for 300 minutes. After a furnace cool in hydrogen, the specimens were placed in a vacuum furnace and vacuum sintered at 1200°C for 2 hours. The specimens were then encapsulated for HIPing. Specimens were wrapped in Ta or Nb foil and vacuum encapsulated in Ti HIP cans. The foil was used to prevent reaction between the $MoSi_2$ and the Ti can. The HIP cycle was 1500°C, for 2 hours at 172 MPa. Depressurization and cooling occurred slowly (from 1500°C to 300°C in 60 minutes,

followed by depressurization to atmospheric pressure and cooling
to room temperature over the next 60 minutes). The cross section
of an aligned $MoSi_2$-20v%Al_2O_3 composite is shown in Fig. 2.

2.2 Hot Isostatic Pressing

Niobium was added to $MoSi_2$ in the form of particles, random
chopped fibers and aligned continuous fibers. Irregular shaped
Nb particles (-80 mesh, microtrac diameter 108μm) were obtained
from Teledyne-Wha Chang in Albany, Oregon. Twenty volume percent
(or 25 wt%) Nb was mixed into $MoSi_2$ powder (H.C. Stark-Grade C).
Niobium wire also was obtained from Teledyne-Wha Chang. The
diameter of the wires was 812μm. The wire was chopped to
approximately 12.5mm in length. Twenty volume percent of Nb wire
was mixed with $MoSi_2$ powder. Mixing occurred in 1 hour with a
turbula type mixer. The mixed powder and wire were placed in a
polyuerethane cold isostatic press (CIP) mold bag (23mm in
diameter by 70mm long). The CIP bag was lined with Ta or Nb foil
prior to the placement of the powder into the bag. Specimens
were CIPed to 240 MPa. The specimens were then vacuum
encapsulated in Ti HIP cans and HIPed for 3 hours at 1350°C at
172 MPa pressure. Depressurization and cooling occurred over a
three hour period. A typical microstructure appears in Fig. 3.

Continuous aligned Nb-reinforced $MoSi_2$ composites were
produced via a combination hand layup-powder infiltration
technique. A CIP mold lined with either Ta of Nb foil was filled
to one half of its capacity with $MoSi_2$ powder. Wires cut to
70mm length were carefully placed in the powder. Then the CIP

6

bag was filled to capacity with $MoSi_2$ powder, infiltrating the wires. The amounts of powder and wires used were determined prior to layup of the wire, such that loading of the wire was 20v% (25 wt%). These specimens were CIPed and HIPed as above.

In each case, a reaction zone was noted between $MoSi_2$ and Nb. Microprobe analysis results are shown in Fig. 4 for fiber-reinforced $MoSi_2$. The Mo_5Si_3 phase, contaminated with Fe, was identified. The source of contamination is unknown; it might have originated in the wire as Fe was not detected in particulate composites. Other researchers have noticed similar chemical interactions between Nb and $MoSi_2$[3]. For any practical engineering application Nb must be coated to prevent inter-diffusion.

Bend specimens were electrodischarge machined from the ingots (6.36mm in dia. by 38mm in length). The bend bars were re-HIPed at 1350°C for three hours. Specimens were polished through 0.3 μm Al_2O_3 powder. Specimens were tested in three point bend at a cross head velocity of 0.127 mm/sec. The span length between the supports on the three point bend jig was 25.4 mm.

Compressive creep tests in air were carried out at 1050-1450°C in a band load apparatus previously described[4]. Stresses ranged from 10-100 MPa. Grain sizes of both $MoSi_2$ and $MoSi_2$-20v%Nb particulate composites were about 23μm.

2.3 Plasma Spray

A commercial plasma spray unit has been modified to permit

deposition onto a substrate. Dual injection ports allowed spraying of two different powder types, Al_2O_3 and $MoSi_2$.

Composites were formed by sequential deposition of $MoSi_2$ and Al_2O_3. Both powders were -325 mesh grade. The plasma gun was operated inside a glove box supporting an inert argon environment which is monitored for oxygen and kept below 4 ppm during the spray deposition. The plasma equipment used is a Miller plasmadyne system with a SG-100 gun using the 175 anode, 129 cathode and a 113 gas injector. The arc gas pressure was kept at 60 psi, the feed gas pressure at 35 psi and the arc current varied. The equipment was modified by running separate feed lines from each hopper directly to the gun, eliminating the check valve supplied by the vendor which was shown to cause cross contamination of the layers.

The gun was kept 8.8 cm away from the rotating (30 RPM) cast iron substrate. At this distance some heat enters into the deposit and provides some stress relief to the laminate structure. Residual porosity is evident in these films, being caused by argon entrapment between successively deposited splats and also by unmelted powders. To remove this porosity hot isostatic pressing and vacuum annealing were used. Vacuum annealing at 1500°C for 1 hour was found to fully densify the $MoSi_2$ layer.

The composites have been characterized by density measurements, back-scattered electron microscopy, Vickers microhardness and X-ray diffraction. The $MoSi_2$ solidifies as a

8

hexagonal phase which is a non-equilibrium phase at room temperature[5], as shown in the X-ray traces of Fig. 5. The transition to the equilibrium body centered hexagonal phase occurs on annealing between 700°C and 900°C.

A general view of a plasma sprayed $MoSi_2/Al_2O_3$ laminate appears in Fig. 6. The density of the deposits increased from 82% to 96% with increasing arc current between 300 and 500 amps, with no further increase at 700 amps. A higher magnification view of as-sprayed material appears in Fig. 7. Note the large inhomogenieties and porosity, as well as non equilibrium phases present.

Transmission electron microscopy of the as sprayed material showed several interesting features, including an amorphous interface phase, Fig. 8a), and particles (as yet unidentified) in the $MoSi_2$, Fig. 8b).

3. Mechanical Properties

3.1 $MoSi_2-Al_2O_3$ Composites

Both powder processed and plasma sprayed composites were produced. Room temperature hardness results indicate that Al_2O_3 might improve the fracture resistance of $MoSi_2$. Figures 9a)-d) show Rockwell "A" hardness indentions (60kg load, Brale) in HIPed $MoSi_2$, plasma sprayed $MoSi_2$, $MoSi_2$-20v% FP composite produced by PIM and $MoSi_2/Al_2O_3$ laminate produced by plasma spray, respectively. The actual hardness results were 87.6, 90.2 and 85.7 HRA for $MoSi_2$, $MoSi_2/20v\%$ FP and $MoSi_2/Al_2O_3$ laminate, respectively. Notice that while cracks propagate from the

9

indentations in each of the composite specimens, absent are large areas of adjacent fractured material as displayed in the monolithic specimen, Figs. 9a) and 9b).

Microhardness values also have been obtained from each phase in plasma sprayed $MoSi_2/Al_2O_3$ composites, see Fig. 10[6]. Hardness and density increased with arc currents for both $MoSi_2$ and Al_2O_3.

3.2 $MoSi_2/Nb$ Composites

The mechanical behavior of $MoSi_2$-Nb composites was determined by means of three point bend tests at room temperature and compressive creep tests at elevated temperatures. Fig. 11a) shows room temperature flexural stress versus displacement curves for $MoSi_2$ and $MoSi_2/20v\%$ Nb particulate composite. Note that these curves exhibit only elastic behavior. Fig. 11b) shows the curves for $MoSi_2$ with 20v% short random Nb fibers. Note the large variability in shape of these curves; however, each displays some "non-elastic" deflection or strain. This indicates crack blunting and improvements in toughness with additions of the random short fibers. Fig. 11c) shows bend deflection curves for $MoSi_2/20v\%$ Nb aligned continuous fibrous composite. Clearly, these curves indicate that the aligned fibers will impart the greatest improvement in toughness. Fig. 12a-c) shows fracture surfaces for $MoSi_2$ and the Nb fibrous composites. Fig. 13a-c) shows high magnification of the Nb fracture surface in each of the composites (particulate random fibrous and aligned continuous fibrous). Note from Figs. 12 and 13 that for the

10

random fibrous and particulate composite, failure of Nb occurred primarily by transgranular cleavage, while for the aligned fibrous composite the Nb failed in a ductile mode. This would indicate that there is a large orientation effect for toughening $MoSi_2$ with ductile phases.

Creep tests have been carried out in compression to date only on Nb- particulate reinforced $MoSi_2$. Typical creep curves at 1200°C for $MoSi_2$ and $MoSi_2$-20v%Nb particles are shown in Fig. 14[4]. Note the much more rapid creep rate of the composite. Activation energies, Q, of 232 kJ/mole for $MoSi_2$ and 119 kJ/mole for the composite were noted from the data in Fig. 15. Sadananda et al[7] showed similar creep rates for 20 MPa stress, but with a much higher activation energy, also shown in Fig. 15.

The matrix creep rates measured in the present work are on the same order of magnitude as those reported by Sadananda et al[7] over the same temperature range, at different stresses (10 MPa versus 20 MPa) and for material of similar grain size. The exact amount of glass in the samples of Sadananda et al was not reported, so small differences in the creep rates may be due to differences in the glass content or composition.

The rapid creep of the $MoSi_2$/Nb composite demonstrates that it is not attractive for high temperature structural applications. The Nb is responsible for the faster creep rate, either due to the creep of the Nb particles themselves or because of the deformation of the reaction zone. Meschter[8] had suggested that a Nb particulate composite might have low

toughness due to the formation of a brittle $(Mo,Nb)_5Si_3$ reaction zone with a weak interface which does not permit ductile-phase crack bridging. However, no cracking was observed at the reaction zone in the creep samples and neither the particles nor the reaction zone were visibly deformed.

The creep rate of niobium is strongly time-dependent, exhibiting a $t^{1/3}$ dependence[9]. The creep strain of the composite was found to fit equation (1);

$$\epsilon = a_o + a_1 t^{1/2} + a_2 t \qquad (Eq. 1)$$

which contains a $t^{1/2}$ term and a term linear with time. A term in $t^{1/3}$ plus a linear time term also gave good fit. The $MoSi_2/Nb$ creep rate therefore may be the sum of a constant $MoSi_2$ deformation rate and a time dependent Nb creep rate.

Summary and Conclusions

Several processing techniques have been shown to provide fully dense $MoSi_2$-base composites with various forms of Al_2O_3 and Nb reinforcements. Unfortunately, the powders of $MoSi_2$ that are commercially available carry with them significant amounts of SiO_2. In the case of plasma spraying, annealing without pressure is sufficient to fully densify laminates, but for P/M processed material HIPing is necessary.

Preliminary observations of the microstructure of plasma sprayed $MoSi_2$-Al_2O_3 laminates by TEM reveal an unidentified amorphous phase at interphase boundaries as well as many defects in the $MoSi_2$ (dislocations, twins, second phase particles). The influence of deposition conditions and annealing on these defects

12

is currently being studied.

The mechanical properties evaluations also are still preliminary, but it is evident that continuous Nb filaments are necessary to produce significant toughening at 23°C. However, it is also highly likely that such fibers will lead to degradation of creep properties, as with Nb particles. Coatings such as Y_2O_3 are reported to inhibit interdiffusion between $MoSi_2$ and Nb[10] but may not improve creep resistance.

References

1. E. Fitzer and W. Remmele in Proc. Int. Conf. Composite Matls. ICCM-V, (W.C. Harrigan, J. Strife and A.K. Dhingra eds.) TMS-AIME, Warrendale, PA, 1985, p. 515.

2. D.E. Alman and N.S. Stoloff in Low Density High Temperature Powder Metallurgy Alloys (W.E. Frazier, M.J. Koczak and P.W. Lee, eds), TMS-AIME, Warrendale, PA, 1991, p. 109.

3. E. Fitzer and F.K. Schmidt, High Temperatures-High Pressures, 1971, (3), 445-460.

4. A.P. Hynes, M.S. Wilenski and R.H. Doremus in Proc. Am. Soc. for Composites, Technonic Publ. Co. Inc., Lancaster, PA, 1991, p. 591.

5. A.B. Gokhale and G.J. Abbaschian, Binary Alloy Phase Diagrams, (T.B. Massalski, ed), p. 1631, ASM, Materials Park, OH, 1986.

6.   K.G. Shaw, Rensselaer Polytechnic Institute, unpublished.

7.   K. Sadananda, H. Jones, J. Feng, J.J. Petrovic and A.K.
      Vasudevan, "Creep of Monolithic and SiC reinforced $MoSi_2$",
      to be published.

8.   P.J. Meschter and D.S. Schwartz, <u>J of Metals</u>, 1989(11),
      p. 52.

9.   J.B. Conway and P.N. Flagella, "Creep Rupture Data for the
      Refractory Metals to High Temperatures", General Electric
      Company Report No. R-69-NSP-9, 1969.

10.   T.C. Lu, A.G. Evans, R.J. Hecht and R. Mehrabian, <u>Acta
      Metall. 39</u>, (1991) 1853.

Figure Captions

1. Schematic of injection molding process.

2. Cross sectional view of $MoSi_2$-20v%Al_2O_3 composite produced by injection molding.

3. Cross sectional view of random $MoSi_2$-20v%Nb wire composites, HIPed at 1350°C, 3 hrs at 172 MPa pressure.

4. a) Reaction zone in $MoSi_2$-Nb random wire composites.

    b) Microprobe traces across reaction zone, showing phases present. Note iron contamination in reaction zone.

5. X-ray traces of $MoSi_2$ in plasma sprayed laminates.

6. Plasma sprayed $MoSi_2$-Al_2O_3 laminates.

7. Higher magnification view of as-deposited laminate in SEM backscatter mode.

8. TEM views of plasma sprayed MoSi-Al_2O_3 laminate
    a) interface region, b) second phase particles in $MoSi_2$.

9. Rockwell "A" hardness indentations, a) HIPed $MoSi_2$
    b) plasma sprayed $MoSi_2$, c) injection molded $MoSi_2$-Al_2O_3
    d) plasma sprayed $MoSi_2$-Al_2O_3.

10. Hardness of $MoSi_2$ and Al_2O_3 as a function of arc current.

11. Flexural stress vs. displacement curves, a) $MoSi_2$ and $MoSi_2$-20v%Nb particles, b) $MoSi_2$-20v% random Nb fibers, c) $MoSi_2$-20v% aligned continuous Nb fibers.
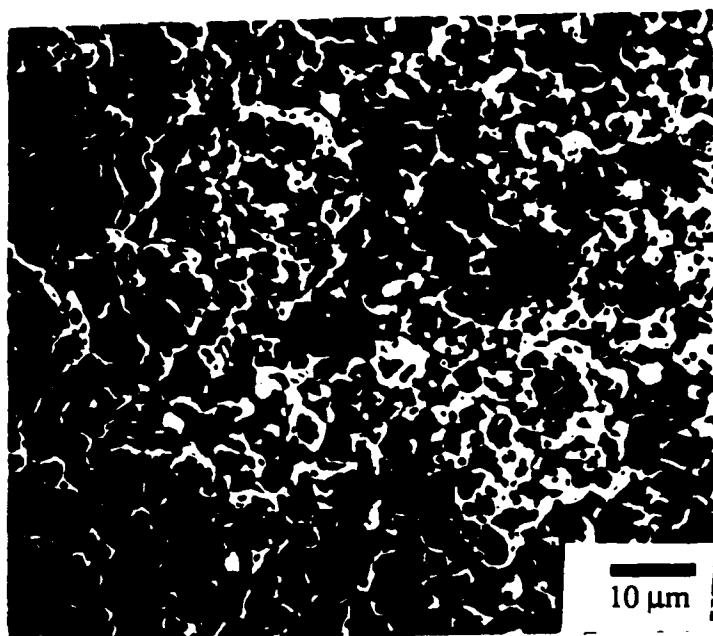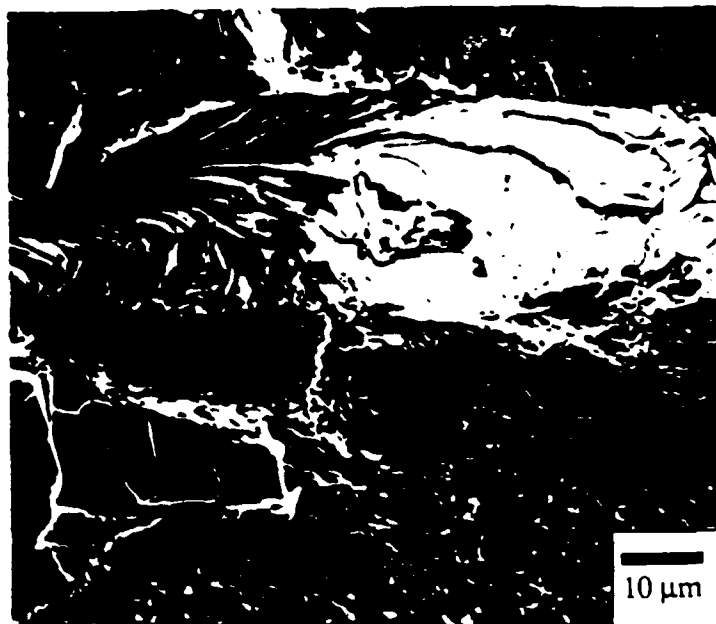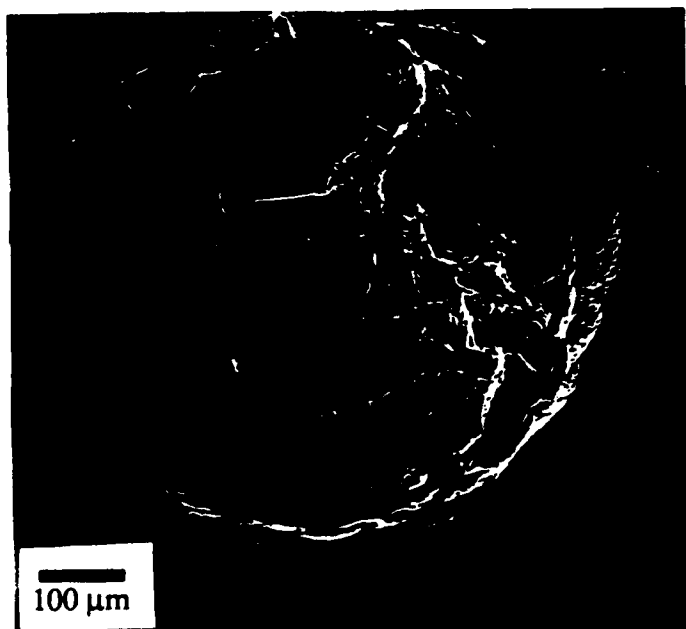
12. SEM fractographs of bend specimens, a) $MoSi_2$, b) $MoSi_2$-20v% random Nb fibers, c) $MoSi_2$-20v% continuous Nb fibers.
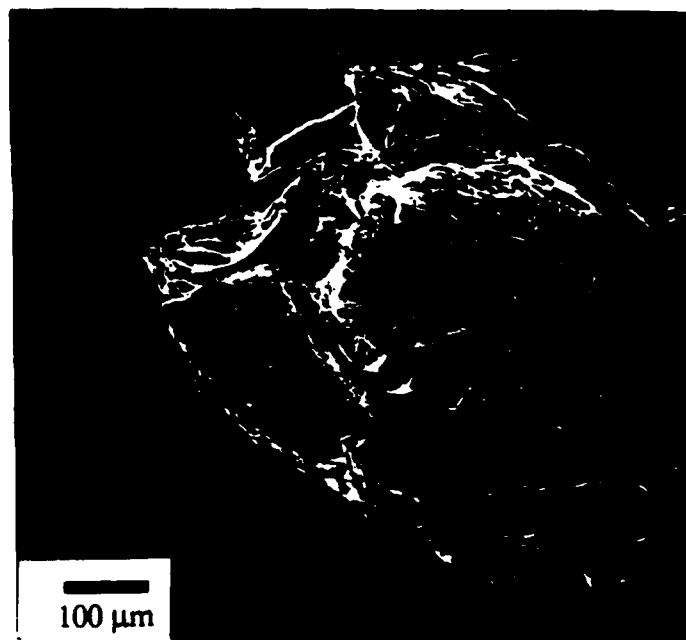
13. SEM fractographs of bend specimens, a) $MoSi_2$, b) $MoSi_2$-20v% particles, c) $MoSi_2$-20v% short random fibers, d) $MoSi_2$-20v% continuous fibers.
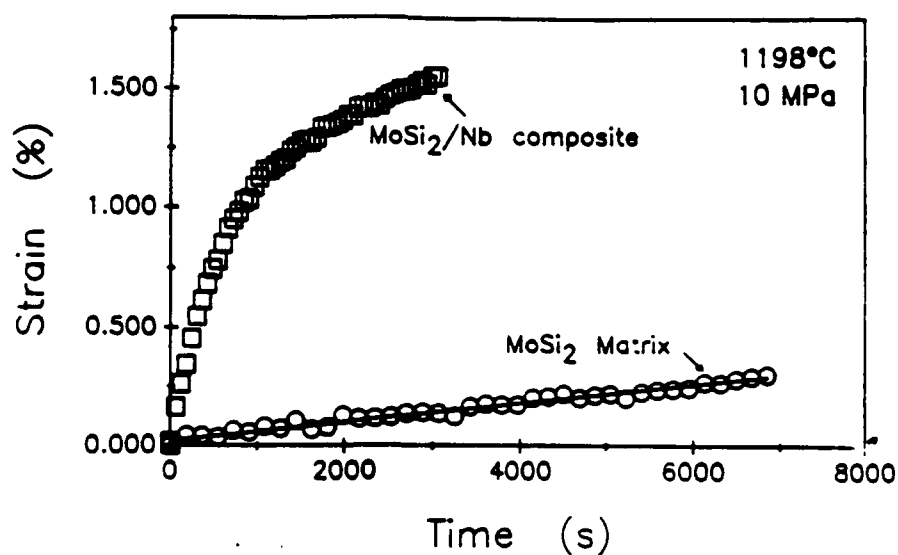
14. Creep curves for $MoSi_2$ and $MoSi_2$-20v%Nb particles, 1200°C, σ=10 MPa[4].

15. Creep rates vs. temperature, σ=10 MPa. Data for Sadananda et al[7] shown for comparison.
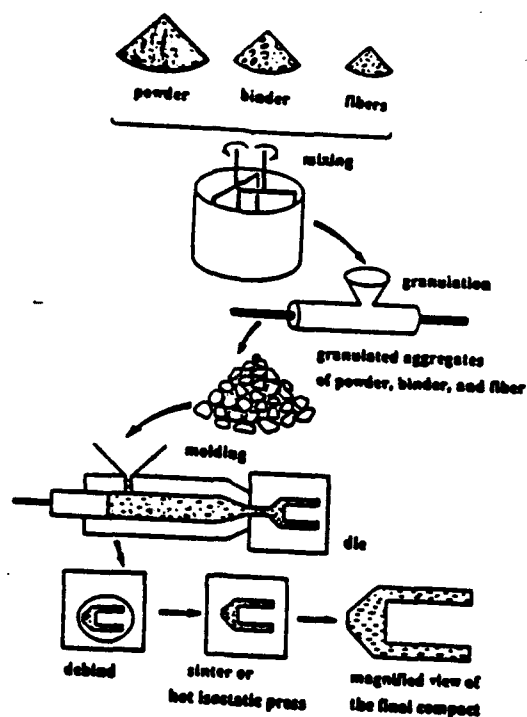
Fig. 1.   Schematic of injection molding process.
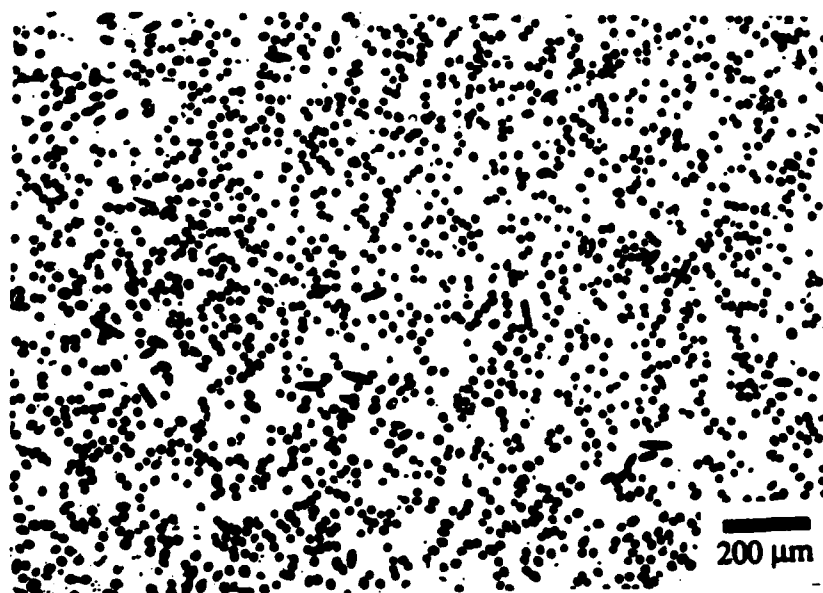
Fig 2.   Cross sectional view of $MoSi_2$-20v%Al_2O_3
          composite produced by injection molding.

Fig. 3. Cross sectional view of random $MoSi_2$-20v%Nb wire composites, HIPed at 1350°C, 3 hrs at 172 MPa pressure.
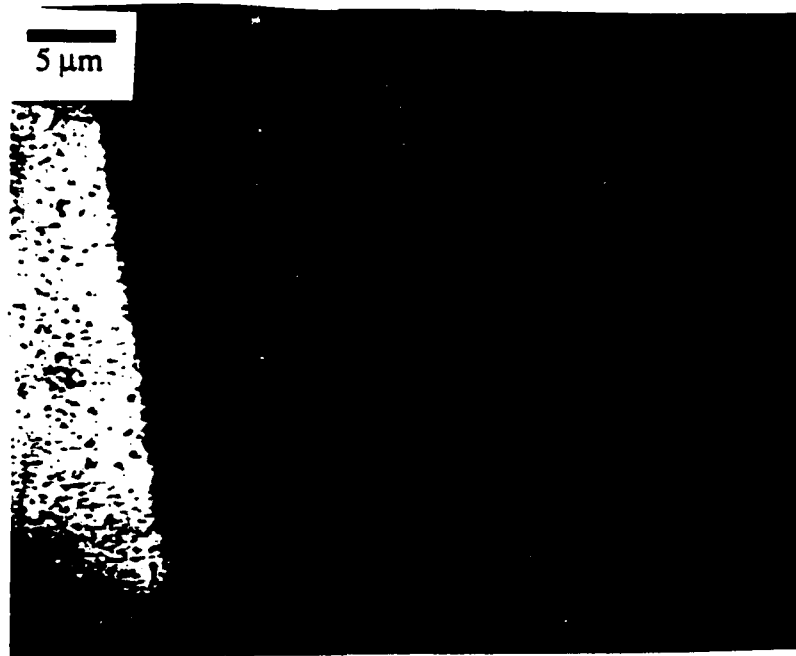
a)
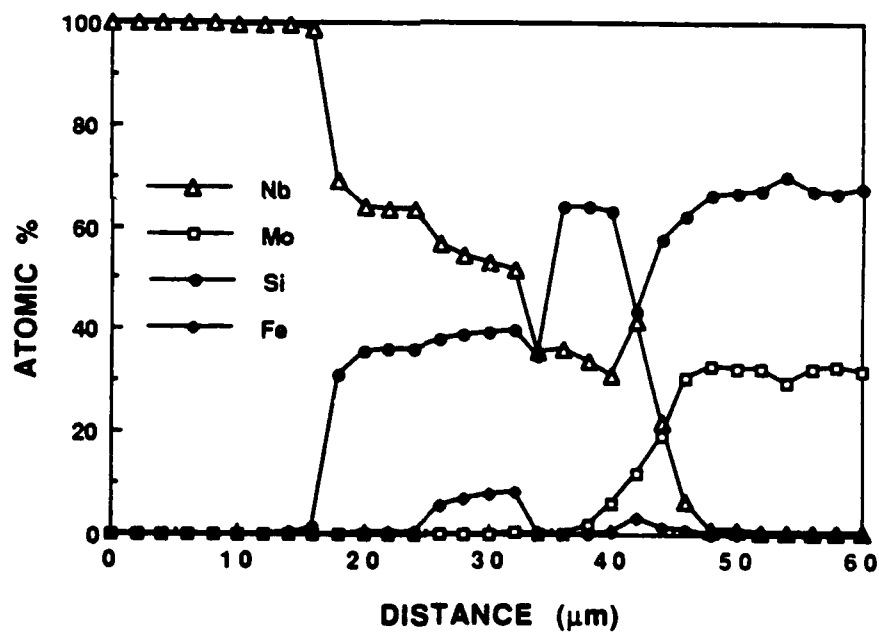
b)

Fig. 4.   a) Reaction zone in MoSi$_2$-Nb random wire composites.

b) Microprobe traces across reaction zone, showing phases present. Note iron contamination in reaction zone.

18
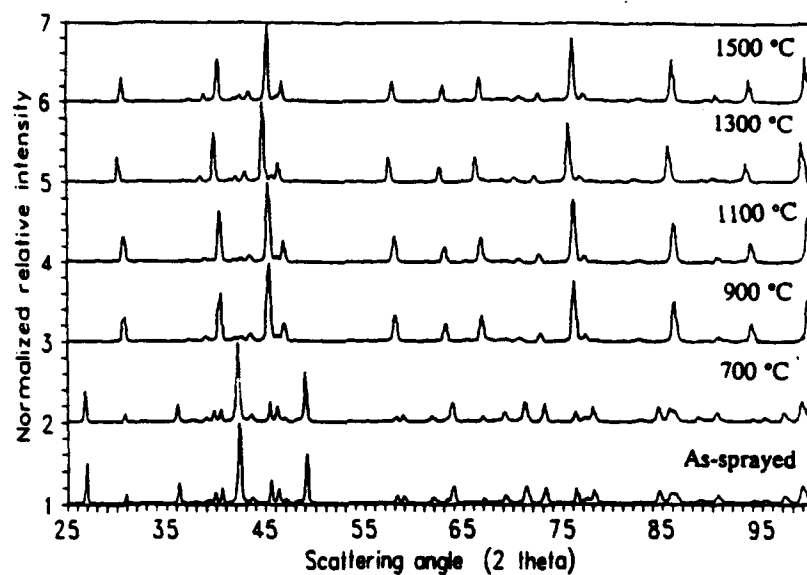
Fig 5.   X-ray traces of MoSi$_2$ in plasma sprayed laminates.
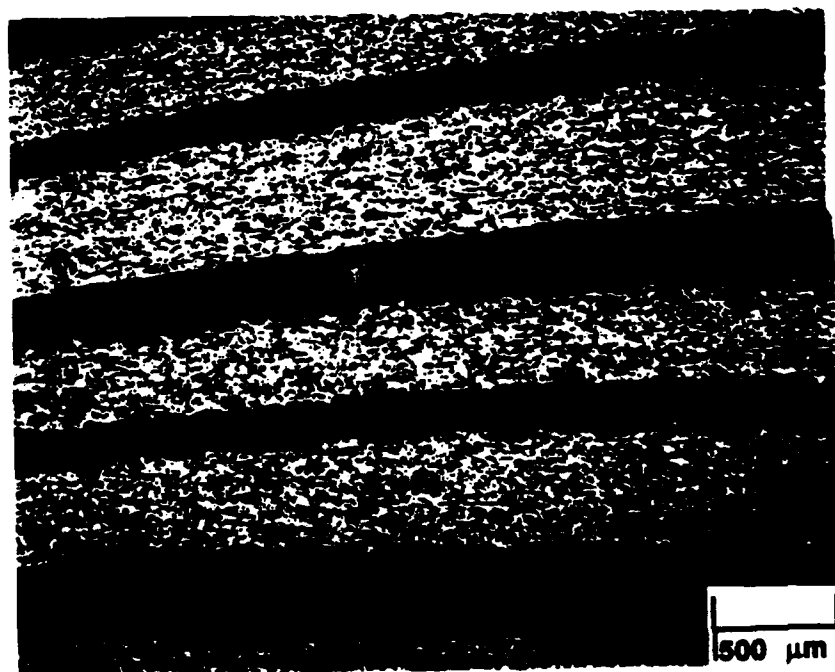
Fig. 6.   Plasma sprayed MoSi$_2$-Al$_2$O$_3$ laminates.
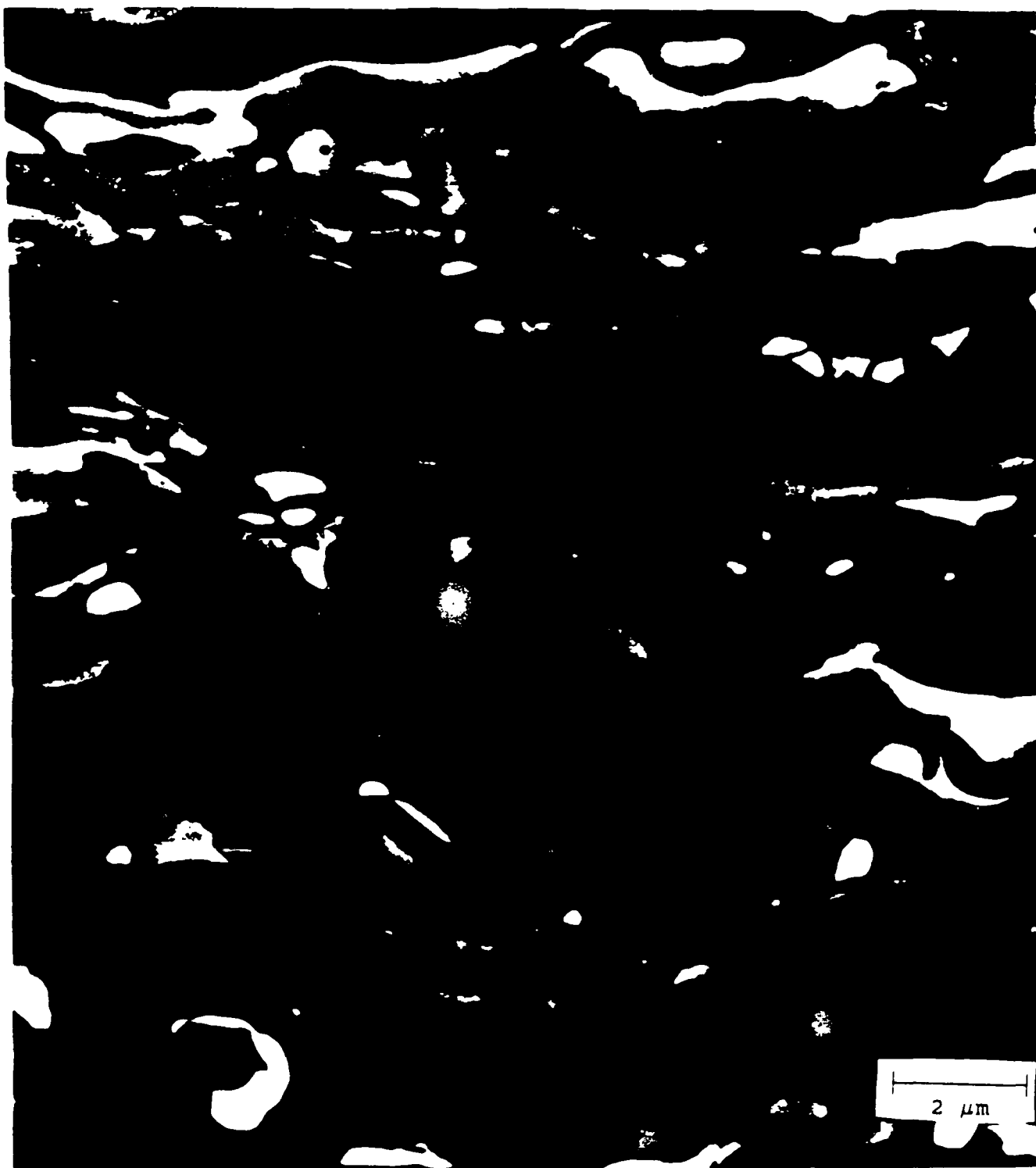
Fig. 7.   Higher magnification view of as-deposited
           laminate in SEM backscatter mode.
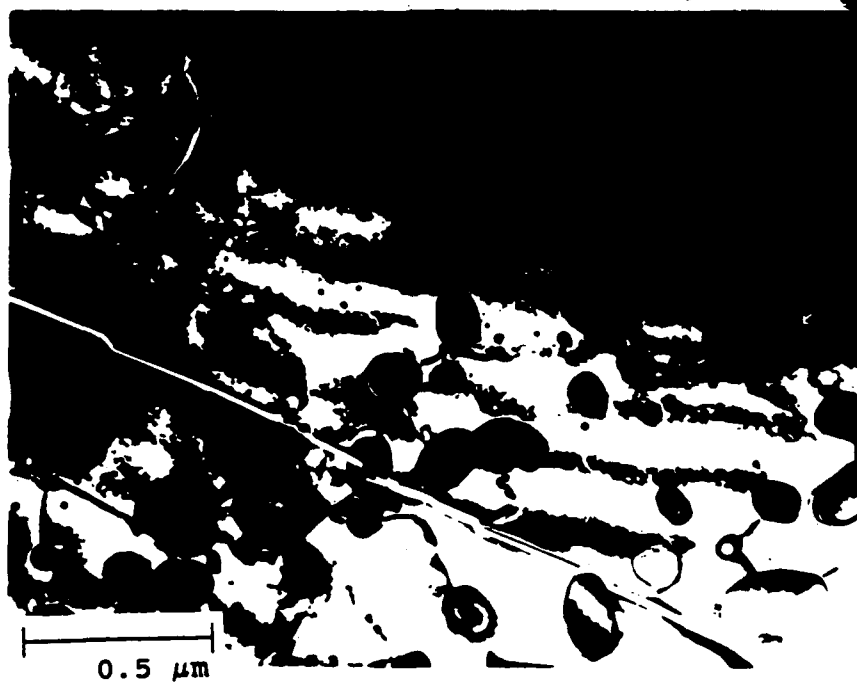
Fig. 8.   TEM views of plasma sprayed $MoSi-Al_2O_3$ laminate a) interface region, b) second phase particles in $MoSi_2$.

21
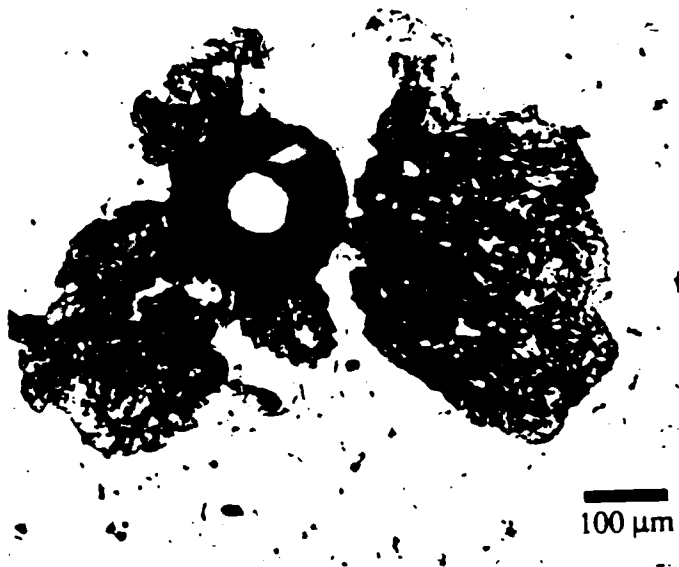
a)
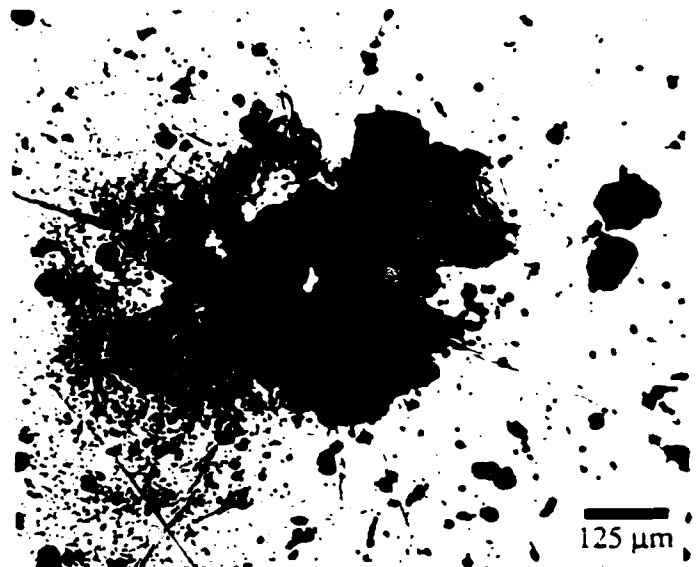
b)
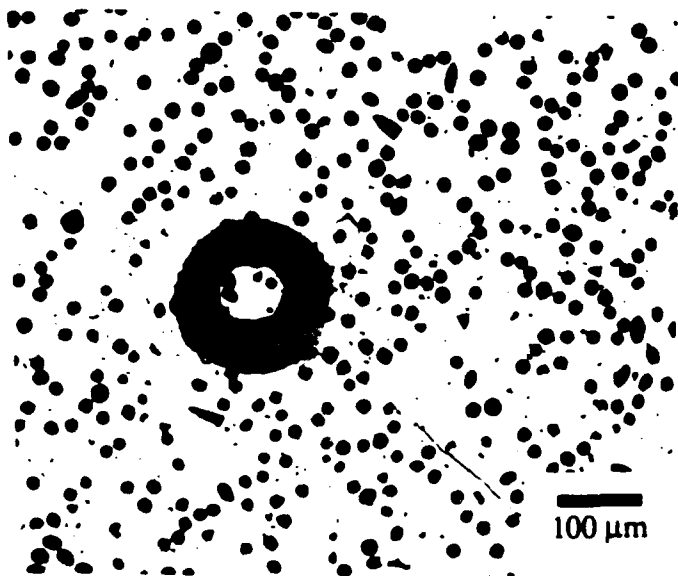
c)

d)

Fig. 9. Rockwell "A" hardness indentations, a) HIPed $MoSi_2$, b) plasma sprayed $MoSi_2$, c) injection molded $MoSi_2-Al_2O_3$, d) plasma sprayed $MoSi_2-Al_2O_3$.

Fig. 10.   Hardness of MoSi$_2$ and Al$_2$O$_3$ as a
           function of arc current.
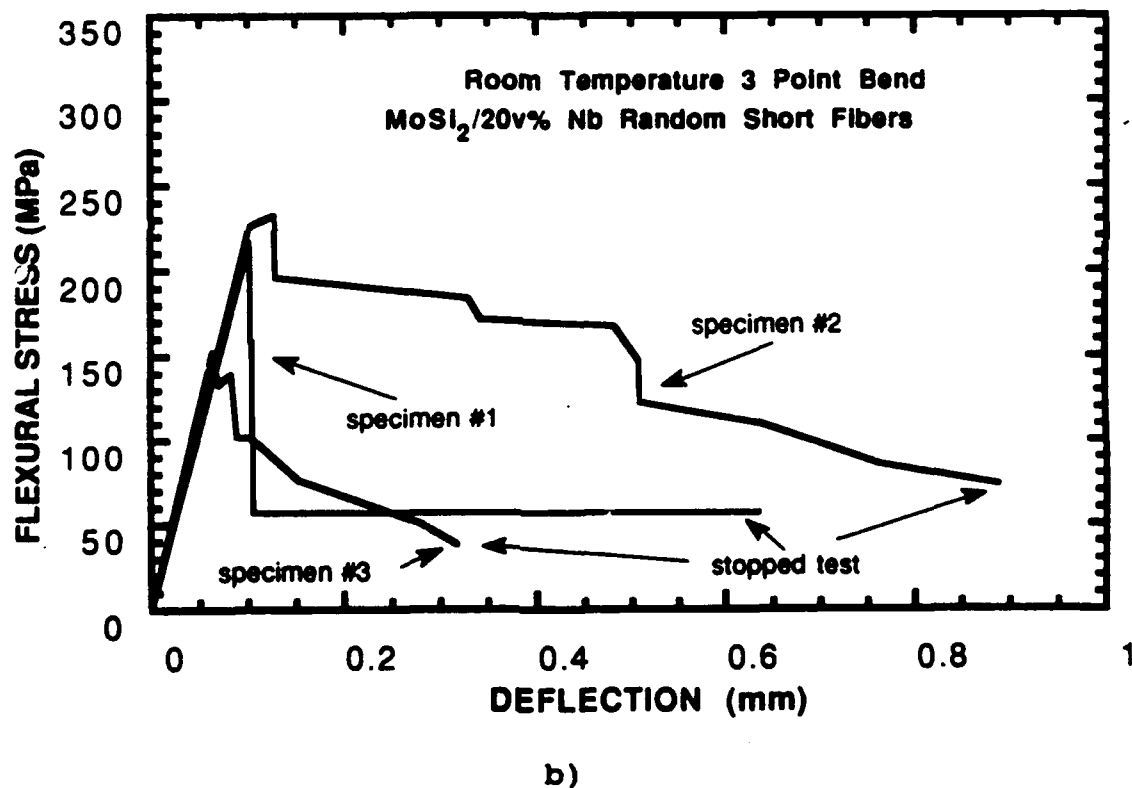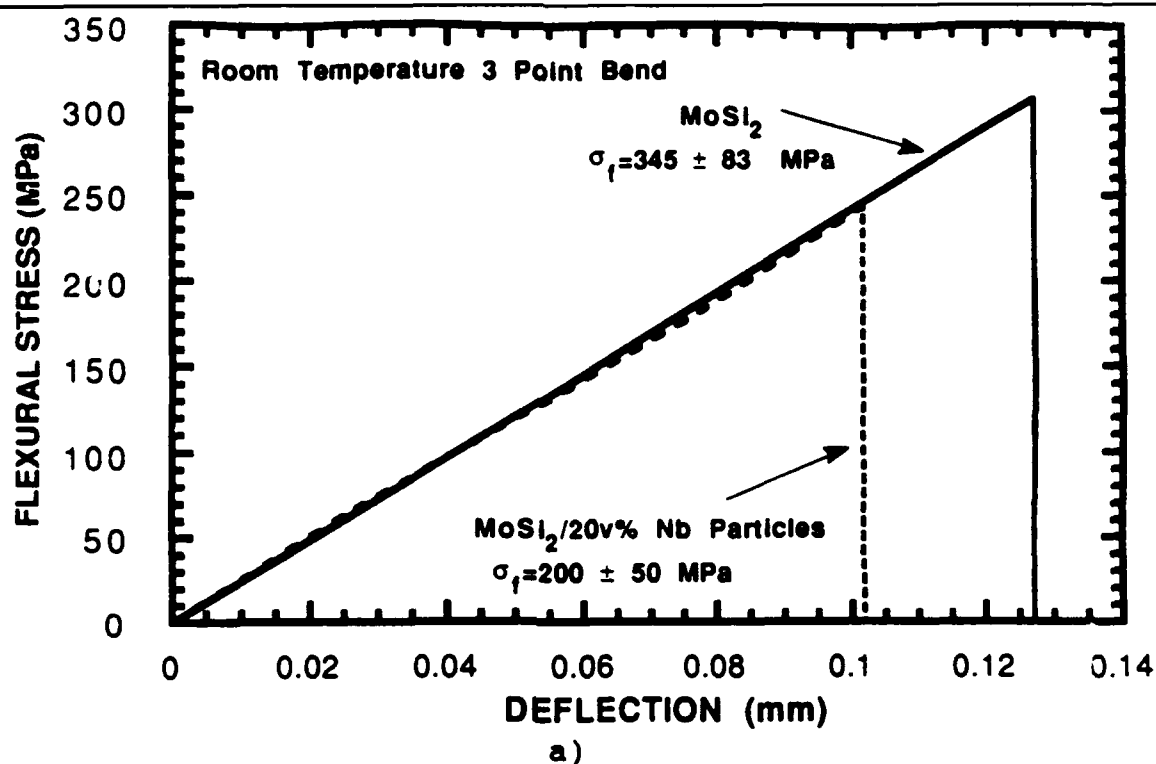
23

Fig. 11. Flexural stress vs. displacement curves, a) MoSi$_2$ and MoSi$_2$-20v%Nb particles, b) MoSi$_2$-20v% random Nb fibers, c) MoSi$_2$-20v% aligned continuous Nb fibers.

Room Temperature 3 Point Bend
MoSi$_2$/20 Nb Continuous Aligned Fibers
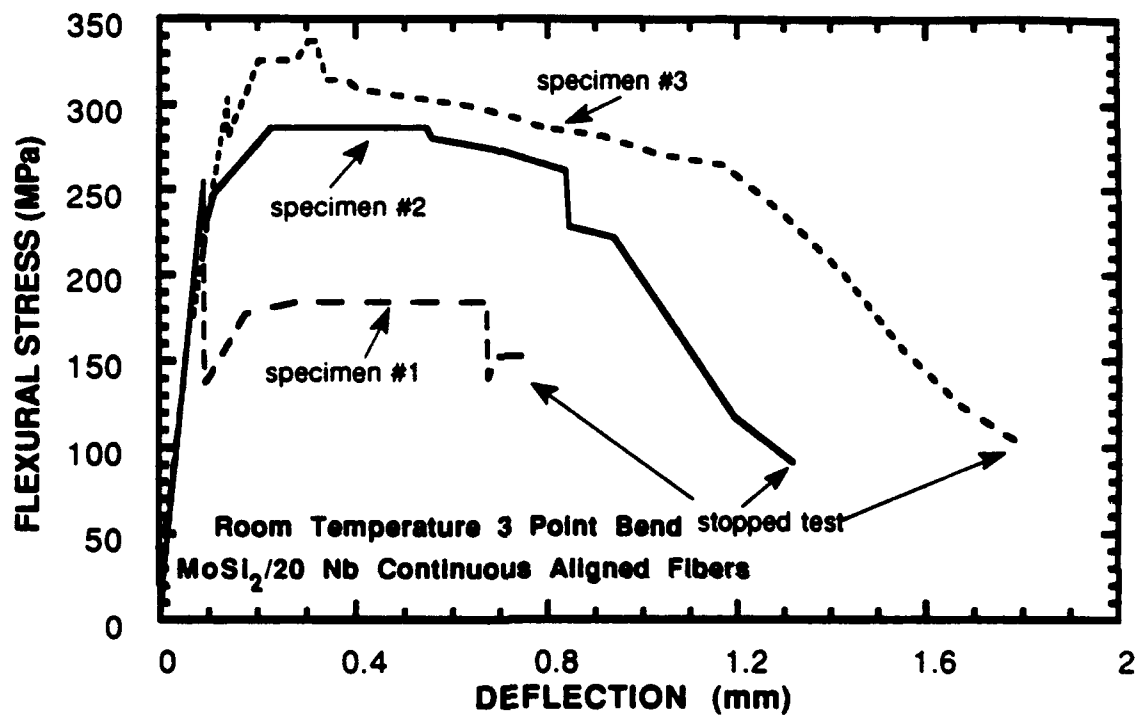
c)

Fig. 11. Flexural stress vs. displacement curves, a) MoSi$_2$
and MoSi$_2$-20v%Nb particles, b) MoSi$_2$-20v% random
Nb fibers, c) MoSi$_2$-20v% aligned continuous Nb
fibers.
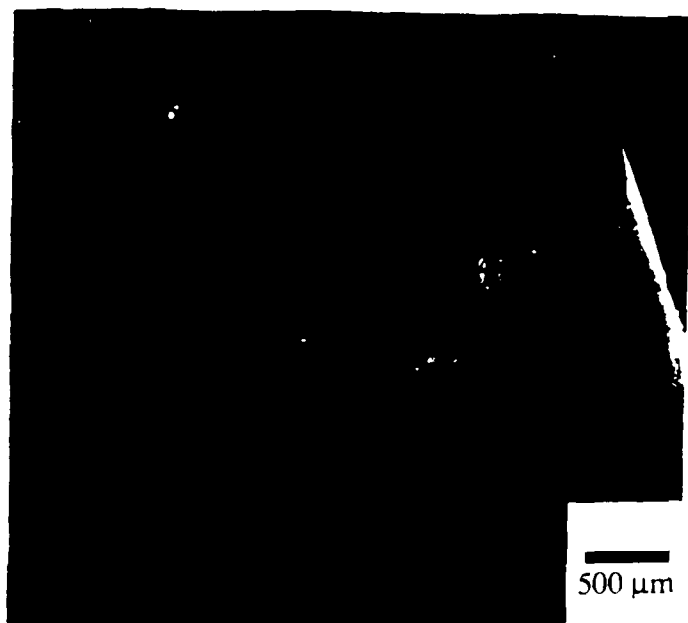
Fig. 12. SEM fractographs of bend specimens, a) $MoSi_2$, b) $MoSi_2$-20v% random Nb fibers, c) $MoSi_2$-20v% continuous Nb fibers.

26

Fig. 13. SEM fractographs of bend specimens, a) $MoSi_2$, b) $MoSi_2$-20v% particles, c) $MoSi_2$-20v% short random fibers, d) $MoSi_2$-20v% continuous fibers.

27

Fig. 14. Creep curves for MoSi₂ and MoSi₂-20v%Nb particles, 1200°C, σ=10 MPa[4].
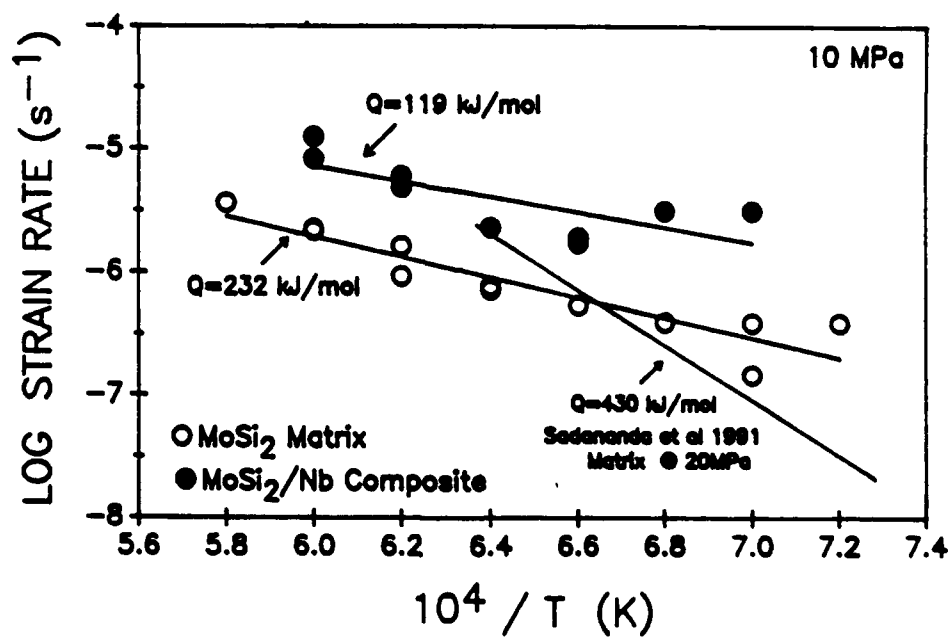
Fig. 15. Creep rates vs. temperature, σ=10 MPa. Data for Sadananda et al[7] shown for comparison.

28

PROCESSING AND PROPERTIES OF INTERMETALLIC MATRIX COMPOSITES

D.E. Alman and N.S. Stoloff
Materials Engineering Department
Rensselaer Polytechnic Institute
Troy, New York 12180-3590

ABSTRACT

This paper is concerned with the processing and mechanical properties of intermetallic-matrix composites. The effects of processing variables on fabrication of compounds including Ni_3Al, NiAl, $TiTaAl_2$, $MoSi_2$ and their composites is described. A key concern is with processing effects on microstructure, selection of compatible ceramic reinforcing phases, and whisker alignment through injection molding.

INTRODUCTION

Intermetallic compounds with low densities (<7.0 g/cm^3) and high melting temperatures ($>1600°C$) are attractive for potential high temperature structural applications. However, before these compounds can be exploited for this purpose their low toughness and inadequate creep strength must be improved. Composite strengthening, in particular in the form of fibrous reinforcement, is an approach that can improve both toughness and creep strength. Thus, the fabrication and properties of intermetallic matrix composites are under intense investigation, as evidenced by a recent Materials Research Society conference devoted to the subject [1].

To date, intermetallic matrix composites in our laboratory and elsewhere have largely been fabricated by powder metallurgical techniques. Therefore, this paper will emphasize various powder consolidation methods. The preparation of intermetallic matrix composites by liquid or vapor routes has been described in a recent review paper [26] and in several other chapters of ref. 1.

Table I is a summary of powder processing techniques that have been applied to IMC's. Noteworthy is the use of both elemental powders (reactive sintering or reactive HIPing) as well as prealloyed powders. Most of these techniques have been applied to aluminides, although considerable attention has been devoted also to $MoSi_2$. The properties of alloys to be described in this paper are listed in Table II.

REACTIVE PROCESSING

Our research has emphasized reactive sintering for forming several aluminides and their composites. Reactive sintering [2,3] involves reacting elemental powders to form the desired compound. Upon heating a powder mixture to the lowest liquidus temperature (commonly either a eutectic, or melting temperature of one of the constituents) a transient liquid forms. This liquid rapidly spreads through the component, consuming the elemental powders and precipitating a solid intermetallic compound. The driving force for this process is the thermodynamic stability of the high melting temperature of the intermediate compound. Consequently, these reactions are exothermic in nature, which results in the temperature of the component being sintered to be markedly increased. This process is spontaneous, self driving and persist only for a few seconds; it has also been termed in the literature as high temperature self propagating synthesis(SHS). Like other transient liquid phase sintering treatments the liquid provides a capillary force on the structure which leads to densification [4]. However, if the solubilities are unbalanced, swelling can occur due to the formation of Kirkendall porosity.

Reactive synthesis is ideally suited for a system in which the lowest liquidus temperature is an eutectic, such as the Ni-Al system (Fig. 1a). Notice that as Ni diffuses into Al, the liquidus temperature initially decreases; therefore, diffusion will enhance the formation of a liquid phase and the compounds in this system are readily formed. In a system in which the lowest liquidus temperature is the melting temperature of one of the constituent elements, such as in Ti-Al (see Fig. 1b) diffusion impedes the

formation of the liquid phase [5]. As Ti diffuses into Al notice that the liquidus temperature is increased; therefore the reactive synthesis of compounds is inhibited. Thus, reactive sintering is sensitive to processing parameters such as heating rates, interfacial cleanliness, green density, and particle size. Because of the rapid spreading and reaction of the liquid, pore formation at prior particle boundaries is common, especially in systems with large particle sizes and large exotherms. Furthermore, dimensional control proves difficult if an excess of liquid is formed. Because of such problems, the applications of reactive sintering have been limited. However, as demonstrated here, the process is well suited to forming dense intermetallic compound composite structures.

Reactive sintering has been applied in various forms to produce composites based upon NiAl, Ni$_3$Al, TaAl$_3$, NbAl$_3$ and TiAl. In one variant, compound formation and densification is achieved in separate steps by mixing elemental powders, reacting, pulverization (grinding), compaction, and subsequent sintering. Variations on this basic scheme involved hot pressing and pressure assisted sintering. Stoichiometry control is important and if often achieved using an excess of the more volatile ingredient or intermediate chemical leaching to remove unreacted constituents. The current reactive sintering approach circumvents these problems by using commercial elemental powders, low processing temperatures, short process cycles with a classic press and sinter technology. Small particle sizes generally proved most useful [2,6,7].

To date, most work in our laboratory on reactive sintering of composites has been carried out on the NiAl-TiB$_2$ system. In general, tensile or compressive strength is much improved by the addition of up to 40vtTiB$_2$; however, toughening cannot be achieved by the use of brittle particles, so we have devoted recent efforts to preparing fibrous composites, utilizing Al$_2$O$_3$ reinforcements.

Recently, we have noted an apparent "dispersion softening" effect in NiAl-TiB$_2$ to which Hf has been added for solid solution strengthening of the matrix, see Fig. 2. Note that although TiB$_2$ strengthens NiAl, it weakens NiAl+Hf; similar results have been reported for XD NiAl/Ni$_2$AlTi-TiB$_2$ composites, by Whittenberger et al [8].

The dispersion weakening phenomenon occurs in highly creep-resistant alloys between 0.3 and 0.7 T$_m$. Edwards et al [9] theorized that the particle-matrix interface becomes a source of mobile dislocations which leads to the weakening phenomenon. The creep resistance of NiAl has been markedly improved by alloying with Hf, with creep resistance approaching that of Ni base superalloys [10].

Al$_3$Ti alloys to which 9% Cr has been added to produce a fcc structure have been reinforced with 10 and 30vt chopped Al$_2$O$_3$ fibers through reactive HIPing [11]. Compressive yield strengths of the matrix are increased appreciably by the presence of 30vtAl$_2$O$_3$ at 25 and 600°C, the only temperatures at which samples have been tested, see Fig. 3a). However, ultimate strengths in compression are actually decreased at 25°C and are little different than that of the matrix at 400 and 600°C, as shown in Fig. 3b. This indicates that the randomly oriented fibers, by acting as crack initiators, decrease the load carrying capacity of the matrix. Similar effects had been noted previously in random short fiber composites of Ni$_3$Al with FP Al$_2$O$_3$ [12].

TABLE I

POWDER CONSOLIDATION

Hot Press
Reactive Processes
  Sinter
  HIP
  Press
XD
Dynamic Compaction
High Energy Rate Forming
Powder Cloth
Mechanical Alloying
Microstructural Toughening
Injection Molding

TABLE II

PROPERTIES OF INTERMETALLICS STUDIED AT RPI

Compound	Crystal Structure	Melting Point °C	Density g/cm³	Modulus GPa
Ni_3Al	L12	1390	7.50	178.5
NiAl	B2	1640	5.86	294.2
TiAl	L1o	1460	3.91	175.6
$NbAl_3$	DO22	1600	4.54	—
$TaAl_3$	DO22	1550	6.90	167
$MoSi_2$	C11	2030	6.3	359

a)   b)
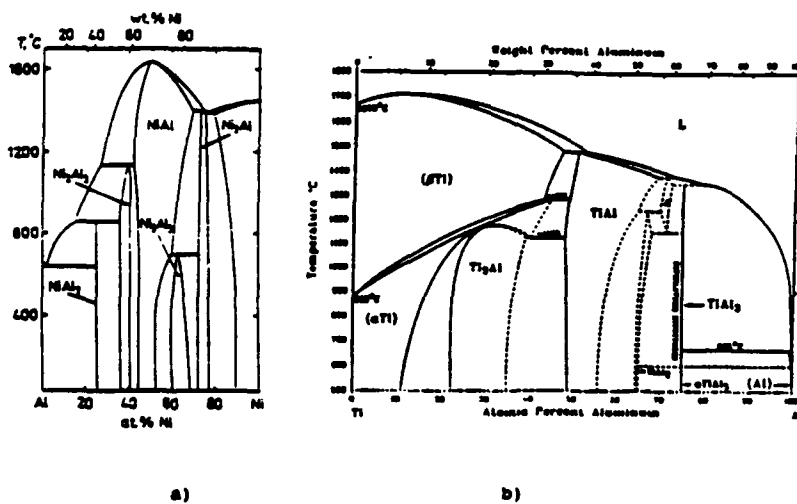
Fig. 1.   Phase diagram of intermetallic systems a)Ni-Al b)Ti-Al.
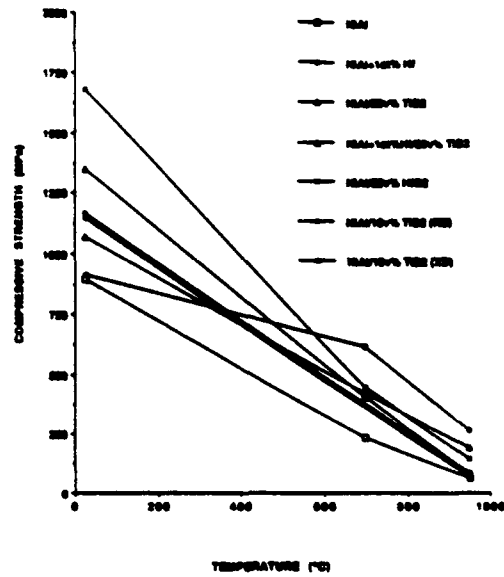
Fig. 2   Compressive flow stress vs. temperature for several NiAl alloys.

a)   b)
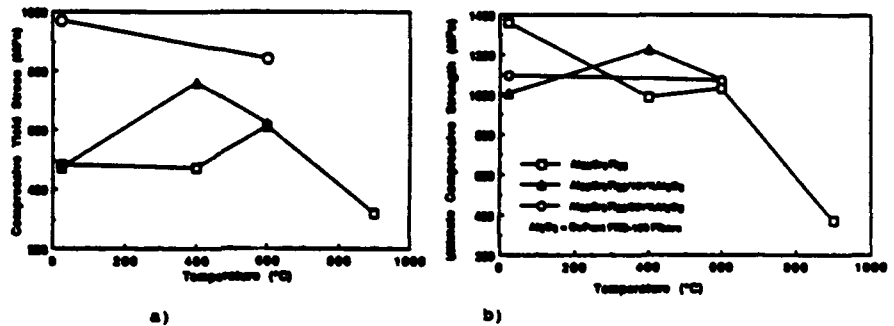
Fig. 3. Mechanical properties of $Al_3Ti.Cr-Al_2O_3$ composites.
    a)compressive yield stress vs. temperature.
    b)compressive ultimate stress vs. temperature.

POWDER INJECTION MOLDING (PIM)

Unless reactive sintering is combined with a layup of fibers or a preform, alignment of continuous fibers is not achievable. However, aligned short fiber composites can be made by combining powder injection molding (powder extrusion) with a subsequent reactive sintering or HIPing cycle [2,3,13]. The method consists of passing a heated mixture of a polymeric binder, a matrix in powder form and chopped fibers through a tapered die to achieve alignment. The technique has been applied to NiAl, MoSi, and Al_3Ta base composites reinforced with Al_2O_3 fibers. Experimental details are reported elsewhere [13]. Suffice it to note here that complete binder removal is critical to avoid contamination of the alloy.

Extrusion is performed at temperatures above the softening point of the polymer binder. With the proper die design complex shapes can be fabricated. However, the major shortcoming of the method is that continuous composites cannot be produced.

NiAl Base Composites

NiAl reinforced with 15vt%Al$_2$O$_3$ fibers produced by extruding from a small die and CIPing the wires together. Porosity remains in the microstructure after reactive sintering indicating that pressure is necessary to consolidate the composites. A HIP cycle proved sufficient for densification, see Fig. 4.

Figures 5a) and b) show microstructures of as-HIPed NiAl reinforced with 10 and 20vt% Al$_2$O$_3$ fibers respectively. Extrusion was performed with a large die, which avoided misalignment due to CIPing. An increased number of misaligned and agglomerated fibers is present in the composite with 20vt% Al$_2$O$_3$.

A longitudinal section of NiAl-20vt%Al$_2$O$_3$ is shown in Fig. 6a). Note that the morphology of the fiber ends is either conical or square. This indicates that the alignment is not perfect. If 100 percent alignment existed, all the fiber ends would be square if the section were cut in the plane of the extrusion direction or conical if the section were not in plane. For comparison, a microstructure of Al$_3$Ta reinforced with 40vt% Al$_2$O$_3$ fabricated by Anton [14] by hot pressing and sectioned at RPI is shown in Fig. 6b). Superior alignment was obtained by the hand layup technique of Anton. Another feature to notice, from the microstructures in Figs. 6 is the number of broken fibers that result from powder processing. It appears that more fibers are damaged in composites fabricated by PIM than by the hand layup technique.

Figures 4 through 6 indicate that reactive synthesis coupled with PIM is a viable route for the consolidation of these composites. The effectiveness of short fibers in improving the mechanical properties of NiAl was determined by tensile tests. Tensile bars were electrodischarge machined (EDM) from NiAl-15vt% Al$_2$O$_3$ HIP bars. Tests were performed in air at a strain rate of 1.67×10^{-4} sec^{-1} on a servohydraulic machine. Results at 800°C, which is above the ductile to brittle transition for reactively synthesized NiAl [6] are reported in Table III. Modest increases in strength resulted from the fibers, but the ductility was markedly reduced. Fracture surfaces for NiAl and the composite are shown in Figs. 7a) and b), respectively. Fiber pullout is prevalent in the composite, with some fibers being totally separated from the matrix. It appears that at this temperature a weak interface exists between the fiber and matrix. However, a strong interface is required for strengthening a ductile matrix by a brittle fiber. Below the ductile to brittle transition (<700°C) [6], NiAl fails by brittle cleavage (Fig 8a). The stress-strain curve of the composite also resembled that of a brittle material. However, fiber pullout was observed on the fracture surface (Fig. 8b). The clam shell markings initiating from the fibers on the fracture surface suggests that fiber failure caused fracture, indicating a strong bond. Also, the separation between the matrix and fiber is not as extensive as it is at 800°C (compare Figs. 7b) and 8b), indicating that the strength of the interface increases with decreasing temperature. Composite properties also are governed by the strength of the fiber matrix interface. A weak interface is necessary for improvements in toughness for a brittle fiber-brittle matrix composite.
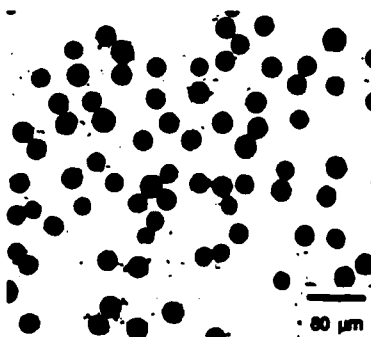

Fig. 4   Fully dense NiAl-15vt%Al$_2$O$_3$ produced by injection molding plus HIPing.
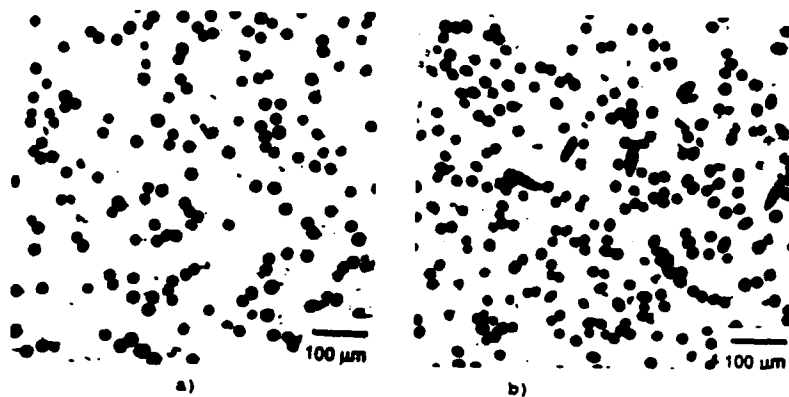
80 μm

Fig. 5   Cross section of NiAl-Al₂O₃ composites produced by molding in a large
         die plus HIPing. a)10v%Al₂O₃ b)20v%Al₂O₃.

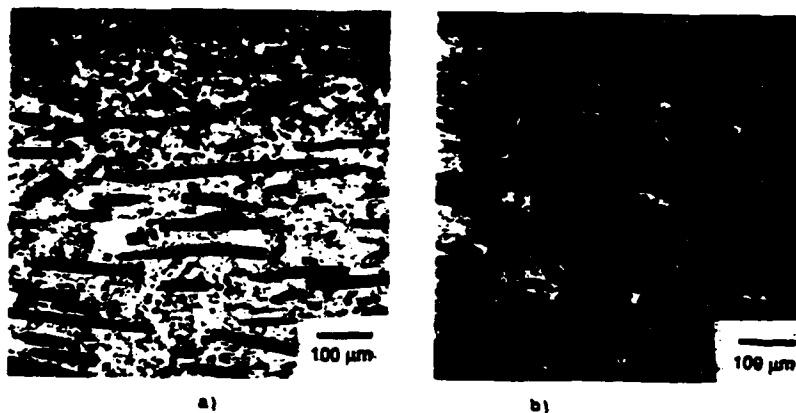Fig. 6.   Longitudinal section of composites produced by differing techniques
          a)NiAl-Al₂O₃, injection molding b)Al₃Ta-Al₂O₃, reactive hot pressing.

TABLE III

800°C Tensile Properties of Reactively Processed NiAl Matrix Composites

	σ_{ys} (MPa)	UTS (MPa)	Reduction Area (%)
NiAl	135	154	14
NiAl 15v% Al₂O₃ Fibers	142	163	3
NiAl 20v% TiB₂ Particles	190	207	12.5
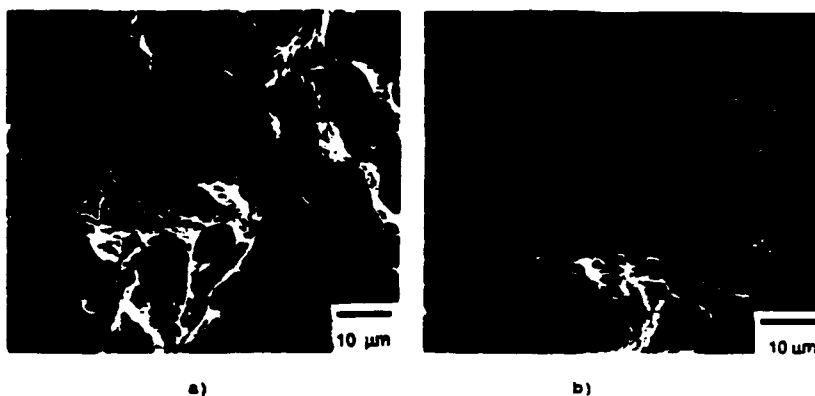
Fig. 7 Fracture surfaces at 800°C a)NiAl b)NiAl-15vt%Al$_2$O$_3$ composite.
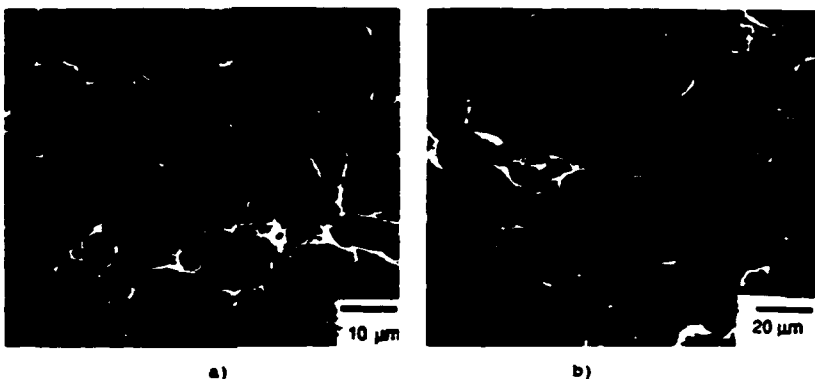
Fig. 8 Fracture surfaces at 700°C a)NiAl b)NiAl-15vt%Al$_2$O$_3$ composite.

Included in Table III are values of strength and ductility for NiAl reinforced with 20vt TiB$_2$ particles (13µm in size) fabricated by reactive synthesis [6]. It would appear that TiB$_2$ particles are more effective in improving high temperature strength than the short Al$_2$O$_3$ fiber.

MoSi$_2$-Base Composites

The microstructure of MoSi$_2$ reinforced with 20vt Al$_2$O$_3$ is shown in Figure 9. Due to lack of material only small specimens could be produced by the extrusion and CIP method. Room temperature hardness results indicate that Al$_2$O$_3$ might improve the toughness of MoSi$_2$. The hardness improved from 87.6 to 90.2 on the Rockwell "A" scale with the addition of the aligned fibers. Hardness values for powder processed MoSi$_2$ have been reported to range from 80 to 87 Rockwell "A" [15,16]. Fig. 10a) and b) show the actual indentations. While cracks propagated from the hardness indentation in the composite specimen, absent were large craters of fractured material observed in the matrix. These results indicate that the DuPont FP fibers may improve the fracture toughness of MoSi$_2$. Attempts to obtain fracture toughness values from Vickers hardness indentations failed, as cracks did not propagate from the indentations.
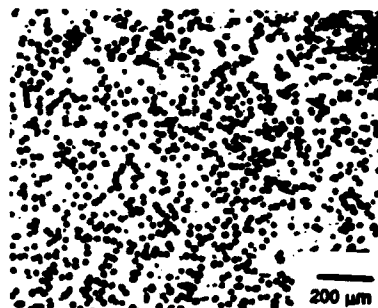
Fig. 9 Microstructure of MoSi$_2$-20v%Al$_2$O$_3$ fabricated by PIM.

a)   b)
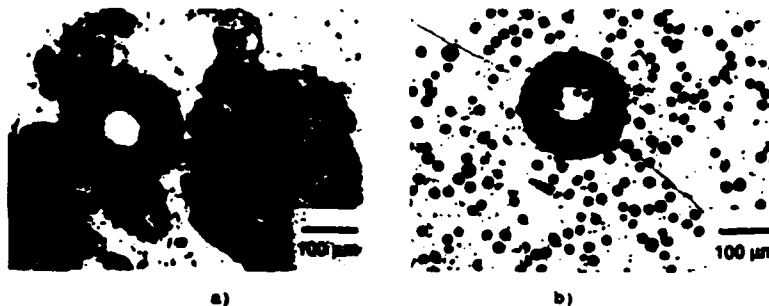
Fig. 10 Hardness indentations in a)MoSi$_2$ b)MoSi$_2$-Al$_2$O$_3$

TaTiAl$_2$ Base Composites

This alloy is a two phase(σ'+γ') derivative of Al$_3$Ta. The monolithic alloy and its composites, see Fig. 11, were HIPed in stainless steel cans at 1250°C, 172 MPa pressure for 2 hours. Note that good alignment of PRD 166 Al$_2$O$_3$ fibers is achieved, Fig. 11a), but that some agglomeration of fibers has occurred. Fig. 11b) shows that the fibers and matrix do not significantly react with each other. Compressive properties of TaTiAl$_2$ and a composite with 10v%Al$_2$O$_3$ particles (<5μ) are shown in Fig. 12. Note that the particles strengthen and also appear to toughen the matrix. This surprising result, which cannot be attributed to a grain refining effect, needs to be verified by further work. Tensile tests on this system are planned for the near future.

DISCUSSION

Certain advantages and disadvantages are inherent in powder processing. The most notable advantage is much lower furnace temperatures than required for melting (even though exothermic reactions may drive the compact temperature to well above the melting point). In addition, powder processing is flexible, in that a range of sizes and shapes can be produced from either elemental powders, which are cheap, or prealloyed powders, which are not. Also, the powder process provides finer grained, more homogeneous material than can be achieved in most melting processes. With anisotropic alloys such as non-cubic MoSi$_2$ and Al$_3$Ta, cooling of powder compacts with little or no cracking is possible, while arc melted buttons of these alloys are prone to cracking.

These advantages are somewhat counterbalanced by the increased likelihood of incorporating impurities, especially oxygen, that can be very detrimental to mechanical behavior. Porosity can be a problem, but is usually easily overcome by HIPing. The fine grain size inherent with powder processing is advantageous for low temperature strength and toughness, but is undesirable for good high

temperature creep resistance. Nevertheless, the inherent versatility of powder processes has led to the many innovative techniques that have been applied to or developed for intermetallic matrix composites. We shall now consider specific aspects of various processes described earlier.

Reactive Sintering

The key to successful reactive consolidation is the use of fine powders, the existence of a finite controllable exotherm and the lack of formation of intervening compounds (as in the Al-Ti system cited above). When full density is not achieved by reactive sintering, subsequent consolidation by HIP can be employed, although in these cases a single stage RHIP operation is more efficient. However, RHIP material tends to be less homogeneous.

Injection Molding

Injection molding, coupled with reactive sintering or HIPing, has proven to provide near perfect alignment and full density for NiAl, MoSi$_2$ and TaTiAl$_2$ composites. However, the method suffers from several shortcomings. These include the need for fine spherical powders, proper selection of binder, complete binder removal, and one or more post extrusion steps. In addition, only short fiber reinforcement is possible, and the fibers may be cracked during molding. Nevertheless, the process offers the potential for near-net shape processing of test specimens and of larger parts, such as turbine airfoils. The effectiveness of short fibers as strengtheners and toughness enhancers has not yet been demonstrated; tests are planned in the near future.

Other Powder Processing Techniques

We now consider other powder approaches to consolidation of NiAl and MoSi$_2$ matrix composites. The XD process developed by Martin Marietta has generally been utilized to produce multiphase alloy powders which are subsequently hot pressed to full density. The process can incorporate both hard (strengthening) and soft (toughening) phases of various sizes. Morphologies ranging from whiskers to platelets can be obtained by appropriate process control. The most common reinforcement has been TiB$_2$, which has been incorporated as 1 μm diameter particles into matrices in the form of a weakly bonded compact [17,18]. However, other ceramic reinforcements: carbides, nitrides and silicides, have been incorporated into Nb-Ti-Al matrices [19]. After synthesis the samples usually are broken up, milled and then consolidated by hot pressing or HIPing [20].
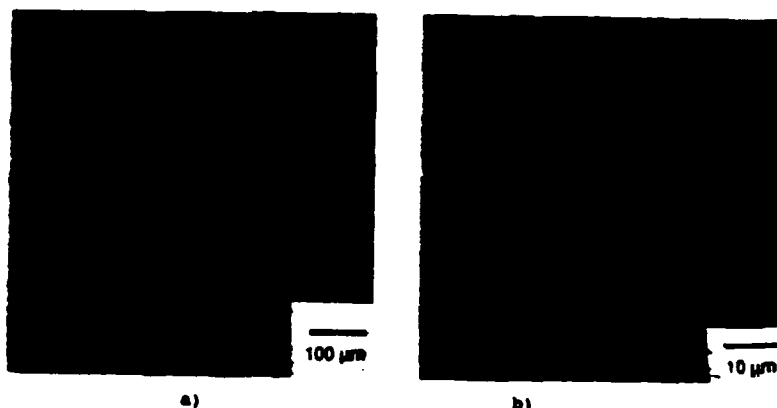

Fig. 11 Microstructures of TaTiAl$_2$-Al$_2$O$_3$ a)general cross section b)reaction-free interfaces.
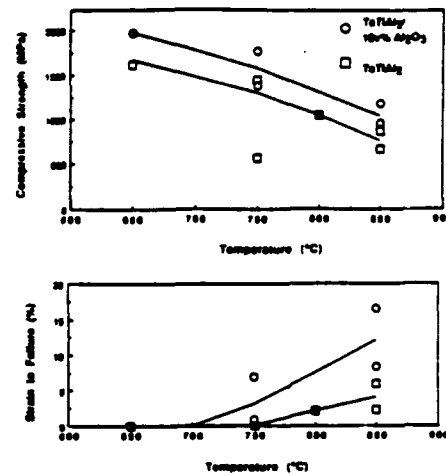
Fig. 12 Compressive Properties vs. temperature for TaTiAl$_2$-Al$_2$O$_3$ particulate composite.

Kampe et al [21] have shown that random short fiber reinforcements of (Ti,Nb)B$_2$ provide higher yield and creep strengths but lower ductility than particulate reinforcements of TiB$_2$ in TiAl-base composites. In our own work, on NiAl, Table III, aligned fibers did not provide higher strength than particles. Since 15vt Al$_2$O$_3$ fibers in NiAl were compared with 20vt TiB$_2$ particles in Table III, the relative merit of particles vs aligned or random fibers of the same reinforcement cannot yet be established.

Petrovic and Honnell [22] have extensively studied the mechanical properties of hot pressed MoSi$_2$ reinforced with SiC whiskers. The strength of MoSi$_2$-base composites can be further strengthened by alloying with WSi$_2$. Anton [14] has utilized vacuum hot pressing of reactive powders with continuous Al$_2$O$_3$ fibers to form full density composites that are stronger and tougher than unreinforced Al$_3$Ta.

The processes described above have almost exclusively been applied to composites strengthened by brittle ceramic particles or fibers. However, several techniques have been utilized to incorporate ductile particles, fibers or tubes into a brittle matrix so as to improve toughness. A few examples follow:

Hot pressing of prealloyed powders has been utilized to prepare ductile phase-toughened alloys such as Nb$_5$Si$_3$-Nb [23], γTiAl-Ti-33aNb [24] and MoSi$_2$-Nb [25]. Fitzer and Remmele [27] utilized Nb wires to reinforce MoSi$_2$. The latter authors mixed MoSi$_2$ and MoGe$_2$ powders and prepegs of Nb wires, prepared by a slurry technique. The primary role of the MoGe$_2$ was to reduce sintering temperatures, but it also served to eliminate the pest (embrittlement) reaction. Improved bend strength was obtained with only one or two layers of the Nb-wire prepegs on the tensile side.

A combination of ductile phase toughening and hard particle strengthening has been reported by Hardone [28,29]. Thin-walled tubes of ductile metals have been mixed with powders and a binder to produce multiphase alloys capable of stopping cracks in more than one direction. Composites of NiAl+B$_4$C/304 tubes and MoSi$_2$+Al$_2$O$_3$/Nb-1%Zr tubes have been produced with substantial increases in toughness relative to the monolithic matrices.

SUMMARY

Several powder consolidation methods have been described, with emphasis on reactive processing and powder injection molding. Densification during reactive consolidation has been applied successfully to several aluminides and has the potential to be used for other intermetallic systems. Full density often is achieved only when HIPing is employed subsequent to or concurrently with reactive sintering, especially in systems with a weak exotherm or in two-phase systems.

phase systems. Reactive sintering is favored also by the use of fine powders and controlled atmospheres. Reactive HIPing of injection molded fibrous composites is a feasible method of producing aligned intermetallic matrix composites. Mechanical properties of NiAl-TiB$_2$ composites prepared by reactive synthesis compare well with properties achieved by other powder processes. MoSi$_2$-Al$_2$O$_3$ short fiber composites are both aligned and fully dense after injection molding and appear to be tougher than monolithic MoSi$_2$. Injection molding is adaptable to other composite systems such as NiAl-Al$_2$O$_3$ and TaTiAl$_2$-Al$_2$O$_3$, but mechanical properties need to be determined.

ACKNOWLEDGEMENT

REFERENCES

1. D.L. Anton, R. McMeeking, D. Miracle, and P. Martin, Intermetallic Matrix Composites, MRS 194, Pittsburgh, PA, 1990.

2. A. Bose and R.M. German, Material Sci. and Engr., A107, 107 (1989).

3. A. Bose and R.M. German, Advanced Materials and Manufacturing Process, 1, 37 (1988).

4. R.M. German, "Liquid Phase Sintering", p. 157, Plenum, New York (1985).

5. R. Oddone, M.S. Thesis, Rensselaer Polytechnic Institute, 1989.

6. D.E. Alman and N.S. Stoloff, Int J Powder Metall, to be published, 1991.

7. D. Alman, A. Dibble, A. Bose, R.M. German and N.S. Stoloff in Proc. of Ceramic and Metal Matrix Composites, H. Mostaghaci, Ed., Pergamon, New York, 1989, p. 217

8. J.D. Whittenberger, R.K. Viswanadham, S.K. Mannan and K.S. Kumar, J. Mat. Res. Vol. 4, 1989, p. 1164

9. G.R. Edwards, T.R. McNelley, and O.D. Sherby, Phil. Mag. Vol. 36, 1975, p. 1164.

10. K. Vedula, G. Anderson, V. Pathare, and I. Aslanidis in Modern Developments in Powder Metallurgy, vol. 16, eds. E.N. Aqua, C.I. Whitman, MPIF, 1984, p. 727.

11. M. Otsuki, D.E. Alman and N.S. Stoloff, Rensselaer Polytechnic Institute, 1990, unpublished.

12. B. Moore, M.S. Thesis, Rensselaer Polytechnic Institute, 1988.

13. D.E. Alman and N.S. Stoloff, Proc. Symp. on Low Density High Temperature P/M Alloys, TMS-AIME, 1990, in press.

14. D.L. Anton in "High Temperature/High Performance Composites", p. 57-64, MRS, P.D. Lemkey, et al, MRS 120, P.D. Lemkey, et al, Eds., Pittsburgh, PA, (1988).

15. R. D. Grintal, Powder Met. Bull. 8 186 (1957).

16. Materials and Methods, 43 131 (1956).

17. J.D. Whittenberger, R.K. Viswanadham, S.K. Mannan and K.S. Kumar, J. Mat. Res. 4, 1164 (1984).

18. J.D. Whittenberger, R.K. Viswanadham, S.K. Mannan and B. Sprissler, J. Mat. Sci., 21, 35 (1990).

19. R.M. Aikin, P.S. McCubbin and L. Christodoulou, Intermetallic Matrix

Composites, MRS 194, Pittsburgh, PA, to be published (1990).

20. D. Whittenberger in "Solid State Powder Processing, p. 137, A.H. Clauer and J.J. Barbadillo, Eds. (1990).

21. S.L. Kampe, J.A. Clarke and L. Christodoulou, Intermetallic Matrix Composites, MRS 194, Pittsburgh, PA, to be published (1990).

22. J. Petrovic and R.E. Honnell, Proc. 14th Annual American Ceramic Soc. Conf. on Composites and Advanced Ceramics, Jan. 1990, Cocoa Beach, FL.

23. R. Mikkanti, and D. Dimiduk, in Intermetallic Matrix Composites, MRS 194, Pittsburgh, PA, to be published (1990).

24. G. R. Odette, G. Lucas, W. Sheckherd and E.H. Aigelfinger, in Intermetallic Matrix Composites, MRS 194, Pittsburgh, PA, to be published 1990.

25. L. Xiao, Y.S. Kim and R. Abbaschian, Intermetallic Matrix Composites, MRS 194, Pittsburgh, PA, to be published (1990).

26. N.S. Stoloff and D.E. Alman, Intermetallic Matrix Composites MRS 194, Pittsburgh, PA, to be published (1990).

27. E. Fitzer and W. Remmele in Fifth Int. Conf. on Composite Materials, (ICCM-5) 1985, p. 515.

28. V.C. Nardone, United Technologies Research Center, presented at DARPA program review, P&W Aircraft, W. Palm Beach, FL, March 1, (1990).

29. V.C. Nardone, J.R. Strife and K. M. Prewo, Intermetallic Matrix Composites, MRS 194, Pittsburgh, PA, (1990).

POWDER PROCESSING AND MECHANICAL PROPERTIES OF
INTERMETALLIC MATRIX COMPOSITES

D.E. Alman and N.S. Stoloff[a] and M. Otsuki[b]

a) Department of Materials Engineering, Rensselaer Polytechnic
Institute, Troy, New York 12180-3590

b) Mitsubishi Materials Corporation, Central Research Institute,
1-297 Kitabukuro-cho, Omiya, Saitama 330, Japan

Abstract

Several intermetallic matrix composites containing either
particles or short fibers have been consolidated by powder
metallurgical techniques. NiAl-TiB$_2$ particulate, NiAl-Al$_2$O$_3$ and
Al$_3$Ti-Al$_2$O$_3$ fibrous composites have been produced by reactive
sintering while MoSi$_2$-Al$_2$O$_3$ and TaTiAl$_2$-Al$_2$O$_3$ composites have been
fabricated by conventional prealloyed p/m techniques. Injection
molding techniques were utilized for the alignment of short fibers
in MoSi$_2$ and NiAl.

1. Introduction

Intermetallic compounds with low densities (<7.0 g/cm^3) and
high melting temperatures ($>1600°C$) are attractive for potential
high temperature structural applications. However, before these
compounds can be exploited for this purpose their low toughness and
inadequate creep strength must be improved. Composite strength-
ening, in particular in the form of fibrous reinforcement, is an
approach than can improve both toughness and creep strength. Thus,
the fabrication and properties of intermetallic matrix composites
are under intense investigation, as evidenced by a recent Materials
Research Society conference devoted to the subject [1].

To date, intermetallic matrix composites in our laboratory and
elsewhere have largely been fabricated by powder metallurgical
techniques. Both elemental powders (for reactive sintering or
reactive HIPing) as well as prealloyed powders have been utilized.
Most of these techniques have been applied to aluminides, although
considerable attention has been devoted also to MoSi$_2$. The
properties of alloys to be described in this paper are listed in
Table 1.

2. Reactive Processing

Our research has emphasized reactive sintering for forming
several aluminides and their composites. Reactive sintering [3,4]
involves reacting elemental powders to form the desired compound.
Upon heating a powder mixture to the lowest liquidus temperature
(commonly either a eutectic, or melting temperature of one of the
constituents) a transient liquid forms. This liquid rapidly
spreads through the component, consuming the elemental powders and

TABLE 1

PROPERTIES OF INTERMETALLICS STUDIED

Compound	Crystal Structure	Melting Point °C	Density g/cm^3	Modulus GPa
NiAl	B$_2$	1640	5.86	177-294
TaTiAl$_2$	DO$_{22}$	1800	≈7.00	-
MoSi$_2$	C$_{11}$	2030	6.3	359
Al$_3$Ti,Cr	L1$_2$	1340*	3.37*	-

* Values are for binary Al$_3$Ti

precipitating a solid intermetallic compound. The driving force for this process is the thermodynamic stability of the high melting temperature of the intermediate compound. Consequently, these reactions are exothermic in nature, which results in the temperature of the component being sintered to be markedly increased. This process is spontaneous, self driving and persists only for a few seconds. Like other transient liquid phase sintering treatments the liquid provides a capillary force on the structure which leads to densification [2]. However, if the solubilities are unbalanced, swelling can occur, due to the formation of Kirkendall porosity.

Reactive sintering has been applied in various forms to produce composites based upon NiAl, Ni$_3$Al, TaAl$_3$, NbAl$_3$, TiAl and Al$_3$Ti. In one variant, compound formation and densification is achieved in separate steps by mixing elemental powders, reacting, grinding, compaction, and subsequent sintering. Variations on this basic scheme involved hot pressing and pressure assisted sintering. The current reactive sintering approach uses commercial elemental powders, low processing temperatures, short process cycles with a classic press and sinter technology. Small particle sizes generally prove most useful [3].

3. Particle-Reinforced Composites

NiAl-TiB$_2$

To date, most work in our laboratory on reactive sintering of composites has been carried out on the NiAl-TiB$_2$ system. In general, tensile or compressive strength is much improved by the addition of up to 40v%TiB$_2$. However, toughening cannot be achieved by the use of brittle particles.

Recently, we have noted an apparent "dispersion softening" effect in NiAl-TiB$_2$ to which Hf has been added for solid solution strengthening of the matrix, see Fig. 1. Note that although TiB$_2$ strengthens NiAl, it weakens NiAl+Hf; similar results have been reported for XD NiAl/Ni$_2$AlTi-TiB$_2$ composites, by Whittenberger et al [4].

892

The dispersion weakening phenomenon occurs in highly creep-resistant alloys between 0.3 and 0.7 T_m. Edwards et al [5] theorized that the particle-matrix interface becomes a source of mobile dislocations which leads to the weakening phenomenon. The creep resistance of NiAl has been markedly improved by alloying with Hf, with creep resistance approaching that of Ni base superalloys [6].
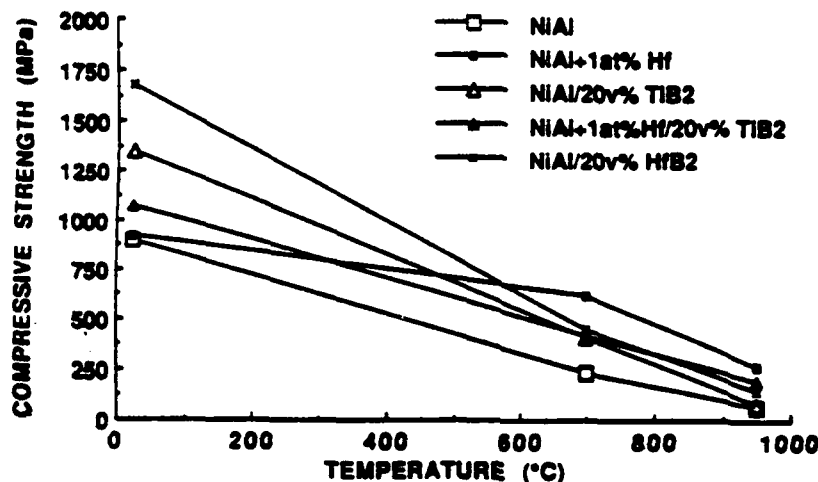

Fig. 1   Compressive flow stress vs. temperature for several NiAl alloys.

TaTiAl₃ Base Composites

TaTiAl₃ is a two phase ($\sigma'+\gamma'$) derivative of Al₃Ta. σ' consists of Ta₃Al alloyed with Ti, while γ' is TiAl alloyed with Ta. Prealloyed TaTiAl₃ powders were HIPed in 304 stainless steel cans at 1250°C, 172 MPa pressure for 2 hours. The resultant microstructure is shown in Fig. 2a. TaTiAl₃ reinforced with fine (<5um) Al₂O₃ particles also were consolidated employing the above conditions (Fig. 2b). Compressive properties vs temperature for these two alloys are shown in Fig. 3. Note that the particles strengthen and also appear to toughen the matrix. This surprising result, which cannot be attributed to a grain refining effect, needs to be verified by further work. Tensile tests on this system are planned for the near future.

4. Random Fiber Composites

Al₃Ti-Base Composites

Al₃Ti alloys were produced by RHIP conditions at 1270°C. Al₃Ti is a tetragonal compound with DO₂₂ crystal structure. In order to improve the chances for toughening of composites based upon this alloy, 9% Cr was utilized to stabilize the fcc L1₂ structure. X-ray results verified the achievement of this structure.

Compressive properties vs temperature for the intermetallic matrix alone are shown in Fig. 4. Note that appreciable compressive ductility is achieved even at 25°C, and that there is a sharp rise in plasticity at temperatures above 500°C.

(a)   b)
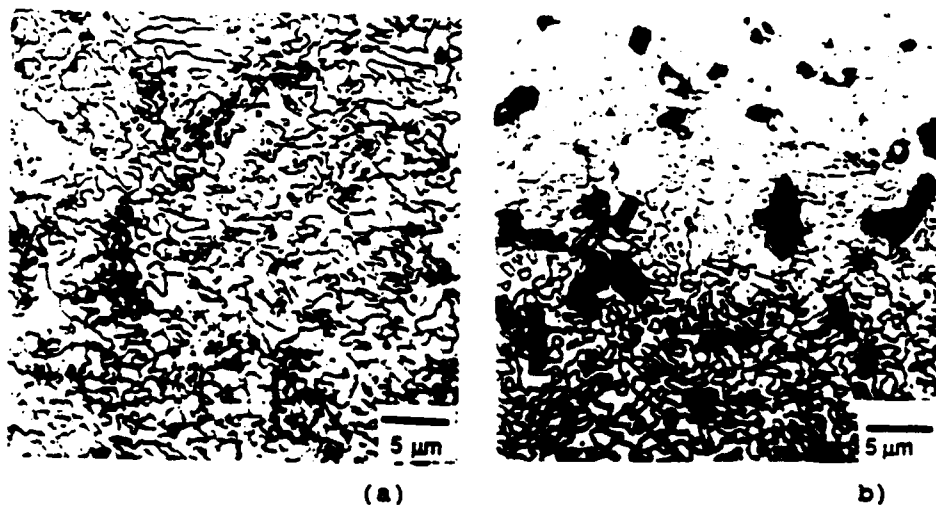
Fig. 2   Microstructures of a) TaTiAl₂ and
          b) TaTiAl₂/10v% Al₂O₃ particulate composite.
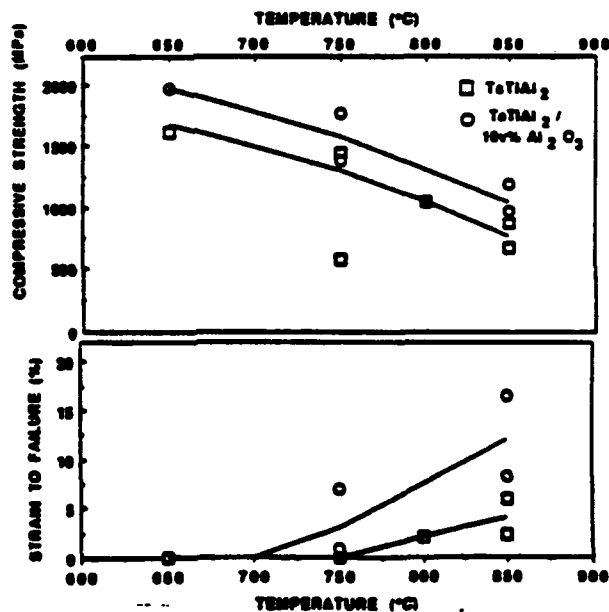
Fig. 3   Compressive Properties vs. temperature for
          TaTiAl₂-Al₂O₃ particulate composite.

The addition of random short fibers of FP Al₂O₃ results in appreciable strengthening but severe loss of ductility at 25°C, see Fig. 5. At 600°C, fibers do not strengthen nearly as much, but the ductility loss is again very severe, also shown in Fig. 5. These observations suggest that randomly oriented fibers act as crack initiators, thereby decreasing the load carrying capacity of the matrix. Similar results have been obtained previously with random short fibers of FP Al₂O₃ in Ni₃Al [7].
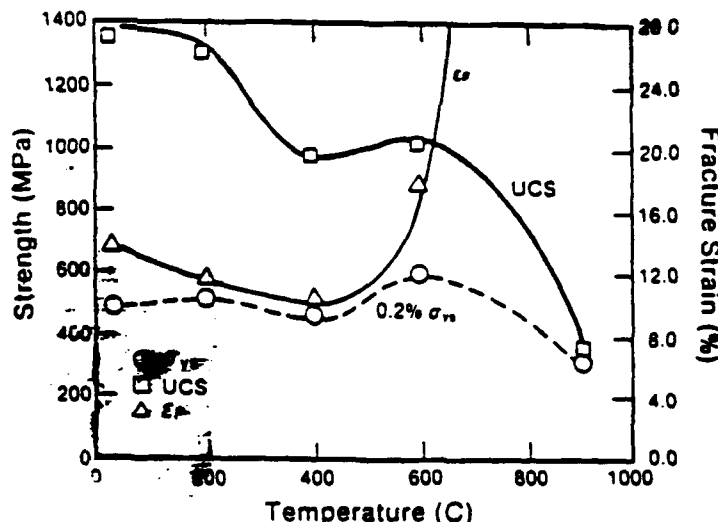
Fig. 4: High temperature compressive properties of Al₆₆Cr.Ti₃₃ RHIPed at 1250°C.

5. Aligned Short Fiber Composites

Aligned short fiber composites can be made by combining powder injection molding (powder extrusion) with a subsequent reactive sintering or HIPing cycle [8-10]. The method consists of passing a heated mixture of a polymeric binder, a matrix in powder form and chopped fibers through a tapered die to achieve alignment. The technique has been applied to NiAl, MoSi₂ and Al₂O₃ base composites reinforced with Al₂O₃ fibers. Experimental details are reported elsewhere [10]. Suffice it to note here that complete binder removal is critical to avoid contamination of the alloy.

Extrusion is performed at temperatures above the softening point of the polymer binder. With the proper die design complex shapes can be fabricated. However, the major shortcoming of the method is that continuous composites cannot be produced.

NiAl Base Composites

NiAl reinforced with FP Al₂O₃ fibers were produced by extruding from a small die and CIPing the wires together. Porosity

remains in the microstructure after reactive sintering, indic::ing
that pressure is necessary to consolidate the composites. A HIP
cycle proved sufficient for densification, see Fig. 6. An
increased number of misaligned and agglomerated fibers was present
in a composite with 20v% Al₂O₃.

The effectiveness of short fibers in improving the mechanical
properties of NiAl was determined by tensile tests. Tensile bars
were electrodischarge machined (EDM) from NiAl-15v% Al₂O₃ HIP bars.
Tests were performed in air at a strain rate of 1.67x10⁻⁴ sec⁻¹ on
a servohydraulic machine. Results at 800°C, which is above the
ductile to brittle transition for reactively synthesized NiAl [11]
are reported in Table 2. Modest increases in strength resulted
from the fibers, but the ductility was markedly reduced.
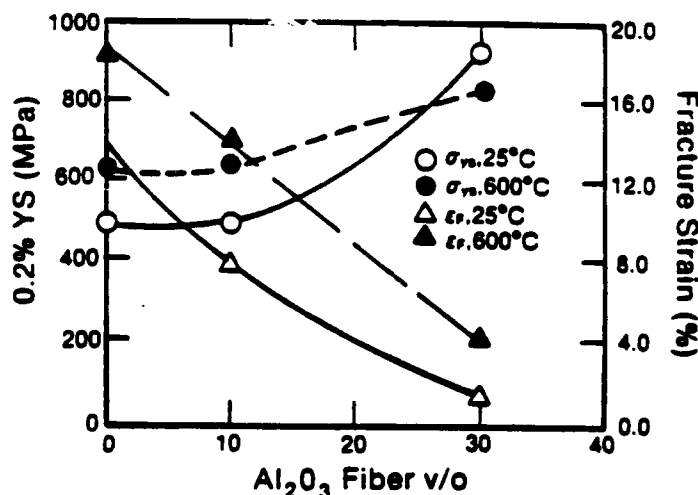
Fig. 5:   Compressive properties of Al₆₆Cr₇Ti₂₇/Al₂O₃ RHIPed at 1270°C
           and tested as function of volume fraction of Al₂O₃ fibers.

MoSi₂ Base Composites

The microstructure of MoSi₂ reinforced with 20v% Al₂O₃ is shown
in Fig.7. Due to lack of material only small specimens could be
produced by the extrusion and CIP method. Room temperature
hardness results indicate that Al₂O₃ might improve the toughness of
MoSi₂. The hardness improved from 802 to 952 Vickers, equivalent
to 87.6 to 90.2 Rockwell "A" with the addition of the aligned
fibers. Hardness values for powder processed MoSi₂ have been
reported to range from 80 to 87 Rockwell "A" [12,13]. While cracks
propagated from the Rockwell "A" hardness indentation in the
composite specimen, large craters of fractured material observed in
the matrix were absent. These results indicate that the DuPont FP

fibers may improve the fracture toughness of MoSi$_2$. Attempts to obtain fracture toughness values from micro hardness indentations failed, as cracks did not propagate from the indentations.

TABLE 2

Tensile Properties of Reactively Processed NiAl Matrix Composites - 800°C

	σ_{ys} (MPa)	UTS (MPa)	Reduction in Area (%)
NiAl	135	154	14
NiAl-15v%Al$_2$O$_3$ Fibers	142	163	3
NiAl-20w% TiB$_2$ Particles	190	207	12.5

Fig. 6. NiAl-15v%Al$_2$O$_3$,
injection molded
plus HIP.
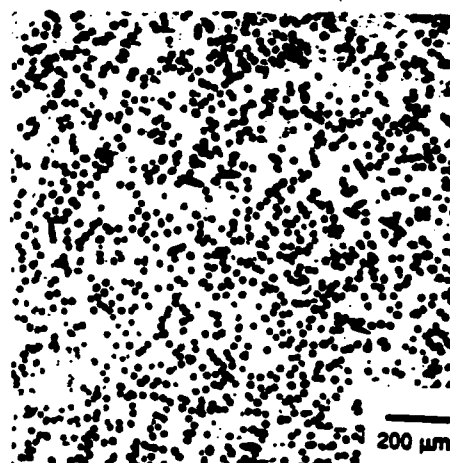
Fig. 7: MoSi$_2$-20v%Al$_2$O$_3$,
injectin molded
plus HIP.

6. Discussion

Certain advantages and disadvantages are inherent in powder processing. The most notable advantage is much lower furnace temperatures than required for melting (even though exothermic reactions may drive the compact temperature to well above the melting point). In addition, powder processing is flexible, in that a range of sizes and shapes can be produced from either elemental powders, which are cheap, or prealloyed powders, which are not. Also, the powder process provides finer grained, more

homogeneous material than can be achieved in most melting processes. With anisotropic alloys such as non-cubic $MoSi_2$ and Al_3Ta, cooling of powder compacts with little or no cracking is possible, while arc melted buttons of these alloys are prone to cracking.

These advantages are somewhat counterbalanced by the increased likelihood of incorporating impurities, especially oxygen, that can be very detrimental to mechanical behavior. Porosity can be a problem, but is usually easily overcome by HIPing. The fine grain size inherent with powder processing is advantageous for low temperature strength and toughness, but is undesirable for good high temperature creep resistance. Nevertheless, the inherent versatility of powder processes has led to the many innovative techniques that have been applied to or developed for intermetallic matrix composites.

The key to successful reactive consolidation is the use of fine powders, the existence of a finite controllable exotherm and the lack of formation of intervening compounds. When full density is not achieved by reactive sintering, subsequent consolidation by HIP can be employed, although in these cases a single stage RHIP operation is more efficient. However, RHIP material tends to be less homogeneous.

Injection molding, coupled with reactive sintering or HIPing, has proven to provide near perfect alignment and full density for $NiAl$, $MoSi_2$ and $TaTiAl_2$ composites. However, the method suffers from several shortcomings. These include the need for fine spherical powders, proper selection of binder, complete binder removal, and one or more post extrusion steps. In addition, only short fiber reinforcement is possible, and the fibers may be cracked during molding. Nevertheless, the process offers the potential for near-net shape processing of test specimens and of larger parts, such as turbine airfoils. The effectiveness of short fibers as strengtheners and toughness enhancers has not yet been demonstrated; tests are planned in the near future.

7. Summary

Several powder consolidation methods have been described, with emphasis on reactive processing and powder injection molding. Densification during reactive consolidation has been applied successfully to several aluminides and has the potential to be used for other intermetallic systems. Full density often is achieved only when HIPing is employed subsequent to or concurrently with reactive sintering, especially in systems with a weak exotherm or in two-phase systems. Reactive sintering is favored also by the use of fine powders and controlled atmospheres. Reactive HIPing of injection molded fibrous composites is a feasible method of producing aligned intermetallic matrix composites. Mechanical properties of $NiAl-TiB_2$ composites prepared by reactive synthesis compare well with properties achieved by other powder processes. $MoSi_2-Al_2O_3$ short fiber composites are both aligned and fully dense after injection molding and appear to be tougher than monolithic $MoSi_2$. Injection molding is adaptable to other composite systems

such as NiAl-Al$_2$O$_3$ and TaTiAl$_2$-Al$_2$O$_3$, but mechanical properties need to be determined. Al,Ti,Cr is strengthened by random Al$_2$O$_3$ fibers, but compressive ductility is sharply reduced.

8. Acknowledgment

9. References

1. Intermetallic Matrix Composites, D.L. Anton, R. McMeeking, D. Miracle and P. Martin, Eds., MRS vol 194, Pittsburgh PA, (1990).

2. R.M. German, Liquid Phase Sintering, Plenum, NY (1985) 157.

3. D. Alman, A. Dibble, A. Bose, R.M. German and N.S. Stoloff in Processing of Ceramic and Metal Matrix Composites, H. Mostaghaci, Eds., Pergamon, NY, (1989) 217.

4. J.D. Wittenberger, R.K. Viswanadham, S.K. Mannan and K.S. Kumar, J. Mat. Res. 4, (1989) 1164.

5. G.M. Edwards, T.R. McNelley, and O.D. Sherby, Phil. Mag., 36, (1977) 1164.

6. K. Vedula, G. Anderson, V. Pathare and I. Aslanidis in Modern Developments in Powder Metallurgy, vol. 16, E.N. Aqua and C.I. Whitman, Eds., Metal Powders Industries Federation, Princeton, NJ, (1984) 727.

7. B. Moore, M.S. Thesis, Rensselaer Polytechnic Institute, (1988).

8. A. Bose and R.M. German, Material Sci. and Engr. A107, (1989) 107.

9. A. Bose and R.M. German, Advanced Materials and Manufacturing Processes, 3, (1988) 37.

10. D.E. Alman and N.S. Stoloff, Proc. Symp. on Low Density High Temperature P/M Alloys, TMS-AIME, in press (1991).

11. D.E. Alman and N.S. Stoloff, Int J Powder Metall, 27 (1991) 29.

12. R.D. Grintal, Powder Met. Bull. 8 (1957) 186.

13. Materials and Methods, 43 (1956) 131.

CONSOLIDATION AND MECHANICAL BEHAVIOR OF INTERMETALLIC MATRIX COMPOSITES

D.E. Alman and N.S. Stoloff, Rensselaer Polytechnic Institute, Materials Engineering Department, Troy, NY 12180-3590

ABSTRACT

Composite strengthening is being investigated in an attempt to improve the mechanical behavior of high melting temperature ($T_m > 1600°C$) intermetallics. NiAl/TiB$_2$, NiAl/Al$_2$O$_3$, MoSi$_2$/Al$_2$O$_3$, and TaTiAl$_2$/Al$_2$O$_3$ particulate or fibrous composites have been fabricated successfully by powder metallurgical techniques. NiAl matrix composites were consolidated by reactive synthesis techniques, while MoSi$_2$ and TaTiAl$_2$ matrix composites were consolidated by conventional prealloyed powder metallurgical techniques. The powder injection molding technique has been evaluated for the alignment of short fibers in these matrices. Presented are results of tension and compression tests performed on these composites.

INTRODUCTION

Intermetallic compounds are being studied as possible high temperature, oxidation resistant structural materials for aerospace and turbine applications. Aluminides and silicides are particularly attractive, with high melting points, low density, high strength, good corrosion and oxidation resistance, nonstrategic elements, and relatively low cost. In some cases these intermetallics exhibit improved strength with temperature (1). Most importantly, recent research has demonstrated improved ductility in some intermetallic systems (2-4). Thus, fabricability and reliability have been improved, leading to new interest in the use of these compounds as matrices for composites.

Melt processing techniques have proven successful for the fabrication of fibrous reinforced intermetallic matrix composites (5-10). However, as the melting temperature of the matrix increases, powder methods for consolidation of composites become more attractive. Powder metallurgical techniques have been successfully applied to fabricate aligned, continuous fibrous reinforced intermetallic matrix composites, as has been demonstrated in the Ti$_3$Al + Nb/SiC(SCS-6) (11) and Al$_3$Ta/Al$_2$O$_3$ (DuPont PRD-166) (12) composites. This paper reviews various powder metallurgical techniques for the fabrication of intermetallic matrix composites. Reactive processing as well as conventional prealloyed powder metallurgical techniques are considered for consolidation approaches. Powder injection molding can be employed to align short fibers in various matrices. The effectiveness of both fibers and particles in strengthening these compounds also is discussed.

BACKGROUND

Reactive sintering involves formation of a transient liquid phase (13,14). The initial compact is composed of mixed elemental powders which are heated to a temperature where they react to form a compound product. Often the reaction occurs on the formation of a first liquid, typically a eutectic liquid at the interface between contacting particles. Fig. 1 shows a schematic binary phase diagram for a reactive sintering system, where a stoichiometric mixture of A and B powders is used to form an intermediate compound product AB. At the lowest eutectic temperature a transient liquid forms and spreads through the compact during heating. Heat is liberated because of the thermodynamic stability of the high melting temperature compound. Consequently, reactive sintering is nearly spontaneous once the liquid forms. By appropriate selection of temperature, particle size, green density and composition, the liquid becomes self-propagating through the compact and persists for only a few seconds. Like other transient liquid phase sintering treatments, the liquid provides a capillary force on the structure which leads to densification (13). However, if the solubilities are unbalanced, swelling can occur due to the formation of Kirkendall porosity. If isostatic pressure is applied during consolidation the process is termed reactive hot isostatic pressing (RHIP).

In injection molding a mixture of powders, short fibers and a binder is extruded through a tapered die to achieve fiber alignment, (15). Extrusion must be performed above the softening temperature of the binding. After extrusion the binder is removed (thermally or by wicking action) and the compact is consolidated to approximately full density. Apart from the alignment of fibers, which is achieved only when the particles are small in diameter, this process offers the possibility of producing complex P/M parts.

• start with a mixture of A and B powders
• finish with a sintered compact of AB compound
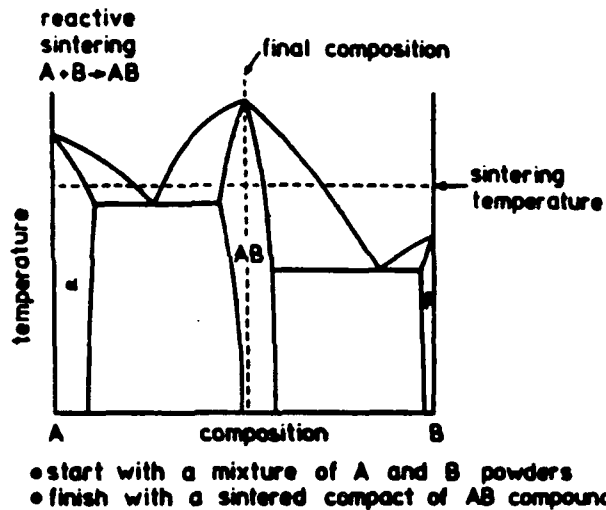
Fig. 1 Schematic of a binary phase diagram.

However, the principal disadvantages are the difficulty of complete binder removal and the inability to produce continuous fiber reinforced composites.

Three intermetallic compounds have been studied as matrices: NiAl, MoSi$_2$ and TaTiAl$_2$. NiAl (ordered B2 crystal structure) was chosen partly because of a large body of literature that exists detailing the properties of this compound. Therefore, measurements of properties can be compared to previous results. Also, besides a high melting temperature (1640°C) and low density (5.86 g/cm^3), NiAl exhibits excellent oxidation resistance. Depending on factors such as grain size, deviations from stoichiometry, strain rate and impurity content, the ductile to brittle transition has been reported to be between about 400 and 600°C (16). MoSi$_2$ (ordered noncubic C11b crystal structure) warrants study due to its melting point alone (>2000°C). It possesses a low density (6.3 g/cm^3) and has useful oxidation resistance to 1700°C; however it exhibits the pest phenomenon below 600°C. The ductile to brittle transition temperature of MoSi$_2$ is approximately 1000°C (17). The properties (25,26) of the ternary alloy TaTiAl$_2$ are as follows: TaTiAl$_2$ is a two phase alloy consisting of σ'plus γ' σ'is Ta$_2$Al alloyed with Ti while γ'is TiAl alloyed with Ta. The melting temperature of this alloy is near 1800°C, and the density is approximately 7g/cm^3. TaTiAl$_2$ exhibits excellent oxidation resistance up to and above 1500°C.

In this study NiAl matrix composites were fabricated by reactive synthesis while MoSi$_2$ and TaTiAl$_2$ matrix composite were fabricated from prealloyed powders. Fibers and particles were chosen on the basis of commercial availability and literature citations concerning thermodynamic stability.

EXPERIMENTAL PROCEDURES

Reactive Processing of NiAl

Elemental Ni and Al powders were mixed to a composition corresponding to Ni-49 at % Al (30wt%Al). For particulate strengthened specimens the appropriate amount of reinforcement phase was blended with the matrix mixture. Mixing was performed with a turbula type mixer for one hour. The mixed powder was then cold isostatically pressed (CIP) to 210 MPa in a cylindrical polyeurethane mold bag. Specimens were then vacuum encapsulated in 304 stainless steel. Prior to encapsulation the specimens were degassed in vacuum at 300°C for 10 hours. RHIP conditions were 172 MPa, 750°C or 1200°C, for one hour.

Consolidation of MoSi$_2$ and TaTiAl$_2$

Prealloyed powder tends not to CIP well; therefore, either loose powder was poured into the HIP container and vibrated to allow for the loose powder to reach tap density, or the powder was pressed into the HIP can directly, with the aid of a hydraulic press. For TaTiAl$_2$ stainless steel cans were employed. The HIP conditions were 1250°C for two hours at 172 MPa. Owing to the high melting temperature of MoSi$_2$, Ti or Nb HIP cans were utilized. Material placed in Ti cans was wrapped with Ta or Nb foil to prevent a reaction with the can. The HIP conditions were either 1500°C or 1600°C for Ti and Nb cans respectively and 172 MPa pressure for two hours.

uniform dispersion of fibers is necessary for maximum strengthening; therefore, proper blending of the fiber and powder is crucial. The chopped fibers tended to agglomerate, but the alcohol slurry was useful for dispersing the fibers. Appropriate amounts of powder were then added to the slurry of fibers and mixed in a turbula type mixer for one hour. The alcohol was then allowed to evaporate. Volume fractions of fibers ranged from 10 to 20 percent. The fiber powder mixture was added to melted binder while being mixed. For small quantities (50 g or less) mixing was performed by hand using a stirring rod. For larger amounts a double planetary type rotating mixer was employed. Typical loading of the feedstock was 65 to 70% by volume of solid (powder plus fiber).

A tapered die used for fiber alignment decreased in diameter from 1.27 to 0.15 cm. The extruded "wires" 0.15 cm in diameter were carefully placed in a polyeurethane mold and cold isostatically pressed (CIPed) at 208 MPa, to produce a cylindrical specimen 1.27 cm in diameter. This allowed for a sample of significant size to be produced. A hand press was utilized for extruding from the dies which were preheated above the softening point of the binder (90°C).

All samples were placed in (Al$_2$O$_3$) wicking powder and debinding was performed in flowing hydrogen. The debinding cycle consisted of heating at 2°C/min to 450°C. After 300 minutes the NiAl composites were allowed to furnace cool. MoSi$_2$ and TaTiAl$_2$ specimens were heated at 10°C/min to 1200°C and held for 60 minutes before being allowed to furnace cool. After debinding, NiAl samples were placed in a vacuum furnace and reactively sintered at 700°C for 15 minutes. MoSi$_2$ and TaTiAl$_2$ specimens were vacuum annealed at 1000°C for one hour. The samples were consolidated by HIP using the cycles described previously.

RESULTS

The exothermic reaction between Ni and Al is so vigorous that melting and loss of specimen shape commonly occurs during reactive sintering. As a consequence, it is usually necessary to mix 10 to 25% prealloyed powders with the elemental powders to dampen the reaction. The optimum amount of prealloyed powder depends on particle size distribution of the powder (18). Alternatively, an inert phase such as TiB$_2$ or Al$_2$O$_3$ (as particles or fibers) can be used for the same purpose. Pressure applied during the reaction between Ni and Al results in an inhomogeneous material, see Fig. 2. This problem can be alleviated by reactive sintering, followed by HIPing (Fig 3). Various TiB$_2$ particulate composites were then fabricated (10, 15, 20 and 40 v%). A typical microstructure is shown in Fig. 4. Compressive yield vs. temperature for these composites are shown in Fig. 5. Tensile properties vs. temperature for NiAl and NiAl/20TiB$_2$ are shown in Fig. 6. Note that strengthening occurs even though the particles are relatively coarse. Virtually no strengthening is observed from the particles above 900°C.

Fig. 7 shows a typical microstructure of NiAl/15v% Al$_2$O$_3$ (DuPont FP) fibers produced by injection molding. The tensile properties of this composite at 300°C, compared to those of NiAl and NiAl/TiB$_2$ are shown in Table 1. The fibers caused modest strengthening at the expense of ductility.

Fig. 8a) and b) show the microstructures of TaTiAl$_2$ and TaTiAl$_2$/10v% Al$_2$O$_3$

particulate composite, respectively. Fig. 9 shows the compressive properties of TaTiAl$_2$ and the particulate composite versus temperature. Somewhat surprising is the "apparent" increase in strain to failure with the addition of the particles, even though there appears to he no grain refinement in the microstructure of the composite.
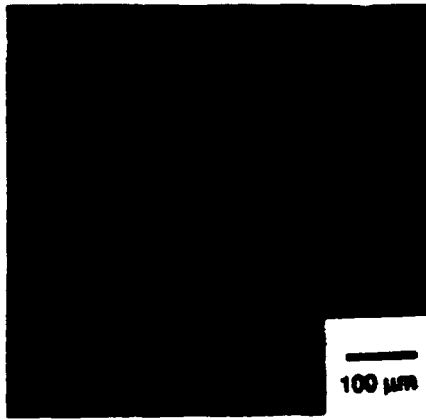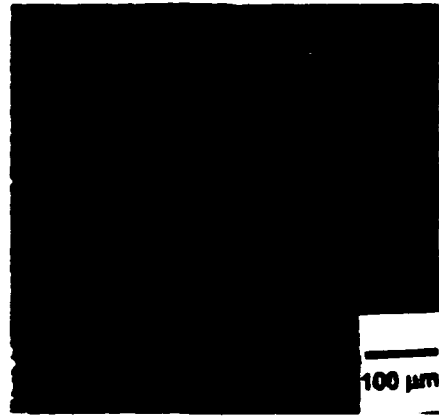

Fig. 2   RHIP NiAl

Fig. 3   Reactive Sintered and HIP NiAl
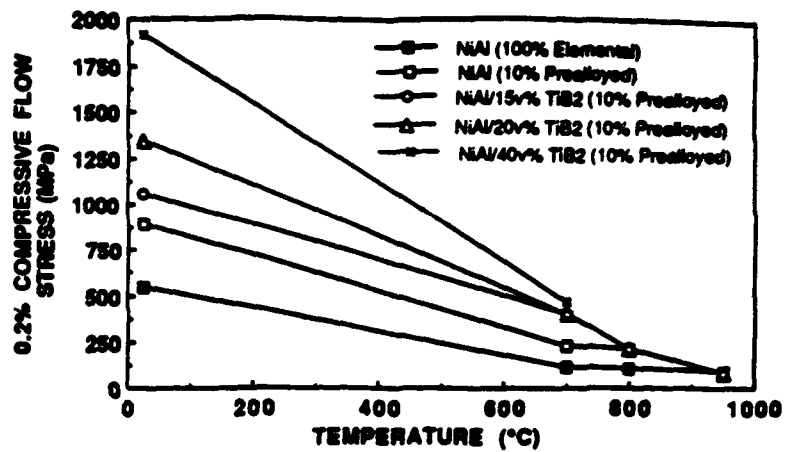

Fig. 4 Microstructure of NiAl reinforced with 20v% TiB$_2$

Fig. 5 Compressive strength versus temperature for NiAl and NiAl/TiB$_2$.
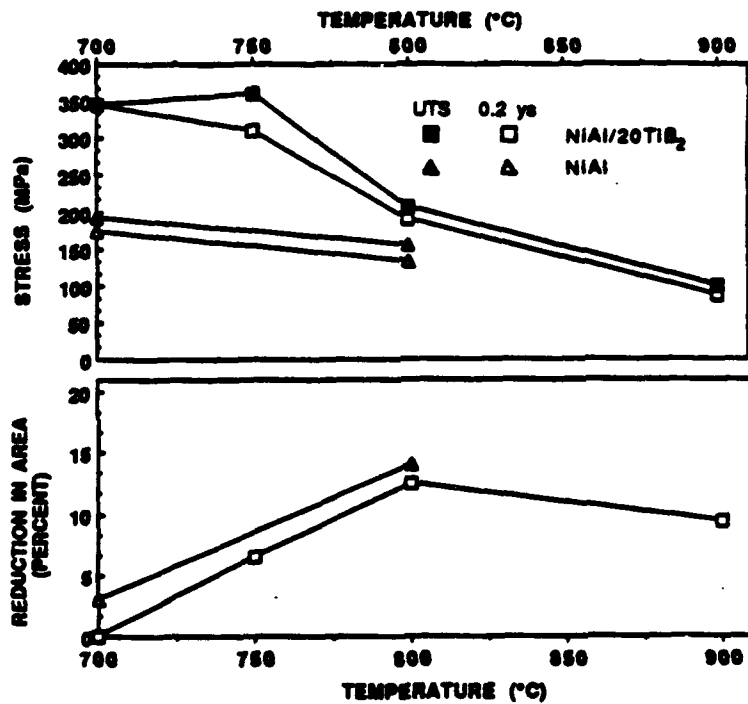
Fig. 6 Tensile properties versus temperature for NiAl and NiAl/20v% TiB$_2$.

TABLE 1

802°C Tensile Properties of Reactively Processed NiAl Matrix Composites

	σ_{ys} (MPa)	σ_{UTS} (MPa)	Reduction Area (%)
NiAl	135	154	14
NiAl 15v% Al_2O_3 Fibers	142	163	3
NiAl 20v% TiB_2 Particles*	190	207	12.5
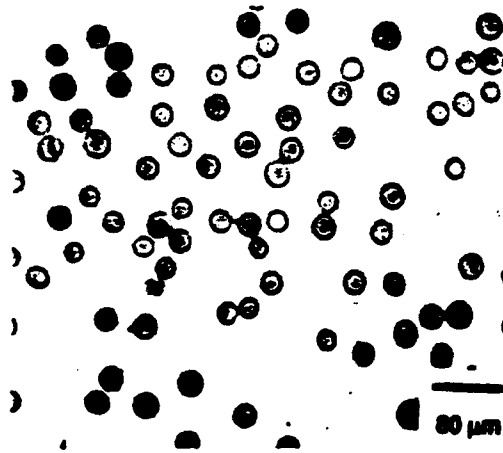
Fig. 7 Microstructure of injection molded NiAl/15v% FP.

(a)   b)
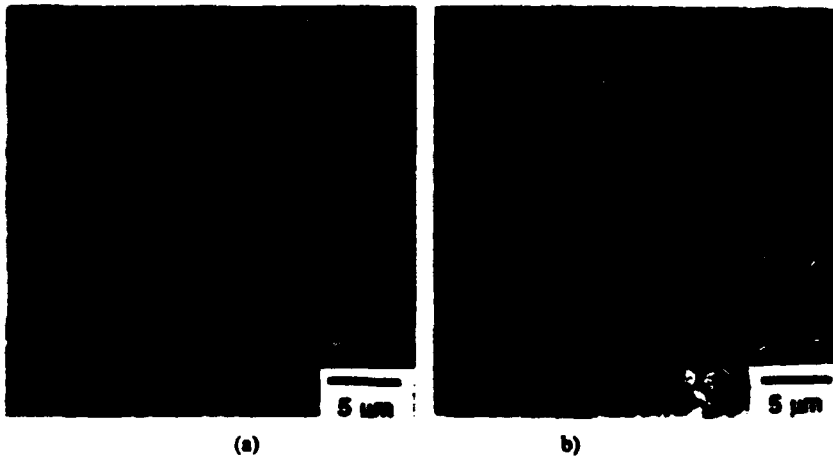
Fig. 8   Microstructures of a) TaTiAl₃ and b) TaTiAl₃/10v% Al₂O₃ particulate composite.
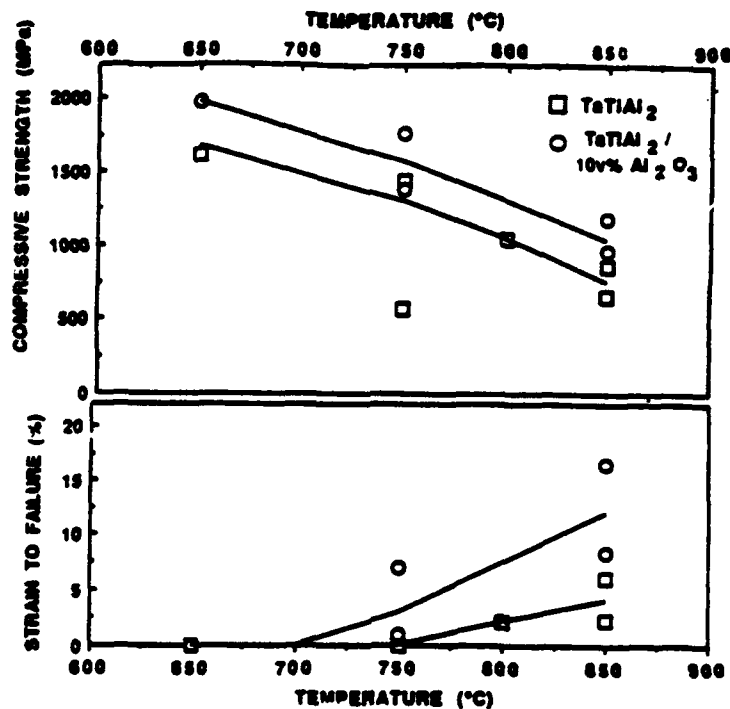
Fig. 9 Compressive strength versus temperature for TaTiAl₂ alloys.

DISCUSSION

Control over the exotherm associated with the formation of NiAl was attained by adding a high melting temperature particulate to elemental powders. For the case of monolithic NiAl, prealloyed NiAl powder was used to dilute the reaction. The application of pressure during reactive sintering caused the transient liquid phase to become non-uniformly dispersed, which led to the inhomogeneity. Similar inhomogeneities have been found during HIPing in the presence of a liquid phase in the W-Ni system (19).

Some of the strengthening with the addition of the TiB_2 particles to NiAl arises from grain refinement. The grain sizes were reduced from 30μm to 5μm with the addition of the particles. A Hall-Petch analysis reveals the contribution of strengthening due to grain size (see Table 2). The remaining strengthening is attributed to the particles.

The "poor" elevated temperature strength of reactively sintered NiA/TiB_2 can be

attributed to the large TiB_2 particles. NiAl/10v% TiB_2 powder produced by XD synthesis was obtained from Martin Marietta Research Laboratories. XD is a proprietary in situ process in which fine 1-3μm TiB_2 particles have been dispersed in a variety of intermetallic matrices (21). This material was HIPed at RPI (1250°C, 2 hours, 172 MPa). The XD microstructure has a finer TiB_2 dispersion than the reactively synthesized material. Table 3 summarizes the mechanical behavior of these composites at 25°C and 900°C. Clearly, fine TiB_2 particles are more effective in strengthening NiAl at elevated temperature.

Both prealloyed and elemental powders were used to fabricate injection molded specimens. However, experience revealed that elemental powders, which are spherical in shape, are less difficult to extrude. The alignment produced by injection molding is not as good as can be produced by infiltration or melt techniques (22).

Due to lack of $MoSi_2$ powder only small aligned composite specimens could be fabricated by the extrusion technique. Room temperature hardness results indicate that Al_2O_3 might improve the toughness of $MoSi_2$. The hardness improved from 87.6 to 90.2 on the Rockwell "A" scale with the addition of the 20v% FP aligned fibers. Hardness values for powder processed $MoSi_2$ have been reported to range from 80 to 87 Rockwell "A" (23,24). Figure 10 shows the actual indentations. While cracks propagated from the hardness indentation in the composite specimen, absent were large craters of fractured material observed in the matrix. These results indicate that the DuPont FP fiber may improve the fracture toughness of $MoSi_2$. Attempts to obtain fracture toughness values from Vickers hardness indentations failed as cracks did not propagate from the indentations.

The compression behavior of $TaTiAl_2$ and $TaTiAl_2/Al_2O_3$ particulate composites is puzzling. To date, no plausible explanation exists for the apparent increase in ductility with the addition of the particles, without any decrease in grain size.

TABLE 2

Contribution of Grain Refinement to Room Temperature Compressive Yield Stress

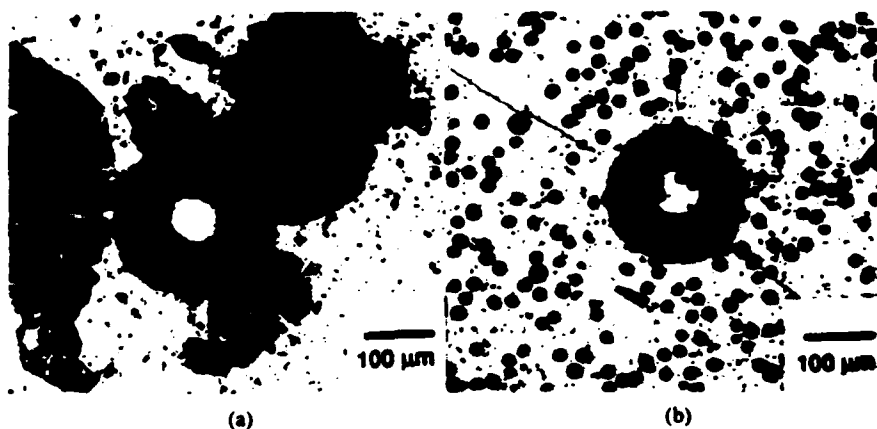|	Grain Size (um)	Yield Stress (MPa)
NiAl (10% Prealloyed)	30	890
NiAl (10% Prealloyed) Calculated from Hall Petch*	5	1000
NiAl (10% Prealloyed) 15 Vol% TiB_2	5	1060
NiAl (10% Prealloyed) 20 Vol% TiB_2	5	1350

Hall Petch slope from Schulson[20]

Fig 10. Hardness indentation a) MoSi$_2$, b) MoSi$_2$/20v% FP.

TABLE 3

Mechanical Behavior of XD and Reactive Synthesized (RS) NiAl/10v% TiB$_2$
Consolidated at Rensselaer Polytechnic Institute

		Test	σ_{ys} (MPa)	σ_{uts} (MPa)	Reduction Area (%)
ROOM TEMP	XD	compression	1150		
	RS	compression	1160		
900°C	XD	tension	143	153	2
	RS	tension	76.5	82.4	14

Tensile tests performed in Vacuum, at a strain rate of 1.67×10^{-4} sec^{-1}.
Compression tests performed in Air at a strain rate of 3.3×10^{-4} sec^{-1}.

Advanced Composite Materials

CONCLUSIONS

Intermetallic matrix components based upon NiAl, MoSi₂ and TaTiAl₂ may be produced by several powder techniques. Random fibers or particles can be incorporated by reactive sintering or HIPing of either prealloyed or elemental powders. Alignment of short fibers is achievable by powder injection molding, full consolidation is then accomplished by HIPing. Preliminary mechanical properties measurements indicate strengthening due to fibers or particles, but little or no toughening can be achieved without alignment of fibers.

ACKNOWLEDGEMENT

REFERENCES

1. N.S. Stoloff, "Ordered Alloys - Physical Metallurgy and Structural Applications", Int Met Rev 29, pp. 123-167, 1984.
2. K. Aoki, and O. Izumi, J. Jpn Inst Met 43, pp. 1190-1193, 1979.
3. C.T. Liu, and V. Sikka, "Nickel Aluminides For Structural Use", J. Met 38 (5), pp. 9-21, 1986.
4. A.I. Taub, S.C. Huang and K.M. Chang, "High Temperature Ductility in Rapidly Solidified Ni₃Al+B", pp. 221-228, in High Temperature Ordered Intermetallic Alloys, eds. C.C Koch, C.T. Liu and N.S. Stoloff, MRS 39, Pittsburgh, PA, 1985.
5. S. Nourbakhsh, F.L. Liang and H. Margolin, "Interaction of Al₂O₃ and ZrO Fibers with Ti-Al Matrix During Pressure Casting", Met. Trans A, 21A, pp. 213-219, 1990.
6. S. Nourbakhsh, F.L. Liang and H. Margolin, "Pressure Casting of Ni₃Al/Al₂O₃ Composites", pp. 459-464, in High Temperature Ordered Intermetallic Alloys III, eds. C.T. Liu A.I. Taub, N.S. Stoloff, and C.C. Koch, MRS 133, Pittsburgh, PA, 1989.
7. S. Nourbakhsh, F.L. Liang and H. Margolin, "Fabrication of Ni₃Al/Al₂O₃ and Ni/Al₂O₃ Composites By Pressure Casting", pp. 195-205, in Processing of Ceramic and Metal Matrix Composites, H. Mostaghci, ed., Pergamon Press, NY.
8. S. Nourbakhsh, F.L. Liang and H. Margolin, "An Apparatus for Pressure Casting Fibre Reinforced High Temperature Metal-Matrix Composites", J. Phys. E: Sci. Instrum, 21, pp. 898-902, 1988.
9. S. Nourbakhsh and H. Margolin, "Microstructural Observation of Pressure Cast Ni₃Al/Al₂O₃ Composites", Met. Trans. A, 20A, pp. 2159-2166, 1989.
10. J.L. Walters and H.E. Cline, "Stability of the Directionally Solidified Eutectic NiAl-Cr and NiAl-Mo", Met Trans., 4, pp. 33-39, 1973.
11. P.K. Brindley, "SiC Reinforced Aluminide Composites", pp. 419-424, in High Temperature Ordered Intermetallic Alloys II, eds. N.S. Stoloff C.C. Koch, C.T. Liu and O. Izumi, MRS 81, Pittsburgh, PA, 1987.

12. D.L.Anton, "High Temperature Intermetallic Composites", pp. 57-64, in High Temperature/High Performance Composites, eds. F.D.Lemkey, S.G. Fishman, A.G. Evans and J.R. Strife, MRS, 120, Pittsburgh, PA, 1988.

13. D.M.Sims, A. Bose and R.M.German, "Reactive Synthesis of Nickel Aluminide", Prog. Powder Metall. 43, pp. 575-593, 1987.

14. R.M.German, "Liquid Phase Sintering", Plenum, New York, p 157, 1985.

15. A. Bose and R.M.German, "Fabrication of Intermetallic Matrix Composites", Material Sci. and Engr., A107, pp. 107-116, 1989.

16. A. Ball and R.E. Smallman, "The Deformation Properties and Electron Microscopy Studies of the Intermetallic Compound NiAl", Acta Met, 14, 1349-1355, 1966.

17. M.J. Maloney, DARPA/ONR Contract No. N00014-87-0862 Program Review, Pratt and Whitney Aircraft, W. Palm Beach, FL., Feb. 28, 1990.

18. D.E.Alman, A. Dibble, B. Moore, A. Bose, R.M.German and N.S. Stoloff, "Powder Processing of Intermetallic Matrix Composites", pp 217-227, in Processing of Ceramic and Metal Matrix Composites, H. Mostaghaci, ed., Pergamon Press, NY, 1989.

19. A. Frisch, W.A.Kaysser and G. Petzow, "Densification Maps and Defect Healing During Sinter/HIP of Polyphase Materials", pp. 193-204, in "Advances in Powder Metallurgy - 1989", MPIF, Princeton, NJ, 1989.

20. E.M.Schulson, "The Effect of Grain Size on the Flow and Fracture of Long Range Ordered Alloys", pp 193-204, in "High Temperature Ordered Intermetallic Alloys", eds. C.C. Koch, C.T. Liu and N.S. Stoloff, MRS 39, Pittsburgh, PA, 1985.

21. K.S.Kumar, S.K. Mannan, J.D. Whittenberger, R.K. Viswanadham, and L.Christodoulou, "Nickel Aluminides/Titanium Diboride Composites Via XD Synthesis", MML-TR-89-102(C), 1989.

22. D.E. Alman and N.S. Stoloff, "Fabrication of Intermetallic Matrix Composites by Powder Injection Molding (PIM) Techniques", in Low Density, High Temperature P/M Alloys, ed. W.E. Frazier, TMS, Warrendale, PA, to be published.

23. R.D. Grintal, "Effect of Some Metal Additions on Molybdenum Disilicide", Powder Met. Bul., 8, pp 18-22, 1957.

24. "Try Molybdenum Disilicide for Strength, Oxidation and Corrosion Resistance", Materials and Methods, 43, pp. 131-133, 1956.

25. "Development of High Temperature Metallics For Structural Aerospace Applications", United Technologies Corporation, Pratt Whitney Engine Business, West Palm Beach, FL., FR-20756, June 20, 1989.

26. L.W.Graham, personal correspondence, R.P.I., April 1990.

Fabrication and Mechanical Properties of Powder Injection Molded Intermetallic Matrix Composites

D.E. Alman and N.S. Stoloff

ABSTRACT

Powder Injection Molding or binder assisted extrusion allows for the alignment of discontinuous fibers in a powder matrix. This technique has been applied to produce composites in various intermetallic matrices ($NiAl/Al_2O_3$, $MoSi_2/Al_2O_3$, $MoSi_2/SiC$ and $TaTiAl_2/Al_2O_3$). Tensile test results indicate that discontinuous Al_2O_3 (DuPont FP) fibers will not toughen NiAl. However, cracks propagating from hardness indentation indicate that Al_2O_3 fibers (DuPont FP) may toughen $MoSi_2$ and $TaTiAl_2$.

INTRODUCTION

Many intermetallic compounds possess desirable properties for high temperature applications such as low density, high melting point, ductility at elevated temperatures and oxidation resistance. However, inadequate creep and fracture resistance of these intermetallics must be improved before they can be exploited for such purposes. Fibrous reinforcement can improve both fracture toughness and creep resistance. Therefore, intermetallic compounds are emerging as potential matrix materials for elevated temperature structural composites.

Powder techniques are ideal for processing high melting temperature materials because processing is performed in the solid state. Powder techniques such as powder cloth [1], and powder infiltration [2] have been applied successfully for fabricating aligned continuous reinforced intermetallic-matrix composites. The powder cloth technique consists of interspersing cloths of powder with fiber tapes. The cloths are produced by rolling the powder with binder into thin sheets. Consolidation is by hot pressing. This technique is limited in that only thin flat plates can be produced. The powder infiltration technique can produce larger specimens, but during consolidation by hot pressing agglomeration of fibers is common (for instance see Fig. 2. in ref. 2). This agglomeration tends to degrade the mechanical properties of the composites [2].

An alternative powder technique is powder injection molding or binder assisted extrusion. Composites are produced by mixing powder and chopped fibers with a polymer binder. The mixture is heated above the softening point of the binder. The heated mixture is then either extruded through a tapered die or injected into a mold cavity. The binder is then removed and the composite is consolidated. The result is a composite that has aligned discontinuous fibers and in the case of the injection molding, near net shape.

This paper describes ongoing research aimed at determining the effects of processing variables and the mechanical properties of powder injection molded intermetallic matrix composites based upon the intermetallics NiAl, $MoSi_2$ and $TaTiAl_2$.

Materials Engineering Department, Rensselaer Polytechnic Institute, Troy, New York, 12180-3590.

SYSTEMS INVESTIGATED

Table 1 lists some properties of the the three matrices employed in this study. All three compounds have high melting temperatures(>1600°C), low density (<7 g/cm^3) and each has excellent oxidation resistance. Note that TaTiAl$_2$ is a two phase material, consisting of γ' (TiAl alloyed with Ta) and σ' (Ta$_2$Al alloyed with Ti). In this study NiAl matrix composites were consolidated by reactive synthesis techniques and MoSi$_2$ and TaTiAl$_2$ by conventional prealloyed powder metallurgical techniques. Reactive synthesis consists of reacting elemental powders together to form the compound. This technique has been employed successfully to produce NiAl and NiAl matrix composites [3]. Two types of fibers were employed in this investigation: DuPont FP Al$_2$O$_3$ fiber and Avco-Textron SCS-6 SiC fiber. Composites produced were NiAl/Al$_2$O$_3$, MoSi$_2$/Al$_2$O$_3$, MoSi$_2$/SiC and TaTiAl$_2$/Al$_2$O$_3$.

FABRICATION PROCEDURE

Table 2 lists the characteristics of the fibers and powders employed for this study. The fibers were chopped manually and had aspect ratios of 10 to 100. The fibers were dispersed into the powder by mixing in alcohol. The fiber, powder and alcohol slurry were mixed in a turbula type mixer for 1 hour, after which the alcohol was evaporated. The powder plus fiber mixture was then added to melted binder. The binder used in this study is based on low molecular weight polypropylene and paraffin wax whose exact composition is proprietary. For small quantities of powder and fibers (50 grams) mixing was performed by hand in stainless steel crucibles. For larger quantities (200 grams) mixing was performed with the aid of a double planetary type mixer, again in stainless steel crucibles.

For small quantities of powder and fiber the die used for alignment decreased in diameter from 1.27 to 0.15 cm. Extrusion was performed with a hand press from a die preheated to above the softening point of the binder (90°C). The extruded wires were carefully placed in a polyeurethane mold and cold isostatically pressed (CIP) to 208 MPa. This allowed for a cylindrical sample 1.27 cm in diameter to be produced. For larger quantities the extrusion die was tapered from 5.08 to 1.27 cm in diameter. This avoided the CIPing stage. Also, near net shape tensile and bend bars (Fig. 1) were produced with a reciprocating screw-type injection molding machine.

All samples were placed in Al$_2$O$_3$ powder to remove the binder by wicking action, and debinding was performed in flowing hydrogen. The debinding cycle consisted of heating at 2°C/min to 450°C and holding at temperature for 4 hours. NiAl matrix composites were heated in vacuum (10^{-5} Torr) to 700°C to allow for the Ni and Al to react to form NiAl. TaTiAl$_2$ and MoSi$_2$ were presintered in vacuum at 1200°C for 1 hour.

Consolidation of all the samples was carried out by Hot Isostatic Pressing (HIP). NiAl and TaTiAl$_2$ composites were vacuum encapsulated in 304 stainless steel and HIPed at 1250°C at a pressure of 172 MPa for 2 hours. Owing to its higher melting temperature, MoSi$_2$ composites were HIPed in titanium cans at 1500°C at a pressure of 172 MPa for 2 hours. To prevent a reaction between the can and MoSi$_2$, the specimens were wrapped in tantalum foil prior to encapsulation in the can. In an attempt to prevent cracking due to thermal expansion mismatch depressurization and cooling were carried out slowly (from temperature to 300°C in 60 min. with pressure decreasing only as a result of decreasing temperature; over the next 60 min. depressurization to atmospheric pressure and cooling to room temperature occured).

RESULTS AND DISCUSSION

Figures 2a-c) show microstructures for TaTiAl$_2$/10v% Al$_2$O$_3$, NiAl/15v% Al$_2$O$_3$ and MoSi$_2$/20v% Al$_2$O$_3$ composites, respectively, produced by extrusion in the small die. Note that the alignment appears to be good in all three composites, even though the morphology of the powders used was different; spherical for NiAl as opposed to irregular for TaTiAl$_2$ and

MoSi$_2$. This indicates that the technique is widely applicable to various powder shapes. German and Bose [4] report that in an Fe/Al$_2$O$_3$ composite, alignment of the Al$_2$O$_3$ fibers was superior when spherical Fe powder was smaller in diameter (5μm) instead of larger (70μm). Clearly, powder size plays a larger role in alignment than does powder morphology. However, powder morphology can effect the rheological behavior of the feedstock during extrusion or injection molding [5]. Since many intermetallic powders are not available in small sizes, the elemental powder approach of reactive synthesis for consolidation appears ideally suited for coupling with binder assisted extrusion or injection molding. Elemental powders tend to be readily available in small sizes.

The effect of fiber volume fraction is assessed in the microstructures shown in Fig 3a) and b). These NiAl/Al$_2$O$_3$ composites were produced from the large die; therefore, misalignment due to CIPing has been avoided. Note that agglomeration and misalignment appears to increase at the higher volume fraction of fiber loading. This is a major detraction of this technique, since the volume fraction of fibers that can be aligned appears to be limited.

Figure 4 shows an as HIPed microstructure of MoSi$_2$ with aligned SCS-6 SiC fibers produced from the small die. Note that the cracks propagate radially from fiber to fiber. This has been attributed to the mismatch between the coefficient of thermal expansion of the fiber and matrix [6]. However, note that these fibers also appear aligned, indicating that large diameter fibers also can be aligned by the binder assisted extrusion or powder injection molding technique.

One advantage of powder injection molding is that near net shapes can be produced (as shown in Fig. 2). Fig. 5 shows various views of the fibers flowing with the powder and binder in the the screw-gate-runner section of the die. The fibers appear to follow the flow of the binder and powder around the corners well. Fig. 6 shows a cross section of an NiAl/10v% Al$_2$O$_3$ tensile bar in the as reactive sintered condition; pores are clearly visible. The alignment of the fibers in the gauge section of the tensile bar appears satisfactory. In the bend specimen the alignment of the fibers was unsatisfactory. Clearly, a key to alignment coupled with near net shape processing is for the die to be designed so that flow of the feedstock always converges.

Table 3 compares the tensile properties of NiAl/15v% Al$_2$O$_3$ with monolithic NiAl and NiAl/20v% TiB$_2$ particles produced by reactive synthesis[3]. The results indicate that short FP fibers will not toughen this matrix at low temperatures, and are not as effective as particles in improving elevated temperature tensile strength. Fracture surfaces show limited pull out at 700°C (Fig. 7). At 800°C (Fig. 8) extensive decohesion between the fibers and matrix has occured. However, both the length of fibers and the strength of the fiber/matrix interface plays a role in the composite mechanical behavior. To date, no reported tensile tests on continuous aligned NiAl/FP Al$_2$O$_3$ fibers have been reported. Therefore, it is unclear if the short length of the fibers or the interface is causing the poor mechanical response of the composite samples.

Figures 9a-c) show hardness (Rockwell "C") indentations in TaTiAl$_2$, TaTiAl$_2$/10v% Al$_2$O$_3$ particulate composite and an TaTiAl$_2$/10v% Al$_2$O$_3$ aligned fibrous composite, respectively. Note the large craters of fractured material adjacent to the indentation in the monolithic and particulate specimens. In the fibrous composite specimen, cracks propagate from the indentation, but no large craters of fractured material are visible. This indicates that the fibers do, in fact, impede crack propagation and may improve fracture toughness. MoSi$_2$ and an MoSi$_2$/20v% Al$_2$O$_3$ aligned fibrous composite displayed similar behavior. Large craters of fractured material existed adjacent to hardness indentations in the monolithic alloy but not in the fibrous composite. Clearly, further testing is warranted in the MoSi$_2$/Al$_2$O$_3$ and TaTiAl$_2$/Al$_2$O$_3$ systems to determine if the short aligned fibers will indeed improve fracture toughness. It should be mentioned that in the monolithic NiAl alloy, while cracks propagated

from hardness indentation, no large craters of fractured material were present. In an NiAl/15v% fibrous composite cracks propagated around the fibers, yet no improvement in toughness as displayed in a stress-strain curve was detected when this composite was tested in tension at 700°C.

SUMMARY

Powder injection molding has been successfully applied to align discontinuous fibers in several intermetallic systems. Both small and large diameters fibers have been aligned. The key to successful alignment appears to have been small starting powders. The morphology of the powders has little effect on the degree of alignment. Tensile tests indicate that that NiAl will not be toughened by discontinuous Al_2O_3 (FP) fibers. Hardness indentations indicate that the discontinuous FP fibers may improve fracture resistance in $MoSi_2$ and $TaTiAl_2$.

ACKNOWLEDGEMENTS

REFERENCES

1   Brindley, P.K., "SiC Reinforced Aluminde Composites", in High Temperature Ordered Intermetallic Alloys II, N.S. Stoloff, C.C. Koch, C.T. Liu, and O. Izumi, Eds., Materials Research Society, 86, Pittsburgh, PA, 1987, 419-426.

2.   Anton, D.L., "High Temperature Intermetallic Composites", in High Temperature/High Performance Composites, F.D.Lemkey, S.G. Fishman, A.G. Evans and J.R. Strife, Eds., Materials Research Society, 120, Pittsburgh, Pa, 1988, 57-64.

3.   Alman, D.E., and Stoloff, N.S., "Powder Fabrication of Monolithic and Composite NiAl", International Journal of Powder Metallurgy, 27 (1991), 29-41.

4.   German, R.M., and Bose, A., "Fabrication of Intermetallic Matrix Composites", Materials Science and Engineering, A107 (1989), 108-116.

5.   German, R.M., Powder Injection Molding, MPIF, Princeton, NJ, 1990, 163-172.

6.   Shah, D.M., Anton, D.L., and Musson, C.W., "Feasibility Study of Intermetallic Composites", in Intermetallic Matrix Composites, D.L. Anton, P.L. Martin, D.B. Miracle, and R. McMeeking, Eds., Materials Reserach Society, 194, Pittsburgh, PA, 1990, 333-340.

TABLE 1
SELECTIVE PROPERTIES OF INTERMETALLIC COMPOUNDS INVESTIGATED

Matrix	Crystal Structure	Melting Point (°C)	Density (g/cm³)	DBTT(°C)
NiAl	B2	1660	5.86	400-600
$MoSi_2$	C11$_b$	2030	6.30	1000
$TaTiAl_2$	α+γ'	>1800	7	---

TABLE 2
MATERIALS

Powder	Source/Designation	Shape	Size
Ni	Novamet/4sp-10	Spherical	3μm
Al	Valimet/H-3	Spherical	3μm
$MoSi_2$	H.C.Stark/Grade C	Irregular	4μm
$TaTiAl_2$	Pratt and Whitney	Irregular	9μm

Fiber	Source/Designation	Diameter
Al_2O_3	DuPont/FP	20μm
SiC	Avco-Textron/SCS-6	127μm

TABLE 3
TENSILE PROPERTIES OF REACTIVE SYNTHESIZED NiAl AND NiAl MATRIX COMPOSITES

	Temp(°C)	σ_{ys}(MPa)	σ_{uts}(MPa)	R.A.(%)
NiAl	700	173	191	3
NiAl/15v%Al_2O_3 aligned fibers	700	196	196	0
NiAl/20v%TiB_2 particles	700	344	344	0
NiAl	800	135	154	14
NiAl/15v%Al_2O_3 aligned fibers	800	142	163	3
NiAl/20v%TiB_2 particles	800	190	207	12.5

TENSILE BAR DIE CAVITY

SPRUE/RUNNER/ GATE

BEND BAR DIE CAVITY

2 cm
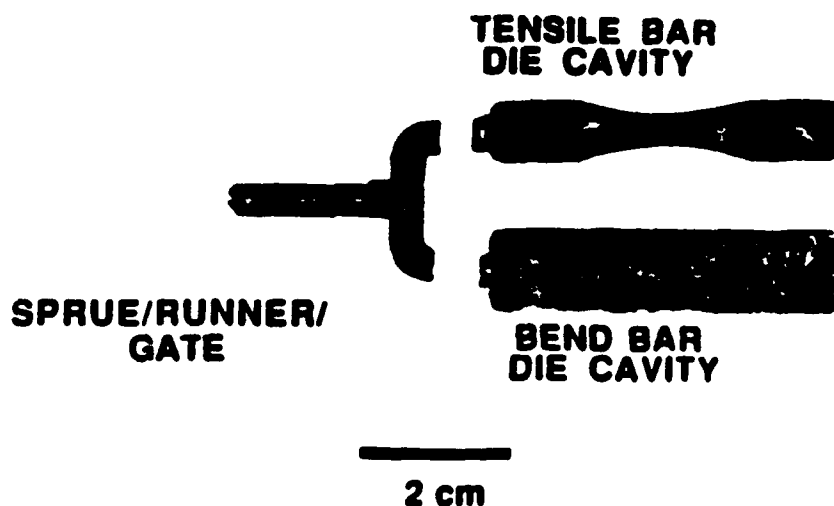
Fig. 1 Near net shaped specimens produced by Injection Molding
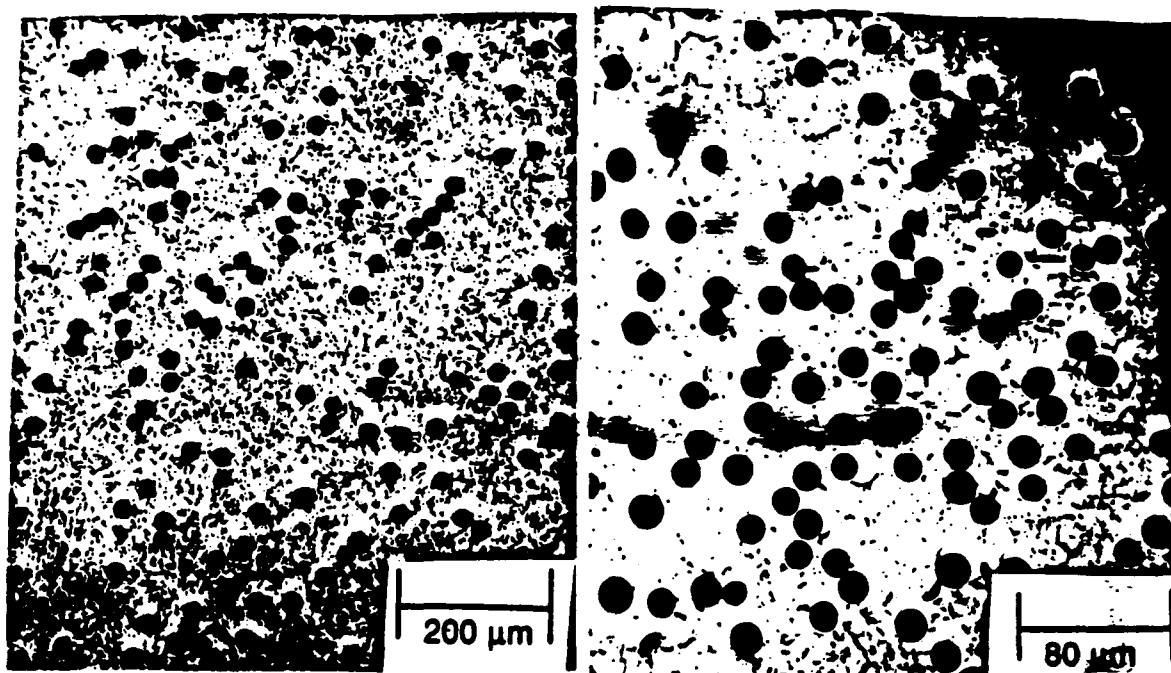
(a)

(b)
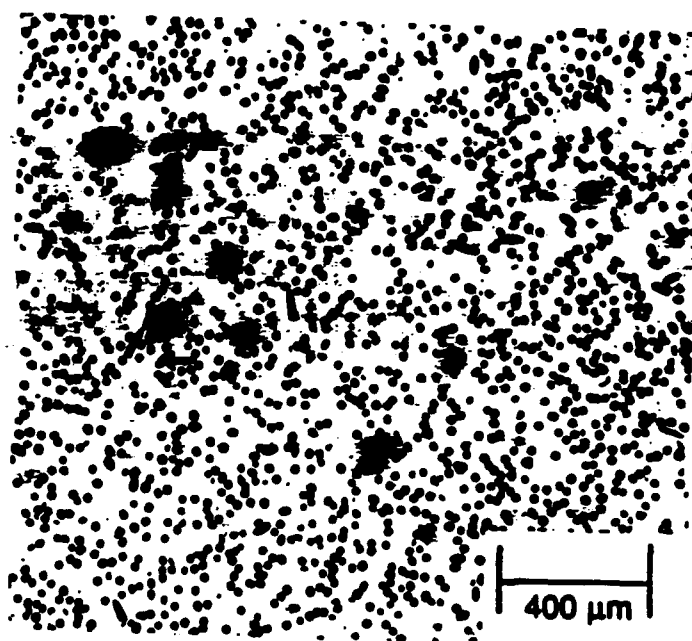
(c)

Fig. 2 Cross sections of composites produced from the small die. (a)TaTiAl₂/10v% Al₂O₃ (b)NiAl/15v% Al₂O₃ (c)MoSi₂/20v% Al₂O₃.
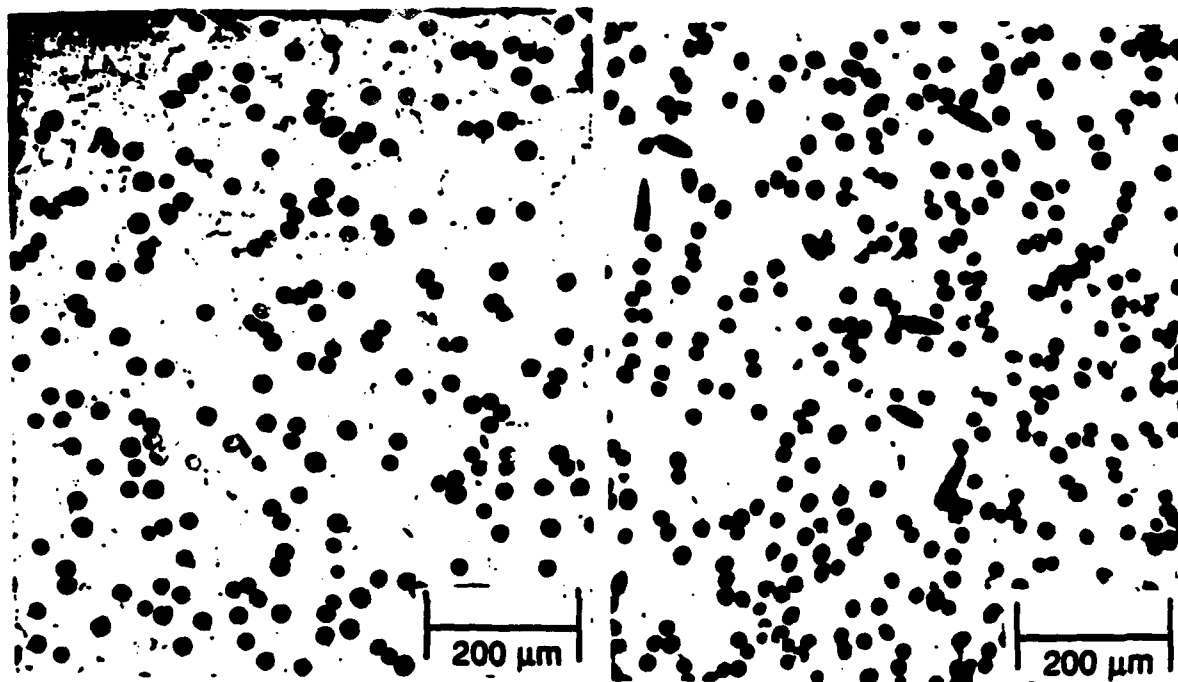
Fig. 3   Cross sections of composites produced from the large die
(a)NiAl/10v% Al₂O₃ (b)NiAl/20v% Al₂O₃.
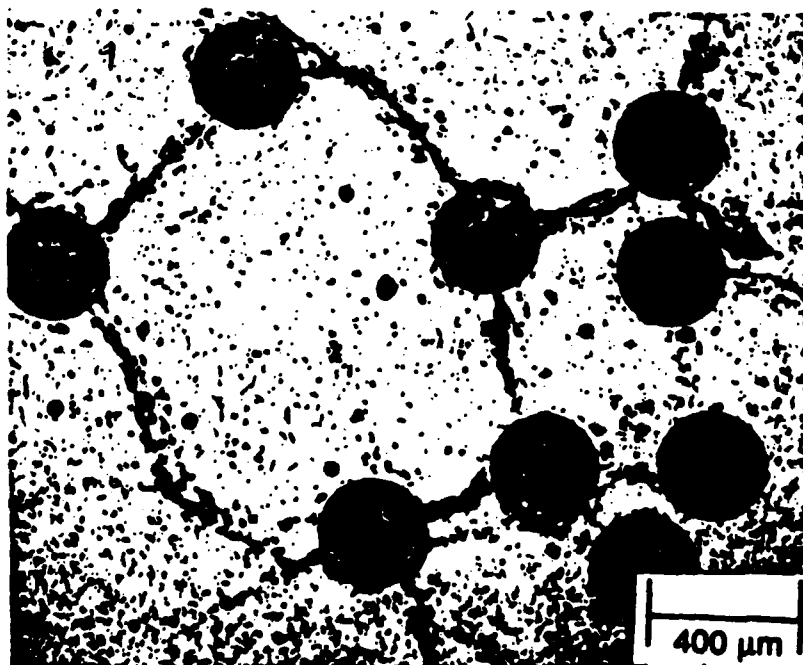
Fig. 4   Cross section of MoSi₂/SCS-6 composite.
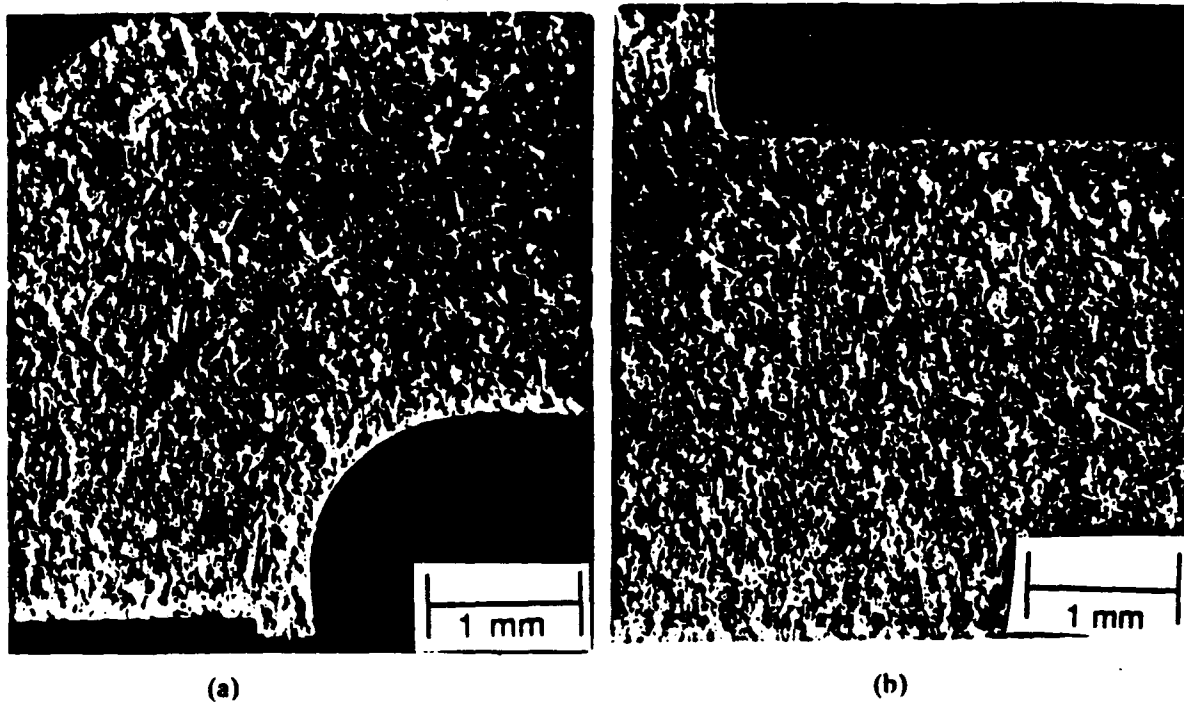
(a)   (b)

Fig. 5 Various views of fibers in screw/gate/ runner section of injection molding die.
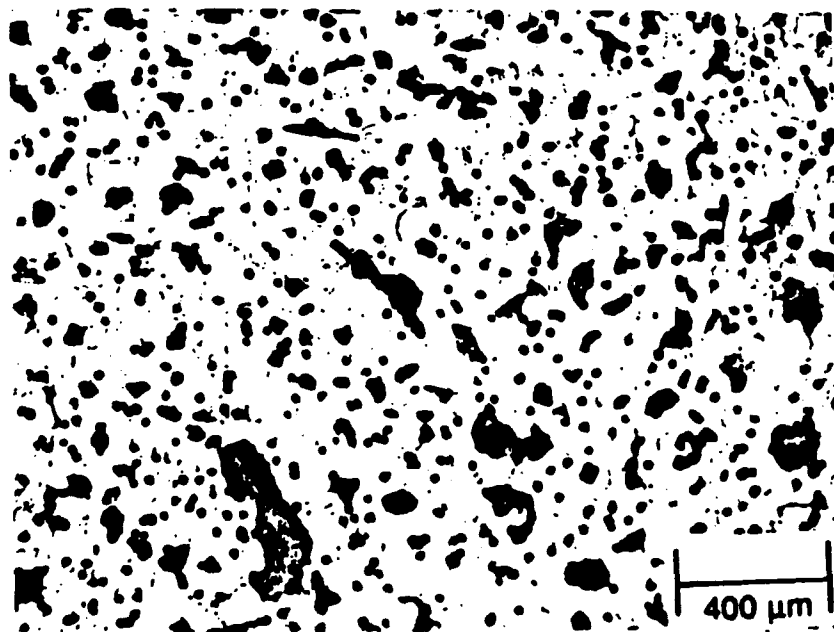
Fig. 6 Cross section of NiAl/15v% Al₂O₃ injection molded tensile bar.

Fig. 7 Fracture surface of NiAl/15v% Al₂O₃ in tension at 700°C.
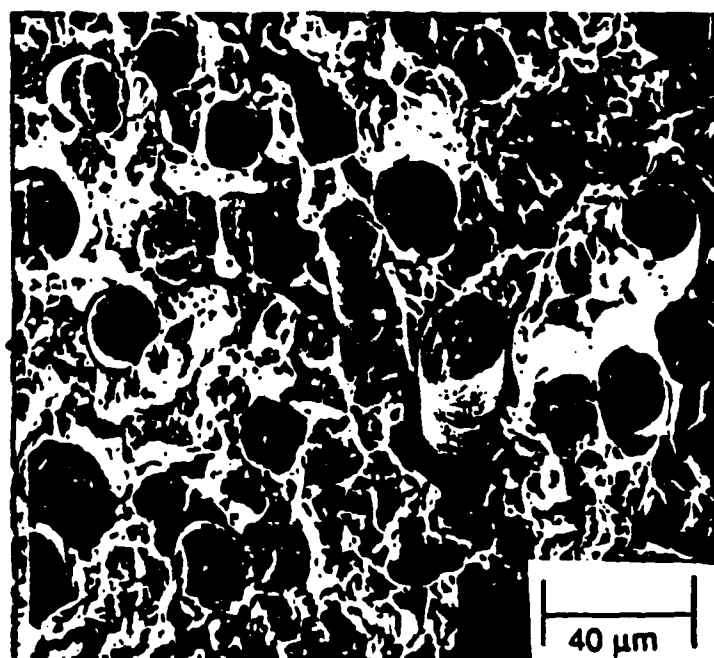
Fig. 8 Fracture surface of NiAl/15v% Al₂O₃ in tension at 800°C.
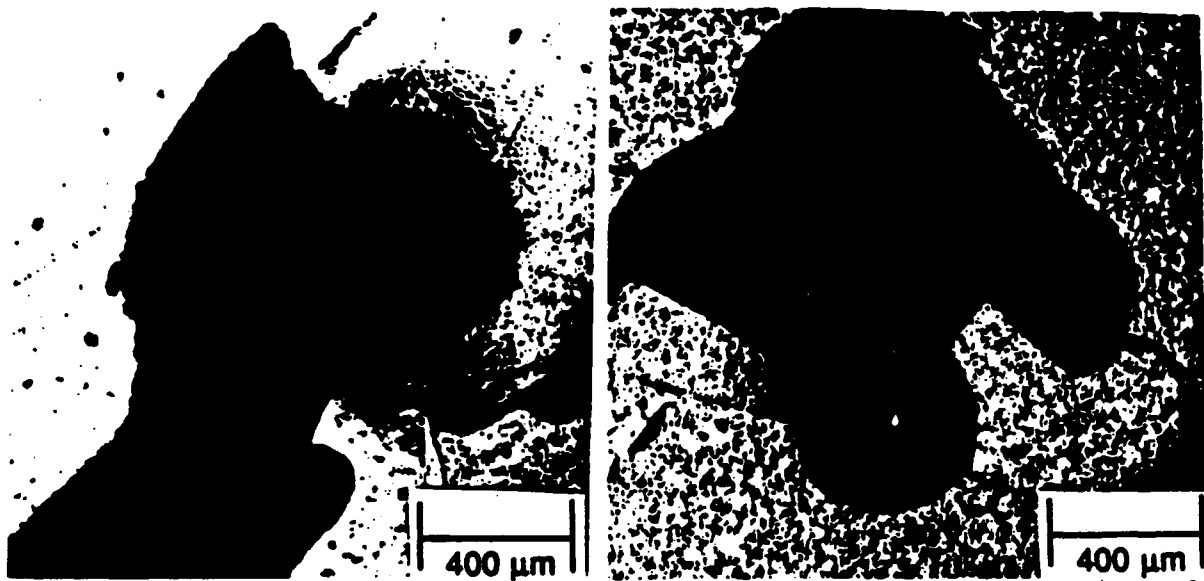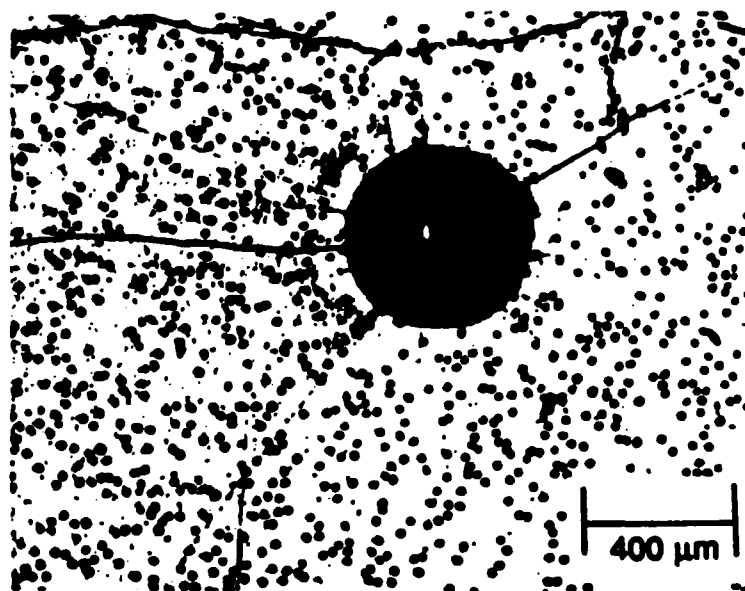
Fig. 9 Hardness indentation in (a)TaTiAl$_2$ (b)TaTiAl$_2$10v% Al$_2$O$_3$ particles and (c)TaTiAl$_2$/10v% fibrous composite.

EFFECT OF DUCTILE PHASE REINFORCEMENT MORPHOLOGY ON TOUGHENING OF MoSi$_2$

D.E Alman and N.S. Stoloff
Materials Engineering Department. Rensselaer Polytechnic Institute, Troy NY 12180

ABSTRACT

Niobium was added to MoSi$_2$ in the form of particles, random short fibers and continuous aligned fibers. It was found that the morphology of Nb played a role in the toughening that occurred (as measured by the area under load displacement curves from room temperature three point bend tests and the examination of fracture surfaces). The Nb particles did not toughen MoSi$_2$. The random short fibers appeared to toughen MoSi$_2$ via crack deflection along the fiber matrix interface. Aligned fibers imparted the greatest toughness improvements, as toughening resulted from fiber deformation. However, larger diameter fibers displayed a greater ability to toughen MoSi$_2$ than smaller diameter fibers. This was attributed to the constraint resulting from the interfacial layer between the MoSi$_2$ matrix and the Nb fiber. Maximum toughness occurs when the fiber is able to separate from the matrix and freely deform.

INTRODUCTION

The attractive combination of low density (6.25 g/cm^3), high melting temperature (2030°C) and excellent resistance to oxidation (up to 1700°C) makes the compound MoSi$_2$ very attractive as a potential elevated temperature structural material. Recent research employing MoSi$_2$ as a matrix material for composites has resulted in improving the inadequate creep resistance and poor low temperature fracture toughness of monolithic MoSi$_2$. Petrovic and co-workers [1] have reinforced MoSi$_2$ with SiC whiskers. The SiC whiskers markedly improved the mechanical behavior of MoSi$_2$ at elevated temperatures. More importantly, the room temperature fracture resistance of MoSi$_2$ has been improved by the addition of Nb fibers, first reported by Fitzer and Remmele [2] in 1985. Room temperature fracture toughness for MoSi$_2$ with Nb fibers has been reported to be 12 MPa·m$^{1/2}$, compared to 3.3 MPa·m$^{1/2}$ for monolithic MoSi$_2$ [3]. These successes have generated enormous research activity on MoSi$_2$ and other silicides over the past few years, as evidenced by a recent workshop devoted solely to structural silicides [4].

Other researchers have published results on MoSi$_2$/Nb foil composites tested in tension in situ in the scanning electron microscope [3,5]. In these studies, the Nb foils would deform during testing. However, when powder-consolidated composites with Nb filaments [3] or particles [5] were tested in bending at room temperature, the Nb reinforcement showed limited ductility. The explanation for the behavior of Nb was a combination of both embrittlement of the Nb by oxygen and the stress state around the Nb reinforcement [5].

The goal of the present effort was to systematically study the role of Nb reinforcement morphology on the mechanical behavior of MoSi$_2$/Nb composites. Thus, MoSi$_2$ was fabricated reinforced with Nb particles, random Nb fibers, and aligned Nb fibers with two different diameters.

EXPERIMENTAL PROCEDURE

The characteristics of the starting powders, particles and fibers are listed in

Table I. The powders and particles were sized using a laser light scattering technique (microtrac) and shapes determined by viewing the powders or particles with a scanning electron microscope. Short fibers were produced by manually chopping the fibers to roughly 10 mm in length.

Particulate and random short fiber composites were produced by incorporating the appropriate amount, twenty volume percent, of Nb with $MoSi_2$ powder with the aid of a turbula mixer (mixing was performed for 60 minutes). Continuously aligned composites were produced by a combination hand layup-infiltration technique described in detail in a previous publication [6]. Briefly, a Cold Isostatic Press (CIP) mold bag was filled to half its capacity with $MoSi_2$ powder. The fibers were layed up within the CIP mold, after which, the CIP mold was filled to capacity with $MoSi_2$ powder infiltrating the fibers. The amounts of powder and fiber were determimed prior to layup and infiltration so to produce a composite with 20 v% fibers.

The mixtures were then CIPed at a pressure of 241 MPa. Cylindrical CIP bars were produced, approximately 25 mm in diameter and 65 mm long. CIP mold bags were lined with Nb foil. The Nb foil had two purposes, first to prevent fragmentation of the CIP bar, since $MoSi_2$ powder tend not to press well. Second to prevent a reaction with the Hot Isostatic Press (HIP) cans and the $MoSi_2$ powder during consolidation. Specimens were vacuum degassed at 600°C for 10 hours and then vacuum encapsulated in Ti HIP cans. Consolidation occurred by HIP at parameters 1350°C-172 MPa.

Smooth bar bend specimens (cylindrical, 6.35 mm in dia. by 38 mm long) were produced by electrodischarge machining (EDM). All bend specimens were containerless re-HIPed after EDM at 1350°C-172 MPa for 3 hours after which they were mechanically polished though $0.3\mu m$ Al_2O_3 powder. Room temperature three point bend tests were performed at a crosshead velocity of 0.127 mm/sec. The distance between the lower supports of the bend jig was 25.4 mm.

TABLE I
MATERIALS

POWDER	SOURCE/DESIGNATION	SHAPE	SIZE
$MoSi_2$	H.C. Stark Grade C Germany	Angular	$2\mu m$
Nb	Teledyne -80 Mesh	Angular	$108\mu m$
FIBER	SOURCE	DIAMETER	
Nb	Teledyne	800 μm	
Nb	NRC	400 μm	

RESULTS AND DISCUSSION

Typical microstructres of the consolidated composites are shown in Fig. 1. Results of the bend tests are shown in Fig. 2. Note, that no toughening was observed from the Nb particles. The maximum toughening (as measured by area under the load displacement curves) occurred with the continuously aligned, large diameter Nb fibers. Examination of fracture surfaces reveals that the Nb particles fractured by cleavage and did not deform in the $MoSi_2$ during testing. The graceful failure exhibited by the random short fibrous composite resulted from extensive crack deflection by decohesion at the $Nb/MoSi_2$ interface (Fig. 3a) for fibers that were off axis and for fibers which perchance happened to be on-axis (aligned perpendicular to the motion of bending) by fiber fracture. For the small diameter continuous aligned specimen the toughening mechanism appears to be fiber failure, with extra energy required to either fracture or deform the fiber (Fig 3b). However, note from Fig. 3c that both fiber failure and considerable separation between the fiber and the matrix occurred with the large diameter fibers.

Microprobe traces across the interface between MoSi2 and Nb indicate that the size and chemical nature (mixed silicides) of the reaction layer were identical in both the large and small diameter fiber composites. Oxygen traces across the interface reveal similar oxygen contents in both fibers and even a lower oxygen content in the Nb particles, implying that the Nb is not being embrittled by oxygen during consolidation. Therefore, the differences in the observed mechanical behavior of the composites cannot be attributed to differences in the matrix/reinforcement interfaces that develop.

The results indicate that maximum toughening will occur when fiber deformation is accompanied by fiber matrix separation (debonding), as occurred with the large diameter continuous aligned Nb fibers. Similar observations have
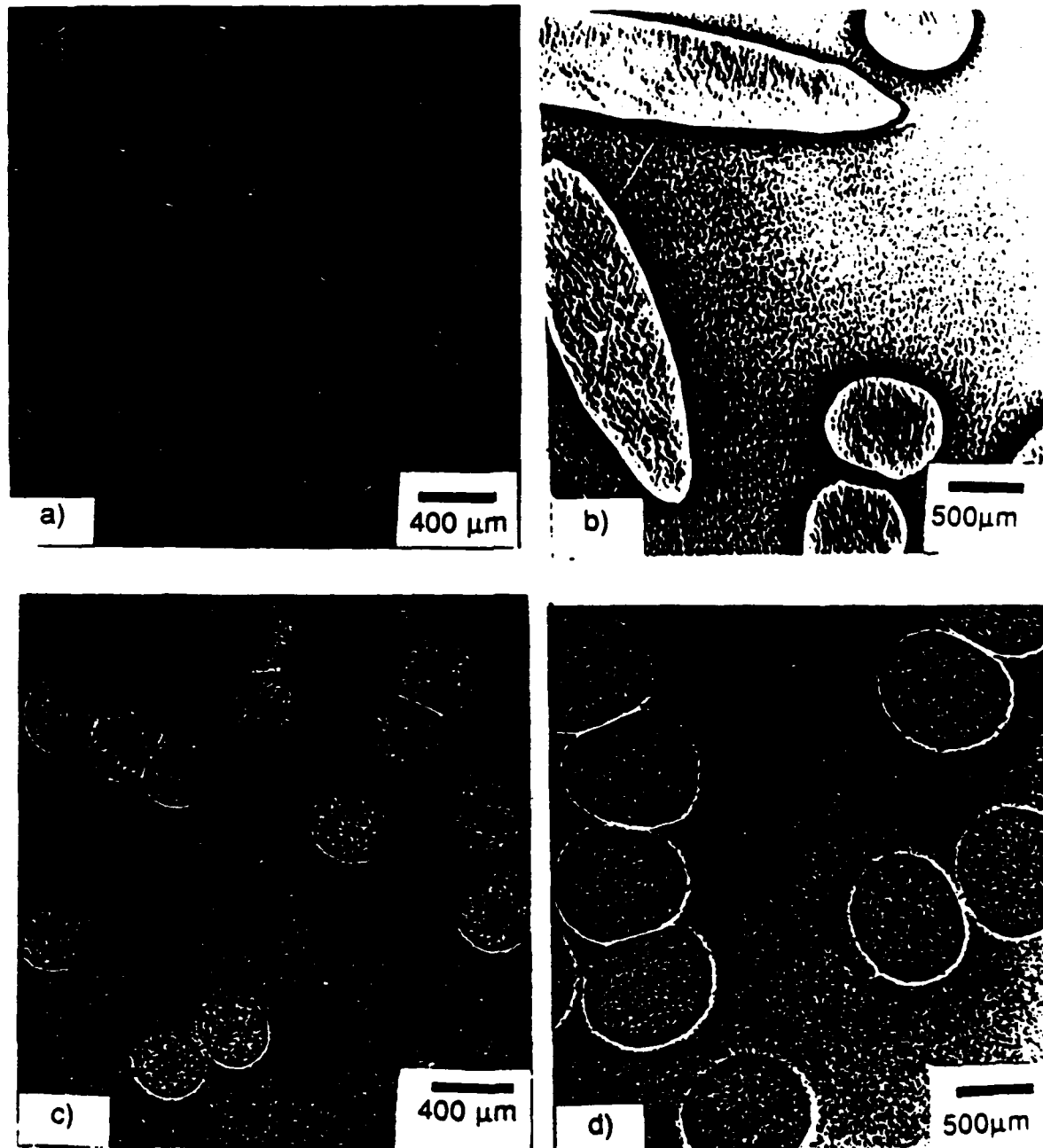
Fig. 1 Typical microstructures of MoSi2/20v% Nb a) Nb particles b) random Nb fibers c) continuous aligned 400μm dia. Nb fibers d) continuous aligned 800um dia. Nb fibers.

been noted for other brittle matrices reinforced with refractory fibers (Si_3N_4/Ta [7] and Al_3Nb/Nb[8]). For fiber matrix separation to occur a critical fiber diameter must be exceeded so that the fibers may deform. This critical diameter results from a balance between the interfacial strength, which impedes fiber-matrix debonding and prevents the fiber from deforming, and the load carrying capacity of the fiber. The smaller diameter fiber did not exceed this diameter and thus failed without debonding.

Fig. 4 shows a comparison of actual composite behavior to the calculated rule of mixtures (ROM) behavior. Note, the actual composite behavior appears to be superior to the calculated behavior. ROM calculations assume that once a crack propagates through the matrix all load is transfered to the fiber; there is no contribution of force necessary to debond the fiber from the matrix. The force necessary to pull the fiber from the matrix results in an added energy required to fracture the composite. This suggests that any coating applied to Nb fibers to prevent a reaction with the matrix should be designed to provide some chemical bonding to both the fiber and the matrix.
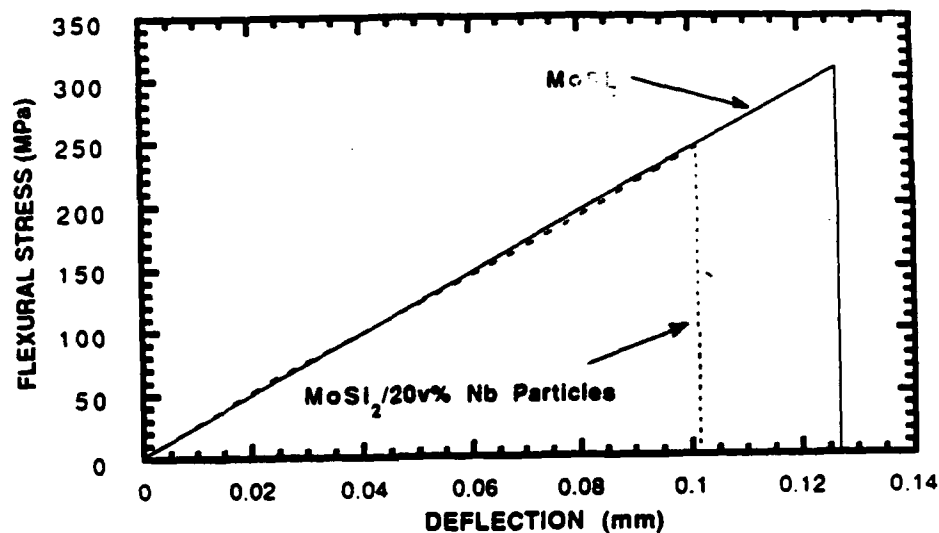
(a)
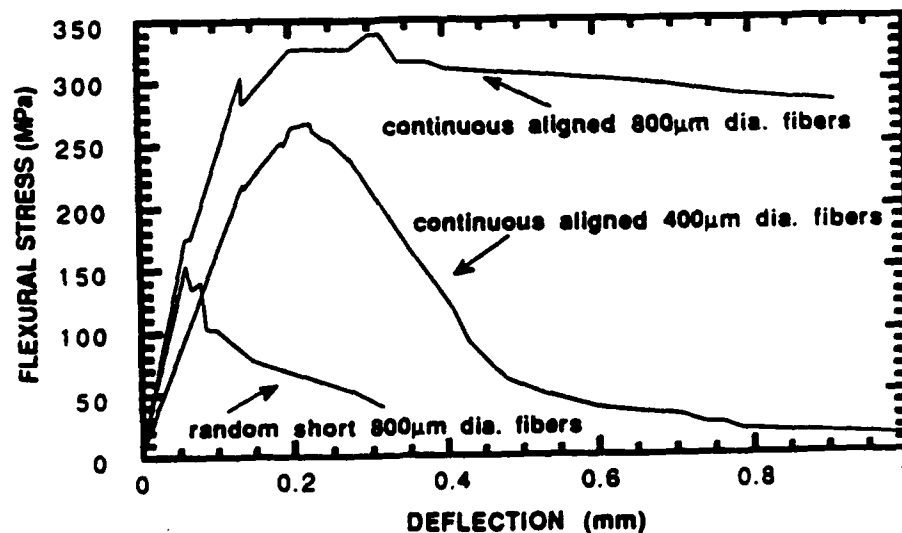
(b)

Fig. 2   Results of room temperature bend tests on $MoSi_2$/20v% Nb composites a) monolithic $MoSi_2$ and $MoSi_2$/Nb particles b) $MoSi_2$ /Nb fibers.
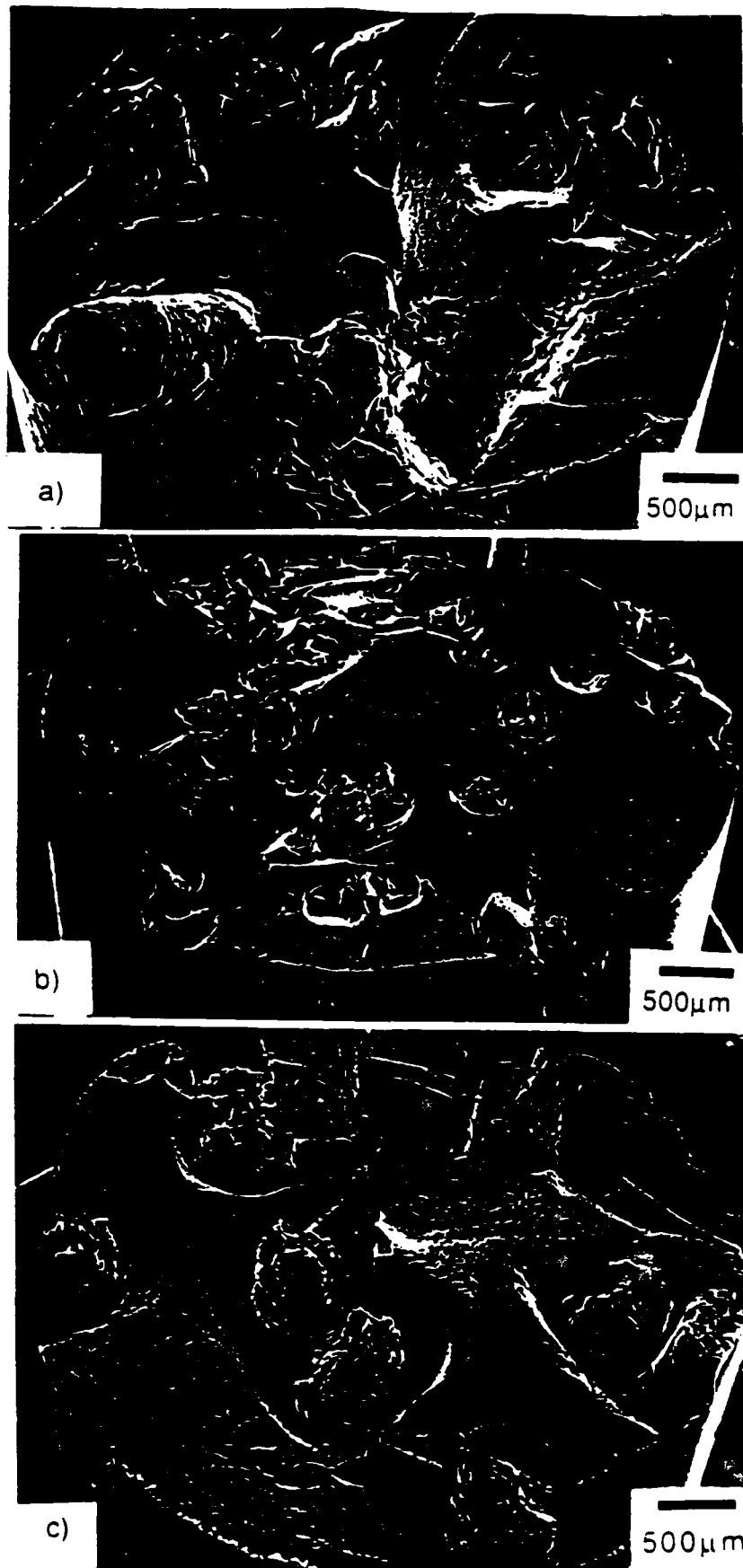
Fig. 3 Fracture surfaces of MoSi$_2$/20v% Nb tested in bending at room temperature a) random Nb fibers   b) Nb continuous aligned 400μm dia. fibers   c) Nb continuous aligned 800μm dia. fibers
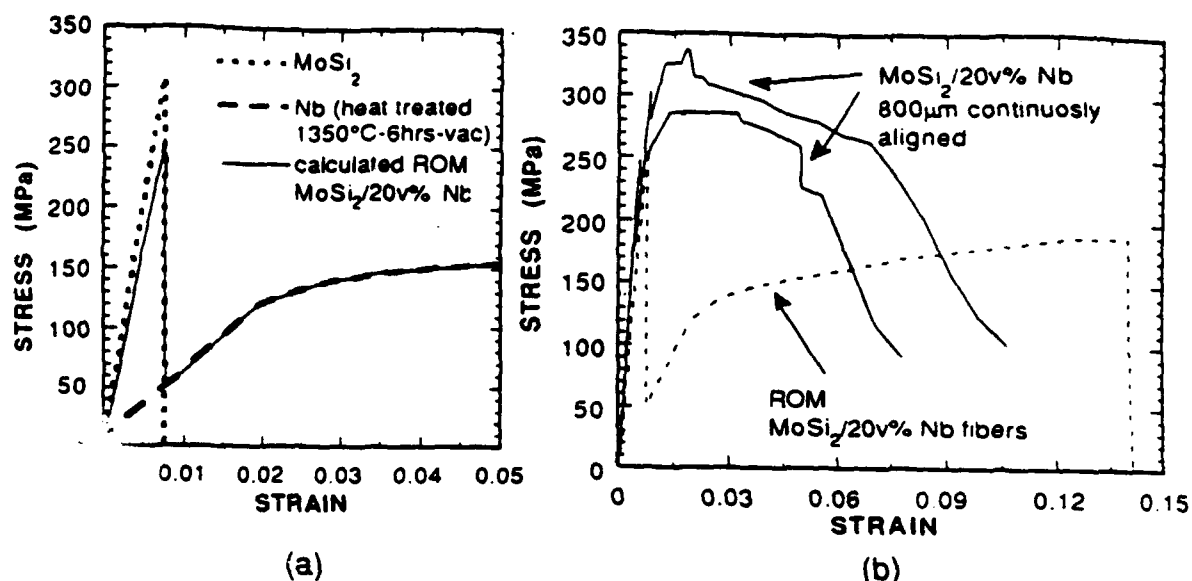
Fig. 4 Comparision of calculated rule of mixtures (ROM) to actual composite behavior. (a) ROM calculation (b) comparison to composite behavior

CONCLUSIONS

The morphology of the Nb reinforcement plays a large role in the toughening mechanisms that occured in MoSi₂/Nb composites. The large diameter aligned Nb fibrous composites had the highest toughness (as measured by area under a load displacement curve) due to a combination of fiber deformation and separation at the fiber-matrix interface.

Maximum toughness will occur in brittle matrices reinforced with ductile phases when the reinforcement phase is able to separate from the matrix and freely deform. The behavior of these types of composites is very much dependent on interfacial properties.

ACKNOWLEDGEMENTS

REFERENCES

1. D.H. Carter, W.S. Gibbs and J.J. Petrovic, in Proc. 3rd. Intl. Symp. on Ceramic Matls & Components for Engines (the American Ceramic Society, Westerville, OH, 1989) p. 977.
2. E. Fitzer and W. Remmele, in Proc. 5th Intl. Conf. on Composite Materials, ICCM-V, edited by W.C. Harrigan, J.Strife and A.K. Dhingra (TMS, Warrendale, PA. 1985) p. 515.
3. L. Xiao, Y.S. Kim, R. Abbaschian and R.J. Hecht, Mater. Sci. and Engr. A144, 277 (1991).
4. High Temperature Structural Silicides WorkShop, Gaithersburg MD, Nov. 4-6, 1991 (proceedings to be published in Mater. Sci. and Engr., 1992).
5. T.C. Lu, A.G. Evans, R.J. Hecht and R. Mehrabian, Acta Metall. 39, 1853 (1991).
6. D.E. Alman. K.G. Shaw, N.S. Stoloff and K. Rajan, presented at the High Temperature Structural Silicides WorkShop, Gaithersburg MD, Nov. 4-6, 1991 (to be published in Mater. Sci. and Engr., 1992).
7. J.J. Brennan, in Special Ceramics 6, edited by P. Popper (The Brittish Ceramic Research Association, Stoke-On-Trent, England, 1975) p. 123.
8. L. Lu, Y.S. Kim, A.B. Gokhale and R. Abbaschian, in Intermetallic Matrix Composites, edited by D.L. Anton, P.L. Martin, D.B. Miracle and R. McMeeking (Mater. Res. Soc Proc. 194, Pittsburgh. PA. 1990) p. 79

Tensile Properties of Ordered and Disordered Ni$_3$Fe Intermetallic Compound and Composite

A. Bose[1], G. Camus[2], R. M. German,
D. J. Duquette and N. S. Stoloff

Materials Engineering Department
Rensselaer Polytechnic Institute
Troy, NY 12180-3590

1. Currently Senior Scientist, Southwest Research Institute, San Antonio, Texas

2. Currently Research Scientist, Laboratorie des Composites Thermostructuraux, Peassac, France

ABSTRACT

Ni$_3$Fe is a compound that exhibits long range ordering below 500°C and a disordered structure above that temperature. Thus, Ni$_3$Fe allows study of the effect of ordering on the mechanical properties This paper discusses the tensile properties of Ni$_3$Fe produced via powder metallurgy. Fabrication of Ni$_3$Fe started with elemental nickel and iron powders that were solid state sintered followed by containerless hot isostatic compaction. Ordering was done by heat treating at 470°C for 200 hours. Disordering was attained by heating to 800°C for 2 hours followed by a water quench. Composites of Ni$_3$Fe with 5 v/o Y$_2$O$_3$ were prepared by pre-sintering cold isostatically pressed rods followed by containerless hot isostatic pressing. Similar ordering and disordering treatments were carried out on these composites to evaluate the effect of particulate additions. Ordering of Ni$_3$Fe increases both strength and hardness with a small affect on ductility. For the Ni$_3$Fe - Y$_2$O$_3$ composite, the increase in the strength and hardness when the material is ordered is accompanied by a loss in ductility.

1

INTRODUCTION

This research is focussed on the effect of long range order on the properties of the Ni_3Fe intermetallic compound. A majority of the intermetallic compounds for example, Ni_3Al, FeAl, Nb_3Al exhibit long range order up to the melting point of the compound. Thus, it is impossible to study the effects of ordering on the properties. This is equally true for intermetallic matrix composites where the effect of ordering has not been reported.

The compound Ni_3Fe has a Ll_2 structure which exhibits long range order below 500°C and is disordered at temperatures above that. Thus, this compound offers the opportunity to study ordering effects on the properties of a ductile intermetallic [1,2]. The addition of 5 v/o Y_2O_3 to Ni_3Fe yields a composite whose matrix can be ordered or disordered, allowing assessment of ordering effects on the composite properties. In this study, Powder processing techniques have been applied for the fabrication of ductile Ni_3Fe and a composite having Ni_3Fe as the matrix. Tensile tests were performed on both materials in the ordered and disordered conditions.

EXPERIMENTAL

The nickel-iron binary phase diagram is shown in Figure 1. An alloy with a composition of 76.5 at. % Ni was chosen for this study. This alloy is in the ordered phase field below 500°C and can be ordered by proper heat treatments.

A mixture of carbonyl iron and nickel powders was used to fabricate the compound. The characteristics of the elemental powders are given in Table I. The powders were mixed in a Turbula mixer in 200g batches and die compacted into flat tensile specimens using a double action floating

2

die. The die wall was lubricated with zinc stearate and the compaction pressure was 300 MPa. The resulting compacts were 5mm thick, 645mm^2 in pressing area, and 5mm wide in the gauge section. These compacts were sintered at 1410°C for 1h in dry hydrogen (-42°C dew point). During the last 10 min of sintering the atmosphere was shifted to dry argon (-48248C dew point) to minimize hydrogen embrittlement [3,4]. These P+S (press and sintered) samples were 95% dense with uniformly distributed closed pores.

Full density Ni_3Fe compacts were fabricated by cold isostatic compaction of mixed elemental powders at 210 MPa to form 18mm diameter by 75 mm long rods These rods were given the same sintering treatment, followed by containerless hot isostatic compaction (103 MPa in argon at 1200°C for 30 min). These 100 dense rods were machined into 4mm diameter tensile bars with a 15 mm gauge length. Composites consisting of 5 vol. % Y_2O_3 (15 μm mean particle size obtained from Cerac) were prepared from mixed powders using the same compact, sinter, hot isostatic compaction, and machining sequence.

Disordered samples were prepared by heating in argon at 10 K/min to 880°C, holding this temperature for 2h, with a water quench. Ordering was performed by vacuum encapsulating the specimens in glass with a Zr setter and then soaking for 200h at 470°C. The degree of order was estimated at 0.95 [5].

All of the tensile tests were performed at room temperature in tension using a crosshead speed of 0.12 mm/min. The fracture surfaces were examined using scanning electron microscopy and typical metallographic cross sections were prepared for assessment of pore and grain structures.

3

RESULTS AND DISCUSSION

A. Material Evaluation

The resulting microstructures of the as sintered Ni_3Fe and the hot isostatically pressed Ni_3Fe, with and without yttria particulate reinforcement, are shown in Figure 2. Note the variation in magnification necessary to account for the grain size differences. Figure 2a shows that the sintered Ni_3Fe has a finer grain structure with an average grain size of 80 μm compared with 450 μm for the hot isostatically pressed material shown in Figure 2b. Moreover the sintered alloy exhibits a uniform distribution of fine porosity of about 5 μm in size whereas the hot isostatically pressed samples show a fully dense microstructure. Therefore, it appears the HIP process has effective closed the remaining porosity present in the as-sintered material. Pore elimination has decreased the inhibiting effect on grain growth due to a pining of the grain boundaries. The large increase in grain size has also probably been favored by the relatively high HIP temperature.

The Y_2O_3 reinforced HIP Ni_3Fe has a finer microstructure than the parent alloy (see Figure 2C). The dispersion of the yttria particles within the NI_3Fe alloy appears to be fine and uniform. Density measurements show that there is no essentially remaining porosity after the HIP process. The large inhibition of grain growth observed in the HIP reinforced NI_3Fe is attributed to the fine oxide dispersion. The ordering or disordering temperatures were too low to significantly affect the scale of the microstructure beyond the growth during the sintering of HIP treatments.

B. Mechanical Properties

The tensile properties obtained with the three different processing

conditions, in both ordered and disordered conditions, are listed in Table II. The ordered condition has a significantly higher yield strength and ultimate tensile strength and only a slightly lower ductility than the disordered condition. The engineering stress strain curves in Figure 3 graphically illustrate these trends and show that the onset of order also increases the strain hardening rates. The increases in yield strength, strain hardening rate, and ultimate tensile strength can all be associated with ordering. Ordered alloys generally deform by the motion of superlattice dislocations, resulting in intense planar slip and restricted cross-slip, while disordered alloys show more diffuse slip. The fact that ordering does not appreciably reduce ductility is rather unusual. Behavior has been previously reported for Ni_3Fe (6,7). This compound possess the Ll_2 structure in its ordered state, i.e. a structure with a sufficient number of independent slip systems to obey the Von Mises criteria, and shows non-inherent brittleness, unlike other Ll_2 intermetallic alloys such as Ni_3Al or Ti_2CuAl_5.

If the three alloys show similar trends in the effect of order on the tensile properties the differences in microstructure give rise to important variations in tensile behavior and fracture when compared one to each other.

Porosity effect

By comparing date for both ordered and disordered alloys, either HIP or P+S, it appears that the elimination of residual porosity results in a significant increase in the yield strength but very little changes in the ultimate tensile strength and elongation. This is shown by the respective engineering stress-strain curves in Figure 3 a and b. The strain hardening rate is nearly unaffected in the disordered condition,

5

but is increased in the first part of the curve by the suppression of the residual porosity in the ordered condition.

The onset of necking is increased in the case of the fully dense HIP material. The strain begins to localize at about the same strain for both the ordered and disordered Ni_3Fe. However, the disordered alloy is able to avoid linkup to fracture until a larger value of total strain. For the P+S specimens, strain is localized later than with the HIP specimens. Once slip is localized, the porous Ni_3Fe quickly fails with limited necking in both the ordered and disordered states.

The HIP treatment removed the residual porosity and gave a large increase in the average grain size from 80 μm to 450 μm. Both effects are responsible, for the observed changes in tensile properties. Grain growth is responsible for lowering the strain at which necking starts to occur since large grains promote shear instability process. The limited necking of the P+S alloys is related to their porosity. On the other hand, determining the mechanism involved in the observed increase of yield strength through HIP is not so straightforward. The residual porosity in the P+S alloys has two possible detrimental effects on yield strength. Slip may initiate near the individual pores as plastic zones form due to concentrated stresses, and thus leading to a lower flow stress. The porous alloys may be regarded as damaged material in which the observed flow stress is inferior to the effective flow stress of an equivalent undamaged material. It is unlikely these effects related to the porosity would have compensated and even overpassed the large drop in yield strength that should have occurred with grain growth. A possible explanation is that a substructure might be present within these large grains after the HIP operation.

6

An increase in the porosity in the range of 2 to 5 percent voids decreases the strength, but has a negligible effect on the tensile ductility (8,9). Ductility is dependent on a shear instability process involving the linking of a critical number of pores/voids and the path of high void content. Therefore, due to the low probability of linking a critical number of pores/voids to failure in materials with porosity in the range of 2.5 to 5%, the ductility of the porous ordered and disordered alloys is not affected.

Although the strain to failure is about the same for both the fully dense alloy and the specimens with 5% porosity, the path to failure results in different ductile fracture surface characteristics, as shown in Figure 4. Examination of the fracture surfaces indicates that the ordered and disordered material failed by a dimpled transgranular mode of rupture. The mean dimple size seems to be the same for the porous ordered and disordered conditions, and in both cases the residual porosity is apparent at the center of the dimples. This suggests the dimples have been generated by residual pores and indicates that residual porosity is responsible for the limited amount of necking of these alloys. In the fully dense material, the dimples are larger, especially in the case of the disordered alloy which exhibited the larger amount of necking on the stress-strain curve.

As shown in Figure 5, the very large grains in the fully dense material show slip bands in the deformed grains near the fracture surface. The ordered alloy exhibits the expected large amount of planarslip (Figure 5a), while the disordered alloy shows diffuse slip (Figure 5b).

7

Reinforcement effect

Comparisons between the unreinforced and yttria reinforced HIP alloys (Table II), show that yttria has a major effect on the tensile properties in both the disordered and ordered states; the yield stress increases by 80 to 85 MPa and the ductility is reduced from near 40% to approximately 10%. The strain hardening rate is also increased, this effect being more pronounced for the ordered alloy. The fracture surface are shown in Figures 6a and 6b. These exhibit a ductile dimpled transgranular appearance, with smaller dimples than in the case of the parent unreinforced alloy. In both conditions, most of the dimples appear to be centered around the yttria particulates, and to some extent the dimples are larger in the disordered condition.

The drop in ductility and the increases in yield strength and strain hardening rate associated with the introduction of particulates is commonly reported for oxide dispersion strengthened superalloys as well as other intermetallic alloys (10,11). Thus, the yttria particles used as reinforcement in this study strengthen the alloys mainly through their inhibiting effect on grain growth. For particles of a 15 μm size the contribution to strengthening by the Orowan mechanism is small (12). Similarly, coarse dispersoids create problems of compatibility of deformation and large stress gradients can be generated in their vicinity (11). This accounts for the observed large drop in ductility and explains dimples centered around the yttria particles on the fracture surface.

SUMMARY

The elimination of the last 5% residual porosity in Ni_3Fe prepared by powder metallurgy has a large benefit to the yield stregnth. With 5% residual porosity neither the tensile strength nor the elongation

8

are effected. In contrast, the inclusion of 5% Y_2O_3 (15μm particle size) in fully densified Ni_3Fe increases both the yield and tensile strength, but degrades the elongation to failure. Comparisons between mechanical properties in the ordered and disordered states for Ni_3Fe and the yttria reinforced Ni_3Fe brings up an important point concerning the interaction between order and reinforcement. Both ordering and reinforcement give strengthening with lower ductility. When considered in terms of relative ductility loss, the ductility decrease between the disordered and ordered states is more from the parent alloy to the reinforced alloy. From Figure 6, the fracture paths of the yttria reinforced alloy in both ordered and disordered conditions shows more particulates on the fracture surface of the ordered alloy, suggesting decohesion of the matrix/particulate interface is easier in the ordered condition. The only effects truly related to this coarse particulate reinforcement are on ductility and fracture. Thus, it appears that the onset of order in a dispersoid alloy enhances the effects of the dispersion on the tensile properties. This might be related to the particular mode of deformation of ordered alloys, through the motion of superlattice dislocations, resulting in intense planar slip and restricted cross-slip.

ACKNOWLEDGMENTS

REFERENCES

1.   G. M. Camus, N.S. Stoloff and D. J. Duquette, Acta Met. **37**, 1497-1501, (1989).

2. D. G. Morris, G. T. Brown, R. C. Piller and R. E. Smallman, Acta Met. 24, 21 1976.

3. A. Bose, B. Moore, R. M. German and N. S. Stoloff in "Proc. conf. on PM aerospace materials", Luzern, Switzerland, Nov. 2-4, 1987, 41-47, 1988, Shrewsbury, England, MPR, Publ. Services Ltd.

4. A. Bose, D. Sims, R. M. German and N. S. Stoloff, in "Proc. Conf. on high temperatures structural composites: Synthesis, characterization and properties," Hoboken, N.J., 1987.

5. G. M. Camus, D. J. Duquette, and N. S. Stoloff, submitted to Scripta Met. (The Article on H-embrittlement of Ni_3Al with an oxide dispersion).

6. Y. Calvayrac and M. Fayard, Phys. Stat. Sol., 17, 407, 1973.

7. T. Takasugi and O. Izumi, Acta Met., 33, 1247, 1989.

8. E. M. Dubensky and D. A. Kioss, Metall Trans., 18A,

9. R. Haynes, The Mechanical behavior of sintered alloys, Freund Publishing house, London, UK, 1981.

10. J. L. Strudel, "Mechanical Properties of Multiphase Alloys" in Physical Metallurgy 3rd edition, ed. by R. W. Cahn and P. Haasen North Holland 1983, p. 1860.

11. C. C. Koch, High Temperature Ordered Intermetallic Alloys II, ed. by N. S. Stoloff, C. C. Koch, C. T. Liu, and O. Izumi, MRS Symposia Proceedings 81 (1987) p. 369.

12. N. S. Stoloff, (The review on Ni_3Al, should be published by now).

Table I

Powder Characteristics

Property	Ni	Fe	Y_2O_3
vendor	INCO	GAF	Cerac
designation	123	HP	
purity, %	99.99	99.50	
Fisher subsieve size, μm	3	3.0	
mean size, μm	3	11	15
specific surface area, m^2/g	2.19	0.88	
apparent density, g/cm^3	2.15	2.20	
major impurities (ppm)	Ca(10) Fe(30) Si(40)	Ca(600) Al(600) Si(300) O(300) Mn(2000)	

11

Table II

Mechanical Properties of Ordered and Disordered Ni_3Fe Compacts

condition	disordered			ordered		
	YS,MPa	UTS,MPa	E,%	YS,MPa	UTS,MPa	E,%
P+S	111	490	43	180	627	37
HIP	172	487	43	247	627	37
5%Y_2O_3	250	513	14	333	649	10

YS = yield strength, UTS = ultimate tensile strength, E = elongation, P+S = press and sinter, HIP = hot isostatic press, 5% Y_2O_3 = HIP with 5 vol. %

Figure Captions

1. The binary phase diagram for the Fe-Ni system showing the Ni_3Fe compound as being ordered below approximately 500°C.

2. Optical micrographs of the Ni_3Fe samples; a) press and sinter (P+S), b)hot isostatically pressed (HIP), and c) HIP wityh 5 vol.% yttria ($5\%Y_2O_3$), molybdic acid etch.

3. Engineering stress-strain curves for NI_3Fe compounds in both the ordered and disordered conditions prepared by three routes; a) P+S, b) HIP, and c) 5% Y_2O_3.

4. Scanning electron microgrpahs of the fracture surfaces of the pressed and sintered (P+S) Ni_3Fe compacts in the disordered (a) and ordered (b) conditions, and HIP Ni_3Fe in the disordered condition.

5. Scanning electron micrographs of HIP Ni_3Fe showing planare ship bands in the ordered condition (a) and diffuse slip bands in the disordered condition (b).

6. Scanning electron micrographs of the fractrure surfaces of HIP NI_3Fe containing 5 vol. % yttria (Y_2O_3) in the diisordered (a) and ordered (b) conditions.

INTERMETALLIC COMPOUNDS

ENVIRONMENTAL EFFECTS AND OXIDATION

FATIGUE/CREEP INTERACTIONS IN Ni₃Al-BASE ALLOYS

G.M. Camus, D.J. Duquette and N.S. Stoloff
Materials Engineering Department
Rensselaer Polytechnic Institute
Troy, New York 12180-3590

ABSTRACT

Stress-controlled fatigue tests and fatigue crack growth rate tests
respectively have been carried out on two Ni₃Al Cr/Zr alloys, IC 218 at
600°C and 800°C, and IC 221 at 800°C, in vacuum, at various test frequen-
cies. Decreasing the test frequency and/or increasing the temperature
leads to a decrease in the number of cycles to failure, and a gradual dis-
appearance of a fatigue fracture zone. In fatigue crack propagation tests,
the crack growth rate only decreases at the lowest frequency and remains
constant in the major part of the frequency range investigated. The fatigue
propagation mode in all cases is intergranular. These trends are shown in
both cases to be related to a true creep component but, under fatigue crack
growth test conditions, crack blunting intervenes gradually as the frequency
is decreased, leading therefore to a less severe frequency effect.

INTRODUCTION

Large improvements in high temperature ductility have been achieved
in boron-doped Ni₃Al through additions of chromium [1,2]. Creep/stress-
rupture properties have been improved through additions of zirconium [2,3].
Simultaneously it has recently been shown [4] that these Ni₃Al alloys
also have improved fatigue properties in terms of crack initiations as well
as crack propagation. However, little work has been done on the creep-
fatigue behavior of Ni₃Al alloys. This phenomenon, in which during
cyclic stresses at elevated temperature, both fatigue and creep damage
interact to reduce a specimen's fatigue life is of major interest for
eventual high temperature applications. In their recent study of a
directionally solidified Ni₃Al (B,Hf) alloy, Bellows et al. [5,6] have
concluded that there is a very good intrinsic creep/fatigue resistance at
450°C and 760°C under stress-controlled fatigue in vacuum. They were not
so sure of the eventual behavior of an equiaxed polycrystal Ni₃Al since
some intergranular failures were noted. Also, a study of the fatigue crack
propagation behavior of a Ni₃Al+B alloy containing some substantial addi-
tions of cobalt and hafnium, at 400°C, has shown no frequency effect on the
crack growth rate in vacuum, but a strong dependence upon the frequency when
the tests are performed in air [7].

The purpose of the present work was to investigate frequency effects
on the high temperature stress-controlled fatigue life and fatige crack
propagation properties of IC 218 and IC 221, respectively, two Ni₃Al
B/Cr/Zr alloys, in vacuum. In the case of the IC 218 alloy, temperature
and stress-range were additional experimental variables.

EXPERIMENTAL PROCEDURE

The IC 218 and IC 221 alloys were provided by Oak Ridge National
Laboratory. Processing, chemical compositions (at %), heat treatments
performed on these alloys and the resulting grain size are listed in
Table I.

TABLE I

	Composition (at %)					Processing	Heat Treatment (Vacuum<3.10^{-4}Pa)	Grain Size (µm)
	Ni	Al	Cr	Zr	B			
IC 218	Bal.	8.45	8.13	0.90	0.027	VIM Cast + extruded	1050°C 1 hr + 800°C 24 hrs	14
IC 221	Bal.	9.01	7.97	1.77	0.020	HIPed + extruded	1160°C 30 m + 800°C 24 hrs	8

Fatigue specimens with a 3.0 mm diameter by 11.3 mm long reduced cylindrical gage section and compact tension specimens with W=25.4 mm, B=3.0 mm were directly machined from the IC 218 and IC 221 rods, respectively, prior to heat treatment. Both alloys were tested in a closed loop machine under stress-controlled fatigue, using a triangular wave function and a stress ratio value R=$\sigma_{min}/\sigma_{max}$ of 0.1, in a vacuum of less than 1.5 10^{-3} Pa. The IC 218 alloy was tested at different frequencies ranging from 0.2 Hz to 20 Hz at 600°C with $\Delta\sigma$=724 MPa and 800°C with $\Delta\sigma$=690 MPa as temperature and stress range conditions, under stress-controlled fatigue. Fatigue crack growth experiments were conducted on IC 221 specimens at a unique temperature of 800°C for different frequencies ranging from 0.02 Hz to 20 Hz, using a calibrated direct current potential drop technique to monitor the instantaneous crack length.

Informations on fracture surfaces and crack morphologies were obtained by optical metallography and by Scanning Electron Microscopy.

RESULTS

Stress-Controlled Fatigue (IC 218)

The influence of frequency on the number of cycles to failure at 600°C and 800°C is shown in Fig. 1. Data show a permanent decrease in the number of cycles to failure for each ten-fold reduction in frequency at the two temperatures investigated. The magnitude of this decrease appears to increase at higher temperature. For a given frequency, raising the temperature from 600°C to 800°C also appears to reduce strongly the fatigue life in terms of cycles to failure, in spite of the lower stress-range used at 800°C. On the same figure also appear the data plotted in terms of time to failure versus frequency: in this case, only the tests run at 800°C exhibit a constant decrease of the fatigue life with the frequency. Ductility, measured as reduction in cross-sectional area and as the total elongation in the gage length after tests (Fig. 2) always increases with decreasing frequency, with the exception of the test performed at 800°C/0.2 Hz where a plateau seems to be reached. The decrease is greater at the lowest temperature, but the values obtained for both elongation and reduction in area are much higher at 800°C than at 600°C.

The observed fracture mode varies with temperature and, to a lesser degree, with frequency. Samples tested at 600°C exhibit surface-connected crack initiation with a relatively flat initial intergranular crack propagation zone, but the overall size of the fatigue zone decreases as the frequency is decreased, see Fig. 3. At 800°C, no presence of a definite fatigue zone is observed at any of the three frequencies investigated. Cracks always initiate internally with the major portion of the fracture occurring by microvoid growth and coalescence, leading to the fracture path exhibited in Fig. 4.
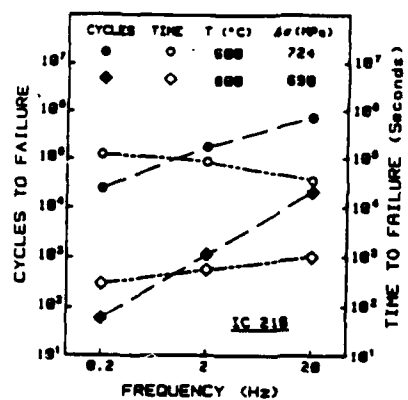
Figure 1. Effect of frequency on fatigue lives of IC 218 at 600°C and 800°C in vacuum.
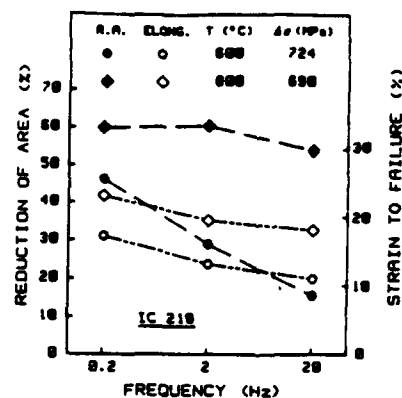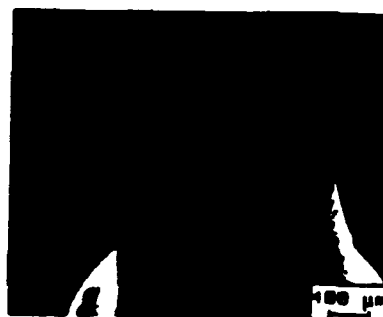

Figure 2. Changes in ductility for IC 218 as a function of temperature and test frequency.

a)

b)

c)

Figure 3. SEM fractographs of IC 218 tested at 600°C
a) ν = 20 Hz   b) ν = 0.2 Hz
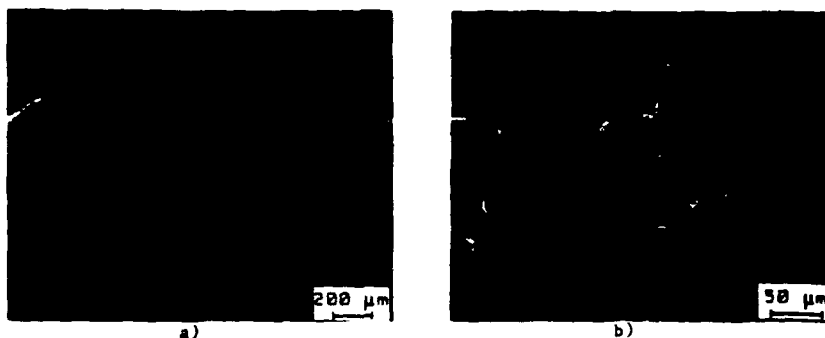c) Crack initiation and fatigue zone, ν = 2 Hz

a)   b)

Figure 4. a) SEM fractograph of IC 218 tested at 800°C/2 Hz

b) Higher magnification on the central region

Fatigue Crack Propagation (IC 221)

Results of crack growth experiments carried out at 800°C on IC 221 for a set of frequencies ranging from 0.02 Hz to 20 Hz are shown in Fig. 5. The rate of crack growth is nearly insensitive to test frequency between 20 Hz and 0.2 Hz but increases at the lowest frequency of 0.02 Hz. When the data are plotted as a function of the test frequency, under a given cyclic stress intensity of $\Delta K=25$ MPa$\sqrt{m}$ (Fig. 6), the same trend obviously remains in terms of crack growth rate per cycle, da/dN, but the crack growth rate calculated per time, da/dt, shows a consistent decrease with a decrease in the test frequency, even at 0.02 Hz.

The observed fatigue propagation mode always remains identical to the one exhibited in Fig. 7 at any of the frequencies investigated, i.e. an intergranular path where the grain boundaries appear to be rounded and not as sharp as when an intergranular failure occurs under a tensile condition. Optical micrographs taken on re-polished sides of broken specimens show an
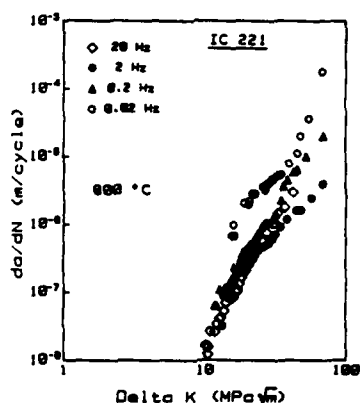
Figure 5. Crack growth rates da/dN vs. ΔK for IC 221 at various frequencies.
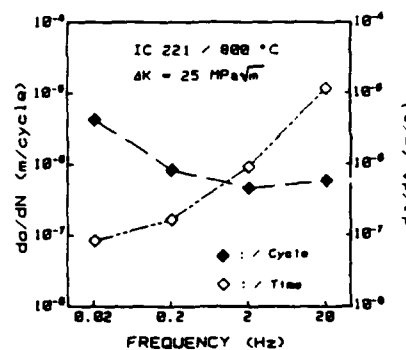
Figure 6. The frequency dependence of da/dN and da/dt for IC 221 at a given ΔK.
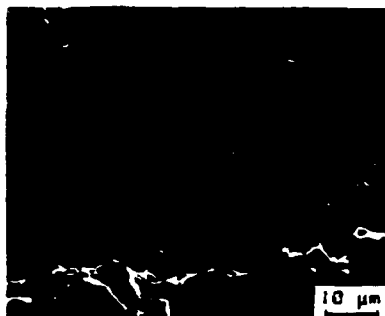
Figure 7. SEM fatigue fracture surface of IC 221 tested at 800°C/ 2 Hz.

Figure 8. Transverse optical fractograph of fatigue crack in IC 221 tested at 800°C/0.2 Hz.

increased tendency for the occurrence of secondary cracks developing perpendicularly to the propagation direction as the frequency is decreased (Fig. 8). Moreover, the fracture path itself appears more erratic at lower frequencies.

DISCUSSION

Decreased fatigue life and, to a lesser degree, increased crack propagation rate for respectively IC 218 and IC 221 are noted as test frequency is reduced. This behavior has been commonly reported in many systems and has been related to a creep interaction, an environmental interaction and/or the combination of the two [8,9]. Although with the medium range vacuum used in this study environment effects cannot be neglected, the experiments reveal considerable evidences for a true creep component.

IC 218 tested under stress-controlled fatigue conditions exhibit at 800°C a fracture mode initiated internally by microvoid growth and coalescence at any of the frequencies employed. Limited fatigue zones decrease in size as the frequency is lowered at 600°C. Moreover, the large increase in ductility occurring with decreasing the frequency at both temperatures is particularly strong evidence for the role of creep in the fatigue process. On the other hand, if creep alone was the principal mechanism for failure, the time to failure would not be expected to be a function of frequency. Thus, taking into account the evolution of the fracture mode and the observed increase of time to failure with a decrease in the frequency (with a lower amplitude at the lowest frequency), it is believed that, within the stress range and frequency conditions used, creep starts to interact at 600°C on a still predominant fatigue failure mode. At 800°C, the absence of a well-defined fatigue zone on the fracture surface and the relatively weak frequency effect on the time to failure show that creep is largely predominant.

Fatigue crack growth experiments conducted on IC 221 at 800°C result in an intergranular fatigue path at all of the frequencies investigated. The relatively non angular shape of the grain boundaries indicates that grain boundary sliding, i.e. a creep related mechanism, is largely involved in the fatigue propagation mode. However, the weak frequency effect on da/dN and the persistent decrease of da/dt with decreasing frequency, at a given ΔK, suggests that a secondary mechanism simultaneously occurs. The increased tendency for the development of secondary cracks with a decrease in the frequency seems very likely to be this interacting phenomenon.

Thus, it is believed that creep plays a significant role in the FCP of
IC 221 at 800°C, but the development of secondary cracks contributes to
limiting any visible frequency effect.

CONCLUSIONS

Frequency effects on the high temperature behavior of two Ni_3Al
B/Cr/Zr alloys, IC 218 and IC 221, in stress-controlled fatigue and fatigue
crack growth tests, respectively, have been studied at 600°C and/or 800°C.
Fractographic studies reveal that in both cases a creep component acts in
conjunction with the fatigue mechanisms, but frequency effects influence
much more the fatigue life than the fatigue propagation rates. The
relative role of creep and fatigue on the fatigue life of IC 218 is temper-
ature and frequency dependent, with creep interacting more strongly as the
temperature is raised and/or the frequency is lowered. The increased ten-
dency for the development of secondary cracks with a decrease of the fre-
quency during crack propagation of IC 221 contributes to limit strongly
frequency effects on the propagation rates.

REFERENCES

1. C.T. Liu and V. Sikka, J. of Metals, 38, 19-21 (1986).
2. V.K. Sikka and E.A. Loria, in Superalloys 1988, edited by S. Reichman
    et al. (Proc. of 6the Int. Conf. on Superalloys, AIME, PA, 1988,
    pp.203-212.
3. S.E. Hsu, N.S. Hsu, C.H. Tong, C.Y. Ma and S.Y. Lee in High Temperature
    Ordered Intermetallic Alloys II, edited by N.S. Stoloff, C.C. Koch,
    C.T. Liu and O. Izumi (Mater. Res. Soc. Proc. 81, Pittsburgh, PA 1987)
    pp.507-512.
4. W. Matuszyk, M.S. Thesis, Rensselaer polytechnic Institute, Troy, NY,
    1988.
5. R.S. Bellows, E.A. Schwarzkopf and J.K. Tien, Met. Trans. A., 19A,
    479-486, (1988).
6. R.S. Bellows and J.K. Tien, Scripta Met., 21, 1659-1662 (1987).
7. K.M. Chang, S.C. Huang and A.I. Taub in High Temperature Ordered
    Intermetallic Alloys II, edited by N.S. Stoloff, C.C. Koch, C.T. Liu
    and O. Izumi (Mater. Res. Soc. Proc. 81, Pittsburgh, PA, 1987),
    pp.303-308.
8. E. Blank and N.S. Stoloff, Acta Met., 35, 2255-2264 (1987).
9. N.S. Stoloff and D.J. Duquetta, in Creep-Fatigue-Environment Inter-
    actions, edited by R.M. Pelloux and N.S. Stoloff (TMS-AIME Proc.
    Warrendale, PA, 1980), pp.178-194.

THE EFFECT OF ORDER ON HYDROGEN
EMBRITTLEMENT OF Ni₃Fe

G. M. CAMUS, N. S. STOLOFF and D. J. DUQUETTE

Materials Engineering Department, Rensselaer Polytechnic Institute, Troy, NY 12180-3590, U.S.A.

Abstract—The susceptibility of a cold pressed and sintered Ni₃Fe alloy to hydrogen embrittlement has been investigated by means of room temperature tensile tests in air and with hydrogen charging in both fully ordered and disordered conditions. Pre-charging with hydrogen and simultaneous charging with hydrogen resulted in a fracture morphology which ranged from a mixed transgranular/intergranular mode to a totally intergranular depending on the type of exposure to hydrogen and the degree of ordering. Associated reductions in the tensile elongations as well as in the ultimate tensile strengths were also observed. Hydrogen diffusion along the grain boundaries led to intergranular fracture concentrated near the surfaces of the alloy when cathodic pre-charging conditions were used, with a deeper penetration due to higher hydrogen diffusivity in the case of the disordered alloy. Susceptibility to hydrogen embrittlement has been found to be largely promoted by ordering under simultaneous charging conditions with a resulting totally intergranular fracture. The results suggest that enhanced diffusitivity of hydrogen to grain boundaries, associated with dislocation transport, occurs in combination with planar slip in the ordered alloy.

Résumé—La sensibilité d'un alliage Ni₃Fe, comprimé à froid et fritté, à la fragilisation par l'hydrogène est étudiee à l'aide d'essais de traction à température ambiante dans l'air et dans une atmosphère chargée en hydrogène dans des conditions d'ordre et de désordre parfaits. Le chargement préalable et le chargement simultané d'hydrogène conduisent à une morphologie de rupture qui va d'un mode mixte transgranulaire/intergranulaire à un mode totalement intergranulaire selon le type d'exposition à l'hydrogène et le degré d'ordre. On a observé des réductions associées pour les élongations en tension ainsi que pour les charges de rupture. La diffusion de l'hydrogène le long des joints de grains conduit à une rupture intergranulaire concentrée près des surfaces de l'alliage quand on a utilisé des conditions de chargement cathodique préalable, avec une pénétration plus profonde due à une plus grande diffusivité de l'hydrogène dans le cas de l'alliage désordonné. On trouve que la sensibilité à la fragilisation par l'hydrogène est largement favorisée par l'ordre dans des conditions de chargement simultané avec une rupture résultante totalement intergranulaire. Les résultats suggèrent qu'il se produit une diffusiveité renforcée de l'hydrogène vers les joints de grains, associée à un transport par les dislocations, en combinaison avec un glissement planaire dans l'alliage ordonné.

Zusammenfassung—Die Neigung einer kaltgepreßten und gesinterten Ni₃Fe-Legierung zur Wasserstoffversprödung wurde mit Zugversuchen an Luft bei Raumtemperatur untersucht; dier Wasserstoffbeladung erfolgte im vollständig geordneten wie auch im entordneten Zustand. Wasserstoffbeladung vor und während des Versuches führte zu einer Bruchmorphologie, die von einer gemischt transgranular/intergranularen Mode vis zu einer vollständig intergranularen Mode reichte, je nach der Art der Wasserstoffexposition und dem Grad der Ordnung. Damit zusammenhängend waren Verlängerung und absolute Festigkeit im Zugversuch verringert. Die Diffusion des Wasserstoffs entlang den Korngrenzen führte zu einem intergranularen Bruch, der in der Nähe der Oberflächen der Legierung konzentriert war, wenn vorher katodisch beladen worden war. Die Eindringtiefe des Wasserstoffs war wegen der höheren Wasserstoffdiffusivität in der entordneten Legierung größer. Die Neigung zur Wasserstoffversprödung wird unter sonst gleichen Beladungsbedingungen durch Ordnung stark gefördert, wobei sich ein vollständig intergranularer Bruch ausbildet. Die Ergebnisse legen nahe, daß die verstärkte Diffusion des Wasserstoffs an die Korngrenzen, unterstützt durch Transport entlang von Versetzungen, zusammen mit planarer Gleitung in der geordneten Legierung auftritt.

INTRODUCTION

The susceptibility of long-range ordered intermetallic compounds to hydrogen embrittlement, especially those ordering in an L1₂ superlattice, has now been well established [1–4]. Comparative studies performed by Kuruvilla and Stoloff [1, 4], who first reported the effect, also have shown that embrittlement is much more severe for ordered alloys vs. disordered alloys of identical composition. Therefore, it appears that long-range order, which has been known to substantially affect the mechanical response of intermetallic compounds, primarily through a change in the dislocation configuration, enhances the susceptibility of these alloys to hydrogen embrittlement. Different theories explaining this behavior have been proposed by several investigators, virtually all of them suggesting changes in the cohesive strength of the grain boundaries, since the observed fractures have always been at least partly intergranular in the
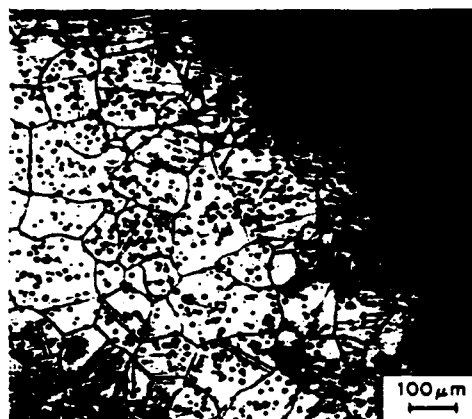
Fig. 1. Optical microstructure of the Ni–23.4 wt% Fe alloy.

presence of hydrogen. For example, Kuruvilla and Stoloff have proposed that planar slip, which is characteristic of ordered intermetallic compounds, provides a rapid transport path of hydrogen from the matrix to the grain boundaries and reduces the cohesive strength of the boundary. Takusugi *et al.* [3] have suggested that the hydrogen is channelled along the grain boundary surfaces and/or the crack surfaces from the sample surface and directly operates to reduce the cohesive strength of the boundaries.

Since Ni₃Fe is known to exhibit appreciable ductility in both the ordered and disordered conditions [5, 6], i.e. there is no inherent brittleness of the grain boundaries, it represents an ideal model alloy for a study of the effects of order, and accordingly slip character, on hydrogen embrittlement.

EXPERIMENTAL

An alloy of composition Ni–23.4 at.% Fe (22.5 wt% Fe) was cold pressed and sintered using elemental powders of nickel and iron. Sintering was performed at 1410°C for 1 h, in successive gaseous atmospheres of hydrogen (50 min) and argon (10 min). Sintered samples were annealed at 800°C for 2 h in flowing argon, followed by a water quench, in order to obtain a fully disordered structure. At this stage of processing, the samples exhibited a uniform grain size of ~80 μm and a uniform distribution of residual micropores of ~5 μm diameter (Fig. 1) resulting in a measured density of 95% of theoretical. The presence of the micropores had no appreciable effect on the mechanical properties of the alloys examined in this study; ductility was high in both the

ordered and disordered conditions. An ordering heat treatment was carried out on specimens which were encapsulated in vacuum under a pressure of ~10⁻⁵ torr with Zr getters, at a temperature of 470°C for 200 h. The degree of order, S, achieved by this heat treatment has been shown to be about 0.95 [7].

All tensile tests were conducted at room temperature on 2.23 × 0.51 × 0.46 cm gage section specimens, using a screw-driven Instron machine at a crosshead speed of 0.012 cm/min. Hydrogen was introduced into the material either by cathodically pre-charging for 45 min or by cathodic charging simultaneously with testing, at a current density of 50 mA/cm², in a solution of 1 N H₂SO₄ containing 0.05 g/l of NaAsO₂ as a hydrogen recombination poison. Fracture surfaces were examined in a scanning electron microscope.

RESULTS

The results of the tensile tests performed in air, and with pre-charging and/or simultaneous charging of hydrogen during testing are summarized in Table 1 and in Fig. 2(a) and (b). When tested in air, the alloy displayed a yield strength, a strain hardening rate, and an ultimate tensile strength which were greater in the ordered condition than in the disordered condition. However, the ductility was comparable for both the ordered and disordered conditions, i.e. 37 and 43% elongation respectively. Examination of the fracture surfaces indicated that the material failed in both conditions by a dimpled transgranular mode of rupture, Fig. 3(a) and (b).

When precharged with hydrogen and tested in air, the tensile strength and the ductility were reduced by 10.5 and 29% respectively in the disordered condition, and by 4.5 and 14% in the ordered condition. The fracture surfaces, as shown in Fig. 4(a) and (b), exhibited a mixed mode of failure for both heat treatment conditions, with an intergranular fracture path concentrated in the outer rim of the specimens. The penetration of the intergranular fracture was deeper in the case of the disordered alloy (130 vs 45 μm in the ordered condition).

When hydrogen was simultaneously charged during tensile testing, the ductility was reduced by 59% and the ultimate tensile strength was reduced by 33% for the disordered alloy. For the ordered alloy, the ductility was reduced by 81% and the ultimate tensile strength was reduced by 65%. The fracture surface of the ordered alloy exhibited a completely

Table 1. Tensile properties of Ni₃Fe

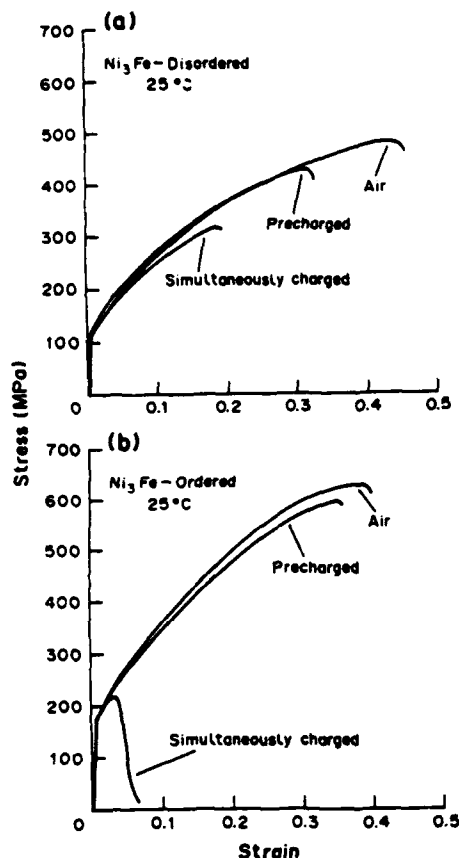|	Disordered			Ordered		
	Air	Precharged	Simultaneously charged	Air	Precharged	Simultaneously charged
σ_n (MPa)	111	112	110	180	176	177
UTS (MPa)	490	439	328	627	598	223
% El.	43	30.5	17.5	37	32	7
Average depth of IG zone (μm)	0	130	590	0	45	Totally IG fracture

Fig. 2. Engineering stress-strain curves for Ni₃Fe tested under several conditions. (a) Disordered, (b) ordered.

cations, resulting in intense planar slip and restricted cross-slip. This mode of deformation accordingly introduces high stress concentrations at grain boundaries. Hydrogen dissolved in the alloys ·is believed to interact with the stress concentrations at the grain boundaries, thus reducing boundary cohesive strength, resulting in intergranular fracture.

The present study shows that Ni₃Fe, in either the ordered or disordered condition is severely embrittled by hydrogen. Failure occurs either in a mixed mode and/or a completely intergranular mode of fracture with significant reductions in ductility, as has been observed for other intermetallic alloys. Also, hydrogen has no appreciable effect on the yield stress of the alloys in either condition. Thus, it appears that dislocation motion is a prerequisite for hydrogen induced failure in this class of alloys. However, the relationship between order and embrittlement has been shown to be dependent on the mode or path of hydrogen entry. The susceptibility to hydrogen embrittlement is greatly enhanced by order when hydrogen is charged simultaneously during the tests. For pre-charging conditions, however, disordered alloys show a larger decrease in ductility when compared to ordered alloys.

The results of the tensile tests performed in laboratory air, without hydrogen, are consistent with the intergranular fracture path, with smooth grain boundary facets [Fig. 5(a)]. The fracture surface of the disordered alloy exhibited a mixed mode of fracture [Fig. 5(b)]. Brittle intergranular fractographic features were concentrated in the outer rim, as in the former case for hydrogen precharging, but with an average depth of penetration of ∼ 590 μm.

It also should be noted that hydrogen did not affect the yield stress for any of the conditions examined.

DISCUSSION

Recent studies have shown that L1₂ intermetallic alloys are commonly susceptible to hydrogen embrittlement, exhibiting significant reductions in ductility as well as in ultimate tensile strength. The fracture paths of these alloys are generally partly and/or entirely intergranular when hydrogen is introduced into the alloys [1-4]. The susceptibility to hydrogen embrittlement also has been shown to be greater in the ordered condition compared to the disordered condition [1, 4]. This behavior has been attributed to the inhomogeneity of the dislocation substructure associated with the ordered condition. Ordered alloys generally deform by the motion of superlattice dislo-
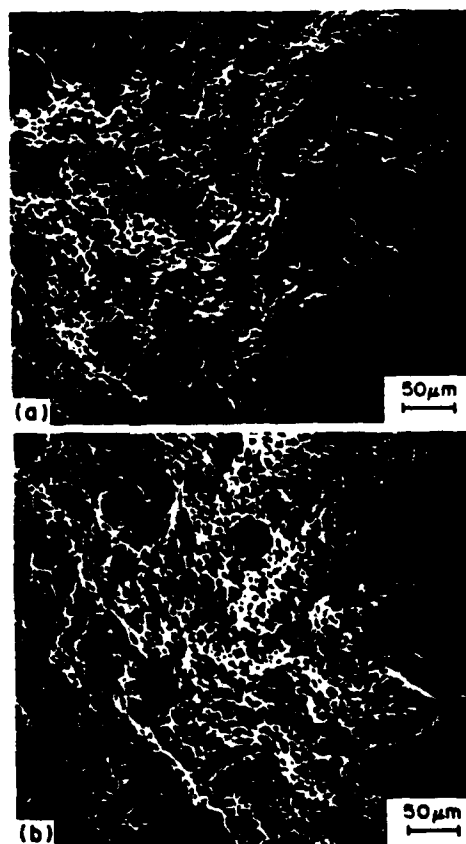

Fig. 3. SEM fractographs of samples tested in air. (a) Disordered, (b) ordered.
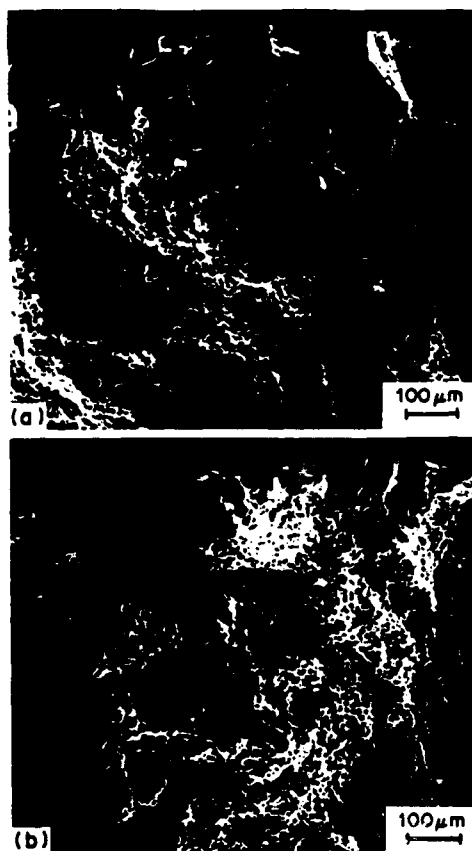
Fig. 4. SEM fractographs of samples precharged and tested
in air. (a) Disordered (b) ordered.

condition. The observation that the inter anular
fracture associated with hydrogen embrittlement is
concentrated in the outer rim of the samples indicates
that, under pre-charging conditions, concentrations
of hydrogen in the grain boundaries are established
prior to testing either through lattice or grain
boundary diffusion. Thus, the depth of hydrogen
penetration due to diffusion and the associated lack
of ductility in the alloy near-surface region are a
function of hydrogen diffusivity, the depth of pene-
tration being reduced in ordered alloys when com-
pared with disordered alloys.

When the tests are performed under simultaneous
charging conditions, embrittlement is much more
severe in the case of the ordered alloy and total
intergranular separation occurs. The disordered
alloy, on the other hand, exhibits a mixed trans-
granular/intergranular mode of failure which tends to
be concentrated towards the surface of the sample.
Thus, under simultaneous charging and tensile defor-
mation, it appears that the highly planar slip which
occurs in the ordered condition effectively "delivers"
hydrogen to the grain boundaries by dislocation
transport. For the disordered alloy, on the other
hand, diffuse slip appears to homogeneously dis-
tribute the hydrogen throughout the matrix, with no
appreciable increase in the hydrogen concentration at

results of Calvayrac and Fayard [5]. That is, the
observed increases in yield strength, strain hardening
rate and ultimate tensile strength can all be associated
with ordering and the effect of ordering on slip
character. On the other hand, ordering does not
appreciably reduce ductility; the overload failures are
essentially transgranular and occur by dimpled rup-
ture. This behavior is not surprising for Ni₃Fe since,
even in the ordered condition, this alloy has a
sufficient number of independent slip systems, as do
other L1₂ intermetallic alloys such as Ni₃Al or Ni₃Si.
However, the latter two alloys exhibit inherent brit-
tleness in the absence of hydrogen. Recent studies
have shown that the wide range of fractures occurring
for nominally the same type of L1₂ intermetallic
compounds can be correlated with differences in
valence, electronegativity and atomic radii between
the two elements of the compounds [6, 8]. The
tendency toward brittle behavior appears to increase
with differences in the above factors.

When cathodically pre-charged with hydrogen, the
Ni₃Fe alloy shows a greater degree of embrittlement
when disordered, with a greater reduction in ductility
and tensile strength and a larger amount of inter-
granular fracture. Dus and Smialowski [9] have
shown that the diffusion rate of hydrogen into Ni₃Fe
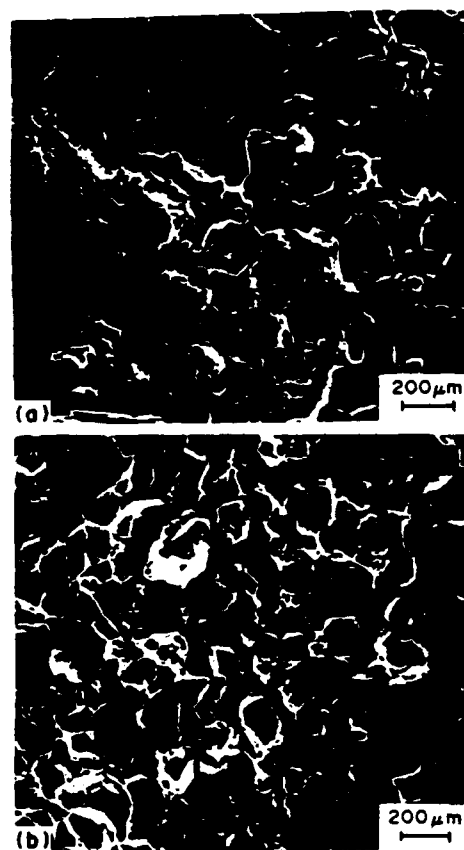is higher in the disordered state than in the ordered

Fig. 5. SEM fractographs of samples charged while testing.
(a) Disordered (b) ordered.

grain boundaries. For the disordered condition, only hydrogen which preferentially diffuses into the grain boundaries during the tensile tests results in embrittlement. These experiments do not indicate if the disordered alloy is intrinsically embrittled by hydrogen; however, the limited reduction in ductility and UTS which are observed during simultaneous charging with hydrogen strongly suggests that embrittlement only occurs at grain boundaries. As for most alloy systems, the specific mechanism(s) for grain boundary embrittlement is largely unknown.

It should be noted that the extent of surface related grain boundary fracture, in the disordered condition, for tests performed under stimultaneous charging was greater than that observed for pre-charging, $(590 \mu m / 50 \mu m)$ even when the time of pre-charging was extended to 70 min, the time period of a typical tensile test under simultaneous charging condition. Thus, it appears that dislocation transport of hydrogen to grain boundaries also occurs during dynamic straining of disordered samples when hydrogen is continuously supplied. However, the extent of this transport process is greatly reduced when compared to that in ordered alloys.

In summary, the present work confirm previous conclusions, based on tests performed on (Fe, Ni)₃V, that c d . enhances the susceptibility to hydrogen embrittlement in $L1_2$ intermetallic alloys [1]. The data reported for Ni₃Al [2] also indicated that there was no effect of hydrogen on the yield strength, suggesting that dislocation motion is a prerequisite to embrittlement and that hydrogen–dislocation interactions with the grain boundaries are involved.

Since this alloy is embrittled by hydrogen in both the ordered and disordered conditions, the present study does not address the hypothesis that enhanced embrittlement in the ordered state (under simultaneous charging) might be due to hydrogen–dislocation interactions at the grain boundaries through a higher build-up of stress caused by planar slip rather than by a simple increase in hydrogen transport to grain boundaries. However, the previous studies performed on the $L1_2$ intermetallic (Fe, Ni)₃V [1] have shown that the latter explanation is more likely since, in contrast to the present study, no hydrogen embrittlement was noticed in the disordered condition for (FeNi)₃V. Therefore, even when hydrogen is present at the grain boundaries, the non-planar slip associated with disordered (FeNi)₃V inhibits embrittlement. Bond *et al.* [10] have directly observed extensive dislocation pileups at grain boundaries between unfavorably oriented grains in boron-doped Ni₃Al. Therefore, while pileups can induce grain boundary fracture even in the absence of hydrogen, the presence of hydrogen exacerbates the effect.

CONCLUSIONS

1. Ni₃Fe is severely embrittled by hydrogen. Unlike other intermetallic compounds previously studied, this embrittlement occurs in both ordered and disordered conditions.

2. Under cathodic pre-charging conditions, diffusion of hydrogen occurs along the grain boundaries which leads to intergranular fracture concentrated near the surfaces of the alloy. Greater penetration of hydrogen and a larger region of embrittlement are observed for the disordered alloy because of the higher diffusivity of hydrogen.

3. Under "dynamic" simultaneous charging conditions, ordering largely promotes susceptibility to hydrogen embrittlement through enhanced penetration associated with dislocation transport and planar slip. These results, in conjunction with previous studies, indicate that the enhanced embrittlement observed upon ordering also may be due to a higher build-up of stress at the grain boundaries associated with planar slip and restricted cross slip.

REFERENCES

1. A. K. Kuruvilla, S. Ashok and N. S. Stoloff, *Proc. Third Int. Congr. on Hydrogen in Metals*, Paris, Vol. 2, p. 629. Pergamon Press, Oxford (1982).
2. A. K. Kuruvilla and N. S. Stoloff, *Scripta metall.* **19**, 83 (1985).
3. T. Takasugi and O. Izumi, *Acta metall.* **34**, 607 (1986).
4. A. K. Kuruvilla and N. S. Stoloff, *Proc. Symp. High-Temperature Ordered Intermetallic Alloys*, MRS Symp. Proc., Vol. 39, p. 229 (1985).
5. Y. Calvayrac and M. Fayard, *Physica status solidi* **17**, 407 (1973).
6. T. Takasugi and O. Izumi, *Acta metall.* **33**, 1247 (1985).
7. D. G. Morris, G. T. Brown, R. C. Piller and R. E. Smallman, *Acta metall.* **24**, 21 (1976).
8. C. T. Liu, *Proc. Symp. High-Temperature Ordered Intermetallic Alloys II*, MRS Symp. Proc., Vol. **81**, p. 355 (1987).
9. R. Dus and M. Smialowski, *Acta metall.* **15**, 1611 (1967).
10. G. M. Bond, I. M. Robertson and H. K. Birnbaum, *J. Mater. Res.* **2**, 436 (1987).

Influence of Long Range Order on Ni_3Fe and
$Ni_3Fe-Y_2O_3$ Composites

A. Bose[1], G. Camus[2], R. M. German,
D. J. Duquette and N. S. Stoloff

Materials Engineering Department
Rensselaer Polytechnic Institute
Troy, NY 12180-3590

1. Currently Senior Research Engineer, Southwest
   Research Institute, San Antonio, Texas

2. Currently Research Scientist, Laboratorie des
   Composites Thermostructuraux, Peassac, France

ABSTRACT

Ni_3Fe is a compound that exhibits long range ordering below 500°C
and a disordered structure above that temperature. Thus, Ni_3Fe allows
study of the effect of ordering on the mechanical properties. This paper
discusses the tensile properties of Ni_3Fe produced via powder
metallurgy. Fabrication of Ni_3Fe started with elemental nickel and iron
powders that were solid state sintered, with some samples subsequently
densified by containerless hot isostatic compaction. Composites of
Ni_3Fe with 5 v/o Y_2O_3 were prepared by pre-sintering cold
isostatically pressed rods followed by containerless hot isostatic
pressing. Similar ordering and disordering treatments were carried out on
these composites to evaluate the effect of particulate additions.
Ordering of Ni_3Fe increases both strength and hardness with a small
effect on ductility. For the Ni_3Fe - Y_2O_3 composite, the increase
in the strength and hardness when the material is ordered is accompanied
by a loss in ductility.

INTRODUCTION

This research is focussed on the effect of long range order on the properties of the Ni_3Fe intermetallic compound. Many intermetallic compounds, for example: Ni_3Al, $FeAl$, $NiAl$, and Nb_3Al exhibit long range order up to the melting point of the compound. Thus, it is impossible to study the effects of ordering on the properties. This is equally true for intermetallic matrix composites where the effect of ordering have not been reported.

The compound Ni_3Fe has a Ll_2 structure; it exhibits long range order below 500°C and is disordered at temperatures above that. Thus, this compound offers the opportunity to study ordering effects on the properties of a ductile intermetallic [1,2]. The addition of 5 v/o Y_2O_3 to Ni_3Fe yields a composite whose matrix can be ordered or disordered, allowing assessment of ordering effects on the composite properties. In this study, powder processing techniques have been applied for the fabrication of ductile Ni_3Fe and a composite having Ni_3Fe as the matrix. Tensile tests were performed on both materials in the ordered and disordered conditions.

EXPERIMENTAL

The nickel-iron binary phase diagram is shown in Figure 1. An alloy with a composition of 76.5 at. % Ni was chosen for this study. This alloy is in the ordered phase field below 500°C and can be ordered by proper heat treatments.

A mixture of carbonyl iron and nickel powders was used to fabricate the compound. The characteristics of the elemental powders are given in Table I. The powders were mixed in a Turbula mixer in 200 g batches and

die compacted into flat tensile specimens using a double action floating die. The die wall was lubricated with zinc stearate and the compaction pressure was 300 MPa. The resulting compacts were 5 mm thick, 645 mm^2 in pressing area, and 5 mm wide in the gauge section. These compacts were sintered at 1410°C for 1 h in dry hydrogen (-42°C dew point). During the last 10 min of sintering the atmosphere was shifted to dry argon (-48°C dew point) to minimize hydrogen embrittlement [3,4]. These P+S (press and sintered) samples were 95% dense with uniformly distributed closed pores.

Full density Ni_3Fe compacts were fabricated by cold isostatic compaction of mixed elemental powders at 210 MPa to form 18 mm diameter by 75 mm long rods These rods were given the same sintering treatment, followed by containerless hot isostatic compaction (103 MPa in argon at 1200°C for 30 min). These 100% dense rods were machined into 4 mm diameter tensile bars with a 15 mm gauge length. Composites containing 5 vol. % Y_2O_3 (15 μm mean particle size obtained from Cerac) were prepared from mixed powders using the same compact, sinter, hot isostatic compaction, and machining sequence.

Disordered samples were prepared by heating in argon at 10 K/min to 880°C, holding this temperature for 2 h, followed by a water quench. Ordering was performed by vacuum encapsulating the specimens in glass with a Zr getter and then soaking for 200 h at 470°C. The degree of order was estimated at 0.95 [5].

All of the tensile tests were performed at room temperature in tension using strain rate of $1.33 \times 10^{-2}s^{-1}$. The fracture surfaces were examined using scanning electron microscopy, metallographic cross sections were prepared for assessment of pore and grain structures.

3

RESULTS AND DISCUSSION

A. Material Evaluation

The resulting microstructures of the as sintered Ni_3Fe and the hot isostatically pressed (HIP) Ni_3Fe, with and without Y_2O_3 reinforcement, are shown in Fig. 2. Note the variation in magnification necessary to account for the grain size differences. Fig. 2a shows that the sintered Ni_3Fe has a finer grain structure with an average grain size of 80 μm compared with 450 μm for the hot isostatically pressed material shown in Fig 2b. Moreover, the sintered alloy exhibits a uniform distribution of fine porosity of about 5 μm in size whereas the HIP samples show a fully dense microstructure. Therefore, it appears the HIP process has effectively closed the remaining porosity present in the as-sintered material. Pore elimination has decreased the inhibiting effect on grain growth due to pinning of the grain boundaries. The large increase in grain size has also probably been favored by the relatively high HIP temperature.

The Y_2O_3 reinforced HIP Ni_3Fe has a finer microstructure than the parent alloy (see Fig. 2c). The dispersion of the Y_2O_3 particles within the Ni_3Fe alloy appears to be fine and uniform. Density measurements show that there is essentially no remaining porosity after the HIP process. The large inhibition of grain growth observed in the HIP reinforced Ni_3Fe is attributed to the fine oxide dispersion. The ordering or disordering temperatures were too low to significantly affect the scale of the microstructure beyond grain growth during the sintering or HIP treatments.

B. Mechanical Properties

The tensile properties obtained with the three different processing

conditions, in both ordered and disordered conditions, are listed in Table II. The ordered condition displays a significantly higher yield strength and ultimate tensile strength and only a slightly lower ductility than the disordered condition. The engineering stress strain curves in Fig. 3 graphically illustrate these trends and show that the onset of order also increases the strain hardening rate. The increases in yield strength, strain hardening rate and ultimate tensile strength all can be associated with ordering.

Among Ll_2 alloys, Ni_3Fe, Co_3Ti, and $(FeCoNi)_3V$ are ductile in the ordered condition, while Ni_3Si, Ni_3Al, Ni_3Ge and Ni_3Ga are not. The former group (except for Co_3Ti) can be disordered by heat treatment, while the latter can not. For each of these alloys the Ll_2 structure permits satisfaction of the Von Mises' criterion for polycrystalline plasticity when {111} <110> slip systems operate. It is beyond the scope of this paper to discuss the factors which make some Ll_2 alloys ductile and others brittle. However, we can point out that ductility in the ordered condition for Ni_3Fe and other ductile Ll_2 alloys always is accompanied by a dimpled rupture fracture mode for tests in air or inert environments.

Although the three Ni_3Fe alloys show similar trends in the effect of order on the tensile properties the differences in microstructure give rise to important variations in tensile behavior and fracture when compared one to each other.

Porosity effect

By comparing data for both ordered and disordered alloys, either HIP or P+S, it appears that the elimination of residual porosity results in a significant increase in the yield strength, but causes very little

5

change in the ultimate tensile strength and elongation. This is shown by the respective engineering stress-strain curves in Figs. 3 a and b. The strain hardening rate is nearly unaffected in the disordered condition, but in the ordered condition is increased in the first part of the curve by the suppression of the residual porosity.

Necking occurs earlier for fully dense HIP material. Deformation begins to localize at about the same strain for both ordered and disordered Ni_3Fe. However, the disordered alloy is able to avoid linkup to fracture until a larger value of total strain. For the P+S specimens, deformation is localized later than with the HIP specimens. Once slip is localized, the porous Ni_3Fe quickly fails with limited necking in both the ordered and disordered states.

The HIP treatment removed the residual porosity and produced a large increase in the average grain size, from 80 μm to 450 μm. Both effects are responsible for the observed changes in tensile properties. Grain growth causes a lowering of the strain at which necking starts to occur since large grains promote shear instability. The limited necking of the P+S alloys is related to their porosity, which causes fracture to occur soon after strain localization begins.

Determining the mechanism involved in the observed increase of yield strength through HIP is not so straightforward. The residual porosity in the P+S alloys has two possible detrimental effects on yield strength. Slip may initiate near the individual pores as plastic zones form due to concentrated stresses, thus leading to a lower flow stress. The porous alloys may be regarded as damaged material in which the observed flow stress is lower than the effective flow stress of an equivalent undamaged material. It is unlikely that these effects related

6

to porosity would have compensated and even surpassed the large drop in yield strength that should have occurred with grain growth. Alternatively, a substructure might be present within these large grains after the HIP operation, thereby leading to increased stength.

An increase in the porosity in the range of 2 to 5 percent voids decreases the strength, but has a negligible effect on the tensile ductility (8,9). Ductility is dependent on a shear instability process involving the linking of a critical number of pores/voids and the path of high void content. Therefore, due to the low probability of linking a critical number of pores/voids to failure in materials with 2.5 to 5% porosity, the ductility of the porous ordered and disordered alloys is not affected.

Although the strain to failure is about the same for both the fully dense alloy and the specimens with 5% porosity, the path to failure results in different ductile fracture surface characteristics, as shown in Fig. 4. Examination of the fracture surfaces indicates that the ordered and disordered materials failed by a dimpled transgranular mode of rupture. The mean dimple size is the same for the porous ordered and disordered conditions, and in both cases the residual porosity is apparent at the center of the dimples. This suggests that the dimples have been generated by residual pores and indicates that the residual porosity is responsible for the limited amount of necking of these alloys. In the fully dense material the dimples are larger, especially in the case of the disordered alloy, which exhibited the greater degree of necking on the stress-strain curve.

As shown in Fig. 5, the very large grains in the fully dense material show slip bands in the deformed grains near the fracture

surface. The ordered alloy exhibits the expected large amount of planar slip (Fig. 5a), while the disordered alloy shows wavy slip (Fig. 5b). These differences in slip character are typical of superlattices that can be disordered.

Reinforcement effect

Comparisons between the unreinforced and Y_2O_3 reinforced HIP alloys (Table II), show that Y_2O_3 has a major effect on the tensile properties in both the disordered and ordered states; the yield stress increases by 80 to 85 MPa and the ductility is reduced from near 40% to approximately 10%. The strain hardening rate also is increased, this effect being more pronounced for the ordered alloy. The fracture surfaces are shown in Figs. 6a and 6b for disordered and ordered samples, respectively. These exhibit a ductile dimpled transgranular appearance, with smaller dimples than in the case of the parent unreinforced alloy. In both conditions, most of the dimples appear to be centered around the Y_2O_3 particles, and to some extent the dimples are larger in the disordered condition.

The reduced ductility and increased yield strength and strain hardening rate associated with the introduction of particles is commonly reported for oxide dispersion strengthened superalloys as well as other intermetallic alloys (10,11). As in other alloy systems, the Y_2O_3 particles strengthen the alloys mainly through their inhibiting effect on grain growth. For 15 μm diameter particles the contribution to strengthening by the Orowan mechanism is small (12). Similarly, coarse dispersoids create problems of compatibility of deformation and large stress gradients can be generated in their vicinity (11). This accounts for the observed large drop in ductility and explains dimples centered

around the yttria particles on the fracture surface.

The elimination of the last 5% residual porosity in Ni_3Fe prepared by powder metallurgy sharply increases yield stress. With 5% residual porosity neither the tensile strength nor the elongation are affected compared to fully dense material. In contrast, the inclusion of 5% Y_2O_3 in fully densified Ni_3Fe increases both the yield and tensile strength, but degrades the elongation to failure. Comparisons between mechanical properties in the ordered and disordered states for Ni_3Fe and the Y_2O_3-reinforced Ni_3Fe brings up an important point concerning the interaction between order and reinforcement. Both ordering and reinforcement provide strengthening with lower ductility. When considered in terms of relative ductility loss, the ductility decrease between the disordered and ordered states is more from the parent alloy to the reinforced alloy. From Fig. 6, the fracture paths of the Y_2O_3 reinforced alloy in both ordered and disordered conditions shows more particles on the fracture surface of the ordered alloy, suggesting decohesion of the matrix/particle interface is easier in the ordered condition. The only effects truly related to this coarse particle reinforcement are on ductility and fracture. Thus, it appears that the onset of order in a dispersion strengthened alloy enhances the effects of the dispersion on the tensile properties. This might be related to the particular mode of deformation of ordered alloys, through the motion of superlattice dislocations, resulting in intense planar slip and restricted cross-slip.

SUMMARY

Powder metallurgical techniques have been used to prepare Ni_3Fe and a Ni_3Fe-5 vol.% Y_2O_3 alloy. Tensile properties have been

9

determined at room temperature. Increased strength of Ni_3Fe is achieved by ordering or by the addition of 5 vol.% Y_2O_3. However, Y_2O_3 reduces the ductility of Ni_3Fe. The onset of necking is affected by the same variables. These effects can be explained via strain localization arguments. Fracture in all alloy conditions was by dimpled rupture. The elimination of porosity principally affects yield stress, with little or no effect on tensile strength or ductility.

ACKNOWLEDGMENTS

REFERENCES

1. G. M. Camus, N.S. Stoloff and D. J. Duquette, Acta Met. 37, 1497, 1989.

2. D. G. Morris, G. T. Brown, R. C. Piller and R. E. Smallman, Acta Met. 24, 21, 1976.

3. A. Bose, B. Moore, R. M. German and N. S. Stoloff in Proceeding of the Conference on PM Aerospace Materials, (Luzern, Switzerland, Nov. 2-4, 1987), 41-47, 1988, Shrewsbury, England, MPR Publ. Services Ltd.

4. A. Bose, D. Sims, R. M. German and N. S. Stoloff, unpublished research, presented at the Conference on High Temperatures Structural Composites: Synthesis, Characterization and Properties, Hoboken, N.J., 1987.

5. G. M. Camus, D. J. Duquette, and N. S. Stoloff, J. Mat. Res., 5, 950, 1990.

6. Y. Calvayrac and M. Fayard, Phys. Stat. Sol. 17, 407, 1973.

7. T. Takasugi and O. Izumi, Acta Met., 33, 1247, 1989.

8. E. M. Dubensky and D. A. Koss, Metall Trans., 18A, 1587, 1987.

9. R. Haynes, The Mechanical Behavior of Sintered Alloys, Freund
    Publishing House, London, UK, 1981.

10. J. L. Strudel, in Physical Metallurgy, 3rd edition, ed. by R. W.
    Cahn and P. Haasen, North Holland, Amsterdam, Netherlands, 1983,
    p. 1860.

11. C. C. Koch in High Temperature Ordered Intermetallic Alloys II, ed.
    by N. S. Stoloff, C. C. Koch, C. T. Liu, and O. Izumi, MRS Symposia
    Proceedings, vol. 81 MRS, Pittsburgh, PA, 1987 p. 369.

12. N. S. Stoloff, Int. Mat. Rev., 34, 153, 1989.

Table I

Powder Characteristics

Property	Ni	Fe
vendor	INCO	GAF
designation	123	HP
purity, %	99.99	99.50
Fisher subsieve size, μm	3	3.0
mean size, μm	3	11
specific surface area, m^2/g	2.19	‚ 0.88
apparent density, g/cm^3	2.15	2.20
major impurities (ppm)	Ca(10)	Ca(600)
	Fe(30)	Al(600)
	Si(40)	Si(300)
		O(300)
		Mn(2000)

Table II

Mechanical Properties of Ordered and Disordered Ni_3Fe Compacts

condition	disordered			ordered		
	YS,MPa	UTS,MPa	E,%	YS,MPa	UTS,MPa	E,%
P+S	111	490	43	180	627	37
HIP	172	487	43	247	627	37
5%Y_2O_3	250	513	14	333	649	10

YS = yield strength, UTS = ultimate tensile strength, E = elongation, P+S = press and sinter, HIP = hot isostatic press, 5% Y_2O_3 = HIP with 5 vol. %

Figure Captions

1. The binary phase diagram for the Fe-Ni system showing the Ni_3Fe compound as being ordered below approximately 500°C.

2. Optical micrographs of the Ni_3Fe samples; a) press and sinter (P+S), b) hot isostatically pressed (HIP), and c) HIP with 5 vol.% Y_2O_3, molybdic acid etch.

3. Engineering stress-strain curves for Ni_3Fe compounds in both the ordered and disordered conditions prepared by three routes; a) P+S, b) HIP, and c) 5% Y_2O_3.

4. Scanning electron micrographs of the fracture surfaces of the pressed and sintered (P+S) Ni_3Fe compacts in the disordered (a) and ordered (b) conditions, and (c) HIP Ni_3Fe in the disordered condition.

5. Scanning electron micrographs of HIP Ni_3Fe showing planar slip bands in the ordered condition (a) and wavy slip bands in the disordered condition (b).

6. Scanning electron micrographs of the fracture surfaces of HIP Ni_3Fe containing 5 vol. % Y_2O_3 in the disordered (a) and ordered (b) conditions.

Temperature (°C)

δ

1500

L

1400

900

γ

700

Ni₃Fe

α

500

Ni₃Fe

300

0   20   40   60   80   100

Fe   wt.% Ni   Ni
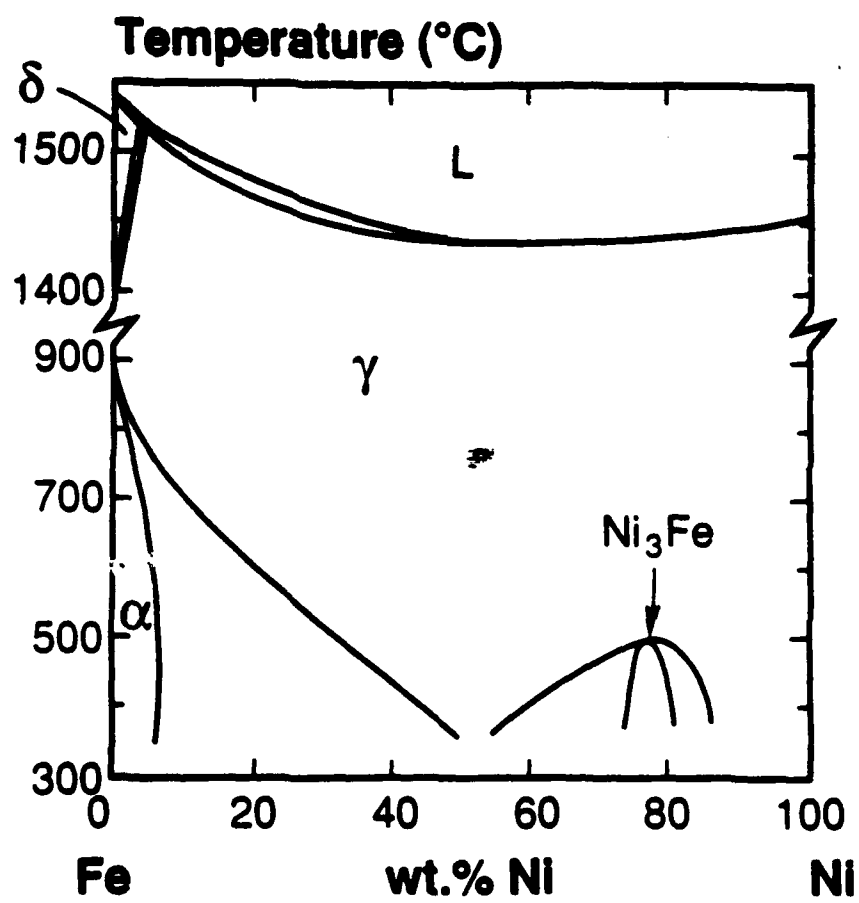
Figure 1
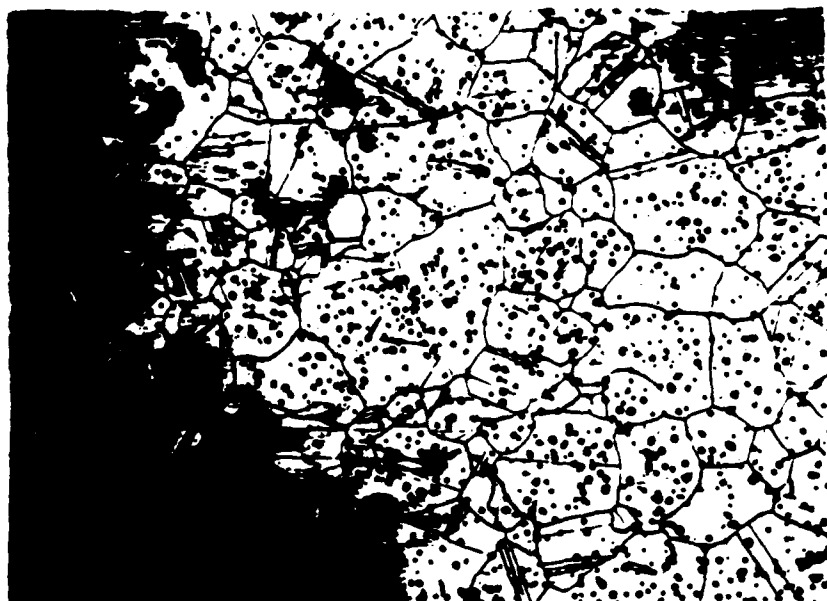
Figure 2a
100 μm

Figure 2b
200 μm
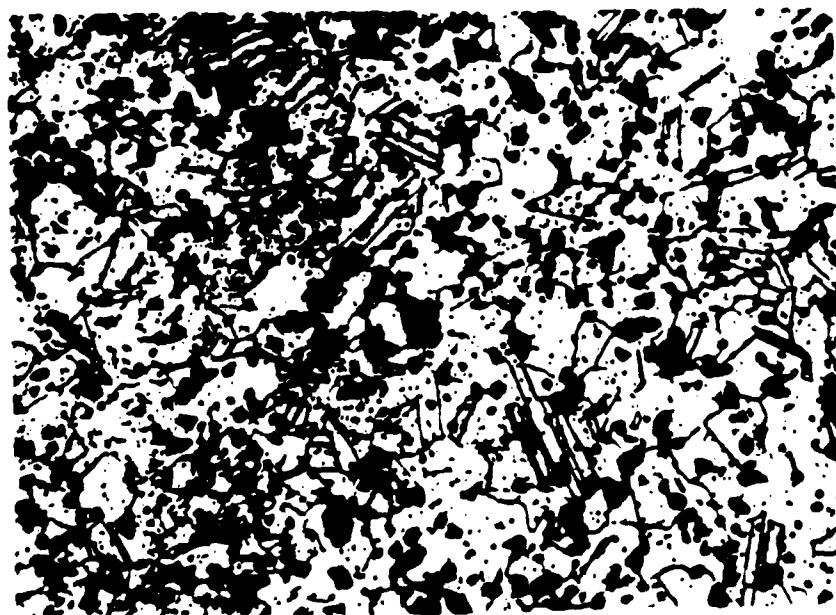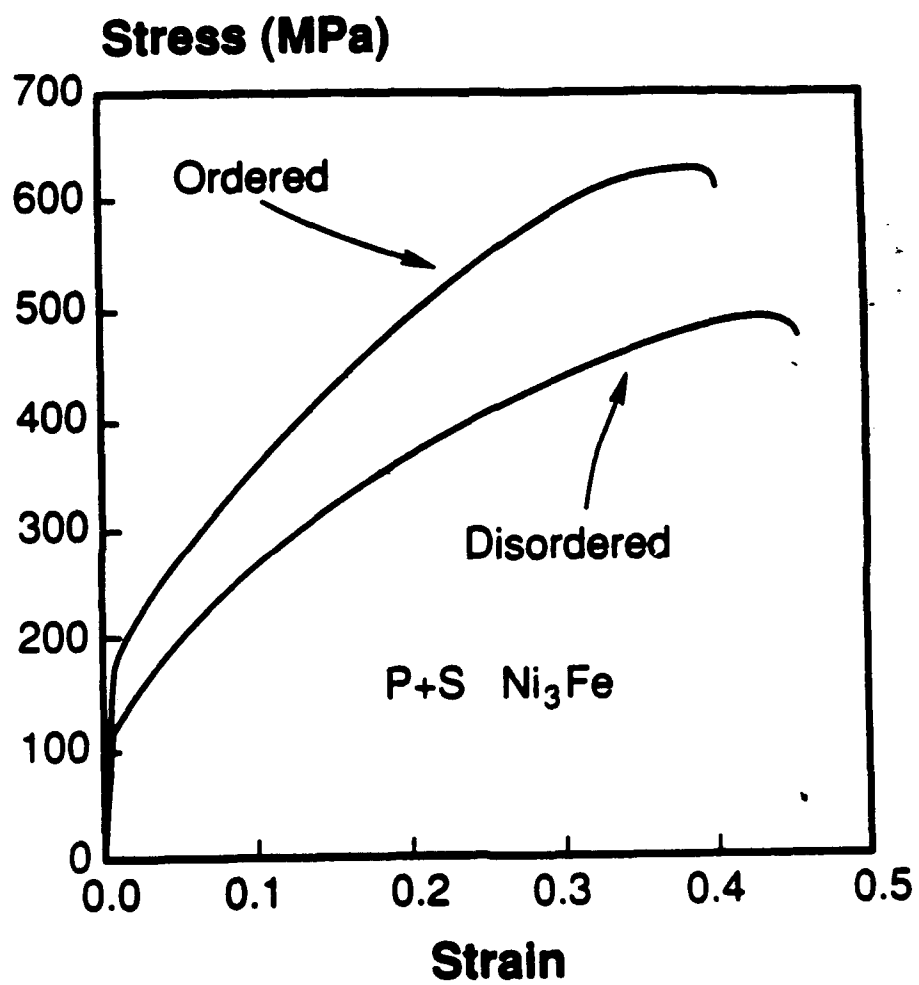
Figure 2c
50 μm
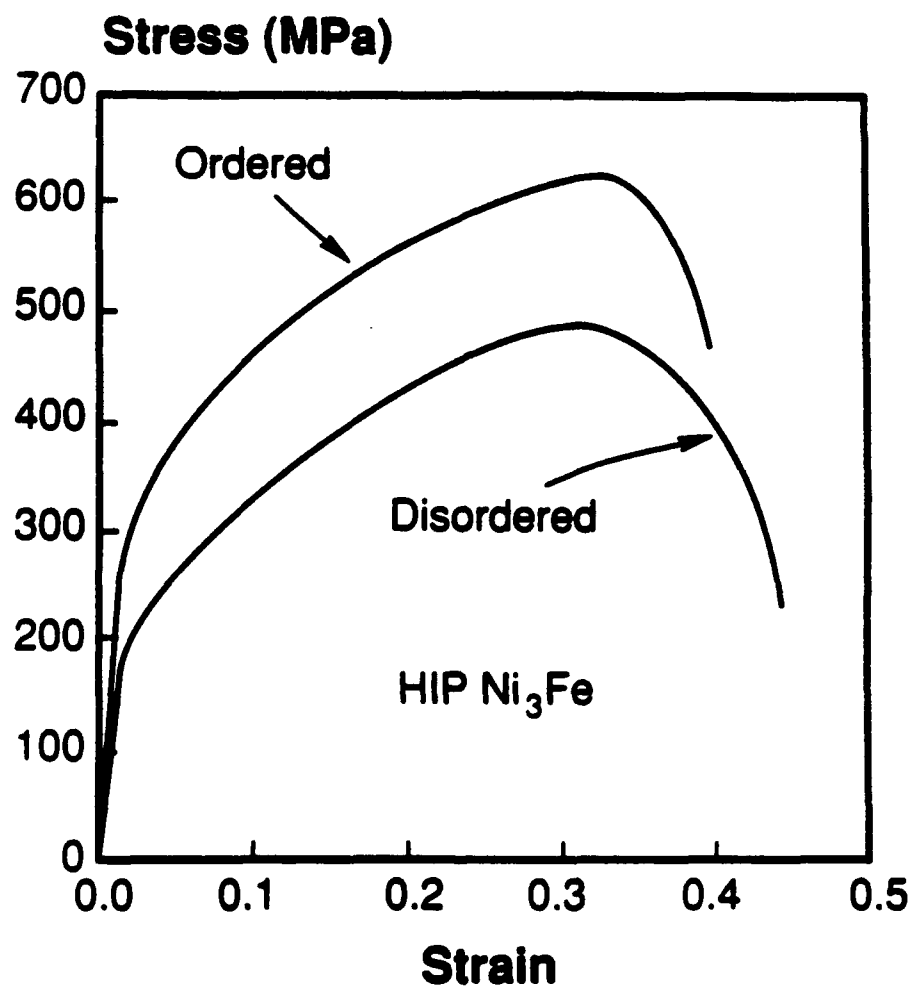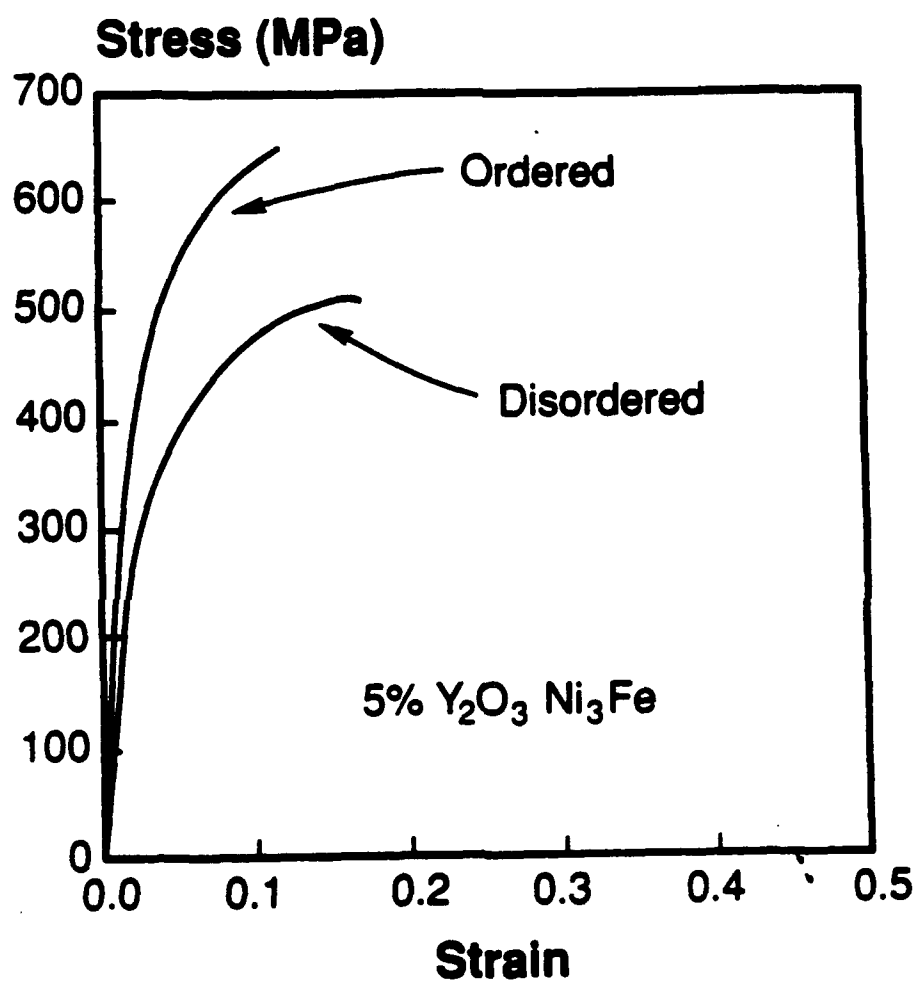
Figure 3a

Figure 3b

Figure 3c

Figure 4a
50 μm
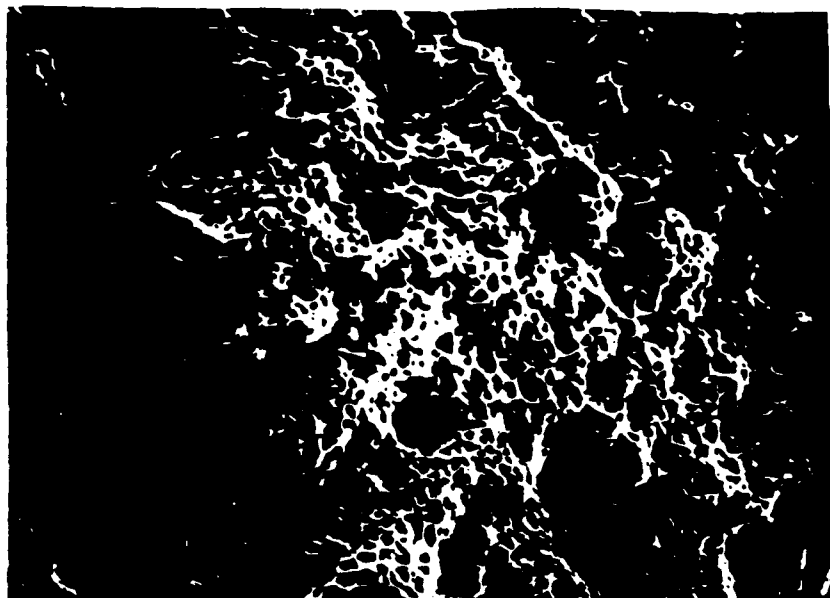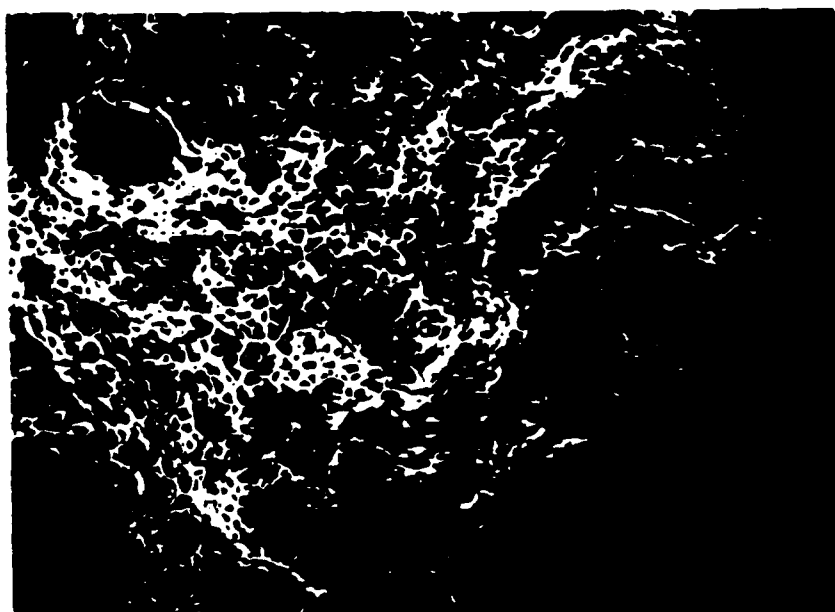
Figure 4b
50 μm
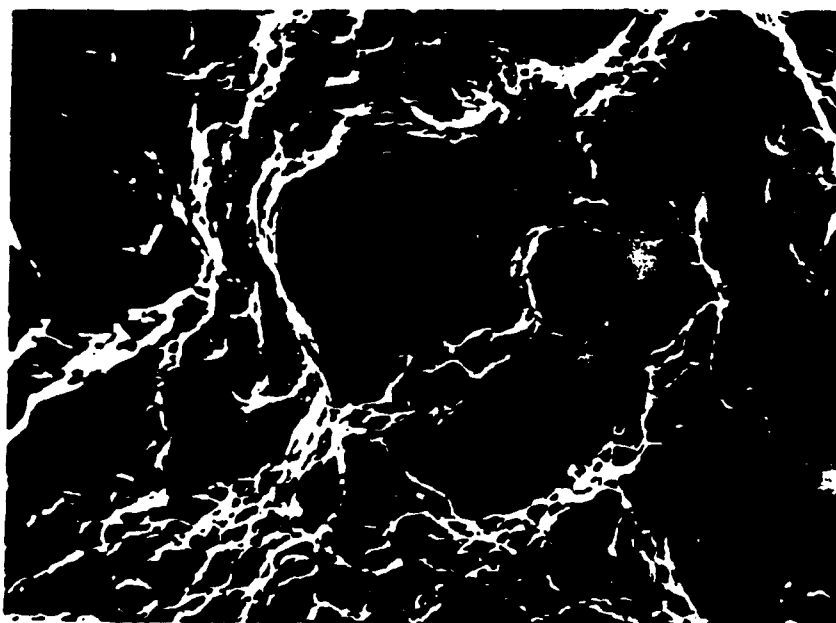
Figure 4c
50 μm
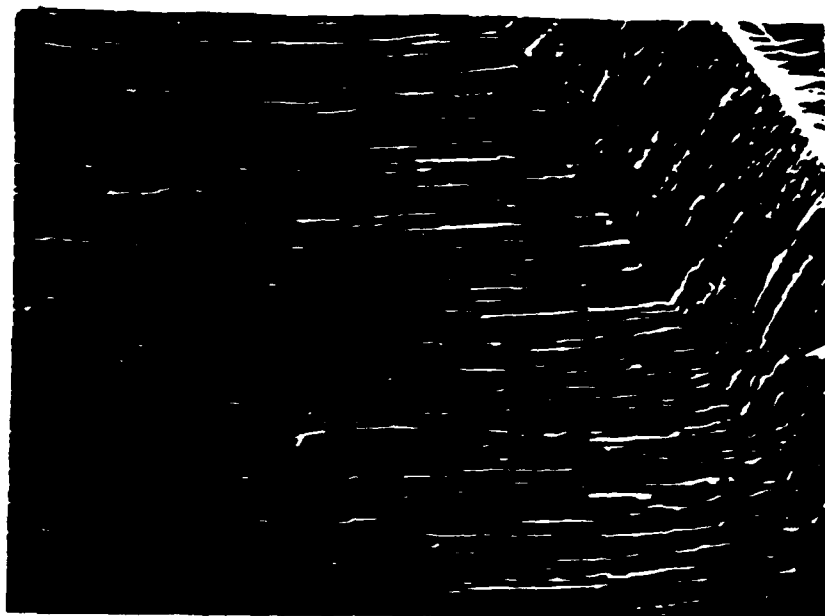
Figure 5a
20 μm

Figure 5b
20 μm
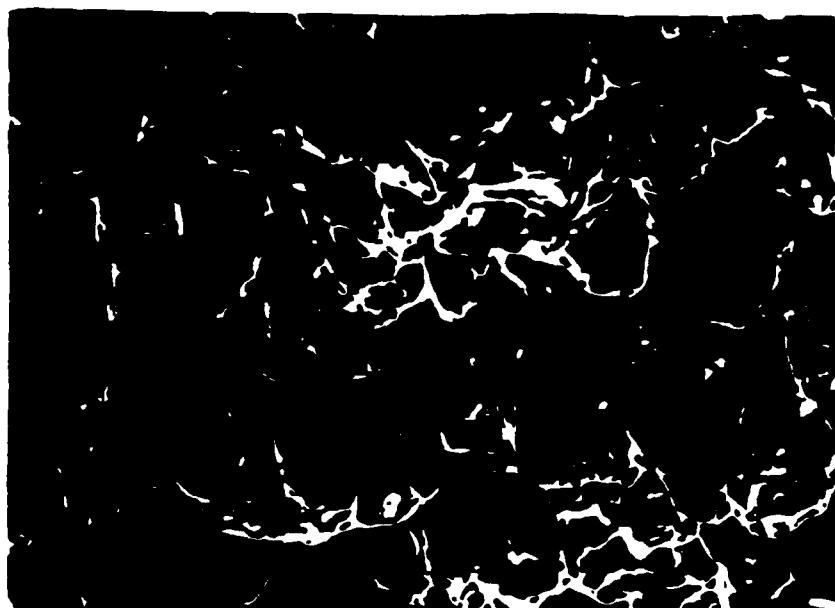
Figure 6a
10 μm

Figure 6b
10 μm

Effect of an oxide dispersion on the hydrogen embrittlement of a Ni₃Al base alloy
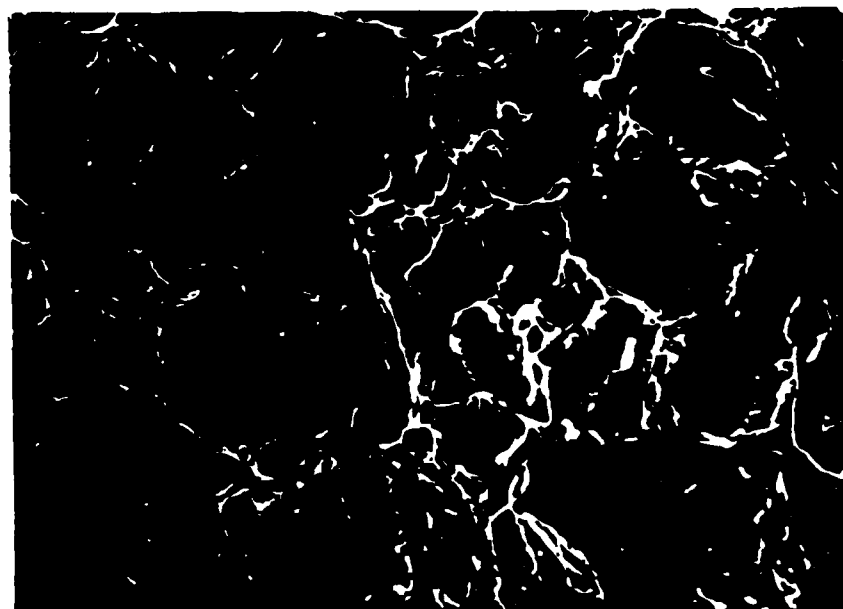
Effect of an oxide dispersion on the hydrogen embrittlement of a Ni_3Al base alloy

G. M. Camus, D. J. Duquette, and N. S. Stoloff

Materials Engineering Department, Rensselaer Polytechnic Institute, Troy, New York 12180-3590

The susceptibility of a hot isostatically pressed Ni_3Al, Cr, Zr alloy to hydrogen embrittlement has been studied. The base alloy and a second alloy containing 5 vol. % Y_2O_3 particles were tested by cathodically charging with hydrogen prior to or simultaneously with tensile testing. Embrittlement of both alloys was noted under both charging conditions, but was much more severe for simultaneous charging. Intergranular fracture due to hydrogen was noted in the base alloy, while the dispersoid-containing alloy failed along prior particle boundaries. The results are explained by a dislocation transport mechanism in which hydrogen is delivered to interior fracture sites by mobile dislocations. Much greater penetration of hydrogen is achieved under simultaneous charging conditions.

I. INTRODUCTION

Since the intermetallic Ll₂ alloy Ni_3Al has been successfully ductilized through microalloying with boron,[1] an increasing interest in its use as a potential high temperature structural material has led to the development of alloys based on Ni_3Al with improved strength, creep resistance and resistance to high temperature, and oxygen induced embrittlement.[2,3] More recently, oxide dispersion strengthened as well as fiber reinforced alloys, with a Ni_3Al alloy as a matrix, have also begun to be developed in an attempt to provide further increases in yield strength, toughness, and creep resistance.[4-6] However, many intermetallics possessing the Ll₂ structure, among them Ni_3Al + B[7] and $Ni_3(Al, Mn)$,[8] have shown a strong susceptibility to hydrogen embrittlement.[9-11] The presence of particles or fibers can be expected to provide a large number of hydrogen trapping sites, with a possible concomitant effect on the susceptibility of the alloys to hydrogen embrittlement. This work is concerned with some preliminary studies on the hydrogen susceptibility of alloys based on Ni_3Al reinforced with yttria particles. Hydrogen embrittlement studies also have been performed on the unreinforced matrix for comparison.

II. EXPERIMENTAL PROCEDURE

An intermetallic alloy of composition Ni-16.4 at. % Al-8% Cr-0.5% Zr-0.1% B was hot isostatically pressed (HIPed), extruded from powder, and supplied in rod form by Oak Ridge National Laboratory, which has designated this alloy as IC-218.

An identical alloy, containing 5 vol. % of yttria particles as reinforcement, was prepared at Rensselaer by powder processing. Prealloyed powders of the alloy (average size 70 μm) and of Y_2O_3 (average size 15 μm)

were mixed in a Turbula mixer, then HIPed at 1100 °C/25 MPa for 1 h. This material was then heat treated at 1050 °C for 2 h followed by 800 °C for 24 h under a vacuum of less than 5.2×10^{-4} Pa (4×10^{-6} Torr). This heat treatment resulted in a microstructure consisting of a uniform grain size of 14 μm and a dispersion of coarse yttria particles surrounding the prior particle boundaries (Fig. 1). The base alloy (with no dispersoids) was heat treated at 1160 °C for 4.5 h and then at 800 °C for 24 h, under the same vacuum in order to obtain the same average grain size (14 μm) for direct comparison (Fig. 2). It should be noted, from the microstructures shown in Figs. 1 and 2, that both alloys exhibit a two-phase γ/γ' microstructure commonly observed in Ni_3Al–Cr alloys.[2]

All tensile tests were conducted at room temperature on specimens with 0.3 cm diam × 1.13 cm long nominal gage dimensions, using a screw-driven Instron machine at a crosshead speed of 2×10^{-4} cm/s. Hydrogen was either cathodically precharged for 1 h or charged simultaneously while testing at a current density of 50 mA/cm² in a solution of 1 N H_2SO_4 containing 0.05 g/l of $NaAsO_3$ as a hydrogen recombination poison. Fracture surfaces were examined in a scanning electron microscope.

III. RESULTS

The results of the tensile tests performed in air, with precharging and/or simultaneous charging of hydrogen during testing, are summarized in Table I and in Fig. 3.

The Ni_3Al based alloy exhibited an elongation of 28.5% along with ultimate tensile strength (UTS) of 1343 MPa when tested in air, and the fracture surface exhibits a ductile (dimpled) transgranular fracture [Fig. 4(a)]. When a sample was precharged for 1 h and
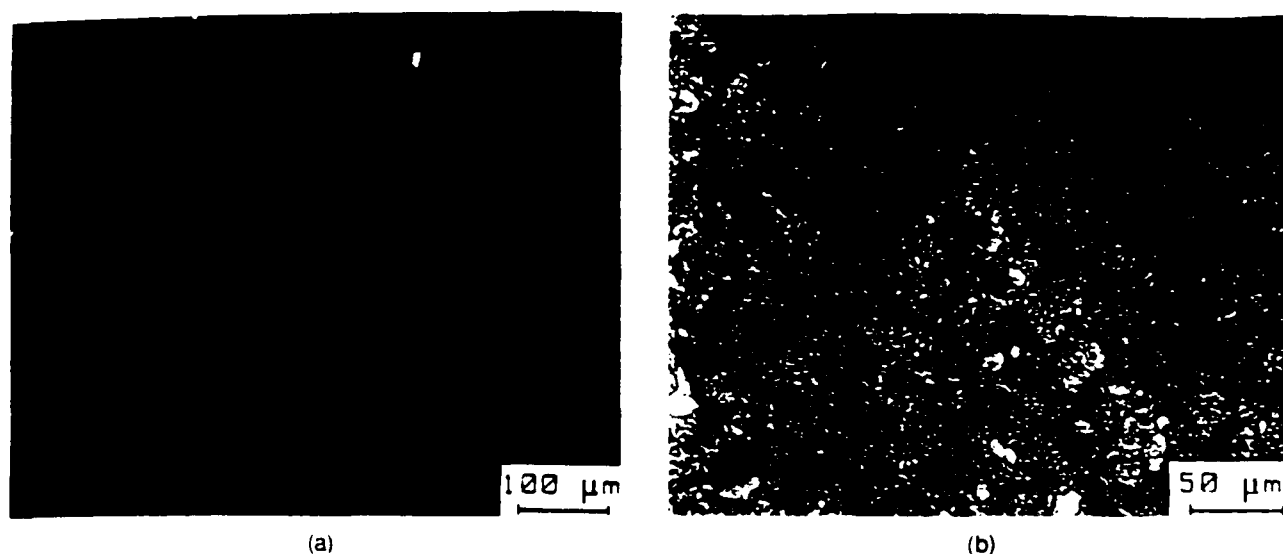
(a)

(b)

FIG. 1 Microstructure of IC-218 + 5 vol. % Y₂O₃ after heat treatment: (a) unnotched and (b) higher magnification, etched.

tested in air, the ductility and the UTS decreased by about 24% and 5%, respectively, and the fracture surface, shown in Fig. 4, displayed a mixed mode of failure, with an intergranular fracture path concentrated in the outer rim of the specimen. When hydrogen was charged simultaneously with tensile testing, the elongation decreased to 3%, the UTS was decreased by 57%, and the fracture path appeared to be entirely intergranular [Fig. 4(c)]. Previous work on a Cr-free Ni₃Al + B alloy had shown that simultaneous charging and testing causes complete loss of ductility.[7]

The alloy containing 5 vol. % Y₂O₃ showed an elongation of 5.9% and an ultimate tensile strength of 744 MPa when tested in air. When precharged with hydrogen for 1 h and tested in air, these values remained nearly unchanged. However, when simultaneous charg-

ing and tensile testing are performed, the elongation was reduced to less than 1% and the UTS was reduced by almost 29%. The fracture surfaces remain similar in the three conditions used, with a fracture path propagating along the matrix prior particle boundaries (Fig. 5).

It should also be noted that, for both alloys, charging with hydrogen either prior to or simultaneously with the tensile test did not affect the yield stress. Furthermore, the yttria-containing alloy displayed a yield stress averaging 33% higher than the yield stress of the unreinforced alloy (Table I).

Effect of processing on strength and ductility

The tensile yield strength in air, 374 MPa, of IC-218 HIPed at 1100 °C, see Table I, is considerably lower than that observed for hot pressed (at 1150 °C) IC-218 by McKamey et al.[15]: 551 MPa average of two points. However, the ultimate tensile strengths were identical. The elongation in air also was considerably lower for the HIPed alloy (28.5%) elongation vs 43.2–53% for hot pressed material. Grain sizes of the two alloys were similar. The differences in yield strength and elongation cannot readily be explained by differences in oxygen content since the yield strength should increase while ductility should decrease as oxygen content increases. Porosity does not seem to be a factor, either, since fully dense material was obtained in both investigations. Since McKamey et al. report that their P/M samples of IC-218 had strength and ductility similar to as-cast alloys of the same composition, it must be concluded that our HIPing cycle adversely affects mechanical properties, perhaps due to the presence of prior particle boundaries in HIPed material (see Fig. 1), or to differences in substructure produced by the two P/M
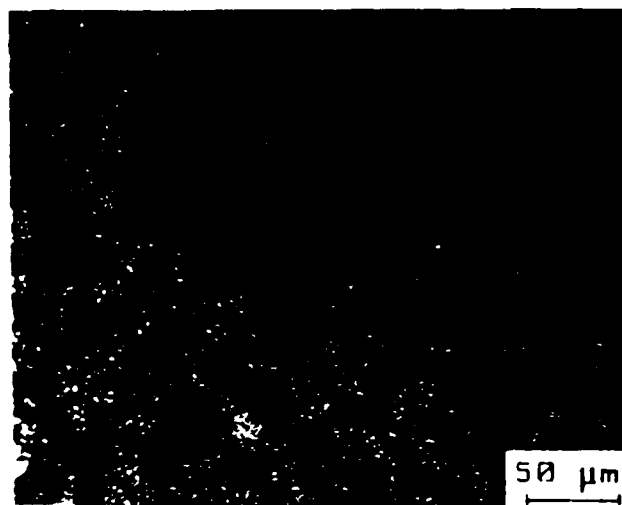

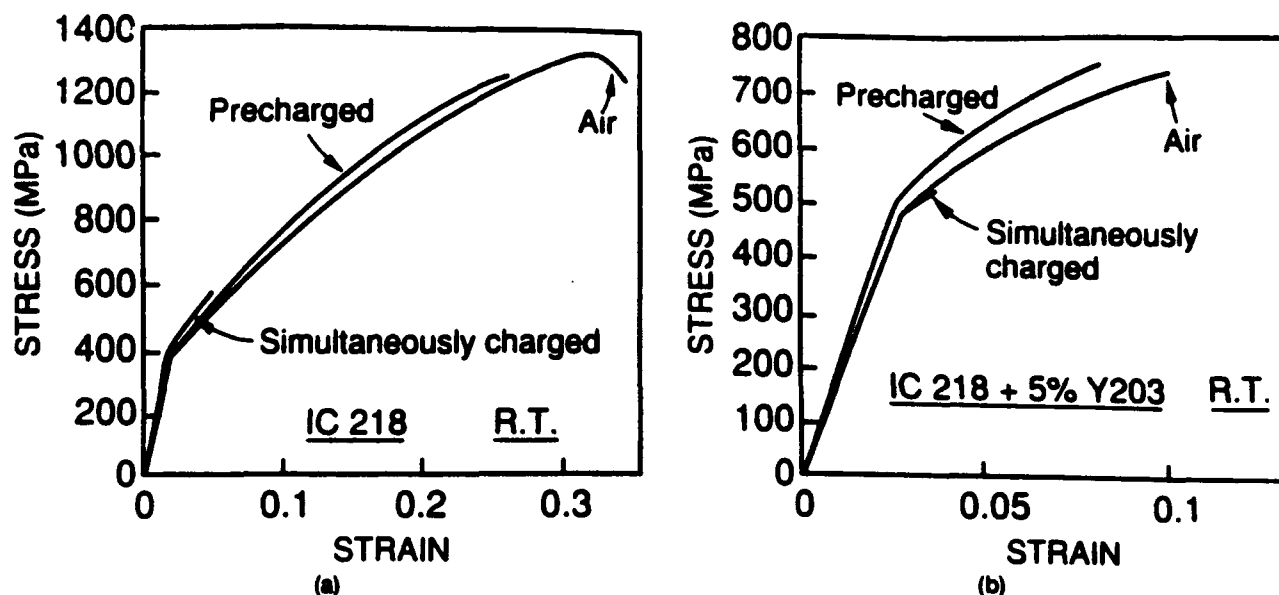FIG. 2 Microstructure of IC-218 after heat treatment

FIG. 3. Engineering stress-strain curves for tests performed under different conditions on (a) IC-218 and (b) IC-218 + 5 vol. % Y₂O₃.

processes. For example, the prior particle boundaries may act as enhanced dislocation sources. If this hypothesis is correct, the yield stress can be expected to be decreased relative to that reported by McKamey and his co-workers, while the tensile strength should be relatively unaffected, as is observed. Similarly, the prior particle boundaries of HIPed materials, which may provide initiation sites for ductile rupture, can be expected to lower the ductility once necking commences (i.e., at the UTS) when compared with hot pressed materials.

IV. DISCUSSION

A. Effect of a Dispersoid of Yttria on the Tensile Properties

Comparisons between the tests performed in air show that alloying of the intermetallic alloy with yttria has a major effect on the tensile properties as well as on the fracture mode; the elongation is reduced from 28.5% to 5.9% and the yield stress increases by nearly 125 MPa. The fracture surface of the parent alloy exhibits a ductile dimpled transgranular appearance,

while that of the alloy containing the dispersoid follows the prior powder particle boundaries where the yttria particles are located. This observation indicates that the fracture path of the alloy containing the dispersoid is governed by decohesion between the yttria particles and the matrix. The large drop in ductility with the introduction of particles or fibers has been reported also for other Ni₃Al alloys.[4,6] On the other hand, the large increase in yield strength is quite surprising, considering the basic alloy microstructure and the rather large size and spacing of the yttria particulates used in this study. It is likely that the strengthening of the alloy containing the dispersoid is linked to the heat treatment required to obtain the same grain size in both alloys, and perhaps to the pickup of oxygen during processing.

B. Effect of hydrogen on tensile properties

The intermetallic alloy examined in this study, as well as other L1₂ intermetallics,[7-11] is severely embrittled by hydrogen. Moreover, the fractographic features of this embrittlement are similar to those which were

TABLE I. Effect of hydrogen on tensile properties of IC-218 and IC-218 + 5% Y₂O₃.

	IC-218			IC-218 + 5% Y₂O₃		
	Air	Precharged	Simultaneously charged	Air	Precharged	Simultaneously charged
σ_{ys} (MPa)	374	371	367	491	501	492
UTS (MPa)	1343	1273	579	744	765	532
% El.	28.5	21.8	3.0	5.9	4.5	0.9
% RA	43.8	26.8	8.4	8.0	8.9	3.3

862
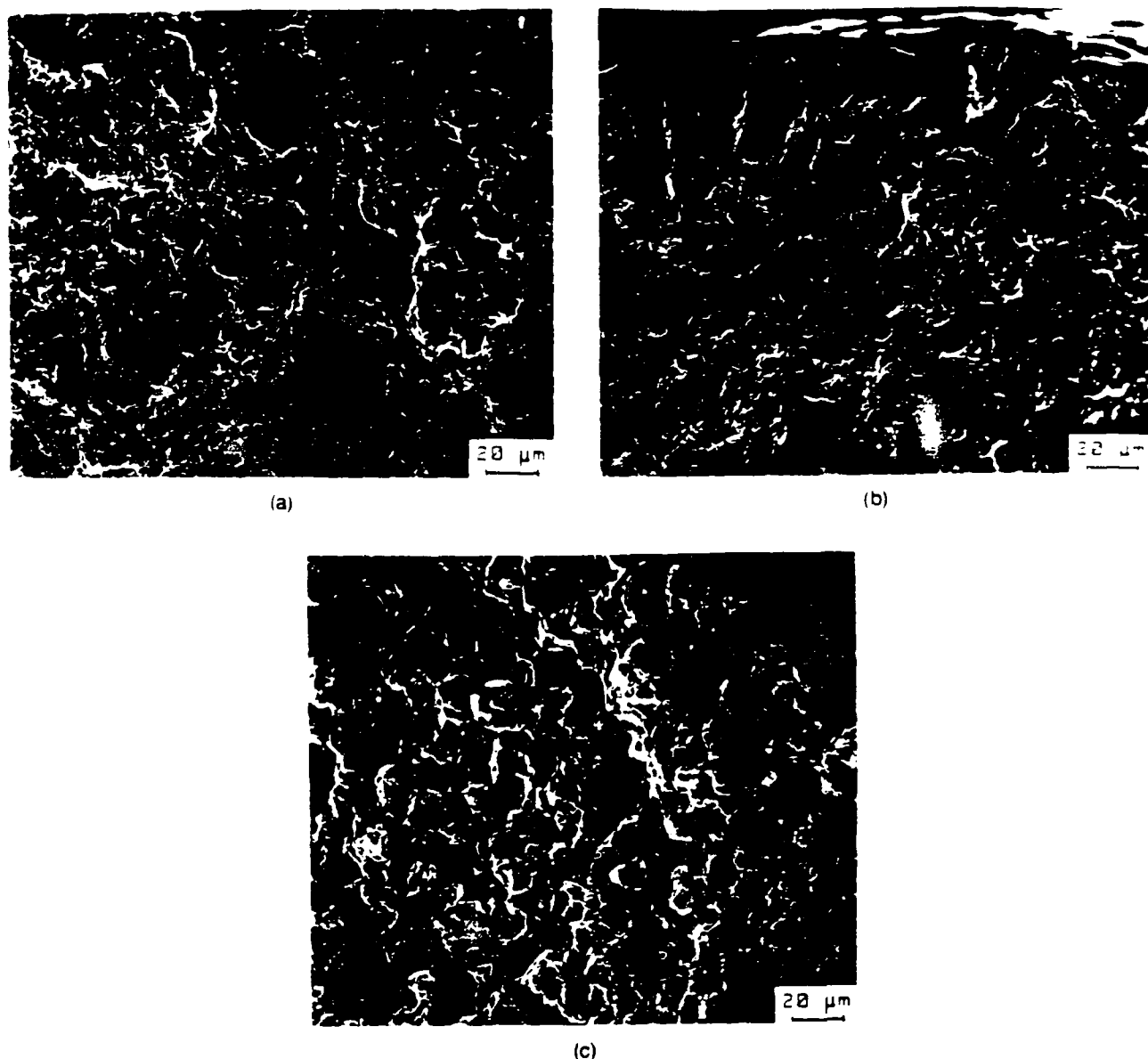
J. Mater. Res., Vol. 5, No. 5, May 1990

(a)

(b)

(c)

FIG 4 SEM fractographs of IC-218 samples tested under different conditions: (a) in air, (b) precharged and tested in air, and (c) simultaneously charged.

observed for other intermetallic compounds: an inter-granular path concentrated in the outer rim of the fractured surface when the specimen was precharged prior to testing, and a completely intergranular fracture when the alloy was tested while simultaneously charged. Although the specific mechanism(s) for grain boundary embrittlement is largely unknown. a correlation between order and hydrogen embrittlement of Ni₃Fe recently has been demonstrated.[11] According to the model suggested in that work, hydrogen transport is facilitated by the highly planar slip of superlattice dislocations which occurs in ordered lattices, and the hydrogen, once delivered to the grain boundaries, exacerbates the effect of the large local pileup stresses also associated

with planar slip, suggesting that dislocation motion is required for significant embrittlement to occur. The macroscopic yield stress is unaffected by precharging with hydrogen or by simultaneous charging during testing. After precharging, only the surface-connected grain boundaries, which act as short circuit diffusion paths, are embrittled. On the other hand, when hydrogen charging and dynamic tensile testing are performed simultaneously, dislocation transport of hydrogen to the grain boundaries results in embrittlement of all of the boundaries.

An alternative point of view has been presented by Bond and co-workers,[12] who suggest that embrittlement of Ni₃Al + B is caused simply by a reduction in cohe-

FIG. 5. SEM fractograph of IC-218 + 5 vol. % Y₂O₃ tested in air. Fracture surfaces of samples tested in the presence of hydrogen are identical.

sion of grain boundaries in the presence of hydrogen. *In situ* observations of grain boundaries by TEM revealed no discernible changes in dislocation arrangements which could be attributed to hydrogen; therefore, it was concluded that the stress concentrations at grain boundaries should not be markedly influenced by hydrogen. There seems to be little doubt that decohesion by hydrogen is the underlying mechanism in hydrogen embrittlement of intermetallics, as recently concluded also for Co₃Ti single crystals.[13] Whether or not pileup stresses facilitate decohesion remains an open question. We shall now consider the case of particle/matrix fracture.

In the present work, severe embrittlement also occurs for the alloy containing yttria when hydrogen is simultaneously charged, as shown by the large reductions in ductility and UTS. However, the fracture surfaces remain identical to those displayed by the sample tested in air. This behavior is not surprising, since the test performed in air has shown that the matrix/particle interface is weak and hydrogen is known to segregate to the weakest interface.[14] Thus, it is very likely that dislocation transport of hydrogen, in this case to matrix/particle interfaces, assists an already easy decohesion process. For the case of precharging, the more numerous trapping sites introduced by the yttria particles also have probably led to a decrease in the hydrogen diffusivity in the alloy. This may explain why, when hydrogen is precharged under the same conditions where surface embrittlement of grain boundaries at the surface is observed for the parent alloy, no embrittlement is observed for the dispersion strengthened alloys [see Fig. 4(b)].

A noteworthy feature of this work is that it further demonstrates the very high susceptibility of Ni₃Al to

hydrogen embrittlement under simultaneous charging and testing conditions even when chromium is present. Chromium is known to suppress oxygen induced embrittlement of Ni₃Al + B,[2] but seems to have only a modest effect on hydrogen ingress or embrittlement. This effect may be due to the presence of the disordered second phase in IC-218, which could be somewhat less susceptible than Ni₃Al to embrittlement.

V. CONCLUSIONS

An intermetallic alloy based on Ni₃Al and the same alloy containing 5 vol. % yttria particles have been shown to be severely embrittled by hydrogen under "dynamic" simultaneous charging conditions. As in the case of other Ll₂ alloys, decohesion is the probable bond breaking mechanism, perhaps assisted by enhanced diffusivity through dislocation transport under conditions of planar slip. Locally high stresses at the grain boundaries and/or at the matrix/particle interfaces also may contribute to embrittlement by enhancing hydrogen solubility.

ACKNOWLEDGMENT

REFERENCES

[1] K. Aoki and O. Izumi, J. Jpn. Inst. Met. 43, 1190 (1979).
[2] C. T. Liu and V. Sikka, J. of Met. 38 (5), 19 (1986).
[3] C. T. Liu and C. L. White, in *High Temperature Ordered Intermetallic Alloys* (Proc. Mater. Res. Soc. Symp.) (Materials Research Society, Pittsburgh, PA, 1985), Vol. 39, p. 355.
[4] B. Moore, A. Bose, R. M. German, and N. S. Stoloff, in *High Temperature/High Performance Composites* (Proc. Mater. Res. Soc. Symp.) (Materials Research Society, Pittsburgh, PA, 1988), Vol. 120, p. 51.
[5] J. S. C. Jany and C. C. Koch, Scripta Metall. 22, 677 (1988).
[6] G. L. Povirk, J. A. Horton, C. G. McKamey, T. N. Tiegs, and S. R. Nutt, J. Mater. Sci. 23, 3945 (1988).
[7] A. K. Kuruvilla and N. S. Stoloff, Scripta Metall. 19, 83 (1985).
[8] N. Masahashi, T. Takasugi, and O. Izumi, Metall. Trans. A 19A, 353 (1988).
[9] A. K. Kuruvilla, S. Ashok, and N. S. Stoloff, Proc. 3rd Int. Congress on Hydrogen in Metals, Paris (Pergamon, 1982), Vol. 2, p. 629.
[10] T. Takasugi and O. Izumi, Acta Metall. 34, 607 (1986).
[11] G. M. Camus, N. S. Stoloff, and D. J. Duquette, Acta Metall. 37, 1497 (1989).
[12] G. M. Bond, I. M. Robertson, and H. K. Birnbaum, Acta Metall. 37, 1407 (1989).
[13] Y. Liu, T. Takasugi, O. Izumi, and T. Yamada, Acta Metall. 37, 507 (1989).
[14] S. Ashok, D. J. Duquette, N. S. Stoloff, and C. Verpoort, Scripta Metall. 15, 1329 (1981).
[15] C. J. McKamey, G. L. Povirk, J. A. Horton, T. N. Tiegs, and E. K. Ohriner, in *High Temperature Ordered Intermetallic Alloys III* (Proc. Mater. Res. Soc. Symp.) (Materials Research Society, Pittsburgh, PA, 1989), Vol. 133, p. 609.

The influence of test frequency, temperature, and environment on the fatigue resistance of an $Ni_3Al-B/Cr/Zr$ intermetallic alloy

G. M. Camus
Laboratoire des Composites Thermostructuraux, U.M.R. 47 CNRS/SEP/UB1, 3 Avenue Leonard de Vinci, 33600 Pessac, France

D. J. Duquette and N. S. Stoloff
Materials Engineering Department, Rensselaer Polytechnic Institute, Troy, New York 12180-3590

Stress-controlled fatigue tests have been carried out on an $Ni_3Al-B/Cr/Zr$ alloy, at 600 °C and 800 °C in air and in vacuum at various test frequencies. Decreasing the test frequency and/or increasing the temperature leads to a decrease in the number of cycles to failure and a gradual disappearance of a fatigue fracture zone. This trend is shown to be related to a true creep component. Environment has a weak interacting effect on fatigue life but strongly influences the fracture path in the fatigue zones, with fracture becoming partly or entirely intergranular when the environment is changed from vacuum to air. It is suggested that most of the fatigue life is spent in initiating a crack. Comparisons are made with some creep data in terms of fracture paths and time to rupture. Fatigue life at 800 °C is shown to be entirely controlled by creep damage at the lowest test frequency of 0.2 Hz.

I. INTRODUCTION

The $L1_2$ intermetallic compound Ni_3Al, successfully ductilized through microadditions of boron,[1] displays good high temperature strength and oxidation resistance. These properties have generated extensive interest in Ni_3Al as a potential candidate for high temperature structural applications. The physical and mechanical properties of Ni_3Al and its alloys have been extensively studied and recently reviewed.[2] However, the majority of recent studies have concerned the boron ductilizing effect,[3] processing techniques,[4] and mechanical behavior, including tensile properties,[5] fatigue,[6,7] and creep/stress-rupture properties.[8] Very little has been reported on creep-fatigue-environment interactions. This phenomenon, in which cyclic stresses at elevated temperature, creep, and environment damage interact to reduce the material's fatigue life is, however, extremely important for eventual high temperature applications. In a recent study of Ni_3Al (B, Hf) single crystals and directionally solidified alloys, Bellows *et al.*[9,10] have concluded that there is very good intrinsic creep/fatigue resistance at 450 °C and 760 °C under stress-controlled fatigue in vacuum. Doubt was raised as to creep fatigue resistance for equiaxed polycrystals of Ni_3Al + B, due to the detrimental effect of environment on its ductility at high temperature.[11] Also, a study of the fatigue crack propagation behavior, at 400 °C, of a Ni_3Al + B alloy containing substantial additions of cobalt and hafnium, has shown no frequency effect on the crack growth rate in vacuum, but a strong dependence upon the frequency when the tests were performed in air.[12] On the other hand, recent investigations[13,14] have shown that additions of chromium in the optimum amount of 8 at.% dramatically improved high temperature ductility, and creep/stress-rupture properties have been improved through additions of zirconium.[14,15] Also, it has recently been shown[16] that these $Ni_3Al-B/Cr/Zr$ alloys have improved fatigue properties in terms of crack initiation as well as crack propagation. This alloy class was, therefore, selected for study of fatigue-creep-environment interactions. This research has been conducted by examining the effects of frequency on stress-controlled fatigue resistance of a $Ni_3Al-B/Cr/Zr$ alloy at elevated temperatures. It has been shown in the past[17] that, in the presence of creep and/or environmental interactions, a decrease in frequency can substantially decrease fatigue resistance at elevated temperatures. Test temperature, environment, and, to a lesser degree, stress-range were additional experimental variables.

II. EXPERIMENTAL PROCEDURE

The Ni_3Al alloy used in this study was provided by Oak Ridge National Laboratory and is designated IC 218. The nominal composition is listed in Table I. The oxygen and carbon contents were less than 150 and 100 ppm, respectively. The alloy was supplied in the form of a 1 cm diameter rod produced from a vacuum indication melted (VIM) cast ingot which had been hot extruded at 1100 °C and cold swaged in a stainless steel can. Fatigue specimens with a 3.0 mm diameter by 11.3 mm long reduced cylindrical gage section were machined from the rod. The samples were then heat

TABLE I. Composition (at. %) and tensile properties of IC 218 (for a cast + extruded alloy, 14 μm grain size).[14,16]

Composition (at. %)				
Ni	Al	Cr	Zr	B
Bal.	8.45	8.13	0.90	0.027

Tensile properties (*in a vacuum of less than 1.5×10^{-3} Pa)

T (°C)	Y.S.0.2% (MPa)	UTS (MPa)	Elongation (%)
25 °C	640	1405	34.5
*600 °C	650	1025	26.1
*800 °C	576	710	19.8

Normalized stress ranges used

T (°C)	$\Delta\sigma$ (MPa)	$\Delta\sigma/\sigma_y$
600	690	1.06
600	724	1.11
800	690	1.19

treated in a vacuum of less tnan 3×10^{-4} Pa at 1050 °C for 1 h, and at 800 °C for 24 h, resulting in the microstructure exhibited in Fig. 1. Due to the Cr content the alloy displayed a γ/γ' two phase microstructure.[18] The alloy was fully recrystallized and the average grain size, measured by a mean linear intercept method, was approximately 14 m. After abrasive polishing using 0.3 m alumina powder in the final step, the samples were tested in an Instron closed loop machine under stress-controlled cyclic loading, in laboratory air or in a vacuum of less than 1.5×10^{-3} Pa. Test frequencies selected were
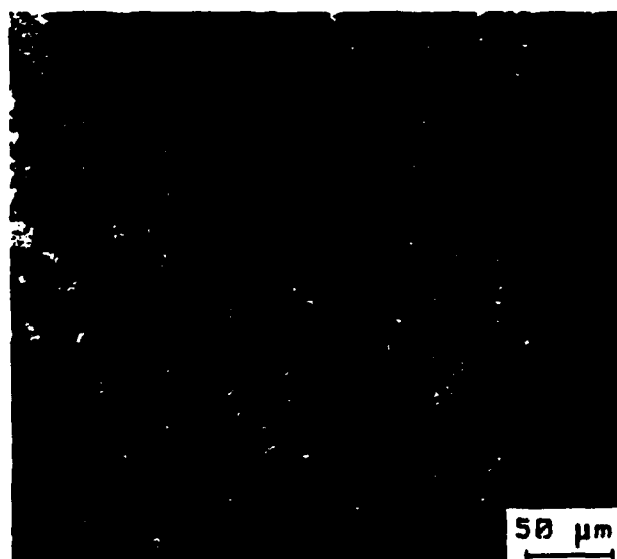
FIG. 1. Microstructure of IC 218 after heat treatment.

20 Hz, 2 Hz, and 0.2 Hz, at temperatures of 600 °C or 800 °C. A stress range of 690 MPa initially was selected for all tests but a higher value of 724 MPa was later used at 600 °C in order to maintain the duration of the tests performed at the lowest frequency in a suitable range. The stress ratio, R (minimum to maximum stress), was held constant at 0.1. Tensile data obtained from other sources[14,16] on an identical material similarly processed and possessing the same grain size of 14 m. also are listed in Table I along with the stress ranges used in this work (normalized by the yield stress). In order to have a suitable comparison for the mechanism(s) involved, some stress-rupture tests were performed at 800 °C in vacuum, using the same electrohydraulic closed-loop machine under constant load control. Fracture surfaces were examined in a scanning electron microscope to determine the failure initiation sites and fracture modes. Foils for transmission electron microscopy (TEM) were prepared from the cross section of the gage lengths of a number of fractured specimens to examine possible differences in the deformation substructures.

III. RESULTS

A. Fatigue tests

Results of the stress-controlled fatigue tests performed under different conditions of frequency, temperature, stress-range, and environment are listed in Table II.

The influence of frequency on the number of cycles to failure as a function of temperature and environment is shown in Fig. 2. The data show a monotonic decrease in the number of cycles to failure with decreasing frequency for every condition of temperature, environment, and stress-range investigated. For a given frequency, raising the test temperature from 600 °C to 800 °C markedly reduces the fatigue life measured as cycles to failure and the reduction in fatigue life is accentuated at lower test frequencies. An air environment has little effect on the number of cycles to failure at any frequency. When the data are replotted in terms of time to failure versus frequency, only the tests performed at 800 °C show a decrease of the fatigue life with decreasing frequency. Time to failure is relatively insensitive to test frequency at 600 °C.

Ductility, measured as reduction in cross-sectional area and as the total elongation of the gage length after test, see Fig. 3, appears to increase monotonically with a decrease in the frequency, with the exception of the tests performed at 800 °C/0.2 Hz in both vacuum and air, for which a plateau seems to be reached. The values of both elongation and reduction in area are much higher at 800 °C than at 600 °C (see Table II). Ductility of the samples tested in air was always lower when compared with the same tests performed in vacuum, this trend being enhanced by an increase of the test temperature.

TABLE II. IC 218 tested under stress-controlled fatigue for different conditions of temperature, frequency, stress range, and environment.

Conditions	ν (Hz)	N_f	R.A. at failure (%)	Elongation at failure (%)	Fracture appearance
600 °C/$\Delta\sigma$ = 690 MPa	20	6 × 10⁶	15.2	7.6	TG fatigue zone, initiated at the surface
Vacuum	2	1.88 × 10⁶	24.4	11.2	TG fatigue zone, initiated at the surface
600 °C/$\Delta\sigma$ = 690 MPa	20	4 × 10⁶	17.3	7.5	Mixed IG + TG fatigue zone, initiated at the surface
Air	2	1.7 × 10⁶	24.9	8.0	TG fatigue zone, initiated inside
600 °C/$\Delta\sigma$ = 724 MPa	20	7.35 × 10⁵	15.6	11.1	TG fatigue zone, initiated at the surface
Vacuum	2	1.76 × 10⁵	28.9	13.2	TG fatigue zone, initiated at the surface
	0.2	2.44 × 10⁴	46.2	17.2	Small TG fatigue zone, initiated at the surface
600 °C/$\Delta\sigma$ = 724 MPa	20	5 × 10⁵	17.4	9.3	Mixed IG + TG fatigue zone, initiated at the surface
Air	2	1.6 × 10⁵	25.6	11.4	IG fatigue zone, initiated at the surface
	0.2	2.12 × 10⁴	31.8	12.4	Very small IG fatigue zone, initiated at the surface IG areas in outer rim
800 °C/$\Delta\sigma$ = 690 MPa	20	2.09 × 10⁴	53.8	18.1	No fatigue zone, dimples at the center
Vacuum	2	1.14 × 10³	60.3	19.5	No fatigue zone, dimples at the center
	0.2	60	59.9	23.1	No fatigue zone, dimples at the c ter
800 °C/$\Delta\sigma$ = 690 MPa	20	1.73 × 10⁴	26.9	10.1	Very small IG fatigue zone, initiated at the surface + small dimple zone in the center
Air	2	9.4 × 10²	51.1	17.1	No fatigue zone, dimples at the center
	0.2	30	47.8	22.4	No fatigue zone, dimples in center, IG areas in outer rim

B. Metallography and fractography

The observed fracture mode varied with temperature and, to a lesser degree, with frequency and environment. Pertinent information concerning the resulting fracture paths for each of the tests conducted is listed in Table II. Samples tested under vacuum at 600 °C exhibit surface-connected crack initiation with a relatively flat initial crack propagation zone, although the overall size of the fatigue zone decreased as the frequency was decreased; e.g., see Fig. 4. The fatigue zones as well as the overload zones were transgranular at 600 °C, as shown in Fig. 5. For tests conducted at 800 °C in vacuum, no indication of a defined fatigue zone was observed at any of the three frequencies investigated. Cracks always initiated internally, with the major portion of the fracture occurring by microvoid growth and coalescence, leading to fracture paths such as that exhibited in Fig. 6.

Samples tested in air at 600 °C also, as in vacuum, exhibited surface-connected crack initiation sites with the fatigue zone shrinking as the frequency was lowered, but the fatigue path was of mixed mode at high frequency changing to a primarily intergranular mode at lower frequencies; see Fig. 7. An exception to this result was observed for the sample tested at 690 MPa/2 Hz, which exhibited a transgranular fatigue zone. In this case, the crack initiated internally, probably at an existing defect. The overload zones for samples tested in air remained

transgranular and were similar to that shown in Fig. 5. Tests performed in air at 800 °C also exhibited internally initiated fracture with dimples in the center of the fracture areas, but the portion of the fracture that occurred by microvoid growth and coalescence was reduced when compared to the same tests run in vacuum. Numerous intergranular areas were present along the outer rim at the lowest frequency (Fig. 8), indicating a very limited intergranular surface-connected fatigue zone.

C. TEM observations

Two fractured samples were examined in the TEM. The test conditions chosen were 600 °C/72 MPa/20 Hz and 800 °C/690 MPa/0.2 Hz as, respectively, temperature, stress-range, and frequency, both in vacuum. These conditions are at both extremities of the range of temperature and frequencies chosen for the present study and should therefore correspond to the maximum differences in the dislocation substructures. Vacuum has been chosen rather than air in order to better isolate possible creep interaction. The sample tested at 600 °C/20 Hz [Fig. 9(a)] exhibits a relatively high density of entangled dislocations. Some straight dislocations also can be seen.

At 800 °C/0.2 Hz, no straight dislocations can be seen [Fig. 9(b)]. Dislocation densities appear to be similar in (a) and (b), but the dislocations tend to be rearranged into a subgrain structure in the latter.
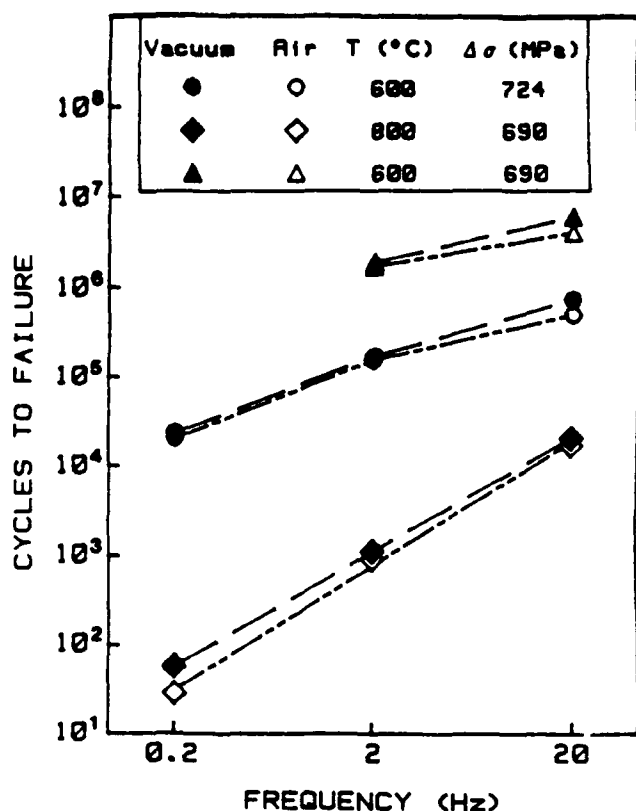
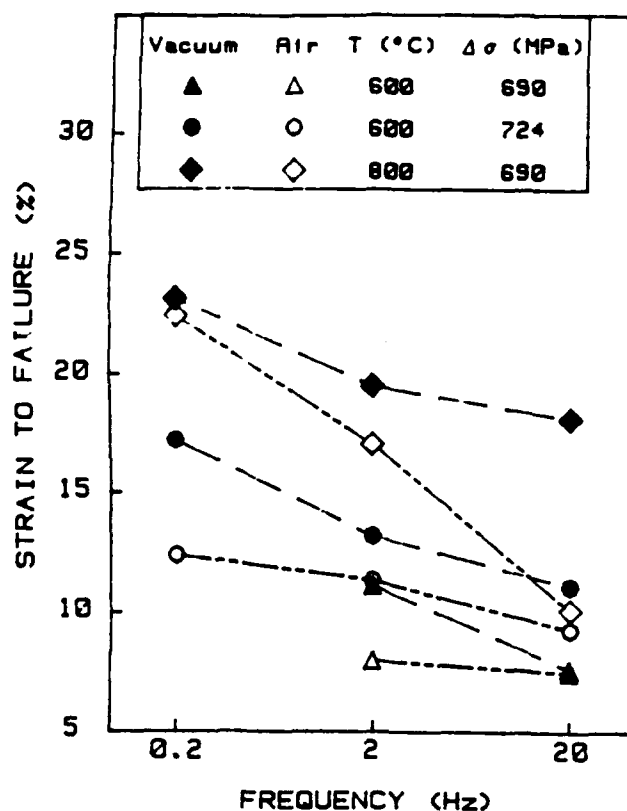FIG. 2. Effect of frequency on fatigue lives at 600 °C and 800 °C in vacuum and in air.

FIG. 3. Changes in elongation as a function of test frequency, temperature. and environment.

IV. DISCUSSION

When alloys are cyclically deformed at elevated temperatures, and only fatigue deformation and crack growth occur, the number of cycles to failure should be independent of frequency; see Fig. 10(a). In this study, however, decreased fatigue lives were observed as the frequency was reduced for all of the conditions investigated. This behavior has been reported in many systems and has been related to a creep interaction, an environmental interaction, and/or the combination of the two.[17,19] Although the moderate vacuum used in this study did not guarantee those tests performed in vacuum were completely free of environmental effects, the results provide considerable evidence for a true creep component at the temperatures of interest.

A. Creep Interaction

Samples tested at 800 °C under vacuum exhibit a fracture initiated internally by microvoid growth and coalescence at each of the frequencies employed. At 600 °C the fatigue zones decreased in size as the frequency was lowered. Moreover, the large increase in ductility observed with decreasing frequency at both temperatures is particularly strong evidence for the role of creep in the fatigue process. Additional evidence for a

creep-fatigue interaction is provided by the experiments conducted in air. Although fatigue lives are slightly shorter compared to the same tests run in vacuum, the general trend of the results in these experiments parallels those obtained in vacuum (i.e., the slopes of N_f and t_f vs ν are identical), indicating that environment plays a minor role in the observed frequency dependence on the stress-controlled fatigue life. Finally, while TEM revealed no major differences in dislocation substructure at the extremes of temperature and frequency, there is some indication of cell formation at the lowest frequency, Fig. 9(b).

On the other hand, if creep alone were the principal mechanism for failure, the time to failure would not be expected to be a function of frequency. A schematic representation of specimen life versus frequency for creep and fatigue-dominated processes is shown in Fig. 10 (after Stoloff[20]). The transient regions between the two "pure" mechanisms are qualitatively represented. In Fig. 10(b), it can be seen that since the lower frequency represents a lower applied stress rate, it is expected that fatigue life measured in elapsed time should increase with decreasing frequency if the process is fatigue-dominated. If creep processes dominate, however, lower applied stress rates should result in
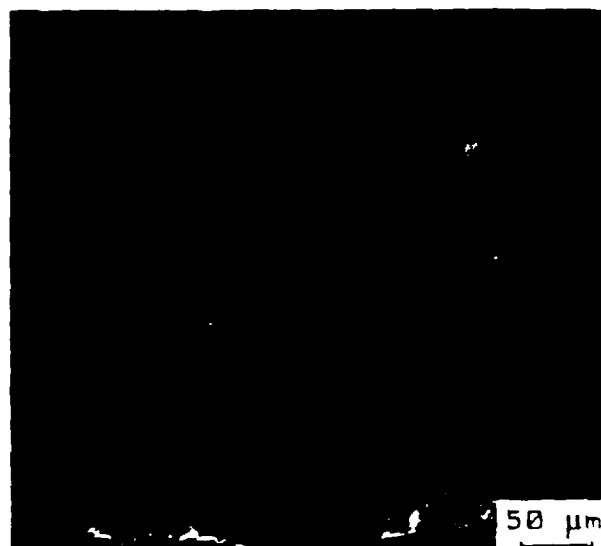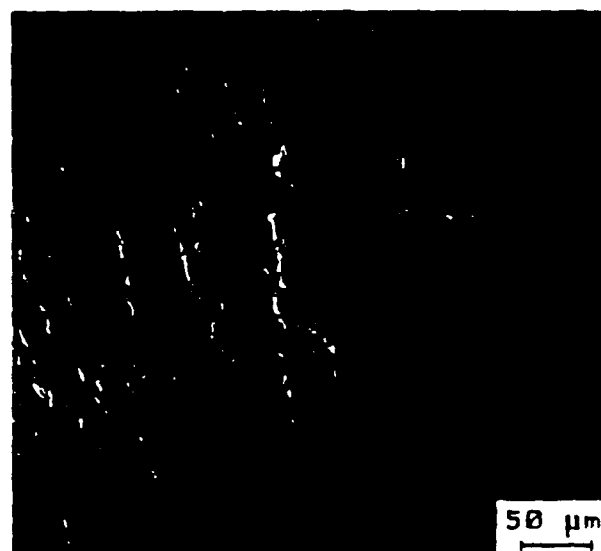
316
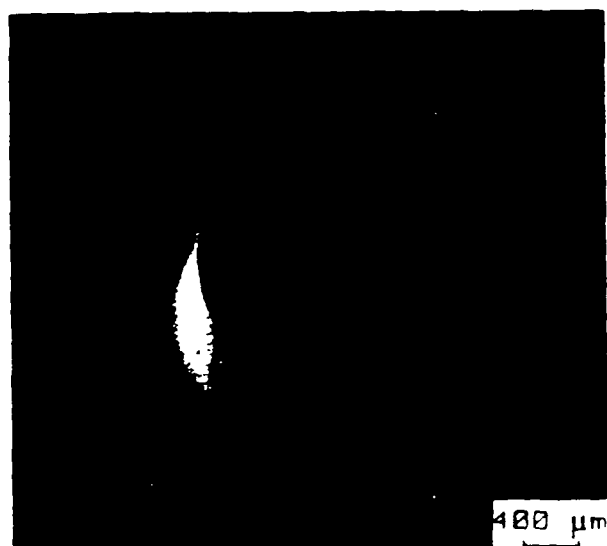
(a)

(b)

FIG. 4. SEM fractographs of samples tested at 600 °C in vacuum at $\Delta\sigma = 724$ MPa (a) $\nu = 20$ Hz and (b) $\nu = 0.2$ Hz.

(a)

(b)

FIG. 5. SEM fractographs of a sample tested at 600 °C in vacuum $\Delta\sigma = 690$ MPa, $\nu = 2$ Hz (a) fatigue zone and (b) overload zone.

decreased lifetimes since a larger fraction of specimen life is spent at high stresses for a fixed number of cycles.

On the basis of this qualitative representation, the evolution of the fracture mode, and the observed increase of time to failure with decreasing the frequency, at the lowest frequency, it appears that creep begins to interact at 600 °C although the primary failure mode is fatigue. At 800 °C, the absence of a well-defined fatigue zone on the fracture surface, the internal initiation of the fractures, and the relatively weak frequency effect on the time to failure indicate that creep is predominant. However, care should be taken in interpreting the temperature

dependence of the magnitude of the creep component since the value of the stress range normalized by the yield stress is higher at 800 °C than at 600 °C (Table I).

B. Environmental effects

Although creep-fatigue interaction largely accounts for the reduction in high temperature fatigue life of IC 218, tests performed in air also reveal some environmental effects. Specimen lives were slightly reduced for the tests run in air. Ductilities, in terms of reductions of area as well as total elongation, were
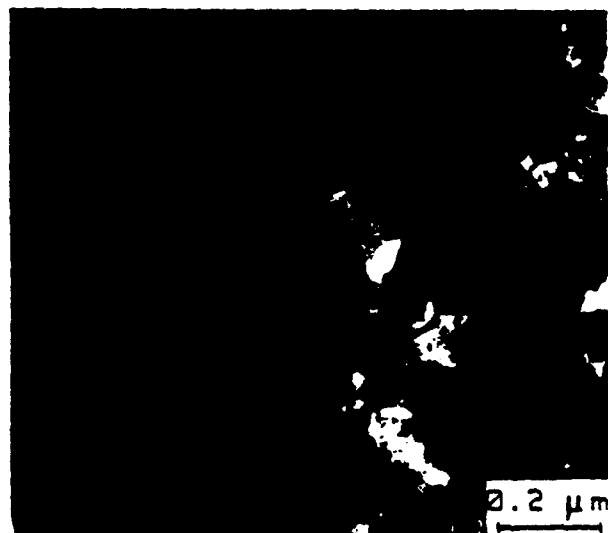
(a)

numerous as the frequency was decreased However, only a weak environmental effect on the fatigue life is observed, although there is a pronounced effect on the ductility and on the fracture surface appearance The former indicates a limited environmental effect on crack nucleation, whereas the latter suggests a strong interaction once the crack is initiated, i.e., on crack propagation. This suggests that most of the fatigue life is spent in initiation. These results also confirm previous studies performed on the same class of chromium-containing Ni$_3$Al alloys.[15,16] That is, by minimizing high temperature oxygen induced embrittlement, chromium

(b)

FIG 6 (a) SEM fractographs of a sample tested at 800 C in vacuum, Δσ 600 MPa ν = 2 Hz (b) Higher magnification on the central region

considerably reduced when compared to the tests performed in vacuum, the trend being enhanced by increased temperature Moreover, major changes in the fracture morphology were observed when comparing air to vacuum At 600 C fatigue zones were consistently transgranular when the tests were performed in vacuum, but were partially or totally intergranular, the degree of intergranular failure increasing with decreasing frequency At 800 C, in air, dimples were still present in the center, although intergranular failure zones around the outside of the sample became more

(a)

(b)

FIG. 9. TEM observations of dislocations in samples tested under two widely different conditions: (a) $T = 600$ °C. $\nu = 20$ Hz. $\Delta\sigma = 724$ MPa and (b) $T = 800$ °C, $\nu = 0.2$ Hz, $\Delta\sigma = 690$ MPa.

additions to Ni_3Al improve high temperature tensile properties as well as high cycle fatigue properties in air. On the other hand, the decreased ductilities and intergranular fatigue zones show that, once a crack is initiated, "dynamic" oxygen embrittlement occurs.

V. CONCLUSIONS

(1) The elevated temperature fatigue resistance of the Ni_3Al–B/Cr/Zr alloy IC 218, tested under load control at 600 ° C and 800 °C, is sensitive to test frequency and temperature. Life decreases with a decrease in the frequency and/or an increase of the temperature.
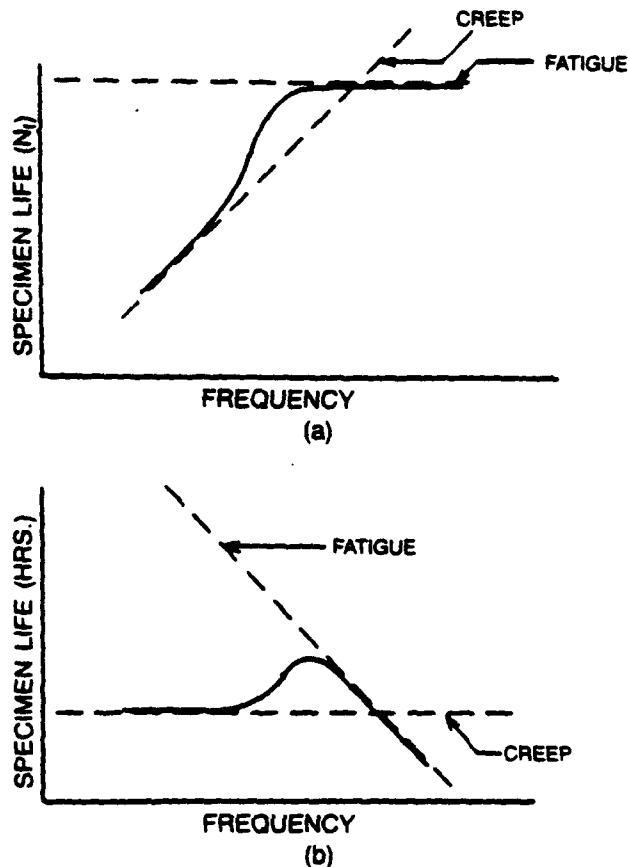
FIG. 10. Schematic diagrams of specimen life versus frequency for creep and fatigue-dominated processes: (a) number of cycles and (b) duration.[20]

(2) The fractographic features as well as enhanced ductility observed with decreasing frequency provide evidence for a creep interaction being the predominant mechanism for these effects.

(3) The relative role of each phenomenon, i.e., creep and fatigue, is frequency and temperature dependent. Within the stress range and frequency conditions used, creep begins to interact at about 600 °C with a still predominant fatigue failure mode, but creep is the major mechanism for failure at 800 °C.

(4) An air environment has a weak effect on crack initiation but strongly influences crack propagation with fatigue zones, when present, becoming partly and/or entirely intergranular.

REFERENCES

1. K. Aoki and O. Izumi, Nippon Kinzoku Gakkaishi **43**, 1190–1196 (1979).
2. N. S. Stoloff, Int. Mater. Rev. **34**, 157–183 (1989).
3. I. Baker, E. M. Schulson, and J. A. Horton, Acta Metall. **35**, 1533–1541 (1987).
4. V. K. Sikka, in *High-Temperature Ordered Intermetallic Alloys II*, edited by N. S. Stoloff, C. C. Koch, C. T. Liu, and O. Izumi (Mater. Res. Soc. Symp. Proc. **81**, Pittsburgh, PA, 1987), pp. 487–493.
5. C. T. Liu and C. L. White, in *High-Temperature Ordered Intermetallic Alloys*, edited by C. C. Koch, C. T. Liu, and N. S. Stoloff (Mater. Res. Soc. Symp. Proc. **39**, Pittsburgh, PA, 1985), pp. 365–380.
6. G. E. Fuchs and N. S. Stoloff, Scripta Metall. **21**, 863–868 (1987).
7. A. K. Kuruvilla and N. S. Stoloff, Scripta Metall. **21**, 873–877 (1987).
8. J. H. Schneibel, G. F. Petersen, and C. T. Liu, J. Mater. Res. **1**, 68–72 (1986).
9. R. S. Bellows and J. K. Tien, Scripta Metall. **21**, 1659–1662 (1987).
10. R. S. Bellows, E. A. Schwarzkopf, and J. K. Tien, Metall. Trans. A **19A**, 479–486 (1988).
11. C. T. Liu and C. L. White, Acta Metall. **35**, 643–649 (1987).
12. K. M. Chang, S. C. Huang, and A. I. Taub, *High-Temperature Ordered Intermetallic Alloys II*, edited by N. S. Stoloff, C. C. Koch, C. T. Liu, and O. Izumi (Mater. Res. Soc. Symp. Proc. **81**, Pittsburgh, PA, 1987), pp. 303–308.
13. C. T. Liu and V. Sikka, J. Metals **38** (5), 19–21 (1986).
14. V. K. Sikka and E. A. Loria, in *Superalloys 1988*, edited by D. N. Duhl, G. Maurer, S. Antolovich, C. Lund, and S. Reichman (AIME, Warrendale, PA, 1988), pp. 203–212.
15. S. E. Hou, N. S. Hou, C. H. Tong, C. Y. Ma, and S. Y. Lee, in *High-Temperature Ordered Intermetallic Alloys II*, edited by N. S. Stoloff, C. C. Koch, C. T. Liu, and O. Izumi (Mater. Res. Soc. Symp. Proc. **81**, Pittsburgh, PA, 1987), pp. 507–512.
16. W. Matuszyk, M. S. Thesis, Rensselaer Polytechnic Institute, Troy, NY, 1988.
17. N. S. Stoloff and D. J. Duquette, in *Creep-Fatigue-Environment Interactions*, edited by R. M. Pelloux and N. S. Stoloff (TMS-AIME, Warrendale, PA, 1980), pp. 178–194.
18. G. L. Povirk, J. A. Horton, C. G. McKamey, T. N. Tiegs, and S. R. Nutt, J. Mater. Sci. **23** (11), 3945–3950 (1988).
19. E. Blank and N. S. Stoloff, Acta Metall. **35**, 2255–2264 (1987).
20. N. S. Stoloff, in *Fatigue Environment and Temperature Effects*, Sagamore Army Conf. Proc. **27**, edited by J. J. Burke and V. Weiss (Plenum Press, New York, 1983), pp. 301–327.

Effects of Temperature and Environment on the Tensile and Fatigue Crack Growth Behavior of a Ni₃Al-Base Alloy

W. MATUSZYK, G. CAMUS, D.J. DUQUETTE, and N.S. STOLOFF

The effects of temperature, frequency, and environment on the tensile and cyclic deformation behavior of a nickel aluminide alloy, Ni-9.0 wt pct Al-7.97 pct Cr-1.77 pct Zr (IC-221), have been determined. The tensile properties were obtained in vacuum at elevated temperatures and in air at room temperature. The alloy was not notch sensitive at room temperature or at 600 °C, unlike Cr-free Ni₃Al + B alloys. In general, crack growth rates of IC-221 increased with increasing temperature, decreasing frequency, exposure to air, or testing at higher R ratios. At 25 °C, crack growth rates were slightly higher than for a previously investigated Cr-free Ni₃Al alloy. However, at 600 °C, the crack growth rates for IC-221 were lower than for the Cr-free alloy. Substantial frequency effects were noted on crack growth of IC-221 at both 600 °C and 800 °C in both air and vacuum, especially at high K. The relative contributions of creep and environmental interactions to fatigue crack growth are discussed.

I. INTRODUCTION

THE Ni₃Al intermetallic has received considerable attention due to its potential for engineering applications at elevated temperatures. Despite such attractive features as increased strength at high temperature and good oxidation and corrosion resistance, applications of polycrystalline Ni₃Al have been limited by its low ductility at room temperature.

Microalloying of Ni₃Al with boron has proven to be very effective in improving ductility.[1,2] Unfortunately, Ni₃Al experiences a ductility loss when tensile tested in an oxidizing environment between 500 °C and 1000 °C, accompanied by a transition in fracture path from transgranular to intergranular.[3] An effective solution to this problem has been to alloy Ni₃Al with moderate amounts of Cr (8 pct).[3,4] The beneficial effect of Cr may be to develop a Cr₂O₃ subscale which could reduce the severity of dynamic embrittlement.[3] Previous studies[2] have indicated that chemisorption of oxygen ultimately results in weakening of atomic bonding across grain boundaries. The present work examines the tensile and fatigue crack growth properties of a Ni₃Al + B alloy containing Cr and Zr. In performing this study, temperature, environment, and frequency (for the cyclic deformation tests) were the principal experimental variables.

II. EXPERIMENTAL PROCEDURE

A. Alloys

A heat of an alloy, designated IC-221, was received from Oak Ridge National Laboratory, Oak Ridge, TN. The composition of the tested alloy is 9.0 wt pct Al, 7.97 pct Cr, 1.77 pct Zr, 0.02 pct B, and bal. Ni. The alloy was hot isostatically pressed (HIP) from prealloyed powders and hot extruded. The ingot was 4.4 cm in diameter by 25.4 cm in length. This material was used for both tensile and crack growth experiments.

B. Metallography and Microstructure

Metallographic samples were mounted in epoxy or bakelite and then mechanically polished through 600 grit SiC paper, 9-μm diamond paste, and a 0.3-μm Al₂O₃ slurry. The samples were then chemically etched with Kallings reagent to reveal their microstructures. The grain size was measured using the linear-intercept technique.

Heat treatments were performed in vacuum at 1150 °C for 0.5 hours with a furnace cool to 800 °C and a hold for 24 hours followed by a furnace cool to room temperature.

The microstructure of the alloy, in the as-received condition, exhibited fine, apparently unrecrystallized grains of <1-μm diameter. The grain size of the heat-treated material was 8 μm (Figure 1). A slight degree of porosity was detected in the alloy, which was not surprising for a powder metallurgy product. At high magnification, a second phase was detected; this phase is reported to be disordered γ.[3]

C. Tensile Testing

Tensile samples were machined from IC-221 prior to heat treatment. The sample geometry is shown in Figures 2(a) and (b) for unnotched and notched samples, respectively. Following the appropriate heat treatment, unnotched tensile samples were mechanically polished in a fashion similar to the metallographic samples. Notched samples were not polished prior to testing.

The samples were tested in a servohydraulic machine with a resistance-heated environmental chamber. This permitted testing up to 800 °C in air or in vacuum. A split wedge-action grip was used. All tests were performed in stroke mode at a strain rate of 4.2×10^{-4} s⁻¹. The temperature was monitored with a chromel-alumel thermocouple in contact with the gage section of the sample. A 20-minute soak was employed once the sample reached test temperature to allow the sample to equilibrate.

W. MATUSZYK is with Knolls Atomic Power Laboratories, Schenectady, NY 12301. G. CAMUS, Research Scientist, is with the Laboratory of Composite Thermostructures, 33600 PESSAC, France. D.J. DUQUETTE and N.S. STOLOFF, Professors of Materials Engineering, are with the Materials Engineering Department, Rensselaer Polytechnic Institute, Troy, NY 12180-3590.
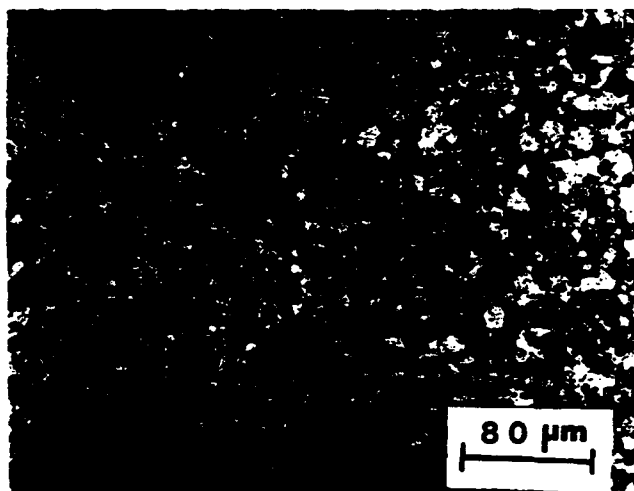Manuscript submitted July 20, 1989.

Fig. 1 — Microstructure of HIP and extruded IC-221 alloy.

Unnotched and notched samples of IC-221 were tested at room temperature in air and at 600 °C and 800 °C in vacuum ($<4.5 \times 10^{-3}$ Pa).

D. Fatigue Crack Growth

The fatigue crack growth properties of IC-221 were examined as a function of temperature, environment, and R ratio (minimum/maximum stress). All crack propagation experiments were conducted on compact tension samples of the geometry shown in Figure 2(c). Electro-discharge machining was used to ensure a sharp notch for precracking. Crack growth was monitored using either a traveling microscope or a dc potential drop technique. During the initial room-temperature tests, crack growth was monitored simultaneously by the dc potential drop technique and the traveling microscope. This provided a calibration curve between the observed potential drop and the actual length measured with the microscope.

Crack growth tests were performed at room temperature in air at $R = 0.1$ and $R = 0.6$. Elevated temperature tests were performed at 600 °C and 800 °C at $R = 0.1$ and $R = 0.6$ in air and in vacuum. The standard test frequency was 20 Hz, except at 800 °C, where frequencies were controlled in the range of 0.02 to 20 Hz. Crack growth was monitored by the potential drop technique only at 600 °C and 800 °C.

III. RESULTS

A. Tensile Tests

Tensile properties of IC-221 are listed in Table I and shown in Figure 3. IC-221 did not display notch sensitivity at room temperature or at 600 °C (Table II). In general, an alloy is considered notch sensitive if the notch sensitivity ratio ($UTS_{notched}/UTS_{unnotched}$) is less than 1.0.

B. Fatigue Crack Growth

The influence of temperature on fatigue crack growth rate (FCGR) for IC-221 tested at a constant frequency
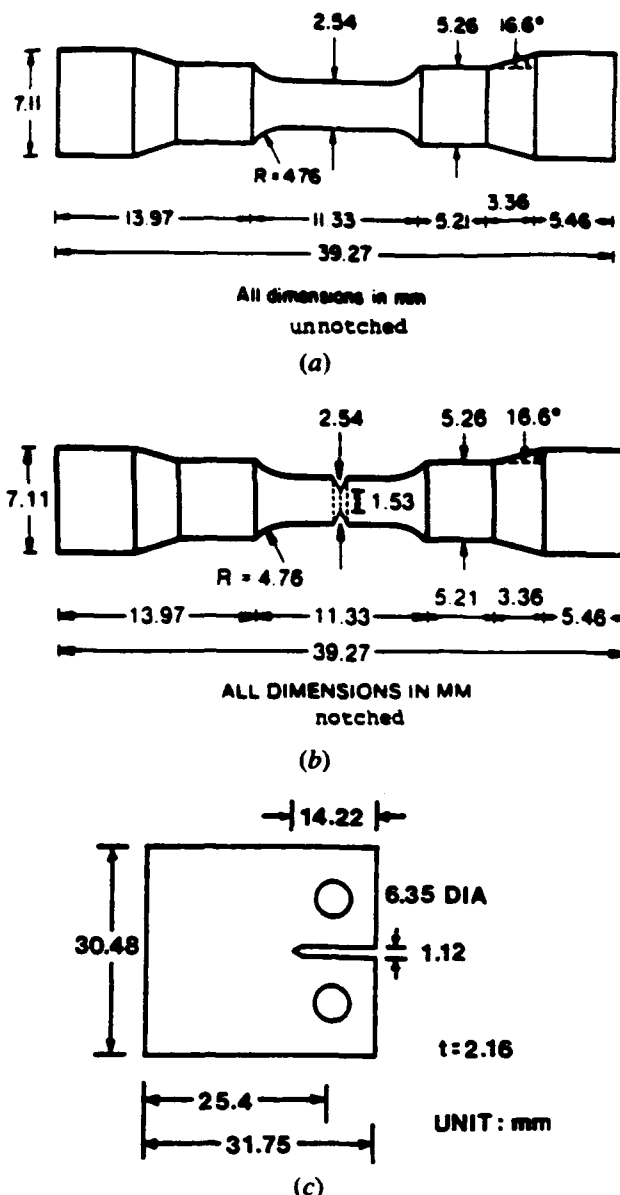

Fig. 2 — Test sample configurations: (a) unnotched tensile, (b) notched tensile, and (c) compact tension.

of 20 Hz is shown in Figures 4(a) and (b) for $R = 0.1$ and $R = 0.6$, respectively. An increase in temperature produces a significant increase in FCGR in similar environments. At 800 °C, crack growth rates are about 100 times higher than at 25 °C. The increase in temperature also results in decreased values of the threshold stress intensity range, ΔK_{th}.

Crack growth rates of IC-221 increased as the environment was changed from vacuum to air at constant R ratio and temperature. Testing in air resulted in only a slight decrease of ΔK_{th} values at $R = 0.1$ (Figure 4(a)). The difference in da/dN between air and vacuum was greater at high K than at low K.

The effects of temperature and R ratio on FCGR of IC-221 in air and in vacuum are individually summarized in Figures 5(a) and (b), respectively. Note that at

Table I. Tensile Data for IC-221 Alloy

Sample	T (°C)	Environment	Yield Strength (ksi)	Yield Strength (MPa)	UTS (ksi)	UTS (MPa)	Ductility (Pct)
IC-221	25	air	94.8	653.2	206.0	1419.3	21.3
IC-221	600	vacuum	116.1	800.0	152.3	1049.3	23.2
IC-221	800	vacuum	101.0	695.9	109.9	757.2	15.2

both 600 °C and 800 °C in air, there is a substantial effect of R ratio on growth rate near threshold, but the effect diminishes with increasing ΔK (Figure 5(a)). In vacuum, on the other hand, there is a strong effect of R on growth rates at all K at 600 °C and no effect at 800 °C (Figure 5(b)).

The effects of test frequency on FCGR at 800 °C in air and in vacuum, at $R = 0.1$, are shown in Figures 6(a) and (b), respectively. Note in Figure 6(a) that crack growth rates in air increase substantially with decreasing frequency at high K but that there is little or no effect of frequency near threshold. In vacuum, a similar effect is noted, but it is not as clear cut (Figure 6(b)). In fact, the curve for $\nu = 0.02$ Hz has an entirely different shape from the other two. The data have been recalculated for $R = 0.1$ on the basis of time-dependent growth in Figures 7(a) and (b), and both da/dN and da/dt are plotted vs frequency at $\Delta K = 25$ MPa·m in Figure 8. A clear trend of decreasing crack growth rate, da/dN, with increasing frequency is seen, with the crack growth rates more than 10 times lower in vacuum than in air at all but 20 Hz. The growth rate based on time, da/dt, shows the opposite trend with frequency, with a higher growth rate at higher frequency in both vacuum and air (Figures 7(a) and (b) and 8).

C. Fractography

Scanning electron microscopic (SEM) examination of samples fractured between 25 °C and 700 °C in vacuum revealed transgranular failure with dimpled regions present. A significant difference in fracture mode was observed in a specimen of IC-221 tested in tension at 800 °C in vacuum (4.5×10^{-3} Pa). The fracture is a mixture of transgranular ductile tearing with intergranular facets (Figure 9).

Crack growth samples of IC-221 showed fracture paths that varied with both temperature and environment. Intergranular fracture was noted for a test at 600 °C in air (Figure 10(a)), while transgranular fracture was noted at 600 °C in vacuum (Figure 10(b)).

At 800 °C in air, IC-221 revealed for all test frequencies and both R ratios a heavily oxidized surface in which the fatigue crack path could not be identified. However, the overload zone invariably was intergranular. In vacuum, a mixed mode of fracture was observed for $R = 0.1$

Table II. Notch Sensitivity Values (NSR) for IC-221

T (°C)	Environment	NSR
25	air	1.02
600	vacuum	1.40

at 20 Hz (Figure 11(a)). At lower test frequencies, the fracture was entirely intergranular in vacuum for $R = 0.1$ or $R = 0.6$, as shown, for example, in Figures 11(b) and (c) for fatigue and overload zones, respectively.

IV. DISCUSSION

A. Tensile Behavior

The tensile results reported here (Figure 3) were obtained primarily to establish the stress levels at which fatigue crack growth tests were to be run and to determine whether the alloys were notch sensitive. It is interesting to note that although the room-temperature ductility of IC-221 is only about 20 pct (Figure 3), there is no sudden drop in ductility at 600 °C and above. The lack of notch sensitivity of IC-221 (Table II) is particularly noteworthy. Previous work has shown that although $Ni_3Al + B$ is ductile at room temperature, it is quite notch sensitive.[5] Manganese also eliminates notch sensitivity in $Ni_3Al + B$, probably through the presence
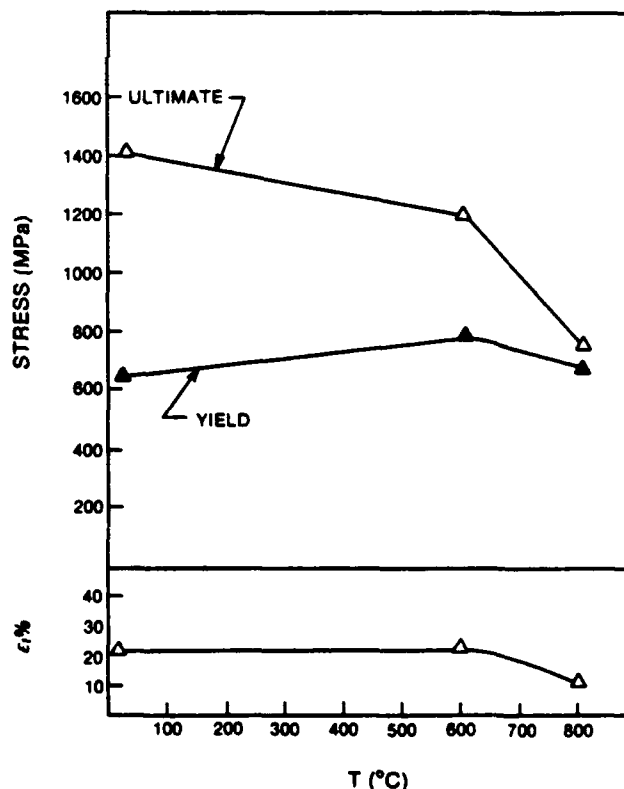

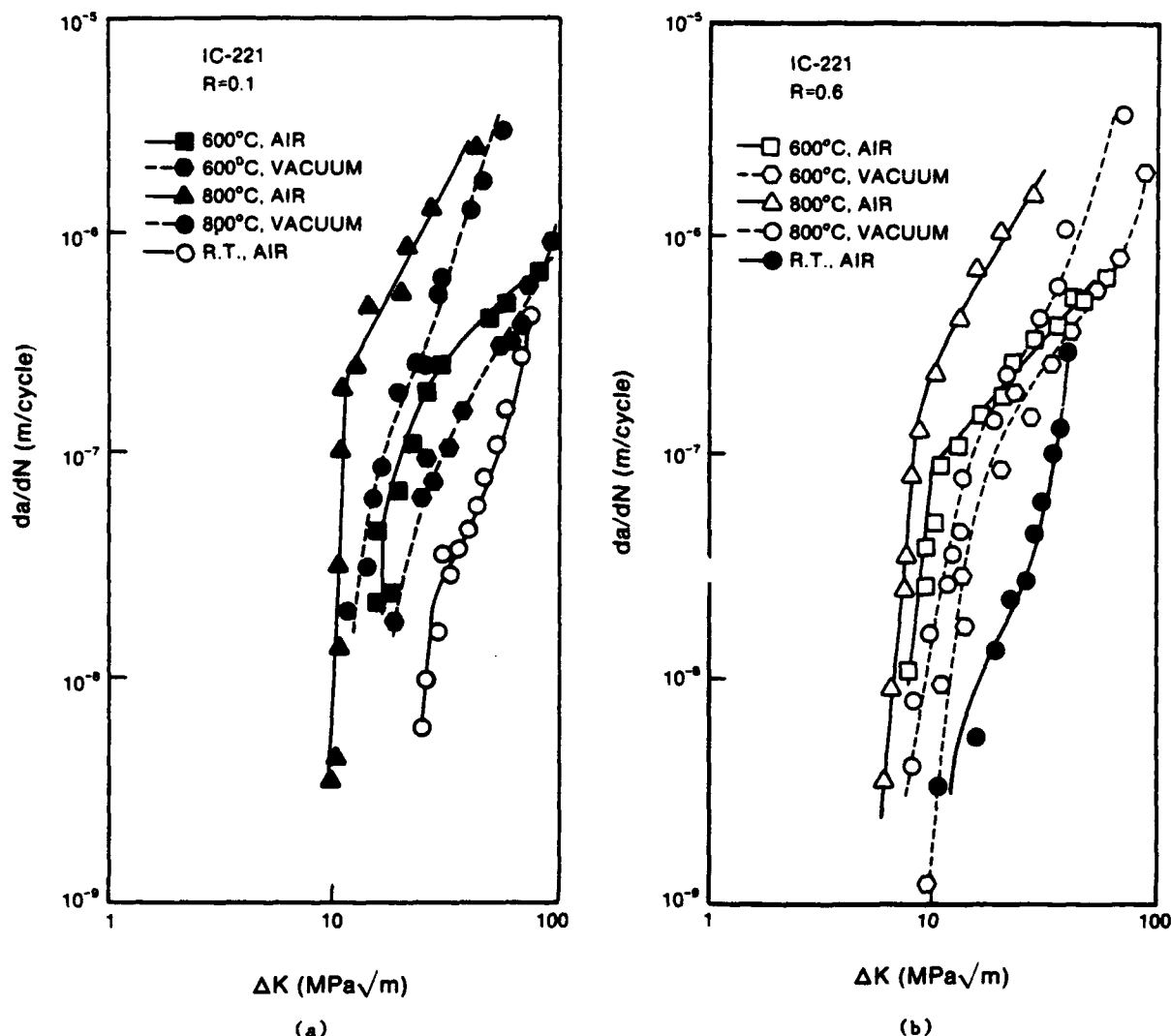Fig. 3—Tensile test results as a function of test temperature for IC-221 alloy.

Fig. 4—Crack propagation rates for IC-221 alloy as a function of ΔK in air and in vacuum at room temperature, 600 °C, and 800 °C; ν = 20 Hz: (a) R = 0.1 and (b) R = 0.6.

of a disordered second phase.[5] The IC-221 utilized in this investigation contains a small amount of disordered γ (Ni-rich solid solution),[3] suggesting the generally beneficial effect of such a phase on notch sensitivity.

B. Fatigue Crack Growth

Plastic zone sizes were estimated according to the Irwin[6] equation:

$$r_y = \frac{1}{2\pi} \left(\frac{\Delta K}{\sigma_y} \right)^2$$

where the cyclic yield stress, σ_y, is estimated to be twice the tensile yield stress (due to cyclic hardening) and r_y is the plastic zone size. Plane strain conditions ($r_y/B <$ 0.02, where B = specimen thickness) were not achieved at ΔK values greater than 25 MPa·m$^{-1/2}$ at 25 °C, 30 MPa·m$^{-1/2}$ at 600 °C, and 26 MPa·m$^{-1/2}$ at 800 °C. Therefore, the results do not conform to ASTM Standard E 637,[7] and the crack growth data can be used only to

analyze trends in properties of this alloy as a function of temperature, R ratio, and environment.

At 25 °C, crack growth of IC-221 occurs slightly faster than for a wrought Cr-free, single-phase Ni$_3$Al-base alloy (IC-50)[8] at low ΔK only, as shown in Figure 12. At high K, crack growth rates for the two alloys are identical. At 600 °C, on the other hand, IC-221 cracks at a lower rate than IC-50, as is also shown in Figure 12. The results of crack growth experiments carried out at 600 °C in vacuum have been compared to those for other high-temperature alloys (Figure 13). Only an ordered (Fe, Ni)$_3$V + Ti alloy, LRO-60[9] Fe-39.5 wt pct Ni, 37 pct Fe, 22.4 pct U, 0.4 pct Ti, and IN X-750,[10] possesses lower crack growth rates at ΔK = 20 MPa·m$^{-1/2}$. At high ΔK, IC-221 displays lower crack growth rates than all the other high-temperature alloys shown in Figure 13.

Crack growth rates increased for IC-221 between 25 °C and 800 °C in spite of an increasing yield stress over the same temperature range. One possible explanation for the high growth rates at elevated temperature is an environmental effect due to adsorbed oxygen at the crack
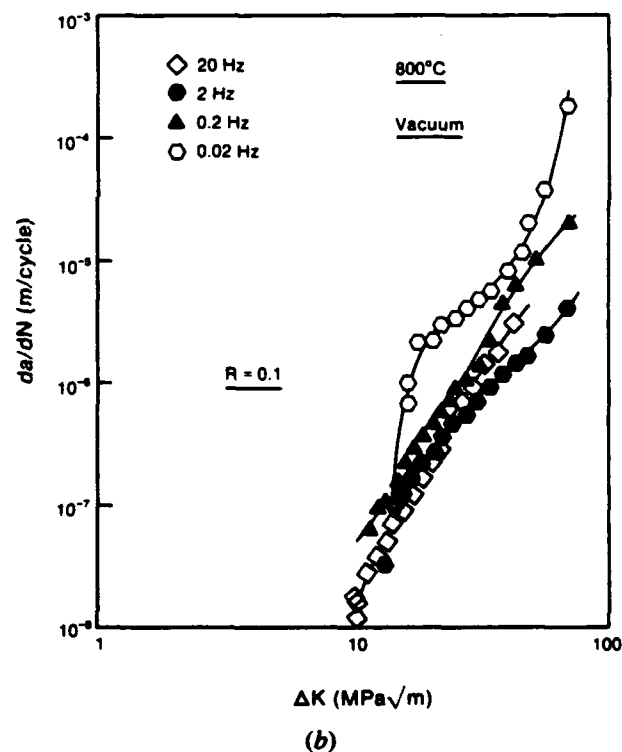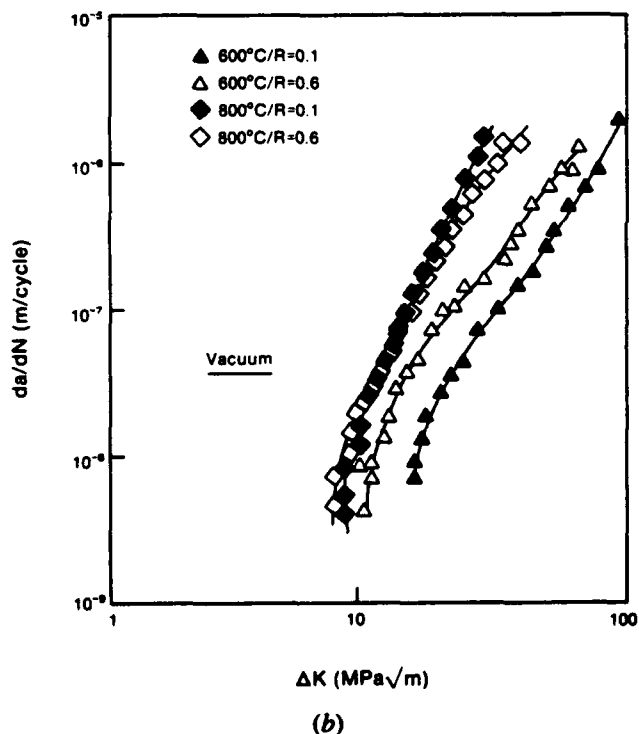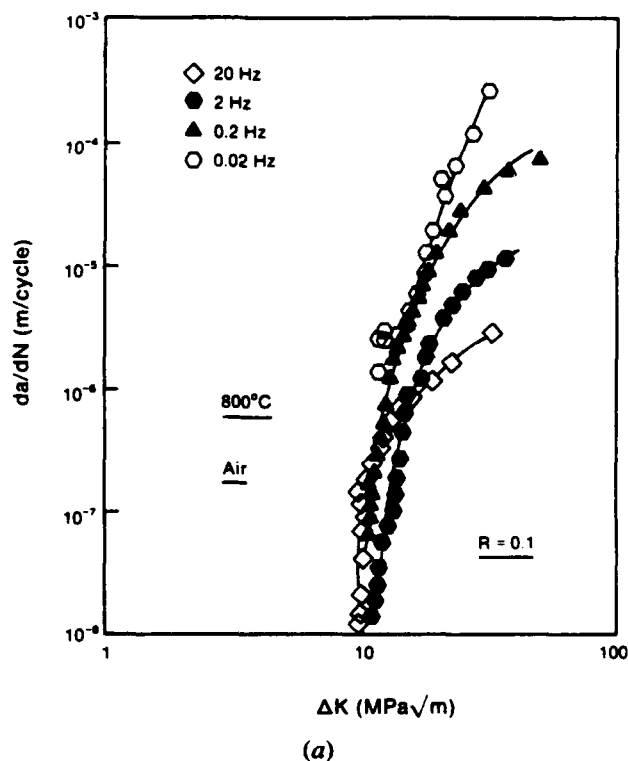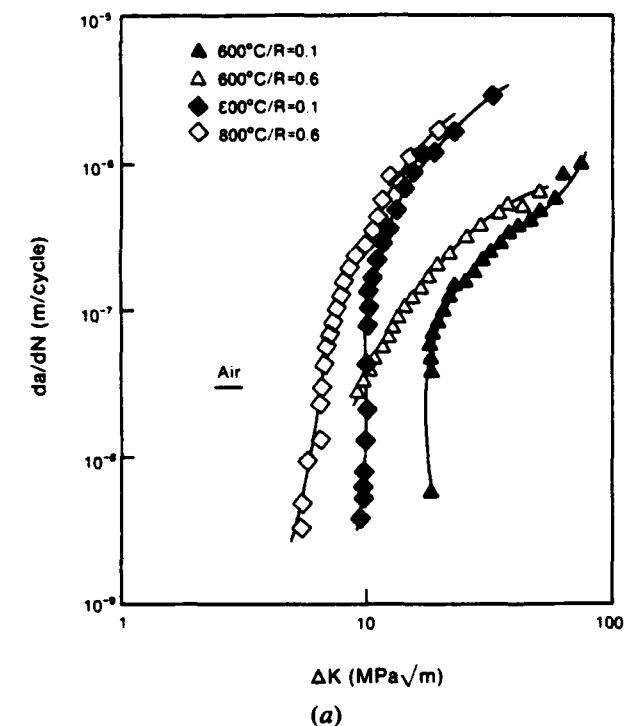
Fig. 5—Crack propagation rates for IC-221 alloy as a function of ΔK and R at 600 °C and 800 °C; $\nu = 20$ Hz: (a) in air and (b) in vacuum.

Fig. 6—Crack propagation rates for IC-221 alloy as a function of ΔK and frequency at 800 °C: (a) in air and (b) in vacuum.

tip.[14] The crack propagation experiments on IC-221 were carried out both in air and in moderate vacuum ($<4.5 \times 10^{-3}$ Pa). Although the surfaces of the specimens tested in vacuum appeared to be shiny after the test, fractography revealed oxide formation in the fatigue zones (Figure 10(b)).

The values of ΔK_{th} decreased with increasing load ratio for IC-221 at all temperatures. The effect of load ratio on near threshold crack propagation rates may be rationalized by crack closure. At the threshold levels, crack tip opening displacements (CTOD) are small. Hence,

Kmax (MPa√m)

(a)

Kmax (MPa√m)

(b)
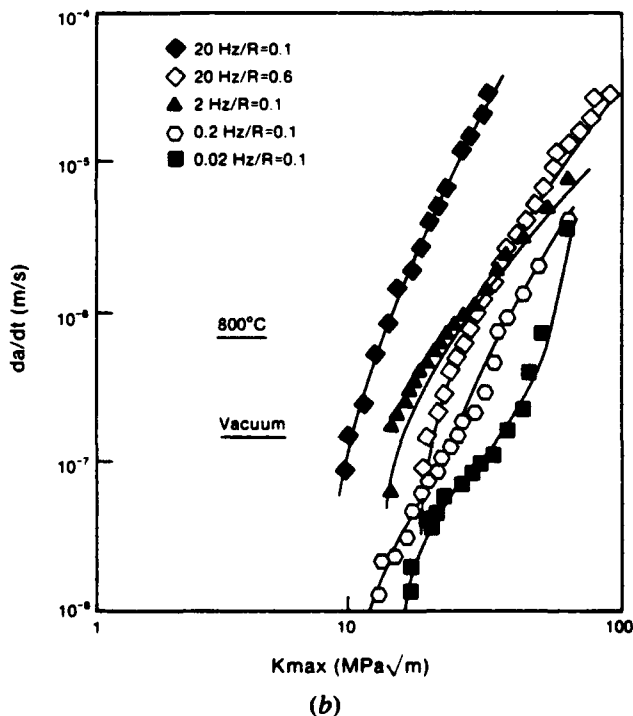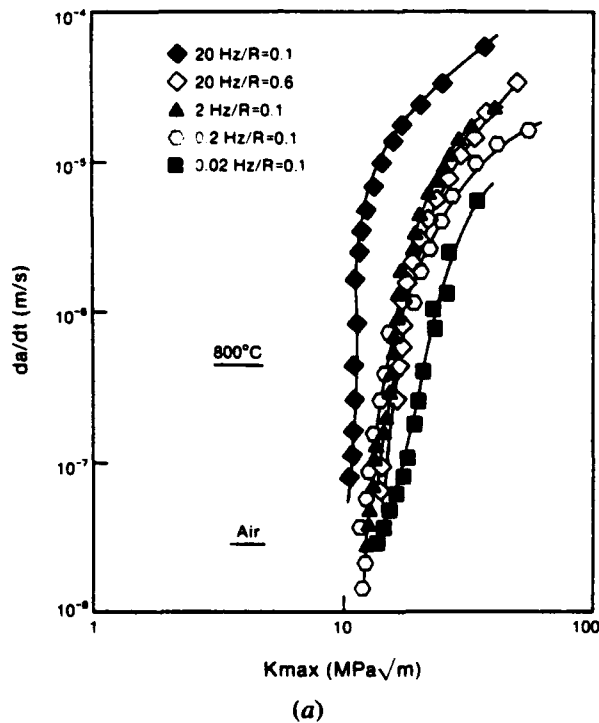
Fig. 7—Time-based crack propagation rates for IC-221 alloy as a function of the maximum stress intensity, frequency, and R ratio at 800 °C: (a) in air and (b) in vacuum.

oxide debris with a thickness comparable to the CTOD or fracture surface roughness with a mismatch between the mating facets will cause early contact of fracture surfaces and raise the crack closure loads. The greater the oxide thickness or the rougher the fracture surface, the higher will be the degree of crack closure. This results in a reduction of the effective crack tip stress intensity,
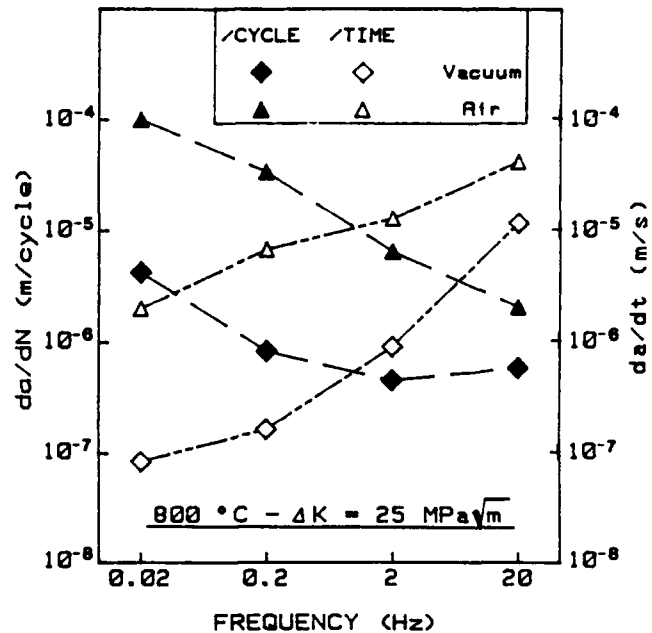
Fig. 8—Influence of frequency and environment on crack growth rates of IC-221 at 800 °C; $\Delta K = 25$ MPa·m.

ΔK_{eff}, thus increasing the apparent value of ΔK_{th}. Oxide- and roughness-induced closure are significant only at low R values, since high load ratios minimize crack closure.

At both 600 °C and 800 °C, with an R ratio of 0.1, ΔK_{th} values are virtually identical in both air and vacuum. At high ΔK, both air and vacuum curves also tend to merge, with a maximum difference in da/dN being observed at intermediate ΔK ranges. These data indicate that at these temperatures, where oxidation rates are low, oxide affected crack closure does not influence the values of ΔK_{th}. At high ΔK, crack propagation rates are sufficiently high so that the cracks are driven primarily by cyclic mechanical driving forces, i.e., pure fatigue. In the intermediate ΔK range, air increases the FCGR when compared to vacuum, and the fracture path is changed from transgranular in vacuum to intergranular
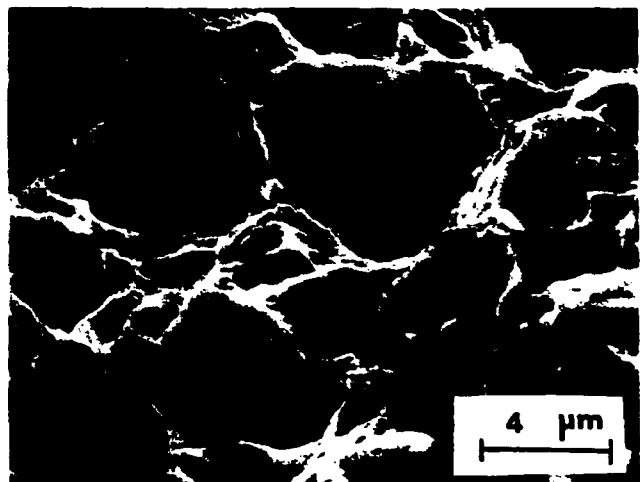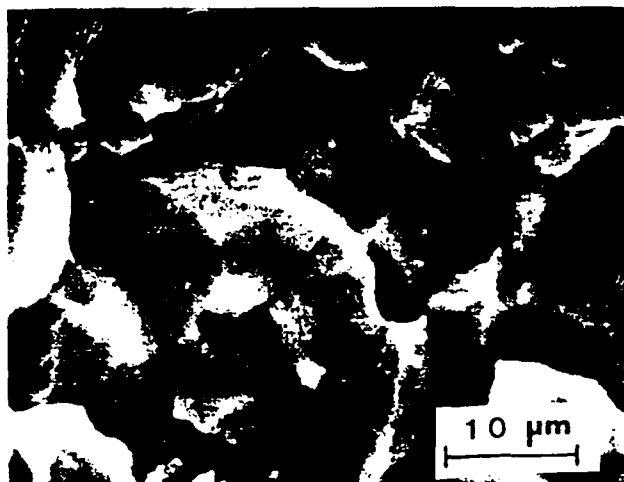

Fig. 9—SEM fractograph of IC-221 showing transgranular ductile tearing with intergranular cleavage facets; tensile test, 800 °C, vacuum.
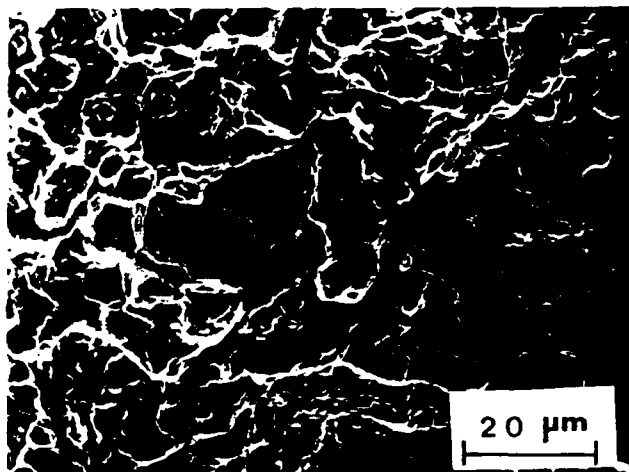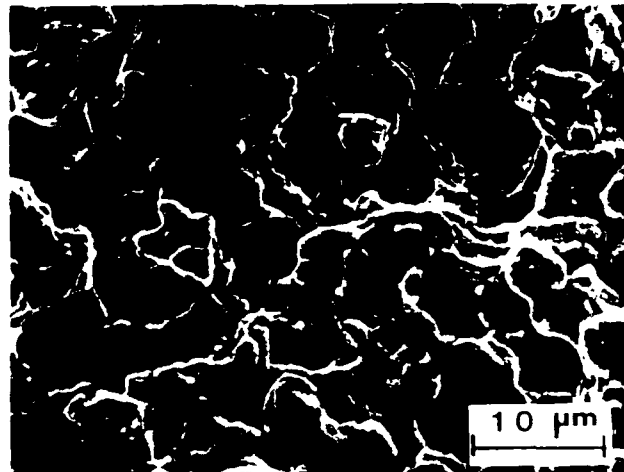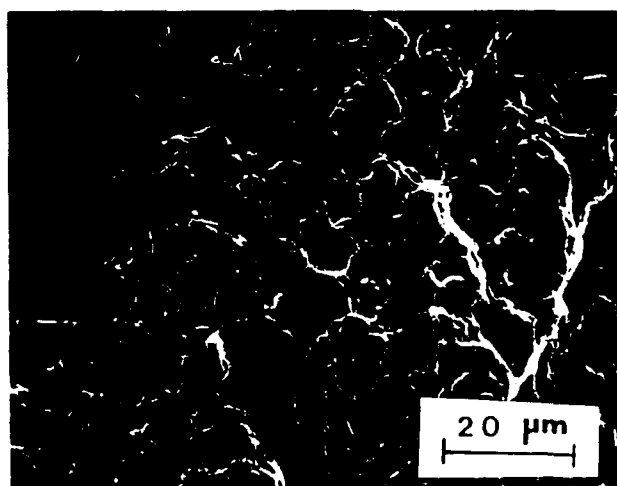
(a)

(b)

Fig. 10 — SEM fractographs of crack growth samples of IC-221 with ν = 20 Hz and R = 0.1. (a) intergranular (600 °C, air) and (b) transgranular (600 °C, vacuum).

(a)

(b)

(c)

Fig. 11 — SEM fractographs of IC-221 tested at 800 °C in vacuum at various frequencies. (a) 20 Hz, fatigue zone, (b) 0.02 Hz, fatigue zone, and (c) 0.02 Hz, overload zone.

Table III. Activation Energies for Crack Growth of IC-221

Environment	K_{max} (MPa·m)	Temperature Range	Q (kJ/m)
Air	20	600 to 800	89
Air	30	600 to 800	82
Vacuum	20	600 to 800	96
Vacuum	30	600 to 800	100

in air. A similar effect has been observed in an $(Fe, Ni)_3V + Ti$ alloy (LRO-42) which has essentially the same composition as alloy LRO-60, data for which are included in Figure 13. The increase in growth rates in air relative to vacuum may be attributed to the adsorption of oxygen at the crack tip, leading to intergranular embrittlement of the alloy.[14]

At 600 °C and 800 °C with an R ratio of 0.6, ΔK_{th} is larger in air than in vacuum. As for an R ratio of 0.1, the FCGR's in air and in vacuum tend to merge at high ΔK, and the differences between them are maximized at intermediate ΔK's (Figure 4(b)). These data indicate that the absence of closure due to a high R ratio results in a greater interaction of the alloy with oxygen at the crack tip at low K and, thus, results in some embrittlement. As for an R ratio of 0.1, high K's show little effect of environment, indicating that crack propagation effectively outpaces oxidation processes.

The specific effects of environment and R ratio are shown in Figure 5, which verifies that in air, the R ratio is only important at low to intermediate ΔK. In vacuum, on the other hand, the R ratio is only important at 600 °C,

Fig. 13—Comparative crack propagation rates as a function of ΔK for IC-221 and a number of commercial and experimental alloys between 550 °C and 650 °C.[10,11]

over the entire ΔK range. At 800 °C, increasing the R ratio from 0.1 to 0.6 has little perceptible effect on FCGR's at any ΔK. These data confirm the concept that only when ΔK's are low can oxidative processes affect FCGR's. Moreover, the tests performed in vacuum indicate that the cyclic stress range, rather than the maximum stress, provides the driving force for crack growth at 800 °C. At 600 °C, there is an apparent effect of R which appears to contradict this observation. However, at the vacuum levels used in this study, it is likely that some oxygen embrittlement has occurred, since the FCGR is considerably lower than at 800 °C, thus providing more time for oxidative reactions.

The effect of environment also can be determined by examining the effects of cyclic frequency shown in Figures 6 and 7. In air, ΔK_{th} is independent of frequency, while FCGR's increase at intermediate to high ΔK's. These effects are due to the increased oxidation time available at the crack tip during slower cycling, and when the data are plotted as da/dt rather than da/dN, it can be seen that, except at the highest frequencies, the data are relatively independent of either frequency or R ratio. The apparent discrepancy at the highest frequency is believed to be due to crack propagation which is more rapid than oxygen-induced embrittlement in the process zone ahead of the crack. When tests are performed in vacuum, frequency has little or no effect on FCGR's, except at the lowest frequency of 0.02 Hz. It is likely that the moderate vacuum used in these experiments was not sufficient to inhibit environmental interactions at this low frequency.

As shown in Figure 8, there is a pronounced increase in growth rate (da/dN) at 800 °C with decreasing frequency to 2 Hz in vacuum and to 0.02 Hz in air. The
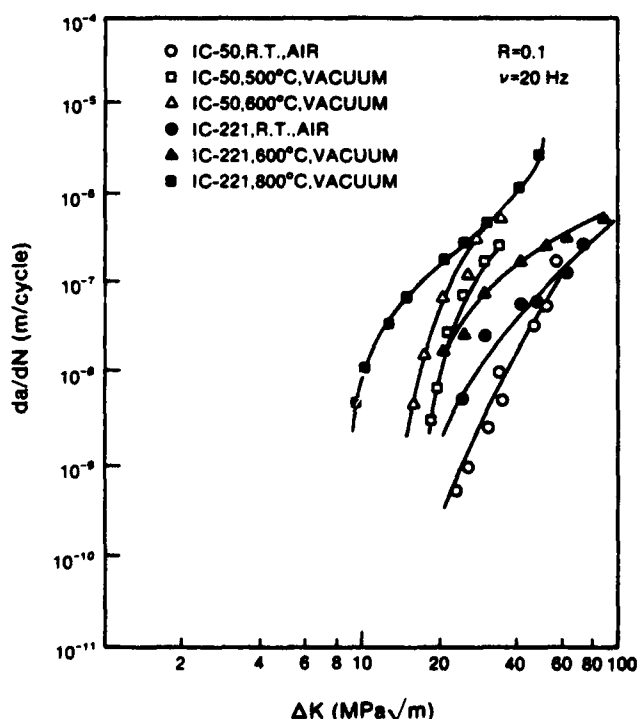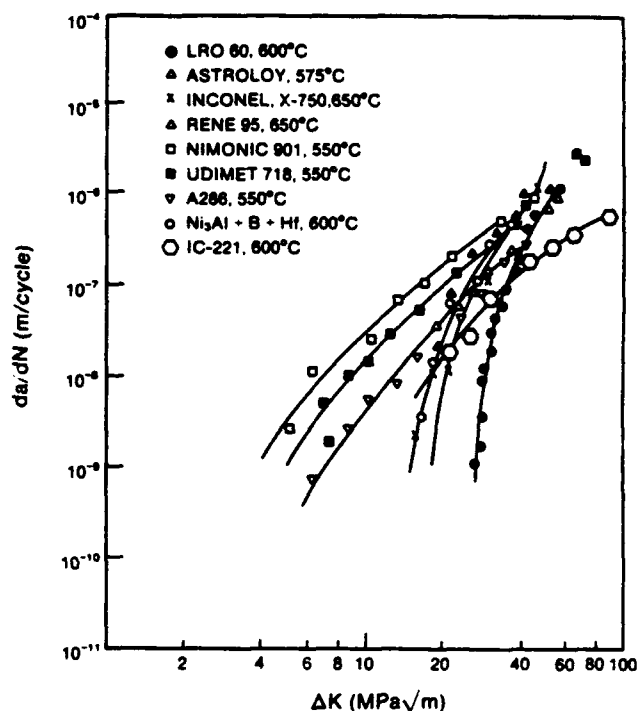

Fig. 12—Comparative crack propagation rates as a function of ΔK for alloys IC-50 and IC-221 at room temperature, 600 °C, and 800 °C in air and in vacuum.

absolute value of growth rate remains higher in air at all frequencies, but the differences in growth rate narrow at high frequency. Previous work on a similar alloy, IC-218, Ni-85 wt pct Al-76 pct Cr-0.83 pct Zr, under stress controlled high cycle fatigue conditions revealed a decrease in the number of cycles to failure with decreasing frequency at both 600 °C and 800 °C.[12] Strain to failure and reduction in area also increased with decreasing frequency, suggesting a contribution of creep to deformation during the fatigue tests.[13] However, it is clear from the oxidized intergranular fracture surfaces obtained at all frequencies that environmental attack occurs even in the vacuum employed for these experiments. Therefore, the frequency effect on growth rate probably reflects a combination of environmental (oxygen) attack and creep processes, although it is believed that environmental interactions are dominant. Also noted at low frequencies was an increased number of secondary cracks. Such cracks also were noted by Hippsley and DeVan[14] in their static fatigue tests on a Ni-22.9 at. pct Al-0.5 pct Hf-0.24 pct B alloy (IC-50) carried out in air. The fact that these cracks were noted in our work only at low frequencies suggests that diffusion of oxygen is necessary for these cracks to appear.

It is instructive to compare our crack growth results under cyclic loading with the crack growth data under static loading in air reported by Hippsley and DeVan[14] for IC-50 in the temperature range of 500 °C to 760 °C. Fracture in the latter alloy occurred by stable intergranular cracking, with an apparent activation energy of 110 kJ/mol for the process. That value is smaller than that for oxygen diffusion along grain boundaries in pure nickel in the absence of stress ($\sim$311 kJ/mol).[15]

Utilizing crack growth data for IC-221 at 600 °C and 800 °C (from Figure 5(a)) at a stress intensity range of 20 MPa·m$^{1/2}$ (comparable to the stress intensity of 15.8 MPa·m$^{1/2}$ used in the static fatigue tests), apparent activation energies of 89 kJ/mol for tests in air and 96 kJ/mol for tests in vacuum are obtained. Similar numbers are obtained for ΔK = 30 MPa·m$^{1/2}$ (Table III). Since IC-221 contains 7.97 wt pct Cr, while IC-50 is Cr-free, one might expect a lower crack growth rate for IC-221 in a similar temperature range (500 °C to 760 °C), with perhaps a transgranular crack path for IC-221. However, it is clear from Figure 10(a) that Cr is unable to prevent intergranular slow crack growth in air at 600 °C. With regard to activation energies, the lower activation energies obtained in both environments for cyclic crack growth of IC-221 than for static crack growth of IC-50 in air might be accounted for by one or more of the following factors:

(a) if oxidation is rate controlling, oxide formation may be more rapid in IC-221 than in IC-50 due to the effects of Cr[16] and Zr[16] in promoting the formation of a surface film;
(b) cyclic crack growth, in which the oxide film is broken by repeated loading and unloading of the crack, may allow oxygen more ready access to the crack tip than would static growth; or
(c) cracking may be controlled by some mechanism other than oxygen diffusion.

Recent research in our laboratory on oxidation of IC-221

in the range of 900 °C to 1100 °C revealed that mixed Cr$_2$O$_3$-Al$_2$O$_3$ surface films form with an increased proportion of Al$_2$O$_3$ at higher temperature.[17] An activation energy of 211 kJ/mol for oxidation between 900 °C and 1000 °C was calculated. This value is so much higher than those observed in our work at lower temperatures on crack growth that it must be seriously doubted that oxidation per se is the rate limiting step in crack growth. However, grain boundary diffusion of oxygen, with a lower activation energy, may still explain the intergranular crack growth noted in air. Previous work on a similar alloy, IC-218, Ni-85 wt pct Al-76 pct Cr-0.83 pct Zr, under stress controlled high cycle fatigue conditions revealed a decrease in the number of cycles to failure with decreasing frequency at both 600 °C and 800 °C.[12] Strain to failure and reduction in area also increased with decreasing frequency, suggesting a contribution of creep to the fatigue tests.[13] However, it is clear from the oxidized intergranular fracture surfaces obtained at all frequencies and in both environments that environmental attack occurs, even in the vacuum employed for these experiments. Therefore, the frequency effect on growth rate probably reflects a combination of environmental (oxygen) attack and creep processes.

V. CONCLUSIONS

1. IC-221 was not notch sensitive at room temperature or at 600 °C, probably due to the presence of a disordered second phase.
2. Crack growth rates in IC-221 increased with testing in air relative to vacuum and with testing at a higher R ratio.
3. The rate of crack propagation in IC-221 increases with increasing temperature, paralleling an increase in yield stress with temperature. This behavior is attributed primarily to an environmental effect at the crack tip, as previously noted by others[14] for crack growth under static loading in Cr-free Ni$_3$Al + B.
4. Crack growth rate (da/dN) increased with decreasing test frequency, both in air and in vacuum, at 800 °C, indicating creep contributions to the environmental effects on crack growth. Secondary cracking is enhanced at lower frequencies.
5. IC-221 displays excellent resistance to fatigue crack propagation and compares favorably with other structural alloys tested under similar conditions at 600 °C.

ACKNOWLEDGMENTS

REFERENCES

1. K. Aoki and O. Izumi: *Nippon Kinzoku Gakkaishi*, 1979, vol. 43, p. 1190.
2. C.T. Liu, C.L. White, and J.A. Horton: *Acta Metall.*, 1985, vol. 33, pp. 213-19.
3. C.T. Liu and V.K. Sikka: *J. Met.*, 1986, vol. 38, pp. 19-21.
4. C.T. Liu: in *High Temperature Ordered Intermetallic Alloys II*, Materials Research Society Symposium Proceedings, Pittsburgh, PA, 1987, vol. 81, pp. 355-67.
5. G.E. Fuchs and N.S. Stoloff: *Proc. 8th Int. Conf. on Strength of Metals and Alloys (ICSMA 8)*, Pergamon Press, Oxford, 1988, vol. 1, pp. 665-70.
6. G.R. Irwin: *Handbuch der Physik*, Springer-Verlag, Berlin, 1958, p. 551.
7. *Annual Book of ASTM Standards*, vol. 03.01, Easton, MD, 1987.
8. A.K. Kuruvilla and N.S. Stoloff: *Scripta Metall.*, 1987, vol. 32, pp. 873-77.
9. A.K. Kuruvilla and N.S. Stoloff: *Proc. 7th Int. Conf. on Strength of Metals and Alloys*, Montreal, Canada, Pergamon Press, Oxford, 1985, vol. 2, pp. 1335-42.
10. E. Hoffelner and M.O. Speidel: *Creep and Corrosion*, Cost-50 Second Round, CH-1 Final Reports, Brown-Boven and Co., Baden, Switzerland, 1981.
11. A.K. Kuruvilla and N.S. Stoloff: *Metall. Trans. A*, 1985, vol. 16A, pp. 815-20.
12. W. Matuszyk: M.S. Thesis, Rensselaer Polytechnic Institute, Troy, NY, 1988.
13. G. Camus, D.J. Duquette, and N.S. Stoloff: in *High Temperature Ordered Intermetallic Alloys III*, Materials Research Society Symposium Proceedings, Pittsburgh, PA, 1989, vol. 133, pp. 579-84.
14. C.A. Hippsley and J.H. DeVan: *Acta Metall.*, 1989, vol. 37, pp. 1485-96.
15. R. Barlow and P.J. Grundy: *J. Mater. Sci.*, 1969, vol. 4, p. 797.
16. S. Taniguchi and T. Shibata: *Oxidation of High Temperature Intermetallics*, T. Grobstein and J. Doychak, eds., TMS, Warrendale, PA, 1988, pp. 17-29.
17. J. Montrym: M.S. Thesis, Rensselaer Polytechnic Institute, Troy, NY, 1988.

Isothermal and Cyclic Oxidation

of TiAl Composites

Abstract

Titanium Aluminide and TiAl matrix composites reinforced with
alumina fibers (PRD166) were fabricated by powder metallurgy.
During isothermal oxidation at 950 and 1070°C, Composites containing
PRD166 fibers exhibited larger weight gains than monolithic TiAl;
the composites showed evidence of oxidation along the perimeter of
the fibers. A fiber reaction, which was observed after oxidation in
air, is believed to result from internal oxidation. The reaction
was suppressed by heat treating in vacuum and increasing the
aluminum content of the matrix. The oxide adherence on TiAl was
improved by the addition of alumina (PRD166) fibers.

1.Introduction

Titanium Aluminides are being considered for high temperature
structural applications, such as the National Aerospace Plane and
rotors in automobile superchargers. However, similar to other
intermetallics, TiAl suffers from a lack of room temperature
ductility, inadequate creep resistance, and susceptibility to
hydrogen embrittlement. Fiber reinforcement is being studied as a
means to improve the damage tolerance, creep resistance, and
specific strength of titanium aluminides.

The maximum operating temperature of titanium aluminides will
be limited by oxidation resistance rather than by creep or strength
retention[*]. Therefore, an understanding of the oxidation
mechanisms of these materials is essential. Oxidation of binary Ti-
Al alloys produces mixed oxides of Al_2O_3 and TiO_2. During oxidation
at 1100 °C in air, a continuous alumina film is formed only on Ti-Al

[*] Compositions are in wt.%

alloys containing more than 42-45%[*] aluminum[2].

While several studies of the mechanical properties of titanium aluminide composites have been conducted, very little research has been published on the oxidation behavior of these composites. The purpose of this study was to examine the oxidation behavior of TiAl composites containing alumina reinforcements.

2.Experimental Procedures

The material used in this study was fabricated by powder metallurgy using elemental titanium and aluminum powders. Dupont's advanced alumina fiber, PRD166, was chosen as the reinforcement for the composites. The composition and size of the powders and fibers are shown in Table 1. The Dupont PRD166 fiber contains 15% stabilized zirconia to improve the fiber's creep resistance and ultimate tensile strength[3]. The composition of the monolithic TiAl and the matrix of the composites was 40% (54 at.%) aluminum, which corresponds to single phase gamma on the Ti-Al phase diagram.

Table 1. Powders and PRD166 Fibers

Powder	Diameter (μm)	Composition	Source
Aluminum	8	99⁻% Al	Valimet
Titanium	36	99⁻% Ti	Micron Metals
PRD166	20	85% Al_2O_3, 15% ZrO_2	Dupont

The PRD166 fibers were chopped to lengths of 3 mm and mixed with ethanol to reduce agglomeration. The chopped fibers were then mixed with the elemental titanium and aluminum powders, cold isostatically pressed at 242 MPa (35 ksi), pre-reacted at 800°C for 45 minutes, and then consolidated by hot isostatic pressing at 1350°C and 173 MPa (25 ksi) for two hours.

Oxidation samples were polished to 0.3 μm alumina and ultrasonically cleaned with acetone and ethanol. Isothermal oxidation experiments were performed using alumina boats in dry air over the temperature range of 950 to 1070°C. Cyclic oxidation experiments, to evaluate oxide adherence, consisted of ten hour cycles at temperature followed by cooling in static air. Weight change measurements were used to determine the oxidation resistance of the composites. Oxide morphology, adherence, and composition were evaluated by X-Ray diffraction, scanning electron microscopy (SEM), energy dispersive analysis by X-Ray (EDAX), and electron microprobe analysis (EMPA).

3.Results and Discussion

3.1 TiAl-PRD166 Oxidation

Oxidation weight change measurements of the PRD166 reinforced composites are shown in Figures 1 and 2. The specific weight gain of the composites was greater than that of monolithic TiAl and increased proportionally with the volume fraction of reinforcement.

Figures 3 and 4 show SEM micrographs of the oxide morphology and cross sections of the oxide after oxidation for 100 hours at 1070°C. Approximately 40% of the monolithic sample was covered with a convoluted oxide and the rest of the surface contained a highly faceted oxide. These oxides were identified by X-Ray diffraction and EDAX as Al_2O_3 and TiO_2, respectively. Figure 3 shows that the matrix of the composites was covered by a buckled Al_2O_3 film and that an external oxide was not formed on the surface of the PRD166 fibers.

Based on SEM observations of oxidized samples, a schematic model of the oxidation of TiAl (40% Al) at 1070°C is presented in Figure 5. During the initial stages of oxidation, both rutile and

alumina nucleate on the sample surface. Oxidation exposures for less than one hour indicate that a buckled alumina layer initially forms. Golightly et. al.[4] proposed that compressive stresses, resulting from oxide nucleation and growth within the parent Al_2O_3 film, are responsible for the buckled oxide.

Formation of the alumina film depletes the substrate of aluminum and produces the Ti_3Al zone shown in Figure 4(a). The lower aluminum content of the Ti_3Al promotes internal oxidation, producing Al_2O_3 precipitates and further reducing the aluminum content. As the activity of titanium increases (and the activity of aluminum decreases), titanium oxide formation becomes more favorable than alumina formation. Continued oxidation produces a heterogeneous oxide consisting of alternating layers of rutile and alumina, shown in Figures 5(a) and 6(d).

Depending on the aluminum content, the alumina film shown in Figure 5(b) may be discontinuous; Meier et. al.[2] showed that approximately 42-45% aluminum is necessary for continuous alumina film formation on binary TiAl during oxidation in air at 1100°C. Ti-Al alloys without sufficient aluminum content to produce a continuous Al_2O_3 film form a thick external oxide of TiO_2[5,6]. Figures 4(a) and 5(d) show a TiO_2 oxide which formed over a discontinuous alumina scale. The rutile layer may result from the outward diffusion of titanium through gaps in the Al_2O_3 film or may result from other rapid diffusion paths. Voids, which have been reported at oxide-metal interface[6], may be Kirkendall porosity resulting from outward titanium diffusion and are expected to reduce the integrity of the oxide-metal bond.

In contrast to monolithic TiAl, the PRD166 composites did not develop a stratified oxide or a thick external TiO_2 layer. In

addition, Figure 4(b) shows evidence of oxidation along the perimeter of the fibers. The alumina layer along the the fibers was thickest near the surface of the composite and diminished towards the center, as shown in Figure 6. Oxygen diffusion along the fibers and subsequent oxidation of the matrix along the perimeter of the fibers is believed to be responsible for the increased weight gain of the composites; Tortorelli et. al.[7] reported that Ni_3Al reinforced with PRD166 and FP fibers exhibited larger weight gains than unreinforced Ni_3Al.

3.2 PRD166 Reaction

A fiber-matrix reaction, shown in Figure 7, occurred at some of the fibers, predominantly at fiber clusters, during oxidation at 950, 1020 and 1070°C in air. Measurements of the reaction zone indicate that it grows at a parabolic rate. EMPA revealed that the dark precipitates are Al_2O_3; in addition, the matrix adjacent to the reaction zone was doped with about 2.5% zirconium.

Nourbakhsh et. al.[3] found that TiAl(Mn)-PRD166 composites produced by pressure casting were doped with zirconium and formed zirconia at the fiber-matrix interface. This effect was attributed to creep of the fiber which swept zirconia to the fiber perimeter and into the matrix. However, Nourbakhsh's study did not include any oxidation experiments or report anything similar to the reaction in Figure 7.

The matrix-PRD166 reaction does not result from an inherent fiber-matrix incompatibility. Diffusion couple experiments have shown that Al_2O_3 is stable with gamma $TiAl$[9]. Above 1000°C, zirconia is thermodynamically more stable than alumina[10]. A sample containing 30% PRD166 was heat treated for 100 hours at 1070°C in an evacuated quartz tube, and Figure 7(b) shows that the reaction did

not occur after this heat treatment. Therefore, the reaction is most likely related to oxygen diffusion and reaction with the matrix along the PRD166 fibers.

Wagner[11] derived an expression for the critical aluminum content, N^*_{Al}, necessary to prevent internal oxidation. The critical aluminum content is dependent on the volume fraction of internal precipitates, g, and the ratio of the diffusivity of oxygen and aluminum in the matrix, D_O/D_{Al}. Other variables in equation (1) include the oxygen solubility in the alloy, N_O, and the molar volumes of the oxide, V_{ox}, and of the alloy, V_m. Internal oxidation occurs when the oxygen flux into the alloy is greater than the counter flux of aluminum. At a critical volume fraction of internal precipitates, g^*, the oxygen flux is reduced by the alumina precipitates to allow the formation of a continuous alumina film.

$$N^*_{Al} = \sqrt{\frac{\pi g^* N_O D_O V_m}{3 D_{Al} V_{ox}}} \qquad (1)$$

The following model is presented to explain the matrix-PRD166 reaction and the accelerated weight gain of the composites. As a result of stress assisted diffusion at the high fabrication temperature (1350°C) and pressure (173 MPa), the TiAl matrix is doped with zirconium and a zirconia sheath forms at the perimeter of the fibers. For example, TEM results by Nourbaksh[12] have shown that ZrO_2 is present at the fiber-matrix interface of intermetallic composites produced by pressure casting. Figure 3 shows that the fiber ends are not covered by an oxide film, thus allowing a constant supply of oxygen to the reaction zone surrounding the fibers. The diffusivity of oxygen in zirconia at 1070°C is

approximately eleven orders of magnitude faster than in alumina[13,14]. A previous study has shown that zirconium increases the oxygen diffusivity in titanium[15]. If Zr has the same effect in TiAl, equation (1) indicates that a greater aluminum content will be required to prevent internal oxidation along the fibers.

By increasing the aluminum content of the matrix, it should be possible to prevent the internal oxidation adjacent to the fibers. Two PRD166 composites were fabricated with 44% and 48% aluminum and oxidized in air for 100 hours at 1070°C. The reaction was observed in the sample containing 44% aluminum but not in the TiAl-PRD166 composite containing 48% aluminum.

3.3 Cyclic Oxidation

The results of cyclic oxidation experiments performed at 1070°C are presented in Figure 8. The oxide adherence on monolithic TiAl is poor, as indicated by the spalling and subsequent rapid weight gain. In contrast, none of the composites exhibited any spalling.

Oxide adherence on Ti-Al alloys appears to be associated with the ability to form a contiguous alumina film and the absence of a thick external TiO$_2$ scale. The monolithic TiAl formed a rutile layer which spalled and cracked during thermal cycling. However, the oxide on the composites, which was similar to that produced during isothermal oxidation, was adherent up to 120 hours.

Examination of spalled films indicates that oxide failure typically occurs at the oxide-metal interface. A possible explanation is that this interface has been weakened by Kirkendall voids, resulting from the outward diffusion of titanium. In any case, precluding the formation of TiO$_2$ appears to improve oxide adherence. Perkins[5] showed that a continuous alumina layer,

promoted by chromium and vanadium additions, prevented the formation of an external TiO_2 scale and improved the oxide adherence of the alloy. The cyclic oxidation resistance of TiAl was significantly improved by promoting alumina formation with a low oxygen pressure pre-treatment[17].

According to Wagner's internal oxidation theory, the formation of a continuous film will occur at a critical volume fraction of internal precipitates, g^*. If the alumina reinforcements act as internal precipitates, then it may be possible to form a continuous Al_2O_3 film at a lower aluminum content than without the reinforcements. Thus, alumina fibers may inhibit outward titanium diffusion by promoting a continuous scale of Al_2O_3 and, thereby, improve the cyclic oxidation resistance of TiAl composites.

4. Summary

TiAl reinforced with PRD166 fibers exhibited increased weight gain during oxidation in air, as compared to monolithic TiAl. Oxygen diffusion along the alumina reinforcement formed an Al_2O_3 layer along the perimeter of the fibers. It is postulated that zirconium from the PRD166 fibers increases the oxygen diffusivity in the matrix and promotes internal oxidation adjacent to the fibers; this reaction may be suppressed by heat treating in vacuum or increasing the aluminum content of the matrix.

The addition of PRD166 fibers significantly improves the oxide adherence during cyclic oxidation. One possible explanation is that the fibers promote the formation of a continuous Al_2O_3 film. Further experiments are planned to determine if zirconium is necessary for the improved adherence.

References

1 KIM Y. W., JOM (July 1989) 24

2 MEIER G. H. et. al., in GROBSTEIN T.and DOYCHAK J. (eds.),
Oxidation of High Temperature Intermetallics, (TMS PA, 1989) p. 185

3 LEWIS G. K. and ROMINE J. C., in 32nd SAMPE Symposium (1987)

4 GOLIGHTLY F. A. et. al., J. Electrochem. Soc., 126 (1979) 1035

5 CHOUDHURY N. S. et. al., in FOROULIS Z.A. and PETTIT F.S. (eds.),
Proc. of Symposium on Properties of High Temperature Alloys, (The
Electrochemical Soc., 1976) p.668

6 WELSCH G. and KAHVECI A. I., in GROBSTEIN T.and DOYCHAK J.(eds.),
Oxidation of High Temperature Intermetallics, (TMS PA, 1989) p. 207

7 TORTORELLI P. F. et. al., in ANTON D.L. et. al. (eds.),
Intermetallic Matrix Composites, Vol 194 (MRS PA, 1990) p. 361

8 NOURBAKHSH S. et. al., Metall. Trans. 21A (1990) 213

9 MISRA A. K., Metall. Trans. 22A (1991) 715

10 JANAF Thermochemical Tables, National Bureau of Standards, 1971.

11 WAGNER C., Z. Electrochem.63 (1959) 772

12 NOURBAKHSH S. et. al., Metall. Trans. 22A (1991) 3059

13 DEBUIGNE J., Met. Corros. and Ind. 501 (1967) 186

14 KOFSTAD P., Diffusion and Electrical Conductivity in Binary
Metal Oxides, (Wiler-Interscience, 1972)

15 VYKHODETS V. et. al., The Physics of Metals and Metallography
vol. 68, No. 5 (1989) 145

16 PERKINS R. A. et. al., in GROBSTEIN T.and DOYCHAK J.(eds.),
Oxidation of High Temperature Intermetallics, (TMS PA, 1989) p. 157

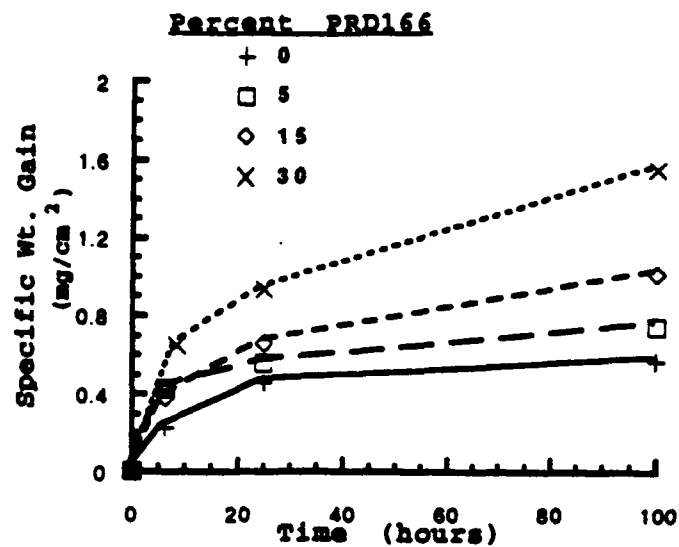17 KOBAYASHI E. et. al., High Temperature Technology vol. 8 (1990)
179

Figure 1   Specific weight gain during isothermal oxidation
at 950°C in air.
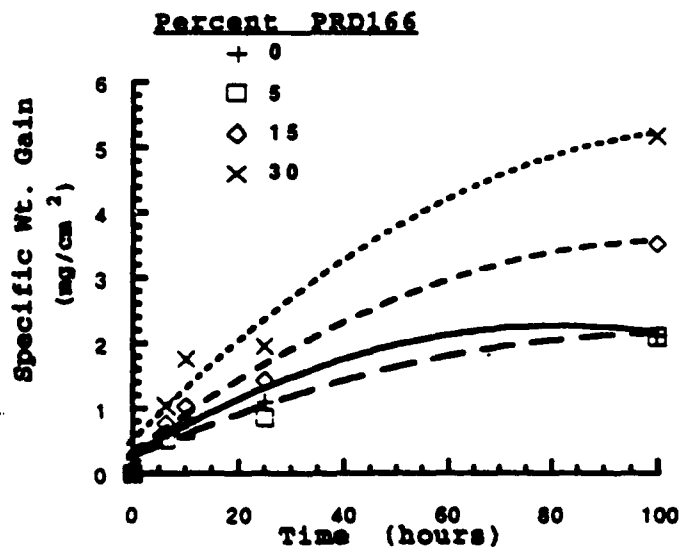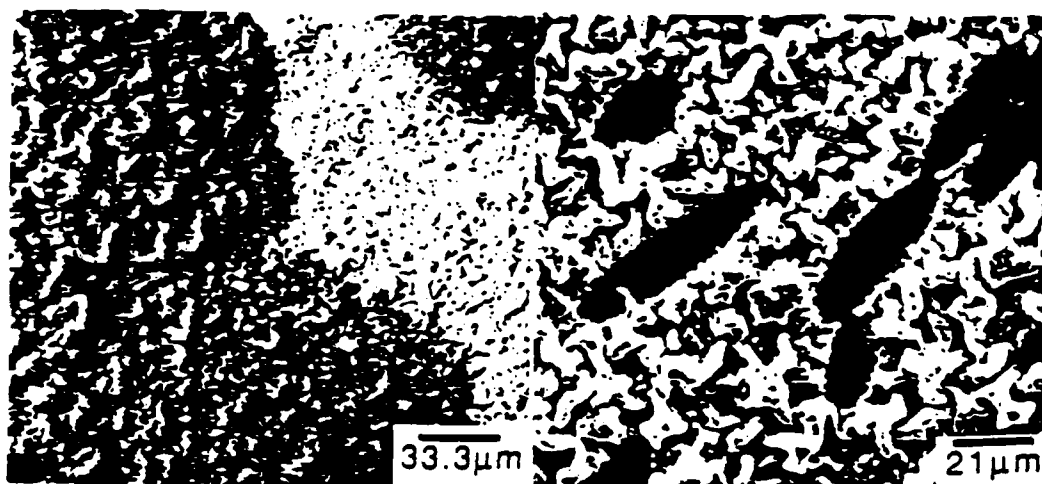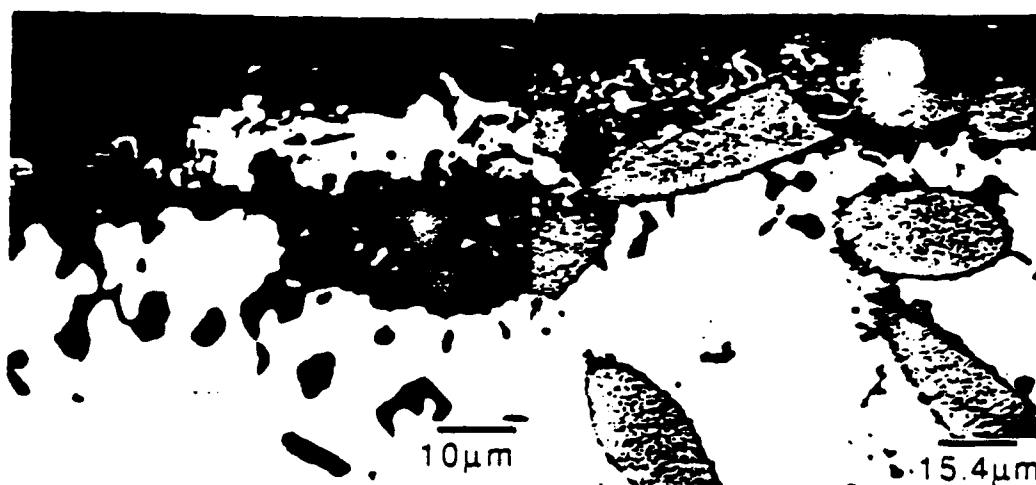

Figure 2   Specific weight gain during isothermal oxidation at
1070°C in air.

(a)   (b)

Figure 3   SEM micrographs (a is a backscattered electron image and b is a secondary electron image) of external oxide morphology after 100 hours at 1070°C. (a- TiAl, b- TiAl-15% PRD166)

(a)   (b)

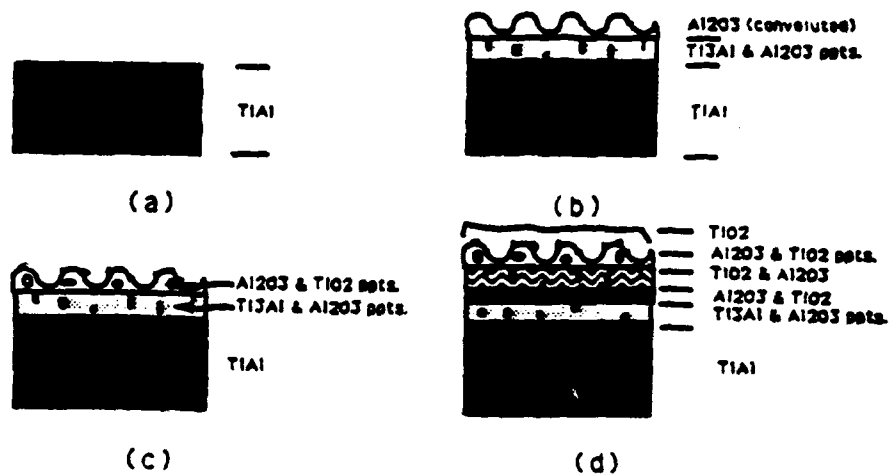Figure 4   Backscattered electron micrographs of oxide cross-sections after 100 hours at 1070°C. (a- TiAl, b- TiAl-15% PRD166)

Figure 5   Schematic model for the oxidation of TiAl at 1070°C.

(a) initial TiAl surface, (b) formation of Al_2O_3 film,

(c) heterogeneous oxide and internal oxidation and (d)
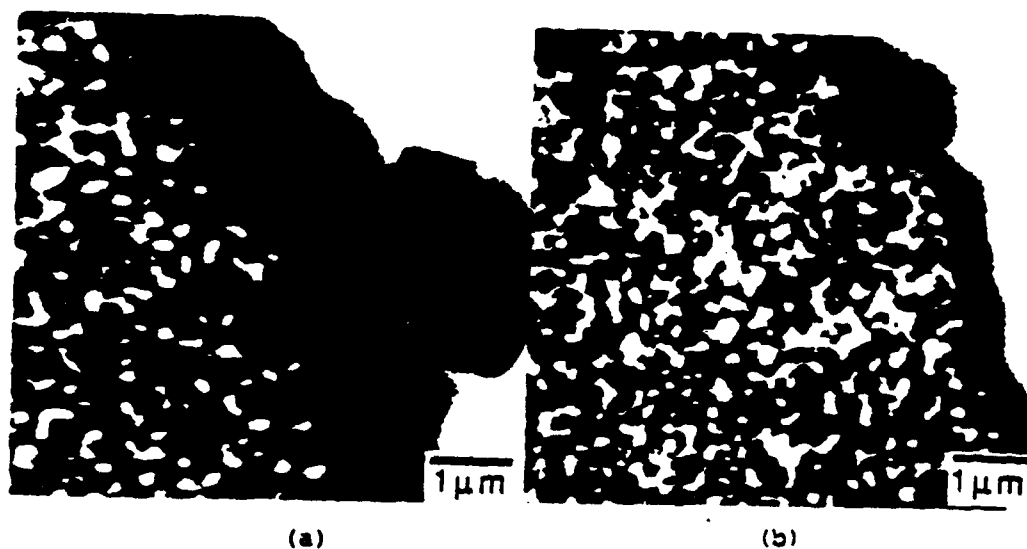
external TiO_2 formation.

Figure 6   Back scattered electron micrograph of alumina layer on

the perimeter of the PRD166 fibers after oxidation for

100 hours at 1070°C.   (a- location near the surface of

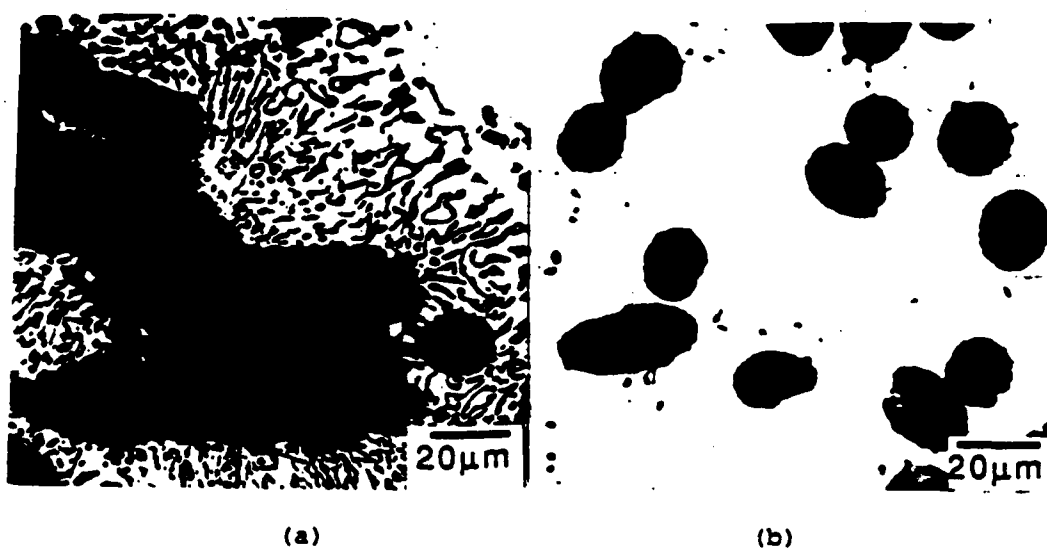the composite, b- location at the center of the

composite).

Figure 7   Microstructure of TiAl-30% PRD166 after 100 hrs. at
            1070°C.(a- air, b- vacuum encapsulated in quartz,
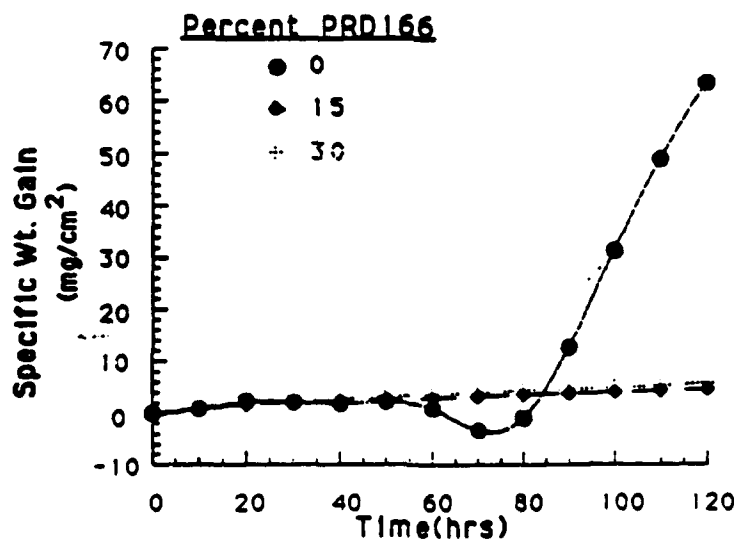   ≈ 10⁻⁷ torr).

Figure 8   Specific weight gain during cyclic oxidation at
            1070°C.(1 cycle= 10 hours).

OXIDATION OF POWDER PROCESSED NbAl₃ MATRIX COMPOSITES

PAUL S. KORINKO AND D.J. DUQUETTE
Rensselaer Polytechnic Institute, Materials Engineering Department, Troy,
New York 12180-3590

ABSTRACT

Niobium aluminide based composites fabricated by powder metallurgy
techniques were tested for oxidation resistance between 1000 and 1400°C.
The oxidation rate of these materials was improved over conventionally
cast or pack aluminized NbAl₃. The inclusion of oxide dispersoids de-
creased the rate constant by an order of magnitude at 1000°C compared to
monolithic NbAl₃ and to a value of the same order of magnitude as NiAl at
1170°C. The most heavily reinforced material studied had a rate constant
an order of magnitude greater than NiAl at 1400°C. The oxide scale was
generally adherent and compact but contained oxide nodules.

INTRODUCTION

Intermetallic compounds are being considered as structural components
for the next generation of aircraft. In these applications it will be
necessary for the components to exhibit superior physical, mechanical and
chemical properties, including resistance to oxidation at elevated tempera-
tures.

It has been shown that, of the niobium aluminides, the intermetallic
compound NbAl₃ has the best oxidation resistance [1]. However, even with
75 atomic percent aluminum, NbAl₃ does not form a compact, a   nt, and
thus protective, scale. A number of efforts have been made to improve the
oxidation resistance of NbAl₃ by alloying. For example, Perkins et al.
added elements which were intended to decrease oxygen solubility and
diffusivity, and to increase the aluminum diffusivity, in an effort to
affect the transition from internal to external oxidation [2]. Hebsur et
al. [3] showed that chromium additions reduced the parabolic rate constant
by a factor of 2.5 and that chromium and yttrium together reduced the rate
constant by a factor of 5.

Oxide dispersions have also been shown to decrease the oxidation rates
of nickel and cobalt based alumina and chromia forming alloys. Reactive
elements, for example, Hf, Sc, Y, Zr, which were preoxidized at a low partial
pressure of oxygen to form internal oxides prior to thermal exposure were
shown to decrease the rate constants [4]. In particular, 0.05% Hf decreased
the weight gain by a factor of 8 in a Co-10Cr-11Al alloy after exposure for
100 hours at 1100°C. In another study a 1% addition of preoxidized Hf in the
same alloy showed a decrease in weight gain by a factor of 4 [5]. Oxide
dispersions included by mechanically alloying Ni-20Cr with 3 volume percent
either Y₂O₃ or CeO₂ showed a decrease in specific weight gain when
compared to similar alloys without the oxide dispersions [6].

In this study the effects of randomly oriented fibers and oxide dis-
persions were investigated in NbAl₃/Al₂O₃ composites manufactured by powder
processing techniques.

EXPERIMENTAL

Two powder metallurgy processing methods were used to fabricate the
materials; conventional hot pressing, (HP), and reactive hot isostatic
pressing, (RHIP). The hot pressed samples were formed by vacuum hot
pressing prealloyed NbAl₃ powders at 21 MPa and 1500°C in a 50 mm diameter

graphite die for 2 hours. The resultant compact contained predominately $NbAl_3$, a small fraction of Nb_2Al (<1%), and 5% Al_2O_3 (determined by quantitative metallography) due to powder contamination. Samples of this composition will be referred to as alloy A.

Reactive hot isostatic pressing was performed by mixing elemental powders of aluminum and niobium in the stoichiometric $NbAl_3$ ratio. The powder was divided into two batches; one batch was used to produce a monolithic compound and a second batch was used to produce the reinforced material. Fifteen volume percent Saffil^{TM} fibers (96-97% Al_2O_3, bal. SiO_2) of diameter $3\mu m$ was added to one batch of powder by means of an ethanol slurry (fibers + ethanol) in order to disperse the fibers. Ethanol was added to the other batch as a control. The powder slurries were mixed for 1 hour in a turbula type mixer. The ethanol was then evaporated at 100°C for 10 hours under vacuum. The loose powders were degassed at 500°C for ten hours and then cold isostatically pressed at 270 MPa in a 13 mm diameter polyurethane die. The green compacts were placed in niobium foil lined welded 304 stainless steel cans, and vacuum encapsulated. The sealed containers were placed in a HIP, which was heated and pressurized to 1200°C and 173 MPa and held for 2 hours [7]. The RHIP sample intended as a monolithic material contained 3-4% Al_2O_3 from oxygen contamination of the powder, and a small fraction of elemental niobium, and will be referred to as alloy B. The matrix of the fiber reinforced RHIP material also had 3-4% Al_2O_3 present. The reinforced alloy is designated as alloy C.

Oxidation samples were electro-discharge machined from the compacts. Samples of alloy A consisted of rectangular slabs, 1.8 mm thick with a surface area of 1.5 cm^2; samples of alloys B and C consisted of disks, 0.7-1 mm thick with a surface area of 0.7 cm^2. The RHIP samples were etched in concentrated HCl + 10% H_2O_2 to eliminate contamination from the HIP can. All of the samples were metallographically polished to $0.3\mu m$ Al_2O_3. The samples were measured, ultrasonically cleaned in an alcohol-50% acetone solution, and weighed on an analytical balance prior to exposure. The specimens were then placed in metallurgical grade alumina combustion boats and loaded into preheated tube furnaces in flowing, dry bottled air (19-22% O_2) at 50 CCM. Single samples were removed after 6.25, 25, and 100 hours and weighed. The sample and any spall which resulted from the thermal cycling were included in the gravimetry. The samples were mounted in epoxy and polished to $1\mu m$ diamond. All the samples were evaluated optically and select samples were examined with a JEOL 733 microprobe or a JEOL 840 SEM in the backscattered electron mode.

The weight gain data was fitted to a parabolic equation of the form:

$$(\Delta W/A)^2 = K_p(time) + C \qquad (1)$$

Where K_p is the parabolic rate constant, C is an integration constant, ΔW is the weight change and A is the surface area.

RESULTS AND DISCUSSION

The data from the isothermal oxidation tests for alloy A are shown in Figure 1. The rate constant was calculated using equation (1).

A micrograph of the sample exposed for 6.25 hours at 1170°C is shown in Figure 2. A generally compact oxide scale was formed, although a number of subsurface cracks were present. These cracks appear along the scale/substrate interface and were present parallel to the interface but further into the substrate. In some areas oxide nodules were formed, as shown in Figure 3. A possible explanation for these sites of severe oxidation is

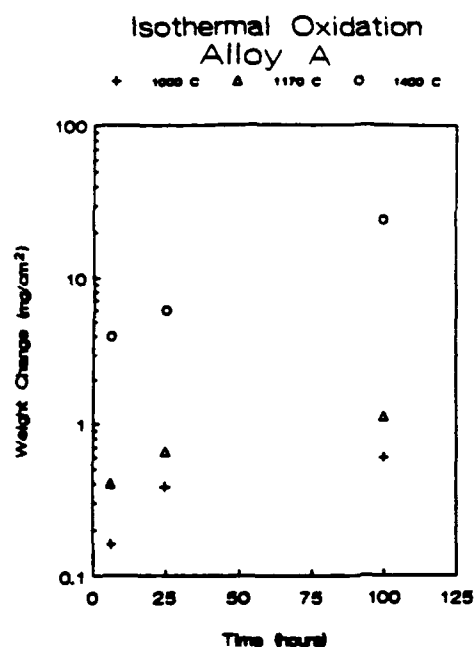^{TM}Saffil is a registered trademark of Imperial Chemical Industries PLC, for alumina fibers.

Isothermal Oxidation
Alloy A

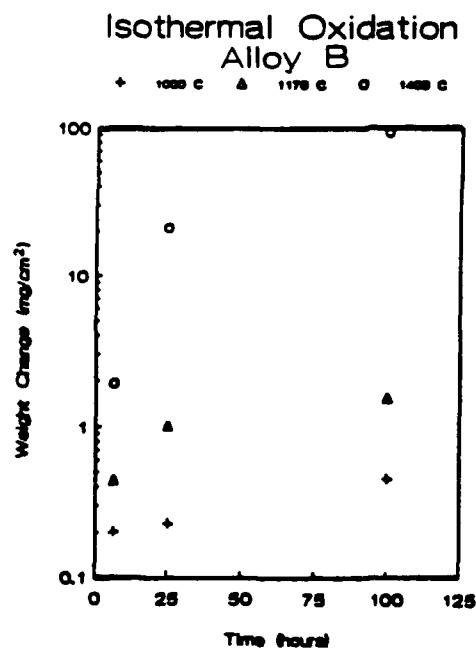+ 1000 C   △ 1170 C   ○ 1400 C

Fig. 1. Isothermal oxidation data for alloy A.

Fig. 2. Backscatterred electron image (BEI) showing oxide scale on alloy A after exposure for 6 hrs. at 1170°C. Crack is parallel to surface at arrow.
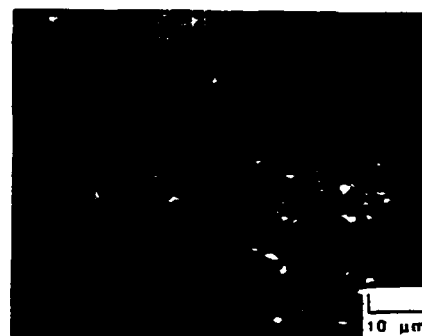

Fig. 3. BEI showing an oxide nodule formed on alloy A after exposure for 25 hrs. at 1170°C. Oxidation occurred along prior particle boundaries. Cracks were also present parallel to the surface, indicated by the arrow.
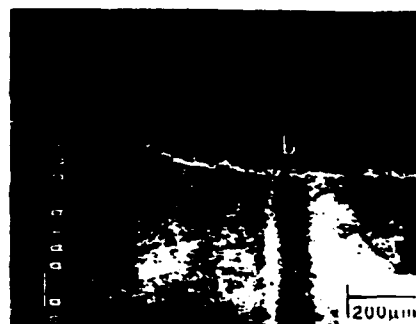
Isothermal Oxidation
Alloy B

+ 1000 C   △ 1170 C   ○ 1400 C

Fig. 5. Isothermal oxidation data for alloy B.

Fig. 4. BEI showing a layered oxide structure formed on alloy A after exposure for 25 hrs. at 1400°C. Dark band in oxide at (a) is Al_2O_3, lighter oxide at (b) is $NbAlO_4$, and subsurface white band (c) is Nb_2Al.

preferential oxidation of the prior particle boundaries leading to debonding of the particle.

A cross-section of the oxide after 25 hours of exposure at 1400°C is shown in Figure 4. Oxidation is much more severe than at the lower temperatures and the oxide scale is thicker. The oxide is layered and consists of NbAlO₄ and Al₂O₃, immediately below the oxide is Nb₂Al.

The oxidation data for alloy B are shown in Figure 5. A macrograph in Figure 6 shows the cross-section of the sample exposed for 100 hours at 1400°C. Almost all of this sample was consumed in this exposure, and only a small unaffected core remained.

The oxide formed at 1000 and 1170°C was generally compact and adherent, but with areas of preferential oxidation. These areas consist of alternating layers of NbAlO₄ and Al₂O₃, a structure similar to the layered oxide shown in Figure 4. Cracking was also present in this alloy. These cracks tended to be parallel to and within the oxide/substrate interface, but not as deep within the substrate as those of alloy A.

The specific weight gain data for alloy C are shown in Figure 7. In contrast to alloys A and B exposed at 1400°C, the surface of alloy C appeared white and feathery. A cross-section of the sample exposed for 25 hours at 1170°C is shown in Figure 8. In addition to the dense and compact oxide shown here; other samples contained regions of enhanced oxidation similar to those found in alloy B. Figure 9 shows a typical region of preferential oxidation of a sample exposed at 1170°C for 6.25 hours. This sample shows a large oxide nodule with a morphology unlike that observed on alloys A and B, shown in Figure 4.
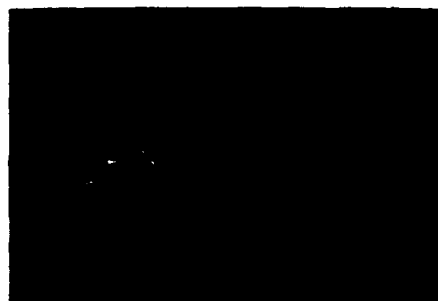

Fig. 6. Macrophotograph of alloy B after 1400°C exposure for 100 hrs. The white is oxide and the shiny core, at arrow, is all that remains of the substrate.
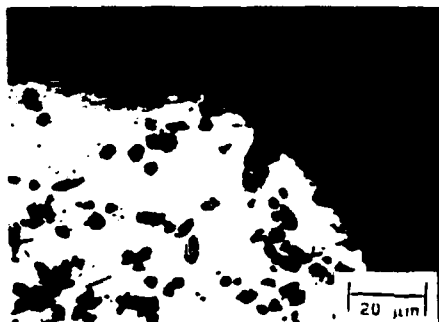

Fig. 8. BEI showing the oxide scale on alloy C after exposure for 25 hrs. at 1170°C. Oxide is shown by (a), fibers by (b) and Nb₂Al by (c).
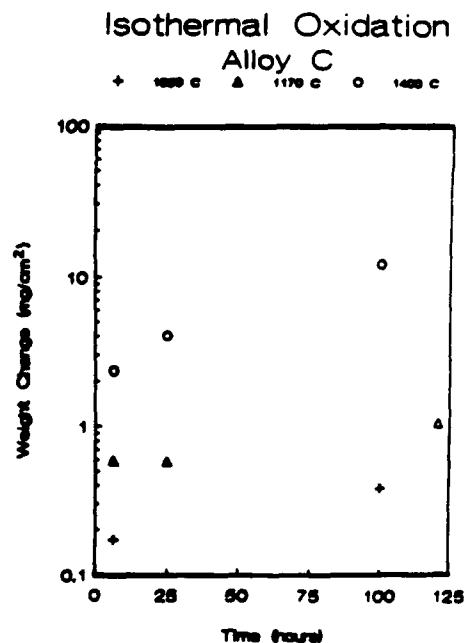

Isothermal Oxidation
Alloy C

Fig. 7. Isothermal oxidation data for alloy C, the composite containing 15 volume percent Saffil^{TM} and 3-4% Al₂O₃ from processing.

Parabolic Rate Constants

Fig. 9. BEI showing an oxide nodule that formed on alloy C after exposure for 6 hrs. at 1170°C. (a) indicates the surface oxide, (b) the nodule and (c) the fibers.
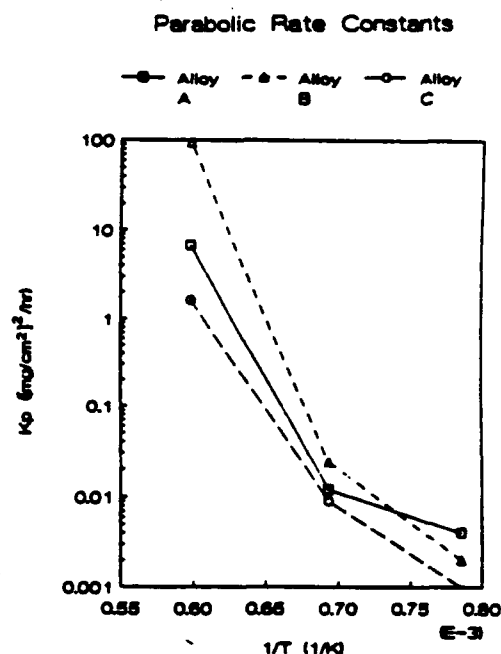
Fig. 10. Arrhenius type plot of rate constants for the materials investigated in this study.

An Arrhenius plot for the rate constants is shown in Figure 10. The apparent change in slope, and the change in oxide morphology, suggest that the oxidation mechanism changes as a function of temperature.

Monolithic $NbAl_3$ produced by pack aluminizing [2] by casting [3] and by reactive sintering [8] form an oxide consisting of alternate layers of Al_2O_3 and $NbAlO_4$. The alloys in the present study showed improved oxide adherence and less propensity to form the alternating layered structure, although the oxide product was nonuniform. This general improvement may be due to the oxide dispersions or fibers contained in the samples. A possible explanation for the improvement due to compositing is suggested from studies on nickel based alloys containing oxides and reactive elements.

The reasons for the improved oxide adherence due to both oxide dispersions and reactive element additions in nickel based alloy systems which form alumina and chromia have been extensively reviewed. For example, Kofstad, compiled the following list of possible mechanisms: (a) improved mechanical properties of the scale/substrate interface; (b) establishment of a graded seal between the main scale and the substrate by formation of a complete layer of a compound of the oxygen active element with favorable thermal expansion characteristics; (c) dispersed oxide particles serve as vacancy sinks and therby reduce or eliminate void formation and loss of oxide adherence; (d) oxide keying or pegging obtained by increased internal and intergranular oxidation due to the presence of the oxygen active elements; (e) an improved chemical bond at the alloy/scale interface by the presence of the oxygen active element [9].

None of the alloys tested in this study contained active elements, thus effectively eliminating (b), (d), and (e). The possibility of improved mechanical properties at the scale/substrate interface is doubtful based on the severity of the cracking found in several of the specimens. From those suggestions, then, the concept of dispersoids acting as vacancy

sinks remains a possibility. Another possibility is that the oxide particles which intersect the surface act as nucleation sites for the external oxide [5], which leads to the formation of the steady state oxide configuration more rapidly. However, a specific mechanism for the decrease in oxidation rate cannot be identified.

SUMMARY

The oxide dispersoids contained in the samples due to processing lead to an improved oxidation resistance in powder metallurgy produced NbAl$_3$. This improvement was even greater for samples that contained randomly dispersed fibers. The fibrous composite exhibited a parabolic rate constant similar to NbAl$_3$ alloyed with Cr and Y. The reasons for the improvement in oxidation resistance are not fully understood.

ACKNOWLEDGEMENTS

REFERENCES

1.   R.C. Svedburg, in Properties of High Temperature Alloys, Edited by Z.A. Foroulis and F.S. Pettit, The Electrochemical Society, 1976, p.331.

2.   R.A. Perkins, K.T. Chiang, and G.H. Meier, Script Metallurgica, 22, 419 (1988).

3.   M.G. Hebsur, J.R. Stephens, J.L. Smialek, C.A. Barrett, and D.S. Fox, NASA TM 101398 (1988).

4.   I.M. Allam, D.P. Whittle, and J. Stringer, Oxidation of Metals, 12, 1, 35 (1979).

5.   I.M. Allam, D.P. Whittle, and J. Stringer, Oxidation of Metals, 13, 4, 381 (1979).

6.   J. Stringer, B.A. Wilcox, and R.I. Jaffee, Oxidation of Metals, 5, 1, 11 (1972).

7.   J. Murray, Master's Thesis, Rensselaer Polytechnic Institute, 1989.

8.   P.S. Korinko and D.J. Duquette, unpublished work (1988).

9.   P. Kofstad, High Temperature Corrosion, Elsevier Applied Science Publishers, New York, 1988, p.404.

OXIDATION OF POWDER PROCESSED NIAL AND NIAL/TIB₂ COMPOSITES

P.S. Korinko, D.E. Alman, N.S. Stoloff, and D.J. Duquette
Rensselaer Polytechnic Institute, Materials Research Center, Troy, NY 12180

ABSTRACT

NiAl and NiAl/TiB₂ composites were tested in air at 800, 1000, and
1200°C. The oxidation resistance of the composites depends on the fabri-
cation route, and subsequently on the reinforcement phase morphology and
distribution. The oxidation resistance of NiAl reinforced with large TiB₂
particles was found to decrease with increasing TiB₂ content. NiAl
reinforced with large TiB₂ particles was completely oxidized at 1200°C after
a 100 hour exposure.

INTRODUCTION

Intermetallic matrix composites have emerged as potential next gener-
ation high temperature structural composites, as evidenced by this
conference and the MRS conference of 1990 [1]. Features such as high
melting temperatures, low densities, and excellent oxidation resistance make
intermetallic compounds attractive for high temperature applications,
especially for the aerospace industry. However, these materials have poor
creep resistance and poor room temperature toughness. Compositing may
improve these material properties and consequently make intermetallics
useful structural materials.

The intermetallic compound NiAl, reinforced with TiB₂ particles,
displays a number of properties that make it attractive for use at elevated
temperatures. For example, NiAl has a high melting temperature, 1640°C, a
low density, 5.86 g/cm³, and excellent oxidation resistance [2]. In
addition, the inclusion of TiB₂ particles has been shown to improve the
mechanical behavior of NiAl. For instance, the creep resistance of
NiAl/10 vol% TiB₂ is markedly improved compared to monolithic NiAl [3],
large increases in the room temperature strength of NiAl/TiB₂ composites
have been reported [4]. Finally, it has been experimentally determined
that NiAl and TiB₂ are thermodynamically compatible at elevated temperatures
[5].

Most research efforts have centered on determining the macromechanical
properties of NiAl/TiB₂ composites [6],[7]. Little work has been
reported on the chemical stability of NiAl/TiB₂ alloys when exposed to an
oxidizing environment, such as air at elevated temperatures, although the
oxidation behavior of binary nickel-aluminum alloys, as a function of
aluminum content, has been extensively studied and is reasonably well
understood [8],[9]. For example, it is well known that a minimum of
17 wt% Al is required to exclusively form a continuous alumina scale on
binary nickel-aluminum alloy [10].

NiAl oxidized at 900°C has a minimum oxidation rate constant at 42at%
Al [11]. This minimum is attributed to the manner in which the activity
of the dissolved Al varies with composition. More recent work [2] did not
show the same compositional dependence of the rate constants, but this work
was conducted at higher temperatures at which an alpha Al₂O₃ forms rather
than the theta Al₂O₃ oxide that forms below 1000°.

Further, the oxide formed on near stoichiometric NiAl has been
observed to spall readily on cooling [12],[13]. Spalling can be

diminished or prevented by appropriate alloying, [2] typically with reactive elements.

In the current work, the oxidation resistance of binary monolithic NiAl and NiAl/TiB$_2$ composites containing 10 and 20 vol% TiB$_2$ produced via powder metallurgy has been determined between 800 and 1200°C.

MATERIALS FABRICATION

For this study, NiAl/TiB$_2$ samples were produced by two powder metallurgical approaches: Reactive synthesis (RS) of Ni, Al and TiB$_2$ powders and conventional hot isostatic pressing (HIP) of XD™ synthesized NiAl/TiB$_2$ powder blends.

Reactive synthesis of NiAl/TiB$_2$

Reactive synthesis involves producing alloys or compounds from elemental constituents. Upon heating the mixture of elemental powders to the lowest liquidus temperature in the desired system (640°C in the Ni-Al system), a transient liquid forms. The liquid phase enhances both diffusion and densification via capillary forces. The high thermodynamic stability (i.e. large heat of formation) provides the driving force for the reaction. The high thermal stability of the forming compound manifests itself by the exothermic nature of the reaction. As a consequence, the reaction becomes self-sustaining. This type of process has been termed self-propagating high temperature synthesis (SHS), and has been used to synthesize NiAl, NiAl/TiB$_2$, as well as other alloys and compounds [4]. It was found that the reaction between Ni and Al to form NiAl was so exothermic that the addition of a dilutant phase (up to 15 wt% either prealloyed NiAl or a high melting temperature second phase) was necessary to prevent melting of the container and sample during the synthesis and pressureless densification stages.

The procedure for the fabrication of reactive synthesized material is as follows: Elemental Ni and Al powders were mixed to a composition corresponding to 51 at% Ni (70 wt% Ni). To decrease the peak temperature and control the reaction 10 wt% prealloyed NiAl was added to the elemental powder mixture. Either 0, 10, or 20 vol% TiB$_2$ was then blended with the Ni, Al, and NiAl mixture. Mixing was performed in a turbula type mixer for 60 minutes. Table I lists the characteristics of the powders used in this study. Cylindrical compacts (31.7 mm diameter by 75 mm long) were produced by cold isostatic pressing the powder to approximately 70% theoretical density. The compacts were encapsulated in 304 stainless steel HIP cans. While attached to a vacuum system the cans were heated to 700°C to allow the Ni and Al to react and densify. The samples were then sealed and HIPed at 1250°C, 172 MPa for either 1 or 2 hours, depending on the sample chemistry, to remove residual porosity. Figures 1a-1c shows the starting microstructures of the RS HIP materials.

Table I. Characteristics of the starting materials.

Powder	Size	Shape	Process
Al	3 μm	spherical	gas atomized
Ni	3-7 μm	spikey surface	carbonyl
NiAl	-325 mesh	angular	—
TiB$_2$	3 μm	—	—

HIP of XD™ Synthesized Powder

XD™ is a proprietary process developed by Martin Marietta Corporation,

Baltimore, MD, in which fine (1-3 μm) TiB_2 particles are dispersed in a
variety of matrices. Details of the process have been described in various
patents [14],[15]. Composite NiAl/10 vol% TiB_2 powder obtained from
Martin Marietta was pressed directly into 304 stainless steel HIP cans (12.5
mm diameter) and vacuum degassed at 300°C for several hours and then
vacuum encapsulated. The HIP conditions were 1250°C, 172 MPa for 2 hours.
Figure 1d shows the microstructure of the XD sample. Note the fine TiB_2
dispersoids compared to the coarser TiB_2 dispersoids found in the
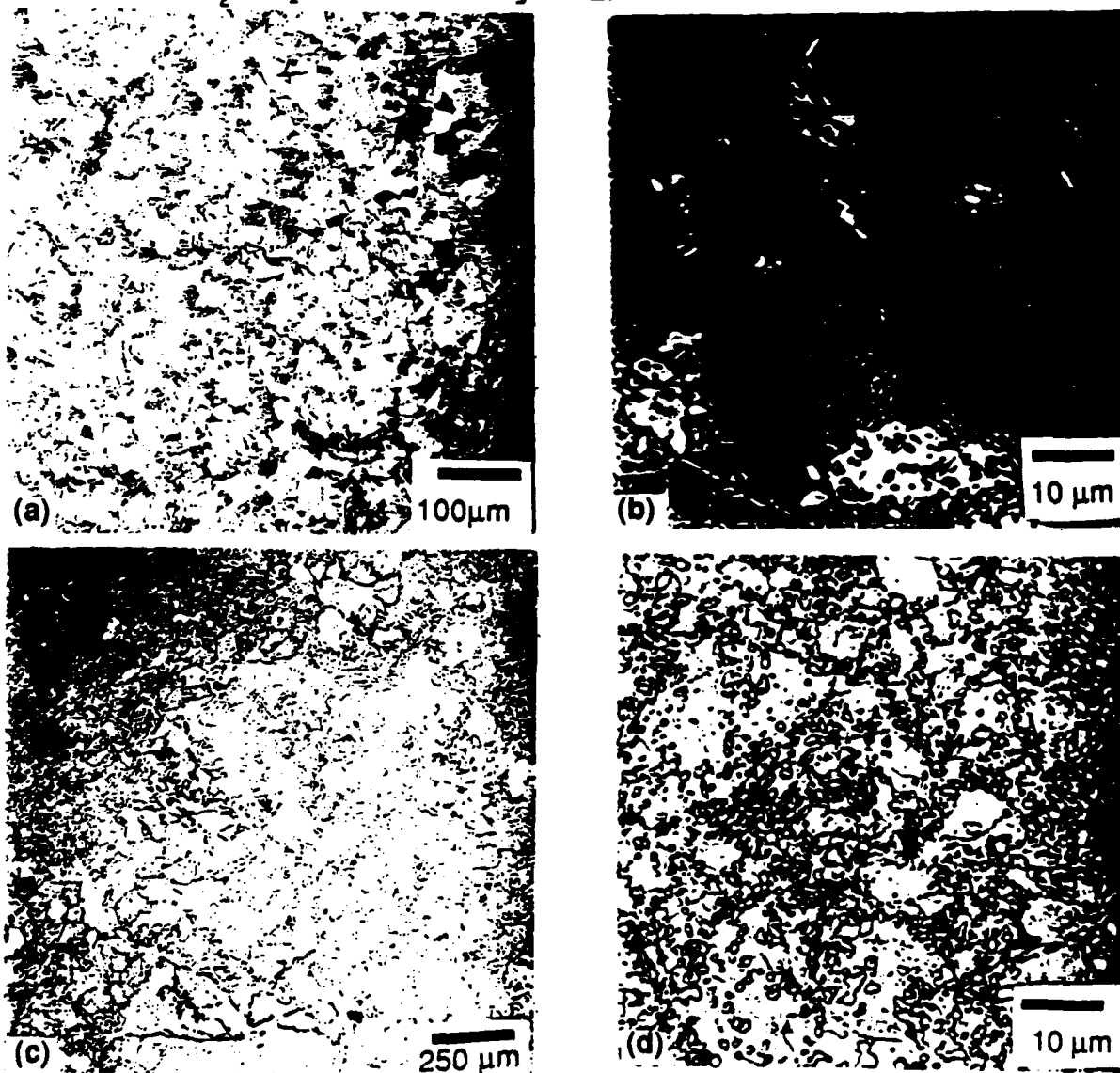RS-10 vol% TiB_2 sample shown in Figure 1b.

Figure 1 showing the initial etched microstructures of the samples used in
this study. (a) RS-monolithic NiAl (b) RS-10TiB₂ (c) RS-20TiB₂ (d) XD-10
TiB_2. Etchant: Kallings Reagent.

OXIDATION SAMPLE PREPARATION

Oxidation samples were prepared by cutting disks of approximately 1
cm^2 of the HIPed material with a diamond saw. The samples were
metallographically polished to 0.3 μm alumina on all sides. After
polishing, the samples were ultrasonically cleaned in alcohol/50% acetone,
measured, and weighed. The samples were placed in alumina combustion boats
and inserted into a preheated furnace. Dry, compressed air was passed
through the furnace tube at 50 cc/min. Thermal exposure was conducted by
placing a single sample in the furnace and removing it after 6.25, 25 or 100

hours. The sample was cooled to room temperature, weighed, and then returned to the furnace until the next interval. The tests were conducted at 800, 1000, and 1200°C. Any loose or lightly adherent oxide was removed before the sample was weighed.

The samples were examined with optical microscopy, scanning electron microscopy (SEM), energy dispersive spectroscopy (EDS), and x-ray diffraction (XRD). Standardless semiquantitative (SSQ) analysis was used in conjunction with the EDS.

RESULTS AND DISCUSSION

The results of the isothermal exposure at 800°C are shown in Figure 2. These results show that the monolithic NiAl (RS-0) initially oxidized slightly and that the weight gain remained nearly constant after the first few hours. The oxide on the sample was so thin that it only showed a slight red-gold heat tint after the 100 hour exposure.

Figure 2 also shows that the inclusion of 10 vol% TiB_2 in to the NiAl, either through the RS process, or the XD process, resulted in only a small reduction of the oxidation resistance compared to the monolithic alloy. However, increasing the TiB_2 content to 20 vol% resulted in an increase of the weight gain of approximately 250%.

The composites had a grayish surface when examined at 10X magnification, however, at 100X magnifications the surface showed islands of grey oxide with a heat tinted oxide on the balance of the surface.
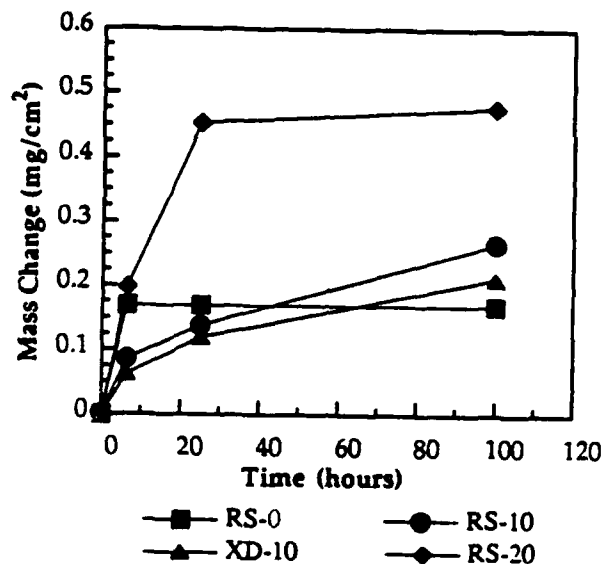

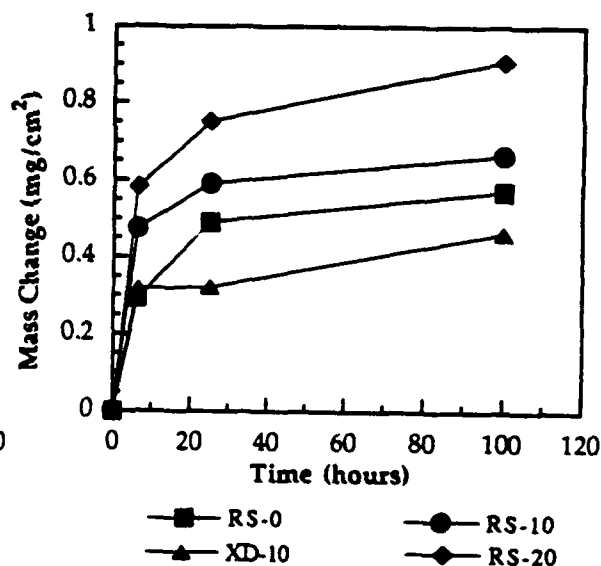Figure 2 Isothermal oxidation data for NiAl and composites at 800°C.

Figure 3 Isothermal oxidation data for NiAl and composites at 1000°C.

X-ray diffraction of the composite samples' surfaces showed predominately NiAl and TiB_2, but also included peaks for Al_2O_3 and TiO_2. The X-ray diffraction pattern from the monolithic samples showed only NiAl, with the oxide peaks at about the same intensity as the background.

The results of the isothermal exposure at 1000°C are shown in Figure 3. The XD-10 sample shows improved oxidation resistance compared to the RS processed materials. This is possibly due differences in alloy composition or morphology of the reinforcing phase. EDS of the oxides on the 10 TiB_2 samples showed that there is a small amount of Ti in the oxide on the XD material but not in the RS material. The RS-0 sample has better oxidation resistance than any of the RS processed composites, and the weight gains increase with increasing volume fraction of TiB_2.
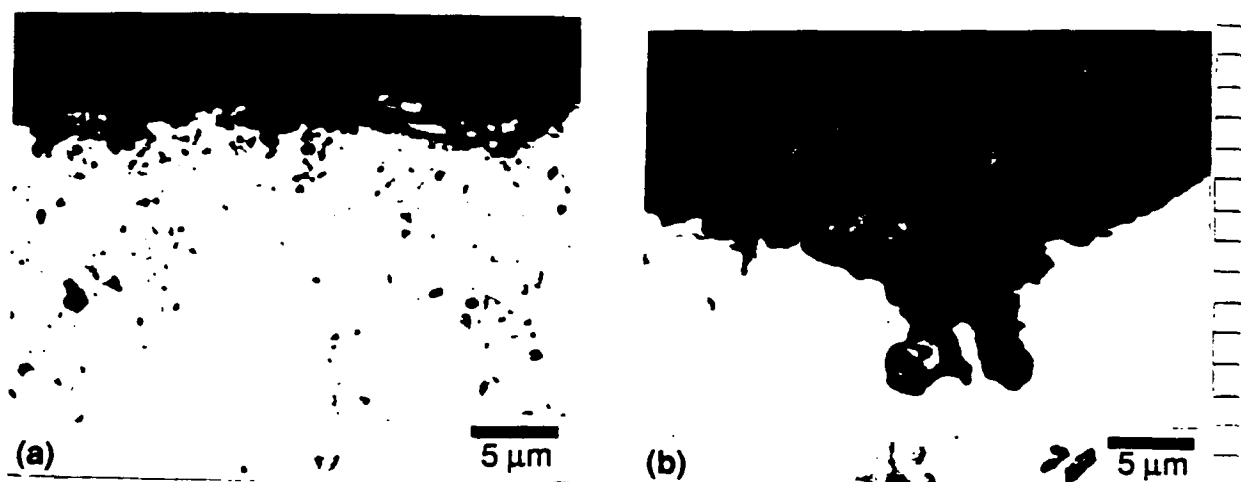
Figure 4 Oxides formed on NiAl/10TiB$_2$ (a) XD processed (b) RS processed SEM backscatter electron images (BEI).

Figures 4a and 4b show the oxide scale formed on the 10 vol% TiB$_2$ composites after a 100 hour exposure at 1000°C. Figure 4a shows the oxide on the XD processed sample. The oxide is generally planar and compact, compared to the oxide formed on the RS sample which tends to be thicker with some oxide intrusions along the TiB$_2$ particles. This difference in reaction product morphology can most likely be attributed to the difference in reinforcement morphology shown in Figures 1b and 1d. Figure 5 shows the isothermal exposure data for the NiAl/TiB$_2$ composites exposed at 1200°C. These data show that the monolithic RS sample is more oxidation resistant than any of the composites, although it spalled after the 25 hour exposure and the test was terminated. The XD-10 sample is more oxidation resistant than the RS-10; in fact, the RS-10 sample was nearly consumed during the testing and only small islands of unoxidized matrix remained, whereas the XD sample retained most of its original characteristics. The RS sample did not
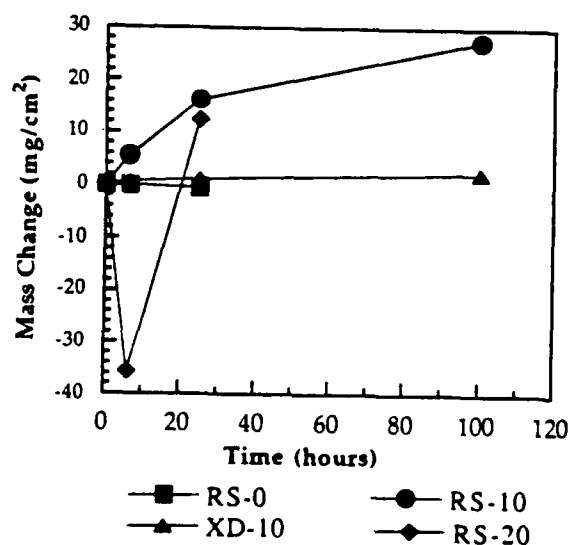

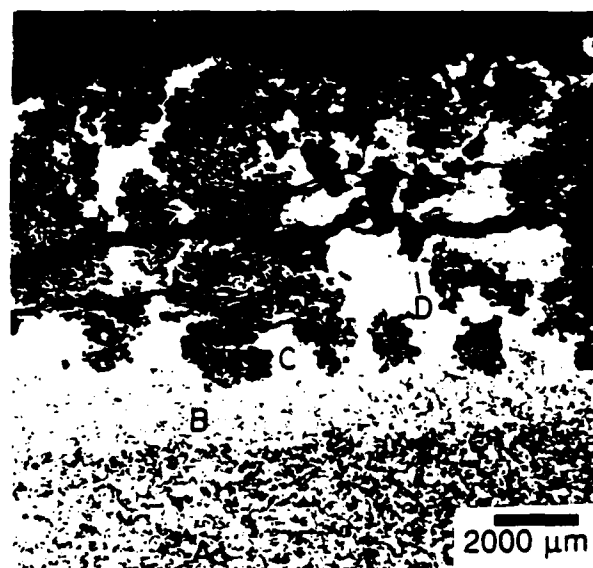Figure 5 Isothermal oxidation data for NiAl and composites at 1200°C.

Figure 6 Photomicrograph of a cross-section of NiAl/20 TiB$_2$ exposed at 1200°C for 25 hours; note the four distinct zones. Kalling's reagent

spall despite the extent of the oxidation.

The RS-20 sample readily spalled after the first cycle. The weight gain for the RS-20 between 6.25 and 25 hours is due to the rapid oxidation and lack of spalling on this thermal cycle. This test was aborted after 25 hours because of the sample's poor performance. Several very interesting reactions occurred during the oxidation testing of this sample. Figure 6a shows a cross section of the RS-20 sample with cracks parallel to the substrate and large areas of internal oxidation. Four distinct regions can also be seen, points A-D. These areas were examined in the SEM using EDS and SSQ; compositions are given in atomic percent. Point A indicates the unaffected base alloy, β NiAl, with 49.6 Ni and 50.4 Al. Point B indicates a narrow dealloyed zone, still β NiAl, with 56.7 Ni and 43.3 Al. Point C indicates a large band with precipitates, γ', with 74.4 Ni and 25.6 Al. And Point D indicates internal precipitates, γ', with 74.8 Ni, 21.2 Al, and 4 Ti.

The oxide also shows variable compositions. These variations are indicated by points E-G in Figure 7, a backscattered electron image (BEI) of the RS-20 sample after a 25 hour exposure at 1200°C. Point E shows a dark continuous phase; presumably Al_2O_3 since only Al was detected. Point F shows a light grey precipitate in the Al_2O_3, most likely TiO_2, since only Ti was detected. Point G shows a white dispersed phase which consisted of 86.25 Ni, 9 Al, and 4.75 Ti.

Table II shows the weight changes after the 100 hour exposure. The specific mass change increases with increasing volume fraction of TiB_2 for the RS processed material.

Table II. Mass changes after 100 hour exposure (mg/cm²).

Sample	800°C	1000°C	1200°C
RS-0	.17	.57	-.42*
XD-10	.21	.46	2.40
RS-10	.22	.66	27.55
RS-20	.48	.91	12.60*+

* test was terminated after 25 hours
+ sample initially spalled

Figure 7 Backscattered electron image of the oxide on NiAl/20 TiB_2 exposed at 1200°C for 25 hours; note the three distinct phases.

SUMMARY AND CONCLUSIONS

1. At 800, 1000, and 1200°C the oxidation resistance of RS NiAl reinforced with TiB_2 decreases with increasing volume fraction reinforcement.
2. The reinforcing phase morphology affects the oxidation resistance with small particles being less detrimental to the oxidation resistance than large ones.
3. NiAl reinforced with large TiB_2 particles is completely oxidized at temperatures in excess of 1000°C, fortunately, the mechanical property limitation for NiAl with large TiB_2 particles also seems to be 1000°C [4],[16].
4. XD-NiAl/10TiB_2 has superior oxidation resistance to the RS-NiAl/10TiB_2 at 1000 and 1200°C.

ACKNOWLEDGEMENTS

REFERENCES

1.   Intermetallic Matrix Composites, Edited by D.L. Anton, P.L. Martin, D.B. Miracle, and R. McMeeking, Vol 194, Materials Research Society, Pittsburgh, PA 1990.

2.   J. Doychak, J.L. Smialek, and C.A. Barrett, in Oxidation of High Temperature Intermetallics, Edited by T. Grobstein and J. Doychak, The Minerals, Metals and Materials Society, 1989.

3.   J.D. Whittenburger, R.K. Viswanadham, S.K. Mannan, and B. Sprissler, Journal of Materials Sciences, Vol 25, pp 35-44, 1990.

4.   D.E. Alman and N.S. Stoloff, International Journal of Powder Metallurgy, Vol 27, No. 1, pp. 29-41, 1991.

5.   M. Saqib, G.M. Mehrotra, I. Weiss, H.Beck, and H.A. Lipsitt, Scripta Metallurgica, Vol 24, pp 1889-1894 1990.

6.   R.K. Viswanadham, S.K. Mannan, K.S. Kumar, and A. Wolfenden, Journal of Materials Science Letters Vol 8, p 409-410, 1989.

7.   R.K. Viswanadham, J.D. Whittenberger, S.K. Kumar, and B. Sprissler, in High Temperature Ordered Intermetallic Alloys III, Edited by C.T. Liu, A.I. Taub, N.S. Stoloff, and C.C. Koch, Materials Research Society, Pittsburgh, PA 1989.

8.   J.S. Wolf and E.B. Evans, Corrosion, Vol 18 pp 129-136, 1962.

9.   F.H. Stott and G.C. Wood, Corrosion Science, Vol 17 pp 647-670, 1977.

10.   F.S. Petit, Transactions of the Metallurgical Society of AIME, Vol 23, pp 1296-1305, 1967.

11.   R.H. Hutchings and M.H. Loretto, Metal Science, pp 503-510, 1978.

12.   H.M. Hindam and W.W. Smeltzer, Journal of the Electrochemical Society, Vol 127, pp 1630-1635, 1980.

13.   J.L. Smialek, Metallurgical Transactions A, Vol 9A, pp 309-320, 1978.

14.   D.C. Nagle, J.M. Brupbacher, L. Christodoulou, U.S. Patent No. 4,774,052 Sept. 27, 1988.

15.   L. Christodoulou, D.C. Naglem and J.M. Brupbacher, U.S. Patent No. 4,751,048, June 14, 1988.

16. D.E. Alman and N.S. Stoloff, in Advanced Composite Materials, Edited by M.D. Sacks, American Ceramics Society, Westerville, OH, 1991

Korinko